eman ta zabal zazu
Universidad del País Vasco
Euskal Herriko Unibertsitatea

ZTF-FCT
Zientzia eta Teknologia Fakultatea
Facultad de Ciencia y Tecnología

ELECTRONIC SPECTROSCOPY OF PROPOFOL, PROPOFOL HOMOMERS AND THEIR HYDRATATED CLUSTERS

By

Iker León Ona

Leoia, July 2011

A ***Thesis*** *Submitted in Fulfillment of the Requirements*

for the degree of

DOCTOR OF PHILOSOPHY

In the Department of Chemical Physics

ISBN: 978-84-695-1248-7

To my parents

‘‘There's real poetry in the real world. Science is the poetry of reality’’

Richard Dawkins (2007)

Abstract

As several works suggest, the action of anaesthetics takes place through direct interaction with membrane receptors. They can interrupt the transmission of the electrical signal along the neuron´s axon by blocking the ion channels or they can dock in the pre/post synaptic receptors, blocking the communication between neurons. In the latter, the action is directly related to that of neurotransmitters, as they bind to the same kind of receptors. Mutagenic studies have already probed the existence of several key amino acids in their respective receptors and thus, the anaesthetic-receptor interaction can be modeled by studying separately the non-covalent interactions between specific residues of the amino acids conforming the active site and the anaesthetic.

There are three main goals in this thesis: first, characterization of the non-covalent interactions that take place between propofol and the residues of the amino acids conforming the active site, i.e. propofol-phenol and propofol-isopropanol have been characterized using a variety of gas-phase spectroscopic techniques. The results obtained shed some light on some of the particularities observed by X-Ray experiments.

Second, the solvation of propofol by water was extensively studied. The whole process of transport and docking of anaesthetics relies in the changes on the Gibb's free energy, which favors the propofol-active site interaction over propofol solvation by the extracellular medium. Therefore, a deep knowledge on the interactions between both propofol and the extracellular medium (water) is required. Consequently, a complete study of propofol with up to nine water molecules, propofol·W_{1-9}, was done.

Third, in order to understand the competition between dispersive forces and hydrogen bond, propofol self-aggregation process was studied (up to $propofol_6$, being one of the greater systems ever explorer by the use of supersonic expansions). Such systems are mainly governed by dispersive forces. In addition, solvation of propofol homomers has also been characterized, introducing water molecules into the previous system: $propofol_2$·W_{1-7}, $propofol_3$·W_1 and $propofol_4$·W_1. Such study has led to unexpected results in both systems, as for the former, formation of nano-micelles was observed, while the latter allows exploring the solvation process of such nano-micelles.

Keywords: anaesthetics, propofol, solvation, hydrogen bond, non-covalent interactions, cooperative effect, spectroscopy, gas-phase biological molecules, supersonic expansions, REMPI, IDIRS, hole burning, *ab initio*, TD-DFT, MMFFs.

Resumen

Estudios recientes demuestran que los anestésicos desempeñan su papel fundamental interaccionando directamente con los receptores de membrana, pudiendo interrumpir la transmisión de la señal eléctrica a lo largo del axón neuronal al bloquear los canales iónicos, o bien pueden acoplarse en los receptores pre/post-sinápticos bloqueando la comunicación entre las neuronas. El último caso está directamente relacionado con la acción de los neurotransmisores, puesto que se unen al mismo tipo de receptores. Varios estudios mutagénicos han demostrado la existencia de aminoácidos clave en sus respectivos receptores, por lo que se puede modelar la interacción anestésico-receptor estudiando por separado las interacciones de carácter no covalente entre los residuos de los aminoácidos clave y el anestésico.

Esta tesis engloba tres objetivos principales: el primero, consiste en el estudio de las interacciones no covalentes que tienen lugar entre el propofol y los residuos de los aminoácidos presentes en el centro activo, es decir, fenol e isopropanol, mediante el empleo de técnicas espectroscópicas en expansiones supersónicas. Los resultados obtenidos sirven para interpretar las estructuras elucidas mediante difracción de rayos-X.

En segundo lugar, se ha estudiado la solvatación del propofol en agua. El proceso completo de transporte y acople de los anestésicos está gobernado por cambios en la energía libre de Gibbs, que favorece las interacciones propofol-centro activo sobre la solvatación por el medio extracelular. Siendo así, es imprescindible el estudio detallado de las interacciones entre el propofol y el medio extracelular, es decir, el agua. Para ello se ha realizado un estudio completo del sistema propofol y hasta nueve moléculas de agua: propofol·W_{1-9}.

En tercer lugar, y siendo como objeto la compresión de la competencia entre fuerzas dispersivas y enlaces de hidrógeno, se ha estudiado la auto-agregación del propofol, llegando incluso al sistema $propofol_6$, que es uno de los mayores sistemas explorados hasta ahora mediante el uso de expansiones supersónicas. Por otro lado, la solvatación de los homómeros ha sido completamente caracterizada al introducir moléculas de agua en los sistemas anteriores: $propofol_2$·W_{1-7}, $propofol_3$·W_1 y $propofol_4$·W_1. Los resultados obtenidos, aparte de la importancia ya mencionada,

permiten alcanzar conclusiones inesperadas al observarse la formación de nano-micelas. Además, el estudio de las especies mixtas, permite la exploración del proceso de solvatación de dichas micelas.

Palabras clave: anestésicos, propofol, solvatación, enlace de hidrógeno, interacciones no covalentes, efecto cooperativo, espectroscopía, moléculas biológicas, expansiones supersónicas, REMPI, IDIRS, *hole burning*, *ab initio*, TD-DFT, MMFFs.

INDEX

Index

CHAPTER 1

INTRODUCTION

1 – INTRODUCTION

Neurons communicate through contacts between the foot of a neuron and the dendrites of the next one, being the space between two neurons called synapses. Some of them are electrical, but by far, the overwhelming majority of synapses in the human brain are chemical synapses. It is the release and capture of neurochemical substances, called neurotransmitters, from one neuron to another, that forms the basis of neural communication (Figure 1.1). Such neurotransmitters (e.g., catecholamines and indoleamines) are present in multicellular animals, which have been found in both vertebrates and invertebrates, and it is known that the central process of brain function is the activation of receptors by this substances.

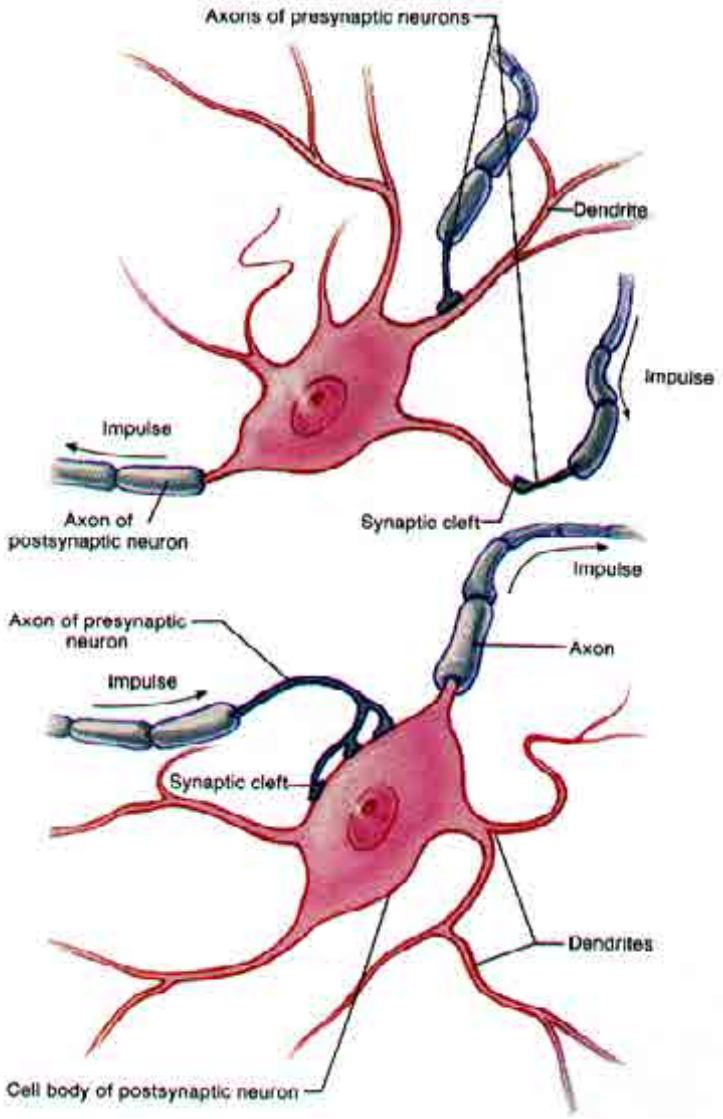

Figure 1.1.*Release and capture of neurochemical substances, neurotransmitters, between neurons forms the basis of neural communication.*

For many years, the molecular mechanism of anesthesia has puzzled scientists, specially taking into account the large number of molecules with anaesthetic action (ethers, haloalkanes, barbiturates, opioids,…, etc), with very different structures. Such diversity of structures, together with the experimental observation of a correlation between the oil/water partition coefficient and the potency of an anaesthetic[1-2] led to conclude that the anaesthetics exert their action by direct interaction with the lipid bilayer. However, such hypothesis fails explaining several experimental observations, such as the different activity of enantiomers.

Following several works on model proteins, a second theory emerged, which explained the action of anaesthetics by their direct interaction with membrane receptors.[3] Such hypothesis was further confirmed by mutagenic studies that demonstrated that the change of a single amino acid in a receptor protein leads to dramatic changes in the anaesthetic action of a molecule.[4] Thus, there are two key points at which the anaesthetic can exert their action. On the one hand, they can dock into the (pre- or post-) synaptic receptors, blocking the communication between neurons[5]. On the other hand, they can interrupt the transmission of the electrical signal along the neuron's axon by blocking the ion channels.[5-6] The action of the first type of anaesthetics is therefore related to that of neurotransmitters, as they bind to the same kind of receptors. For example, $GABA_A$ (gamma-aminobutyric acid) receptors.

The existence of key amino acids suggests that the local anaesthetic (LA) - receptor interaction can be modeled by studying separately the non-covalent interactions that take place in the pore between specific residues of the constituent amino acids conforming the active site and the local anaesthetic. Therefore, using a reductionist approach, it is possible to isolate the intermolecular interactions in anaesthetic–amino acid pairs. Such pairs of interacting molecules can be generated in supersonic expansions and can be probed by using different laser-based spectroscopic techniques. There are many examples in the literature demonstrating the strength of such approach to characterize the non-covalent interactions on molecular aggregates.[7] The expansion cools the molecules to a few K, allowing the formation of the aggregates, isolated from any perturbing interaction, and thus preserving the system's equilibrium structure. On the other hand, several laser-based experimental techniques have been developed, which allow extracting valuable information from the system, like transition energies, vibrational frequencies, number of isomers, ionization thresholds… etc. The work

published by our group[8-15] as well as those of Levy,[16-18] Zwier,[19-22] Simons,[23-35] Mikami,[36-39] Kleinermanns,[40-45] Pratt,[46] Mons,[47-49] de Vries,[50-54] Gerhards,[55-57] Leutwyler,[58-61] Ebata,[62-63] Fuji,[64] and Jouvet[65-67] among others, have already demonstrated the ability of such approach to determine the structure of biological molecules (e.g., neurotransmitters, amino acids, peptides, DNA bases and base pairs, and model systems) and its sensitivity to describe solvation in particular and non-covalent interactions in general.

Quantum chemical studies have also made significant contributions to these determinations. Such studies generate essential information for understanding the core element of neurotransmission: the transmitter/receptor interaction. Comparison of the experimental data with the predictions from high level *ab initio* calculations usually result in a full characterization of the system. Also, the calculations are validated in the process, establishing the minimum calculation level required to obtain a quantitative reproduction of the experimental data. Despite the conditions in the expansions being far from those of the biological medium,[68] this methodology allows one obtaining the intrinsic properties of the interaction forces on the active site, free from the interferences produced by the bulk solvent. In the present work, the above-describe procedure has been employed to study the intermolecular forces between a local anaesthetic, benzocaine, and a general anaesthetic, propofol, and several molecules of biological interest. Our group, has already reported studies on aggregates of benzocaine and other local anaesthetics to investigate their non-covalent interactions, microsolvation (eugenol–water,[69] benzocaine–water[70-71]) and hydrogen bonding (eugenol homodimer[72]) aiming to shed light on their biological action.

Benzocaine (Bz) is a well-known local anaesthetic.[68,73-74] Several studies report the interaction of Bz with the Na^+ voltage-gated ion channels (Figure 1.2) involved in generation and propagation of action potentials, as the basis of its biological interaction. Such receptors have a sub-unit that acts as voltage sensor: when a change in the polarization of the membrane is detected, the ion channel changes its state to open. In such state, benzocaine, which is able to cross the lipid bilayer, blocks the ion pore from inside the axon.[69] Mutagenic studies have demonstrated the importance of the presence of selective amino acids for the process to take place. In fact, in the case of the $Na_{v,1.2}$ domain IV, S6 mutations lead to the largest changes in blocking affinity and, in particular, Phe-1764 and Tyr-1771 have been shown to be critical amino acids that

conform the benzocaine-ion channel interaction site.[70-72] In consequence, a deep knowledge of the interactions between the local anaesthetic and the amino acid residues conforming the interaction site is considered as fundamental to understand their action mechanism. Our group has already studied the interaction of Bz with those key aminoacids,[73,74] pointing out the possible existence of a reaction between Bz and phenol (the residue of tyrosine) in the excited state, which may account for the sensitizing action of benzocaine when employed in sunscreen formulations.

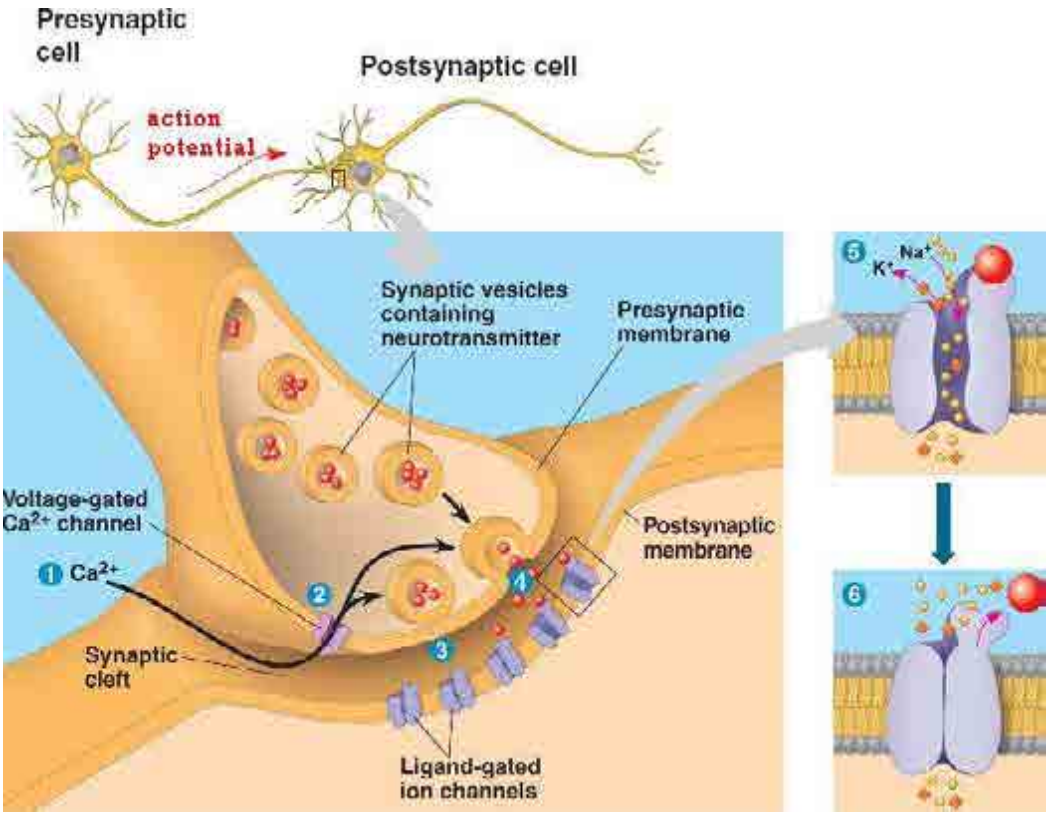

Figure 1.2. *Na^+ Voltage-gated ion channels. This ion channels are integrated in the membrane of proteins and enable the passage of ions across cell membranes, opening and closing in response to changes in transmembrane voltage, and play a key role in electrical signaling by neurons. When the cell membrane is polarized, the interior of the cell is at a negative voltage relative to the exterior and Na+ Voltage-gated ion channels remain closed. If depolarized, these channels open rapidly (less than 1 ms), allowing ions to flow passively down their electrochemical gradients, at near diffusion rates. The pore domain is responsible for the ion selectivity and conduction, and also for channel gating, whereas the voltage-sensing domain triggers a change in conformation of the pore domain in response to changes in transmembrane voltage.*

Benzocaine is also an attractive molecule to explore intermolecular interactions, since it presents two stable conformations (*trans* and *gauche*) and a variety of competing solvation/binding sites at the two ring substituent (ethyl ester and amino group) that can establish hydrogen bonds (Figure 1.3). The ester group has two non-equivalent oxygen atoms that may behave as proton acceptors, whereas the amino group may function as either proton donor or acceptor. In addition, the large polarizability of the aromatic ring yields fairly strong interactions by dispersive forces, i.e., stacking, or weak hydrogen bonds. In this work we have fully characterize the benzocaine·Ar system,[10] which is mainly formed by dispersive forces. Such interaction is not that different from those taking places between benzocaine and aliphatic amino acids like leucine or isoleucine and the interaction between benzocaine and the alkylic chains of the lipids that constitute the cellular membrane. During this study, a complete assembly of a Light Induced Fluorescence (LIF) experimental system has also been carried out to complement the information obtained on the spectroscopy of the S_1 vibronic structure and a stimulated emission pumping (SEP) set up has been implemented.

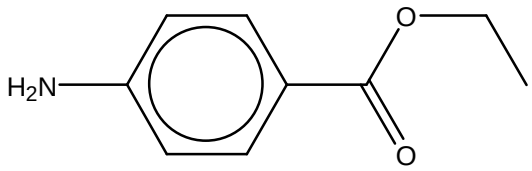

Figure 1.3. *Molecular formula of benzocaine.*

In the second part of this memory, we have explored the spectroscopy of propofol, which probably is the most widely used general anaesthetic. Propofol (2,6-Diisopropylphenol, Figure 1.4) is a widely used, short-acting anesthetic agent, usually administered intravenously. This drug has been recently associated with the death of the famous singer Michael Jackson, according to autopsy.

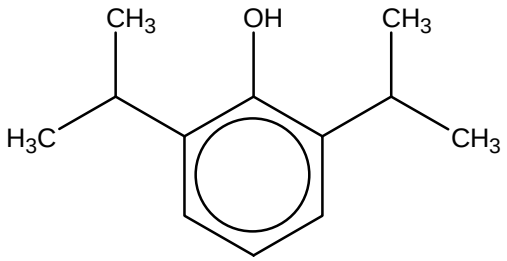

Figure 1.4. *Propofol. Its structure is the same as a phenol with two isopropyl groups in ortho with the OH.*

Propofol usually travels through the body docked to the human serum albumin (HSA)[75] in which two docking sites have been identified (Figures 1.5 and 1.6). Once it arrives to the central nervous system (CNS), propofol interacts mainly with $GABA_A$ receptors[76] blocking their activity[77-79] (Figure 1.7).

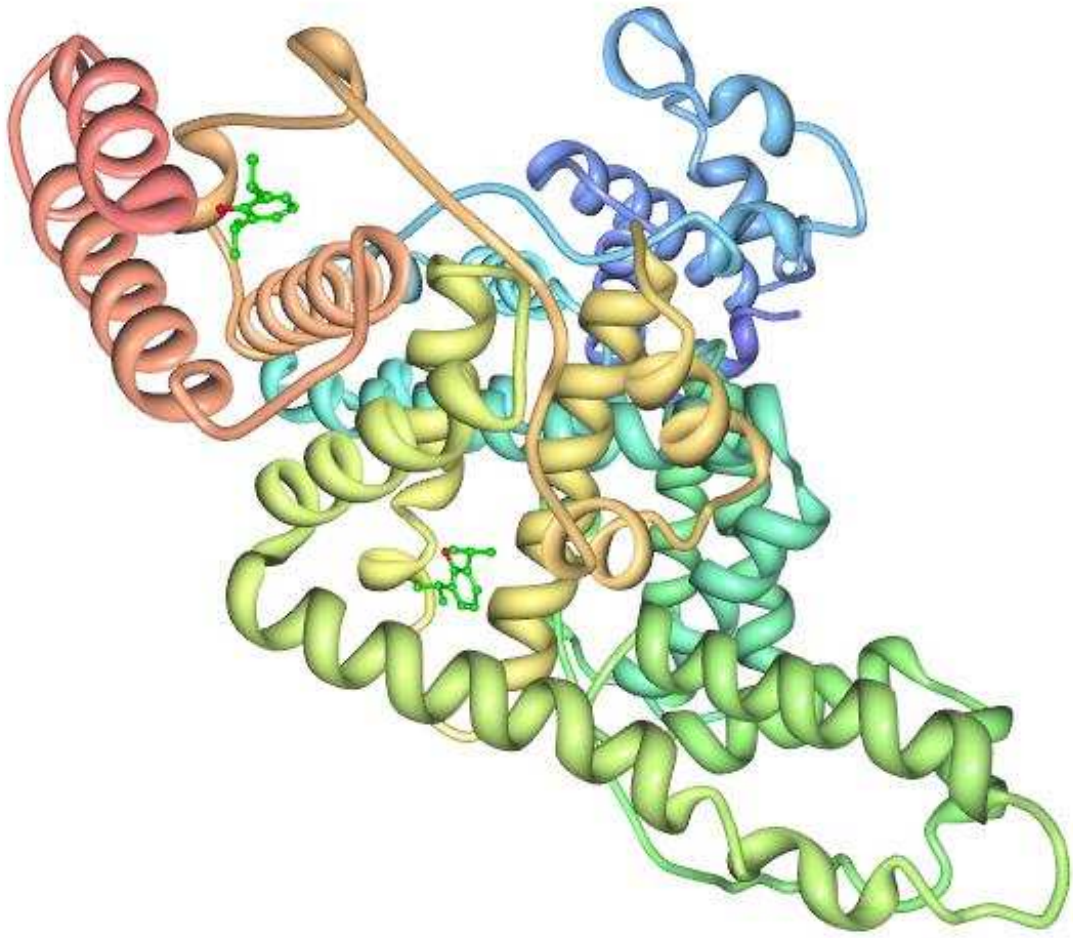

Figure 1.5. *Propofol docking sites with the HSA.[81] Reprinted by permission from American Society for Biochemistry and Molecular Biology: JBC,[81] copyright © (2000).*

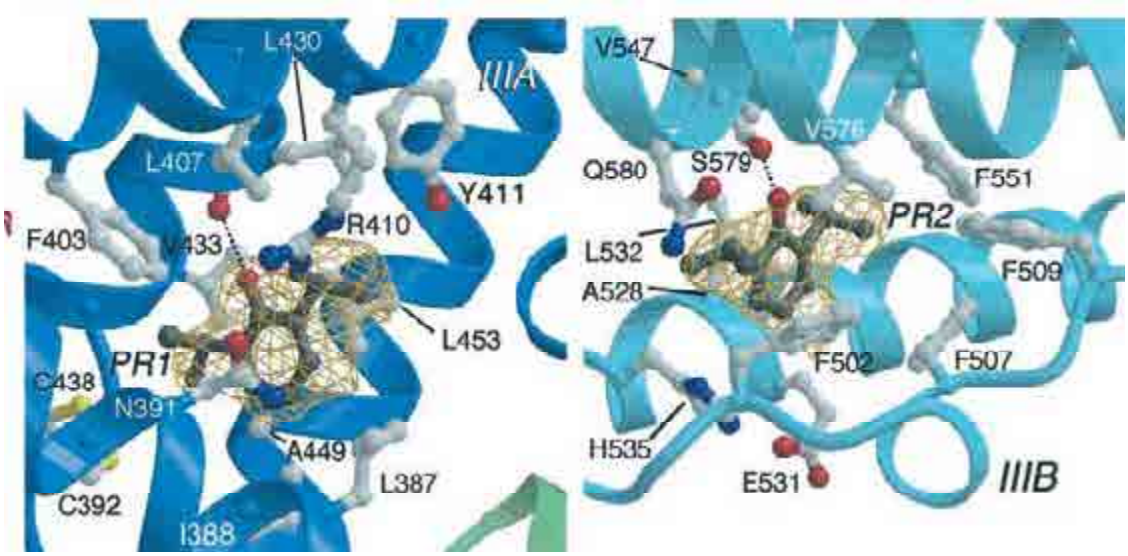

Figure 1.6. *Propofol binding sites on HSA.*[81] *HSA with propofol showing the locations of the two propofol binding sites (A). Site PR1, which is within sub-domain IIIA, and site PR2 (B), which is within sub-domain IIIB. The dashed lines represent hydrogen bonds. Reprinted by permission from American Society for Biochemistry and Molecular Biology: JBC,*[81] *copyright © (2000).*

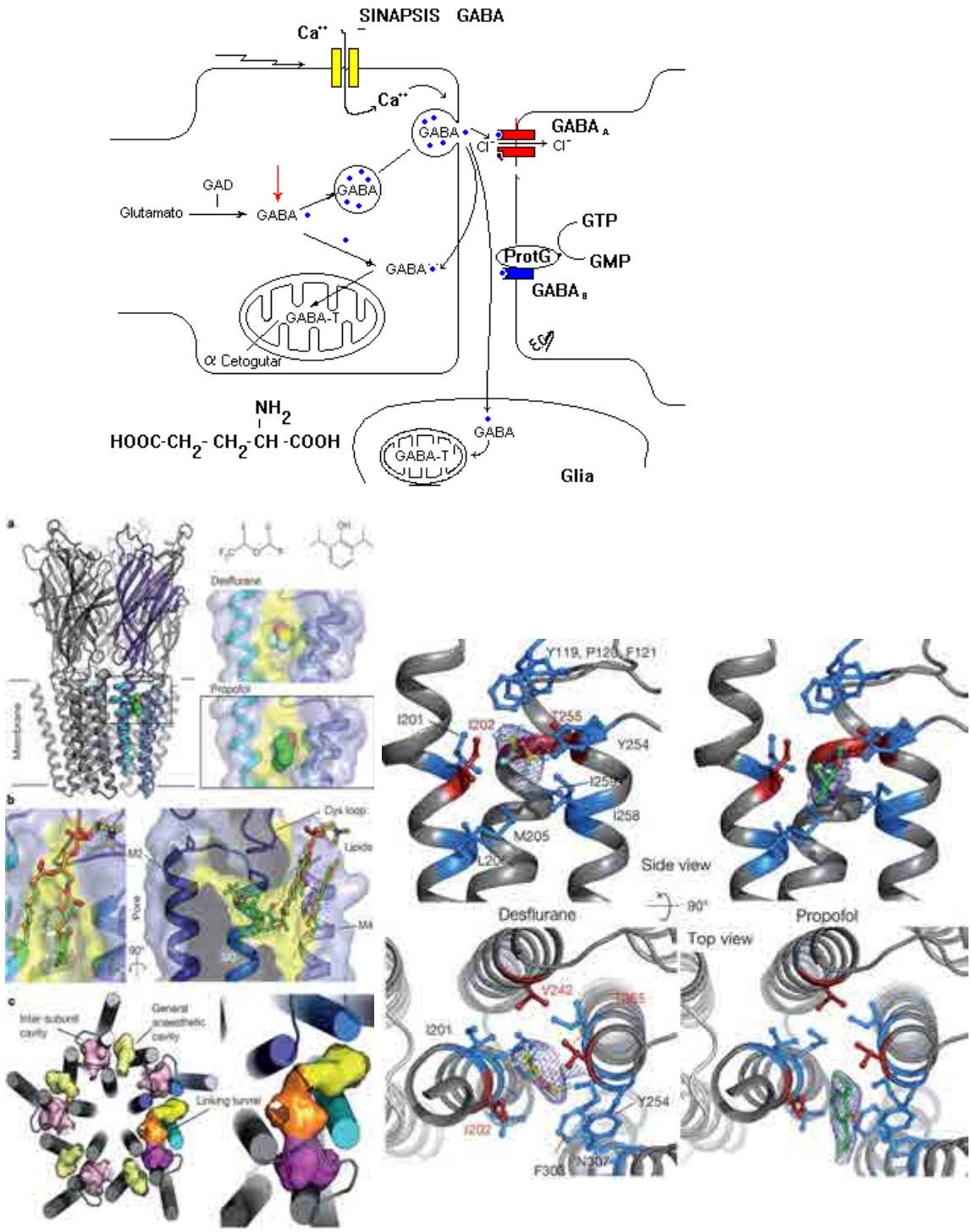

Figure 1.7. *General function of $GABA_A$[86] (upper panel). When a signal reaches the neuron, neurotransmisors are freed (blue spheres) reaching the $GABA_A$ receptors. This opens the gate and the Cl^- pass through them creating a potential difference in the membrane. Interaction between propofol and $GABA_A$ main receptor sites (lower panels).*[88] *When propofol binds to the $GABA_A$ receptor, Cl^- ions are blocked, stopping the signal. Reprinted by permission from Macmillan Publishers Ltd: Nature,*[88] *copyright © (2011).*

Although propofol is one of the most widely used anesthetics[81] and there are many studies in the literature on its precise mechanism of action,[78] it was not until very recently that the structure of the GABA ligand-gated ion channel receptor where propofol docks, has been determined.[82] Conversely with what is observed for inhalational general anesthetic, for which mutagenic studies demonstrate the existence of several key amino acids in their respective receptors, propofol action is strongly dependent on the presence of a single amino acid in the β_3 subunit: β_3 (N265M).[78] Experiments carried out in mice demonstrate that when the amino acid asparagine is replaced with methionine or tryptophan, a reduction in the propofol activity is observed. In the same way, it has been demonstrated that in *Gloeobaster violacoues* bacteria, a tyrosine amino acid plays a key role in the propofol-GLIC (ligand-gated ion channel) receptor interaction.[82] Such experiments also point to an interaction between the hydrophilic side of propofol and an oxygen atom, forming part of an C=O group in asparagine and of an R-OH group in tyrosine, as key interaction in the docking process. The whole process of transport and docking of propofol in particular and of any other anesthetic in general, relies in the changes on the Gibb's free energy, which favors the propofol-active site interaction over the propofol solvation by the extracellular medium. Therefore, understanding the docking process requires of a deep knowledge on the interactions between both propofol and the extracellular medium and propofol and the amino acid residua conforming the active site. Following this reasoning and using a reductionist approach, it is possible to decompose such interactions in pairs (in the case of ligand-active site) or in complexes containing a limited number of water molecules (in the case of ligand-solvation).[83]

In this work, we have extensively studied the solvation of propofol by water. Thanks to a fine-tuning of the experimental conditions, the microsolvation process of propofol with up to nine water molecules has been characterized, obtaining electronic excitation spectra, the number of isomers for each stoichiometry and important vibrational information on the OH/NH stretching region (and in some cases, even in the 500-1700 cm^{-1} region). The experimental results have been completed with extensive quantum mechanics and DFT calculations, obtaining in some cases thousands of possible structures. Comparison of experimental data with the calculated structures allows proposing a very limited number of possible structures for each isomers of a given stoichiometry. The propofol self-aggregation process has also been explored

using the same approach characterizing the homomers up to propofol$_6$, which is one of the largest systems ever solved using the described approach.

Characterization of both types of systems: microsolvated propofol and its homomers has been a key step to tackle mixed systems, containing a variable number of propofol and water molecules. Thus, propofol$_2$·W$_n$ (n=1-7), propofol$_3$·W$_1$, propofol$_4$·W$_1$ have also been studied and solved.

This study would not be completed without the study of some of the interactions that take place between propofol and the GABA$_A$ ionic channel. As has been demonstrated, there are direct interactions between propofol and a tyrosine and a threonine residue. Consequently, we have extended our study to propofol·phenol and propofol·2-propanol. As it will be shown, our data do not replace those from X-ray diffraction but constitute an excellent complement.

In summary we offer here a very complete set of results on the non-covalent interactions that drive propofol from the extracellular water-rich environment into GABA$_A$ active site, where it is able to block the propagation of the pain signal.

1.2 – References

1. K. W. Miller, *International Review of Neurobiology*, **27**, 1-61 (1985).
2. N. P. Franks, W. R. Lieb, *Nature*, **367**, 607-614 (1994).
3. N. P. Franks, *British Journal of Pharmacology,* **147** S72-S81 (2006).
4. D. Belelli, J. J. Lambert, J. A. Peters, K. Wafford, P. J. Whiting, *Proceedings of the National Academy of Sciences of the United States of America*, ***94*** 11031-11036 (1997).
5. S. J. Mihic, Q. Ye, M. J. Wick, V. V. Koltchine, M. A. Krasowski, S. E. Finn, M. P. Mascia, C. F. Valenzuela, K. K. Hanson, E. P. Greenblatt, R. A. Harris, N. L. Harrison, *Nature,* **389** 385-389 (1997).
6. R. Siegwart, R. Jurd, U. Rudolph, *Journal of Neurochemistry,* **80** 140-148 (2002).
7. Schermann, J. P. *Spectroscopy and Modeling of Biomolecular Building Blocks;* Elsevier Amsterdam, 2007.
8. A. Longarte, J. A. Fernandez, I. Unamuno, F. Castaño, "Experimental and Theoretical Study of Methyl p-Aminobenzoate/Ammonia Complexes. II. MAB (NH3)2-4," *J. Chem. Phys.,* **113**, 8549 (2000).
9. J. A. Fernandez, A. Longarte, I. Unamuno, F. Castano, "A Theoretical and Experimental Study of the Ethyl p-Aminobenzoate (H2O)n (n=1-4) Complexes," *J. Chem. Phys.,* **113**, 8531 (2000).
10. J. A. Fernandez, A. Longarte, I. Unamuno, F. Castano, "Laser Mass-Resolved Spectroscopy and Theoretical Study of Methyl-p-Aminobenzoate $(H_2O)_n$ (n=2,3,4) Complexes," *J. Chem. Phys.,* **113**, 5804 (2000).
11. J. A. Fernandez, I. Unamuno, E. Alejandro, A. Longarte, F. Castano, "Structure and Identification of the Amino-p-phenethylamine Conformers," *Phys. Chem. Chem. Phys.,* **4**, 3297 (2002).
12. E. Alejandro, J. A. Fernandez, F. Castano, "Structure of the 4-Aminobenzonitrile/Water Complexes," *Chem. Phys. Ltrs.,* **353**, 195 (2002).
13. A. Longare, I. Unamuno, J. A. Fernandez, F. Castano, "Experimental and Theoretical Study of the Structures and Binding Energies of Eugenol $(H_2O)_n$, n=0-2," *J. Chem. Phys.,* **121**, 209 (2004).
14. I. León, E. Aguado, A. Lesarri, J. A. Fernández, F. Castano, Combined Experimental and Theoretical Study of the Benzocaine/Ar van der Waals System in Supersonic Expansions, *Journal of Physical Chemistry A, **113***, 982-988 (2009).
15. E. Aguado, I. León, E. J. Cocinero, A. Lesarri, J. A. Fernández and F. Castaño, *Phys. Chem. Chem. Phys.*, **11**, 11608-11616 (2009).
16. T. R. Rizzo, D. H. Levy, "The Spectroscopy and Photophysics of the Amino Acid Tryptophan in the Gas Phase," *NATO ASI Series, C, Math. and Phys. Sci.,* **107**, 0258 (1987).
17. J. R. Cable, M. J. Tubergen, D. H. Levy, "Fluorescence Spectroscopy of Jet-Cooled Tryptophan Peptides," *J. Am. Chem. Soc.,* **111**, 9032 (1989).

18. S. J. Martinez, J. C. Alfano, D. H. Levy, "The Electronic Spectroscopy of the Amino Acids Tyrosine and Phenylalanine in a Supersonic Jet," *J. Mol. Spec.,* **156**, 421 (1992).

19. B. C. Dian, A. Longarte, T. S. Zwier, "Conformational Dynamics in a Dipeptide After Single-mode Vibrational Excitation," *Science,* **296**, 2369 (2002).

20. A. Cathrine, D. H. Levy, J. A. Stearns, G. M. Florio, A. Longarte, T. S. Zwier, "Spectroscopic Consequences of Localized Electronic Excitation in Anthranilic Acid Dimer," *J. Phys. Chem. A.,* **108**, 4599 (2004).

21. B. C. Dian, G. M. Florio, J. R. Clarkson, A. Longarte, T. S. Zwier, "Infrared-Induced Conformational Isoerization and Vibrational Relaxation Dynamics in Melatonin and 5-methowy-N. Acetyl Tryptophan Methyl Amide," *J. Chem. Phys.,* **120**, 9033 (2004).

22. B. C. Dian, J. R. Clarkson, T. S Zwier, "Direct Measurement of Energy Thresholds to Conformational Isomerization in Tryptamine," *Science,* **303**, 1169 (2004).

23. B. D. Howells, J. Mccombie, T. F. Palmer, J. P. Simons, and A. Walters, *J. Chem. Soc.-Faraday Trans.*, **88**, 2587 (1992).

24. J. A. Dickinson, M. R. Hockridge, R. T. Kroemer, E. G. Robertson, J. P. Simons, J. McCombie, M. Walker, "Conformational Choice, Hydrogen Bonding, and Rotation of the $S_1 \leftarrow S_0$ Electronic Transition Moment in 2-Phenylethyl Alchohol, 2-Phenylethylamine, and Their Water Clusters," *J. Am. Chem. Soc.,* **120**, 2622 (1998).

25. L. C. Snoek, E. G. Robertson, R. T. Kroemer, J. P. Simons, "Conformational Landscapes in Amino Acids: Infrared and Ultraviolet Ion-Dip Spectroscopy of Phenylalanine in the Gas Phase," *Chem. Phys. Ltrs.,* **321**, 49 (2000).

26. M. Mons, E. G. Robertson, J. P. Simons, "Intra- and Intermolecular π-Type Hydrogen Bonding in Aryl Alcohols: UV and IR-UV Ion Dip Spectroscopy," *J. Phys. Chem. A,* **104**, 1089 (2000).

27. F. O. Talbot, J. P. Simons, "Infrared Ion Dip and Ultraviolet Spectroscopy of 4-phenylimidazole, its Tautomer, 5-phenylimidazole, and its Multiply Hydrated Clusters," *Eur. Phys. J. D: Atomic, Molecular and Optical Physics,* **20**, 389 (2002).

28. N. A. Macleod, J. P. Simons, "Beta-blocker Conformations in the Gas Phase: 2-phenosy Ethylamine, Its Hydrated Cluster and 3-phenoxy Propanolamine," *Phys. Chem. Chem. Phys.,* **6**, 2878 (2004).

29. R. A. Jockusch, R. T. Kroemer, F. O. Talbot, L. C. Snoek. P. Carcabal, J. P. Simons, M. Havenith, J. M. Bakker, I. Compagnon, G. Meijer, G. von Helden, "Probing the Glycosidic Linkage: UV and IR Ion-Dip Spectroscopy of a Lactoside," *J. Am. Chem. Soc.,* **126**, 5709 (2004).

30. Y. Lee, J. Jung, B. Kim, P. Butz, L. C. Snoek, R. T. Kroemer, J. P. Simons, "Alanyl Side Chain Folding in Phenylalanine: Conformational Assignments through Ultraviolet Rotational Band Contour Analysis," *J. Chem. Phys. A,* **108**, 69 (2004).

31. P. Carcabal, R.T. Kroemer, L.C. Snoek, J.P. Simons, J.M. Bakker, I. Compagnon, G. Meijer, G. von Helden, "Hydrated Complexes of Tryptophan: Ion Dip Infrared Spectroscopy in the "Molecular Fingerprint" Region, 100-200 cm^{-1}" *Phys. Chem. Chem. Phys.,* **6**, 4546 (2004).

32. E. C. Stanca-Kaposta, D.P. Gamblin, E.J. Cocinero, J. Frey, R.T. Kroemer, A.J. Fairbanks, B.G. Davis, J.P. Simons, "Solvent interactions and conformational choice in

a core N-glycan segment: Gas phase conformation of the central, branching trimannose unit and its singly hydrated complex." *J. Am. Chem. Soc.,* **130**, 10691-10696 (2008).

33. J. Screen, E.C. Stanca-Kaposta, D.P. Gamblin, B. Liu, N.A. Macleod, L.C. Snoek, B.G. Davis, J.P. Simons, "IR-spectral signatures of aromatic-sugar complexes: Probing carbohydrate-protein interactions." *Angewandte Chemie-International Edition,* **46**, 3644-3648 (2007).

34. R.A. Jockusch, F.O. Talbot, P.S. Rogers, M.I. Simone, G.W.J. Fleet, J.P. Simons, "Carbohydrate amino acids: The intrinsic conformational preference for a beta-turn-type structure in a carbopeptoid building block." *J. Am. Chem. Soc.,* **128**, 16771-16777 (2006).

35. P. Carcabal, I. Hunig, D.P. Gamblin, B. Liu, R.A. Jockusch, R.T. Kroemer, L.C. Snoek, A.J. Fairbanks, B.G. Davis, J.P. Simons, "Building up key segments of N-glycans in the gas phase: Intrinsic structural preferences of the alpha(1,3) and alpha(1,6) dimannosides." *J. Am. Chem. Soc.,* **128**, 1976-1981 (2006).

36. Y. Yamada, T. Ebata, M. Kayano, N. Mikami, "Picosecond IR-UV Pump-Probe Spectroscopic Study of the Dynamics of the Vibrational Relaxation of Jet-Cooled Phenol. I. Intramolecular Vibrational Energy Redistribution of the OH and CH Stretching Vibrations of Bare Phenol," *J. Chem. Phys.,* **120**, 7400 (2004).

37. M. Kayano, T. Ebata, Y. Yamada, N. Mikami, "Picosecond IR-UV Pump-Probe Spectroscopic Study of the Dynamics of the Vibrational Relaxation of Jet-Cooled Phenol. II. Intracluster Vibrational Energy Redistribution of the OH Stretching Vibration of Hydrogen-Bonded Clusters," *J. Chem. Phys.,* **120**, 7410 (2004).

38. T. Ebata, A. Iwasaki, N. Mikami, "Vibrational Relaxation of OH and OD Stretching Vibrations of Phenol and Its Clusters Studied by IR-UV Pump-Probe Spectroscopy," *J. Phys. Chem. A.,* **104**, 7974 (2000).

39. S. Tanabe, T. Ebata, M. Fujii, N. Mikami, "OH Stretching Vibrations of Phenol-$(H_2O)_n$ (n=1-3) Complexes Observed by IR-UV Double-Resonance Spectroscopy," *Chem. Phys. Ltrs.,* **215**, 347 (1993).

40. K. Kleinermanns, C. Janzen, D. Spangenberg, M. Gerhards, "Infrared Spectroscopy of Resonantly Ionized (Phenol)$(H_2O)_n^+$," *J. Phys. Chem. A.,* **103**, 5232 (1999).

41. C. Janzen, D. Spangenberg, W. Roth, K. Kleinermanns, "Structure and Vibrations of Phenol (H2O)7,8 Studied by Infrared-Ultraviolet and Ultraviolet-Ultraviolet Double-Resonance Spectroscopy and Ab Initio Theory," *J. Chem. Phys.,* **110**, 9898 (1999).

42. W. Roth, M. Schmitt, C. Jacoby, D. Spangenberg, C. Janzen, K. Kleinermanns, "Double Resonance Spectroscopy of Phenol (H2O)1-12: Evidence for Ice-like Structures in Aromatic-water Clusters?" *Chem. Phys.,* **239**, 1 (1998).

43. I. Huenig, K. Kleinermanns, "Conformers of the Peptides Glycine-tryptophan, Tryptophan-glycine and Tryptophan-glycine-glycine as Revealed by Double Resonance Laser Spectroscopy," *Phys. Chem. Chem. Phys.,* **6**, 2650 (2004).

44. I, Hunig, K. A. Seefeld, K. Kleinermanns, "REMPI and UV-UV Double Resonance Spectroscopy of Tryptophan Ethylester and the Dipeptides Tryptophan-serine," *Chem. Phys. Ltrs.,* **369**, 173 (2003).

45. C. Pluetzer, K. Kleinermanns, "Tautomers and Electronic States of Jet-Cooled Adenine Investigated by Double Resonance Spectroscopy," *Phys. Chem. Chem. Phys.,* **4**, 4877 (2002).

46. D. W. Pratt, "Perspectives: Molecular Dynamics: Biomolecules See the Light," *Science,* **296**, 2347 (2002).

47. M. Mons, F. Piuzzi, I. Dimicoli, A. Zehnacker, F. Lahmani, "Binding Energy of Hydrogen-Bonded coplexes of the Chiral Melecule 1-Phenylethanol, as Studied by 2C-R2PI: Comparison Between Diastereoisomeric Complexes with Butan-2-ol and the Singly Hydrated Complex," *Phys. Chem. Chem. Phys.,* **2**, 5065 (2000).

48. F. Piuzzi, M. Mons, I. Dimicoli, B. Tardivel, Q. Zhao, "Ultraviolet Spectroscopy and Tautomerism of the DNA Base Guanine and Its Hydrate Formed in a Supersonic Jet," *Chem. Phys.,* **270**, 205 (2001).

49. W. Chin, F. Piuzzi, J.P. Dognon, L. Dimicoli, B. Tardivel, M. Mons "Gas phase formation of a 3(10)-helix in a three-residue peptide chain: Role of side chain-backbone interactions as evidenced by IR-UV double resonance experiments." *J. Am. Chem. Soc.***,** **127**, 11900-11901 (2005).

50. G. Meijer, G. Gerden, W. L. Meerts, H. Hunziker, M. S. de Vries, H. R. Wendt, "Spectroscopy on Triphenylamine and its van der Waals Complexes," *Chem. Phys.,* **163**, 209 (1992).

51. E. Nir, L. Grace, B. Brauer, M. S. de Vries, "REMPI Spectroscopy of Jet-Cooled Guanine," *J. Am. Chem. Soc.,* **121**, 4896 (1999).

52. E. Nir, M. Muller, L. I. Grace, M. S. de Vries, "REMPI Spectroscopy of Cytosine," *Chem. Phys. Ltrs.,* **355**, 59 (2002).

53. J. M. Bakker, I. Compagnon, G. Mjijer, G. von Helden, M. Kabelac, P. Hobza, M. S. de Vries, "The Mid-IR Absorption Spectrum of Gas-Phase Clusters of the Nucleobases Guanine and Cytosine," *Phys. Chem. Chem. Phys.,* **6**, 2810 (2004).

54. M. S. de Vries, P. Hobza, "Gas-phase spectroscopy of biomolecular building blocks." *Annu. Rev. Phys. Chem.,* **58**, 585-612 (2007).

55. K. Schwing, C. Reyheller, A. Schaly, S. Kubik, and M. Gerhards "Structural Analysis of an Isolated Cyclic Tetrapeptide and its Monohydrate by Combined IR/UV Spectroscopy." *Chemphyschem.*, 2011.

56. H. Fricke, K. Schwing, A. Gerlach, C. Unterberg, and M. Gerhards "Investigations of the water clusters of the protected amino acid Ac-Phe-OMe by applying IR/UV double resonance spectroscopy: microsolvation of the backbone." *Phys.Chem.Chem.Phys.,* **12**, 3511-3521 (2010).

57. K. Bartl, A. Funk, K. Schwing, H. Fricke, G. Kock, H. D. Martin, and M. Gerhards "IR spectroscopy applied subsequent to a proton transfer reaction in the excited state of isolated 3-hydroxyflavone and 2-(2-naphthyl)-3-hydroxychromone." *Phys.Chem.Chem.Phys.,* **11**, 1173-1179 (2009).

58. P. Ottiger and S. Leutwyler "Excitonic splittings in jet-cooled molecular dimers." *Chimia (Aarau.),* **65**, 228-230 (2011).

59. J. A. Frey, A. Muller, H. M. Frey, and S. Leutwyler "Infrared depletion spectra of 2-aminopyridine2-pyridone, a Watson-Crick mimic of adenine.uracil." *J.Chem.Phys.,* **121**, 8237-8245 (2004).

60. J. A. Frey, R. Leist, C. Tanner, H. M. Frey, and S. Leutwyler "2-pyridone: The role of out-of-plane vibrations on the S1<-->S0 spectra and S1 state reactivity." *J.Chem.Phys.,* **125**, 114308 (2006).

61. R. Leist, J.A. Frey, P. Ottiger, H.M. Frey, S. Leutwyler, R.A. Bachorz, W. Klopper, "Nucleobase-fluorobenzene interactions: Hydrogen bonding wins over pi stacking." *Angewandte Chemie-International Edition,* **46**, 7449-7452 (2007).

62. R. Kusaka, S. Kokubu, Y. Inokuchi, T. Haino, and T. Ebata "Structure of host-guest complexes between dibenzo-18-crown-6 and water, ammonia, methanol, and acetylene: evidence of molecular recognition on the complexation." *Phys.Chem.Chem.Phys.,* **13**, 6827-6836 (2011).

63. R. Kusaka and T. Ebata. "Remarkable site difference of vibrational energy relaxation in benzene dimer: picosecond time-resolved IR-UV pump-probe spectroscopy." *Angew.Chem.Int.Ed Engl.,* **49**, 6989-6992 (2010).

64. S. Tsuzuki and A. Fujii, *Phys. Chem. Chem. Phys.*, **10**, 2584-2594 (2008).

65. I. Alata, C. Dedonder, M. Broquier, E. Marceca, and C. Jouvet "Role of the Charge-Transfer State in the Electronic Absorption of Protonated Hydrocarbon Molecules." *J.Am.Chem.Soc.*, 2010.

66. N. R. Cheong, S. H. Nam, H. S. Park, S. Ryu, J. K. Song, S. M. Park, M. Perot, B. Lucas, M. Barat, J. A. Fayeton, and C. Jouvet "Photofragmentation in selected tautomers of protonated adenine." *Phys.Chem.Chem.Phys.,* **13**, 291-295 (2011).

67. G. A. Pino, A. N. Oldani, E. Marceca, M. Fujii, S. I. Ishiuchi, M. Miyazaki, M. Broquier, C. Dedonder, and C. Jouvet "Excited state hydrogen transfer dynamics in substituted phenols and their complexes with ammonia: pipi*-pisigma* energy gap propensity and ortho-substitution effect." *J.Chem.Phys.,* **133**, 124313 (2010).

68. Berde, C. B.; Strichartz, G. R. Local anesthetics. In *Anesthesia*, 6th ed.; Miller, R.D., Ed.; **Churchill Livingstone** : New York, 2004.

69. A. Longarte, I. Unamuno, J.A. Fernandez, F. Castano, C. Redondo, "Experimental and theoretical study of the structures and binding energies of eugenol (H2O)(n), n=0-2." *J. Chem. Phys.,* **121**, 209-219 (2004).

70. J.A. Fernandez, A. Longarte, I. Unamuno, F. Castano "A theoretical and experimental study of the ethyl-p-aminobenzoate (H2O)(n) (n=1-4) complexes." *J. Chem. Phys.,* **113**, 8531-8540 (2000).

71. A. Longarte, J.A. Fernandez, I. Unamuno, F. Castano "Structure and ground and first electronic excited state vibrational modes of the ethyl-p-aminobenzoate conformers." *Chem. Phys.,* **260**, 83-93 (2000).

72. A. Longarte, C. Redondo, J.A. Fernandez, F. Castano "IR/UV and UV/UV double-resonance study of guaiacol and eugenol dimers." *J. Chem. Phys.,* **122**, (2005).

73. Edurne Aguado, PhD Thesis, U.P.V. Leioa 2010

74. A. Longarte, J.A. Fernandez, I. Unamuno, F. Castano "Structure and ground and first electronic excited state vibrational modes of the ethyl-p-aminobenzoate conformers." *Chem. Phys.,* **260**, 83-93 (2000).

75. L. L. Brunton, J.S. Lazo, K.L. Parker *Goodman and Gilman's The pharmacological basis of therapeutics;* 11th ed.; New York, 2006.

76. G. M. Lipkind, H.A. Fozzard "Molecular modeling of local anesthetic drug binding by voltage-gated sodium channels." *Mol. Pharmacol.,* **68**, 1611-1622 (2005).

77. V. Yarov-Yarovoy, J. Brown, E.M. Sharp, J.J. Clare, T. Scheuer, W.A. Catterall, "Molecular determinants of voltage-dependent gating and binding of pore-blocking drugs in transmembrane segment IIIS6 of the Na+ channel alpha subunit." *J. Biol. Chem.,* **276**, 20-27 (2001).

78. V. Yarov-Yarovoy, J.C. Mcphee, D. Idsvoog, C. Pate, T. Scheuer, W.A Catterall, "Role of amino acid residues in transmembrane segments IS6 and IIS6 of the Na+ channel alpha subunit in voltage-dependent gating and drug block." *J. Biol. Chem.,* **277**, 35393-35401 (2002).

79. E. Aguado, I. León, E. Cocinero, A. Lesarri, J.A. Fernández, F. Castaño, *Phys. Chem. Chem. Phys.*, **11**, 11608-11616 (2009).

80. I. León, E. Aguado, A. Lesarri, F. Castano, J.A. Fernandez, "Benzocaine·toluene. *Phys. Chem. Chem. Phys (submitted)*.

81. A.A. Bhattacharya, S. Curry, N.P. Franks, "Binding of the general anesthetics propofol and halothane to human serum albumin - High resolution crystal structures." *Journal of Biological Chemistry,* **275**, 38731-38738 (2000).

82. N. Bocquet, H. Nury, M. Baaden, C. Le Poupon, J.P. Changeux, M. Delarue, P.J. Corringer, "X-ray structure of a pentameric ligand-gated ion channel in an apparently open conformation." *Nature,* **457**, 111-114 (2009).

83. R. Siegwart, R. Jurd, U. Rudolph, "Molecular determinants for the action of general anesthetics at recombinant alpha(2)beta(3)gamma(2) gamma-aminobutyric acid(A) receptors." *Journal of Neurochemistry,* **80**, 140-148 (2002).

84. N.P. Franks, "Molecular targets underlying general anaesthesia." *British Journal of Pharmacology,* **147** (S1), S72-S81 (2006).

85. P.L. Chau, "New insights into the molecular mechanisms of general anaesthetics." *British Journal of Pharmacology,* **161**, 288-307 (2010).

86. http://fundacionannavazquez.wordpress.com/2007/08/30/sistema-de-aminoacidos-neurotransmisores/

87. *Molecular and Basic Mechanisms of Anesthesia;* Pabst Science Publishers: Lengerich, 2002.

88. H. Nury, C. Van Renterghem, Y. Weng, A. Tran, M. Baaden, V. Dufresne, J.P. Changeux, J.M. Sonner, M. Delarue, P.J. Corringer, "X-ray structures of general anaesthetics bound to a pentameric ligand-gated ion channel." *Nature,* **469**, 428-431 (2011).

89. J.P. Schermann, *Spectroscopy and Modeling of Biomolecular Building Blocks;* Elsevier: Amsterdam, 2007.

CHAPTER 2

EXPERIMENTAL SETUP

2 – EXPERIMENTAL SETUP

2.1 – Excitation sources

During this work a considerable variety of lasers has been used as excitation sources depending on the availability, resolution requirements, range of frequencies, etc, needed for each technique/experiment. In the following, a short description of the main features of the lasers employed is given:

1 – Nd-YAG Quantel YG-980 Laser (power around 750 mJ/pulse at 532 nm) used to pump a Quantel TDL-90 Dye Laser, with mixing and doubling unit. Pulse duration is around 10 ns and the output beam linewidth is around 0.2 cm^{-1}, although resolution can be improved to 0.1 cm^{-1}, if a beam expander is introduced in the dye's oscillator cavity, at expenses of decreasing the final power density.

2 - Nd-YAG Powerlite Laser (power around 750 mJ/pulse at 532 nm) used to pump a Continuum ND6000 Dye Laser, with doubling unit. Pulse duration is around 10 ns and the output beam linewidth is around 0.2 cm^{-1}, although, as in the case of the TDL-90, resolution can be improved to 0.1 cm^{-1}, if a beam expander is introduced in the dye's oscillator cavity, at expenses of decreasing the final power density. The doubling unit tracking system was not working properly, and therefore, it was replaced by a homemade calibration system.

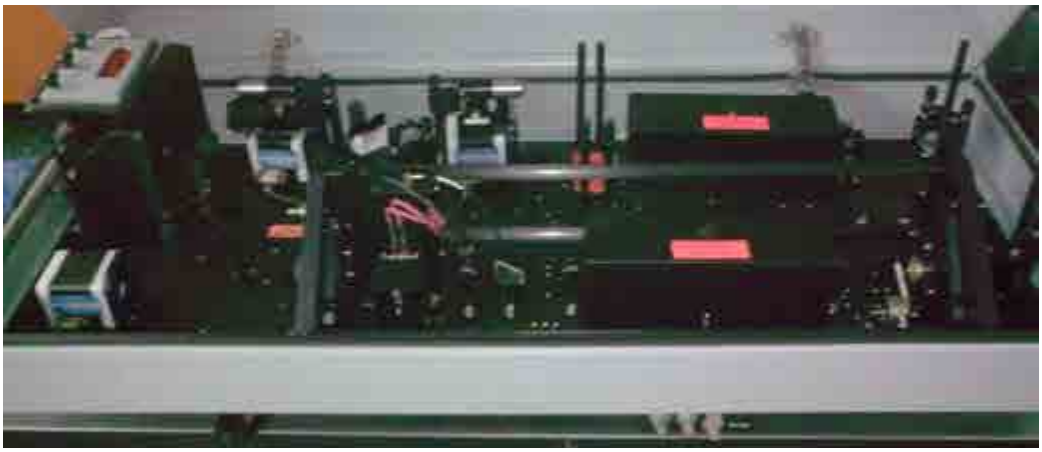

3 –Lambda Physik COMPex Excimer Laser (gas mixture: XeCl) with a maximum output power of 400 mJ/pulse at 308 nm and used to pump a Lambda Physik LPD3000 Dye laser, with mixing unit (BBO1-BBO3). Pulse duration is around 15 ns and the output beam linewidth is around 0.4 cm^{-1}.

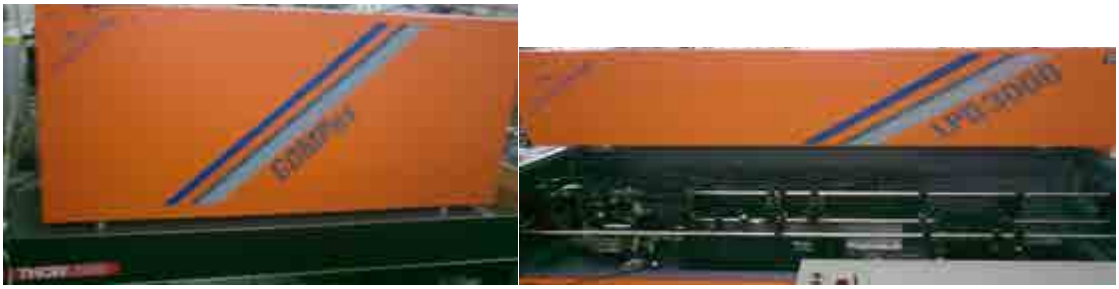

4 –Lambda Physik COMPex Excimer Laser (gas mixture: XeCl) with a maximum output power of 400 mJ/pulse at 308 nm used to pump a Lambda Physik FL3002 Dye, laser with mixing unit (BBO1-BBO3). Pulse duration is around 15 ns and the output beam linewidth is around 0.4 cm^{-1}. During the present work, the Excimer

laser (and the corresponding optical components to pump the dye laser) were replaced by a Quantel Brilliant-b, significantly improving the laser reliability.

5 - Nd-YAG Quantel YG-581 Laser (power around 400 mJ/pulse at 532 nm) used to pump a Quantel TDL-50 Dye Laser, with mixing unit. Pulse duration is around 10 ns and the output beam linewidth is around 0.2 cm^{-1}. This laser was exclusively used to produce IR radiation in the 3000 – 4000 cm^{-1} region using a homemade difference frequency mixing (DFM) unit.

6 – Lambda Physik Scanmate dye laser (pumped by an in-house Nd-YAG Quantel Brilliant-b laser and with an output power of around 400 mJ/pulse at 532 nm), with doubling unit. Pulse duration is around 10 ns and the output beam linewidth is around 0.15 cm^{-1}. Resolution can be improved more than in the Quantel models, down to 0.03 cm^{-1}, using an intra-cavity etalon.

7 – Lambda Physik Scanmate Pro dye laser (pumped by an in-house Nd-YAG Quantel Brilliant-b laser and with an output power of around 400 mJ/pulse at 532 nm), with doubling unit. Pulse duration is around 4.5 ns and the output beam linewidth is 0.1 cm^{-1}. Resolution can also be improved to 0.01 cm^{-1} using an intra-cavity etalon.

8 – Fine adjustment Pulsare Pro -S dye laser (pumped by a Nd-YAG Quantel Brilliant-b laser with a power of around 400 mJ/pulse at 532 nm), with doubling and mixing unit. Pulse duration is around 5.3 ns and the output beam linewidth is around 0.06 cm^{-1}. This laser is also equipped with a mixing unit (DFM) that generates radiation in the 1.4 μm – 5.0 μm region, although with our pump laser sufficient power was only obtained in the 1.4 μm – 3.3 μm region, suitable to record the IR spectra of the systems studied.

2.2 - Dyes employed

In the present work, a wide variety of dyes (Exciton Inc[1]) and their mixtures have been used. Here, a short description of their performance is given. One has to take into account that the optimal concentration of the dyes depends on the type of the pump laser and also on the solvent (methanol, ethanol) employed. The dyes used, sorted by their emission range, which does not always match supplier's specifications, as they tend to be a bit optimistic, are listed in Table 2.1, while Figure 2.1 shows a graphical description of the dyes' tunable range and output laser power. Despite that the concentrations showed in Table 2.1 where used in multiple occasions, at the end of this work, solutions were exclusively prepared with methanol following a trial-and-error procedure (see below).

All dyes were pumped with either an Excimer laser (308nm) or the second harmonic of a Nd:YAG laser (532nm) except Coumarine 540A that has to be pumped with the third harmonic of a Nd:YAG (355nm).

Table 2.1. *Dyes used during this work.*

DYE	MW (g/mol)	Concentration (M)		λ_{range} (nm)	λ_{max} (nm)	Notes
		Oscillator	Amplifier			
Coumarine 540A	309.29	$2.0\ 10^{-3}$	$6.7\ 10^{-4}$	535 - 560	545	Low duration
Rhodamine 575	414.49	$2.8\ 10^{-4}$	$4.1\ 10^{-5}$	547 - 561	553	Average duration
Rhodamine 560	366.80	$2.7\ 10^{-4}$	$3.3\ 10^{-5}$	550 - 570	562	Average duration
Rhodamine 590	543.02	$2.2\ 10^{-4}$	$3.2\ 10^{-5}$	557 - 578	569	Average duration
Rhodamine 590 + Rhodamine 610	543.02 543.02	$1.27\ 10^{-4}$ $+5.63\ 10^{-5}$	$6.26\ 10^{-5}$ $+2.28\ 10^{-5}$	570 - 592	580	Average duration
Rhodamine 610	543.02	$1.97\ 10^{-4}$	$6.89\ 10^{-5}$	583 - 612	593	Average duration
Rhodamine 610 + Rhodamine 640	543.02 591.05	$7.9\ 10^{-5}$ $+3.6\ 10^{-5}$	$3.9\ 10^{-5}$ $+1.8\ 10^{-5}$	595 – 620	607	Average duration
Rhodamine 640	591.05	$2.4\ 10^{-4}$	$3.2\ 10^{-5}$	607 – 628	615	Average duration
DCM	303.37	$5.8\ 10^{-4}$	$7.9\ 10^{-5}$	610 – 670	645	Average duration
LDS 698	378.86	$2.0\ 10^{-4}$	$5.0\ 10^{-5}$	667 - 697	684	Long duration
LDS 722	378.86	$3.4\ 10^{-4}$	$1.3\ 10^{-4}$	693 – 740	720	Long duration
LDS 765	550.00	$1.82\ 10^{-4}$	$2.36\ 10^{-5}$	738 – 787	766	Long duration
LDS 765 + Styril 8	550.00 472.00	---	---	745 - 803	785	[ ] varies the tuning range
Styril 8 + Styril 9	472.00 529.09	$1.6\ 10^{-4}$ $+1.2\ 10^{-4}$	$3.2\ 10^{-5}$ $+ 2.4\ 10^{-5}$	755 - 815	785	Average duration

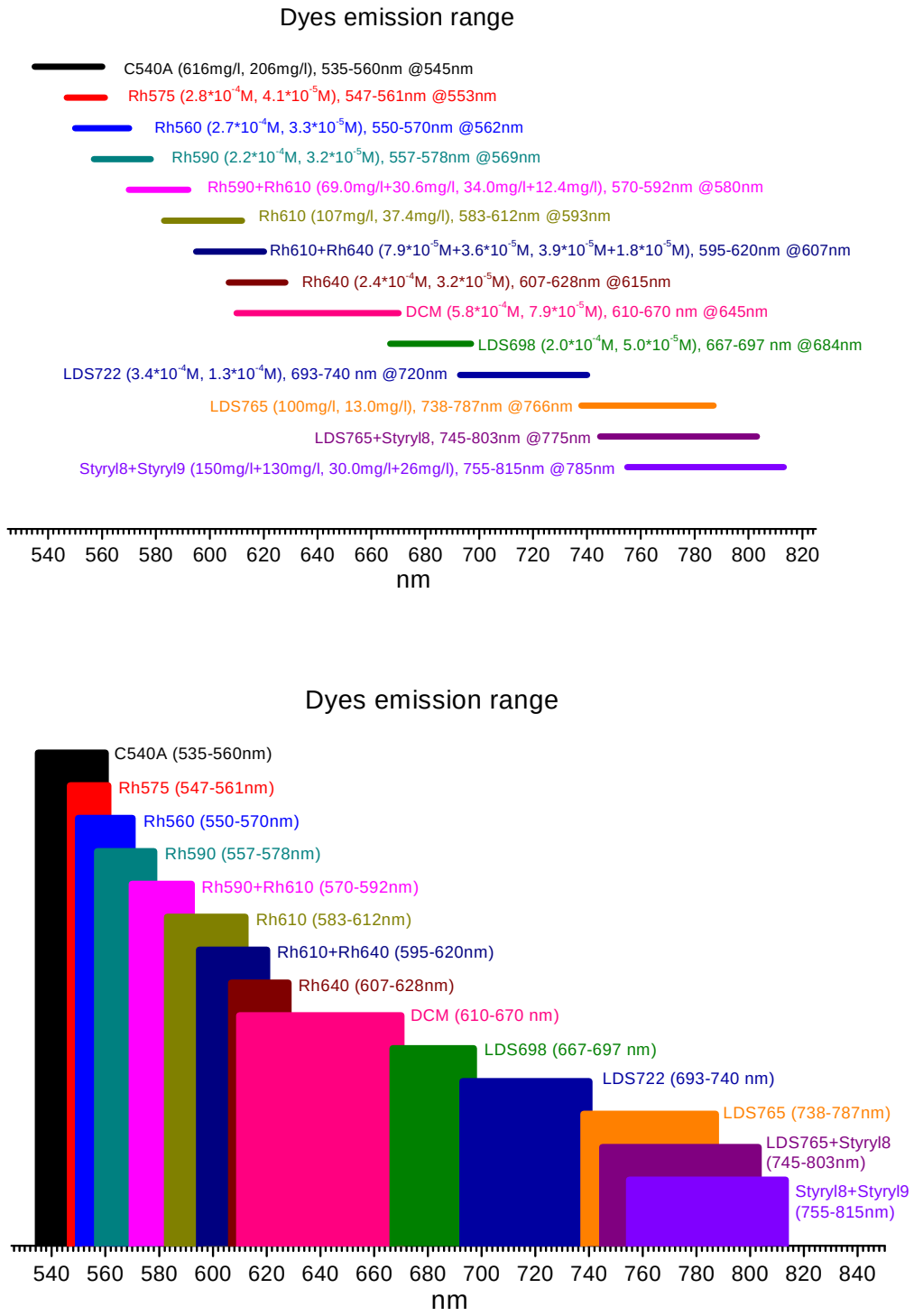

Figure 2.1. *Dyes emission range. Upper panel: optimal concentrations and maximum emission wavelength. Lower panel: histogram of the dyes emission range showing the best dye for a desired wavelength range.*

As previously stated, optimum dyes concentrations vary considerably from one laser to another, and therefore concentration data supplied by the laser dyes' companies are, at most, a rough estimation of the optimum value. Thus, the best procedure to prepare a dye solution is, according to our experience, as follows:

Assuming that the pump laser is properly pre-aligned, first, the dye circulator is filled with the appropriate solvent. In order to align the oscillator, the pump laser is blocked between oscillator and pre-amplifier, and the grating is tuned to the dye's maximum emission wavelength, while the pump laser's energy is decreased to a safe value, to avoid optics burning. The system is now ready to add small amounts of saturated dye concentration, while the output of the oscillator is monitorized using a white cardboard or a white paper. Addition must proceed until the oscillator starts lasing. Once some output energy is observed, laser alignment must be fine-tuned to maximize oscillator laser output. When the user is satisfied with the result, an additional amount of concentrated dye solution may be added to the oscillator's circulator system to increase the oscillator laser output.

Next step is to optimize the preamplifier alignment. For this purpose, it is necessary to unblock the pump laser, so that the preamplifier receives pumping energy, although amplifier must not be pumped yet. In Lambda Physic and Fine Adjustment models, oscillator and preamplifier share the same dye cell, while in Quantel and Coherent models, different cells are employed. Slightly more concentrated dye solution is added to the oscillator's circulating system until there is enough energy to measure the output power. Monitoring the energy of the dye laser, concentrated solution must be added in small amounts until the unwanted Amplified Spontaneous Emission (ASE) becomes significant; around 10% of the total energy is Okay for dyes with emission in the low wavelength region; for the red-most ones, having up to a 30% of ASE is not unusual. At this point we must remark that slight modifications on the optimal dye concentration may result in small shifts in the maximum output wavelength and therefore, it is possible to increase the laser output in the region of interest by altering the concentration: a solution with a higher concentration will slightly red-shift the dye emission curve, while a smaller concentration will slightly blue-shift it.

Adjusting the amplifier concentration is straightforward, once the pumping laser is properly aligned, as the energy will stop increasing with concentration when the optimal value is reached. At this point the work can be considered as finished. A word of caution about concentrations must be added: if the user over concentrates the solution it may have two effects: first, there may be an increase of energy coming out of the amplifier (although not always) but it will mostly be undesired ASE, and secondly and a more important one, the amplifier cell can be severely damaged.

It is important to take into account that every time that the alignment of the pump beam is optimized, the delay between the Flash lamp and the Q-Switch has to be increased so that the pump power goes down, but maintaining enough power to be able to follow the beam path. This is the best procedure to avoid severe damages in the optics due to misalignment of the pump beam, and what is more important, not to get harmed or eye burned. As laser alignment is considerably more difficult wearing eye-protective devices, not all the laser users are responsible enough to wear them during laser operation.

2.3 – Fluorescence Spectroscopy set up

Figure 2.2 shows the experimental setup employed for spectroscopy with optical detection, which consists of an emission source, a vacuum chamber, (with mechanical and turbo-molecular pumps), monochromator, photomultiplier, power supply, oscilloscope, delay generator and a personal computer to record the data and control the measure process.

The molecule(s) to be studied are introduced in a small oven placed outside the chamber; if necessary, they can be gently heated so enough vapor pressure is obtained. Thus, the gas mixture will consist of a small proportion (approximately 1%) of the molecules to be studied and a light and inert buffer gas (He, Ne and/or Ar were used during this work) at pressures of 1-5 bar. This mixture is injected into a vacuum chamber (around 10^{-7} mbar) through a nozzle of approximately 0.5–1.0 mm$^{\varnothing}$, creating a supersonic expansion that cools the problem molecules due to collisions with the buffer gas, greatly reducing the number of populated ro-vibronic states and simplifying the system's spectroscopy. In addition, ideal conditions for studying non-covalent complexes are achieved, because the internal energy of the molecules must be smaller than the complex binding energy or the clusters will not survive.

After the supersonic expansion is created, the molecular beam is interrogated by a pump laser synchronized with the valve's aperture and the emitted fluorescence is collected with appropriate optics, either directly or through a monochromator, and directed towards a photomultiplier (or to a Charge-Coupled Device-CCD-camera). The produced signal is then transferred to a digital oscilloscope (Tektronix TDS 380), which integrates the signal and transfers the resulting value to a personal computer for storage and subsequent analysis.

As it was stated earlier, the sample is deposited in a small oven located outside the chamber and it is heated with a small heating system consisting of two heating cables powered by a continuous current power supply (THANDAR TS3021), while temperature is controlled and stabilized using two thermocouples connected to two differential integers controllers (CEDSAL). To produce the supersonic beam an electromagnetically actionated valve (IOTA ONE, Series 9, General Valve Corporation) with a 0.8 mm orifice is used.

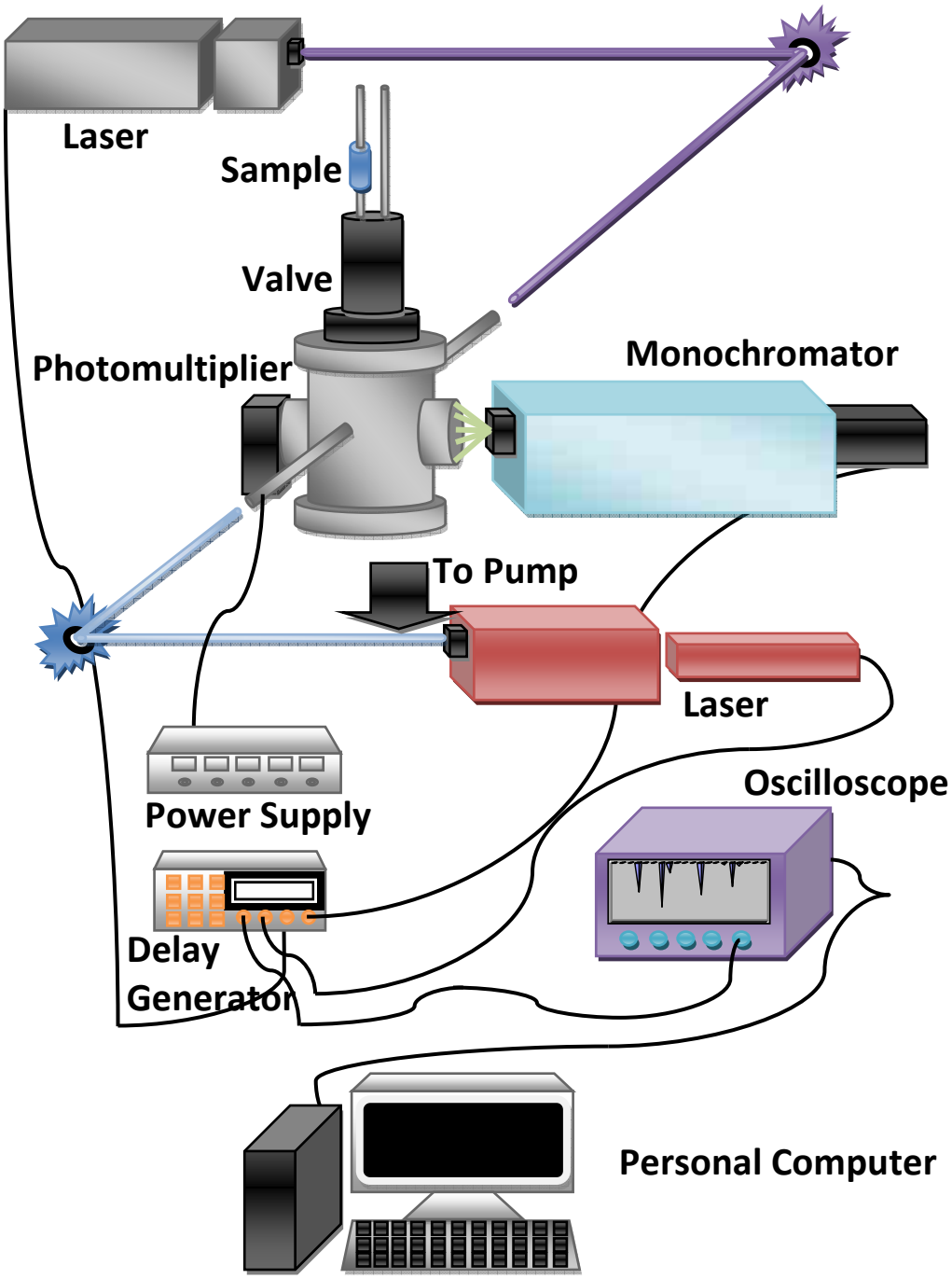

Figure 2.2. *Diagram of the experimental setup for spectroscopy with optical detection.*

The vacuum system consist of a turbomolecular pump (Leybold TW700, 1900 m^3/h) evacuated by a rotary pump (Edwards E2M18, 60 m^3/h). The vacuum in the chamber is maintained at c.a. 10^{-7} mbar and around 10^{-5} mbar during normal operations.

All the experimental components are synchronized with a Delay Generator (Stanford DG535) with a nominal resolution of 10 ps.

During the first part of this work, a fluorescence chamber (Figure 2.3) was designed. The chamber consists of a 10.5 cm diameter, 28 cm height central cylinder, with a valve attached to the upper flange. Two arms 15.5 mm bore and 25 cm length allow aligning the lasers inside the chamber. Two cones with an internal diameter of 4 mm inside the arms reduce the amount of the light scattered by the windows that reach the photomultiplier. Perpendicular to them, two 35.5 mm bore aspheric telescope lenses (Melles Griot, 7.5 cm focal length) are used to collect the fluorescent emission. One of the telescopes is used to collect and focus the fluorescence emitted by the sample into a photomultiplier (EMI 9816B). A *cut off* filter (during this work a WG 305 was used) is usually employed to reduce the laser scattered light. The other telescope focuses the emission into the entrance slit of a monochromator (SPEX 1000M, 0.008 nm resolution) coupled to a photomultiplier (EMI 9816B) to record dispersed emission spectra. In both cases, the signal obtained is sent to a digital oscilloscope (Tektronix TDS 380), integrated and stored in a personal computer. It is possible to attach a CCD camera instead of the photomultiplier to record sections of the spectrum in each laser shot, considerably improving the sensibility of the system.

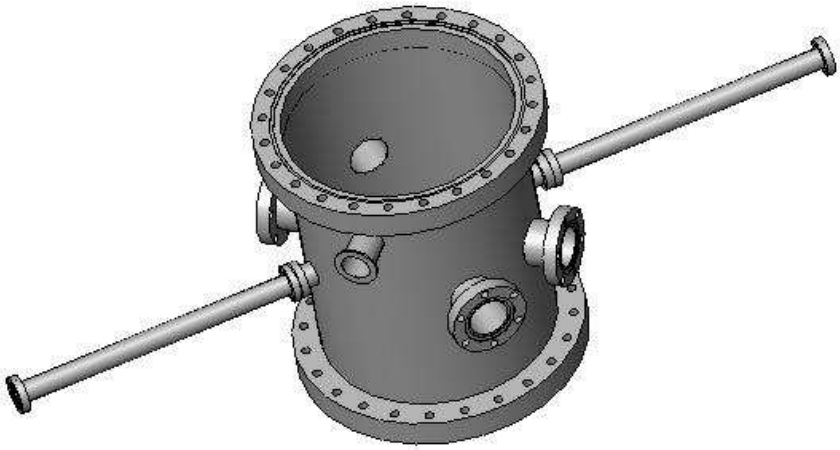

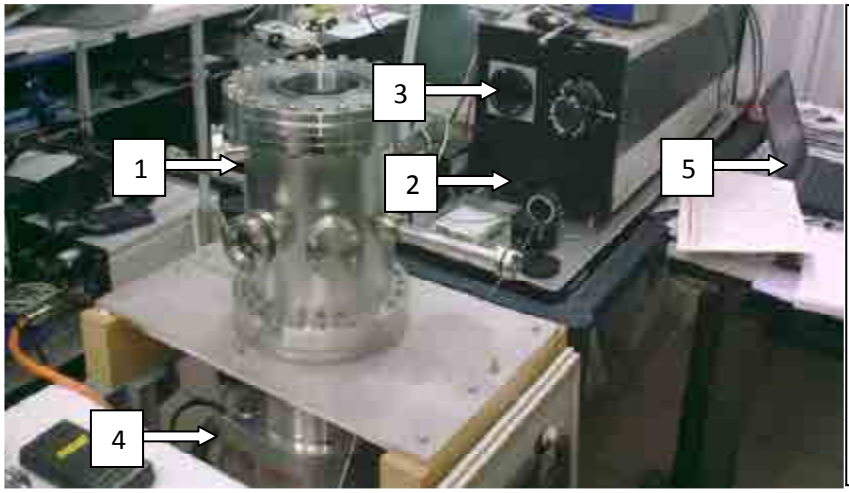

1 – Fluorescence chamber

2 – Monochromator

3 – Photomultiplier part

4 – Vacuum Pumps

5 - Computer

Figure 2.3. *Design of the fluorescence chamber (upper panel). Fluorescence experimental system (down panel).*

2.3.1 – Set up of the Light Induced Fluorescence system: aniline spectroscopy with optical detection

As a part of this work, the light induced fluorescence (LIF) set up available in the laboratory was re-designed to improve its performance, as described in the previous section, and here some experimental results are presented. The performance of the new experimental set up was tested using aniline as calibrant. Aniline, Figure 2.4, has a very well-known spectroscopy and a high fluorescence quantum yield, making it a good choice as calibrant molecule.

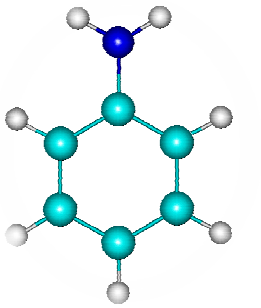

Figure 2.4. *Aniline. It consists of a phenyl ring with an amino substituent; aniline is the prototypical aromatic amine*.

The sample (aniline) is introduced in a receptacle outside the chamber and it is gently heated at around 60ºC. He was used as buffer gas at a typical pressure of 2 bar. The molecular beam is then probed with a laser tuned along the appropriate spectral range and the emitted fluorescence was recorded with the use of a photomultiplier (EMI 9816B). Figure 2.5, exhibits the LIF spectrum of aniline in the 34000 - 34600 cm^{-1} region, obtained with the new set up. Aniline 0_0^0 transition appears at 34043.7 cm^{-1}, in good agreement with previously reported values.[2]

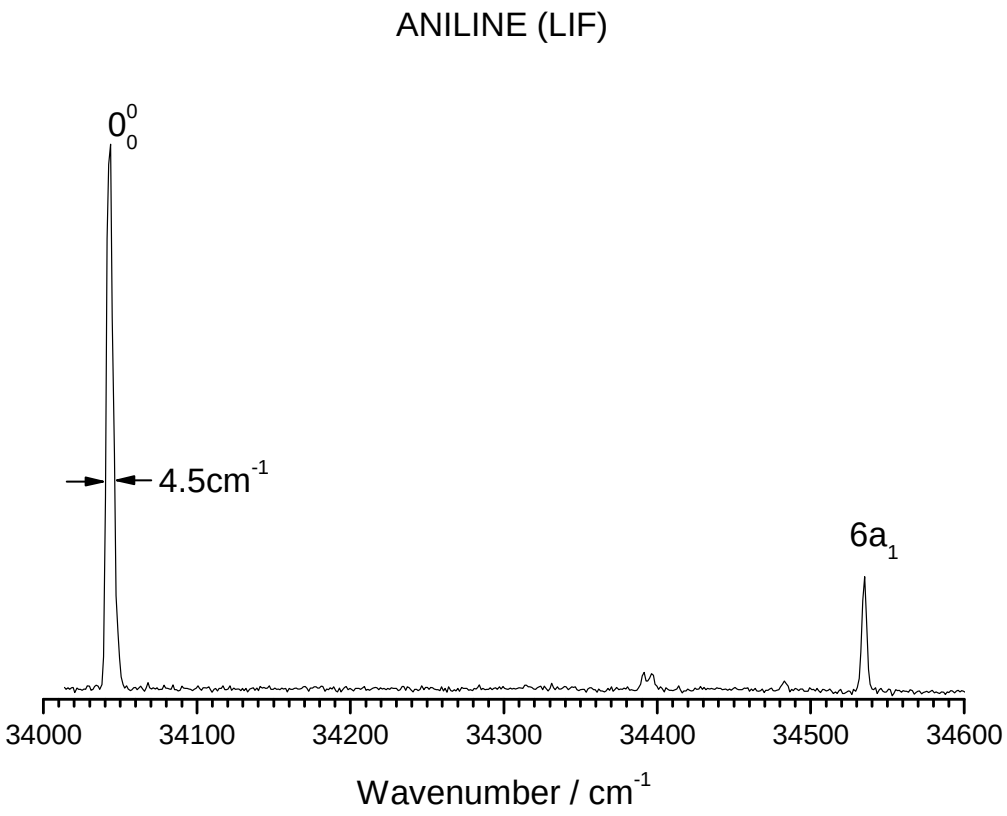

Figure 2.5. *LIF spectrum of aniline between 34000 and 34600 cm^{-1}, recorded in an expansion of 2 bar of He.*

Optimal S/N ration was obtained with the valve at a distance of 15 cm from the probe laser beam, firing the valve 540 microseconds before the laser shot, and using a 7.5 cm focal length lens to collect the fluorescence emission. A *cut off* WG305 filter was employed to minimize the laser light scattering that reaches the detector. With these settings, as can be seen in Figure 2.5, a 4.5 cm^{-1} Full Width at Half Maximum (FWHM) transition is obtained for aniline, which considering that no *skimmer* was used represents a good beam temperature. S/N ratio is c.a. 90:1, demonstrating the system's good performance.

2.4 – Mass resolved excitation spectroscopy (MRES)

The experimental system used for mass resolved excitation spectroscopy (MRES) is shown in Figure 2.6 and includes several lasers, a time of flight mass spectrometer and electronics for synchronization and detection. Most of the results were obtained in this system and the experimental techniques implemented are by far more complicated than in the set up with optical detection.

The molecule(s) to be studied are introduced in a small oven placed outside the chamber, where they can be gently heated to increase vapor concentration. Thus, the gas mixture will be formed by a small proportion (approximately 1%) of the molecules to be studied and a light and inert buffer gas (typically He, Ne and/or Ar) at pressures of c.a. 1-5 bar. The mixture is expanded through the 0.5 mm$^{\emptyset}$ nozzle of a stainless steel pulsed valve (R.M. Jordan, Figure 2.7) into the vacuum chamber of a time-of-flight mass-spectrometer (TOF-MS, R.M. Jordan[3]) at $<10^{-8}$ bar background pressure. The vacuum system consists of three turbo-molecular pumps (a Pfeiffer Vacuum TMU 521 of 1870 m^3/h and two Pfeiffer Vacuum TMU 071 of 200 m^3/h) evacuated by three rotary pumps (a Pfeiffer Vacuum DUO 010M of 10 m^3/h and two Pfeiffer Vacuum UNO 005A of 5 m^3/h). The supersonic expansion freezes the rotational and vibrational degrees of freedom of the complexes to a few K, creating the appropriate conditions to form non-covalent species. The central region of the supersonic beam is skimmed before entering the ionization region of the spectrometer, where the molecules are interrogated and ionized by different methods.

Three parallel plates (A_1, A_2, y A_3) separated 1 cm from each other and set at 4100, 3750 and 0 V, create an electric field that accelerates the ions through the TOF tube (Jordan Inc.) toward the 18 mm$^{\emptyset}$ multichannel plate (MCP, C-0701) detector, where they generate an electrical current. The ions produced by the laser radiation, are repelled by the A_1 grid, extracted by A_2 and finally accelerated by A_3 (Figures 2.8 and 2.9). The signal is routed to a digital oscilloscope (Tektronics TDS 520) with a nominal resolution of 10 ps and further to a PC computer for analysis and storage.

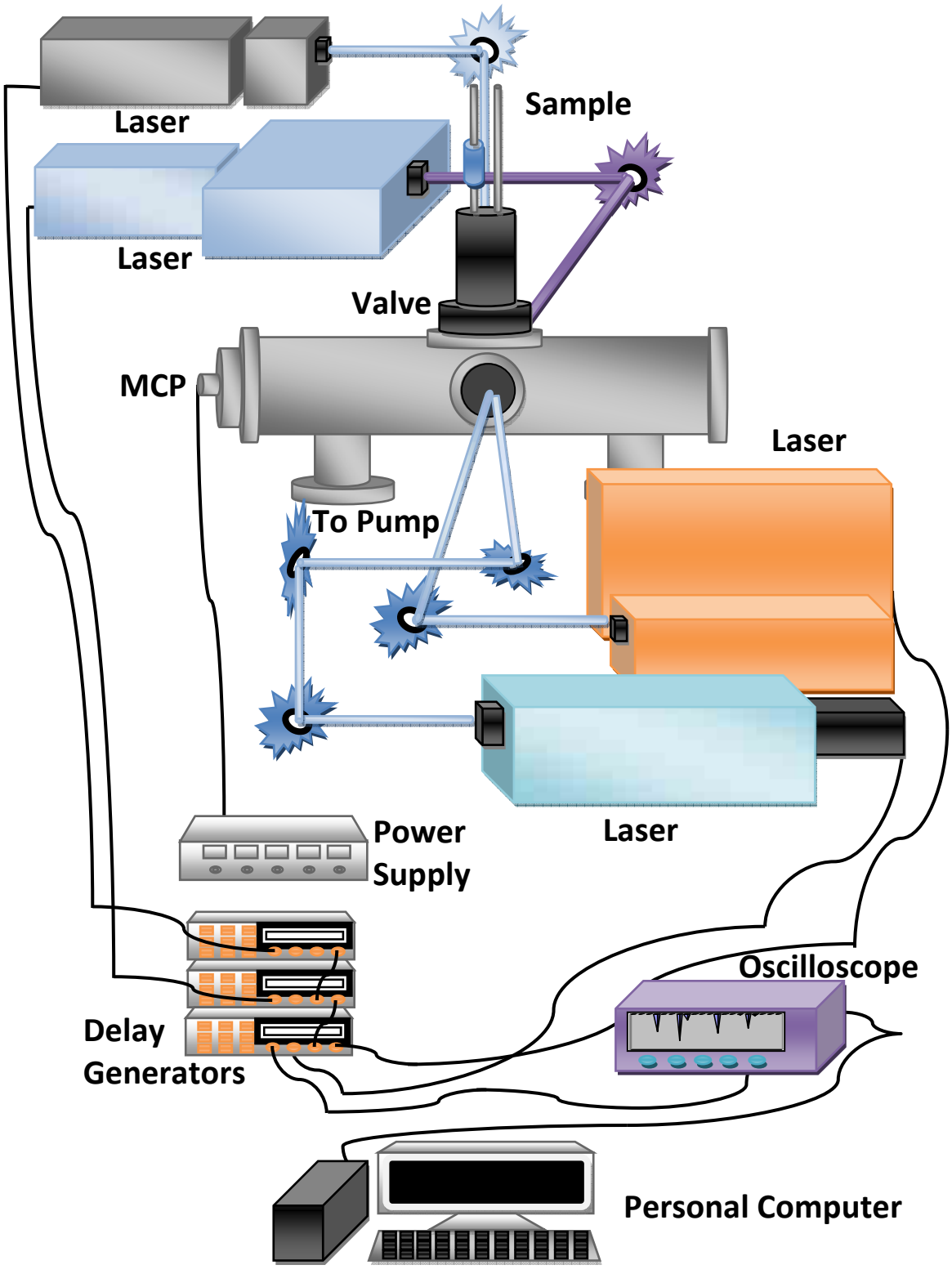

Figure 2.6 a. *Diagram of the MRES setup.*

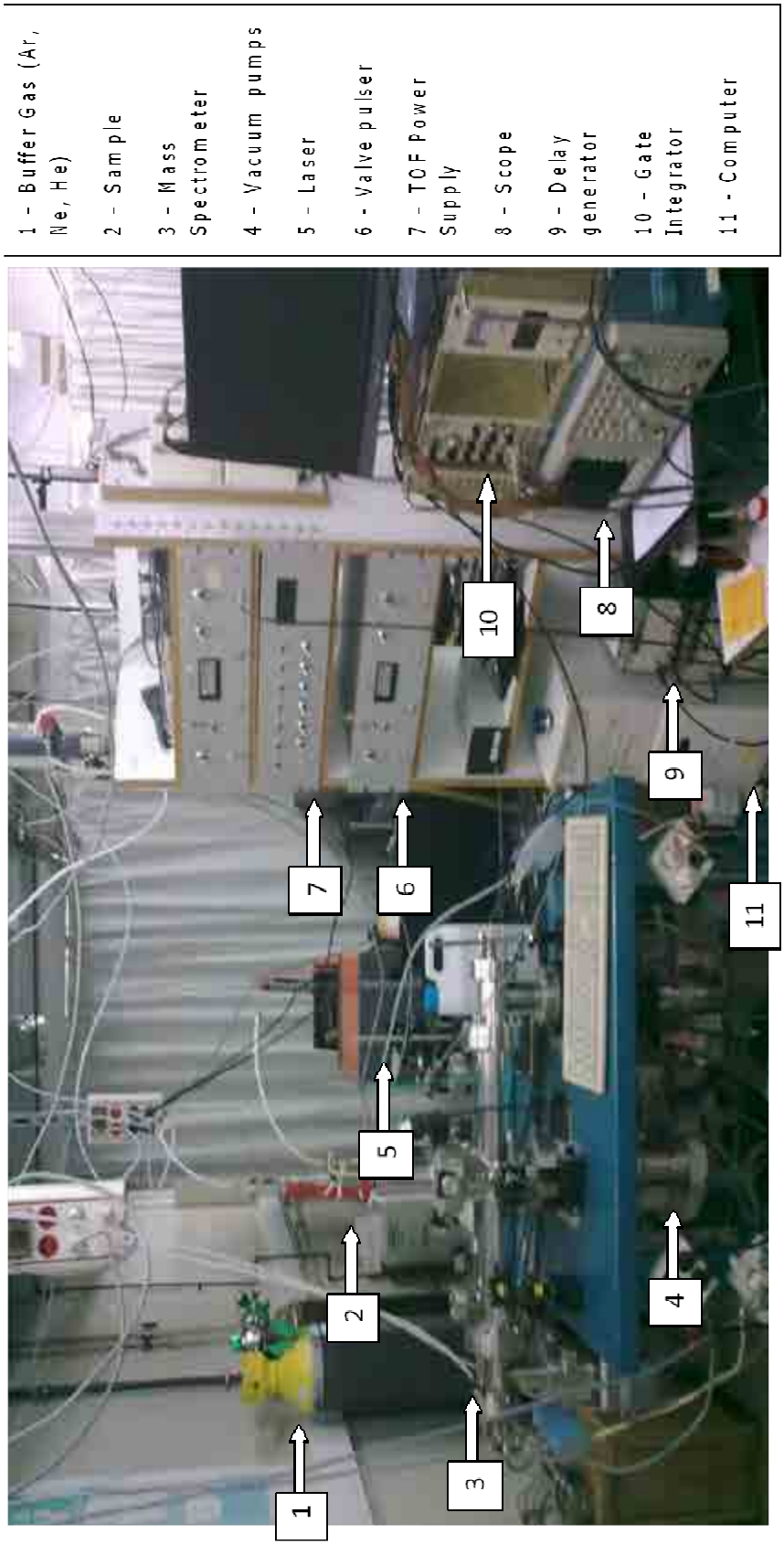

Figure 2.6 b. *MRES experimental system.*

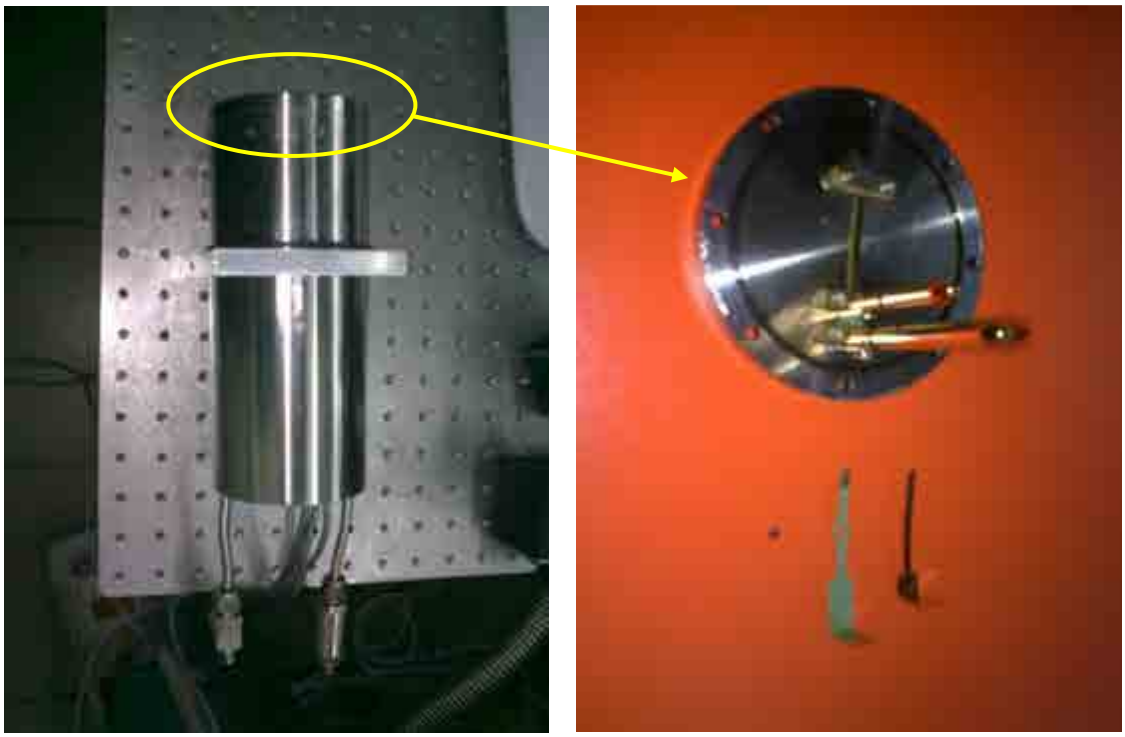

Figure 2.7. *R. M. Jordan stainless steel pulsed valve.*

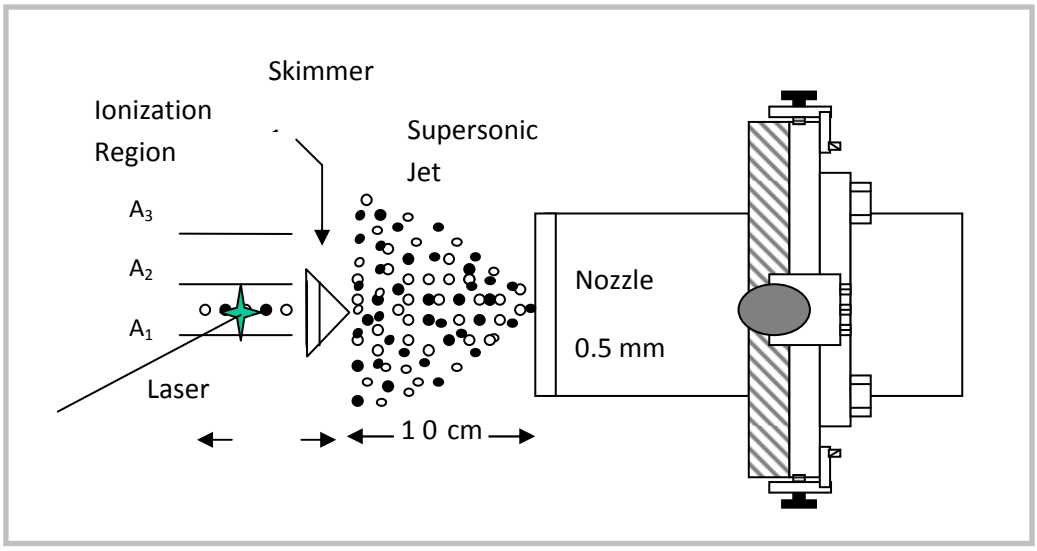

Figure 2.8. *Detail of the mass spectrometer pulsed valve and configuration of the ionization region.*

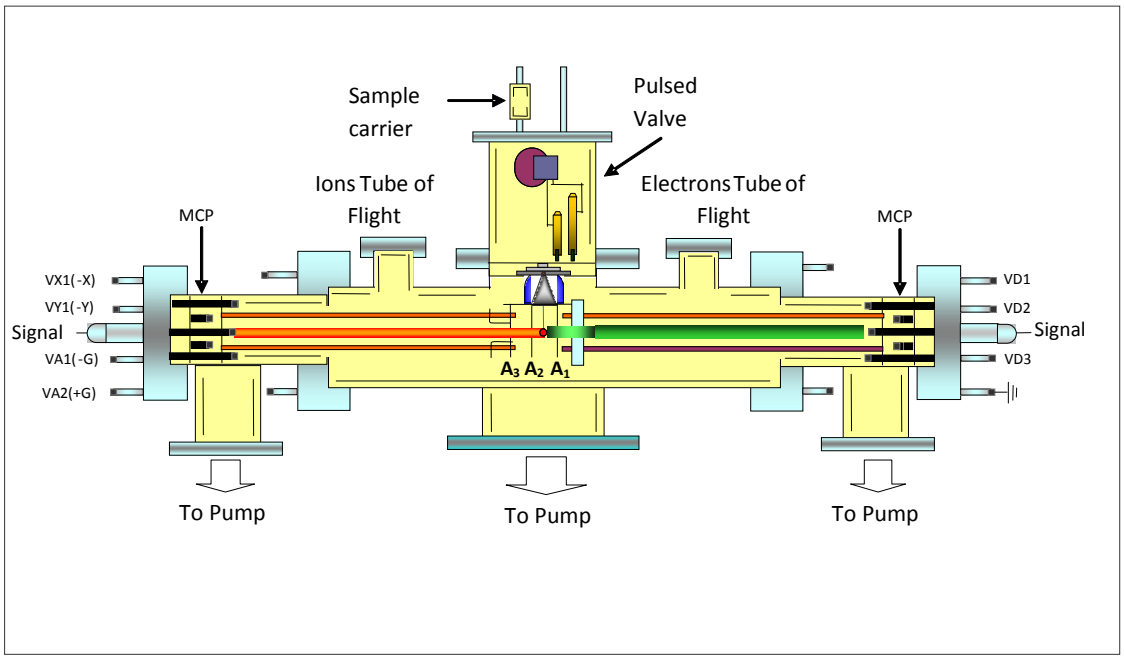

Figure 2.9. *Detail of the mass spectrometer.*

The produced and accelerated ions acquire velocities proportional to their m/z ratio, reaching the detector at different times, according to $(t_1/t_2) = (m_1/m_2)^{1/2}$ where m_i and t_i are the mass and time of flight of the *i*th ion. To minimize ion losses along the flight tube, two Einzel lenses correct their trajectories, focusing the ions into the detector. The voltage on the lenses can be regulated by the user and must be revised in each experiment to maximize the signal.

The temporal resolution of the lineal time of flight spectrometer is determined by the following relation:

$$R_T = \frac{t}{2\Delta t} = \frac{m}{\Delta m}$$

where t is the total time of flight of the ion package of m mass and Δt and Δm are respectively the FWHM of the ion package arrival time and mass. Taking into account that Δt is determined by the spreading of the spatial distribution and the initial kinetic energy of the ions in the acceleration region, the resolution improves when the spatial width of the ionization source (focusing) is reduced and the initial distribution of velocities is narrowed, for example, using a *skimmer*. For the molecules studied in this work, the experimental conditions are set in such a way that it is always possible to resolve species with m mass from the $m+1$ species for most of the clusters.

2.5 – Software

During this work a variety of software packages were used for structure prediction, programming and representation, so a brief description of each one is given bellow.

2.5.1 - *Structure prediction*:

- *Schrödinger*: *Schrödinger*'s[4] suite includes several applications.

a) *Maestro* was used as a molecular modeling environment tool in order to use *Macromodel's conformational search* and *XCluster* programs.

b) *Macromodel* was employed as a molecular visualization tool as well as to run semi-empirical molecular modeling calculations during conformational searching. It has been of an invaluable help to examine the conformational landscape of the system's studied. Some of them are considerably large and present hundreds or even thousands of possible conformational isomers. Thus, it is mandatory to use an automatic tool to explore the conformational landscape.

c) *XCluster* is a *Macromodel* tool that allows analyzing and visualizing the clustering of molecular conformations, given any of several commonly used criteria of molecular similarity. As computational techniques such as molecular dynamics, Monte-Carlo sampling, and conformational search methods produce a large number of conformations of a given chemical structure, *XCluster* is used to define structural classes and to determine the nature of the classes. The program permits classifying hundreds, or even thousands of conformers into a few families.

- *Gaussian*[5] is computational chemistry software with state-of-the-art capabilities for electronic structure modeling. Starting from the fundamental laws of quantum mechanics, Gaussian predicts the energies, molecular structures, vibrational frequencies and other molecular properties of molecules and reactions in a wide variety of chemical environments.

2.5.2 – *Communication and programming*:

- *Agilent VEE*[6] graphical language environment was used during this work for communication between lasers, oscilloscope, and other computers and in general to automate the experiment.

- *NI Labview*[7] graphical programming environment was used to program a control software for a homemade mixing unit for a Continuum dye laser

2.5.3 - *Graphical representation*:

- *Mathematica*[8] was used in this work for different purposes, such as graphical representation or to program some scripts to perform repetitive task on data collections.

- *Origin*[9] was used during the work for data analysis and graphical representation.

- *Chemcraft*[10] was used as a graphical interface for visualization of Gaussian outputs.

2.6 – References

1. http://www.exciton.com/
2. E.R. Bernstein, K. Law, M. Schauer, *J. Chem. Phys*., **80**, 634 (1984)
3. D. M. Lubman, R. M. Jordan, *Rev. Sci. Instrum*., **56**, 373 (1985).
4. http://www.schrodinger.com/about/
5. http://www.gaussian.com/
6. http://www.home.agilent.com/agilent/product.jspx?cc=ES&lc=eng&ckey=1476554&nid=-34095.806312.00&id=1476554&cmpid=20604
7. http://www.ni.com/labview/
8. http://www.wolfram.com/mathematica/
9. http://www.originlab.com/
10. http://www.chemcraftprog.com/

CHAPTER 3

METHODOLOGY

3 – METHODOLOGY

3.1 – EXPERIMENTAL TECHNIQUES

In this section a description of the experimental techniques employed during this work is given, highlighting specific details regarding how they are performed. For a complete description there are several books focused in the subject.[1-3]

3.1.1 – Laser spectroscopy with optical detection

3.1.1.1 - Laser induced fluorescence spectroscopy (LIF)

This technique allows obtaining the excitation spectrum of the molecules with vibrational (and sometimes rotational) resolution. Consists of scanning the excitation laser while the molecules' fluorescence emission is collected (Figure 3.1). In the cool environment of the jet, the electronic transition occurs exclusively from the zero-point level of the electronically ground state.

A limitation of the technique is that the system's lifetime must not be too short (not shorter than approximately 0.1 ns) or the vibrational information is lost due to Heisenberg's principle. On the other hand, if the system's lifetime is too long (longer than a few microseconds) the signal becomes too weak, as molecules will exit the observation window before emitting and there are high chances for non-radiative processes to drag molecules back to the electronic ground state.

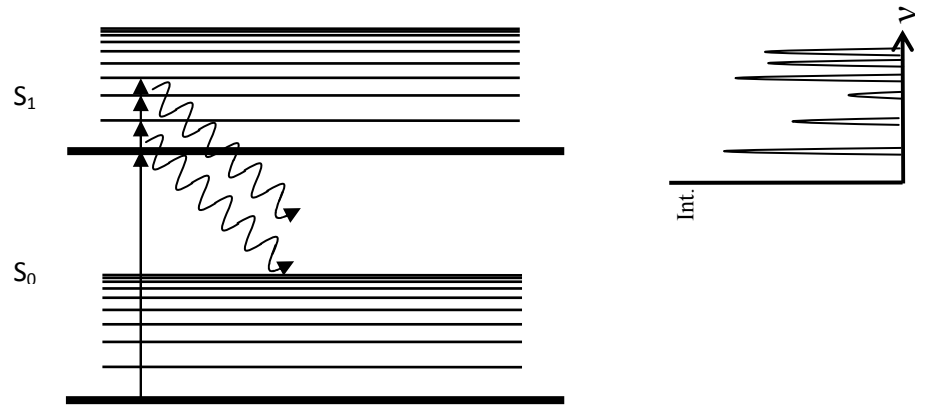

Figure 3.1. *Diagram of a LIF experiment under collision free conditions. The laser (hν) excites the system from the ground state to the vibronic levels of the excited state, while the total fluorescent emission is recorded as a function of the laser wavelength.*

The distribution of intensities and the vibrational structure provides information on structural changes between the states implicated in the transition by means of Franck-Condon Factors (FCF).

3.1.1.2 - Dispersed emission spectroscopy

While LIF yields the excited state vibronic spectrum, it is possible to obtain information on the ground state by using the so-called *dispersion emission spectroscopy*, in which the pump laser is tuned to a vibronic transition and the fluorescent emission of the system is collected. A monochromator is placed in front of the photomultiplier to select the observation wavelength. Changing this value and recording the signal produced in the photomultiplier, the ground state vibronic spectrum is obtained. The dispersed fluorescence (DF) spectrum (Figure 3.2) consists of all allowed transitions from a specific vibronic level of the excited state to the ground state. Because of the absence of hot bands, the low frequency vibrational levels can be recorded with high accuracy.

As the intensity distribution of the allowed transitions is determined by the FCF of the transition, important information on the system's structure can be extracted from this experiment. Changes in the shape of the spectra with the vibronic state give also hints on the system's dynamics: intra-molecular vibrational relaxation (IVR), conical intersections, etc.

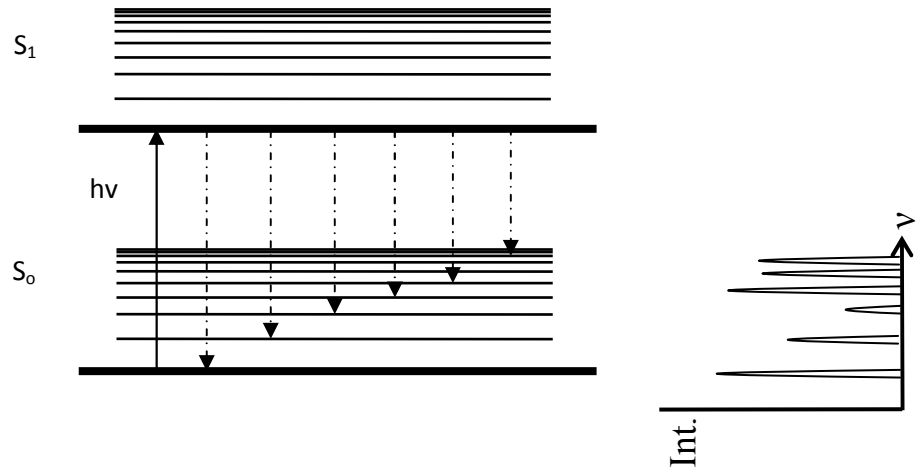

Figure 3.2. *Diagram of a dispersed emission experiment. The pump laser (hv) prepares the system in a vibronic level of the excited state, and the fluorescence emission is recorded as a function of wavelength.*

3.1.1.3 - Hole Burning spectroscopy (HB)

The *Hole Burning* spectroscopy is a double resonance technique that allows discriminating between transitions originated in different vibronic levels, such as conformational isomers, complexes of different stoichiometry and even hot bands. Therefore it is a powerful tool for assignment and characterization of complex spectra, like those of clusters formed by non-covalent interactions.

In this work, the clusters are generated by adiabatic expansion of a mixture of species. In the jet, a number of clusters of various sizes and different isomers of each stoichiometry are simultaneously generated and their electronic states are located quite close. Thus, when an absorption spectrum is measured by laser induced fluorescence (LIF) or resonance enhanced multiphoton ionization (REMPI) (see 3.1.2.1 section), the spectrum may contain overlapped transitions of several species. Colson and coworkers developed this spectroscopic method to discriminate between the spectrum of *cis* and *trans* isomers of m-cresol[4] isolating single absorption bands of a each species from the overlapping electronic spectra of the molecules, generated in a supersonic jet and termed this technique as "*Spectral Hole Burning Spectroscopy*". They also applied it for clusters as phenol·W_2.[5] Since then, this technique has been applied to single out the isomeric forms of molecular clusters such as the van der Waals clusters of large polyatomic molecules.[6-14]

In this technique (Figure 3.3), two lasers are used: the depopulation laser is tuned to the transition to be probed, while a conventional LIF spectrum is recorded, with the pump/probe lasers fired with a 0.1 - 1 μs delay, so both beams probe the same section of the jet. In this work, an active subtraction is also performed to improve *S/N* ratio. The result is a spectrum in which only those transitions originated in the same vibrational level of the electronic ground state of the probed species are present. The process continues probing different bands until all the features are identified.

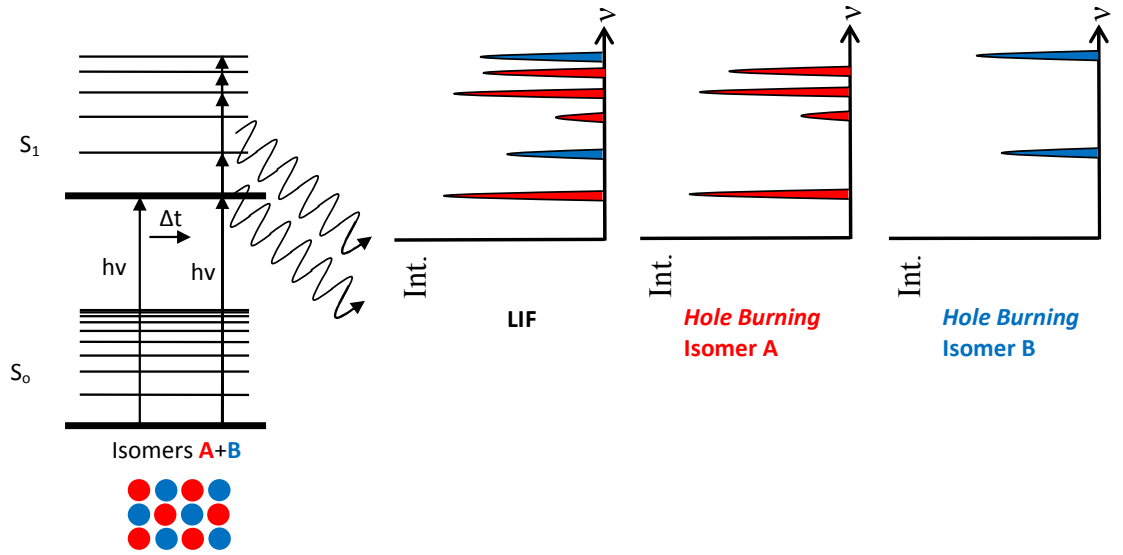

Figure 3.3. *Diagram of a HB spectroscopy experiment. The pump laser is tuned to one of the features of the spectrum, while a LIF spectrum is recorded with a probe laser delayed 0.1 – 1 μs respect to the pump laser. All the transitions that share the ground vibronic level with the transition probed by the pump laser, will present a reduced intensity.*

3.1.1.4 – Fluorescence dip infrared spectroscopy (FDIR)

While LIF is generally applied to electronic transitions, it can be extended to record the vibrational spectrum of the ground state with the employment of infrared–ultraviolet (IR-UV) double resonance spectroscopy. Vibrational spectroscopy is extensively used to study the molecular structure and intermolecular interactions in molecular clusters, thus, allowing the determination of the structures. IR-UV[15-16] double resonance is a highly sensitive and selective method that can be applied to record the vibrational spectra of clusters. Using a $LiNbO_3$ crystal, radiation between 2800 – 3800 cm^{-1} is easily achievable, allowing studying NH and OH stretching vibrations. If an OPO is used instead, it is possible to increase the lower range to approximately 2200 cm^{-1}, and therefore CH stretching vibrations can be also studied.

A set up similar to that in *Hole Burning* experiments is employed for ground state IDIRS experiments, but using an IR laser for depopulation. A probe UV laser monitors the population of specific species in a supersonic jet by LIF using a $S_1 \leftarrow S_0$ transition. Under such condition, an intense, tunable IR laser is introduced some nanoseconds prior to the UV laser pulse to pump molecules from the $v''=0$ to an excited vibrational level. Scanning the IR laser frequency while monitoring the LIF signal, an ion-dip spectrum corresponding to the IR ground state spectrum is obtained. The schematic and experimental setup is depicted in Figure 3.4.

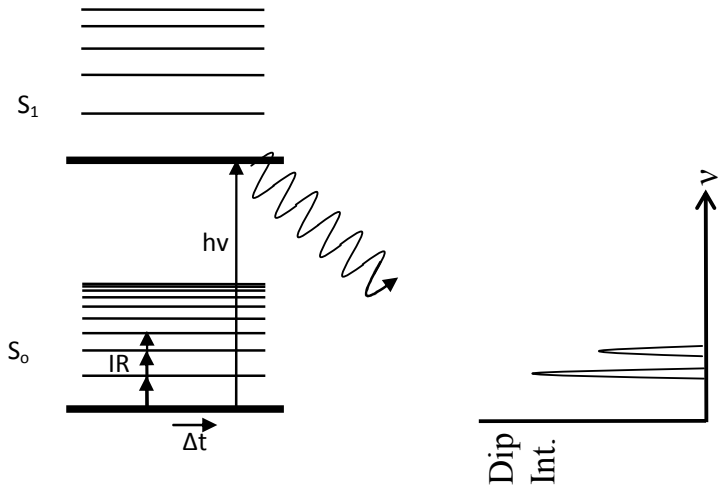

Figure 3.4. *Diagram of an IR-UV spectroscopy experiment. A probe UV laser monitors the population of a given species while the IR laser is scanned, fired some ns before the probe laser. Each time the IR hits a transition, a depletion on the LIF signal is produced.*

3.1.2 – Mass-resolved spectroscopic techniques

Multiphoton ionization (MPI) involves the ionization of a molecule by the absorption of more than one photon. It follows a non-dissociative ionization process in which $X + n*h\nu \rightarrow X^+ + e^-$ where X and X^+ are the parent neutral and the parent ion of interest respectively, and *n* represents the number of photons of h*v* energy required for the ionization process. Once they are ionized, it is possible to accelerate the ions towards the detector. Between the ionization region and the detector, some kind of ion selection device, in our case a time of flight (TOF), is introduced. Each species appear in its mass channel (m/z) allowing discriminating between species having a specific mass, which offers a great advantage over the laser spectroscopy with optical detection, at expenses of a more complex experiment.

3.1.2.1 – One-color REMPI spectroscopy (1+1)

REMPI spectroscopy[17-18] (Resonant Enhanced Multiphoton Ionization) is a refinement of the LIF spectroscopy that allows discriminating between species with different molecular weights. Therefore, it is an excitation technique that gives information on the excited electronic state. In the REMPI process, the molecule needs to absorb a minimum of two photons to be excited from its ground state, S_0, to its first ionization limit. The probability of such excitation process can be considered enhanced if there is a real excited state. Resonance is a necessary but not sufficient condition for state S_1 to cause an enhanced Multiphoton Ionization probability following excitation. It also requires the $S_1 \leftarrow S_0$ photon(s) excitation to have a non-zero transition probability and the state S_1 to be sufficiently long lived for the subsequent one-photon step to have a reasonable probability. If these conditions are met, then the spectrum obtained by measuring the ion yield (or the yield of the accompanying photoelectrons) as a function of the excitation wavelength will provide a signature of the $S_1 \leftarrow S_0$ transition of the neutral molecule with vibrational resolution (Figure 3.5). Usually, such process is described as 1+1, but each of the two steps may involve interchange of several photons, like 2+1 (absorption of two photons to the excited state and another one to produce the ionization), 2+3, etc. Analysis can provide structural and in some cases, dynamical information about the excited state S_1. A multiphoton transition between two states is allowed if the transition moment is non-zero. Multiphoton excitation cross-sections are small so high incident light intensities are necessary in order to compensate it. For

spectroscopic applications, high intensities can usually be achieved by focusing the output of conventional nanosecond pulse tunable dye lasers.

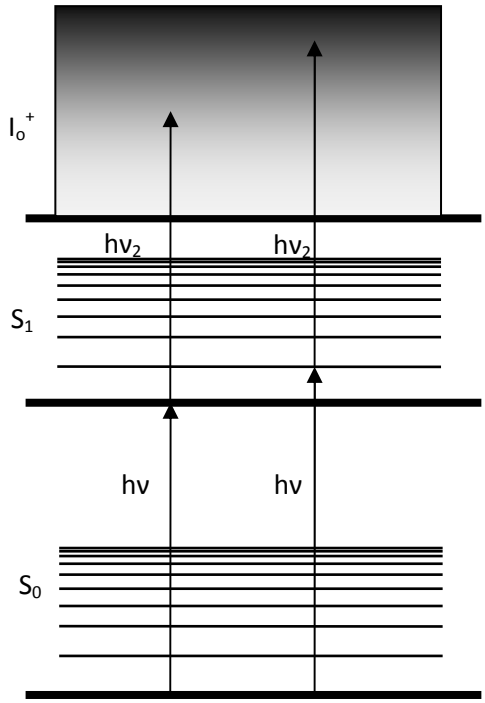

Figure 3.5. *Diagram of the one color REMPI spectroscopy. In a 1+1 process, absorption of one photon promotes the molecule to an intermediate electronic excited state. Absorption of a second photon ionizes the molecule, usually with an excess of energy.*

3.1.2.2 – Two-color REMPI spectroscopy (1+1')

Usually, the one-color REMPI (*1c–REMPI*) process leads to creation of ions with an excess energy because the energy of the $I_o^+ \leftarrow S_1$ transition does not match that of the $S_1 \leftarrow S_0$ transition. While the energy excess is not usually a problem when studying isolated molecules, it may lead to undesired fragmentation processes when the system is a complex of several molecules formed by non-covalent interactions. In order to avoid such problem, the two-color REMPI spectroscopy (*2c-REMPI*)[19-20] was developed, in which the $I_o^+ \leftarrow S_1$ transition is promoted by a photon with a small excess of energy only (Figure 3.6). This implicates that two different lasers must be used, increasing the complexity of the experiment, as both laser beams must overlap spatially and temporally with the gas pulse from the valve.

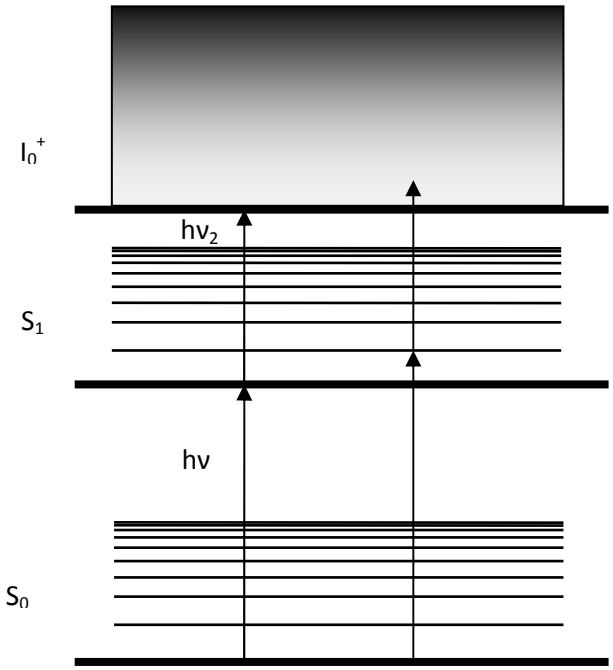

Figure 3.6. *Diagram of two color REMPI spectroscopy. The first photon prepares the molecule in an electronic excited state and a second photon of adequate energy, ionizes the molecule. Recording the ionization signal as a function of the pump laser, a spectrum of the electronic excite state is obtained.*

A comparison between the REMPI spectrum and the *2c-REMPI* spectrum of propofol between 36000 and 37000 cm^{-1} is shown in Figure 3.7. As can be seen, the 1c-REMPI spectrum presents a considerably larger number of bands than the 2c-REMPI spectrum, mainly due to fragmentation of clusters of higher stoichiometry.

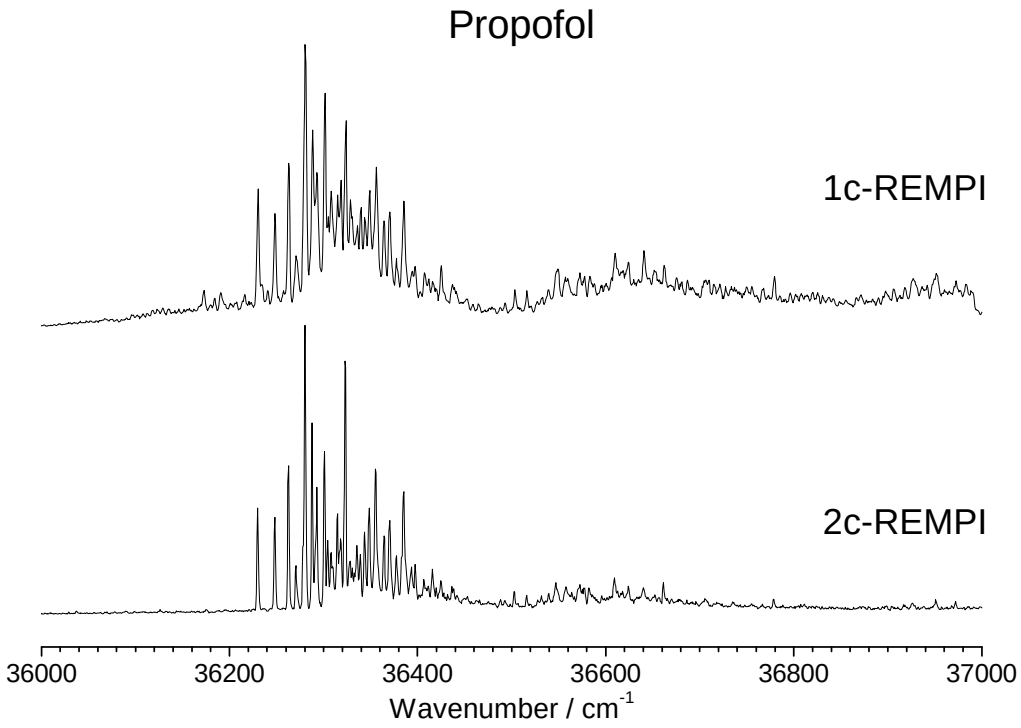

Figure 3.7. *Comparison between a 1c-REMPI spectrum (upper trace) and a 2c-REMPI spectrum (lower trace) of propofol.*

In addition to the excited state spectrum, it is possible to obtain the ionization threshold tuning the pump laser to the 0_0^0 transition and scanning the ionization laser. A technique developed by Giardini's group[21] allows determining the dissociation energy of complexes formed by non-covalent interactions[22] with reasonable accuracy, as long as the $I_0 \leftarrow S_1$ transition does not involve a large change in geometry, and therefore the bottom of the ion potential energy surface can be accessed. In this *fragmentation threshold method* mass-resolved two-color R2PI transitions are used to derive the potential well depths and dissociation energies of the ground, S_0, first excited, S_1 and ion I_0 states (Figure 3.8), or of other electronic state involved in the *REMPI* process.

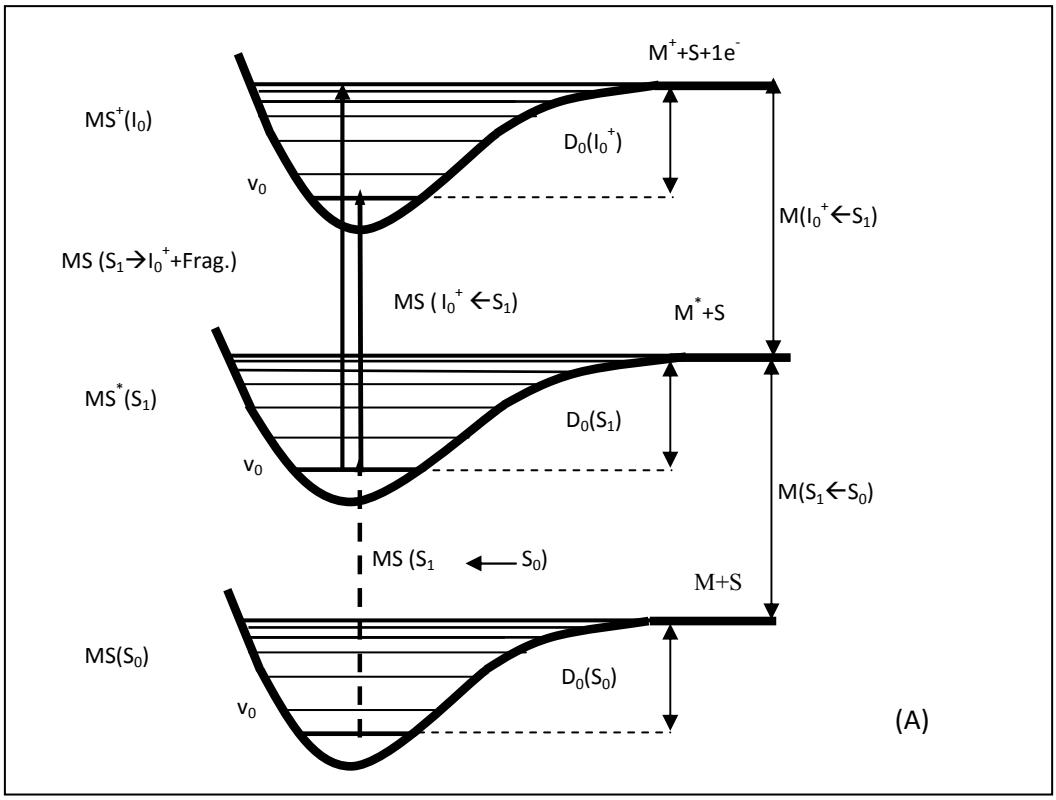

Figura 3.8. *Scheme of the fragmentation threshold method to determine dissociation energies. Mass-resolved two-color R2PI transitions are used to derive the potential well depths and dissociation energies of the ground, S_0, first excited, S_1 and ion I_0 states.*

3.1.2.3 - Hole Burning spectroscopy (HB)

Although multiphoton ionization mass spectrometry can discriminate between species having a given mass, it is sometimes difficult to avoid fragmentation of the clusters after the ionization and it is impossible to discriminate between species having the same mass, such as conformational isomers. Only with the employment of double resonance techniques, like *hole burning*, it is possible to avoid such problems. The theoretical basis of the mass-resolved *hole burning* spectroscopy is similar to the one described in the *optical detection spectroscopy* section, with the only difference that, in this case, a third laser is needed in order to avoid the energy excess produced during ionization. Thus, one laser is used for depopulation and another two for the 2-color detection. The result is the discrimination between spectra of different isomers of a given stoichiometry.

In this technique, three lasers were used: the depopulation laser is tuned to the transition to be probed, while a *2c-REMPI* spectrum is recorded, with the pump/probe lasers delayed c.a. 100-400 ns, so they probe the same section of the molecular beam burned by the depopulation laser. An active subtraction is also performed to improve *S/N* ratio. The result is a spectrum in which only those transitions originated in a common vibrational level of the electronic ground state of the species probed by the pump/probe laser set up are present. It is possible to obtain their spectra separately by repeating the whole process for each species (Figure 3.9).

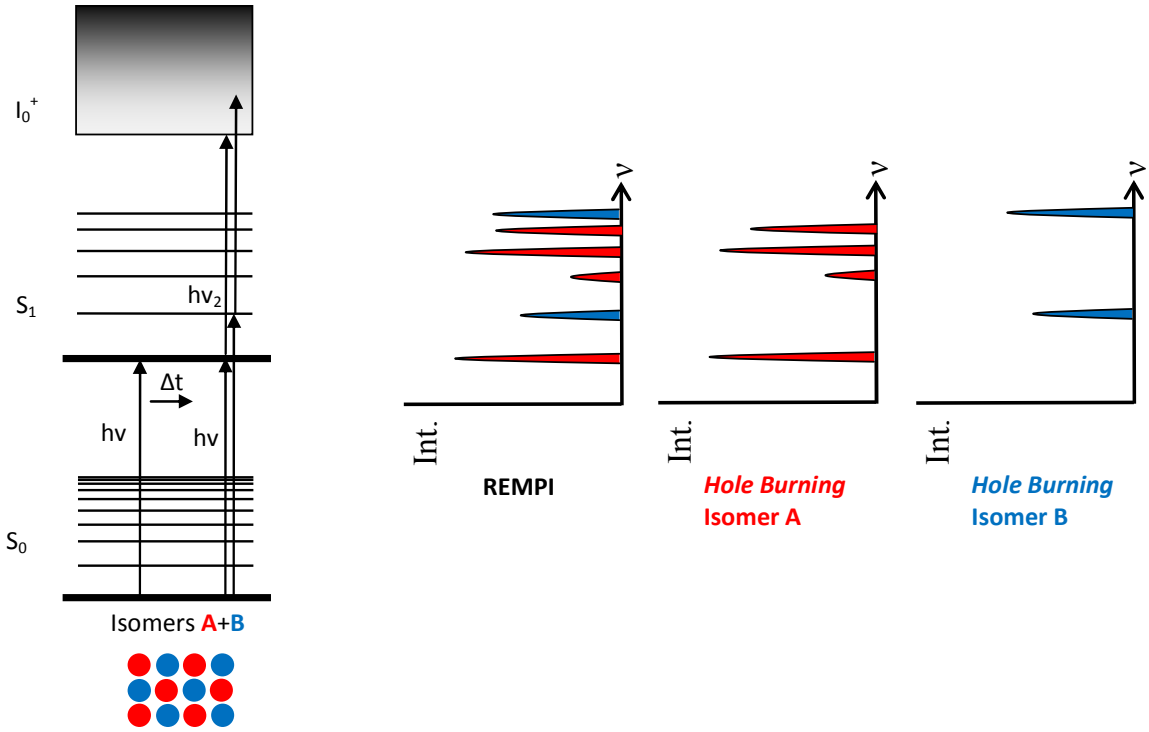

Figure 3.9. *Diagram of a Hole burning spectroscopy experiment. The pump laser is tuned to one of the features of the spectrum, while a 2c-REMPI spectrum is recorded with the pump/probe laser set up delayed 100-400 ns respect to the pump laser. All the transitions that share the ground vibronic level with the transition probed by the pump laser, will present a reduced intensity.*

3.1.2.4 - IDIR spectroscopy

The theoretical basis of the Ion Dip InfraRed Spectroscopy (IDIRS) is similar to that described in the optical detection section but, in this case, the ions produced by the probe laser are detected, instead of the fluorescence. In this work, the detection was carried out using a two-color scheme, as in the hole burning set up, so interference due to fragmentation is avoided.[14] Such refinement yields better spectra in most cases, but it is indispensable in the study of propofol and its high order clusters.

It is worthy to mention the very low power densities used for IDIRS experiments in the present study: usually 100-200 μJ of laser energy are enough to achieve a 70-80% depopulation of the signal. Although such a large dip is not expected in a two levels system, one has to take into account the lifetimes of the vibrationally excited states of the clusters, as if they are short they can follow a fast decay processes, such as intramolecular vibrational redistribution or vibrational predissociation and, that the cluster may dissociate after absorption of an IR photon.

A probe UV laser monitors the population of a specific species in a supersonic jet, using a $S_1 \leftarrow S_0$ transition. Then, an intense tunable IR is introduced some nanoseconds prior to the UV laser. Thus, by scanning the IR laser frequency while monitoring the *2c-REMPI* signal, the ground state IR spectrum is obtained (Figure 3.10). An active subtraction is also performed to improve *S/N* ratio.

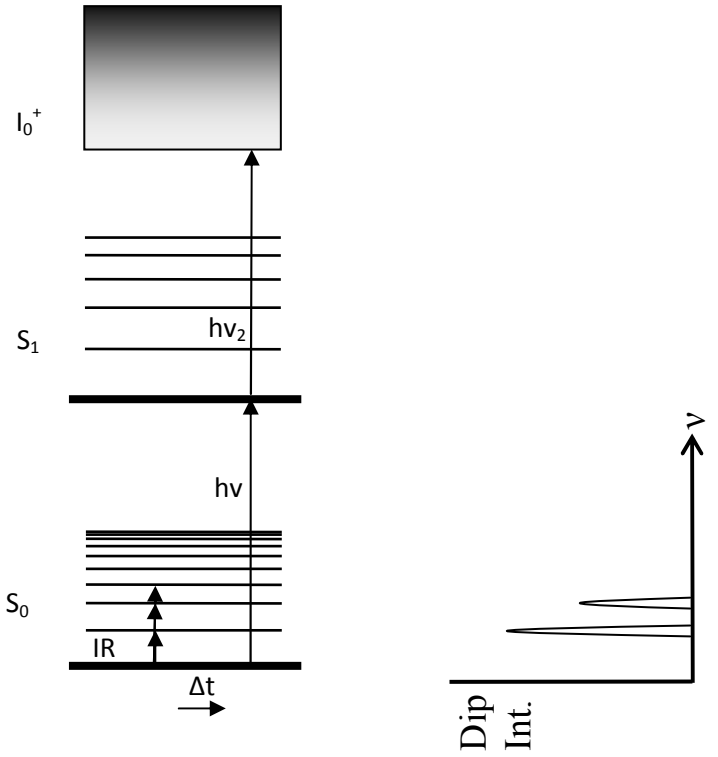

Figure 3.10. *Diagram of an IR-UV spectroscopy experiement. A UV probe laser monitors the population of a specific species, while the IR laser is scanned, delayed some ns respect to the probe laser. Each time the IR laser is resonant with a vibrational transition of the species probed, a depletion of the 2c-REMPI signal is produced.*

It is worthy to mention that, while the 2800 – 3800 cm^{-1} region can be explored with the equipment in our lab, the region around 500-1700 cm^{-1}, the fingerprint region, was scanned using the FELIX[23] free electron laser (Free Electron Laser for Infrared eXperiments), located at the FOM Instituut voor Plasmafysica "Rijnhuizen" (Nieuwegein, The Netherlands) which delivers 60 mJ per macropulse, 5 μs pulse duration, bandwidth 0.2 - 0.5% of central λ.

3.1.2.5 - S_1 IDIR spectroscopy

Using IDIRS it is also possible to record the excited state IR spectrum, by changing the lasers' firing sequence and scanning the IR laser between the two UV lasers (usually 5 ns after the pump laser), which were separated ca. 15 ns (Figure 3.11) for this system.

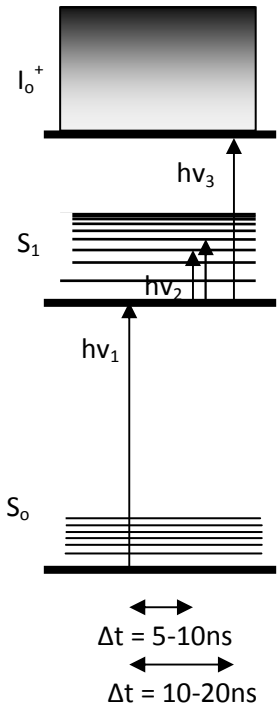

Figure 3.11. *Diagram of a S_1 IDIRS experiment. The first UV photon prepares the molecules in an electronic excited state and after some time (ca. 15 ns) a second photon ionizes the molecules. Between the two UV lasers, an IR laser is scanned and each time the IR laser is resonant with a vibrational transition, a depletion of the 2c-REMPI signal is produced. Recording the ionization signal as a function of the IR laser, an IDIR spectrum of the electronic excited state is obtained.*

3.1.2.6 – IR-IR-UV hole burning spectroscopy

Some molecules or clusters present overlapped electronic spectra and thus, when recording the IDIR spectrum, the transitions from each of the conformers cannot be resolved. In this case, a triple resonance technique, recently developed by Zwier's group,[24] allows separating the IR spectra of the different isomers obtained via double resonance methods.

The technique is similar to that for the IR-UV method, but in this case, another IR laser is needed: a probe UV laser monitors the population of the overlapped electronic transition for two or more specific conformers in a supersonic jet, using a $S_1 \leftarrow S_0$ transition. An IR laser is introduced, at a repetition rate of 5 Hz, some micro-nanoseconds prior to the UV laser and it is fixed to a transition observed in the double resonance method. Then, a third laser is introduced temporally between them, at a repetition rate of 10 Hz. In this way, by scanning the second IR laser frequency while monitoring the *2c-REMPI* signal, an ion-dip spectrum is obtained via active substraction, which corresponds to the IR ground state spectrum of the conformer selected by the first IR laser. The schematic and experimental setup is depicted in Figure 3.12.

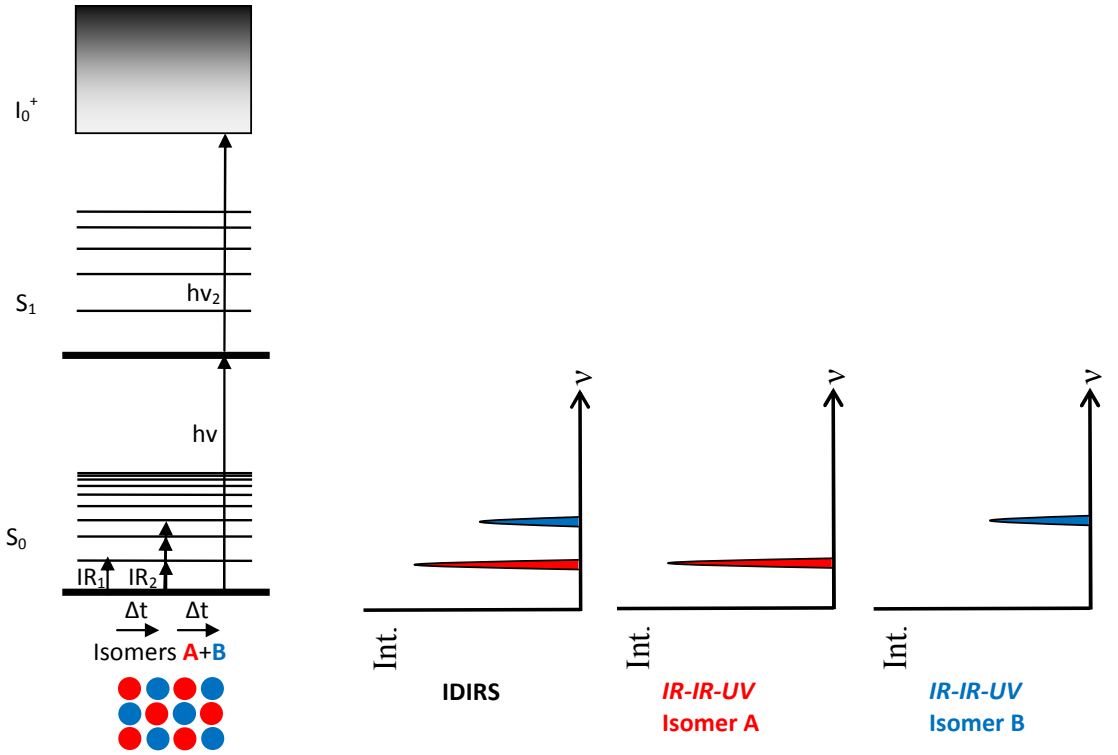

Figure 3.12. *Diagram of a triple resonance IR/IR/UV spectroscopy experiment. A prove UV laser monitors the population of two conformers whose electronic transitions are overlapped. A first IR laser is introduced at 5Hz, some μs prior to the probe laser and fixed to a vibration on the IDIR spectrum while a second IR laser fired between the other two lasers is scanned. Each time the second IR laser is resonant with a vibrational transition of the selected conformer, a net effect is presented due to the gain at the selected transition's constant depletion produced by the first IR laser.*

As the technique is considerably complicated, an example is offered for clarification: an aromatic molecule (X), which consist of carbons, hydrogens and a single OH group, is cooled under supersonic expansion conditions and only two conformers are formed: conformers A and B in a proportion of 4:1 (80% of conformer A and 20% of conformer B). These two conformers share common electronic transitions from the ground state to the excited state's vibrational levels and thus, they cannot be resolved. Consequently, when a IDIR experiment is done by fixing the UV laser in any of the electronic transitions, two OH stretching vibrations appear in the 3000-3800 cm^{-1} region (for example at 3500 and 3600 cm^{-1} for the conformers B and A respectively, Figure 3.13). For the sake of clarity, we will consider that both IR lasers have the same energy which does not fluctuate upon time, they have similar beam profiles and dimensions, and that the second IR laser exactly overlaps with the first IR laser and also

with the UV laser. We also know that the UV laser is continually ionizing 100 molecules of our system, and therefore, 80 ions of conformer A and 20 ions of conformer B reach the detector in each of the UV pulses. In addition, the probability of both OH stretching modes is of 50%. If such conditions are fulfilled, when an IDIR experiment is done 40 molecules of conformer A are vibrationally excited at 3600 cm^{-1} and 10 molecules of conformer B at 3500 cm^{-1} (Figure 5.13a).

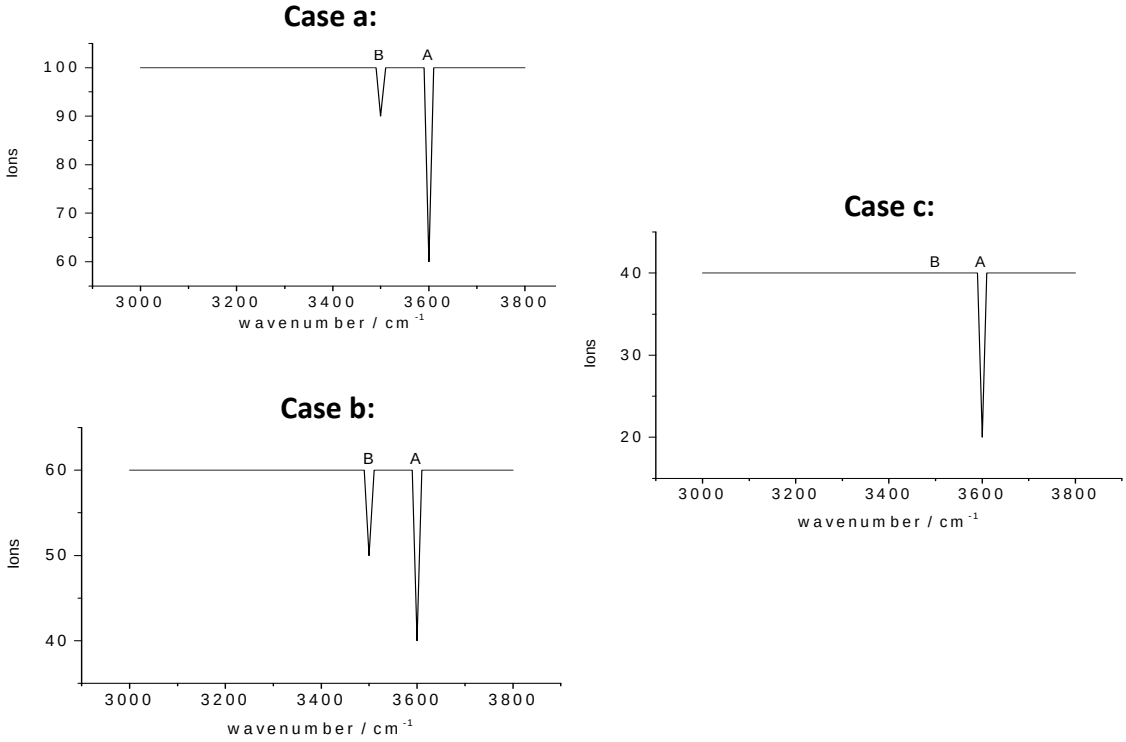

Figure 3.13. *Example of a triple resonance IR/IR/UV spectroscopy experiment. Case a: of the 100 ions reaching the detector, when the first IR laser is off and the second IR laser is resonant with the conformer A and B OH stretching modes, there is a depletion of the signal of 40% and 10% respectively. Case b: If the first IR laser is on and tuned into the OH stretching of conformer A there is a constant depletion, and when the second IR laser resonant with the conformer A and B OH stretching modes, there is a depletion in the remaining ions of 40% and 10% respectively. Case c: If an active substration of both signals is done, a net effect due to the gain in the selected transition's constant depletion is presented.*

When doing the triple resonance method, the same result than in an IDIR experiment (Figure 5.13a) is achieved when the first laser is *off* (one must remember that it is fired at 5Hz while the other IR laser and the UV laser are fired at 10Hz). On the

other hand, when it is *on* we will have three cases resulting in Figure 5.13b: 1) when the second IR laser is not resonant with any of the OH stretching vibrations, and as the first IR laser excites vibrationally 50% of the selected conformer A, a constant depletion of 40 molecules in the signal resulting in a baseline is obtained. 2) when the second IR laser is resonant with a stretching of conformer A, the first IR laser makes a dip of the 50% of the conformer A population, but the second laser depletes an additional 50% of the conformer A remaining population, resulting in a dip of 0.5*80=40 due to IR_1 and 0.5*(0.5*80)=20 due to the second, which amounts for a total dip of 60 molecules of the 100 ionized molecules. 3) when the second IR laser is resonant with a stretching of the conformer B, a depletion of 50% of the conformer A plus a 50% of conformer B is produced, which accounts for a total dip of 50 molecules. Thus, substraction of IR *on* from IR *off* signal results in the case shown in Figure 5.13c.

If fractions are used instead of molecules, the real case is achieved. When this technique is carried out using an active subtraction, a net effect is observed due to the gain in the selected transition's constant depletion caused by the first IR laser. Repeating the procedure for the rest of the OH stretching modes, an IR spectrum of each of the conformers is obtained.

3.1.2.7 – S_1 IR-IR-UV hole burning spectroscopy

With some minor modifications, it is possible to apply the IR-IR-UV technique to the excited state.

The technique is similar to that for the S_1 IR-UV method, but in this case an additional IR laser is introduced prior to the second IR laser: the first IR laser is fixed at an IR transition of the excited state of one of the conformers and the second IR laser is scanned while monitoring the *2c-REMPI* signal due to the second UV laser. The excited state IR spectrum of the conformer selected by the first IR laser is obtained in this way. The schematic and experimental setup is depicted in Figure 3.13.

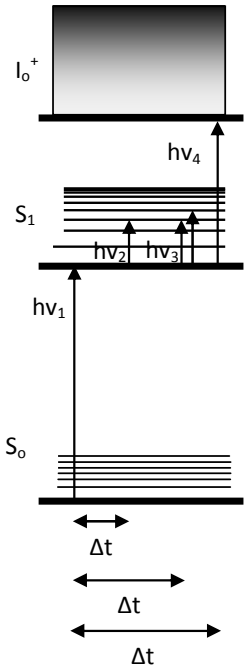

Figure 3.13. *Diagram of an excited state triple resonance IR-IR-UV spectroscopy experiment. An UV laser pumps population of two conformers whose electronic transitions are overlapped. A first IR laser is introduced at 5 Hz, delayed some ns from the pump laser and tuned to a transition on the S_1 IDIR spectrum, while a second IR laser is scanned between the latter and the second/detection UV laser. The delay between the first UV and the first IR lasers is c.a. 5 - 10 ns; the rest of the delays are the maximum allowed by the excited state lifetime having enough signal.*

3.1.2.8 – Stimulated emission pumping

Stimulated emission pumping (SEP) is a powerful tool that gives information on the electronic ground state of the molecules. It allows also for a very accurate determination of dissociation energy values of complexes formed by non-covalent forces. Depending on the optically active vibrational modes, specially on those near the dissociation limit, accuracies of c.a 0.1 kcal are achievable.[25]

In order to carry out such experiment, a laser prepares the molecules in the excited state while a second laser, delayed some nanoseconds (between 15-30 ns), probes the excited state. Between both lasers, another laser is scanned; when a $S_1 \leftarrow S_0$ vibronic transition is hit, stimulated emission is produced and the signal produced by the probe laser decreases (Figure 3.14). In this way, the ground state vibronic spectrum is obtained.

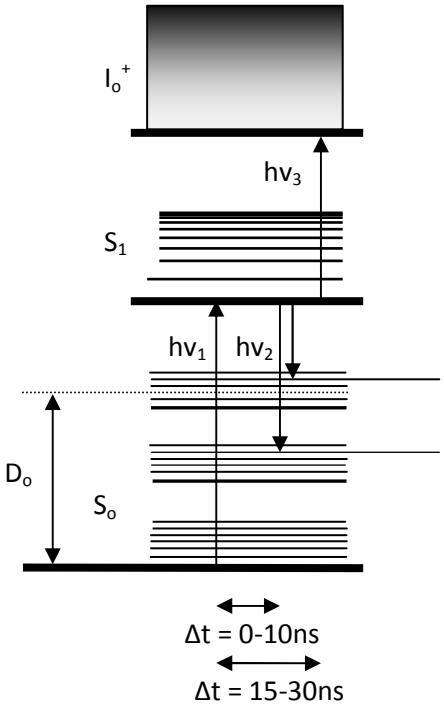

Figure 3.14. *Diagram of a SEP-R2PI spectroscopy experiment. In the first step, the complex is taken to an excited state (pump laser). By the use of a second laser the S_1 excited state population is transferred into intra and intermolecular vibrational levels of the S_0 state. The variation in the excited state population is probed by a third laser, tuned to the $I_0^+ \leftarrow S_1$ transition, as a function of the wavelength of the second laser.*

This experiment can also be conducted doing stimulated emission followed by a R2PI detection. In this second scheme, a first laser prepares the molecules in an electronic excited state, usually using the 0_0^0 transition. Then, a second laser, by stimulated emission, returns part of the population back to the ground state. Scanning the stimulated emission laser to the red of the 0_0^0 transition, it is possible to selectively populate the S_0 vibronic levels. After some time (usually around 1 μs) the presence or absence of vibrationally excited states of the complexes in S_0 is probed with a third laser, tuned to a region of the spectra where hot bands are present. The probe laser produces signal only if the stimulated emission laser is resonant with a vibronic transition. If the energy of the S_0 vibronic level where the molecules are driven into is greater than the dissociation energy $D_0(S_0)$, then vibrational predissociation occurs and no signal is produced by the probe laser. The last peak detected determines the lower limit of the $D_0(S_0)$ value (Figure 3.15).

Although this last method provides more precise dissociation energy values, it is a considerable more complicated technique, especially when trying to locate hot bands in the ground state. Therefore, it has been applied in scarce occasions.[26-27] It was tried for the benzocaine·argon cluster but without any success, maybe due to the nature of the cluster.

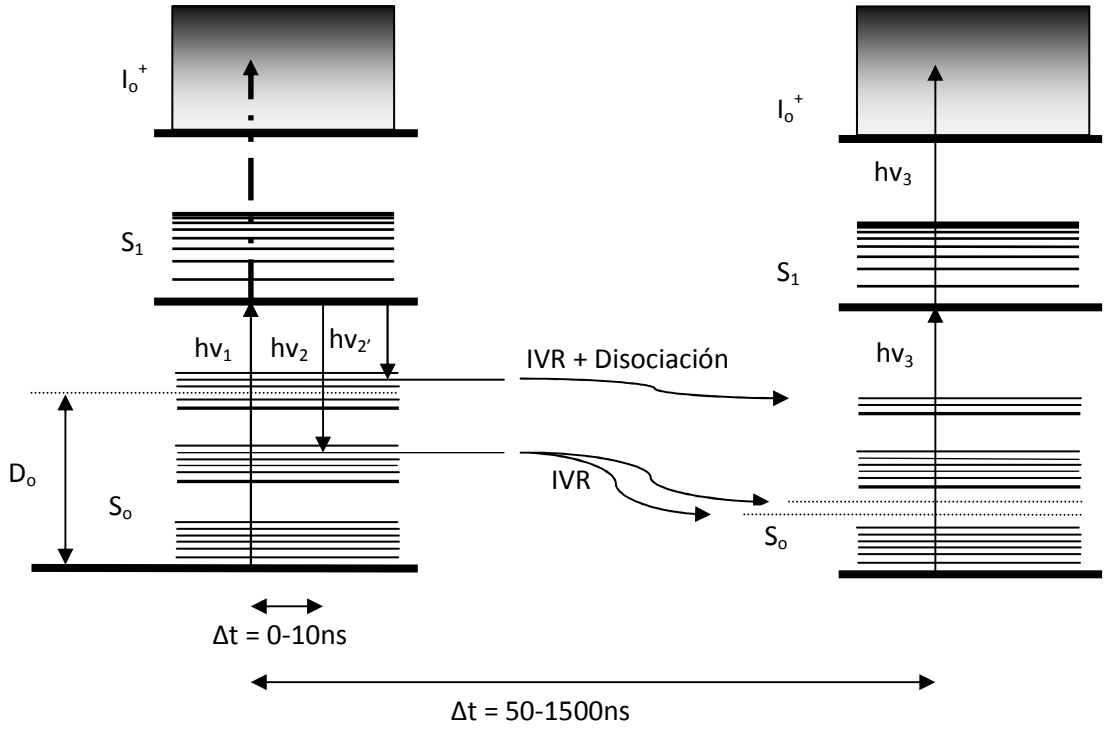

Figure 3.15. *Diagram of a SEP-R2PI spectroscopy experiment. In the first step, the system is taken to the excited state (pump laser). When the second laser drives the population of the S_1 excited state into the intra and intermolecular vibrational levels of the S_0 state bellow D_o, the system evolves during some time (Δt between 50 ns – 15 μs), in which IVR processes lead to population of hot levels. When the second laser moves the population of the S_1 excited state to levels above D_0, the complex dissociates following a vibrational predissociation (VP) during Δt. The increase or decrease in the population of the hot levels is then probed by the use of two-photons 1+1' (R2PI) resonant ionization with the aid of a third laser.*

3.1.2.9 - Lifetimes

Excited electronic state lifetimes give information on the existence of dynamical processes, reactions and other kinds of non-radiative mechanisms that may influence the system's spectroscopy, and therefore they were determined in the present work. The coexistence in the expansion of numerous species with spectra in the same region makes compulsory the employment of a mass-resolved technique for such purpose. Thus, the pump laser is tuned to the 0_0^0 transition of a given species, while the probe laser ionizes the molecules from the S_1 electronic state. The change in the signal intensity with the delay between both lasers is recorded, obtaining the excited state time evolution. A matching of the calculated curves to the measured data, using a nonlinear least-squares analysis, i.e. a iterative reconvolution[28] is done to extract the S_1 lifetime. The goal is to obtain the values of the parameters which provides the best match between the experimental data and the calculated decay, while minimizing the deviation.

3.2 – THEORETICAL CALCULATIONS

3.2.1 – Introduction

Theoretical calculations are an indispensable tool to determine the structures of the systems studied. Thanks to the computational development achieved during the last years, nowadays, big molecular systems with large quantity of electrons can be studied. The information obtained is invaluable: structures, binding energies, vibrational modes, potential energy surfaces (PES) and rotational spectra of the structures present in the beam among other parameters. On the other hand the experimental results are also essential for the estimation of the quality of the theoretical calculations.

The procedure used in the calculations is as follows: first, molecular mechanics calculations are carried out in order to find nearly all the possible conformers in a *stability window*, and classify them into families or most stable structures; second, Quantum Mechanics (Q.M.) or Density Functional Theory (DFT) calculations are performed on the most stable structures to obtain reliable geometries, relative stabilities and a prediction of the vibrational spectrum.

Calculations were conducted on an itanium-based cluster with 794 processors[29] available in the university's computational centre and an Intel QuadCore Xeon Harpertown-based cluster with 1024 processors[30] available at I2Basque in the Basque Government.

3.2.2 – Molecular mechanics

In order to search for all the possible conformational structures, molecular mechanics calculations were carried out. Such kind of calculation are of great help, specially for big systems like propofol·W high order complexes. These calculations can be done in reasonable time even for big systems and serve as criteria to select the best candidates to run *ab initio* and/or DFT calculations.

During this work *MMFFs* force field was used as is one of the most recommended parameterized potentials as to describe the geometries and dissociation energies of clusters[31]. A combination of torsional sampling and Large Scale Low Mode (LLMOD) method was used to explore the conformational landscape. LLMOD search method[32] progressively builds up and refines a collection of conformers. During the search, a conformation is selected and then greatly perturbed in the direction of one of the low frequency normal modes of the molecule. The perturbed structure is then energy minimized and added to a list of conformers if it has a sufficiently low energy. The use of low frequency normal modes ensures that changes in atom positions are coordinated in a direction that has a reasonable chance of leading to another low energy conformation.

Although LLMOD approximation is very good for the systems presented in this work, it has been combined with a Monte Carlo (MC) algorithm. In MC, a new configuration is generated by selecting a random molecule, translating it, rotating it, and performing any internal structural variations. Acceptance of the new configuration is determined by the *Metropolis sampling algorithm*; application over enough configurations yields properly Boltzmann-weighted averages for structure and thermodynamic properties. For molecular dynamic methods (MD), new configurations are generated by application of Newton's equations of motion to all atoms simultaneously over a small time step to determine the new atomic positions and velocities. In both cases, the force field controls the total energy and forces, which determine the evolution of the systems.

3.2.3 – Computational chemistry

Once the conformational landscape is explored, *ab initio* calculations on the structures found in a given stability window are carried out. Due to the size of the system, it is necessary to carefully calibrate the calculation level to obtain reliable results at affordable computational times. DFT is a good method for description of systems with hydrogen bonds. Until recently, one of the most employed functionals was the B3LYP hybrid functional, which has been successfully used in numerous systems,[33-34] but the development of new functionals with implicit description of dispersion interactions, such as M05-2x and M06-2x[35] make B3LYP somehow obsolete. These two functionals yield reliable vibrational modes and binding energies both in systems formed by hydrogen bonds and by dispersive forces.[36] During this work, MP2 (Møller-Plesset second order) perturbation theory was also employed, which usually gives good results, but at a higher computational cost. As MP2 takes into account dispersive forces, comparison with the results obtained with M06-2x allows calibrating the performance of the functional.

Finally, for the excited state Time-Dependent Density Functional Theory (TD-DFT) and Configuration Interaction with Simple and Double excitation (CIS/CID) were used and a comparison between them is offered. With these methods, transitions for the $\pi^* \leftarrow \pi$ first excited state and transition oscillator strengths are obtained.

3.3 – EXAMPLE PROCEDURE

Some of the techniques described can be difficult to follow, so for the sake of clarity, a *cooking receipt-like* description of the experimental work flow is given in this section.

The first step in a *de novo* study of a molecule by MRES (mass-resolved excitation spectroscopy), consists of establishing the warming conditions required to achieve enough vapor pressure to carry out the experiments, and then the expansion conditions to cool the molecules. In case of molecules with high boiling point, warming may result in thermal decomposition. Such is the case of many biological molecules, like amino acids. In that case, an ablation set up is needed to vaporize the sample.

As the TOF is calibrated for a given molecule, using the relation given by expression 3.1, the mass channel to monitorize the molecule of interest is obtained. Scanning the probe laser while the selected mass channel is minimized (different dyes may be needed in order to scan the whole region) the REMPI spectrum of the molecule is obtained, which gives information of the electronic excited state. A second color (if required) can be used tuning the first laser into one of the observed transitions (normally the 0-0 transition), reducing the power of this laser until only a little ionization due to the absorption of two photons is obtained and scanning the second laser (synchronized in space and time). When a reduction in the signal due to the second laser is observed, the ionization threshold is reached.

$$\frac{t_1^2}{t_2^2} = \frac{m_1}{m_2} \qquad \textbf{[3.1]}$$

If the second color is tuned the $I_0^+ \leftarrow S_1$ transition and the first laser is scanned monitoring the signal, a 2c-REMPI spectrum is obtained.

The next step is determining the number of isomers using a *hole burning* spectroscopy. Although the REMPI experiment gives the spectrum of the electronic excited state of the system of interest, different isomers may be present in the expansion. As explained in section 3.1.2.3, the *Hole Burning,* will unveil the number of conformers and the excited state's electronic spectrum of each conformer.

Assuming the following REMPI spectrum:

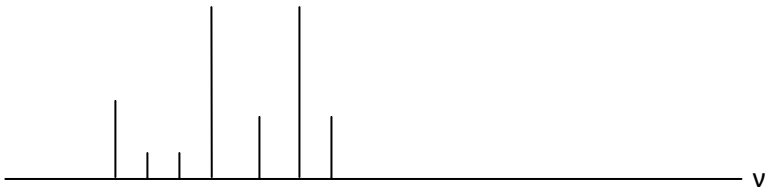

Tuning a first laser into one of the transitions and scanning a second laser while monitoring the signal, gives a depletion of those peaks due to the conformer probed by the first laser. For example:

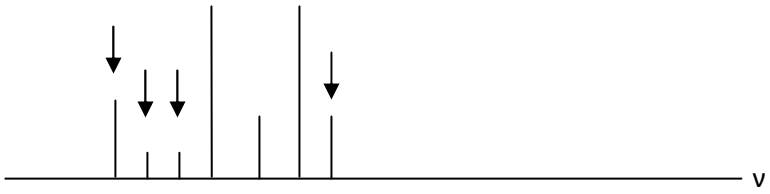

Those peaks noted with an arrow in the Figure are depleted, and therefore, they all belong to the same species, for example conformer A. As not all the peaks are depleted, there is, at least, another conformer. Thus, selecting the first non-depleted transition in the REMPI spectrum and scanning the second laser a result like the following may be obtained:

The reduction in the intensity of the two peaks point to the existence of at least a second conformer, that we will name conformer B. There are still some not depleted transitions in the two *hole burning* scans, so there is still, at least, an additional conformer. Tuning the first laser into the first non-depleted transition and scanning the probe laser:

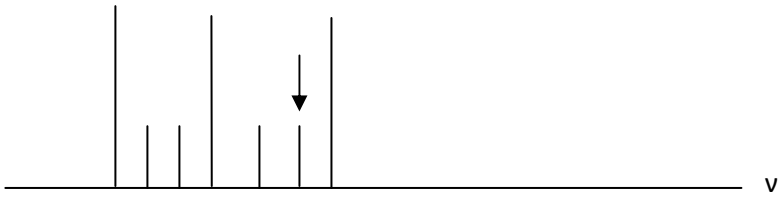

All the peaks that have less intensity compared to the REMPI spectra are due to conformer C. At this point, considering the three *hole burning* experiments, all the transitions in the REMPI spectrum were depleted, so in the supersonic beam 3 conformers are present: conformers A, B and C:

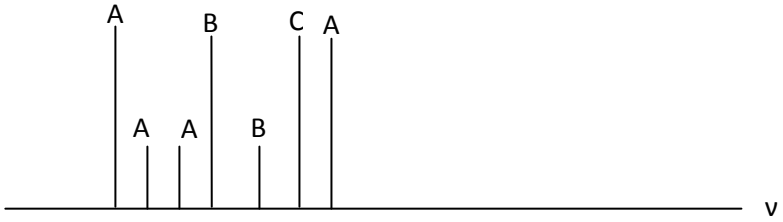

After solving the transitions of the excited state belonging to each conformer, an additional and important step is need: determination of the structure for each conformer. IDIRS is used in this work for that purpose. The experiment is similar to the *hole burning* but, in this case, an IR laser is used instead of a UV laser. As the transitions for each conformer were obtained by *hole burning*, in IDIR spectroscopy, a transition for one of the known conformer is probed and an IR laser is scanned in order to deplete the signal whenever a transition is reached. In this way, an IR spectrum is obtained for a given conformer. Repeating this step for each of the conformers detected in the previous *hole burning* experiment, the IR spectra for each conformer is obtained.

To assign the conformational structures, a comparison with the theoretical calculations is performed, as the OH, NH, etc. vibrational modes are very dependent on the environment. That is, they experiment a shift depending on the inter and/or intramolecular interactions in which they are involved. The comparison with the theoretical calculations may suffice to assign the experimental spectra, but sometimes the information yielded by the spectral shifts, ionization thresholds and any other physical observable that may be obtained in the laboratory are required for a complete characterization of the system.

3.4 – References

1. W. Demtröder, *Laser Spectroscopy*, Springer-Verlag Berlin Heidelberg New York, 2002.
2. W. Demtröder, *Molecular Physics*. Wiley-Vch Verlag GmbH & Co. kGaA, Weinheim Germany. 2005.
3. J. M. Hollas, *Modern Spectroscopy*. 2004.
4. R.J. Lipert, S.D. Colson, *J. Phys. Chem*., **93**, 3894 (1989).
5. R.J. Lipert, S.D. Colson, *Chem. Phys. Lett*., **161**, 303 (1989).
6. W. Scherzer, O. Trätzschmar, H.L. Selzle, E.W. Schlag, *Naturforsch.*, **47a**, 1248 (1992).
7. H.L. Selzle, E.W. Schlag, "Reaction dynamics in clusters and condensed phase" in Proceedings of the 26th Jerusalem Symposia on Quantum Chemistry and Biochemistry. (J. Jortner, R.D. Levine and B. Pullman ed.) Klumer academic publishers, Dordrecht/ Boston/London (1993).
8. M. Pohl, M. Schmitt, K. Kleinermanns, *Chem. Phys. Lett.,* **177**, 252 (1991).
9. M. Schmitt, H. Müller, K. Kleinermanns, *Chem. Phys. Lett*., **218**, 246 (1994).
10. M. Schmitt, U. Henrichs, H. Müller, K. Kleinermanns, *J. Chem. Phys*., **103**, 918 (1995).
11. H. Saigusa, E.C. Lim, *J. Phys. Chem*., **95**, 1194 (1991).
12. R. Takasu, N. Kizu, M. Itoh, *J. Chem. Phys*., **101**, 7364. 117 (1994).
13. M. Kurono, R. Takasu, M. Itoh, *J. Phys. Chem*., **99**, 9668 (1995).
14. Ricardo E. Campos Ramos, STRUCTURE AND EXCITED-STATE DYNAMICS OF AROMATIC NITRILES IN SUPERSONIC FREE JET, Thesis, 2005
15. S. Tanabe, T. Ebata, M. Fujii, and N. Mikami, *Chem. Phys. Lett*., **215**, 347 (1993).
16. M. Mons, E.G. Robertson, C.S. Lavina, J.P. Simons, *Chem. Phys. Lett*., **310**, 423 (1999).
17. D.M Lubman, M.N. Kronick, *Anal. Chem*., **54**, 660 (1982).
18. R. Trembreull, D.M. Lubman, *Anal. Chem*., **56**, 1984 (1984)
19. R. T. Kroemer, K. R. Liedl, J. A. Dickinson, E.G. Robertson, J.P. Simons, D. R. Borst, D. W. Pratt, *J. Anal. Chem. Soc*., **120**, 12573 (1998)
20. J. Yao, H.S. Im, E.R. Bernstein, *J. Phys. Chem. A.,* **104**, 6197 (2000)
21. M. Satta, A. Latini, S. Piccirillo, T. M. Di Palma, D. Scuderi, M. Speranza, and A. Giardini, *Chem. Phys. Lett*., **316**, 94 (2000).
22. S. R. Haines, C. E. H. Dessent, and K. Muller-Dethlefs, *J. Chem. Phys*., **111**, 1947 (1999).
23. http://www.rijnhuizen.nl/felix

24. V.A. Shubert, T.S. Zwier, *Journal Of Physical Chemistry A*, **111**, 13283-13286 (2007).

25. M. Mons, I. Dimicoli, & F. Piuzzi, *International Reviews in Physical Chemistry*, **21**, 101-135 (2002).

26. T. Bürgi, T. Droz, S. Leutwyler, *Chem Phys Lett.*, **225**, 351 (1994).

27. T. Bürgi, T. Droz, S. Leutwyler, Chem. Phys. Lett., **246**, 291 (1995).

28. Joseph R. Lakowicz, *Principles of Fluorescence Spectroscopy*, 97-155 (2006)

29. The SGIker UPV/EHU Facilities, supported by the European Social Funding and MCYT, are acknowledged for computational resources.

30. The i2Basque Facilities, supported by the Vasque Government and EJIE, are acknowledged for computational resources.

31. R.S. Paton, J.M. Goodman, *J. Chem. Inf. Model.*, **49**, 944 (2009).

32. I. Kolossváry, G. M. Keseru, *J. Comp. Chem.,* **22**, 21 (2001).

33. J.A. Fernandez, I. Unamuno, E. Alejandro, A. Longarte, F. Castaño, *Phys. Chem. Chem. Phys.,* **4**, 3297 (2004).

34. C.J. Gruenloh, J.R. Carney, F.C. Hagemeister, T.S. Zwier, J.T. Wood, K.D. Jordan, *J. Chem. Phys.,* **113**, 83 (2000).

35. Y. Zhao, G.D. Truhla, *Acc. Chem. Res.*, **41**, 157 (2008)

36. G.E. Hohenstein , T. S. Chill, C. D. Sherrill, *J. Chem. Theory Comput.*, **4**, 1996 (2008).

CHAPTER 4

BENZOCAINE

4 – BENZOCAINE

Introduction

As it has been previously stated, our group is involved in the study of aggregates of benzocaine (hereafter Bz) and other local anaesthetics to characterize their non-covalent interactions. Thus, we have already studied the microsolvation of benzocaine[1-2] and benzocaine·phenol[3] to shed light on benzocaine biological action. Such systems are formed by hydrogen bonds. Therefore, to extend the study to systems formed by dispersive forces, in this work, benzocaine·argon was studied,[4] as it resembles the kind of interactions between benzocaine and the CH_3 groups present in the isoleucine and leucine aminoacids. Additionally, an important effort was carried out to determine the system´s binding energy. The experimental results are then compared with *ab initio* calculations at MP2 level with 6-31+G(d), and 6-31++G(2d,p) basis sets in order to assign the possible structures.

4.1 – Spectroscopy of benzocaine

Figure 4.1 shows a comparison between the excitation spectrum of benzocaine recorded using *LIF* (upper trace) and *MRES* (lower trace). The origins of both *trans* and *gauche* benzocaine conformers at 34133.2 cm^{-1} and at 34143.1 cm^{-1} respectively, are clearly visible in both spectra, although the *2c-REMPI* trace shows considerably narrower transitions. The better resolution achieved with the *2c-REMPI* spectrum using the *MRES* experimental system recommends continuing the study of the spectroscopy of benzocaine with such technique, despite the additional complication associated.

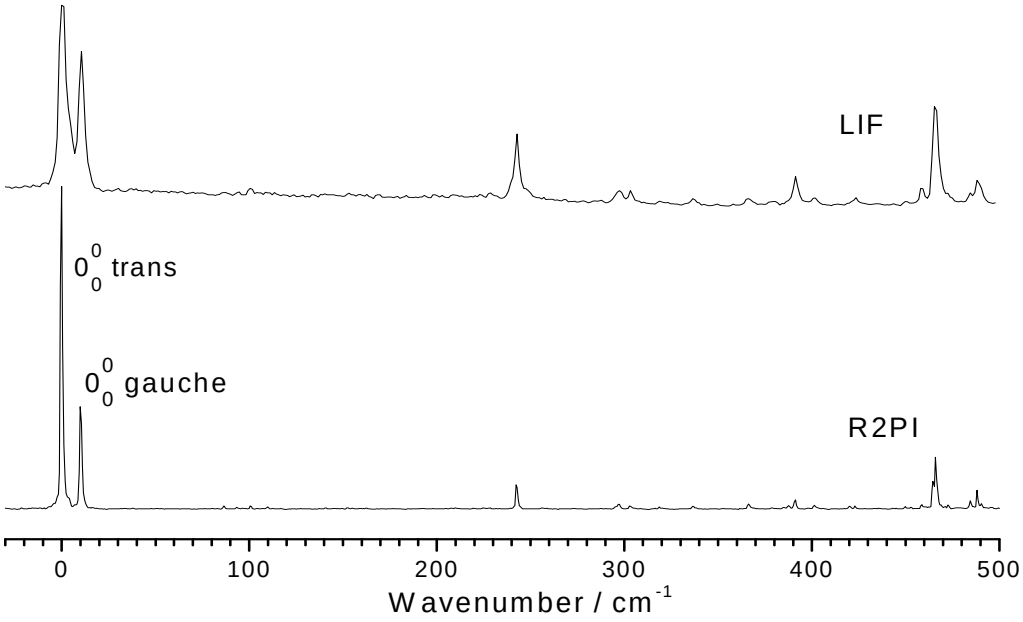

Figure 4.1. *Spectra of benzocaine recorded with a pressure of 1.5 bar He and heating the sample to 105ºC: LIF (upper trace) and 2c-REMPI (lower trace). The scale is in wavenumber relative to the 0-0 transition.*

Figure 4.2 shows the R2PI spectrum of benzocaine between 34000 and 35300 cm^{-1} recorded at a pressure of 1.5 bar in He and at a temperature of the sample of 110ºC. The assignment of the main spectral features is also shown.

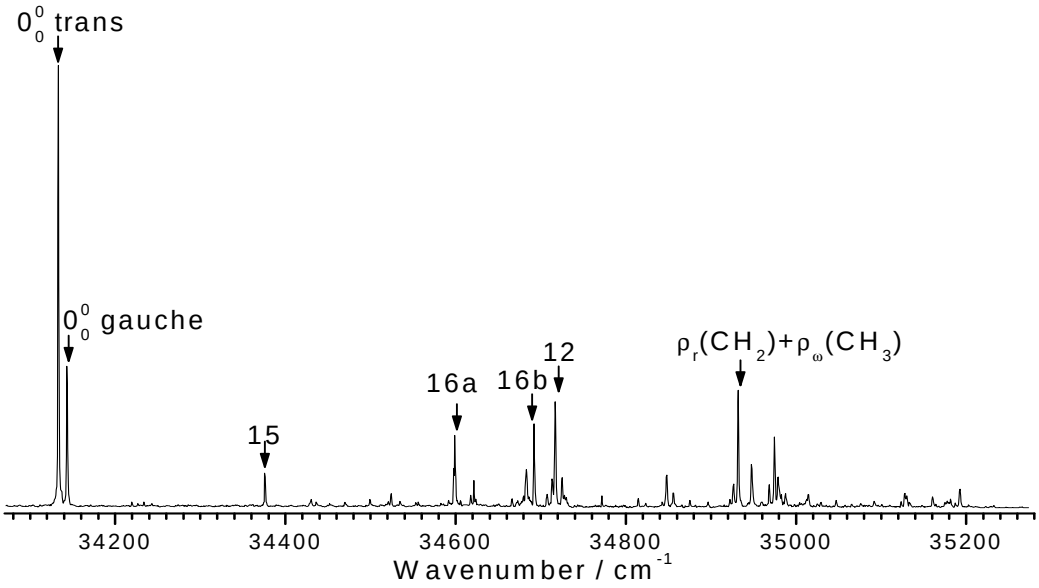

Figure 4.2. *R2PI spectrum of benzocaine in the 34100-35300 cm^{-1} region, recorded with a pressure of 1.5 bar He and heating the sample to 105ºC.*

This R2PI spectrum of benzocaine is in good agreement with previous publications[5-7] and shows transitions due to the two Bz isomers. The barrier between *gauche* and *trans* conformers is so small that the whole *gauche* population can be moved into the more stable *trans* conformer using the more energetic Ar collisions, as can be seen in Figure 4.3, where the spectrum of benzocaine in the 34100 – 34500 cm^{-1} region recorded using pure helium (upper trace) and 5% Ar/He (lower trace) is shown. In the latter, all the transition due to the *gauche* conformer have disappeared. This means that no conformers due to *gauche*-benzocaine·argon complexes will be found.

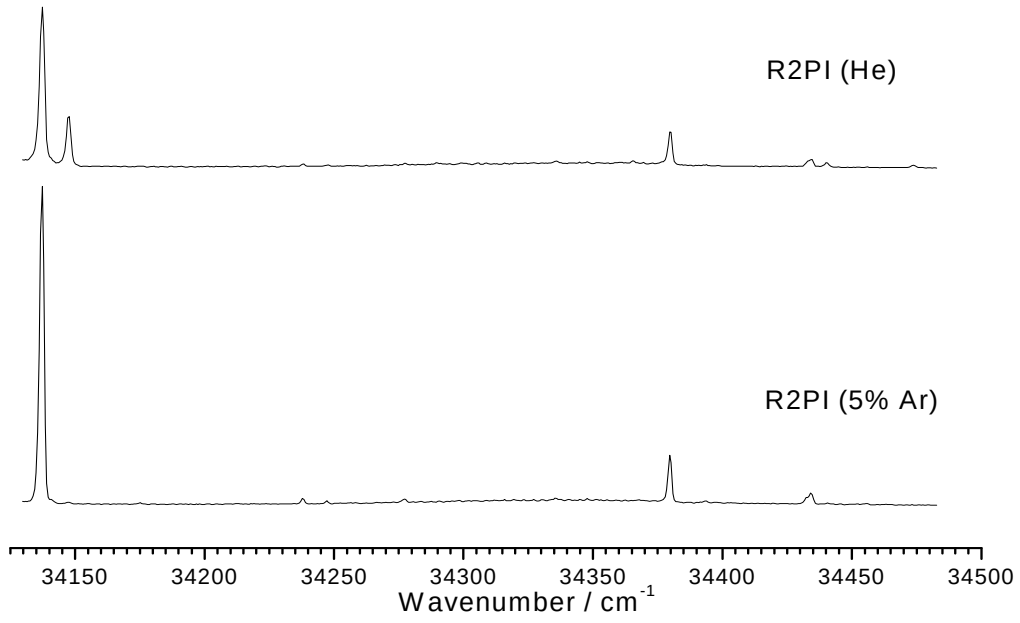

Figure 4.3. *R2PI spectra of benzocaine with He as buffer gas (upper trace) and using 5% Ar in He (lower trace). Depletion of the transitions due to the gauche isomer transitions is clearly observed.*

4.2 – Benzocaine·Ar

In this section mass-resolved spectroscopy techniques are employed to study the dispersive forces between Bz and Ar in order to understand the interaction between benzocaine and the amino acids isoleucine and leucine.

4.2.1 Theoretical calculations

Due to the flatness of the PES for the intermolecular interactions in benzocaine·argon, strict convergence criteria must be imposed during optimization. Besides, frequencies had to be calculated ahead the optimization step (*opt=CalcAll* in Gaussian). Furthermore, the benzocaine·argon complex is formed exclusively by dispersive forces and therefore DFT methods are not recommended,[8] forcing us to use the MP2 calculation level. Different basis set were used, but always including polarization and diffuse functions for a quantitave description of the non-covalent interactions. In total, three different basis: 6-31G(d), 6-31+G(d) and 6-31++G(2d,p) were used. Additionally, two final single point calculations were carried out on the structures obtained at the MP2/6-31++G(2d,p) level, using MP2/6-311++G(2d,p) and MP2/AUG-cc-pVTZ calculation levels. A single optimization at MP2/6-311++G(2d,p) was carried out, obtaining a structure and a Zero-Point Energy (ZPE) correction almost identicals to those obtained at MP2/6-31++G(2d,p) level, validating the calculation procedure.

4.2.2 Experimental results

Figure 4.4 shows the spectrum of Bz, recorded with a 5% Ar in He mixture, and the spectra of Bz·Ar_n n=1-4. The spectra of Bz·Ar and Bz·Ar_2 are in good agreement with those previously reported.[9-10] As described above, the collisions with argon have enough energy to transfer the *gauche*-conformer population to the *trans*-conformer and, in consequence, all the features observed in Figure 4.4 are assigned to the *trans*-benzocaine conformer. In addition, the first ca. 400 cm^{-1} of the Bz·Ar spectrum matches that of *trans*-benzocaine except for a progression on the low frequency intermolecular mode of ca. 11 cm^{-1} developed on the origin band. Also, the chromophore intramolecular vibrations are weaker compared to its 0_0^0 transition than those on the bare benzocaine spectrum, and finally disappear at ~500 cm^{-1}. The highest energy feature of the Bz·Ar appears at 34803 cm^{-1}, i. e., blue-shifted 678 cm^{-1} with respect to

the 0_0^0 band. The rest of the peaks to the blue are associated with fragmentation from the Bz·Ar_2 complex. The 12 cm^{-1} shift between Bz·Ar and Bz 0_0^0 bands suggests a small difference between ground and excited states dissociation energy values.

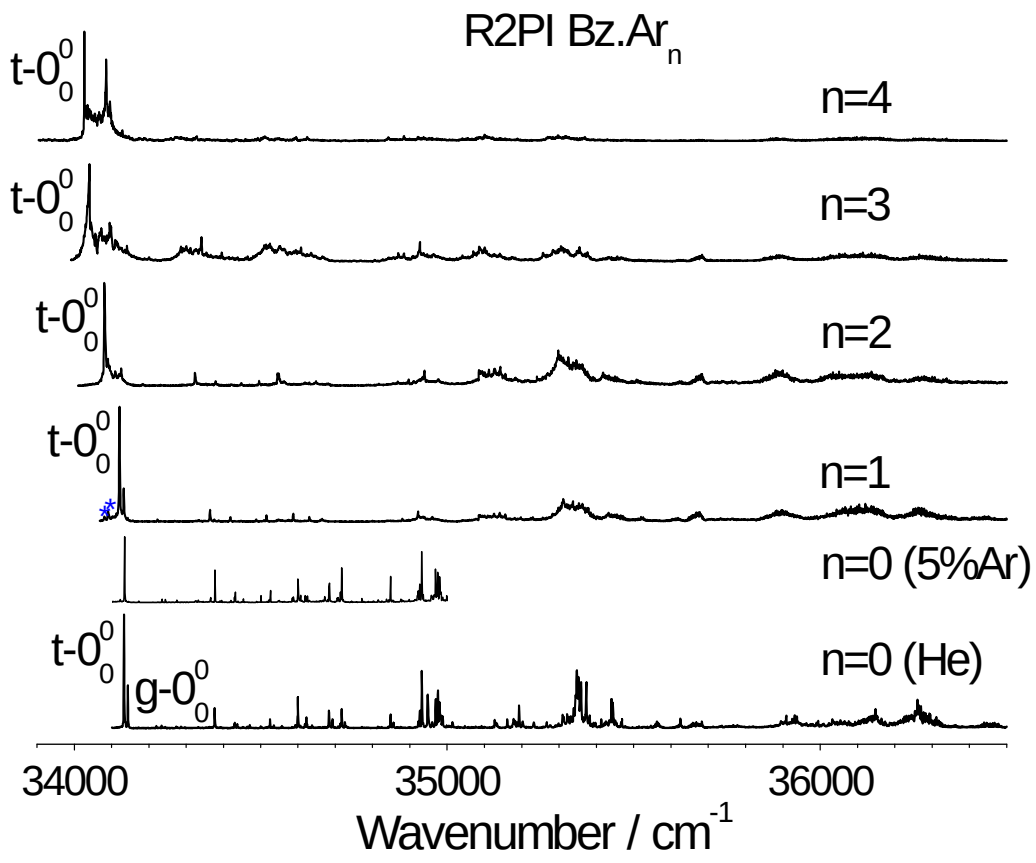

Figure 4.4. *R2PI spectra of Bz·Ar_n n=0-4. For n=0 the R2PI spectrum of Bz with He (lower trace) and with 5% Ar in He (upper trace) are shown. The asterisks indicate the transitions due to fragmentation of higher order clusters.*

The Bz·Ar_2 spectrum has a substantial vibrational activity near the origin band, which we momentarily assign to the red-most peak, at 34081 cm^{-1}. A number of features partly due to intermolecular vibrations add up to form a broad absorption of ~ 60 cm^{-1}, with 5 significant peaks. As in the lowest ~+700 cm^{-1} region of the Bz·Ar, the intensity of the vibrational bands compared to that of the 0_0^0 band is smaller than for Bz. The spectrum extends up to ~2200 cm^{-1}, but it is not possible to discriminate the Bz·Ar_2 bands from those of Bz·Ar_3 fragments and therefore it is not possible to determine the real extension of the 1:2 spectrum.

The spectra of $Bz{\cdot}Ar_3$ and $Bz{\cdot}Ar_4$ complexes have similar overall appearance: a quasi-continuum with no discrete features. $Bz{\cdot}Ar_3$ 0_0^0 band is shifted ca. 40 cm^{-1} with respect to that of $Bz{\cdot}Ar_2$ and the spectrum of the $Bz{\cdot}Ar_4$ has at least two peaks that may be identified as origin bands. Based on the relative shifts of the complexes studied, one would assign the stronger red-shifted peak to the $Bz{\cdot}Ar_4$ 0_0^0 band, i.e. shifted ca. 14 cm^{-1} from the $Bz{\cdot}Ar_3$ 0_0^0 transition, being the partner peak due to fragmentation (marked with asterisks) from higher complexes or to an hypothetic second conformer.

Table 4.1 collects the position of the origin bands of the spectra depicted in Figure 4.4. The shift of the $Bz{\cdot}Ar_2$ 0_0^0 transition relative to that of $Bz{\cdot}Ar$ is - 41 cm^{-1}, which is 3 times larger than the Bz→Bz·Ar shift, indicating that the second argon is not placed symmetrically respect to the first one.

Table 4.1. *Ionization and fragmentation energy values and origin band shifts relative to the bare benzocaine* 0_0^0 *transition. All values are in* cm^{-1}.

	$S_1 \leftarrow S_0$	shift	$D_0^+ \leftarrow S_1$	Fragment$\leftarrow S_1$
t-Bz	34134	0	28981	
g-Bz	34145	11	28991	
$BzAr_1$	34122	-12	28917	29416
$BzAr_2$	34081	-53	28859	29442 (2→1)
				30016 (2→0)
$BzAr_3$	34041	-93		
$BzAr_4$	34027	-107		

Interestingly, the fragmentation of the complexes does not vanish in two-colour laser experiments. Figure 4.5 depicts the ionization and fragmentation onsets of *trans*- and *gauche*-benzocaine, $Bz{\cdot}Ar_1$ and for the more abundant $Bz{\cdot}Ar_2$ conformer, while binding energies estimated for the complexes using the fragmentation threshold method

are collected in Table 4.2. The $D_0^+ \leftarrow S_1$ shift between the benzocaine conformers is 10 cm^{-1}, in good agreement with the energies reported elsewhere.[9] These ionization onsets are affected by the extraction field of the ionization region of the spectrometer, shifting the energy some ~100-200 cm^{-1} and thus they must be taken as lower limits.[11]

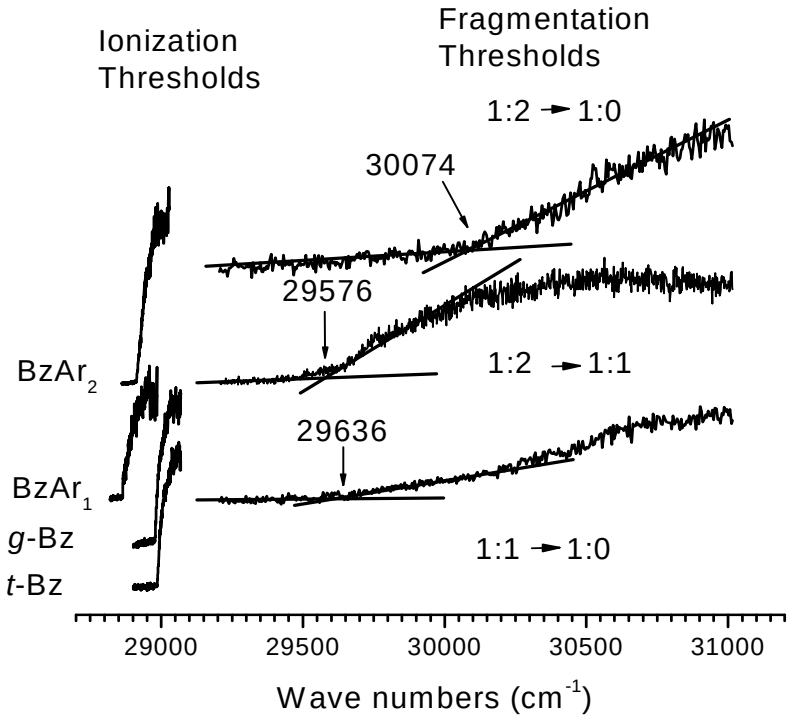

Figure 4.5. *Ionization and fragmentation thresholds of trans-benzocaine, gauche-benzocaine, and Bz·Ar and Bz·Ar₂ complexes.*

Table 4.2. *Binding energies of the Bz.Ar and Bz.Ar₂ complexes derived by different methods. Energies are in cm⁻¹.*

	Binding energy determination method							
	Fragmentation threshold			Calculation (S_0) MP2		S_1 dissociation		SEP (S_0)
	S_0	S_1	D_0^+	6-31+G(d)	6-31++G(2D,P)	S_0	S_1	
$Bz{\cdot}Ar_1$	423	435	499	776 (trans)	664 (trans)	666	678	590
				1016 (gauche)	742 (gauche)			
$Bz{\cdot}Ar_2$	484	525	583	1606 (SS)		733	774	600
	982	1035	1157	1762 (OS)				

Next step is to determine the number of isomers for each stoichiometry so *hole burning* experiments were carried out. Figures 4.6 and 4.7 show the *hole burning*

spectra of both 1:1 and 1:2 species together with the *2-color R2PI* spectra of the complexes for comparison. All major features in the *R2PI* spectrum of the 1:1 complex are mirrored in the *hole burning* trace, confirming the existence of a single isomer. The peaks to the red of the Bz·Ar 0_0^0 band, assigned to Bz·Ar_2 fragments are missing in the *hole burning* trace as expected. On the other hand, the *hole burning* traces on the 1:2 complex clearly demonstrate the existence of at least two conformers, with origin bands shifted 41 and 12 cm^{-1} from the 1:1 0_0^0 transition.

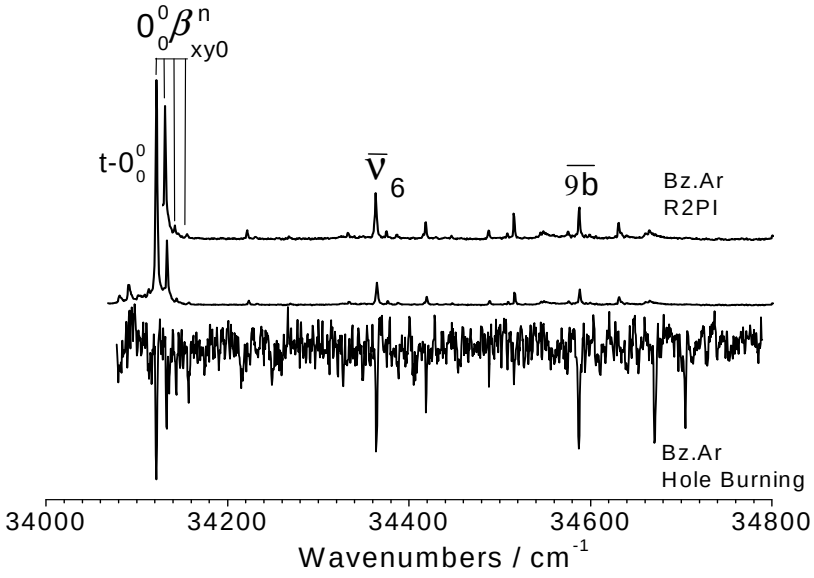

Figure 4.6. *UV-UV hole burning spectrum of Bz·Ar. The R2PI spectrum is also shown for comparison. Only one isomer is found.*

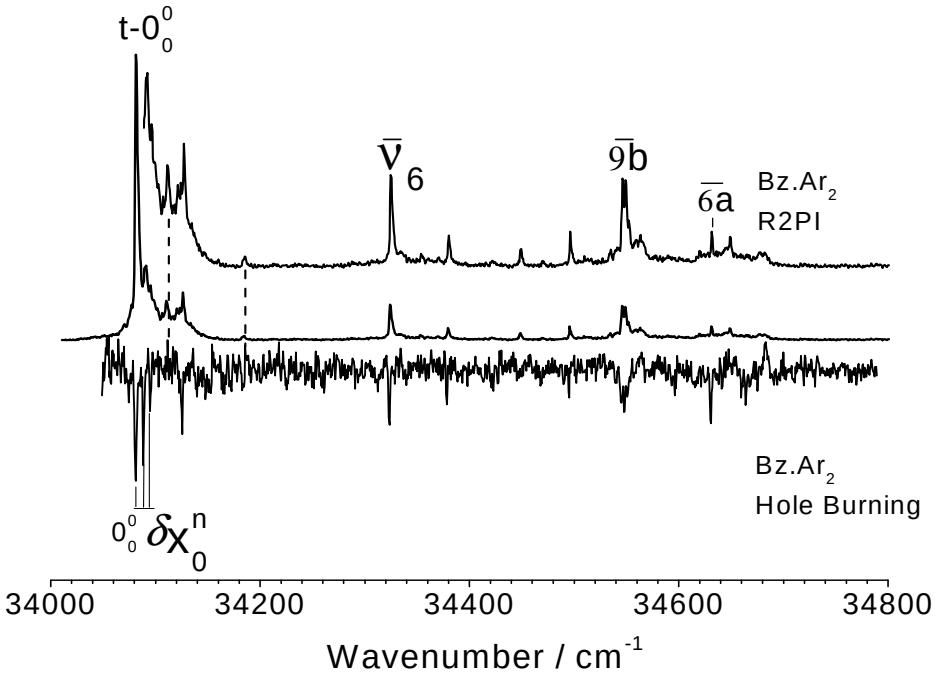

Figure 4.7. *UV-UV hole burning and R2PI spectra of Bz·Ar$_2$ complex. The R2PI spectrum is shown for comparison.*

4.2.3 Discussion and conclusions

The geometry of the Bz·Ar proposed by Simons et al.[12] is based on the *trans*-benzocaine conformer with the argon atom sitting over the aromatic ring. Conversely, calculations at MP2/6-31++G(2d,p) show that the interaction energy in both *trans*- and *gauche*- isomers is very close and therefore one would expect to have both in the supersonic expansion. However, the collisions with argon provide enough energy to initiate the isomerization process, pumping the population to the more stable *trans*-conformer.[10] Consequently, although calculations suggest the existence of both conformers, the complexes derived from the *gauche*-benzocaine conformer are not observed. Figure 4.8 shows *gauche*-benzocaine and *trans*-benzocaine isomers estructure.

Figure 4.8. *Estructures of trans-benzocaine (left) and gauche-benzocaine (right) isomers. The complexes of gauche-benzocaine are not observed due to an isomerization process.*

There are two possibilities for the Bz·Ar_2 structure: both Ar atoms on the same side of the aromatic ring, or on opposite sides (Figure 4.9). According to the calculations, in the latter isomer the second Ar atom does not enter in a symmetric place with respect to the first one and finally lies slightly shifted towards the COOEt substituent. As Bz·Ar_2 0_0^0 band is shifted 41 cm^{-1} with respect to that of Bz·Ar, that in turn is ~3 times larger than the Bz·Ar/Bz pair 0_0^0 bands shift, it suggests a non-symmetric Bz·Ar_2 structure with the Ar atoms on the same side. Here, the second Ar atom ought to enter in a less favorable site, close to the amino moiety, but the extra Ar·Ar interaction compensates the weaker Bz·Ar interaction of the second atom.

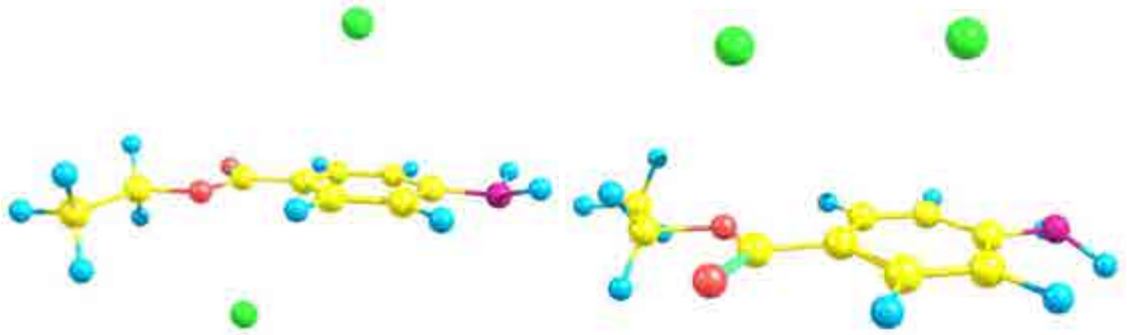

Figure 4.9. *Structures of trans-Bz·Ar$_2$ with both Ar atoms in opposite sides (left) and in the same side (right) isomers. The later is the most probable structure.*

Calculations at MP2/6-31+G(d) level show two Bz·Ar$_2$ isomers of close stability, as the calculated binding energy is 1606 cm^{-1} for the Ar atoms on the same side and 1762 cm^{-1} for both atoms in opposite sides. However, the energy difference is within the computational error. In summary, although the most likely Bz·Ar$_2$ isomer has the Ar atoms on the same side of the aromatic ring of benzocaine, one cannot rule out the structure with atoms on opposite sides, based only on energetic considerations.

The binding energies of the complexes were determined experimentally by four methods: fragmentation threshold, dissociation in the S_1 state, stimulated emission pumping and *ab initio* calculations. The fragmentation threshold provides the lowest binding energies ($D_0(S_0) \approx 420$ cm^{-1} for Bz·Ar and ≈ 980 cm^{-1} for Bz·Ar$_2$). For a safe application of the method, the Frank-Condon window must permit the ν=0 level of the ion to be reached, a constraint frequently fulfilled by the bare molecule, but not always by van der Waals complexes, which seem to be the case in Bz·Ar.

The dissociation energies derived from SEP and R2PI spectra are very similar. The last peak observed in the Bz·Ar S_1 spectra is at ~ 678 cm^{-1}, resulting in a S_0 binding energy of 666 cm^{-1}, S_1 - 0_0^0 shift, not far from the ~600 cm^{-1} derived from the broad emission of the SEP spectrum (see next section, Figure 4.12). Both values are also close to the 664 cm^{-1} value computed at MP2/6-31++g(2d,p) level for the *trans*-Bz·Ar isomer and thus, it may be stated that the ground state binding energy of the Bz·Ar is ~ 660 cm^{-1}. The agreement between binding energies also implies a good coupling between intra- and inter-molecular vibrations.

The dissociation energies of the Bz·Ar_2 complex derived from R2PI and SEP spectra are not as close as those for the Bz·Ar; whilst it increases ~30 cm^{-1} up to 692 cm^{-1} in the R2PI spectrum, it stays unaffected (600 cm^{-1}) in the SEP (see next section). Even if Bz·Ar_2 has a symmetric structure with Ar atoms on both sides of Bz, one would expect a larger interaction energy (consequence of the three-body interactions), although one should keep in mind that the Bz·Ar dissociation energy was estimated from the last peak observed in the spectrum, while that for Bz·Ar_2 was taken from the first peak of Bz·Ar_2 that appears in the Bz·Ar spectrum. In fact, the ~700 cm^{-1} region of the Bz·Ar_2 R2PI spectrum is piled up with many contributions, including fragments from Bz·Ar_3 and hence, assignments are rather uncertain compared with those of Bz·Ar.

It is also feasible to derive the Bz·Ar_2 dissociation energy from the dissociation threshold, estimating the energy required to evaporate 1 or 2 Ar atoms separately. Once again, the method provides the lowest energies but higher than those estimated for Bz·Ar. Likely the bottom of the PES well of the ion is not accessible from S_1, leading to a energy estimate too low by ~100-200 cm^{-1}.

4.3 – Stimulated emission

Figure 4.10 shows the SEP trace of *trans*-benzocaine relative to the 0_0^0 transition, for a gas pressure of 1.5 bar and a sample temperature of 110 ºC.

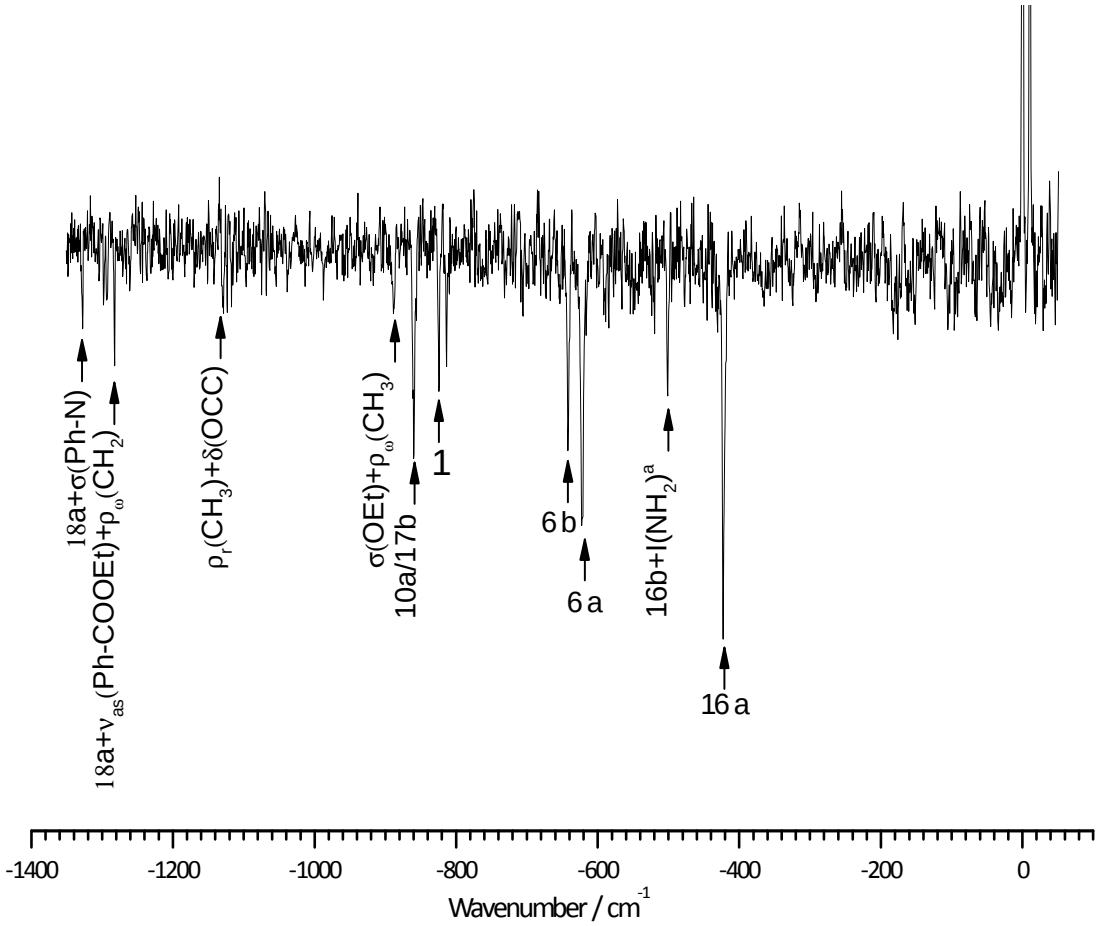

Figure 4.10. *SEP spectra of trans-benzocaine relative to the* 0_0^0 *transition.*

A shift on the vibration wavelengths between ground and excited states is observed (Table 4.3). In addition, a few bands vary their relative intensities. The 0_0^0 band appears as a positive peak because when the depletion laser is resonant with the 0_0^0 transition, the signal increases. However, the SEP transitions appear as negative peaks. The R2PI spectrum presented was pumped just over laser saturation on purpose, in order to highlight the weak bands and to make easier the comparison with the SEP features. The SEP and the dispersion emission spectra of the bare Bz[16] are in good

agreement. Note the lack of bands in the SEP spectrum below ~400 cm^{-1} and the appearance of the first strong band at 423 cm^{-1}.

Bz·Ar and Bz·Ar_2 SEP spectra were also recorded (Figures. 4.11 and 4.12).

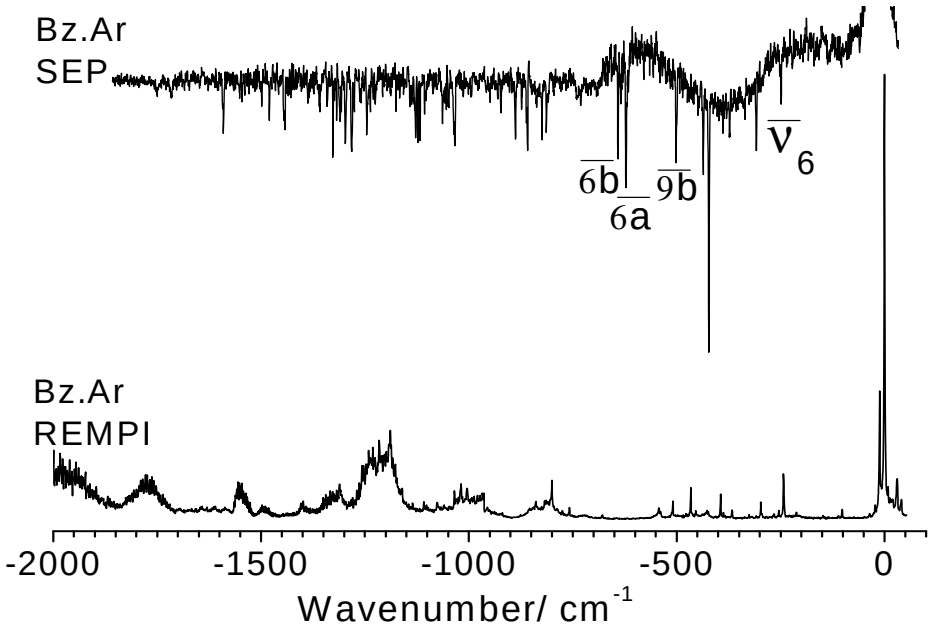

Figure 4.11. *Comparison of the stimulated emission pumping (SEP) and the R2PI spectra of the Bz·Ar complex.*

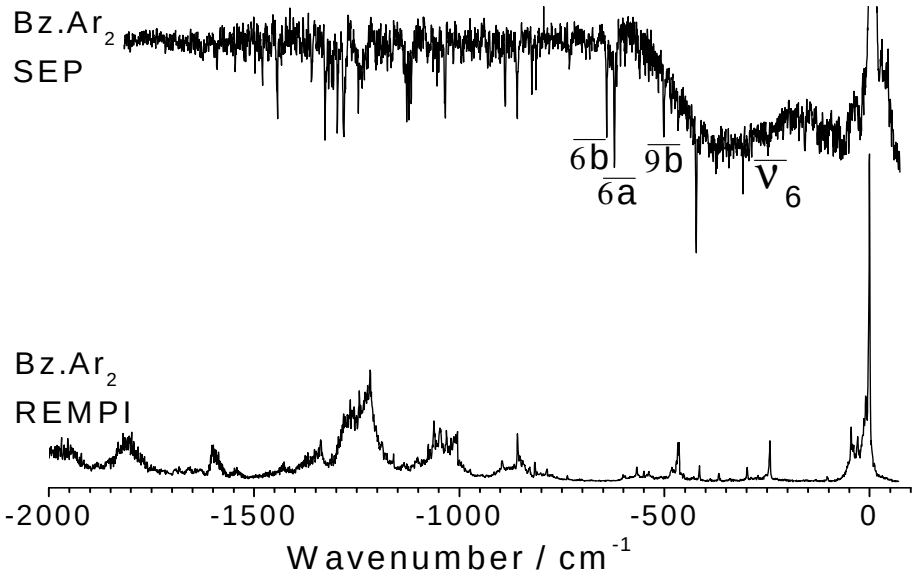

Figure 4.12. *Comparison of the stimulated emission pumping and the R2PI spectra of the Bz·Ar_2 complex.*

As can be seen in Figure 4.11, the SEP spectrum has two regions; at low energies a broad emission of ~590 cm^{-1} comes into sight, on top of which a number of vibronic transitions can be clearly seen. At higher wavenumbers, there is a rise on the baseline until it levels off around 720 cm^{-1}. Well-resolved transitions are observed up to ~2000 cm^{-1} where the band intensities fade out. Note as well the absence of well-resolved intermolecular transitions in the SEP spectrum and that a few of the intramolecular transitions observed bellow 400 cm^{-1} are not seen in bare Bz (Figure 4.2). Both Bz and Bz·Ar SEP spectra above 500 cm^{-1} match reassonably well, except for a decrease in the intensity of the Bz·Ar bands around c.a. 1700 cm^{-1} that finally disappear below 2000 cm^{-1}.

Figure 4.12 shows that the SEP spectrum of Bz·Ar_2 shares some similities with that of Bz·Ar: in the first ~ 590 cm^{-1} both have a broad emission, whose origin is not clear. From the broad emission a few peaks emerge at wavelengths close to those of the Bz·Ar complex. Over 590 cm^{-1} the background disappears and with small changes, the same vibronic lines as for the Bz·Ar are observed, assigned to the chromophore intramolecular modes. The peak intensities weaken above ~1400 cm^{-1} and disappear near ~1600 cm^{-1}.

The broad emissions only present in the argon clusters may be related with the complex dissociation limit. Such hypothesis is reinforced by the absence of intermolecular modes above 422 cm^{-1}. To test such hypothesis the benzocaine·phenol (hereafter Bz·PhOH) SEP spectra have been also recorded (Figure 4.13) for the two detected conformers.[3] No broad emission is observed in any of the two traces which may reinforce the hypotheses. Besides, the spectra extend up to c.a. 2000 cm^{-1}.

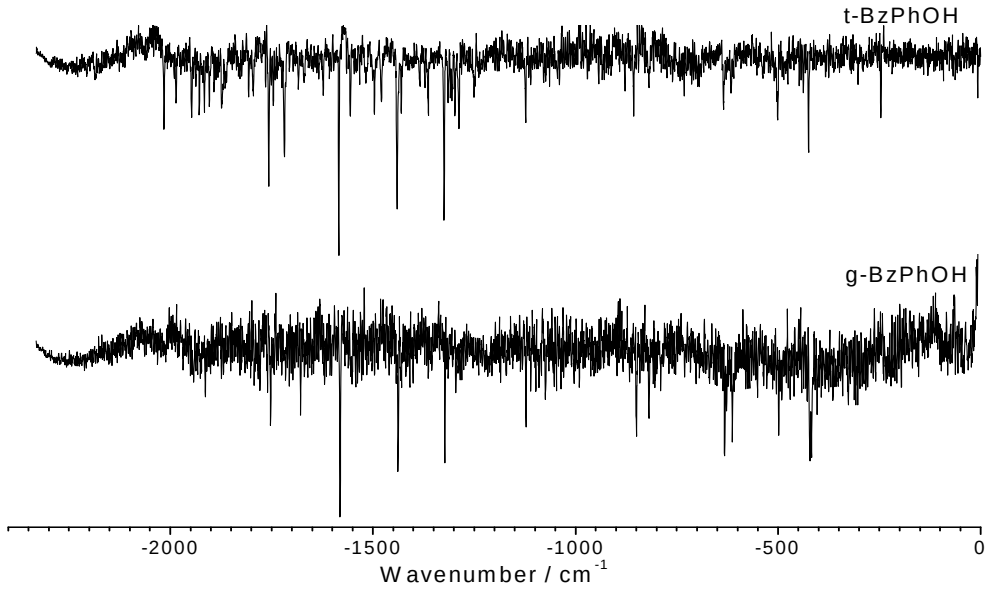

Figure 4.13. *SEP spectra of trans-Bz·PhOH (upper trace) and gauche-Bz·PhOH (lower trace).*

Dissociation energies

Table 4.3 collects the transitions found for S_0 (SEP) and S_1 (*2c-REMPI*) for Bz, Bz·Ar, Bz·Ar_2 and Bz·PhOH. Regarding Bz·Ar, as mentioned above, the dissociation energies derived from SEP and R2PI spectra are close. As the last peak observed in the Bz·Ar S_1 spectrum is at ~ 678 cm^{-1} and in the S_0 spectrum a broad emission can be seen at ~600 cm^{-1}, the dissociation energy may be close to that value, i.e, ~650 cm^{-1}. Theoretical calculations support this value as the energies predicted at MP2/6-31++g(2d,p) level for the *trans*-Bz·Ar isomer are close to the 664 cm^{-1} value. For Bz·Ar_2, unequivocal determination of the dissociation energy can not be done, as discriminating the fragmentation due to higher order clusters was not possible. The SEP experiment for this cluster seems to indicate a dissociation energy close to ~600 cm^{-1} where a broad emission can be seen as happened with the Bz·Ar cluster.

Taking a closer look at the Bz·phenol SEP spectra, it extends for 2000 cm^{-1} where a broad absorption seems to take place, and thus the dissociation energy may be close to this value: 2000 cm^{-1}. This way, if the interaction does not change that much upon electronic excitation, one should expect, at least, a region of 2000 cm^{-1} for the *2c-REMPI* spectrum. Such observation supports the hypothesis of a proton transfer or

chemical reaction in the excited state as the S_1 MRES is considerably shorter. On the other hand, as it was also stated, theoretical calculations predicted a binding energy of ~2000 cm^{-1}, which is also the experimental value obtained from the ionization and fragmentation thresholds, considering the 2000 cm^{-1} difference due to the correlation between the neutral ground state and a transition state in the ion, which is ~2000 cm^{-1} above the minimum of the potential energy curve.

t-Bz		Bz·Ar		Bz·Ar_2		*t*-Bz·PhOH		*g*-Bz·PhOH	
S_0	S_1	S_0	S1	S_0	S_1	S_0	S_1	S_0	S_1
0	0	0	0	0	0	0	0	0	0
423.0	37.9	248.5	22.1	19.3	11.2	246.3	115.1	303.6	5.2
501.2	86.4	308.7	35.5	70.1	29.1	375.5	238.7	326.4	111.0
622.4	100.5	373.2	101.6	101.9	44.8	424.4	297.3	421.0	165.7
642.0	140.4	422.7	147.4	157.8	242.8	500.9	324.0	498.6	215.1
705.9	198.6	501.4	212.1	247.4	298.2	616.4	370.9	613.0	
813.4	242.3	622.0	242.8	308.5	367.5	634.9	426.3	631.6	
824.5	295.0	641.0	254.6	375.4	414.5	819.6	452.0	819.6	
859.9	297.3	730.5	265.2	422.8	464.5	856.1	459.2	990.1	
887.6	366.2	813.4	366.2	501.9	567.5	877.7	468.8	1074.4	
1128.5	387.7	823.9	297.8	622.2	786.2	1123.0	547.4	1122.4	
1282.5	391.2	858.8	326.2	640.6	815.7	1250.5	581.7	1184.9	
1327.8	458.8	888.1	366.6	731.0	858.1	1287.7	726.3	1216.4	
	465.9	922.9	386.9	810.3	894.8	1297.4	796.9	1295.3	
	473.1	1033.3	394.0	823.6	1004.6	1305.0		1322.7	
	485.1	1064.3	426.8	858.4	1030.5	1314.7		1438.0	
	488.1	1122.9	453.8	888.2	1047.1	1324.9		1581.1	
	558.9	1175.6	466.3	1034.1	1062.0	1363.0		1678.3	
	573.5	1245.5	509.4	1053.8	1107.7	1384.5		1752.8	
	583.6	1282.2	543.0	1127.8	1217.0	1430.5		1759.7	
	681.5	1296.7	678.2	1175.0	1242.6	1440.1		1913.5	
	714.9	1318.3	758.3	1203.1	1265.7	1478.6		1942.0	
	742.2	1326.9	800.3	1246.3	1280.7	1496.1			
	798.9	1358.6	817.4	1280.8	1337.7	1555.1			
	814.1	1387.6	838.8	1297.1	1369.1	1583.75			
	841.6	1442.7	967.6	1327.0	1426.4	1622.4			
	845.4	1476.0	987.3	1443.0	1542.2	1718.7			
	854.5	1498.1	1004.0	1479.7	1599.4	1745.0			
	880.8	1546.0	1018.8	1498.3	1655.5	1757.0			
	913.4	1590.5	1031.9	1546.1	1798.5	1796.3			
	931.1	1715.4	1059.6	1589.9	1819.1	1806.2			
	941.1	1750.1	1076.3	1629.5	1953.6	1828.66			
	958.2		1108.6		1969.2	1864.1			
	994.6		1135.3			1874.0			
	1027.3		1189.4			1892.2			
	1048.3		1190.8			1903.6			
	1059.5		1215.6			1916.1			
			1231.3			1947.1			
			1256.9			1985.4			
			1311.4			2015.9			
			1334.1			2184.6			
			1398.3			2205.0			
			1481.8						
			1497.6						
			1552.1						
			1641.6						
			1736.5						
			1762.3						
			1777.7						
			1922.7						
			1983.2						
			2015.8						
			2032.8						

Table 4.3. *Transitions found for S_0 (SEP) and S_1 (2c-REMPI) for benzocaine, Bz·Ar, Bz·Ar_2 and Bz·PhOH.*

4.4 – REFERENCES

1 . J. A. Fernandez, A. Longarte, I. Unamuno, F. Castano, "A theoretical and experimental study of the ethyl-p-aminobenzoate (H2O)(n) (n=1-4) complexes." *J. Chem. Phys*., **113**, 8531-8540 (2000).

2. A. Longarte, J. A. Fernandez, I. Unamuno, F. Castano, "Structure and ground and first electronic excited state vibrational modes of the ethyl-p-aminobenzoate conformers." *Chem. Phys*., **260**, 83-93 (2000).

3. E. Aguado, I. León, E. J. Cocinero, A. Lesarri, J. A. Fernández and F. Castaño. *Phys. Chem. Chem. Phys*., **11**, 11608-11616 (2009).

4. I. Leon, E. Aguado, A. Lesarri, J. A. Fernandez, F. Castano, "Combined Experimental and Theoretical Study of the Benzocaine/Ar van der Waals System in Supersonic Expansions." *Journal of Physical Chemistry A*, **113**, 982-988 (2009).

5. Asier Longarte, PhD Thesis, U.P.V. Leioa 1999.

6. B.D. Howells, J. McCombie, T.F. Palmer, J.P. Simons, A. Walters. *J.Chem.Soc., Faraday transactions*, **88**, 2595 (1992).

7. R. Pereira, T. Calvo, F. Castaño, M.T. Martinez. *Chem. Phys*., **201**, 433 (1995).

8. J. Cerny and P. Hobza, *Phys. Chem. Chem. Phys.*, **9**, 5291 (2007).

9. Idem. Ibid. **88**, 2603 (1992).

10. J. A. Fernandez, A. Longarte, I. Unamuno, and F. Castano, *J. Chem. Phys*., **113**, 8531 (2000).

11. A. Longarte, J. A. Fernandez, I. Unamuno, and F. Castano, *Chem. Phys*., **260**, 83 (2000).

12. E. Aguado, A. Longarte, E. Alejandro, J. A. Fernandez, and F. Castano, *J. Phys. Chem. A*, **110**, 6010 (2006).

13. J. Fabian and R. Zahradnik, *Angewandte Chemie-Int. Ed*., **28**, 677–694 (1989).

CHAPTER 5

PROPOFOL

5 – PROPOFOL

Introduction

The knowledge acquired in the study of Bz·Ar is employed in the study of another anaesthetic: propofol. In this chapter we deal with the electronic spectroscopy of propofol and its clusters with water. More precisely, propofol with up to nine water molecules was completely characterized. The spectroscopy of the homodimers was also solved up to propofol hexamer. Thanks to a careful tuning of the experimental conditions, propofol dimer and its clusters with up to seven water molecules was also studied. Finally, the trimer·water and the tetramer·water clusters were fully characterized. Once the study of propofol and its solvation by water was tackled, propofol·phenol and propofol·isopropanol, as model systems for propofol·tyrosine and propofol·treonine interactions in the $GABA_A$ receptor, were spectroscopically solved.

Thus, this chapter includes the following sections:

-Propofol monomer: section 5.1.

-Propofol and its water clusters: propofol·W_{1-9}: section 5.2.

-Propofol dimer: section 5.3.

-$Propofol_2$ and its water clusters: $propofol_2$·W_{1-7}: section 5.4.

-Propofol homomers: $propofol_{1-6}$: section 5.5.

-Propofol homomers and their water clusters: $propofol_3$·W_1 and $propofol_4$·W_1: section 5.6.

-Interaction of propofol with tyrosine and treonine residues: propofol·phenol and propofol·isopropanol: section 5.7.

The following conventions are adopted along the work:

1 – The large number of structures generated in the exploration of the conformational landscape using Molecular mechanics are named as follows:

- *structure en*: where *n* refers to the relative order in energy, being n=1 the most stable structure.
- If the structure is grouped in a family the nomenclature *structure n* is used instead. In this case, *n* refers to the structure's energetic position within the family.

Thus, apart from being a systematic labeling criterion when referring to the large amount of the calculated structures, it also let us to quickly trace back the species' stability once the *ab initio* calculations are done, which is invaluable to test the molecular mechanics precision.

2 – For most of the systems studied, a large number of stable structures were found, and therefore, it is not possible to present all of them with the text. Therefore, only the eight most stable structures are presented during the analysis of each cluster, while the rest of structures are collected in appendix 7.1. Similarly, only the predicted IR spectra for the most stable conformers are presented during the IDIRS analysis, but all of them are compiled in appendix 7.1. Additionally, a table with the energetic of the calculated is also included.

3 - All the energy values presented in this work are ZPE corrected and the binding energy values include also the Boys and Bernardi[2-3] correction to the basis set superposition error (BSSE).

4 – When more than one conformer is presented, they are named from the red to the blue. That is, *first conformer* refers to the isomer with the red-most electronic transition; *second conformer* refers to the second red-most one, and so on.

5 – When talking about the strength of a hydrogen bond, depending on the field, a controversy may exist. As in this work, we will only refer to hydrogen bonds in gas phase, phenol·water interaction will be considered a strong hydrogen bond.

6 – When talking about the OH stretching vibrations, the following naming criteria has been choosen: σ_t^i (OH_m), where *i* refers to the interaction type (*f* for free, *s* for single, *d* for double, *f-s* for a weak hydrogen bond midaway between single and free stretching, and *O-H*$\cdots\pi$ for that type of interaction), *t* refers to the type within the interaction (*s* for symmetric, *as* for anti-symmetric) and *m* to the molecule responsible for that kind of interaction (*w* for water, *ppf* for propofol).

7 – All the lifetimes determined are collected in appendix 7.2.

8 – Unless said otherwise, all the spectra obtained during this work with propofol and its clusters are recorded with a pressure of 1.5 - 3.0 bar He (depending on the amount of water in the sample) and heating the sample to 60ºC.

5.1 – Spectroscopy of propofol

The relative orientation of the two isopropyl groups and the OH moiety raises nine possible conformations (Figure 5.1), which are reduced to five, due to symmetry (the OH is in the plane of the ring). So the structures Gg and gG, EG and Eg, GE and gE are equivalents. *Ab initio* calculations conducted at MP2/6-311++G(d,p) show that the interaction between the OH group and the CH_3 moieties of the isopropyl groups destabilizes the molecule. Consequently, the most stable conformers are those with the two isopropyl hydrogens on the OH side of the molecule (pointing *forward*). Thus, conformers GG and Gg are almost isoenergetical, as they both have the two hydrogens pointing *forward* (Figure 5.1), differing only in the orientation of the CH_3 moieties. Rotating one of the isopropyl groups until the hydrogen atom points *backwards* decreases the molecular stability in ~ 1.1 kJ/mol if the CH_3 groups interact with the OH lone pairs (EG) or in ~ 4.9 kJ/mol if the interaction is with the OH hydrogen atom (GE conformer).

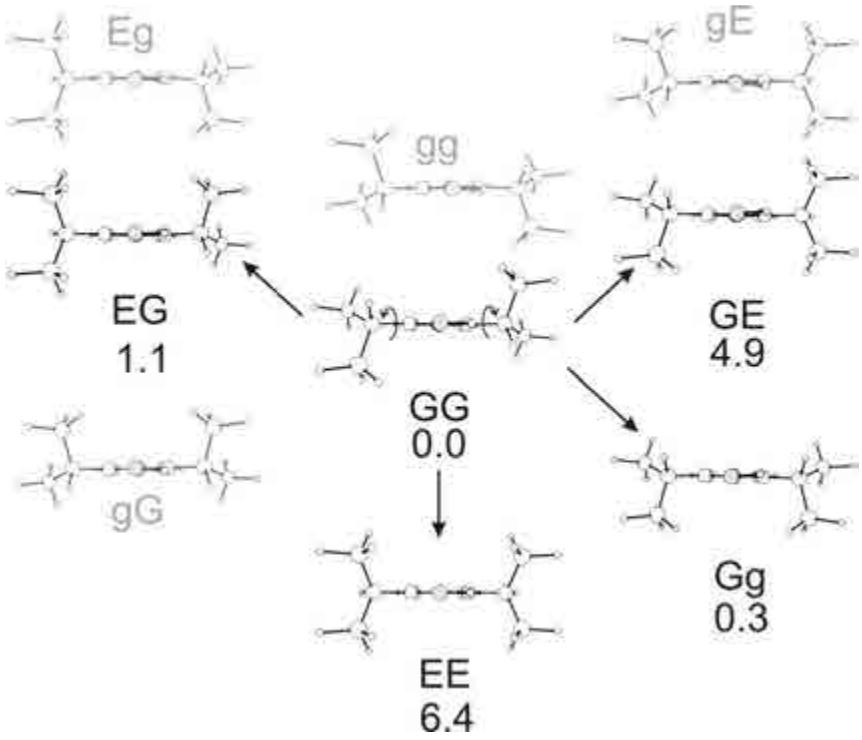

Figure 5.1. *The nine conformers of propofol and their relative stability, as calculated at MP2/6-311++G(d,p) level. Energy values in kJ/mol. Faded molecules are specular images of one of the non-faded ones (e. g. Eg≡EG).*

Finally, the less stable isomer is obtained rotating both isopropyl groups until the hydrogen atoms points *backwards*, resulting in a ~ 6.4 kJ/mol decrease in the molecular stabilization energy (conformer EE). In a recent paper by Pate's group[1], three of the five possible conformers were detected in supersonic expansions, using a pure Ar adiabatic expansion and broadband chirped-pulse microwave spectroscopy: Gg, identified as the most stable conformer, EG and GE. The absence of a GG conformer, predicted as the most stable species by our calculations, was attributed to a low barrier for isomerization, which allows a population transfer during the cooling process. Also, they demonstrated that a correct energetic order of the conformers is obtained if a cc-pVTZ basis set is used instead of the Popple's 6-311++g(d,p) basis set.

Figure 5.2 shows the *2c-REMPI* spectrum for propofol. The red-most band appears at 36222 cm^{-1}, and thus it is taken as the 0_0^0 transition. As can be seen, propofol exhibit a rich spectroscopy of around 400 cm^{-1}.

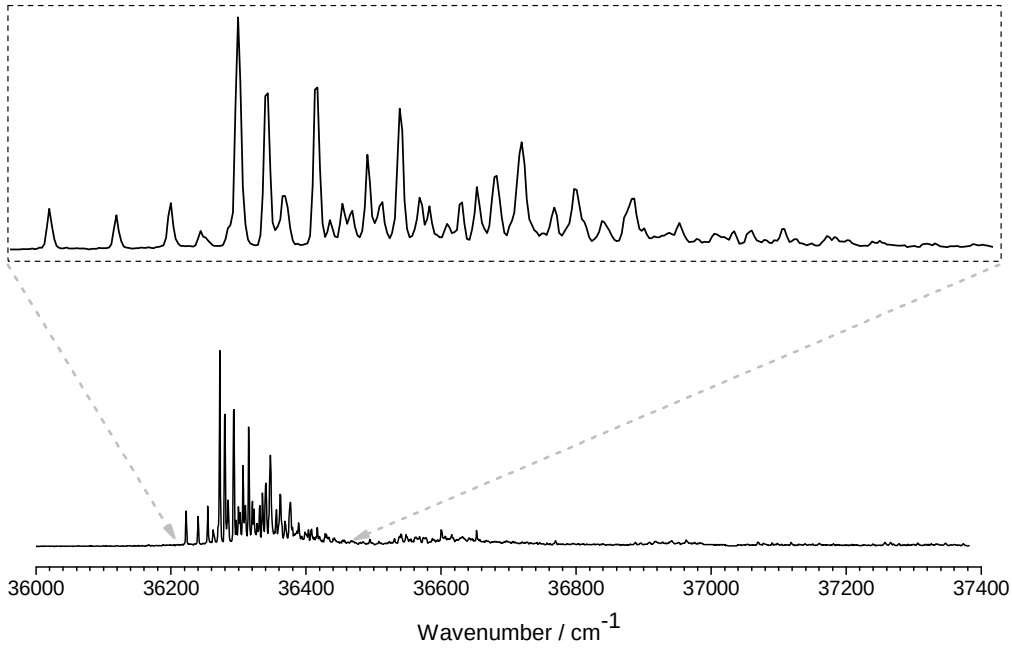

Figure 5.2. *2-color REMPI of propofol, in the 36000-37400 cm^{-1} region, recorded setting the probe laser at 27972 cm^{-1}. The insert shows a detailed view around the origin.*

To determine the number of isomers contributing to the spectrum of each stoichiometry, a *hole burning* experiment was performed (Figure 5.3). As can be seen, at least 3 conformers are present. Figure 5.3 also shows a comparison between the *2c-REMPI* spectra of propofol recorded using He, Ne and Ar as buffer gas, and the *hole burning* traces recorded tuning the probe laser at 32666, 36273 and 36315 cm^{-1} respectively.

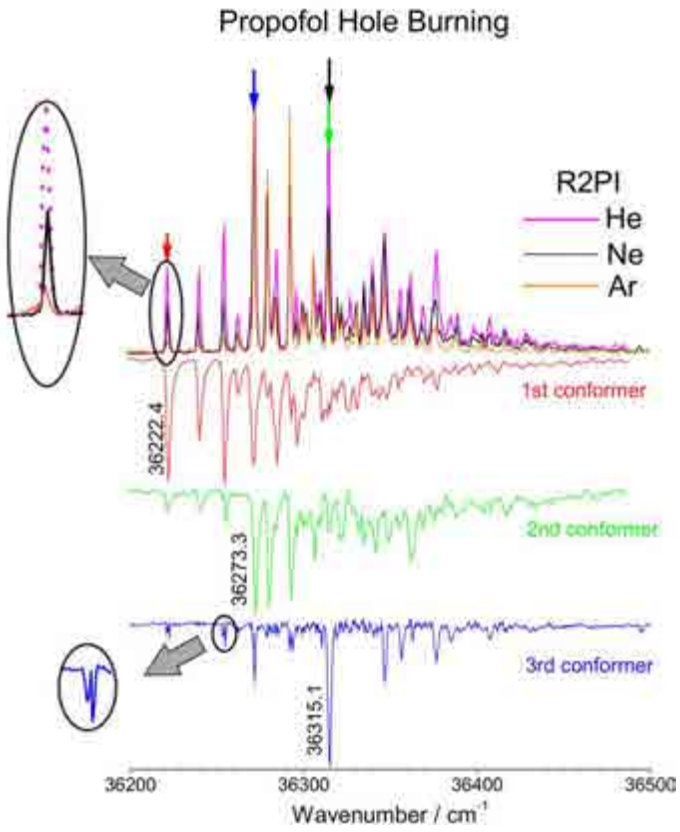

Figure 5.3. *Hole burning traces of propofol recorded tuning the probe lasers (2-color detection) at 36222, 36273 and 36315 cm^{-1} respectively. The 2-color REMPI spectrum recorded using He (solid line), Ne (black) and Ar (orange) as carrier gas is also shown for comparison. A zoom of the origin of the REMPI spectrum and of a peak on the third isomer hole burning trace is also shown. The arrows indicate the transitions employed for recording the IDIRS traces.*

It is worthy to note the intensity distribution: the 0_0^0 transition for the first conformer is the most intense transition, and when going to the blue, the intensity of the transitions decrease. For the second conformer the opposite trend is observed and it becomes more evident when introducing a heavier carrier gas. Such behaviour is due to

a low barrier between GG and Gg conformers. Collisions with Ne or Ar are energetic enough to move part or total of the population to the more stable species.

As can be seen in Figure 5.3, a heavier carrier gas leads to the despopulation of the first conformer of propofol uncovering the transitions due to the second conformer, whose 0_0^0 transition, is not the most intense peak but the one ~ 1.2 cm^{-1} to the red of the first isomer 0_0^0 transition. The existence of this two, very close origins is also visible in the third conformer *hole burning* trace, due to a crossed *hole burning* with first and second conformers. Collisions with Ne move part of the population from the first to the second isomer and the even more energetic collisions with Ar result in a complete depopulation of the first isomer allowing recording the spectrum of the second isomer origin, which is slightly shifted to the red.

Such observations seem to indicate that the experimental second conformer is the calculated Gg structure (the global minimum), and therefore the experimental first conformer should be assigned as the calculated GG structure. This assignment is in agreement with results reported by Pate's group using microwave spectroscopy[1]. The low barrier for the isomerisation process precluded, with their experimental arrangement, detection of the GG conformer.

Following the above assignment and taking into account that Pate's group found Gg, EG and GE isomers, we should then expect to find a fourth conformer. To test it, an IRID experiment on all the detected species was carried out both in the OH stretching region (around 3600 cm^{-1}) and in the fingerprint region (500-1700 cm^{-1}) using a free electron laser and, obtaining the spectra shown in Figure 5.4.

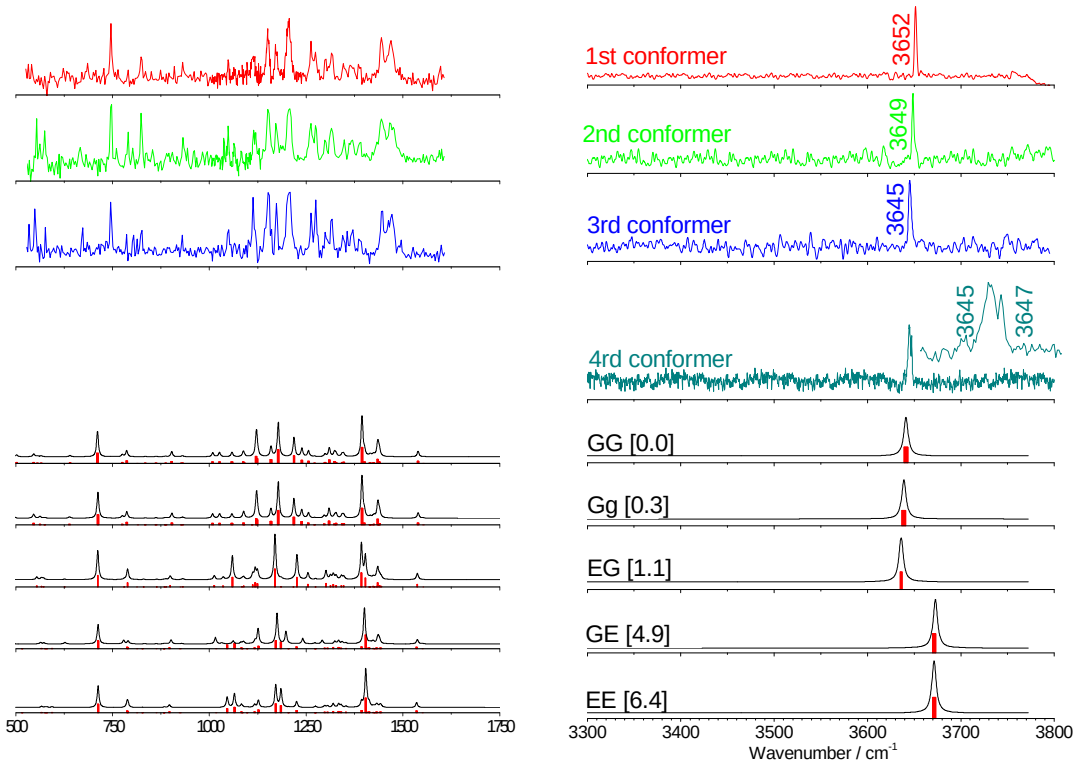

Figure 5.4. *IDIR spectra of propofol recorded tuning the probe laser at 36222, 36273, 36315.2 and 36135.5 cm^{-1} respectively. The fourth isomer IDIR spectrum in the 500-1700 cm^{-1} range could not be isolated from that of isomer 3 and therefore is not shown. The predicted IR spectra for all five calculated structures are also shown for comparison. The numbers in brackets are the relative energies of the calculated conformers, in kJ/mol. The correction factor is 0.943.*

On the right side of Figure 5.4, the IDIR spectra of the three (red, green, and blue) propofol conformers detected by *hole burning* spectroscopy are shown. These spectra are obtained probing the transitions marked with arrows in Figure 5.3, at 36222, 36273 and 36151 cm^{-1}. The fourth (dark cyan) one is obtained probing the third isomer's 0_0^0 transition slightly to the blue, and clearly shows two IR transitions: one due to contribution from the third isomer and the second one due to a fourth isomer, whose spectrum could not be isolated from that of the third isomer; i. e.: all the transitions belonging to third isomer present the peak at 3645 cm^{-1}, but in addition, some of them present a peak at 3647 cm^{-1} that we assign to the fourth isomer.

The position of the OH stretching vibration predicted for all five calculated conformers at MP2/6-311+G(d,p) is also offered for comparison. The calculated traces

are multiplied by a 0.943 scaling factor to match the experimental transitions. It is clear from the Figure, that the calculations overestimate the environment influence over the OH stretching vibration, as they predict a larger separation between the GG, Gg and EG group of isomers and GE and EE, while experimentally, all four vibrations are found in a 7 cm^{-1} window.

Only three IDIR spectra (Fig. 5.4, left side) were recorded in the 1000-1700 cm^{-1}; the fourth one is a broad absorption, due to spectral congestion, because it is not possible to isolate its spectrum from that of third isomer. All three IDIR spectra are very similar, and show a larger number of transitions than the simulated spectra, making difficult to extract any conclusion about the assignment.

In order to find an explanation for the coincidence of GG and Gg 0_0^0 transitions, separated by only ~ 1 cm^{-1} and the difference in the intensity patterns of the vibronic bands between the spectra of both isomers, that while GG 0_0^0 transition is the strongest feature in the GG spectrum, together with the band at 0_0^0+33 cm^{-1}, the Gg band origin is very weak, gaining intensity over 0_0^0 + 55 cm^{-1}, the S_0 potential energy surface (PES) for the rotation of both isopropyl groups was calculated at the B3LYP/6-31++G(d,p) level rotating each isopropyl group in 30 degrees steps and relaxing the rest of the degrees of freedom, obtaining 144 points. Additionally an estimation of the excited state PES was done at TD-DFT level (Figure 5.5) using the 144 structures obtained for S_0.

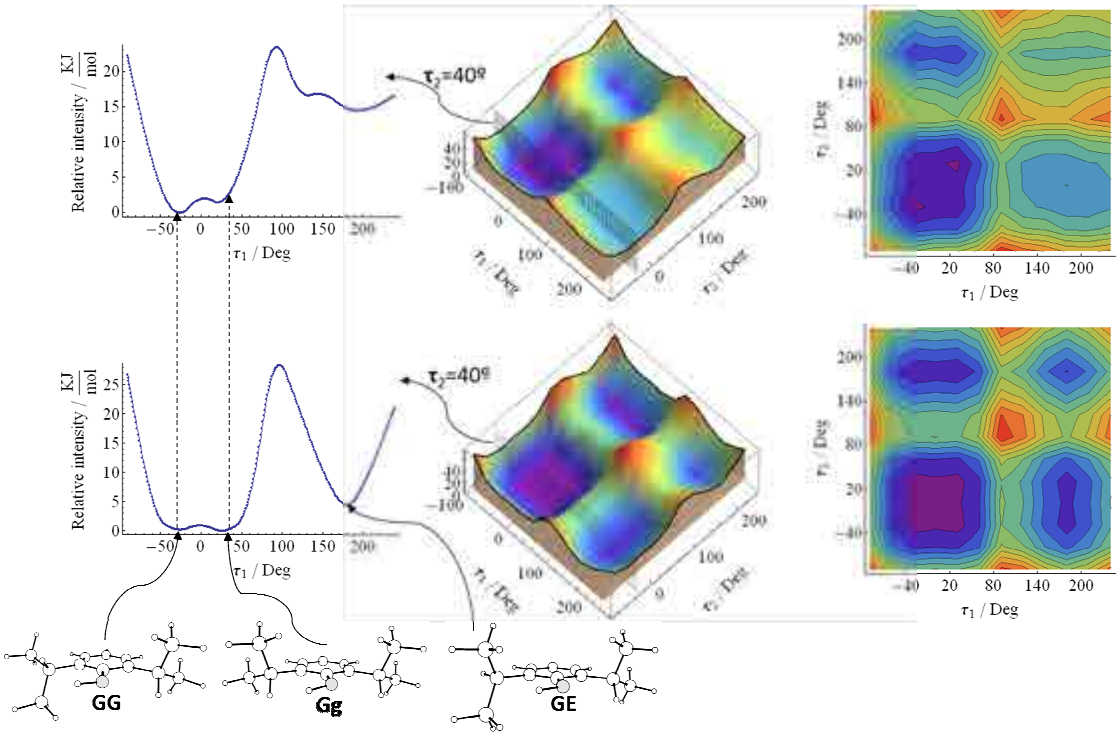

Figure 5.5. *3D representation of the S_0 potential energy surface for the rotation of propofol two isopropyl groups, calculated at B3LYP/6-31++G(d,p) level rotating the isopropyl/benzene angles at 30 degrees steps (= 144 points) and relaxing the remaining degrees of freedom. The S_1 surface is built running a TDDFT calculation on each of the S_0 144 calculated points and therefore, it corresponds to vertical excitations. The 2D projection of each surface is also shown to the right. It is readily noticed that there is a shift in the position of GG and Gg minima from S_0 to S_1 state, and that both access the same potential well in the excited state.*

As can be seen, there is a conformational change in the excited state. The difference between Gg and GG propofol conformers is the orientation of the isopropilic hydrogens: both on one side of the ring plane (Gg) or one in each side (GG). However, in the excited state, there is a change in the geometry and due to Frank-Condon Factors (FCFs), it is possible to access the excited state ground vibronic level when exciting the GG conformer. However, the FCFs penalize the 0_0^0 transition for the Gg conformer, and only above certain vibronic level the transitions gain intensity.

In order to avoid fragmentation due to higher-mass clusters, the ionization threshold was estimated tuning the first color into the 0_0^0 transition for each conformer and scanning the second laser while monitoring the ionization signal (Figure 5.6).

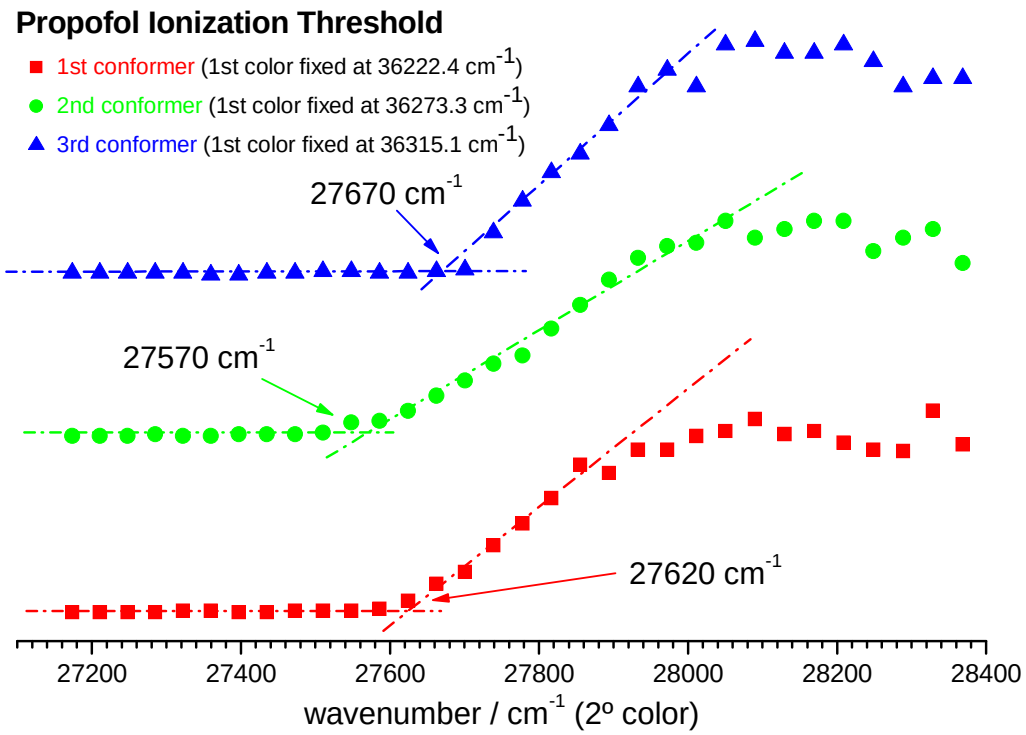

Figure 5.6. *Ionization thresholds obtained for three of the four propofol conformers. The first color is tuned to the* 0_0^0 *transition for each conformer, while the second color is scanned.*

Ionization thresholds of 63842 cm^{-1}, 63843 cm^{-1}, and 63985 cm^{-1} were obtained for the first, second and third conformer respectively. The calculation of the ionization potential for the fourth conformer cannot be performed, as it overlaps with transitions of the other three conformers. As can be seen, values around 28000 cm^{-1}, i.e. 357 nm, are necessary for the probe laser to ionize propofol. Thus the third harmonic of a Nd:YAG laser (355nm) can be used as a probe laser. It is worthy to mention that in order to test such election, the R2PI spectrum of propofol with the probe laser at 355nm and at 357nm were obtained finding no remarkable differences.

5.2 – Propofol·W_n

Once the electronic spectroscopy of propofol has been studied, the solvation with water was investigated, characterizing the hydratation with up to nine water molecules. The *2c-REMPI* spectroscopy of the clusters was recorded and the numbers of conformers present in the beam was determined using *hole burning* spectroscopy. Finally, the structures were elucidated by comparison between IDIR spectroscopy and *ab initio* calculations.

Figure 5.7 shows the mass spectrum of a supersonic expansion of propofol in He saturated with water. Clusters containing with up to 10 water molecules are readily detected not only for propofol, but also for propofol homomers. The 1:n species follow a typical RRKM distribution. However, magic numbers are found for the 2:n and 3:n species, presumably due to the formation of remarkably stable species. Also a propofol fragment due to the loss of a CH_3 group is visible at m/z = 8.1 μs.

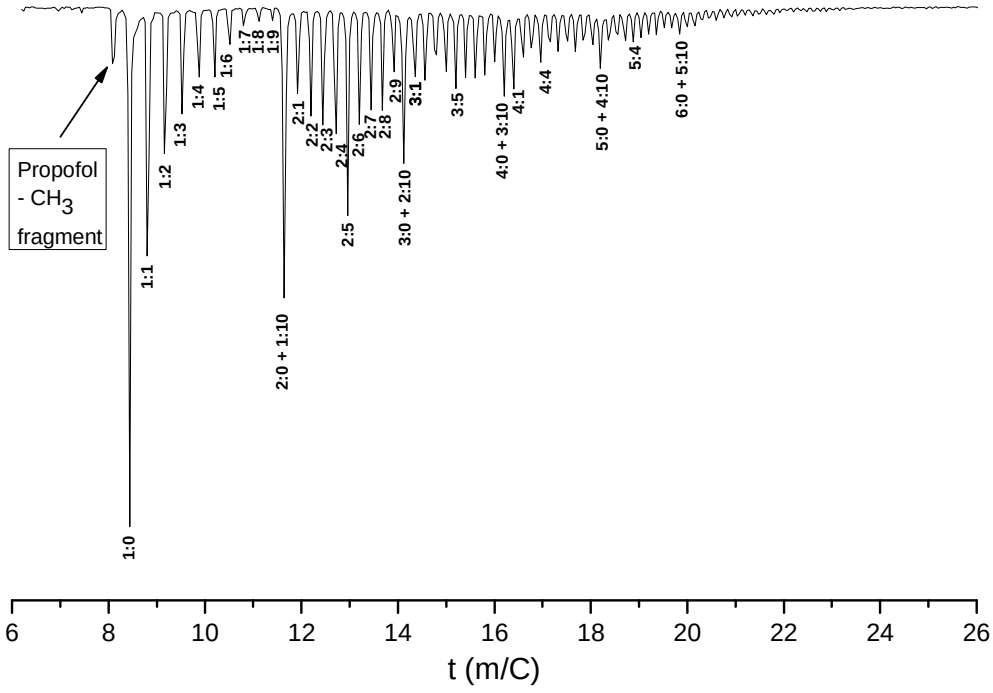

Figure 5.7. *Mass spectrum of an expansion of propofol and water mixture in He.*

The *2c-REMPI* spectra of the 1:n species, which are the subject of the present section, are obtained integrating the corresponding mass-channel (Figure 5.8).

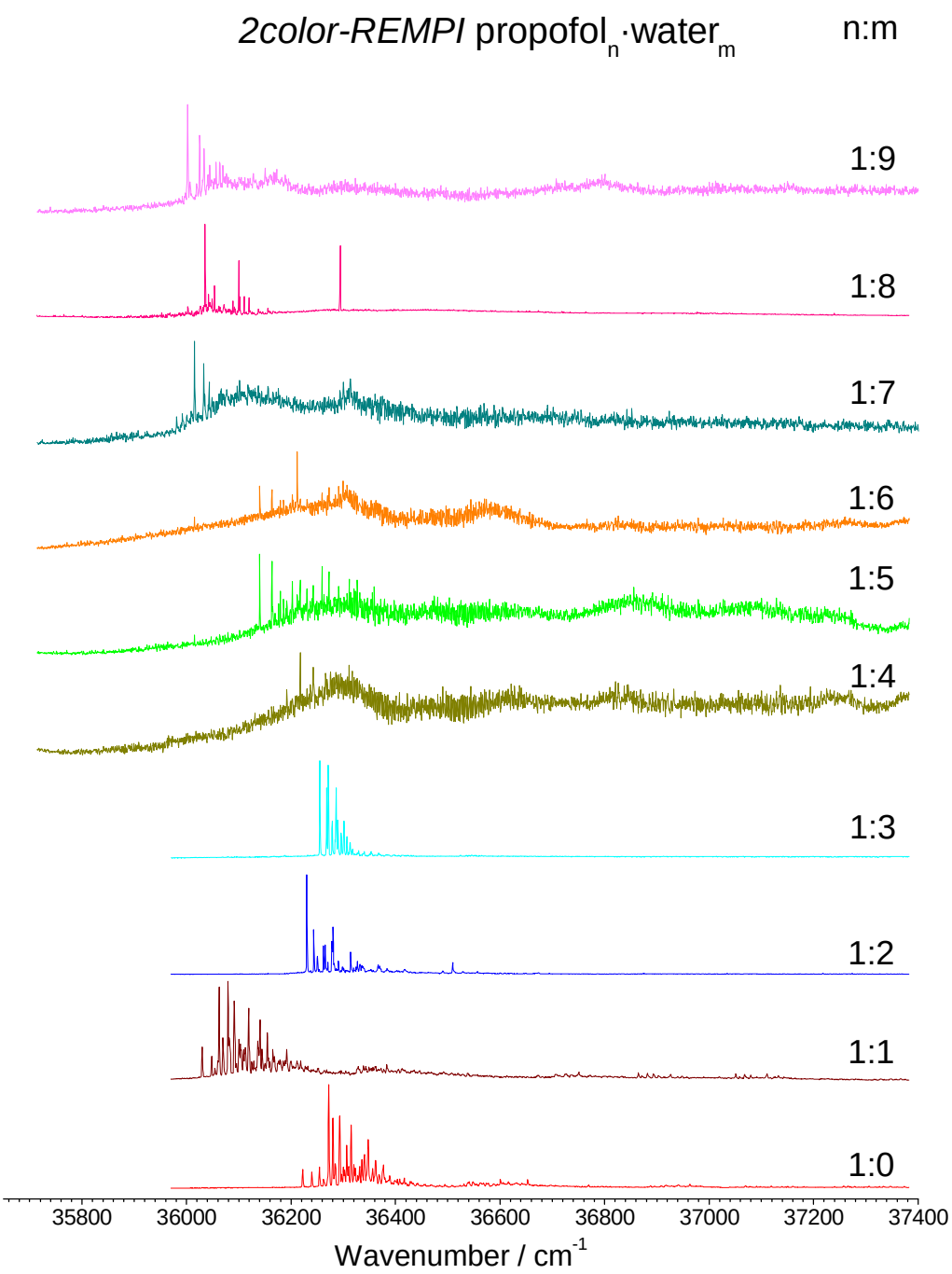

Figure 5.8. *2c-REMPI of propofol·W_n, n=0-9 in the 35700-37400 cm^{-1} region.*

5.2.1 – Propofol·W_1

Introduction of a water molecule leads to a considerably more complicated conformational landscape compared to the bare molecule. The possibility of water acting as either proton-acceptor or donor, either to the OH group or to the aromatic ring, the different orientations that the water molecule can adopt in the complex for a given type of interaction and the bare molecule symmetry-break introduced by the water molecule result in more than twenty isomers in an energy window of 10 kJ/mol. Some of the most representative structures obtained in the calculations are presented in Figure 5.9. As can be seen, the most stable isomers are those with propofol adopting a GG or Gg conformation, and with the water acting as proton acceptor. The water molecule can enter either in an *in-plane* or in an *out-of-plane* configuration. In the latter, the O-H···OH_2 hydrogen bond angle varies between 140-150º, indicating that, due to steric effects, the water can never reach an optimal position to maximize the hydrogen bond interaction, and therefore is forced to adopt a position that is a compromise between hydrogen bond, dipole-dipole, steric effects and several other minor interactions. As observed for the bare molecule, GG- and Gg-based 1:1 isomers are practically isoenergetical. Also, the HO-H···π interaction (structure *10*) is predicted to be only ~ 1.2 kJ/mol less energetically favorable than the main solvation site interaction, and it is preferred over the π···H-O-H···O(H)Ph interaction, according to the calculations.

The complexes based on the bare molecule EG isomer are also very similar to those described above based on Gg and GG conformers, as the water molecule interacts only with the isopropyl group with the H atom pointing *forwards*, and therefore it finds an environment similar to Gg and GG. Therefore, the observed difference in stability is mainly due to the conformation adopted by the bare molecule. Conversely, the GE conformer has the OH on the side of the isopropyl group with the H pointing *backwards*, and therefore, the water molecule finds a more hostile environment, leading to species less stable by ~ 7 kJ/mol or more. Furthermore, only two GE-based monohydrated species bellow 10 kJ/mol were found at the present calculation level.

In addition to the structures reported in Figure 5.9, there is a large number of structures that exhibit small variations in the orientation of, mainly, the free water O-H bond (see appendix 7.1). In any case, due to the small energy difference between most of the structures, which is well within the calculation errors, the final number of species

present in the expansion will mostly depend on the topography of the potential energy surface (PES), and more precisely, on the height of the barriers between the different minima.

In the same line, water finds strong steric hindrances to solvate the OH group when propofol is in EE conformation, and consequently, the EE-based most stable 1:1 species has the water acting as proton-donor to the OH group. The most stable propofol-O-H···OH_2 species is 5.7 kJ/mol higher in energy.

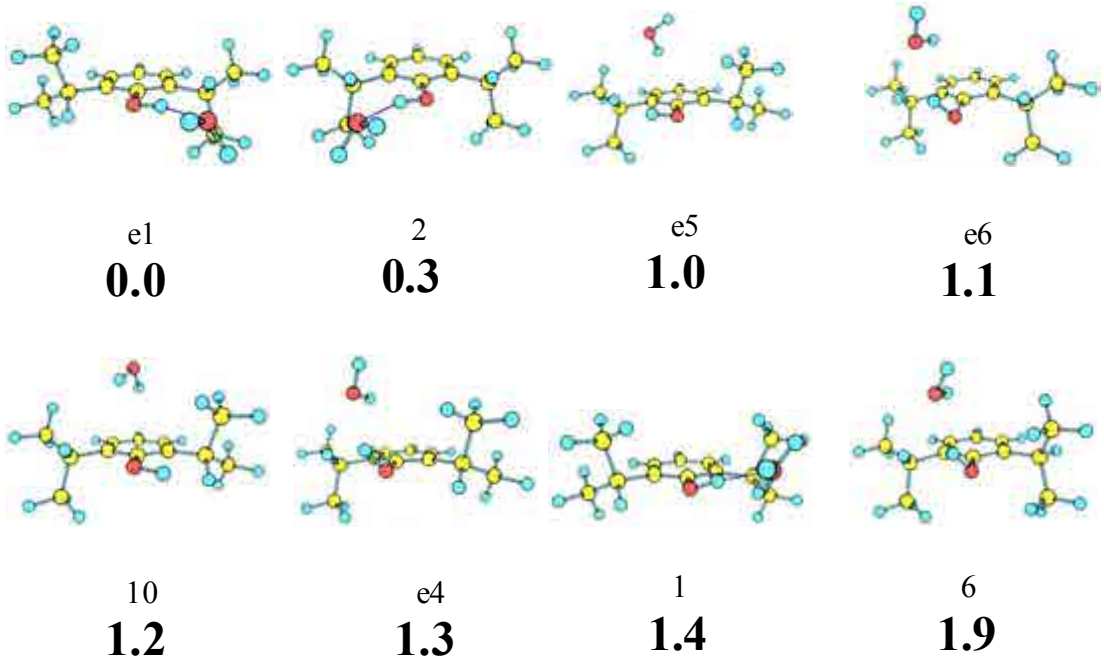

Figure 5.9. *Propofol·W_1 eight most stable isomers calculated at MP2/6-311++G(d,p) level, with their relative energies in bold. Energy values are in kJ/mol. All the calculated structures for this cluster are presented in appendix 7.1 (Figure 7.1).*

Figure 5.10 shows the *2c-REMPI* spectrum of propofol·W_1. The red-most band appears at 36029 cm^{-1}, and thus it is taken as the 0_0^0 transition. As can be seen, the spectrum of the monohydrated species is very similar to that of propofol, although it presents a higher abundance of bands, due to the presence of intermolecular modes. Its red-most feature is shifted ca. 200 cm^{-1} from the bare molecule. Such a shift can be attributed to a change in the inductive effect of the propofol's oxygen atom on the $\pi^* \leftarrow \pi$ transition due to the formation of an R-OH···OH_2 hydrogen bond, indicating that propofol is acting as proton-donor.

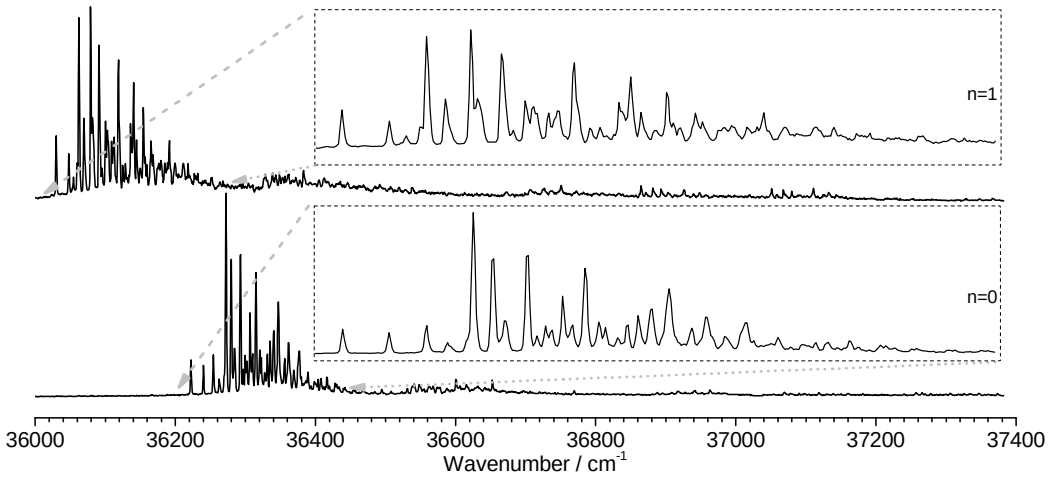

Figure 5.10. *2-color REMPI of propofol and propofol·W_1 in the 36000-37400 cm^{-1} region, recorded setting the probe laser at 27972 cm^{-1}. The inserts show a detailed view around the origin of each species.*

To determine the number of isomers contributing to the spectrum, a *hole burning* experiment is done (Figure 5.11), discovering, at least three conformers. The results share some similarities with what is shown in Figure 5.4: three isomers are found with origins at 36030, 36064 and 36120 cm^{-1}, two of them with a rich spectroscopy, and the third one with considerably less features. When Ne or Ar are used as buffer gas, depopulation of one of the isomers is also observed, while the *hole burning* traces show that the first and second isomers 0_0^0 transitions overlap. As happened with the bare molecule, the more energetic collisions with Ne move part of the population from the first to the second isomer. The even more energetic collisions with Ar result in a complete depopulation of the first isomer, making possible recording the spectrum of the second isomer origin, which is slightly shifted to the red.

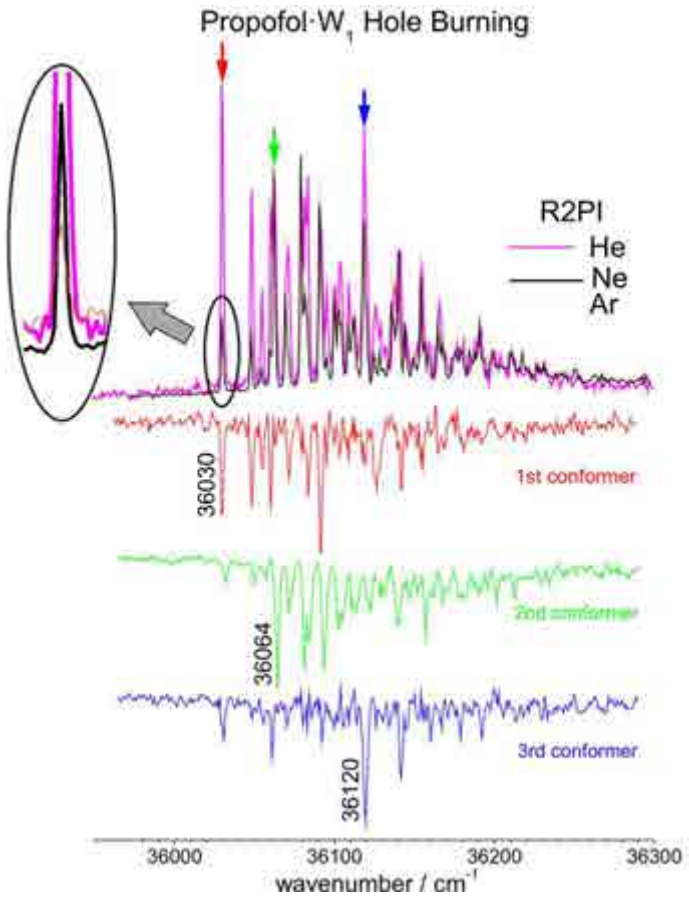

Figure 5.11. *Hole burning traces of propofol·W_1 recorded tuning the probe laser (2-color detection) at 36030, 36064 and 36120 cm^{-1} respectively. The 2-color REMPI spectra recorded using He (pink), Ne (black) and Ar (orange) as carrier gas are also shown for comparison. A zoom of the origin of the REMPI spectrum and of a peak on the third isomer hole burning trace is also shown. The arrows indicate the transitions employed for recording the IDIRS traces.*

Such observations seem to indicate that the experimental second conformer is built on propofol Gg structure, and therefore the experimental first conformer should be assigned to a GG-propofol water structure.

In order to extract the maximum structural information to match the REMPI spectra with the calculated structures, the IDIR spectra of all the detected species were recorded, both in the OH stretching (around 3600 cm^{-1}) and in the *fingerprint* region (500-1700 cm^{-1}) using a free electron laser and, obtaining the spectra shown in Figure 5.12. The *ab initio* predictions for some selected calculated structures are also shown: A Gg propofol·W_1 complex with the water accepting a proton in an *in plane* configuration (structure *e1*), a Gg propofol·W_1 with the water molecule interacting with the aromatic

ring (structure *e5*), and Gg, GG, and EG propofol·W_1 isomers with the water accepting the OH proton in an *out of plane* configuration (structures *e6, e4, 6*). The second type of interaction can be discarded as two peaks, due to the O-H···π interaction, in the 3600-3650 cm^{-1} region should be present.

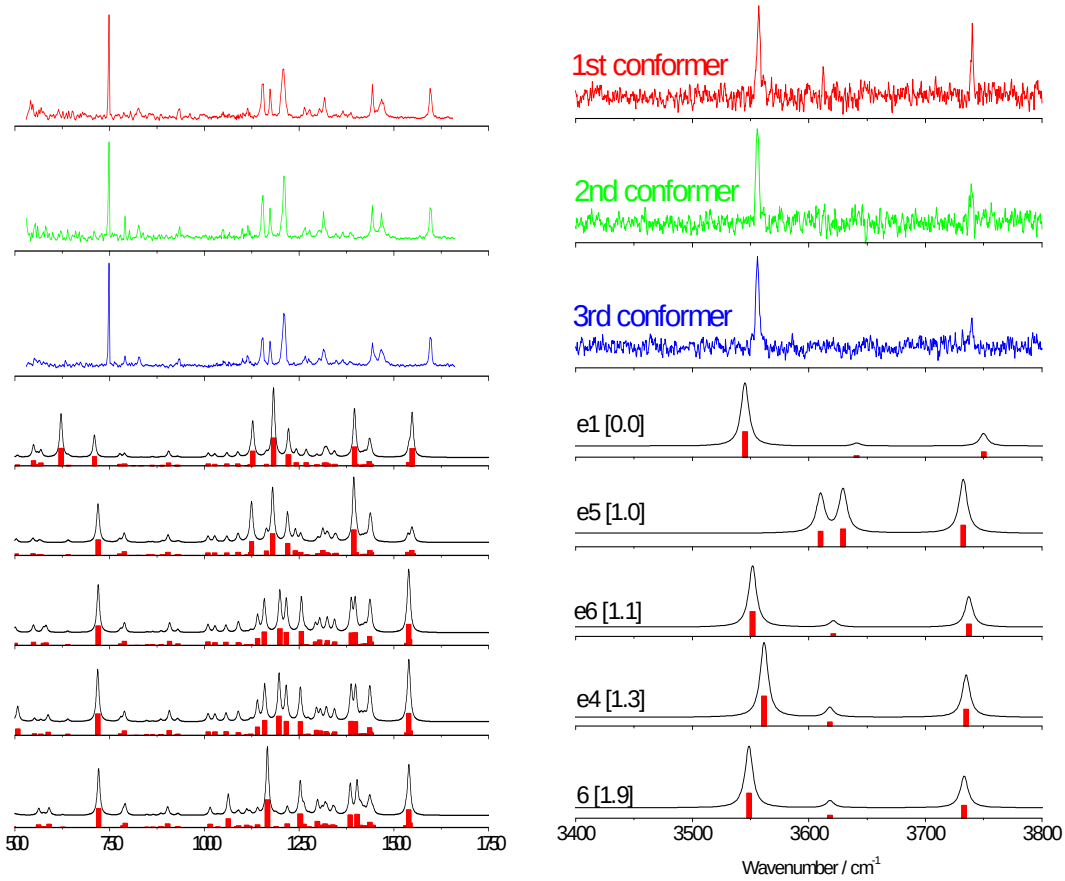

Figure 5.12. *IDIR spectra of propofol·W_1 recorded tuning the probe laser at 36030, 36064 and 36120 cm^{-1}. The predicted IR spectra for some of the calculated isomers are also shown for comparison. The predicted IR spectra for some of the calculated structures are also shown for comparison. The numbers in brackets are the relative energies of the calculated conformers, in kJ/mol. The correction factor is 0.943. The predicted IR spectra of all the calculated structures are recorded in appendix 7.1 (Figure 7.2).*

Changing the delay of the IR laser so that it is fired between the pump and probe UV lasers, information on the structure of the complexes on the excited state is obtained as shown in Figure 5.13. The same experiment could not be performed for the bare molecule, because the excited state short lifetime. The shift to lower frequencies, 105 cm^{-1} from the ν_{OH} in the fundamental state of the complex, that is, twice the shift from the bare molecule, in the propofol OH stretching vibration indicates that propofol becomes more acidic in the S_1 state, as it happens with phenol. As observed in S_0, the spectra of all three isomers are very similar in the excited state.

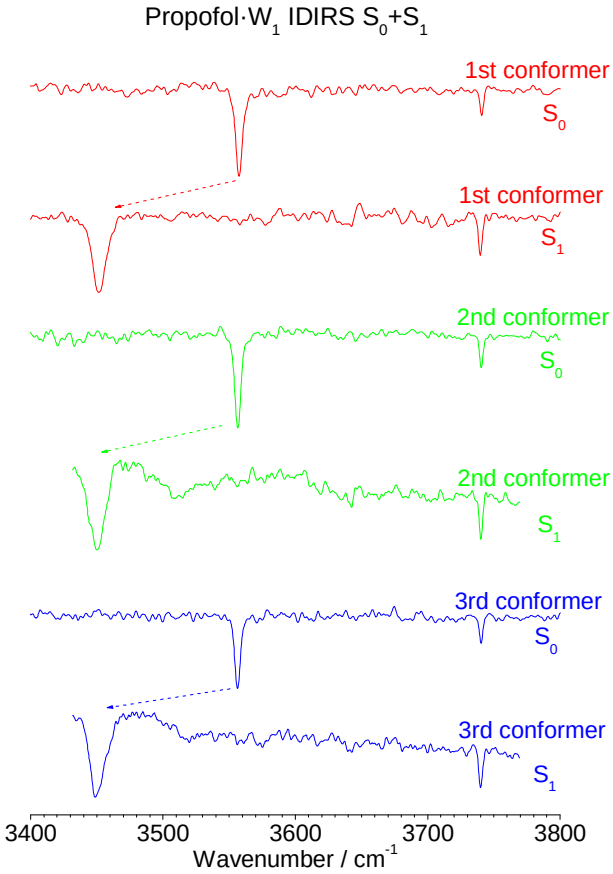

Figure 5.13. *Comparison between ground and excited state IDIRS of propofol·W_1 isomers.*

Assignment

The red shift in the propofol's OH stretching vibration (95 cm^{-1}) observed in the experimental traces indicates that water is acting as proton-acceptor in all three experimental isomers. So only two possibilities are left for the water: to adopt an *in plane* configuration, or to adopt an *out of plane* configuration. Both types of structures present very similar spectra in the 3400-3800 cm^{-1}, hampering the final assignment. However, some differences between both types of structures are observed in the fingerprint region. The simulated spectrum for the Gg-propofol·W_1 complex with the water accepting a proton in an *in plane* configuration shows four peaks in the 500-700 cm^{-1} region, while in the *out of plane* structures that spectral region is dominated by a single, strong peak, resembling the experimental observation. Thus, we can conclude that the water is acting as proton-donor in an *out of plane* configuration, and the only difference between the three isomers is the conformation adopted by propofol. Comparing 1:0 and 1:1 spectra, it is reasonable to assume that the propofol conformation will correlate, due to the similar shift experimented by all three 1:1 0_0^0 transitions respect to the corresponding 1:0 species and the similarity between spectra. Therefore, we assign the 1:1 three isomers as Gg-, GG- and EG-propofol·W_1 with an *out of plane* water-acceptor molecule.

Thus, of the five possible bare molecule conformers, four were detected, differing in the relative orientations of the isopropyl groups, being those with the isopropyl hydrogen atoms pointing *forward* the most stable structures, i.e Gg and GG. The introduction of a water molecule, leads to the formation of three propofol·W_1 conformers leaving out the GE-propofol·W_1 conformer. Consequently, the assignment proposed for the bare molecule is reinforced by the results obtained for the 1:1 species, which clearly show that they are originated in propofol GG, Gg and EG conformers, with a water molecule accepting the OH proton of propofol. In the 1:1 complex the hydrogen bond is placed out of the plane marked by the phenol ring, as demonstrated by the comparison between IDIR traces in the fingerprint region and *ab initio* predicted spectra. A close inspection of the calculations presented in Figure 5.9 shows that the three propofol·W_1 *out of plane* isomers containing GG, Gg and EG propofol conformers are of similar stability, as the water finds a similar solvation site, and therefore, they should exhibit similar 0_0^0 transition shifts upon complexation. Furthermore, GG- and

Gg-propofol·W_1 isomers seem to share a common excited state, as it can be deduced from Figure 5.11, although the calculations on the 1:1 excited state were not done.

GE- and EE-based 1:1 isomers force water to interact with two hydrophobic CH_3 moieties, and therefore, the strength of the interaction, binding distance and probably the expected 0_0^0 transition shift would be different from those of the other three isomers. In addition, according to the calculations, the GE- and EE-based isomers with the water accepting a proton are considerably less stable than those based in GG, Gg and EG conformers, and therefore a significant decreasing in the signal intensity of those species would be expected.

5.2.2 – Propofol·W_2

The introduction of a second water molecule reduces the number of possible isomers in the 10 kJ/mol window (the molecular mechanics calculation yields ~ 30 structures in the 20 kJ/mol window), due to the strong tendency of water to self-aggregate (Figure 5.14). Therefore, the second water reinforces the first water proton-acceptor skills and the only two options left are to form a cycle with the OH moiety or to interact with the aromatic ring. According to the calculations, the second option is energetically more favorable, by ~ 8 kJ/mol. The steric hindrance in the EE-based isomers is stronger for ring formation, as the isopropyl CH_3 groups occupy the space required for the water to enter in the optimal position to establish a hydrogen bond network.

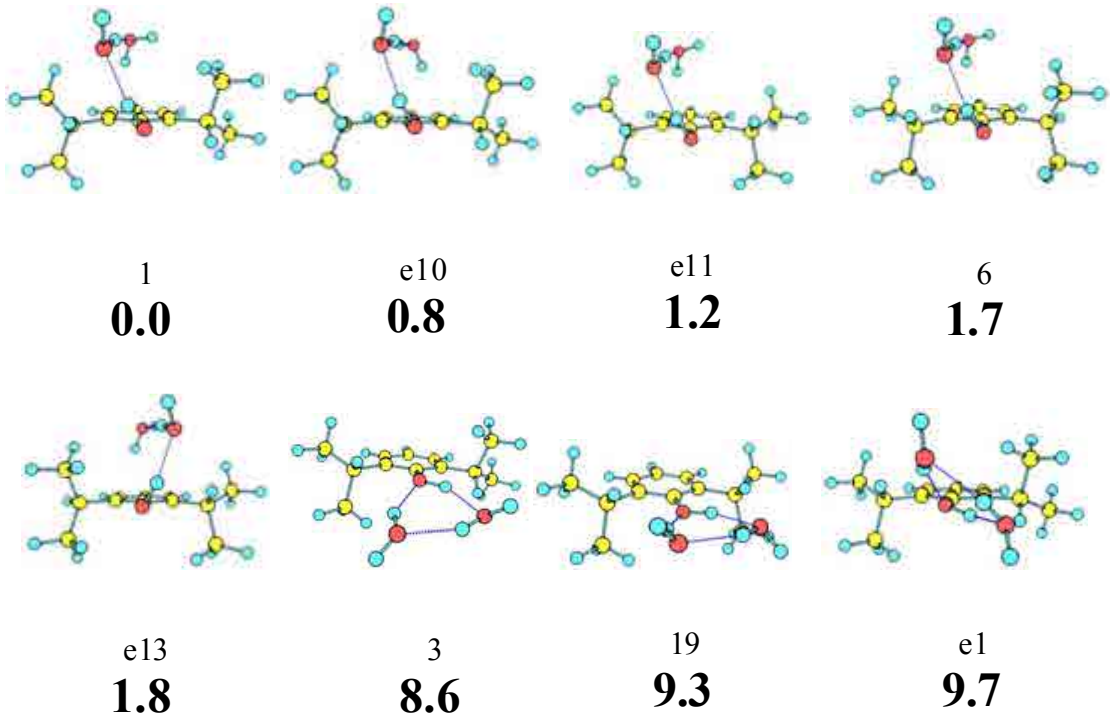

Figure 5.14. *Propofol·W_2 eight most stable isomers calculated at MP2/6-311++G(d,p) level, with their relative energies in bold. Energy values are in kJ/mol. All the calculated structures are presented in appendix 7.1 (Figure 7.3).*

Figure 5.15 shows the *2c-REMPI* spectrum of propofol·W_2 cluster. The red-most band appears at 36230 cm^{-1}, and thus it is taken as the 0_0^0 transition. As can be seen, addition of a second water molecule results in a simplification of the spectrum, which presents considerably less bands than those of the 1:0 and 1:1 species. In addition, the

origin band is located at 36230 cm^{-1}, which means that the 1:2 spectrum 0_0^0 transition is shifted by only ca. 8 cm^{-1} to the blue of that from the bare molecule. Such shift pattern is usually taken as the signature of the formation of a water cyclic structure.

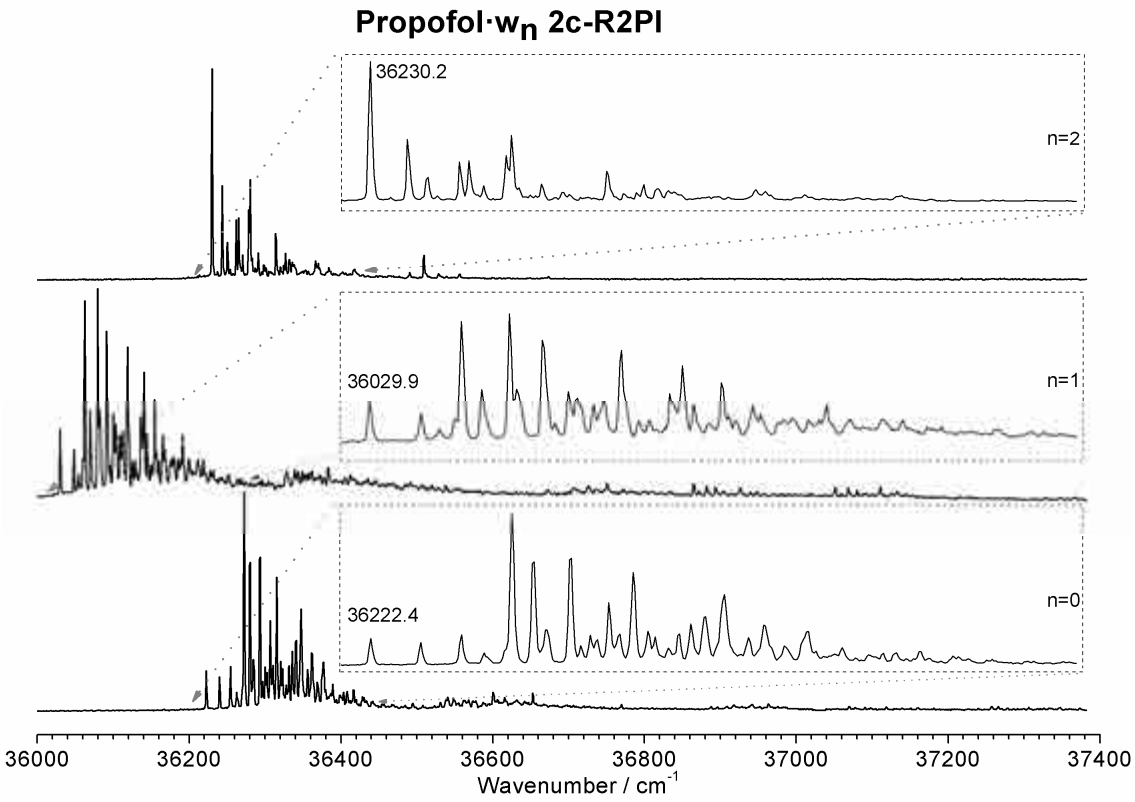

Figure 5.15. *2-color REMPI of propofol·W_n, n=0-2 in the 36000-37400 cm^{-1} region, recorded setting the probe laser at 27972 cm^{-1}. The inserts show a detailed view around the origin of each species.*

To determine the number of isomers contributing to the spectrum of each stoichiometry, a *hole burning* experiment of the 1:2 species is done. Figure 5.16 shows a comparison between the propofol·W_2 *2-color REMPI* spectrum and the *hole burning* traces obtained probing the origins at 36231, and 36244 cm^{-1}. As can be seen, addition of a second water molecule results in a drastic reduction in the number of spectral features and also in the number of conformers, which has been reduced to only two. Furthermore, no signal depletion is observed when Ne or Ar are used as buffer gas and, in addition, the separation between origins is only 13 cm^{-1}. These two observations seem to indicate that the two isomers are based on the same bare molecule conformer, differing only in the position of the water molecules.

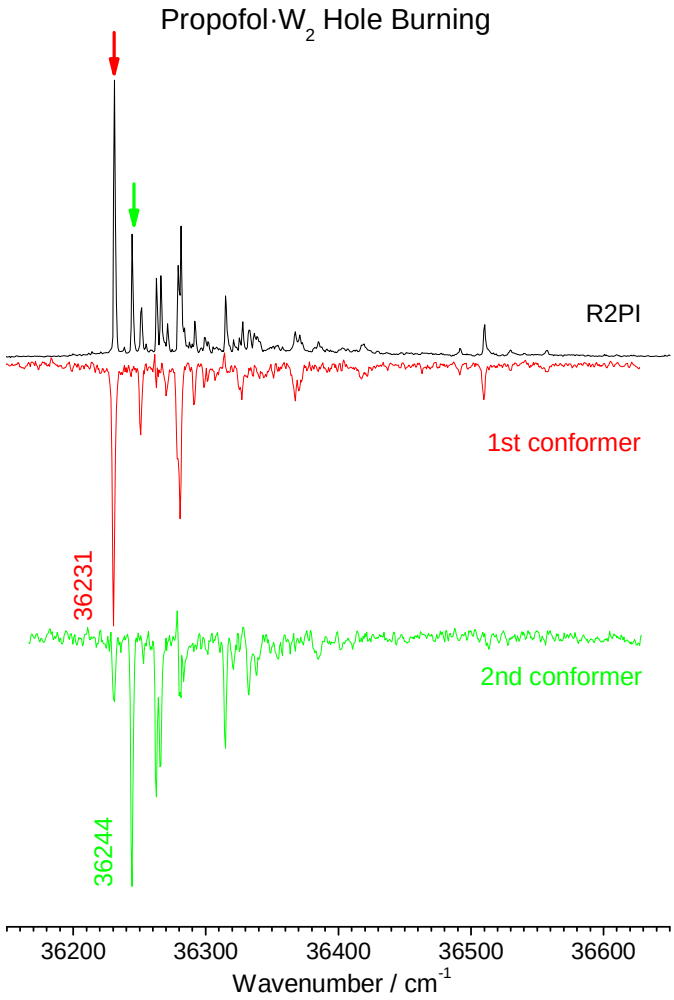

Figure 5.16. *Hole burning traces of propofol·W_2 recorded tuning the probe lasers (2-color detection) at 36231, and 36244 cm^{-1} respectively. The arrows indicate the transitions employed for recording the IDIRS traces.*

In order to extract the maximum structural information to match the *REMPI* spectra with the calculated structures, the *IDIR* spectra of the two conformers detected were recorded, both in the OH stretching region (around 3600 cm^{-1}) and in the fingerprint region (500-1700 cm^{-1}) using a free electron laser, obtaining the spectra shown in Figure 5.17.

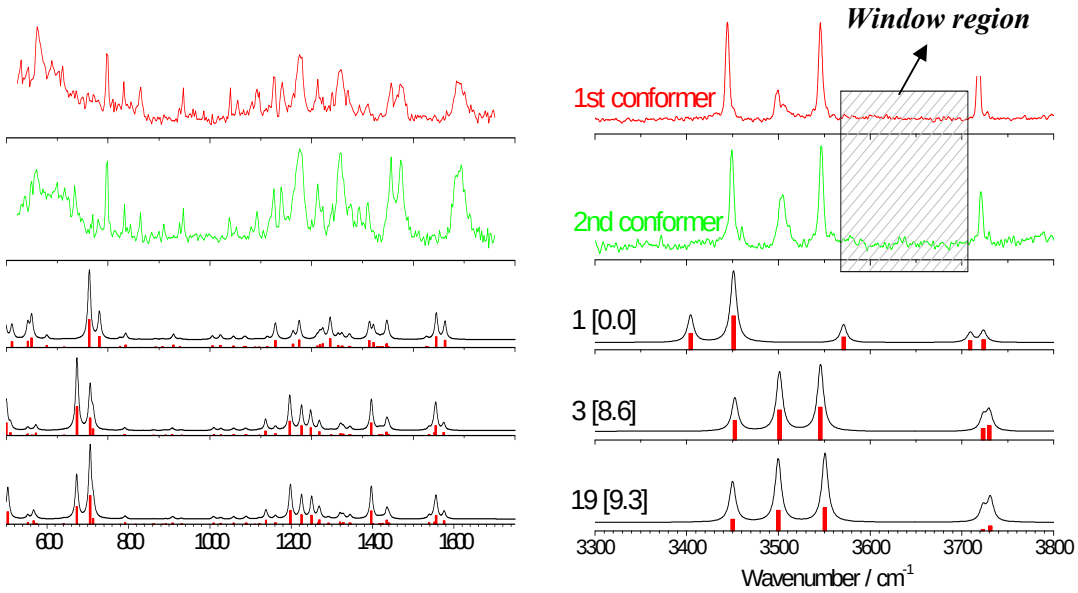

Figure 5.17. *IDIR spectra of propofol·W_2 recorded tuning the probe laser at 36231, and 36244 cm^{-1}. The predicted IR spectra for some of the calculated isomers are also shown for comparison. The numbers in brackets are the relative energies of the calculated conformers, in kJ/mol. A correction factor of 0.943 was applied. The predicted IR spectra of all the calculated structures are recorded in appendix 7.1 (Figure 7.4).*

The comparison between the *IDIR* spectra obtained for the two propofol·W_2 isomers detected and the *ab initio* predictions for some of the selected calculated structures are shown in Figure 5.17. The *IDIR* spectra obtained for both conformers of propofol·W_2 are very similar: both present a large abundance of lines in the 500-1750 cm^{-1} region, and five peaks in the 3300-3800 cm^{-1} window, divided in two groups: two peaks at high frequencies, corresponding to the free OH stretching vibrations of the water molecule, and another three at lower frequencies, corresponding to the stretching of the hydrogen bonded OH groups.

Figure 5.18 shows a comparison between the IDIR spectra of propofol·W_2 S_0 and S_1. It is worthy to note that the same experiment could not be performed for phenol·W_2 cluster by Ebata's group.[7] They concluded that there is fast intracluster vibrational redistribution (IVR), resulting in a anomalously shorter lifetime compared with the rest of phenol·W_n clusters, due to a structural change upon electronic excitation. As can be seen in the IDIRS spectra of the S_1 state, propofol OH stretching

vibration is shifted 110 cm^{-1} to the red, while the OH stretching vibration of the water that is donating a proton to the propofol oxygen atom shifts 30 cm^{-1} to the blue, due to a reduction in the strength of the HO-H··· O(H)-Ph hydrogen bond. Against what happens for the 1:1 complex, the spectra of the 1:2 two conformers are not identical: changes in the relative intensities of the spectral features are observed and an extra peak appears in the spectrum at 3369 cm^{-1} for the second conformer. Fermi resonances could be one explanation but it should be present for both isomers. Another possibility is that the IR photon promotes the system to a high S_1 vibronic level that experiments a fast conversion into a $\pi\sigma^*$ state (presumably S_2). However, according to some authors,[18] S_2 state is c.a. 4500 cm^{-1} above S_1 and therefore, it is not accessible with a single IR photon. Besides, such hypotheses do not explain the absence of such peak in the other isomer. A more plausible explanation is an isomerization in the excited state from the second to the first isomer, resulting in a spectrum which is a combination of the S_1 spectra of both conformers.

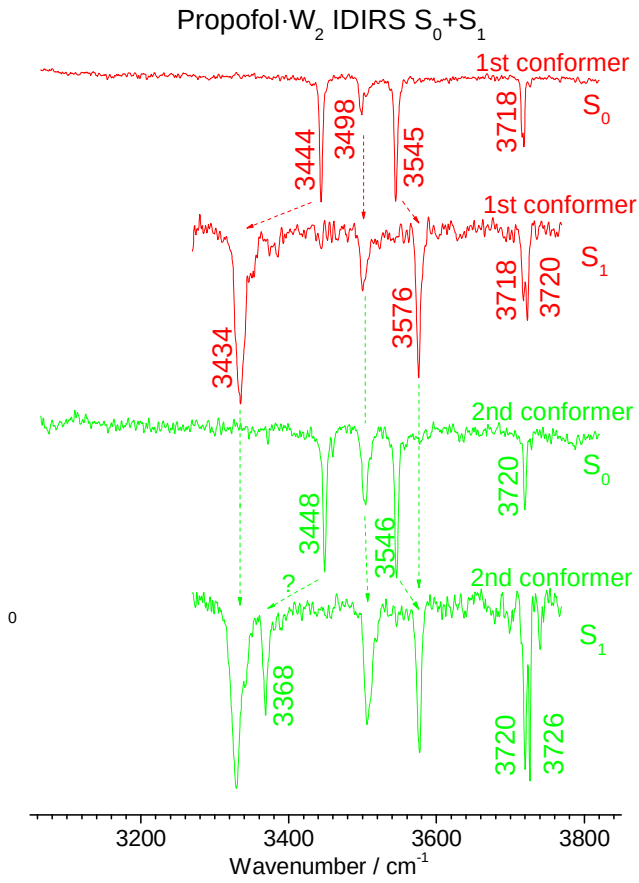

Figure 5.18. *Comparison between ground and excited state IDIRS of propofol·W_2 isomers.*

Assignment

The addition of a second water molecule further reduces the number of possible isomers to only two. For both conformers, the first experimental evidence pointing to the formation of a ring-like is the trend of the shifts in the 0_0^0 transitions from the bare molecule to the propofol·W_1 and propofol·W_2 species. Such shift pattern is normally associated with the formation of cyclic structures in which water is also able to form a six-member ring with the OH group, as it happens in phenol·water.[15] The *window region* between the two groups of peaks in the IR spectrum is also usually taken as an indication of a ring-like structure.[17] Accordingly, only those calculated isomers with ring-like structures are able to reproduce the experimental observations, and therefore, we can conclude that the two water molecules are forming a six-member ring with the propofol OH moiety. Very likely, propofol is adopting a Gg conformation and the difference between the two 1:2 isomers is the relative orientation of the water free OH bonds, as it has been observed for similar systems.[19] Another argument to favour such assignment is that using Ar as buffer gas does not result in the depopulation of one of the two isomers as it would be expected if one of them was based on propofol GG conformer. In addition, the 1:0 and 1:1 GE and EG-based species present very different spectra, while the two spectra recorded for the 1:2 isomers are very similar.

5.2.3 – Propofol·W_3

Molecular mechanics yields a reduced number of structures for this cluster, confirming the strong tendency of water to self-aggregate. In propofol·W_3 (Figure 5.19) either a water network between the propofol's OH and the ring (structures *5, 7*), an eight-member ring with propofol's OH (structures *4*, *2*), or an hybrid between both structures, in which the water molecules form a hydrogen bond network between the propofol's OH and the π cloud, but one of the water molecules closes also a six-member ring over propofol´s OH (structures *28*, *29*). In addition, the cyclic structures can adopt several orientations respect to the aromatic ring: either in the same plane (structure *2*) or perpendicular to it (structure *4*). The calculations, predict again a higher stability for hydrogen bond network structures, but only by ~ 2 kJ/mol. Again, most stable conformers are based on the GG/Gg propofol isomers.

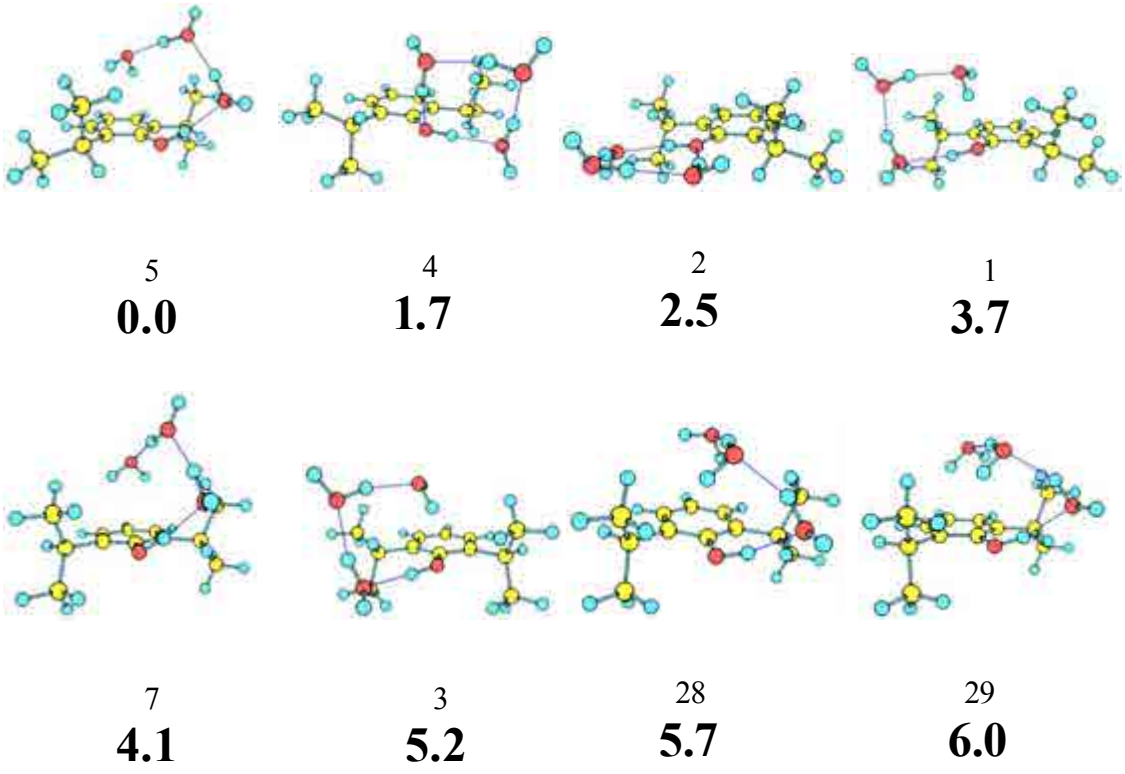

Figure 5.19. *Propofol·W_3 eight most stable conformers calculated at M06-2x/6-311++G(d,p) level, with their relative energies in bold. Energy values, in kJ/mol. All the calculated structures are presented in appendix 7.1 (Figure 7.5).*

Figure 5.20 shows the *2c-REMPI* spectrum of propofol·W_3. Strong transitions starting at 36255 cm^{-1} and extending for only c.a. 100 cm^{-1} are observed. Some weak features to the red, starting at 36185 cm^{-1}, are also present, which disappear when Ne is used instead of He, and therefore they are due to a different species.

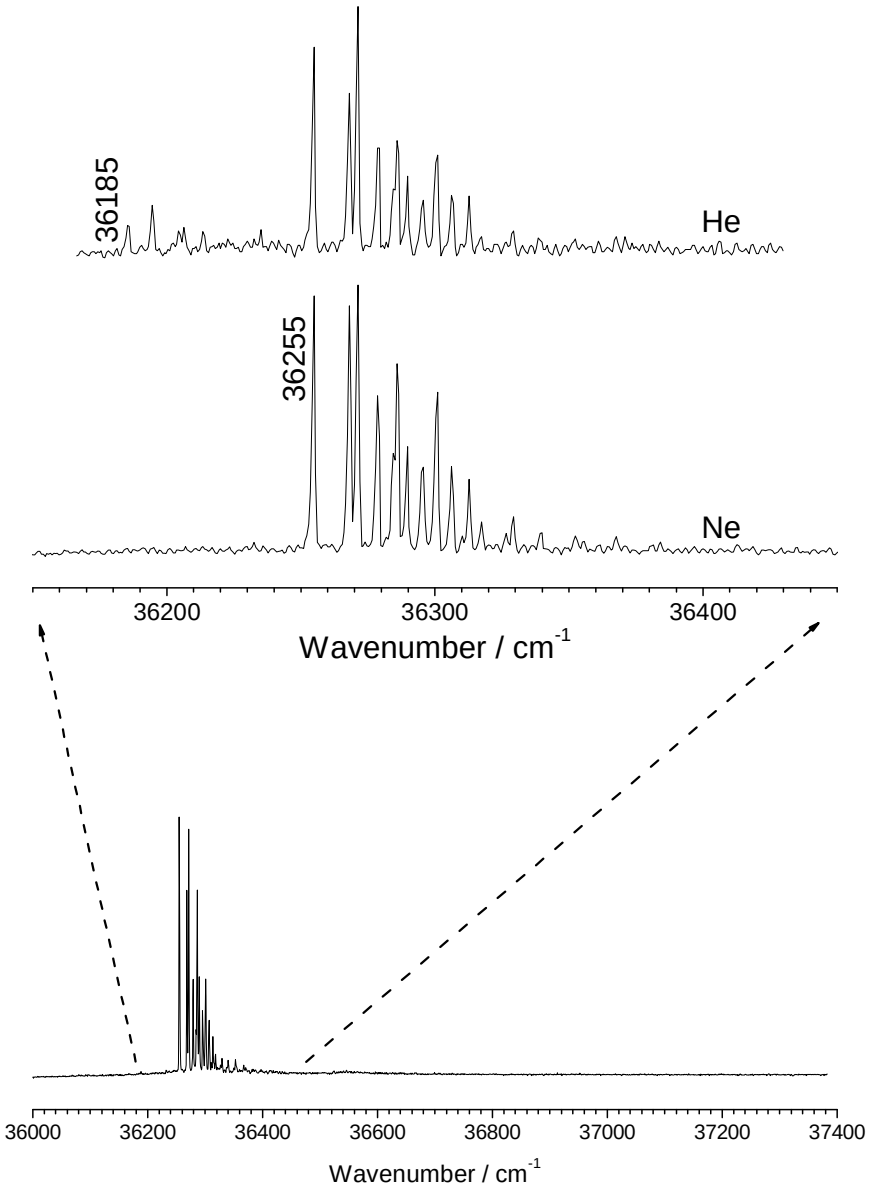

Figure 5.20. *2c-REMPI of propofol·W_3, in the 36000-37400 cm^{-1} region, recorded setting the probe laser at 27972 cm^{-1} (lower trace) and propofol·W_3 using He (upper trace) and Ne (middle trace). Note that most red-shifted transitions disappear when using Ne.*

To determine the number of isomers a *hole burning* experiment on propofol·W_3 is done, and the result is shown in Figure 5.21, where a comparison between the propofol·W_3 *2c-REMPI* spectrum and the *hole burning* traces obtained probing the origins at 36194, and 36255 cm^{-1} is offered. Two isomers are clearly seen, presenting little vibrational activity.

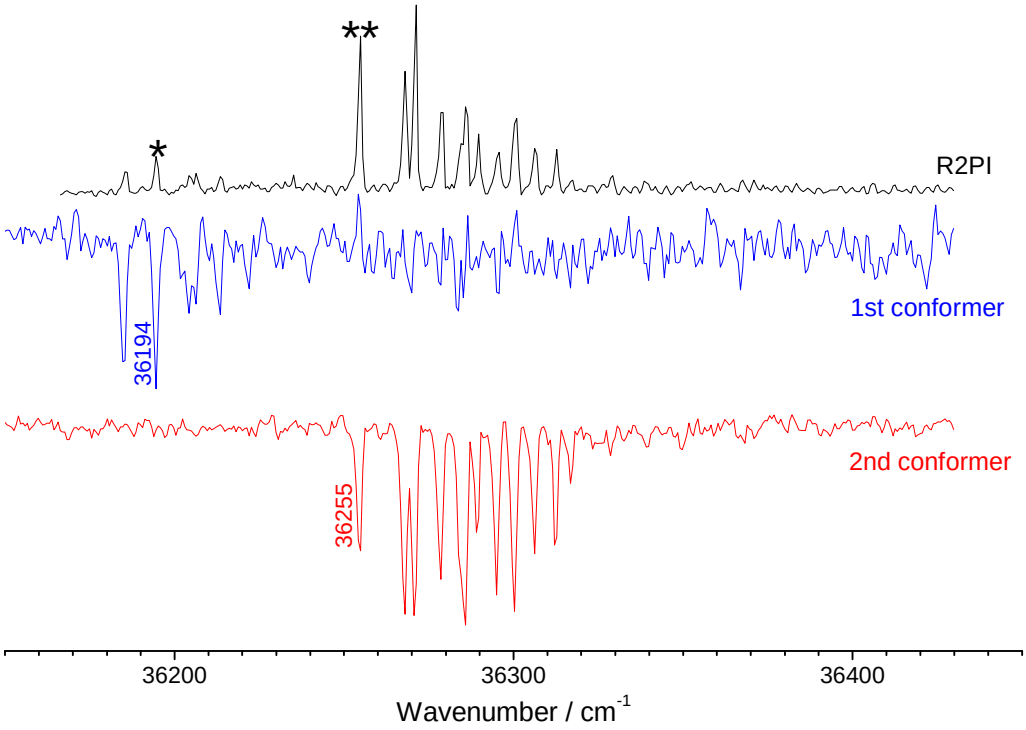

Figure 5.21. *Hole burning traces of propofol·W_3 recorded tuning the probe lasers (2-color detection) at 36194, and 36255 cm^{-1} respectively. The stars indicate the transitions employed for recording the hole burning spectra, as well as the IDIRS traces for each conformer.*

In order to extract the maximum structural information to match the *REMPI* spectra with the calculated structures, the *IDIR* spectra of the two conformers detected was recorded, both in the OH stretching and in the fingerprint regions (500-1700 cm^{-1}), obtaining the spectra shown in Figure 5.22. The predicted spectra for the most stable species are also shown in the Figure. The IDIR spectra obtained for both conformers of propofol·W_3 are very similar: both present a large abundance of lines in the 500-1750 cm^{-1} region, three broad bands which probably consist of four peaks in the 3310-3440 cm^{-1} region, corresponding to the stretching of the OH that take part in hydrogen bonds

and three peaks at higher frequencies, corresponding to the free OH stretching modes of the water molecule. The *window region* between the two groups of peaks is taken as an indication of a ring-like structure[17]. Accordingly, only those calculated isomers with ring-like structures are able to reproduce the experimental observations, and therefore, we can conclude that the three water molecules are forming an eight-member ring with the propofol OH moiety. The fingerprint region also confirms such assignment. Note that the chain-like structures interacting with the aromatic ring present an OH stretching mode at c.a. 3650 cm^{-1} which is usually more intense than the theoretically prediction. Such vibration should be clearly observed in the experimental spectra.

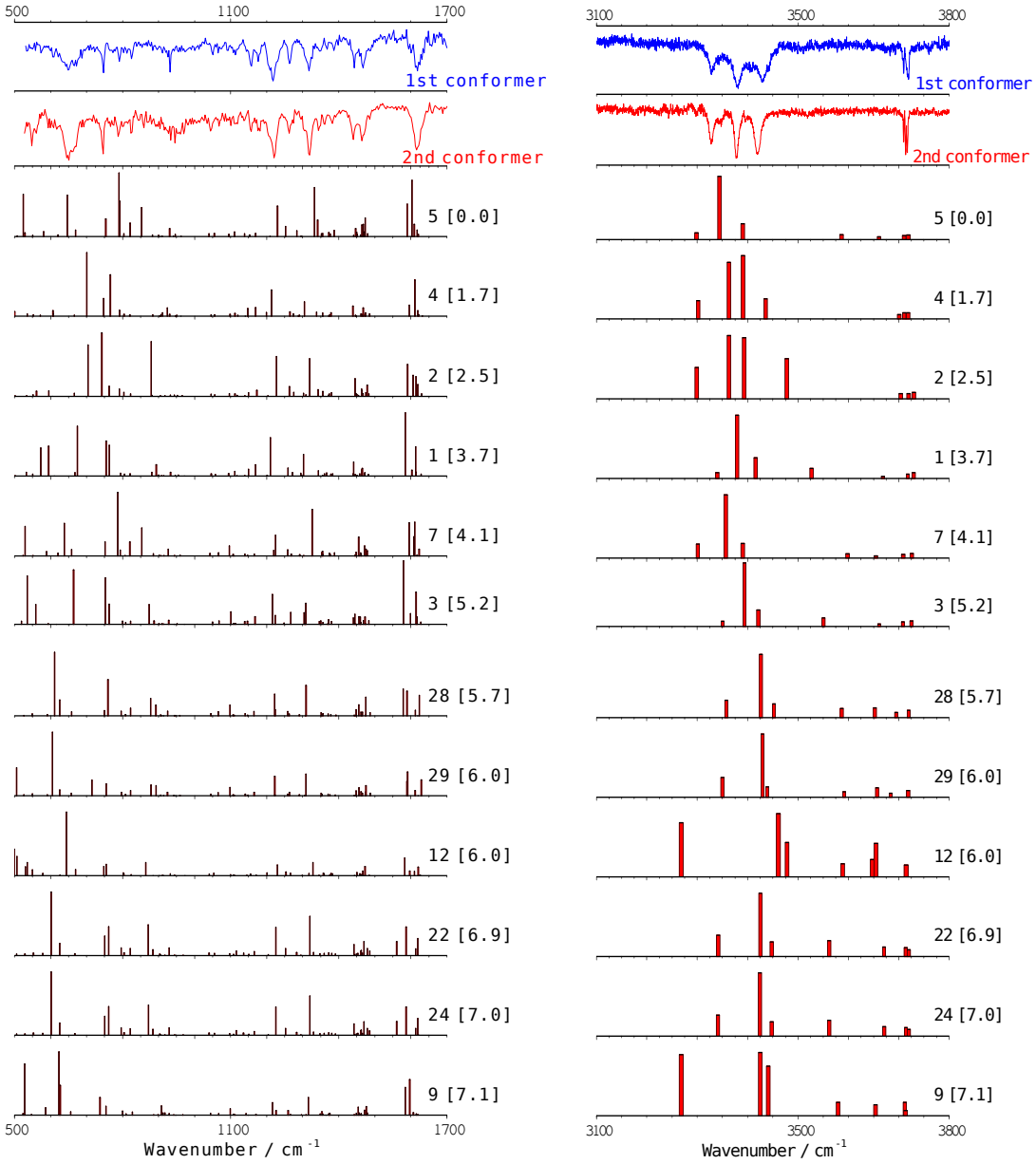

Figure 5.22. *IDIR spectra of propofol·W_3 recorded tuning the probe laser at 36194, and 36255 cm^{-1}. The predicted IR spectra for some of the calculated isomers are also shown for comparison. The numbers in brackets are the relative energies of the calculated conformers, in kJ/mol. A correction factor of 0.938 has been applied. See appendix 7.1, Figure 7.6, for the complete set of simulated spectra.*

The spectra of the complexes on the excited state are presented in Figure 5.23, together with the S_0 trace for comparison. As can be seen, in the *IDIR* spectra of the S_1 state, the electronic excitation causes an increase in one of the OH stretching vibrations

of c.a. 110 cm^{-1} for both conformers. A striking feature is the split of the OH stretching mode at c.a. 3512 cm^{-1} in 4 peaks for the first conformer. The same spectrum has been repeated several times and in all of them such effect was found, which on the other hand, was not found for the second conformer. As it we will discussed, the first conformer could present a change in its geometry in the excited state, which may result in the observed splitting.

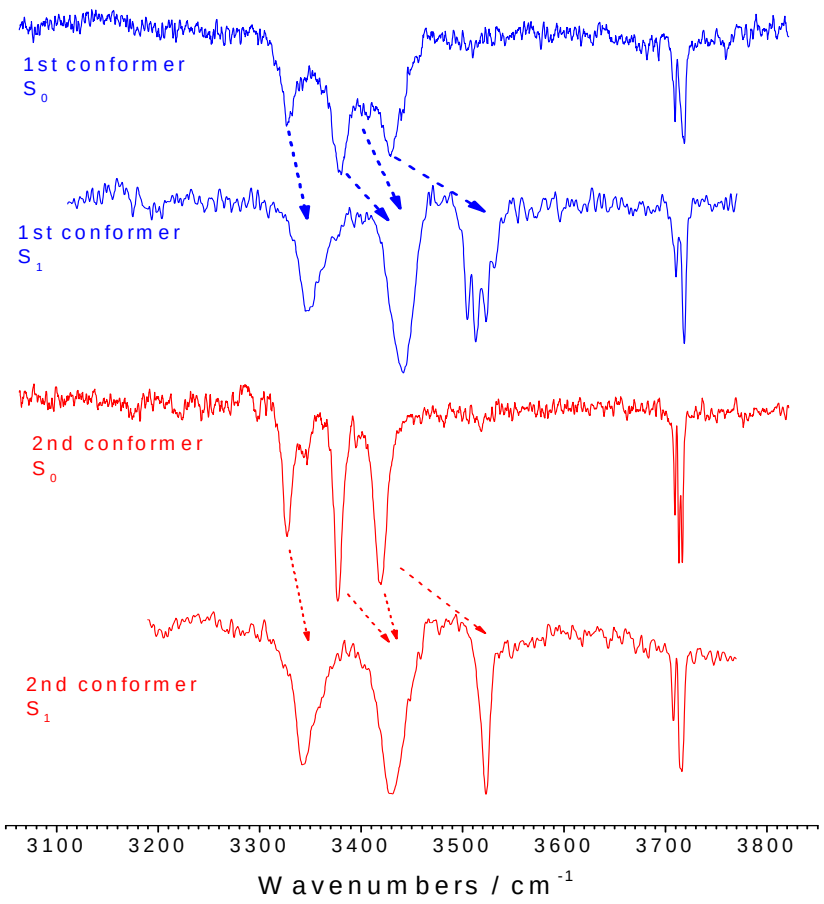

Figure 5.23. *Comparison between ground and excited state IRIDS of propofol·W_3 isomers.*

Assignment

The *2c-REMPI* spectrum of this cluster shows an activity of c.a. 200 cm^{-1} that, as *hole burning* spectrum demonstrates, is due to the presence of two conformers. The intense origin band of the second conformer is located at 36255 cm^{-1}, which means that this conformer is blue-shifted by only ca. 35 cm^{-1} with respect to propofol and propofol·W_2. Such a shift pattern is usually considered as the signature of the formation of a water cyclic structure. On the other hand, the first conformer's origin band, located at 36185 cm^{-1}, is red-shifted ca. 40 cm^{-1} with respect to propofol and propofol·W_2, pointing to a different type of structure.

In order to assign the structures present in the experiments, *IDIR* spectra of both conformers were recorded. The absence of peaks in the 3450-3700 cm^{-1} region clearly indicates that in both conformers water cyclic structures are formed and, as shown in Figure 5.24, only two calculated structures can explain the experimental IR spectrum, i.e. structures *2* and *4* which are shown in Figure 5.25. As can be seen, the only difference between them is the relative orientation of the water cycle respect to the phenolic aromatic ring: in the same plane (structure *2*) and in a perpendicular plane (structure *4*). The small difference between experimental spectra makes difficult to carry out a more precise assignment.

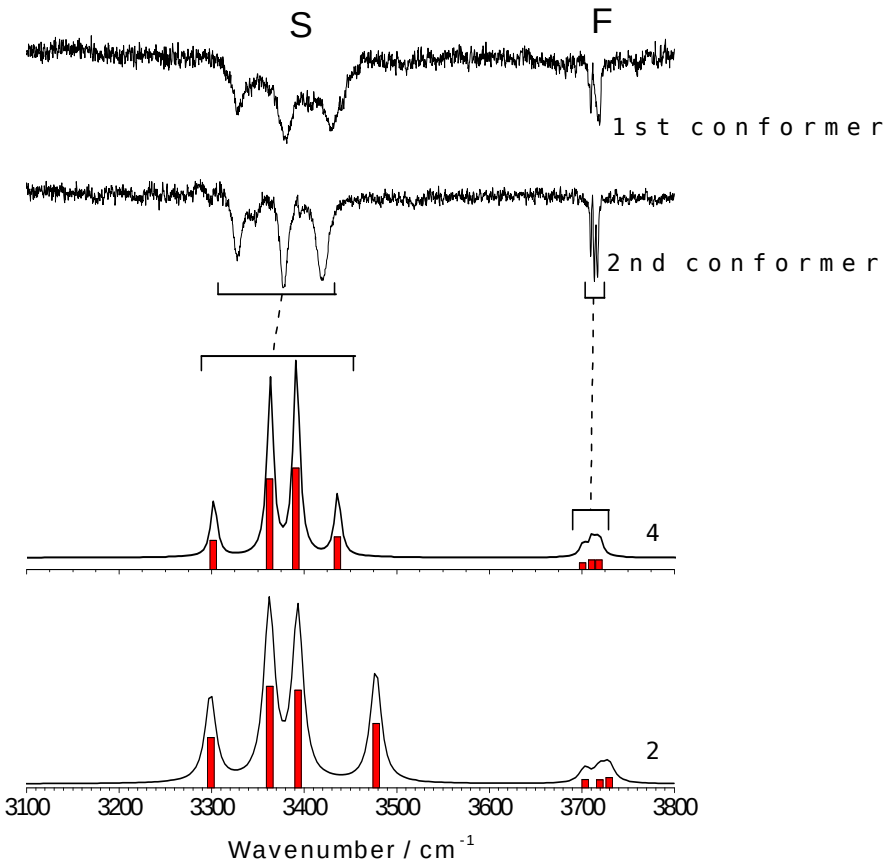

Figure 5.24. *Predicted IR spectra for structures 4 and 2. The experimental IDIR spectra is also shown for comparison. As can be seen the predicted spectra for both structures match reasonably well with the experimental ones for both conformers.*

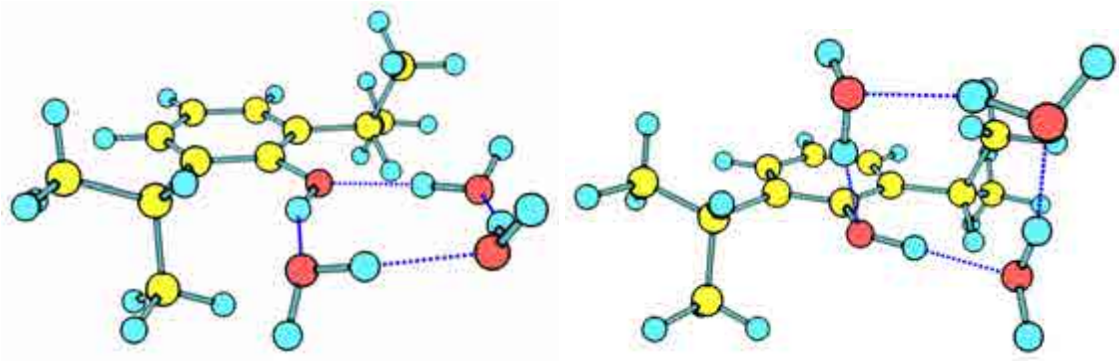

Figure 5.25. *A detailed view of structures 2 (left) and 4 (right), which are the only calculated structures with the water molecules forming a cyclic structure with the propofol OH group, and therefore reproduce the experimental IR spectra.*

However, there are other experimental evidences that may assist in the assignment: the difference in signal intensity between both conformers and the

disappearance of the signal of the weaker conformer when Ne is employed instead of He as buffer gas. The latter, seems to point to a different assignment for the experimental conformers, as it seems to indicate that the detected species present the same water structures, but a different propofol core. On the other hand, such hypothesis would not explain the considerable difference between their origin transitions. To test this hypotheses, a number of calculations were carried out. Figure 5.26. shows the potential energy curve obtained rotating one of the isopropyl groups in 30° steps starting with structure *4*, while the rest of the coordinates are relaxed. A more precise scan was performed around the minimun, taking 10° steps. In this case, the barrier separating GG- and Gg-based structure *4* conformers is ~ 0.2 kJ/mol and therefore is lower than the system's ZPE. The same topography is observed when structure 2 is taken as starting point (Figure 5.27). Consequently, we can rule out the existence of structures based on different bare molecule conformers.

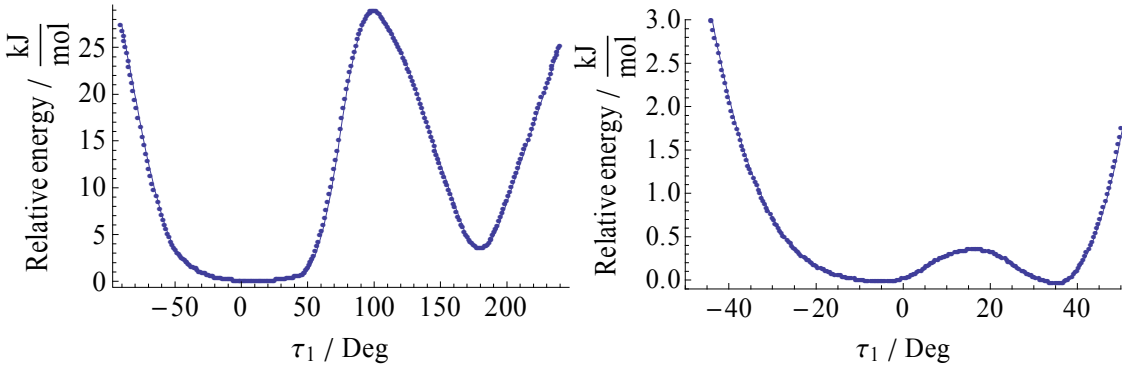

Figure 5.26. *Left: PES calculation of structure 4 rotating one of the isopropyl groups each 30º. Right: a more precise PES calculation of structure 4 rotating one of the isopropyl groups each 10º. Two minima are found with a barrier of only 0.25 kJ/mol between them. Calculations are conducted at B3LYP/6-31++G(d,p) level.*

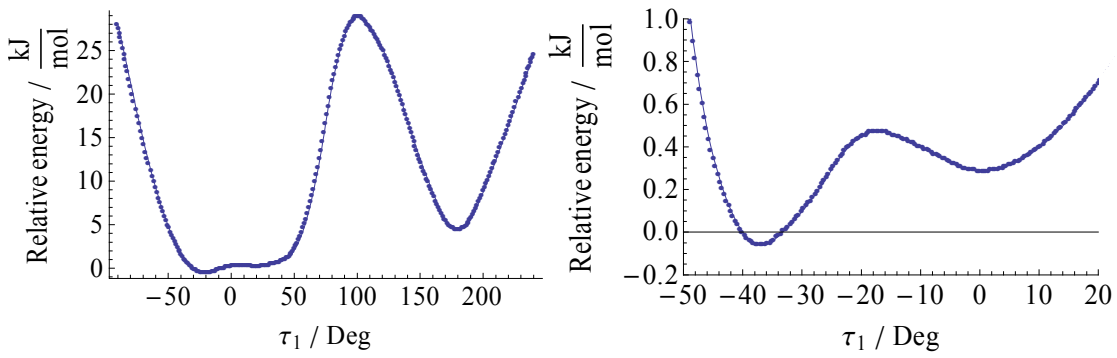

Figure 5.27. *A PES calculation of structure 2 turning one of the isopropyl groups each 30º (left) and 10º (right). Two minima are found with a barrier of only 0.4 kJ/mol between them. Calculations are conducted at B3LYP/6-31++G(d,p) level.*

Then, the behavior of the weaker conformer with the buffer gas must be due to the topology of the PES connecting it with the other conformer. As already stated, the difference between structures *2* and *4* is the orientation of the water ring respect to the aromatic ring. It may well be that, rotating propofol´s OH group around the C-O bond a path connecting both isomers may be found. Figure 5.28 shows the potential energy curve obtained taking structure *2* as starting point and rotating the OH group at 30º steps. It is clear from the Figure that although structure *4* is not reached, a very similar conformer, structure marked in a frame, is separated from structure *2* by a ~ 4 kJ/mol barrier. Repeating the calculation, but using structure *4* as starting point, it is again possible to reach the same structure, surmounting a ~5 kJ/mol barrier, leading to the energy path depicted in Figure 5.29, connecting structures *2* and *4*. The barriers shown in the Figure are high enough to avoid population migration due to collisions with He, although the real topography must be considerably more complicated and one cannot rule out the existence of paths involving changes in a large number of degrees of freedom, such as hydrogen bond distances and angles, that communicate structures *2* and *4*.

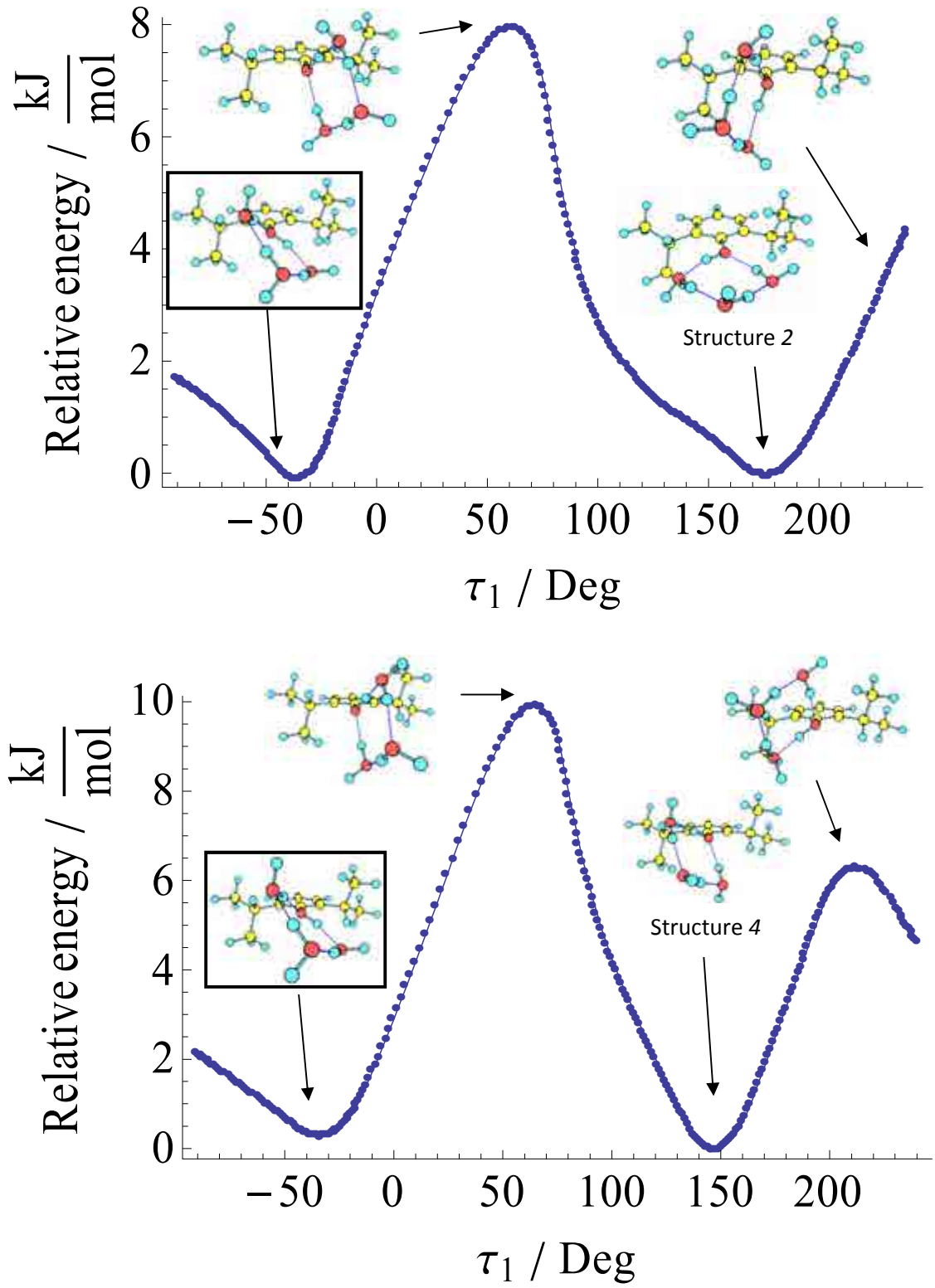

Figure 5.28. *Calculation on the reaction path from structure 2 to structure 4, calculated rotating propofol's OH group in 30° steps. Upper panel: taken structure 2 as stating point, lower panel: taking structure 4 as starting point. Two minima are found in each case, sharing the same transition state at c.a. -40°. Calculations are conducted at B3LYP/6-31++G(d,p) level.*

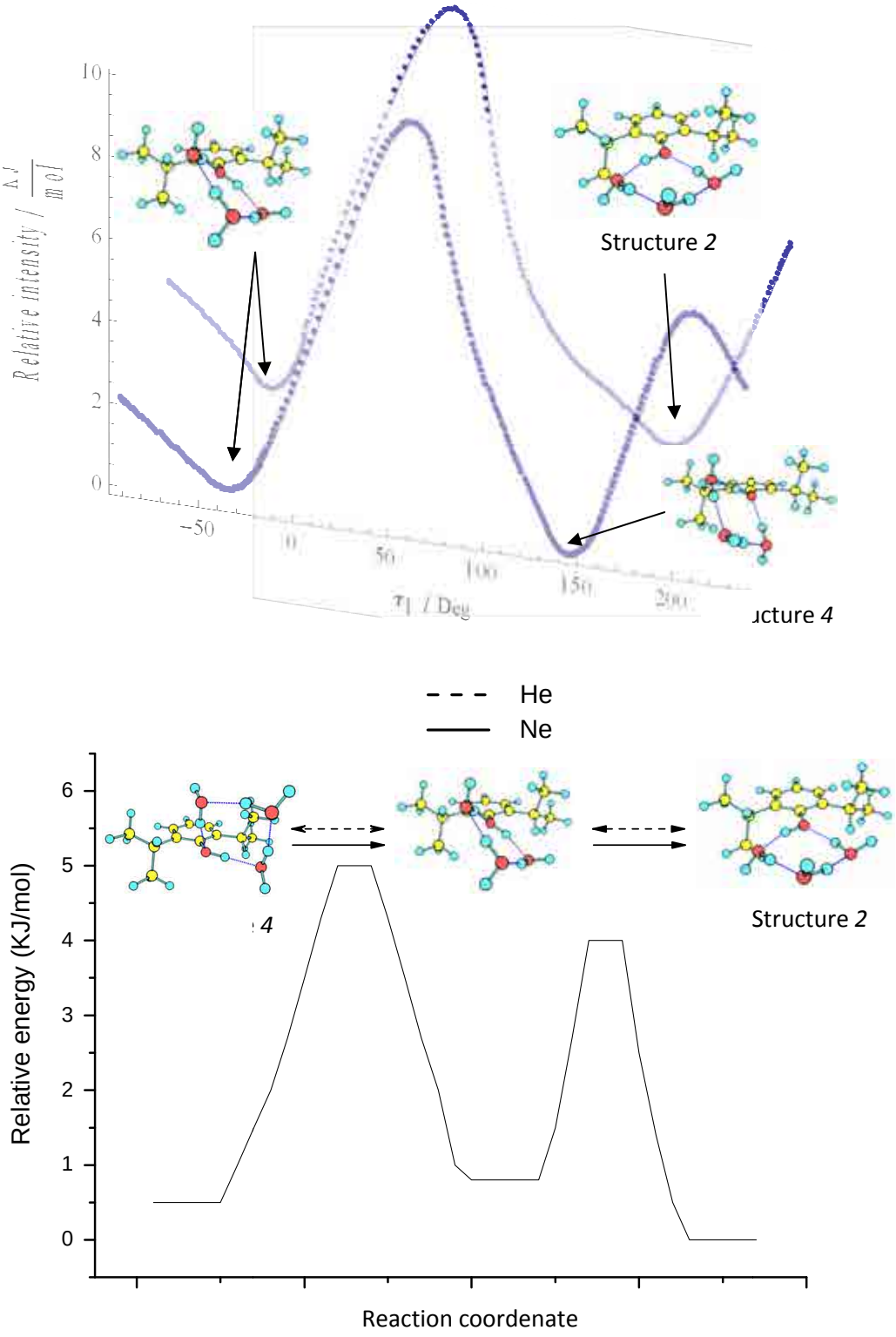

Figure 5.29. *Upper panel: structures 4 and 2 show a common structure, which can be a transition state between both conformers. Lower panel: when using helium (dotted line) both conformers are present, if neon is used instead (solid line), the less stable conformer isomerizes into the most stable and only the latter is found, i.e. structure 2.*

The observed trends in the shifts of the electronic origins of the detected conformers also deserve some attention. As explained before, formation of ring-like structures usually result in a blue shift with the increase in the number of components. However, the first isomer presents a red shift respect to the 1:2 species, which may point to an assignment to a different type of structure. On the other hand, it has been already demonstrated that electronic excitation induces conformational changes in this system and that may well be the present case, hampering a precise location of the 0_0^0 transition. In such situation the more likely explanation is the opening of the water ring, also postulated for other systems.[15] Figure 5.31 shows the calculated reaction path (QST) that connects (ring-like) structure *4* with (open ring) structure *5* (Figure 5.30), calculated at the M06-2x/6-31++G(d,p) level. As can be seen, a small barrier of ~3.5 kJ/mol was found. As in the path between structures *2* and *4*, such value must be taken as an upper limit, as there may exists other trails involving more degrees of freedom with lower barriers. Nevertheless, such value is small enough to justify the absence of structure *5* in the beam. A TD-DFT calculation was carried out in each of the points of the reaction path, and the results are shown in Figure 5.31. The energy order of structures *4* and *5* changes upon excitations, becoming structure 5 considerably more stable.

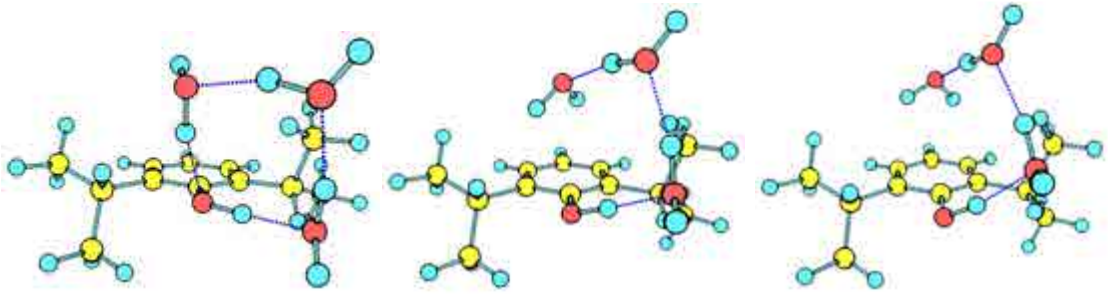

Figure 5.30. *From the left to the right: structure 4, transition state and structure 5.*

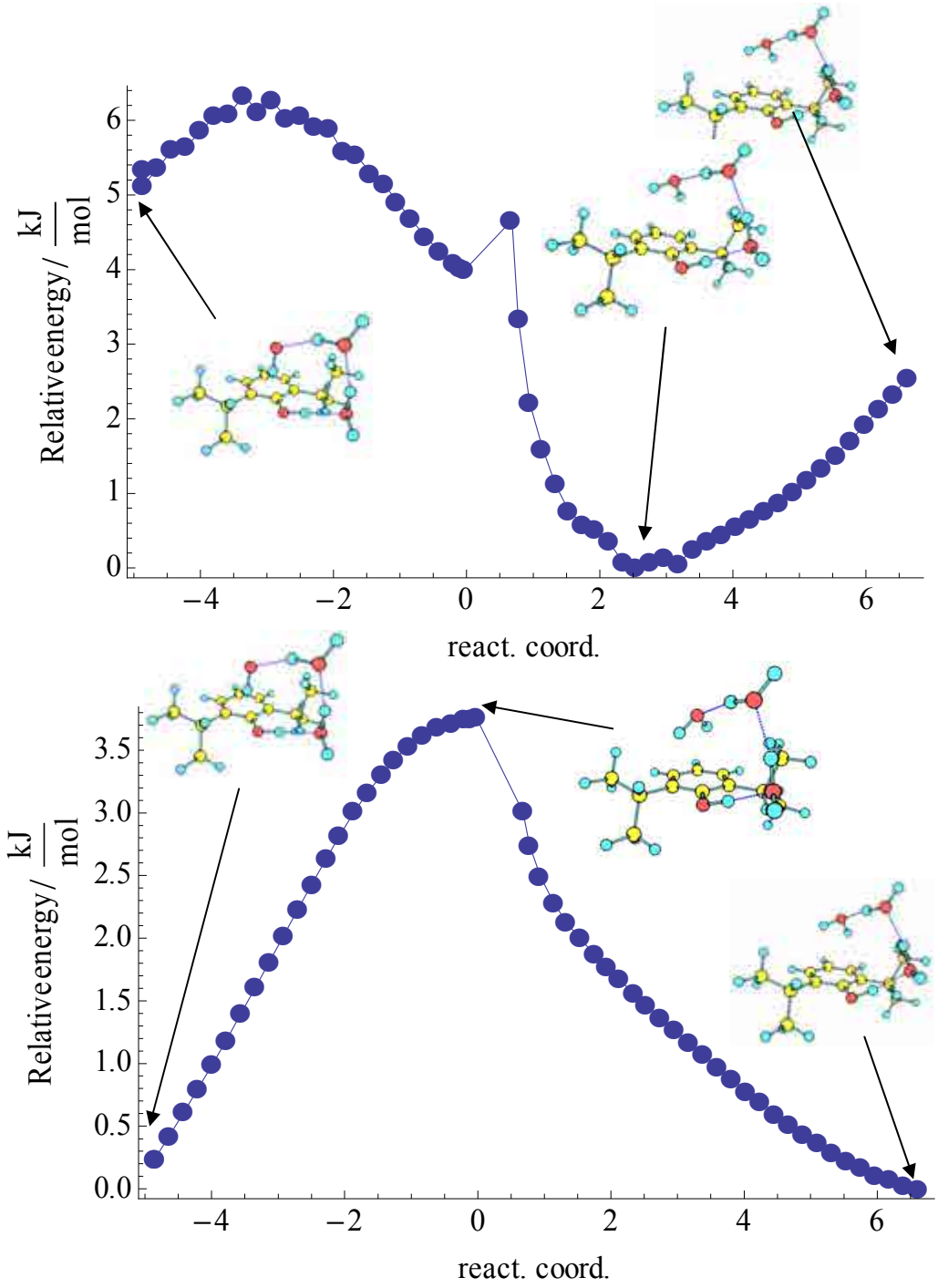

Figure 5.31. *Reaction coordinate along the transition state's negative frequency. For the ground state (lower panel), the transition state corresponds to a maximum for this coordinate but it is a minimum in the rest of the degrees of freedom. Optimization of geometries in each of the extremes of the curve converges into structures 4 and 5. For the excited state (upper panel), the S_0 transition state is close to a minimum.*

Once the conformational change is ruled out as the source of the red-shift observed in the first conformer, the most plausible explanation is the change in the coupling between the phenolic oxygen lone electronic pair and the ring's π cloud with the PhOH angle, leading to a poor coupling and therefore the observed shift may be due exclusively to the HO-H···π interaction in structure *4*. Conversely, in structure *2* there exists a measurable inductive effect, as already reported for similar systems, which result in the observed blue-shifted 0_0^0 transition. The weak intensities found for the first conformer, c.a. 100 times lower than for the second, also indicates that there is a great change in the geometry upon excitation for the former.

5.2.4 – Propofol·W_4

The introduction of a third water molecule increases one order of magnitude the numberof structures in the 20 kJ/mol window. However, only a few structures are statistically meaningful. According to the calculations at M06-2x/6-311++G(d,p) level, the most stable structures (Figure 5.32) are those with the water molecules forming a eight-member ring, which presents a direct interaction with both propofol's aromatic ring and propofol's OH moiety (structures *e33, e16, e157, e25* and *e19* for example) or those structures with a hydrogen-bond network between propofol's OH moiety and the aromatic ring (structures *e32* and *e35*). In the latter, propofol always acts as a proton donor. There is a third type of structures in which the water molecules form a ten-member ring with the propofol's OH moiety, i.e. a macrocycle.

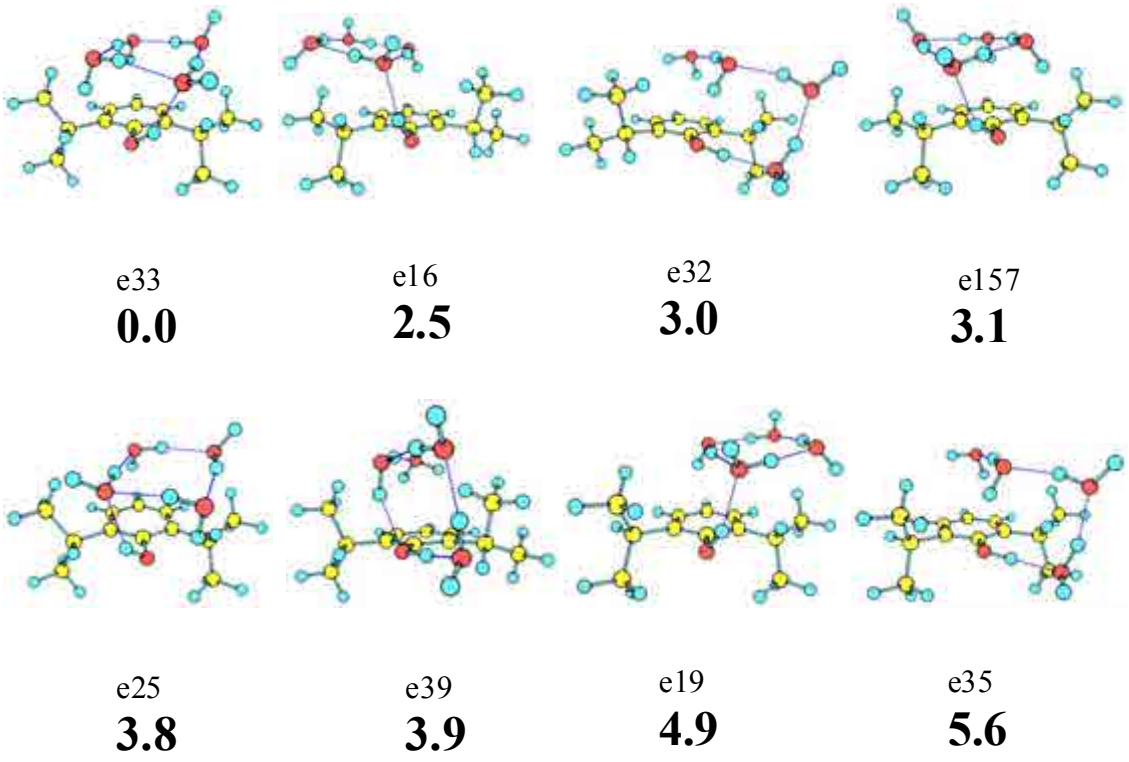

Figure 5.32. *Eight most stable conformers of propofol·W_4 calculated at M06/6-311++G(d,p) level, with their relative energies in bold. Energy values are in kJ/mol. The whole set of structures are collected in appendix 7.1 (Figure 7.7).*

Figure 5.33 shows the *2c-REMPI* spectrum of propofol·W_4, which is considerably different from the rest of the spectra shown so far, as it is mainly a broad absorption, starting at c.a. 35800 cm^{-1} and that extends for more than 1600 cm^{-1}. A few peaks emerge at 36192, 36217 and 36242 cm^{-1}. Comparison with the spectra from

propofol·W_5 and propofol·W_6 species (Figure 5.44) demonstrates that the discrete features are due to fragmentation.

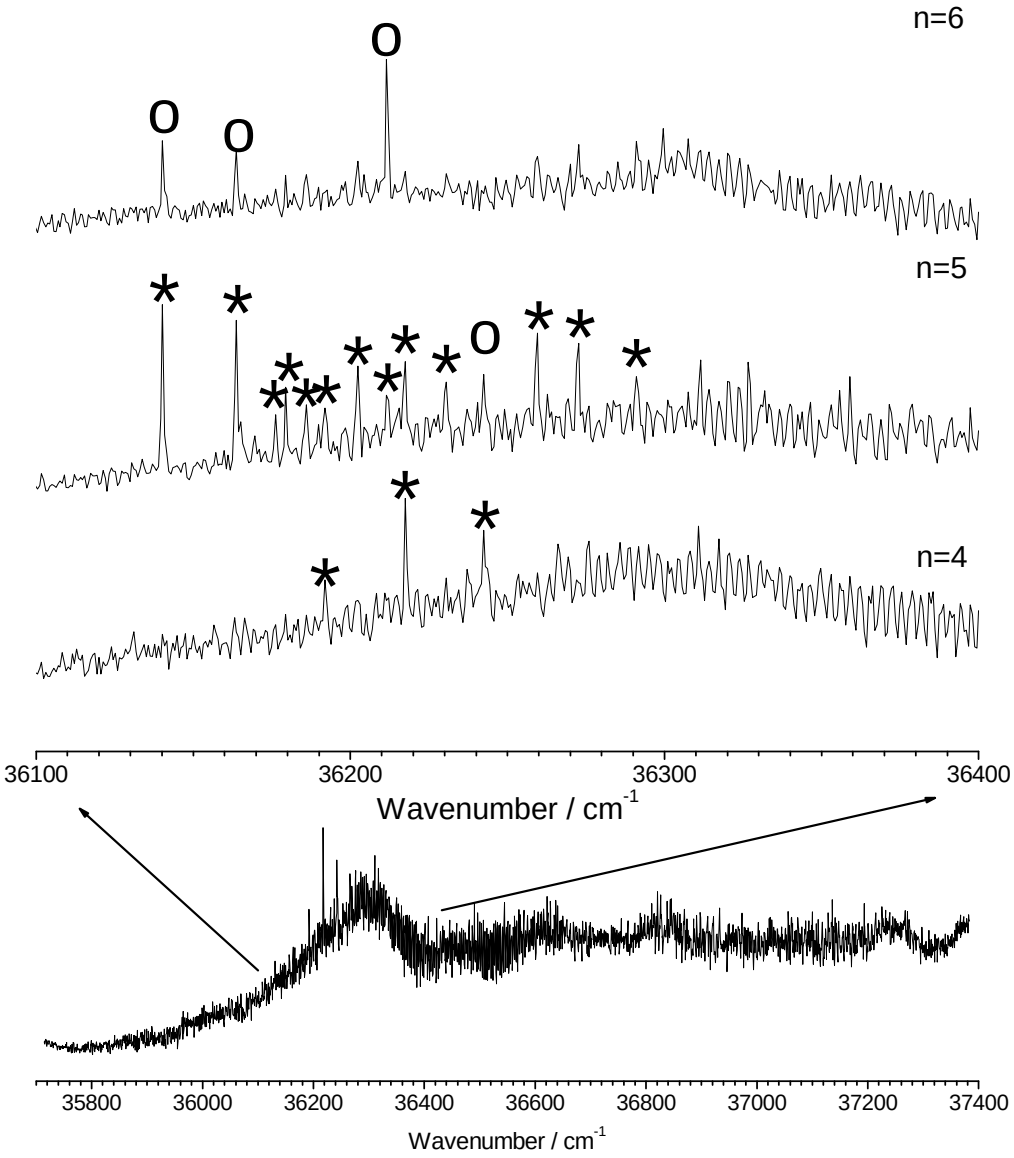

Figure 5.33. *2c-REMPI of propofol·W_4, in the 35700-37400 cm^{-1} region, recorded setting the probe laser at 27972 cm^{-1}. A detailed view of the region with the maximum intensity, together with the same region of the spectra of propofol·W_n n=4-6 is also shown. The peaks labeled with asterisks are due to fragmentation from higher order clusters, while those marked with circles are not. As can be seen, all the peak appearing in propofol·W_4 mass channel, are due to fragmentation, either from propofol·W_5 or propofol·W_6.*

Attempts to record *hole burning* spectra were not successful as a broad absorption was the only result. In order to extract structural information, IDIR spectra setting the laser at different wavelengths along the broad absorption were recorded, obtaining the spectra shown in Figure 5.34. As can be seen, the spectrum seem to be due to propofol·W_4, as it presents the correct number of bands. Also, when studying propofol·W_5 and propofol·W_6 cluster, the broad absorption in the same wavelengths was probed in order to test if this spectrum comes from another cluster but no discrete IR transition was observed, and thus we can conclude that this IR spectrum is due to one conformer of propofol·W_4. As can be seen in Figure 5.34, a peak at 3700 cm^{-1} due to the free OH stretching modes of the water molecules, and surely involving three peaks, is present. The next peak is located at 3623 cm^{-1}, which may be due either to an O-H···π interaction or to a double donor anti-symmetric water OH stretching modes, although in such case, one of the hydrogen bonds must be very weak. The peak located at 3597 cm^{-1} is surely due to the OH anti-symmetric OH stretching mode of a double donor water molecule. The peaks in the red side are due to single donor OH stretching modes and to the propofol's bounded OH.

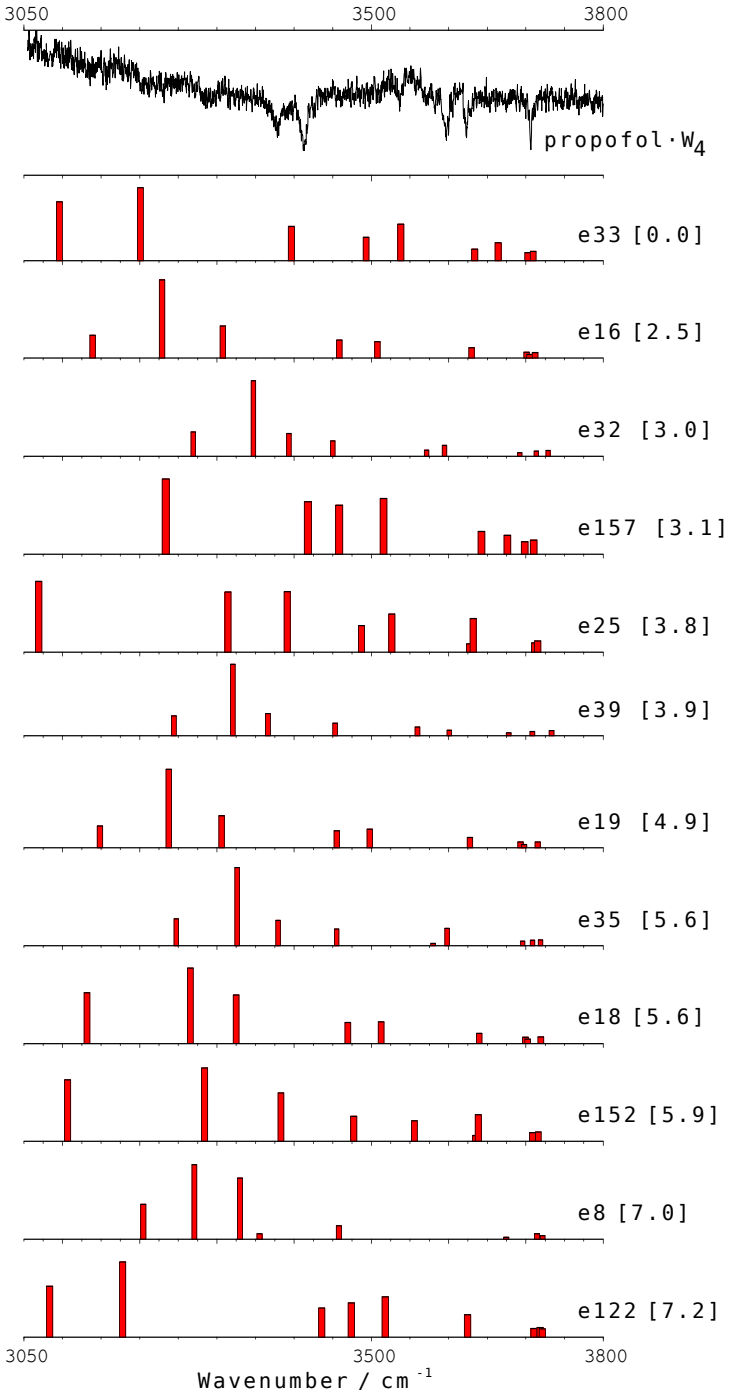

Figure 5.34. *IDIR spectrum of propofol·W_4 recorded tuning the probe laser at 36300 cm^{-1}. The predicted IR spectra for some of the calculated structures are also shown for comparison. The numbers in brackets are the relative energies of the calculated conformers, in kJ/mol. A correction factor of 0.938 is applied to the predicted spectra. The predicted IR spectra of all the calculated structures are collected in appendix 7.1 (Figure 7.8).*

Assignment

The S/N ratio of the IDIR spectrum in Figure 5.34 together with the large number of calculated structures make difficult establishing a univocal assignment for this complex. Therefore we will group the calculated structures with similar predicted spectra before comparing them with the experimental IRID traces.

The **first group** includes those structures in which **the water molecules form an eight-member ring, which presents a direct interaction with both propofol's aromatic ring and propofol's OH moiety**. Structure *e33* (Figure 5.35) is the most stable structure of this group, in which structures *e16, e157, e25, e19, e18, e152, e122, e24, e17, e21, e20, e26, e31 and e120* are also included. We can discard the structures from this group as all of them have some common characteristic which are not present in the experimental spectrum (Figure 5.36): at least two peaks in the 3450–3550 cm^{-1} region and a single peak at c.a. 3625 cm^{-1}. Structures *e146* (Figure 5.35), *15, 14* and *e249* can also be included into this group, although in these structures the propofol molecule is acting as proton acceptor. The predicted spectra for these structures have three separated peaks in the 3300-3425 cm^{-1} region and thus they do not match the observed results either. Also, the red-most peaks over 3600 cm^{-1} do not fit the experimental results.

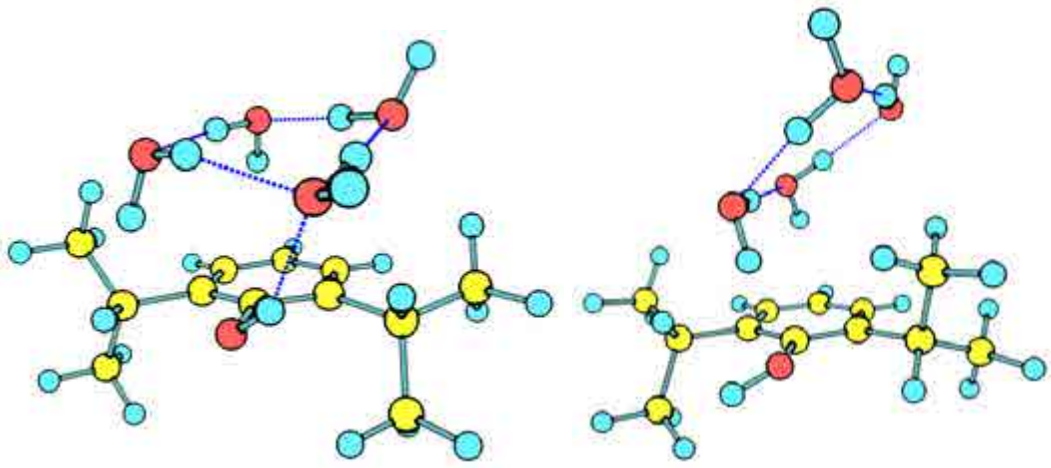

Figure 5.35. *A detailed view of structures e33 and e146 that are representative of the first group, in which the water molecules form a ring, the former with propofol as an acid molecule and as a base in the latter. The structures in this group are also stabilized by an O-H···π interaction.*

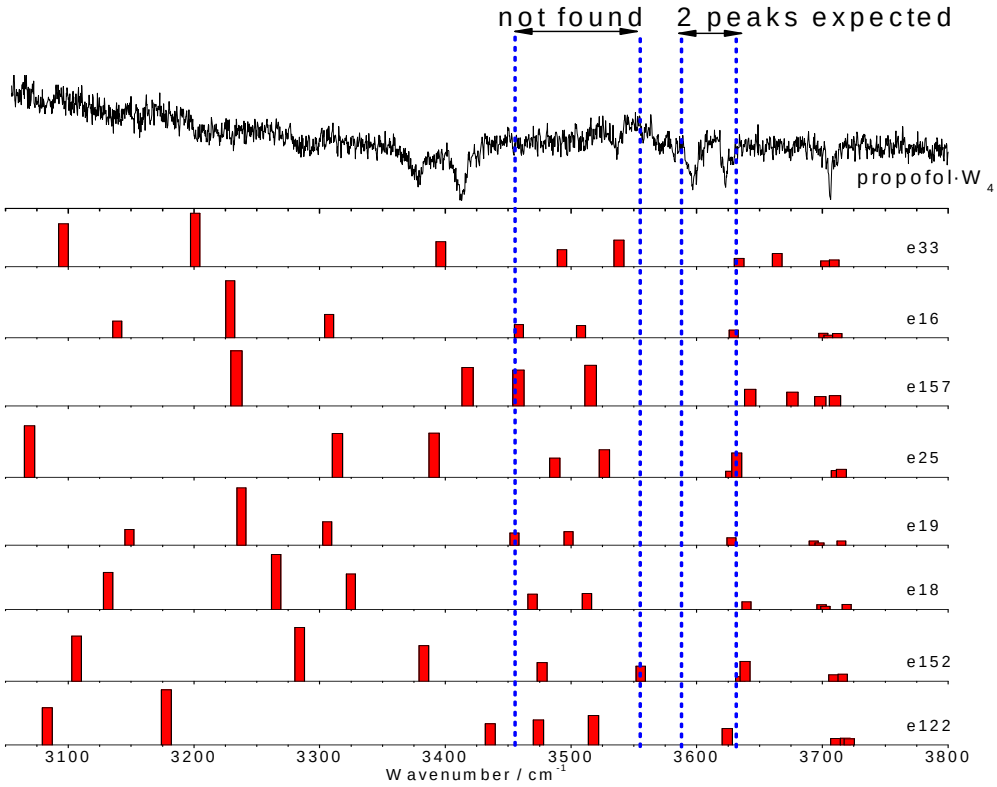

Figure 5.36. *Predicted IR spectra for some of the structures in the first group. The experimental IDIR spectrum is also shown for comparison. As can be seen, the two peaks predicted in the 3450-3550 cm^{-1} region are not found in the experimental trace. Also the experimentally observed peak at 3600 cm^{-1} is missing in the predictions.*

A **second group** consists of the structures forming a **ten-member ring**, involving all the water molecules and propofol's OH moiety, i.e. a **monocyclic** structure.[37] Structures *e8* (Figure 5.37)*, e10, e22, 8, e12* and *e43* belong to this group. The resulting spectra are clearly different from the experimental trace because, as all the molecules are involved in a macrocycle, their OH stretching modes appear very close in frequencies, in the characteristic region for the single-bonded OH stretching, i.e. in the 3100-3450 cm^{-1} range, exhibiting the characteristic *window region*. The two peaks at 3597 and 3623 cm^{-1} clearly show that the molecules are not forming a macrocycle in the detected conformer. Interestingly, the isopropyl groups alters the stability of the cluster, as the structure with the macrocycle in the same plane of the aromatic ring (structure *8,* shown in Figure 5.37) is at 14.5 kJ/mol and a structure where it is placed perpendicular to the aromatic ring (structure *e8*) is at 7 kJ/mol.

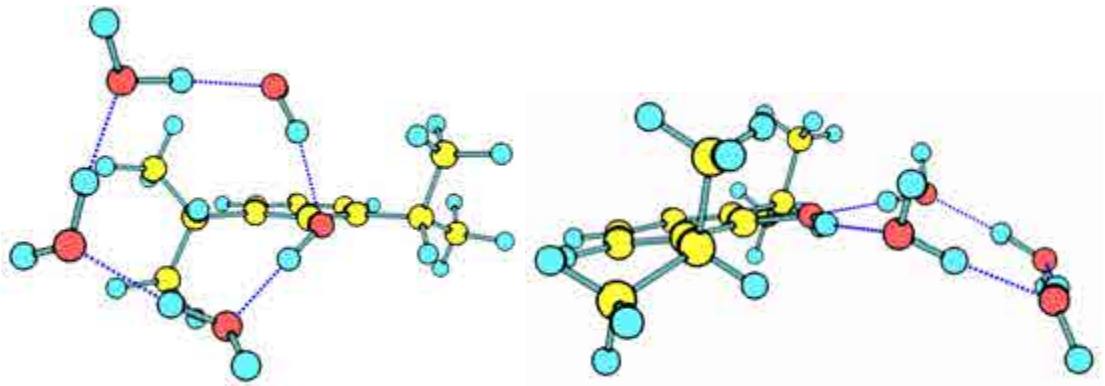

Figure 5.37. *A detailed view of structure e8 (left) and 8 (right) where all the OH moieties are involved in a cyclic structure. This group cannot reproduce the experimental results.*

The **third group** is formed by all the structures in which the water molecules are forming a **hydrogen-bond network** between the propofol's OH moiety and the aromatic ring. There is one water molecule that is interacting with the propofol's OH, group but it is at a distance far from that of an ideal hydrogen bond. Structures *e32, e39, e35* and *e147* belong to this group and, as can be seen in Figure 5.38, the predicted IR spectra **reproduces reasonably well** the experimental results. This structures are also among the most stable ones (*e32, e39* and *e35* are bellow 6kJ/mol). The most stable conformer of this group, *e32*, is shown in Figure 5.39.

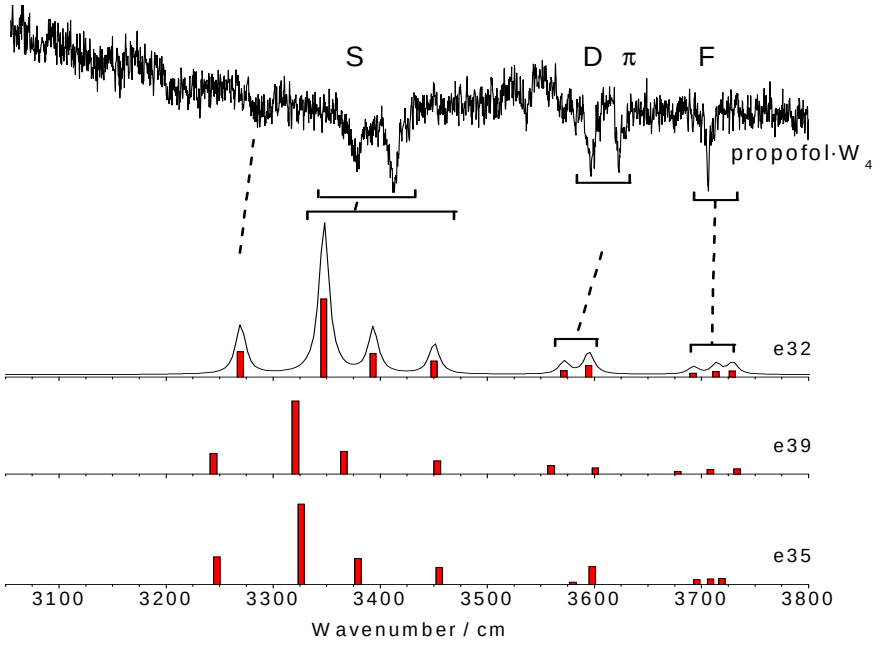

Figure 5.38. *Predicted IR spectra for some of the third group's structures. The experimental IDIR spectrum is also shown for comparison. As can be seen the predicted spectra for this type of structures matches reasonably well with the experimental ones.*

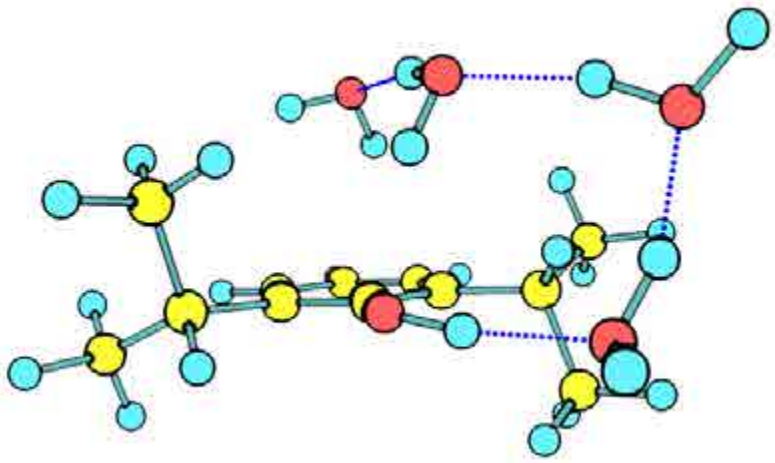

Figure 5.39. *A detailed view of structure e32 that is representative of the third group.*

Structures in the **fourth group** present a 3-dimensional structure that resembles **the *cage* type structure of water$_5$ cluster.**[31] In this group, structures *e121* (Figure 5.40)*, 9, 2, e29, 6, e153, 4* and *e41* are found. Due to the estheric hindrance of the isopropyl groups, the water molecules cannot reach an appropriate position to conform a 3-dimensional structure, and thus, the predicted IR spectra present peaks scattered along

the 3400-3715 cm^{-1} region. Nevertheless, their spectra present at least two peaks in the 3450-3550 cm^{-1} region which are not found in the experimental trace.

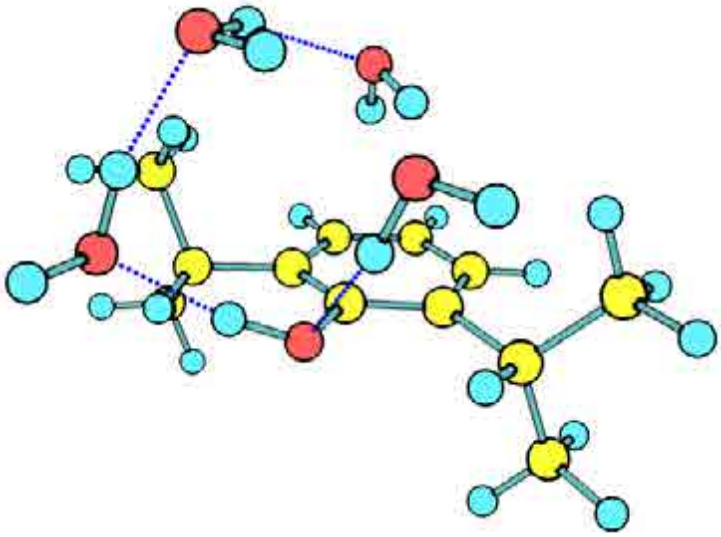

Figure 5.40. *A detailed view of structure e121 that is representative of the fourth group.*

A **fifth group** can be formed with the structures in which the water molecules form an **envelope**[37] with the propofol's OH group. For example, structures *e23* (Figure 5.41) and *e36*. Again, their predicted spectra are considerably different from the experimental one.

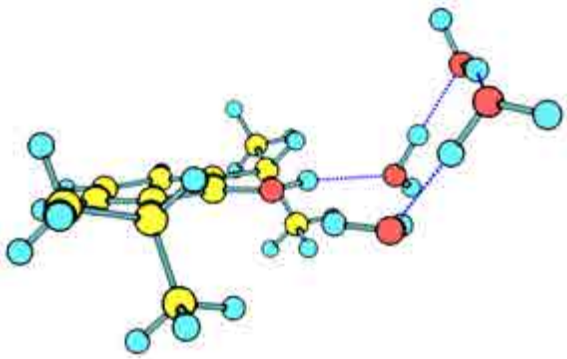

Figure 5.41. *A detailed view of structure e23 that is representative of the fifth group.*

The rest of the structures present their own peculiarities and thus, they cannot be groped: structures where a hydrogen-bond network is attached to the propofol, or nearly-cage type structures over the ring, water chains interacting with the propofol's

OH moiety on one side and another water molecule interacting with the same functional group but from the other side, etc, … they all present different features in the IR region failing in completely reproduce the experimental results.

Thus the IR spectrum of the experimentally found structure corresponds to the third group. Table 5.1 offers a tentative assignment of the IR spectrum, using structure *e32* the most stable structure of the third group, as a guide.

Table 5.1. *Vibrational assignment of propofol·W_4 IR spectrum for structure e32.*

Experimental Peak (cm^{-1})	**structure *e32***		
	Frequency (cm^{-1})	Intensity	Vibrational type
3285	3269	424	σ_s^s (OH_w)
3378 (x2 peaks)	3347	1309	σ (OH_{ppf})
	3393	396	σ_s^s (OH_w)
3412	3450	266	σ_s^d (OH_w)
3596	3572	109	σ_{as}^d (OH_w)
3623	3595	194	$\sigma^{O\text{-}H\cdots\pi}$ (OH_w)
3707 (x3 peaks)	3692	64	σ^f (OH_w)
	3714	91	σ^f (OH_w)
	3729	100	σ^f (OH_w)

5.2.5 – Propofol·W_5

Molecular mechanics calculation yields more than a thousand stable structures for this cluster in a 20 kJ/mol window, which compared to the hundreds of structures found for propofol·W_4, suggest a more complicated landscape. According to the calculations at M06-2x/6-311++G(d,p) level, there are mainly three families of structures (Figure 5.42): one with the water molecules in a *book*-type arrangement (structures *e30, e27, e29, e23*), another one with the water molecules forming a ten-member ring, hydrogen bonded to the propofol's OH moiety (structures *e28, e33*) and a third one in which the water molecules form a pentameric structure with propofol's OH group and the fifth water molecules interacts both with the chain of water and with propofol's aromatic cloud (structure *e46*).

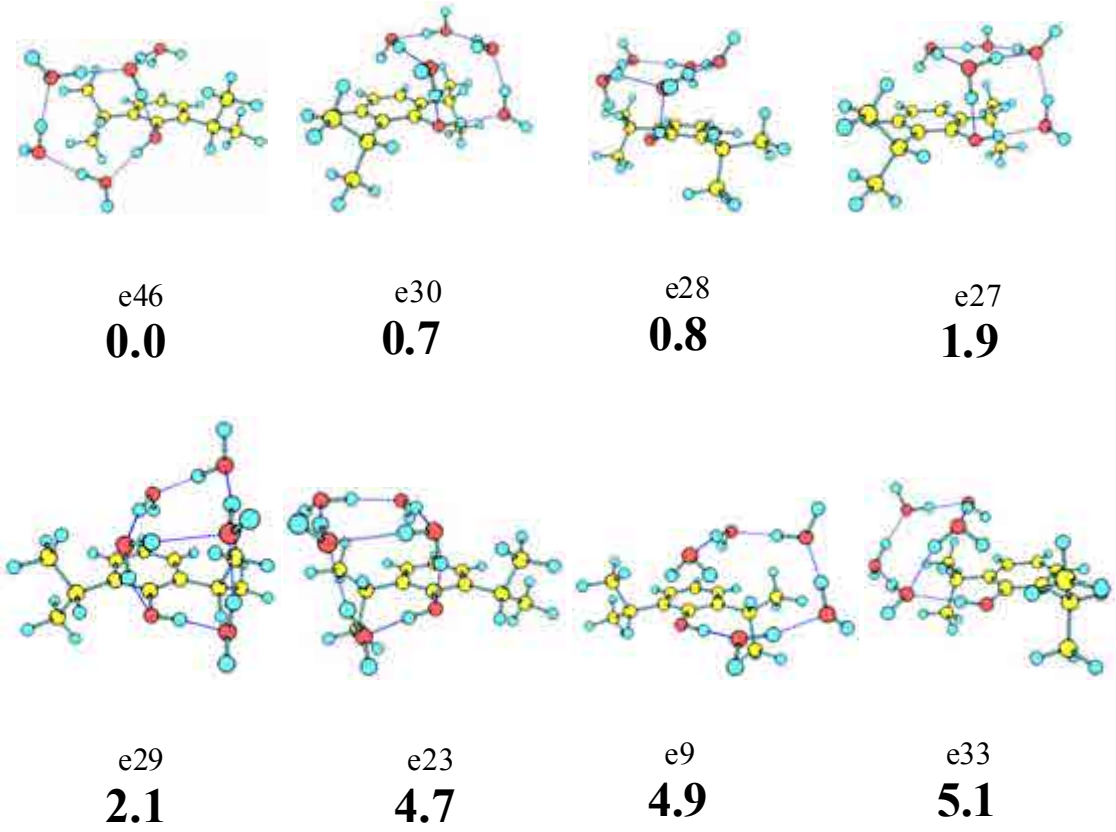

Figure 5.42. *Propofol·W_5 eight most stable conformers calculated at M06-2x/6-311++G(d,p) level, with their relative energies in bold. Energy values are in kJ/mol. The complete set of calculated structures is presented in appendix 7.1 (Figure 7.9).*

Figure 5.43 shows the *2c-REMPI* spectrum of propofol·W_5. Like in propofol·W_4, a broad absorption takes place from 36100 cm^{-1} to 37400 cm^{-1}. Some peaks in the 36140 to 36350 cm^{-1} region can be distinguish, which are close to the bare molecule transition (36224 cm^{-1}). In order to see if fragmentation is taking place, Figure 5.56 shows a comparison between the *2c-REMPI* spectrum of propofol·W_5 and those of propofol·W_6 and propofol·W_7. As can be seen, all but the peaks located at 36242, 36312 and 36327 cm^{-1}, are due to fragmentation.

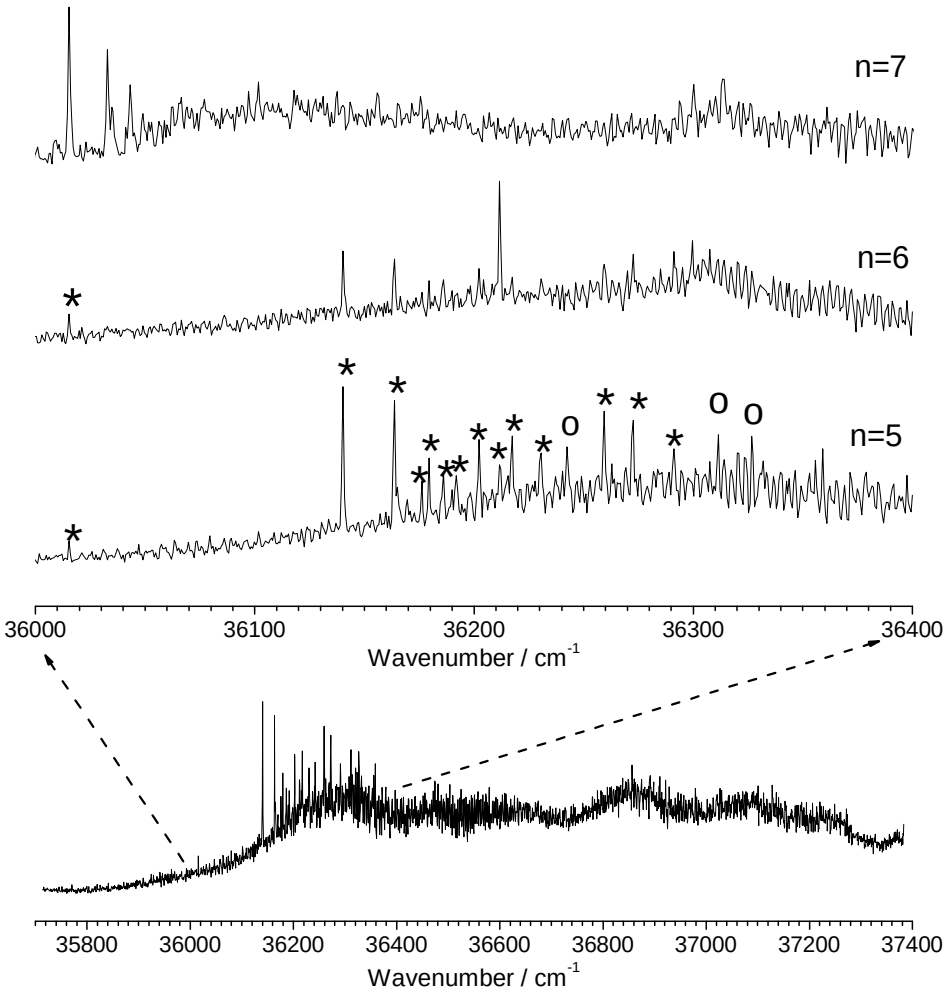

Figure 5.43. *2c-REMPI of propofol·W_5, in the 35700-37400 cm^{-1} region, recorded setting the probe laser at 27972 cm^{-1}. A detailed view of the region with the maximum intensity, together with the same region of the spectra of propofol·W_n n=5-7 is also shown. The peaks labeled with asterisks are due to fragmentation from higher order clusters, while those marked with a circle are not. As can be seen, most of the peaks are due to fragmentation.*

Two conformers were obtained using *hole burning*, probing the transitions at 36242 and 36312 cm^{-1} (Figure 5.44). The S/N ratio of the *hole burning* traces is not as good as for other species and therefore, only a few features, apart from the origin bands, can be identified for each conformer.

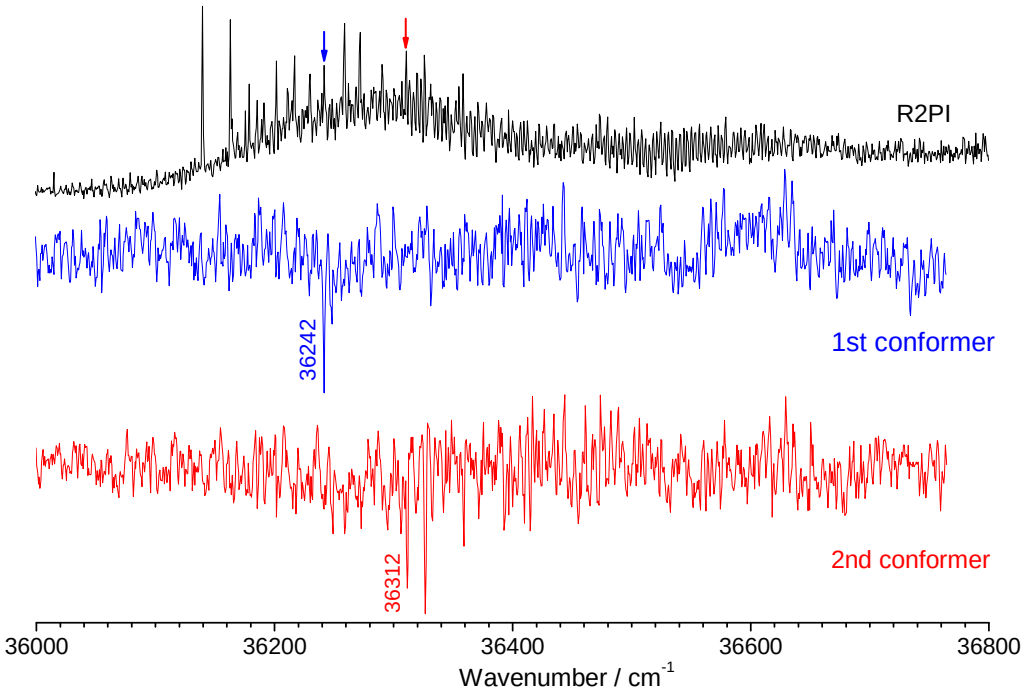

Figure 5.44. *Hole burning traces of propofol·W_5 recorded tuning the probe lasers (2-color detection) at 36242 and 36312 cm^{-1}. The peaks noted with arrows indicate the transitions employed for recording the hole burning spectra, as well as the IDIRS trace for each of the conformers.*

Figure 5.45 shows the IDIR spectra of both conformers, recorded setting the probe laser at 36242 and 36312 cm^{-1}. In order to test if there are additional conformers, different parts of the broad absorption were probed, but no different IR spectra were obtained. The IR spectra of both conformers present some similarities: they both show some peaks, presumably three, in the blue part of the spectrum, at c.a. 3700 cm^{-1}, due to free OH stretching modes of water molecules. They both also present an intense peak at c.a. 3640 cm^{-1} that usually is due to an O-H···π interaction. Some peaks are present in the 3500-3700 cm^{-1} region, which indicate that no window-region is present so the structures are not cyclic. Conversely, double-donor water molecules must be involved in

the structure. The strong and broad peaks in the red part of the spectrum (3250-3450 cm^{-1}) are due to single-donor OH stretching vibrations and to propofol's bounded OH stretching. The main difference between the IR spectra of both conformers is the peak located at 3600 cm^{-1} in second conformer and not seen in the first one, and a peak at 3200 cm^{-1} in the spectrum of the first conformer.

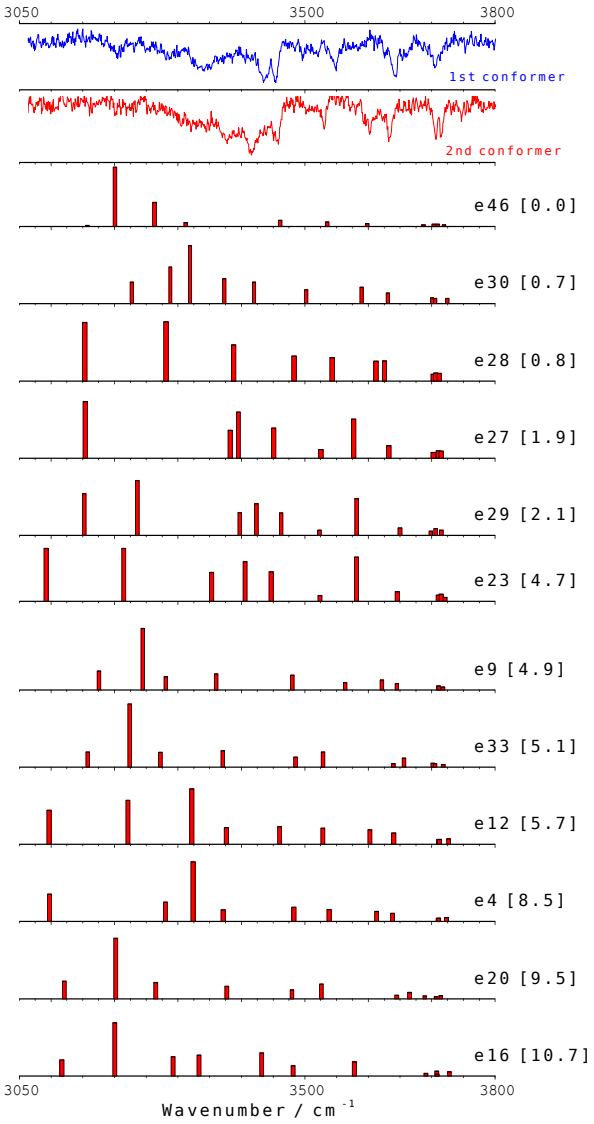

Figure 5.45. *IDIR spectra of propofol·W_5 recorded tuning the probe laser at 36242 and 36312 cm^{-1}. The predicted IR spectra for some calculated structures are also shown for comparison. The numbers in brackets are the relative energies of the calculated conformers, in kJ/mol. A correction factor of 0.938 was applied. The predicted IR spectra of all the calculated structures are recorded in appendix 7.1 (Figure 7.10).*

Assignment

The large number of structures found in the conformational search, some of them differing in the orientation of a single OH bond, makes impractical to carry out a univocal assignment and therefore, we will group the structures into families with similar structures, i.e., with analogous spectra.

The **first group** collects those structures with the water molecules and the propofol's OH moiety **forming a book-type structure**. Such arrangement resembles one of the most stable types for water$_6$[31] (ej. structures *e16 and e6,* Figure 5.46). The predicted IR spectra for this group fail to reproduce the experimental results, as they lack the peak at 3640 cm^{-1}, which is present in both conformers.

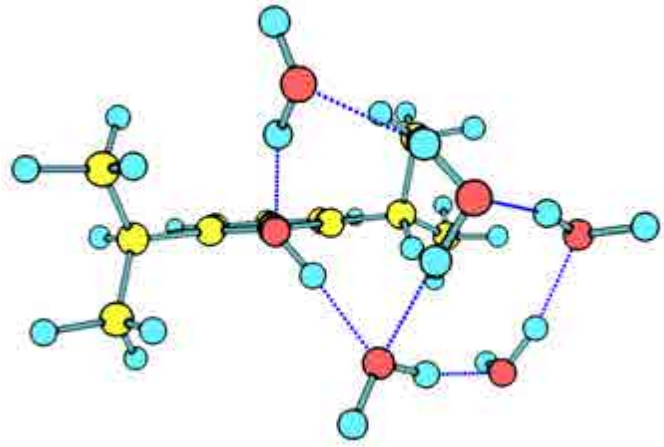

Figure 5.46. *A detailed view of structure e16 that is representative of the first group, where the OH moieties conform a book-type structure interacting with one of the isopropyl groups. This group fails in reproducing the experimental results.*

A family of structures with the water molecule in a ***book*** **conformation constitutes the second group**. The difference with the first group is the **existence of an OH···π interaction**. Structures *e30, e27, e29* and *e23* are components of this group, being the first one the most stable specie (Figure 5.47). As can be seen in Figure 5.48, their predicted spectrum **reproduces very well** the experimental results for **the second conformer**, and therefore, they are taken as the structure of propofol·W_5 second conformer. Additionally, this family contains some of the most stable structures calculated for this stoichiometry, being all of them in a c.a. 5 kJ/mol window.

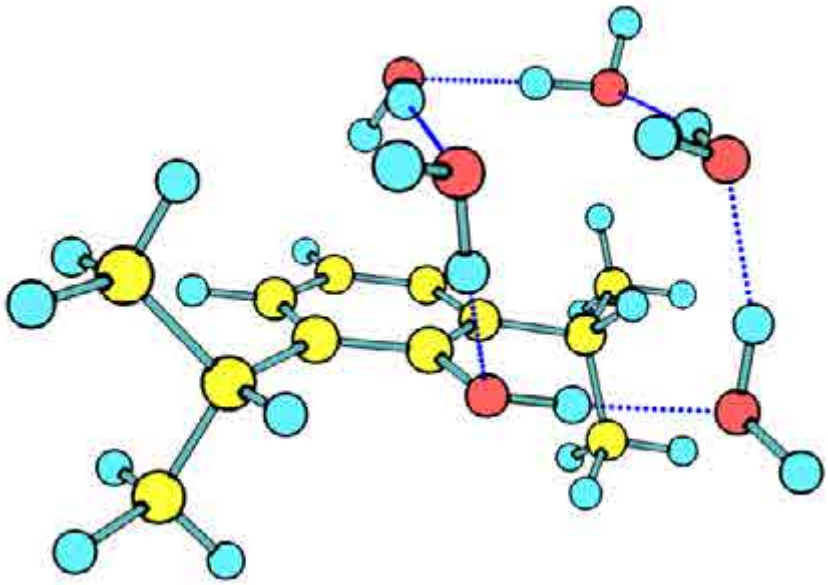

Figure 5.47. *A detailed view of structure e30 that is representative of the second group. The OH moieties conform a book-type structure interacting with the aromatic ring. This kind of structures is able to reproduce the experimental results for the second conformer.*

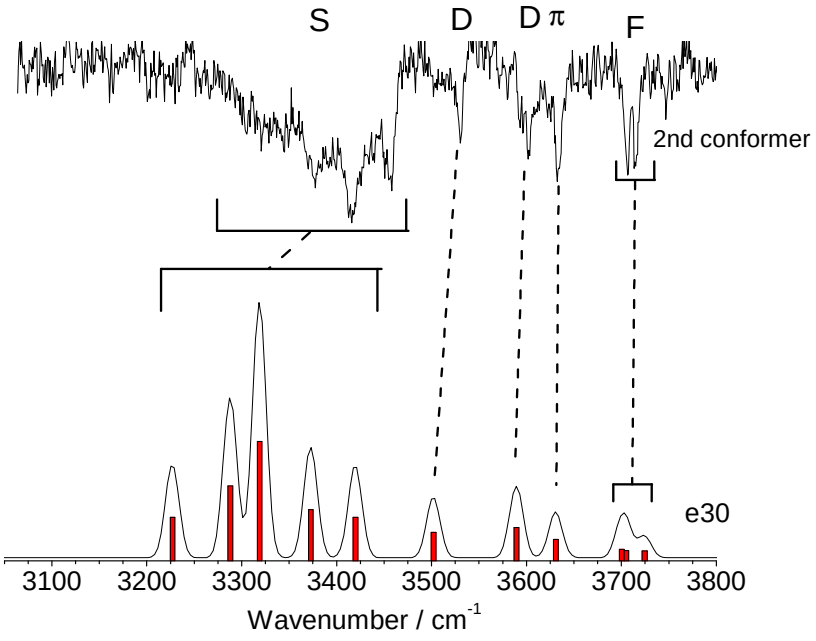

Figure 5.48. *Predicted IR spectrum for structure e30, the global minimum of the second family calculated for propofol·W_5. The experimental IDIR spectrum is also shown for comparison. As can be seen, the predicted spectrum for this type of structures matches the spectrum of the second conformer.*

The **third group** gathers these structures in which the **water** is forming a **pentagon over the propofol** molecule interacting with the OH group (Ph-O-H···OH_2) and with the aromatic ring via an O-H···π interaction. Structures *e28* (Figure 5.49)*, e33, e12, e4, e20* and *e41* are in this group. Their predicted spectra systematically **fail in reproducing** the 3300-3500 cm^{-1} region of the experimental trace. Structures *e7* (Figure 5.49)*, e5, e24, e22, e32* and *11* can also be englobed into this group, with the only difference with the previous being a displacement of the water's pentagon from interacting with the propofol's oxygen and thus, one of the peaks at c.a. 3625 cm^{-1} now appears in the 3700 cm^{-1} region. Being that the only difference, they also fail in predicting any of the experimental conformers.

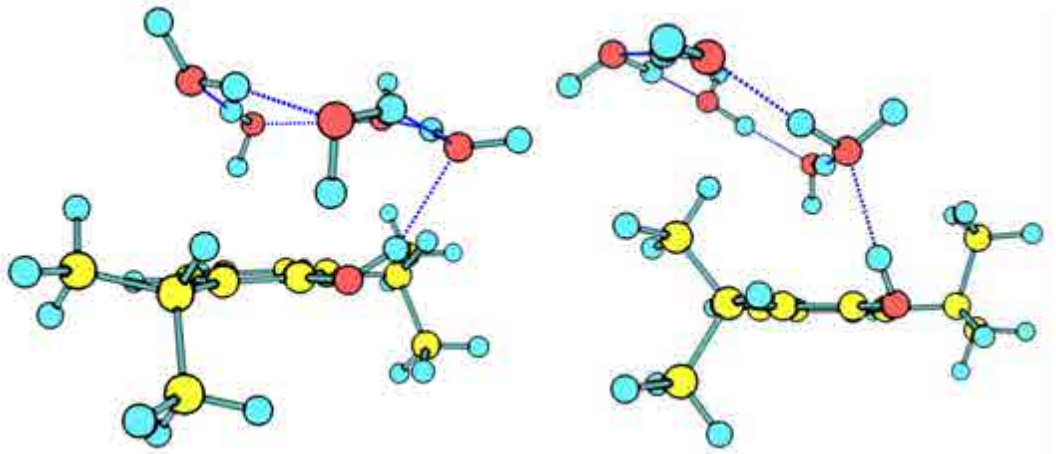

Figure 5.49. *A detailed view of structures e28 (left) and e7 (right) that are representative of the third group. None of them explain the experimental spectra of any of the conformers.*

In structures *1*, *e2*, *e39* and *e15* the water molecules form a hexagon with propofol's OH, i.e. **a macrocyclic structure**, and they form the **fourth group** (Figure 5.50). As all the OH bands are involved in a cyclic structure, the IR region presents the characteristic *window region*. Neither of the two experimentally obtained conformers exhibits such a spectral feature and therefore these structures can be discarded. In addition, such structures are considerably less stable, over 15 kJ/mol, than the global minimum.

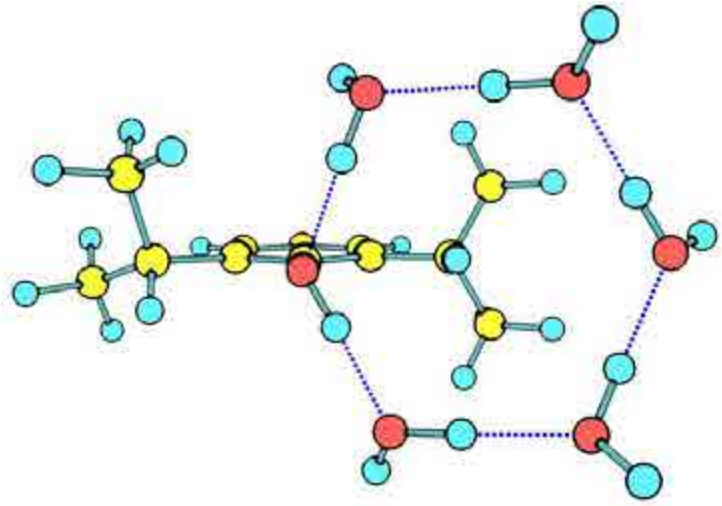

Figure 5.50. *A detailed view of structure 1 that is the fourth group's global minimum. These macrocyclic structures are not able to explain the experimental results for any of the conformers.*

The rest of structures present particular characteristics and thus they form a heterogeneous group. In any case, their spectra cannot reproduce the experimental traces. It is worthy to note that no *prism* or *boat* structures were found for this cluster, the former being one of the most stable structures for the $water_6$ cluster. Most of the structures in this heterogeneous group present several water molecule(s) attached to either the ring or the propofol's OH moiety, or water molecules forming a chain, with the only common characteristic of presenting spectra absolutely different from those recorded.

On the other hand, there is one type of structure that **reproduces** the IR experimental spectrum for **the first conformer** very satisfactorily: **Structure 3** (Figure 5.51), presents four water molecules forming a eight-member ring over the propofol molecule and one of them acts as a proton-donor to the propofol's OH moiety; another one interacts with the aromatic ring via a O-H···π interaction. The remaining water molecule is interacting directly only with the propofol's OH moiety, with the latter acting as a proton donor. This peculiar structure, which is located at a relative high energy almost 30 kJ/mol, reproduces accurately the experimental IR spectrum, as shown in Figure 5.52.

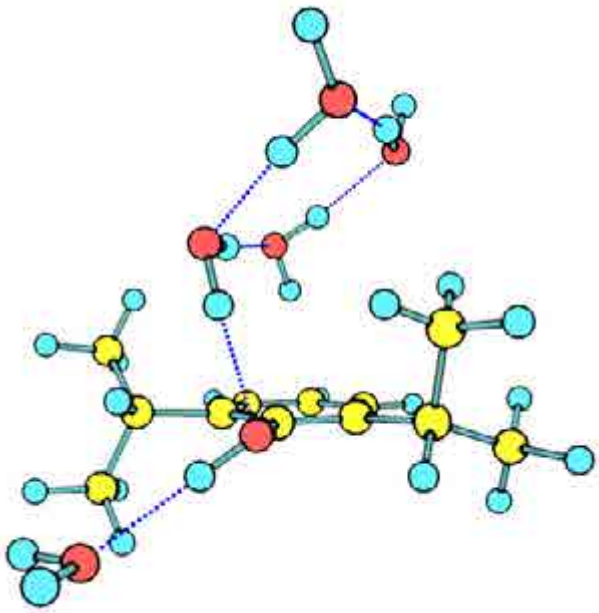

Figure 5.51. *A detailed view of structure 3 that is representative of the third group. The predicted spectrum for this structure matches with that of the first conformer.*

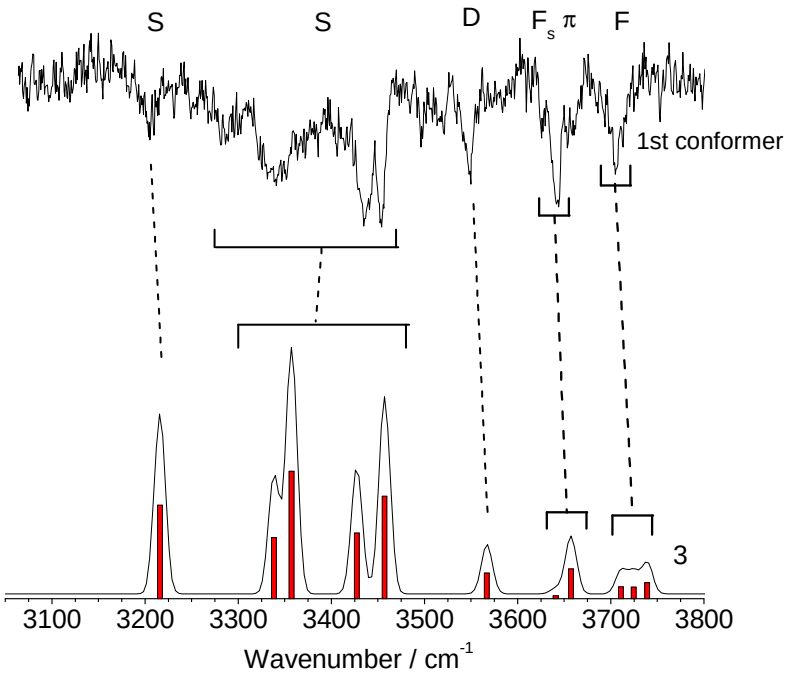

Figure 5.52. *Predicted IR spectrum for structure 3. The experimental IDIR spectrum is also shown for comparison. As can be seen, the predicted spectrum for this structure matches the experimental one for the first conformer.*

Thus, the first conformer corresponds to structure *3* and the second conformer to one of the structures of the second group. The OH stretching modes for each of the conformers are collected in Table 5.2 and compared with the structure *3* for the first conformer and with the most stable conformer in the second group, structure *e30*, for the latter.

Table 5.2. *Experimental vibrational transitions in the IR traces of propofol·W_5 first and second conformers, with a tentative assignment based on a comparison with the calculated frequencies for structures 3 and e30.*

Experimental Peak (cm^{-1})	**structure *3***		
	Frequency (cm^{-1})	Intensity	Vibrational type
3210	3216	650	σ_s^s (OH_w)
3341 (x2 peaks)	3338	426	σ_s^d (OH_w)*
	3357	887	σ_s^s (OH_w)
3436	3427	456	σ_s^s (OH_w)
3452	3457	712	σ (OH_{ppf})
3548	3567	178	σ_{as}^d (OH_w)
3644 (x2 peaks)	3641	20	$\sigma^{f\text{-}s}$ (OH_w)
	3657	209	$\sigma^{O\text{-}H\cdots\pi}$ (OH_w)
3705 (x3 peaks)	3711	85	σ^{f} (OH_w)
	3724	80	σ^{f} (OH_w)
	3739	113	σ^{f} (OH_w)

* This stretching vibration is coupled with the other ring vibrations. This explains its unusual red-shift for a double donor.

Experimental Peak (cm^{-1})	**structure *e30***		
	Frequency (cm^{-1})	Intensity	Vibrational type
3314 (x2 peaks)	3227	384	σ_s^s (OH_w)
	3288	658	σ_s^s (OH_w)
3378	3319	1049	σ (OH_{ppf})
3416	3373	453	σ_s^s (OH_w)
3430	3420	382	σ_s^d (OH_w)
3530	3502	250	σ_s^d (OH_w)
3602	3590	294	σ_{as}^d (OH_w)
3632	3631	188	$\sigma^{O\text{-}H\cdots\pi}$ (OH_w)
3710 (x3 peaks)	3700	103	σ^{f} (OH_w)
	3705	93	σ^{f} (OH_w)
	3725	89	σ^{f} (OH_w)

5.2.6 – Propofol·W_6

Molecular mechanics calculation yields of the order of ten thousand stable structures for this cluster in a 20 kJ/mol window. There is a considerable increase in the number of different structures found for propofol·W_6, which indicates a substantial change in the possibilities of water forming diverse structures around or with the propofol molecule. According to the calculations at M06-2x/6-311++G(d,p) level, the most stable structures (Figure 5.53) are those with a *chair*-type structure[31] (with the propofol's OH involved in the structure, structures *e13, e5, e1, e8*), a *book*-type structure attached to the propofol's OH (structure *e9*), *prism* types (structure *e12*) and other tridimensional structures (structure *e17*).

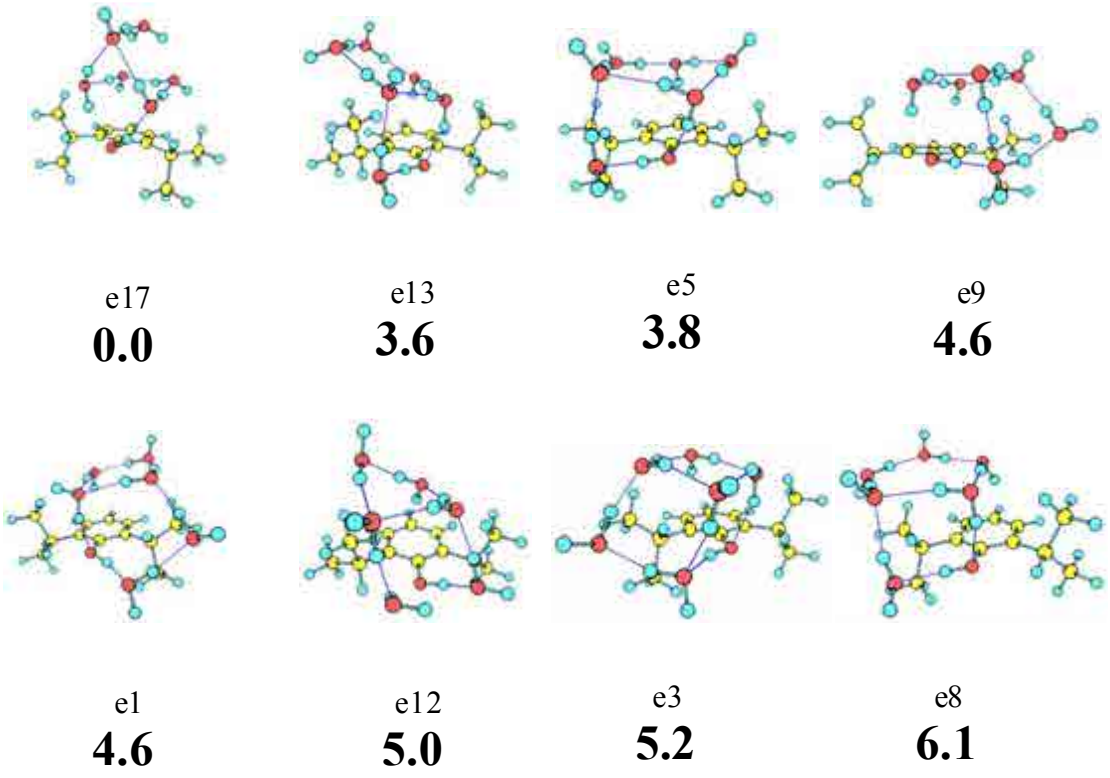

Figure 5.53. *Propofol·W_6 eight most stable conformers calculated at M06-2x/6-311++G(d,p) level, with their relative energies in bold. Energy values are in kJ/mol. The complete set of calculated structures can be found in appendix 7.1 (Figure 7.11).*

Figure 5.54 shows the *2c-REMPI* spectrum of propofol·W_6. As it happens with the previous propofol·W_4 and propofol·W_5 clusters, a broad absorption covers the 36100-37400 cm^{-1} region, where some peaks can be distinguish starting from 36140 cm^{-1}. Figure 5.43 shows a comparison of the *2c-REMPI* spectrum of propofol·W_5 and

with propofol·W_6 and propofol·W_7. A clear reduction on the fragmentation is observed, as only the peak at 36000 cm^{-1} seems to be due to fragmentation. Therefore the peak located at 36140 cm^{-1} is taken as the first transition for this conformer. Fragmentation from higher order clusters can be reduced by decreasing either the probe laser's intensity or either the 2º color laser's intensity, so, in order to record the *2c-REMPI* spectrum of propofol·W_6 cluster very low power of both lasers was used.

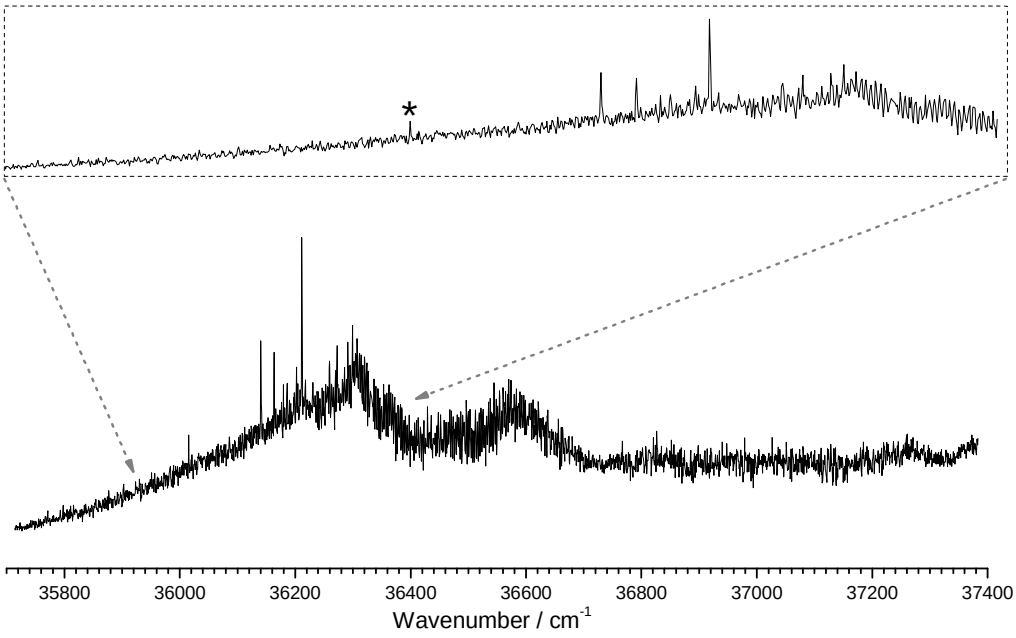

Figure 5.54. *2c-REMPI of propofol·W_6, in the 35700-37400 cm^{-1} region, recorded setting the probe laser at 27972 cm^{-1}. The insert shows a detailed view around the origin. The peak marked with an asterisk is due to fragmentation from propofol·W_7.*

To determine the number of conformers present, *hole burning* experiments were carried out probing the transitions at 36140 and 36212 cm^{-1} and finding two isomers (Figure 5.55). For the first conformer some peaks can be seen clearly, while a single peak is found for the second one.

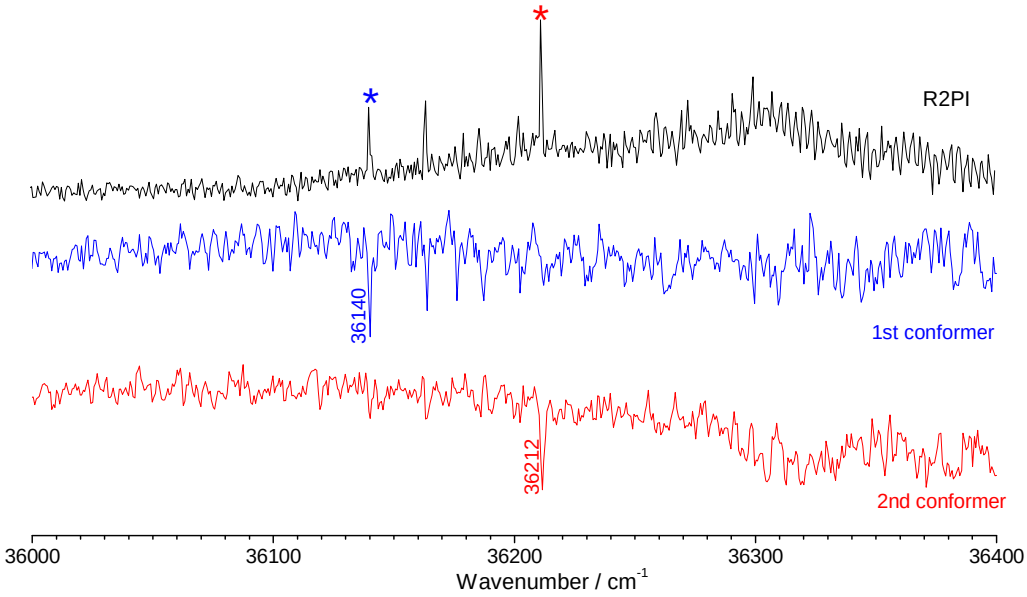

Figure 5.55. *Hole burning traces of propofol·W_6 recorded tuning the probe lasers (2-color detection) at 36140 and 36212 cm^{-1}. The peak noted with asterisk indicate the transitions employed for recording the hole burning spectra, as well as the IDIRS trace for each of the conformers.*

As for previous systems, IDIR spectra of both conformers were done setting the probe laser at 36140 and 36212 cm^{-1} (Figure 5.56), as well as probing at different parts of the broad absorption, but no additional conformers were found. The IR spectra of both conformers are not identical, although they share some similarities: the (presumably three) peaks in the blue region, are due to free OH stretching modes of water molecules. No *window region* is present and, in both cases, the last peaks is found at c.a. 3250 cm^{-1}. The main difference between both IR spectra is a peak located at 3625 cm^{-1}, only present for the first conformer, which most surely is due to an O-H···π interaction.

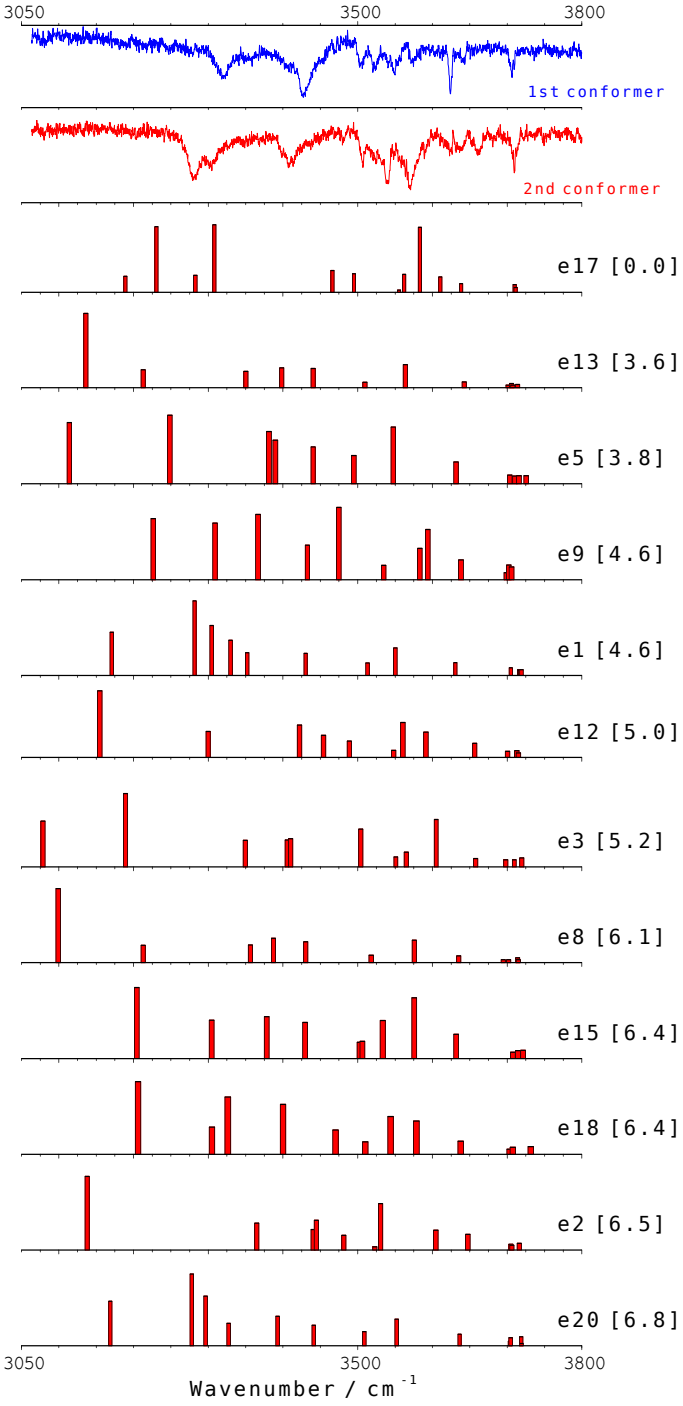

Figure 5.56. *IDIR spectra of propofol·W_6 recorded tuning the probe laser at 36242 and 36312 cm^{-1}. The predicted IR spectra for the calculated structures are also shown for comparison. The numbers in brackets are the relative energies of the calculated conformers, in kJ/mol. A correction factor of 0.938 was applied. The predicted IR spectra of all the calculated structures are recorded in appendix 7.1 (Figure 7.12).*

Assignment

As it happens with propofol·W_6, a considerable amount of structures was found in the calculations, and therefore a univocal assignment is unattainable. Thus, we have grouped the calculated structures in families with similar (or identical) spectra.

The **first three groups** are formed by structures with the water molecules forming a **chair-type** structure **with** propofol's OH, but with **different orientations**: in the first group propofol's OH forms part of the eight-member ring and the ten-member ring is directly over the aromatic ring as is the case for structures *e13* (Figure 5.57)*, e5, e8, e23* and *8*. In the second group, propofol's OH forms part of the ten-member ring while the eight-member ring is interacting with the aromatic ring as seen for structures *e1* and *e20* (Figure 5.57). In the structures of the third group, such O-H···π interaction is not present, see for example structures *e22, e28, e14, e16, e19* and *e2619* (Figure 5.57). These differences result in considerably different predicted IR spectra, and against what it could be expected as this type of structure is within the most stable ones for $water_7$, none of them reproduce the experimental spectra.

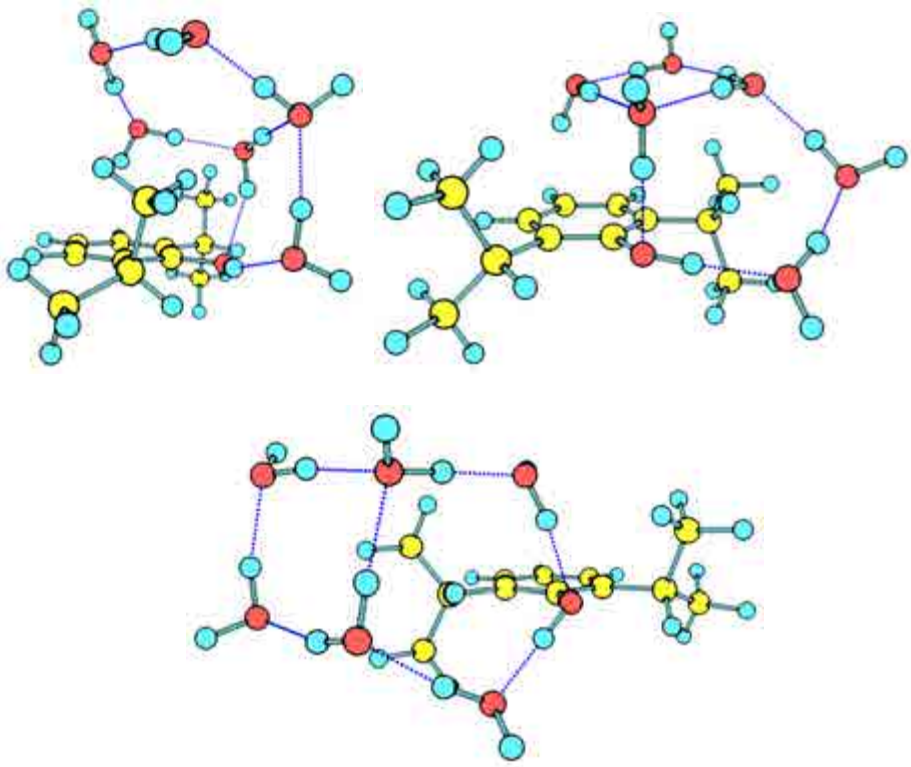

Figure 5.57. *A detailed view of structures e13, e1 and e22 that are representative of the first, second and third groups respectively. They belong to chair-type structures but none of them match the experimental results.*

The **fourth and fifth groups** consist of **prism** structures, **differing** only **in their orientation**: in the forth group, the base of the prism is formed by the propofol's OH and two water molecules, while the top is formed by the remaining four water molecules. In the fifth group, one of the faces of the prism is now composed by propofol's OH moiety, one of the water molecules and the aromatic ring. Structures *e15*, *e2, e12* and *e6* form part of the fourth group and structures *e12, e18* and *11* of the fifth group (Figure 5.58). Both groups **reproduce very well the experimental IR spectra**, but the special feature presented in the structures on the fifth group, the O-H···π interaction, indicates that the **second conformer** has a structure similar to those on the **fourth group** while the **first conformer** structure must be like those on the **fifth group** (Figures 5.59 and 5.60).

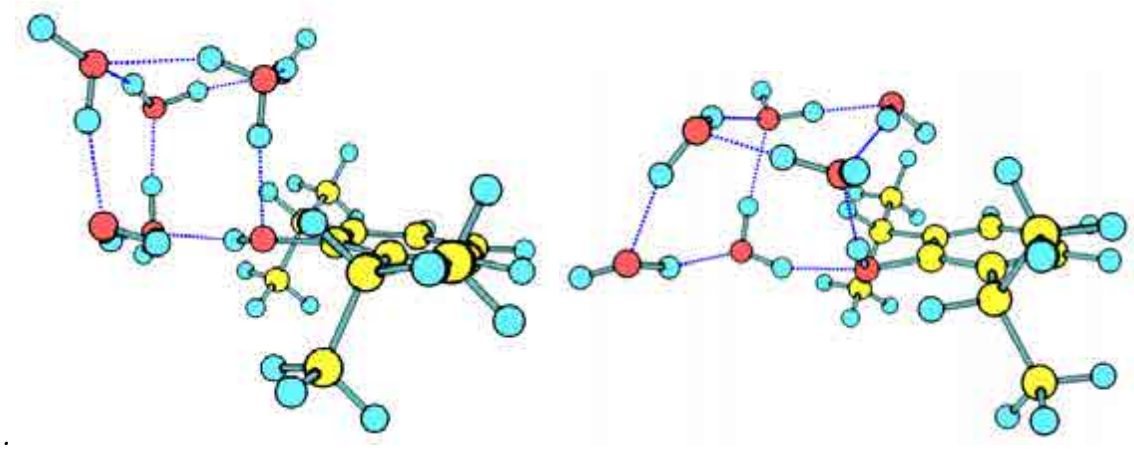

.

Figure 5.58. *A detailed view of structures e6 and e18 that are representative of the fourth and fifth groups respectively. A prism-type structure can be seen.*

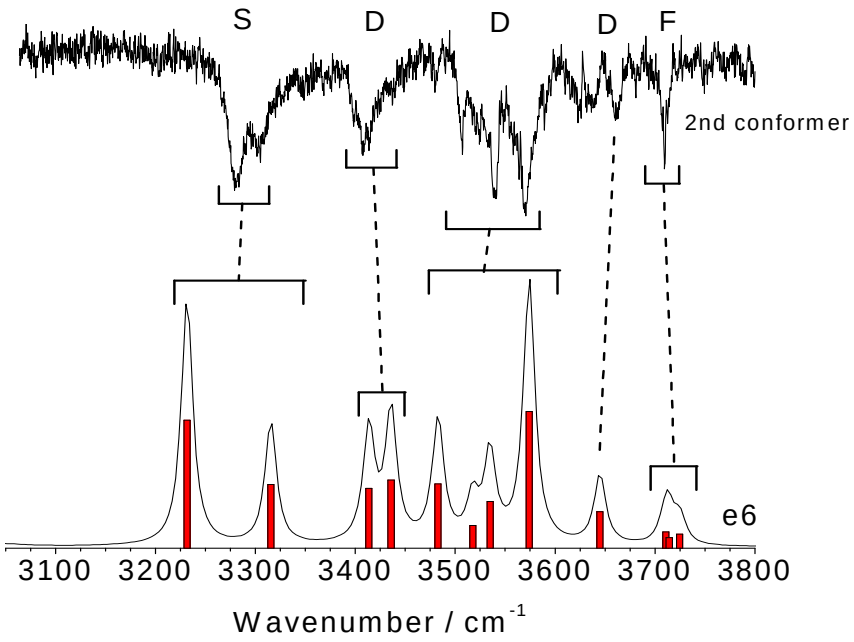

Figure 5.59. *Predicted IR spectrum for structure e6. The experimental IDIR spectrum is also shown for comparison. As can be seen, the predicted spectrum for this structure matches reasonably well the experimental one for the second conformer.*

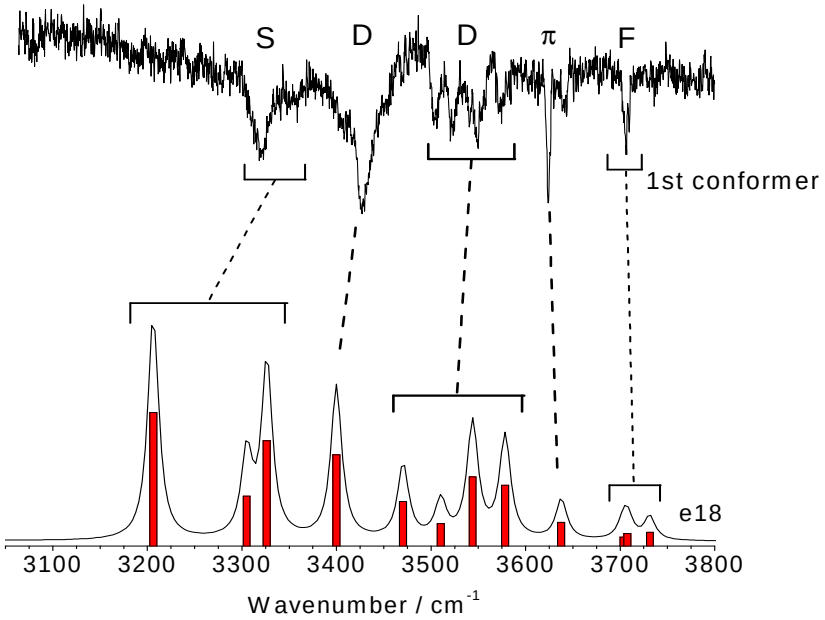

Figure 5.60. *Predicted IR spectrum for structure e18. The experimental IDIR spectrum is also shown for comparison. As can be seen, the predicted spectrum for this structure matches reasonably well the experimental one for the first conformer.*

A **sixth group** can be constructed with those structures in which the water molecules form a **book-type structure, interacting with the propofol's OH moiety**. Structures which belong to this group are *e9* (Figure 5.61), *e4, e7* and *11* but their calculated spectra **fail in reproducing** the 3300-3500 cm^{-1} region.

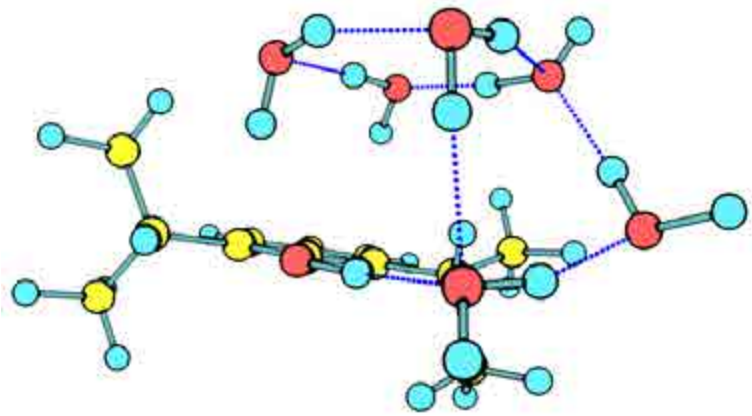

Figure 5.61. *A detailed view of structure e9 that is representative of the sixth group. They do not reproduce any of the experimental spectra.*

Bicyclic structures are gathered into the **seventh group,** although only structure *2* (Figure 5.62) can be found at reasonably low energies, 22.6 kJ/mol over the global minimun. As it is a cyclic structure, its predicted spectrum presents no peak in the 3500-3700 cm^{-1} region is expected and thus, its spectrum is considerably different from the experimental ones.

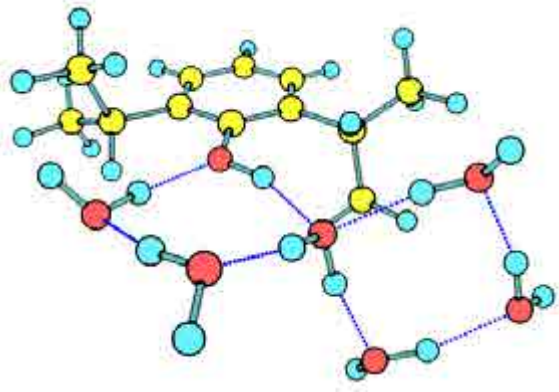

Figure 5.62. *A detailed view of structure 2 that is representative of the seventh group: bicyclic structures. Its spectrum does not reproduce the experimental ones.*

The rest of structures present their own peculiarities and therefore, they compose a heterogeneous group sharing the common characteristic of not matching the

experimental spectra of any of the two conformers. One word must be said concerning the *hexamer-monomer* structure as it was not found within the theoretical results bellow the 33 kJ/mol studied. The closest structure found is structure *e4070*, shown in Figure 5.63.

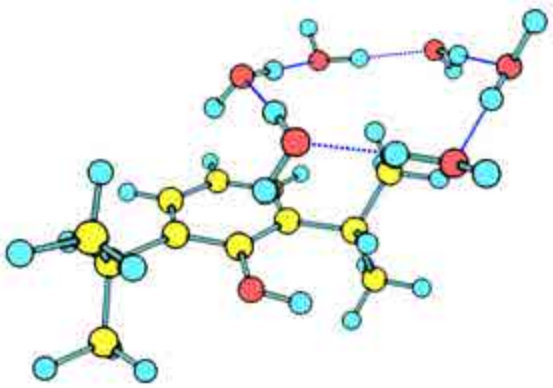

Figure 5.63. *A detailed view of structure e4070.*

The OH stretching modes for each of the conformers are collected in Table 5.3 and compared with the structure *e18* for the first conformer and structure *e6* for the second conformer.

Table 5.3. *Experimental vibrational transitions in the IR traces of propofol·W_6 first and second conformers, with a tentative assignment based on a comparison with the calculated frequencies for structures e18 and e6.*

Experimental Peak (cm^{-1})	**structure *e18***		
	Frequency (cm^{-1})	Intensity	Vibrational type
-----	2848	1503	σ_s^s (OH_w)
3318 (x2 peaks)	3206	971	σ_s^s (OH_w)
	3305	363	σ_s^s (OH_w)
3351	3326	767	σ (OH_{ppf})
3430	3400	664	σ_s^d (OH_w)
3503	3470	324	σ_s^d (OH_w)
3521	3510	164	σ_s^d (OH_w)
3549	3544	504	σ_{as}^d (OH_w)
3575	3578	444	σ_{as}^d (OH_w)
3624	3638	174	$\sigma^{O\text{-}H\cdots\pi}$ (OH_w)
3707 (x3 peaks)	3703	67	σ^f (OH_w)
	3708	92	σ^f (OH_w)
	3731	102	σ^f (OH_w)

Experimental Peak (cm^{-1})	**structure *e6***		
	Frequency (cm^{-1})	Intensity	Vibrational type
-----	2981	924	σ_s^s (OH_w)
3279	3232	805	σ_s^s (OH_w)
3305	3315	400	σ_s^s (OH_w)
	3414	376	σ (OH_{ppf})
3408 (x2 peaks)	3436	428	σ_s^d (OH_w)
	3483	404	σ_s^d (OH_w)
3507	3518	141	σ_s^d (OH_w)
3538	3535	292	σ_{as}^d (OH_w)
3568	3574	859	σ_{as}^d (OH_w)
3662	3645	228	σ_{as}^d (OH_w)
3709 (x3 peaks)	3711	102	σ^f (OH_w)
	3714	67	σ^f (OH_w)
	3725	88	σ^f (OH_w)

Special considerations

The experimental conditions are especially critical for detection of the species studied in this section. A slight change in buffer gas pressure or laser intensity results in a drastical signal reduction and a loss of spectral features. Thus, very low power densities were used in order to avoid fragmentation. Tight control of the probe laser energy is also required to avoid fragmentation. Conversely to what is observed for higher-order cluster, like propofol·W_8 and propofol·W_9, it was not possible to record propofol·W_6 spectrum using its fragmentation on a different mass channel. Furthermore, attempts to record the propofol·W_7 or propofol·W_8 clusters' excited state spectrum in the propofol·W_6 cluster's mass channel were also unsuccessful, as only a broad background can be seen with no discrete structure. Despite such difficulties, it was possible to perform *hole burning* experiments, confirming the existence of at least two conformers.

5.2.7 – Propofol·W_7

As it will be shown, the introduction of a seventh water molecule produces a substantial change in some aspects. The number of possible isomers rises, mostly due to the numerous ways in which the water molecules can organize. Molecular mechanics calculations yield of the order of ten thousand structures in a 20 kJ/mol window, being those with water cubes, the most stable ones (Figure 5.64). The cube can also be deformed to ease the formation of an O-H···π hydrogen bond. Such possibility does not implicate a reduction in the cluster's stability. The first non-cubic structures appear at 11kJ/mol.

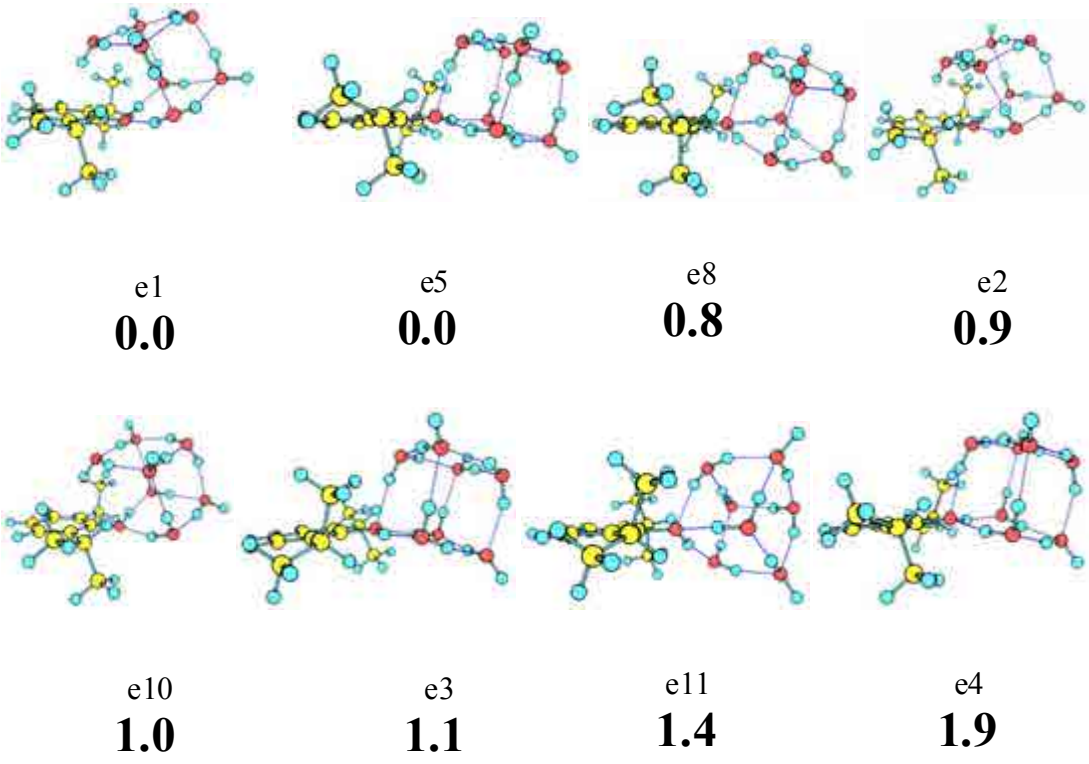

Figure 5.64. *Propofol·W_7 eight most stable conformers calculated at M06-2x/6-311++G(d,p) level, with their relative energies in bold. Energy values are in kJ/mol. The complete set of calculated structures can be found in appendix 7.1 (Figure 7.13).*

Figure 5.65 shows the *2c-REMPI* spectrum of propofol·W_7. As in the previous three clusters, a broad absorption is present, from which some prominent peaks appear. A reduction in the intensity of the background respect lower-order clusters is also observed. The red-most band appears at 35981 cm^{-1} and is taken as the origin band. Figure 5.65 also shows a comparison of the *2c-REMPI* spectrum of this cluster, and

propofol·W_8 and propofol·W_9 clusters, demonstrating the absence of fragmentationfrom higher order clusters.

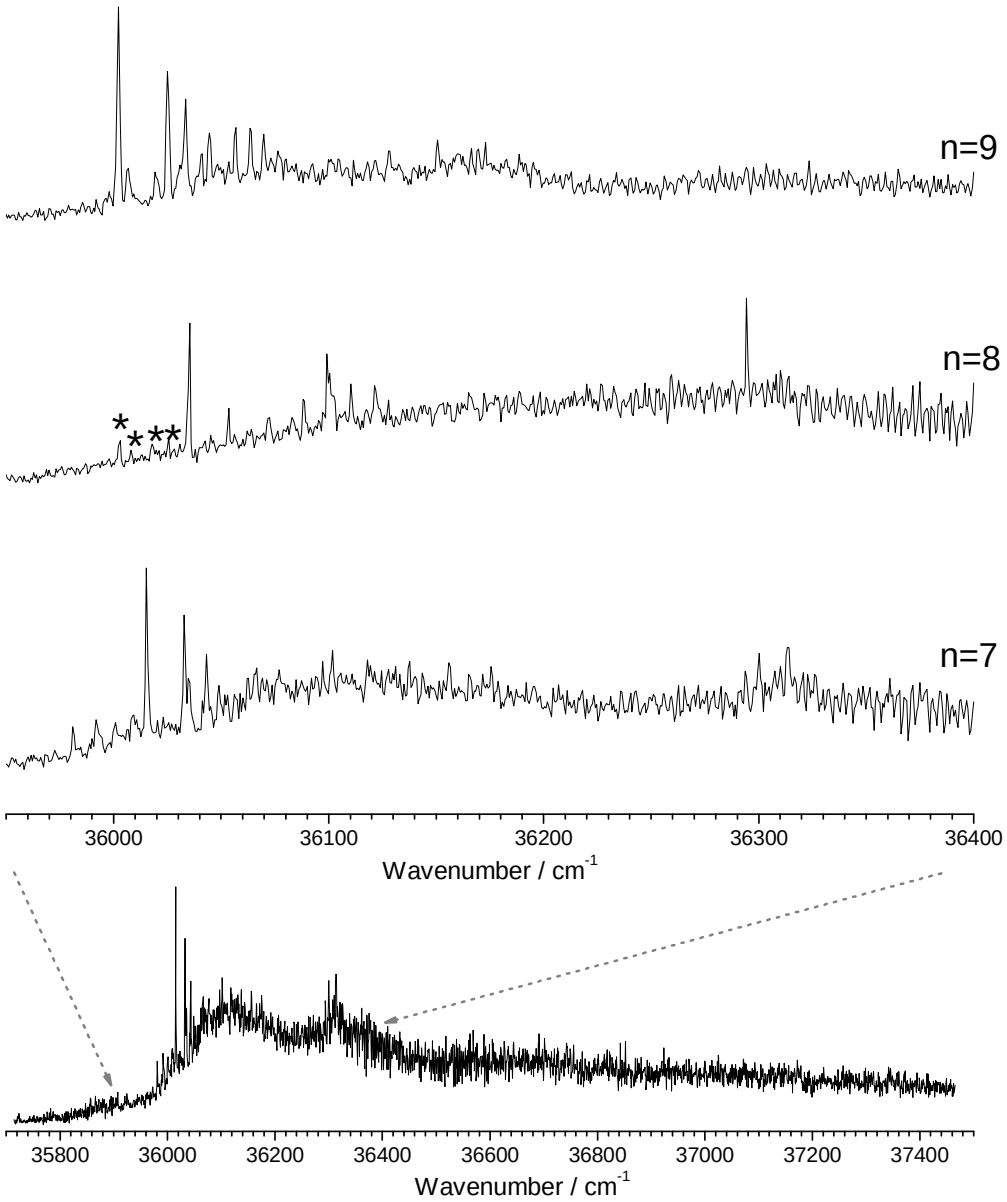

Figure 5.65. *2c-REMPI of propofol·W_7, in the 35700-37500 cm^{-1} region, recorded setting the probe laser at 27972 cm^{-1}. The zoom shows a detailed view around the origin with a comparison of propofol·W_n (n=7-9) 2c-REMPI spectra. Peaks marked with an asterisk are due to fragmentation from higher order clusters.*

The *hole burning* experiment (Figure 5.66) demonstrates that there is contribution from at least two isomers to the 1:7 spectrum, with origins at 36015 and 36293 cm^{-1}.

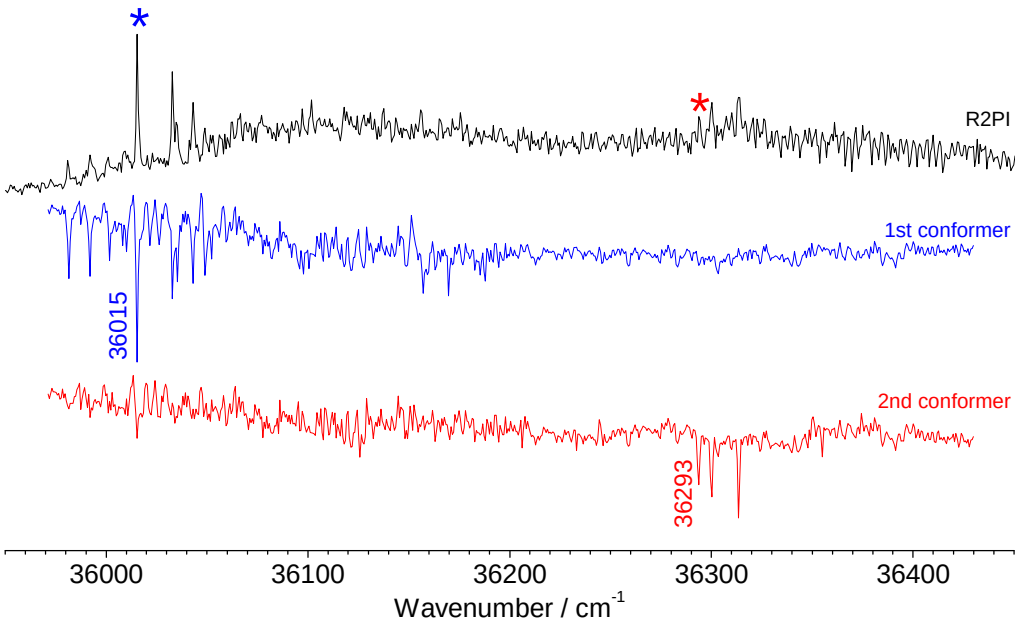

Figure 5.66. *Hole burning traces of propofol·W_7 recorded tuning the probe lasers (2-color detection) at 36015, and 36293 cm^{-1} respectively. Asterisks indicate the transitions employed for recording the hole burning spectra, as well as the IDIRS traces for each conformer.*

To extract the maximum structural information, the *IDIR* spectra of the two conformers detected was recorded in the OH stretching region, obtaining the spectra shown in Figure 5.67. The IR spectra are similar, indicating that the structure of both isomers is not that different. Only the O-H···π bond at 3610 cm^{-1} in the first conformer and a band at 3458 cm^{-1} also for the first conformer, indicate that probably the water superstructure adopt different orientations respect to the chromophore in both isomers. No enough tunable IR radiation was obtained to record the IR spectra bellow 3100 cm^{-1} and therefore the predicted peaks bellow that wavenumber are missing in the experimental traces.

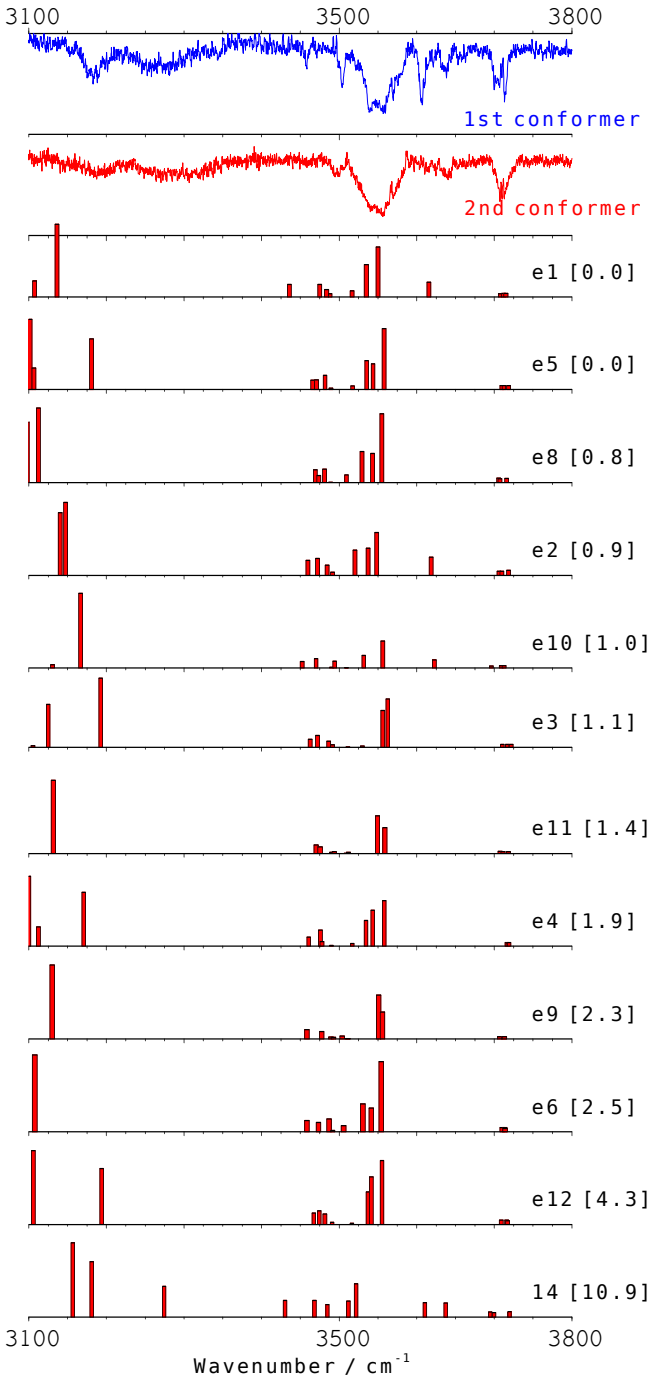

Figure 5.67. *IDIR spectra of propofol·W_7 recorded tuning the probe laser at 36015, and 36293 cm^{-1}. The predicted IR spectra for the 12 structures bellow 24 kJ/mol of the calculated isomers are also shown for comparison. The numbers in brackets are the relative energies of the calculated conformers, in kJ/mol. A correction factor of 0.938 was applied. The predicted IR spectra of all the calculated structures are recorded in appendix 7.1 (Figure 7.14).*

Assignment

As the IR spectrum shows, only those isomers based on the predicted most stable structures are able to reproduce the experimental results. Among such **cubic structures**, structures *e1* (Figure 5.68)*, e2 and e10*, closely **reproduce the first conformer's** IR spectrum and structure *e5* (Figure 5.68)*., e8, e3, e11, e4, e9, e6* and *e12*, **reproduce the second conformer's** IR spectrum**.**

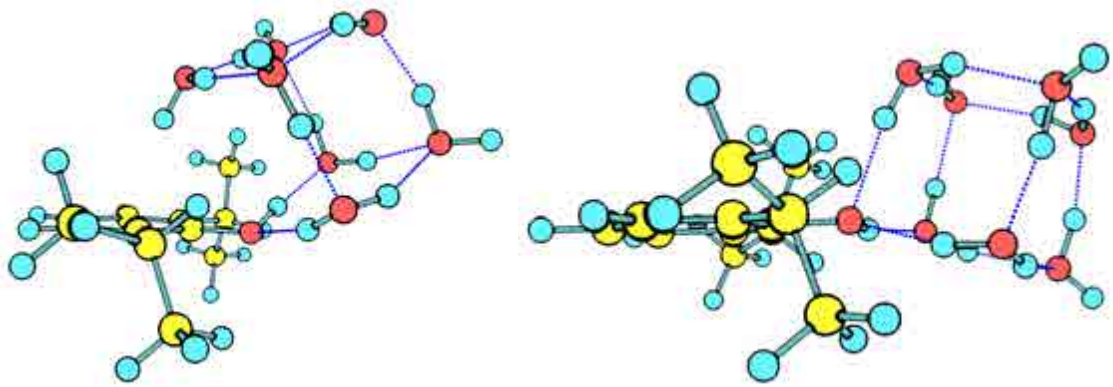

Figure 5.68. *The two conformers of propofol·W_7 are based on cubic structures: the most red-shifted conformer presents an O-H···π interaction (structure e1, left), while the second conformer (structure e5, right) does not.*

Once a ground assignment is carried out, some aspects of the assigned structures deserve attention. Nearly 11 almost identical conformers are found bellow 5 kJ/mol with similar predicted spectra. Conversely, water octamer can only form two almost-isoenergetical cubic isomers, namely S_4 and D_{2d}.[21,22] The difference lies in the symmetry break induced by the propofol molecule and that the water cube can adopt several orientations respect to the bare molecule, without a significant modification of the system's total energy. For example, structures *e5* and *e8* (Figure 5.69) are both S_4 but only differ in the orientation of homodromic faces with respect the propofol. Another clear example is presented by structures *e1* and *e2* (Figure 5.70) where both structures are S_4-type, but in the former the homodromic face is perpendicular to the aromatic ring, while it is parallel in the latter.

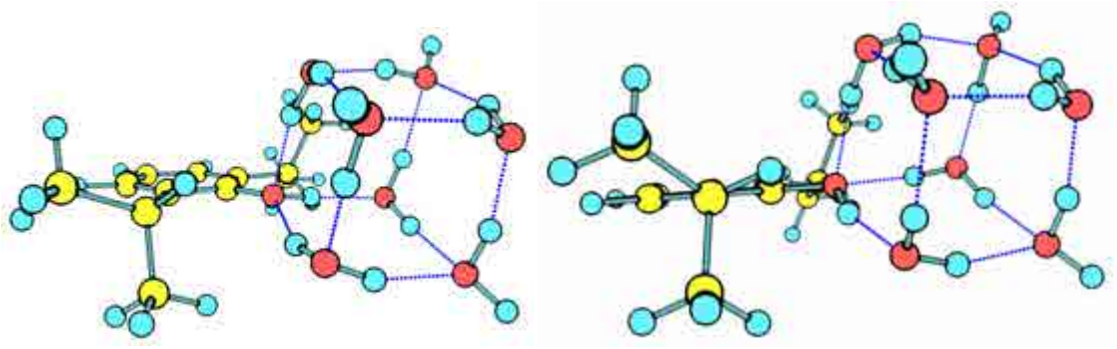

Figure 5.69. *Structures e5 and e8, they only differ in the orientation of the homodromic faces.*

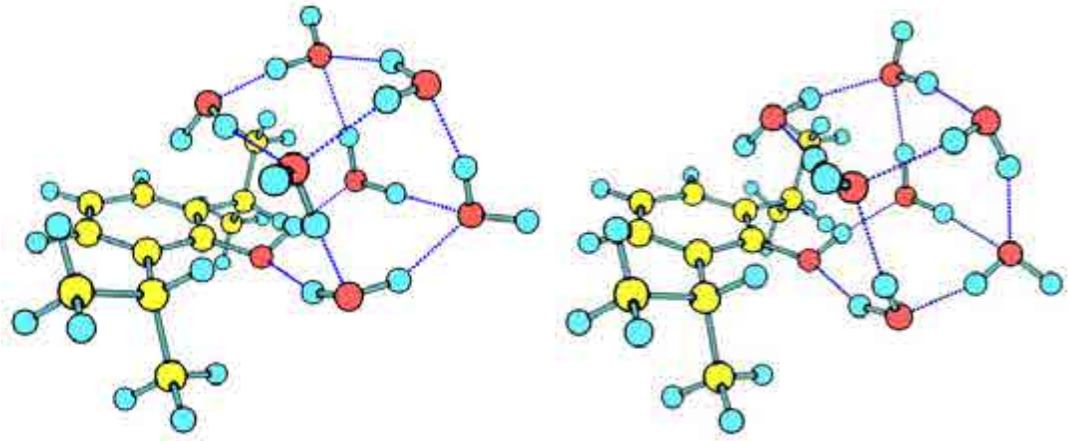

Figure 5.70. *Structures e1 and e2 as both S_4 types, but they differ in the orientation of the water molecules in the homodromic faces.*

In summary the existence of water cubes of S_4 and D_{2d} symmetries, the different orientations of the water cube respect to the bare molecule and the symmetry break induced by the propofol in the water cube results in a large number of almost iso-energetic conformations.

Keeping this in mind, a more precise assignment may be attempted for the second conformer. In structures *e5*, *e3* and *e4* the cube is formed nearly in the plane of the aromatic ring while in structures *e8* and *e11* the cube is rotated with respect to the aromatic ring, leading to the appearance of a characteristic peak at 3185 cm^{-1} in the predicted spectrum, corresponding to the bonded propofol's OH stretching. Such a feature is not found in the experimental trace and, therefore, one can safely discard such possibilities (structures *e8* and *e11*). Therefore, we can conclude that the **second**

conformer has a nearly **in-plane cubic S_4 symmetry structure**, like those in structures *e5*, e3 or *e4* (Figure 5.71).

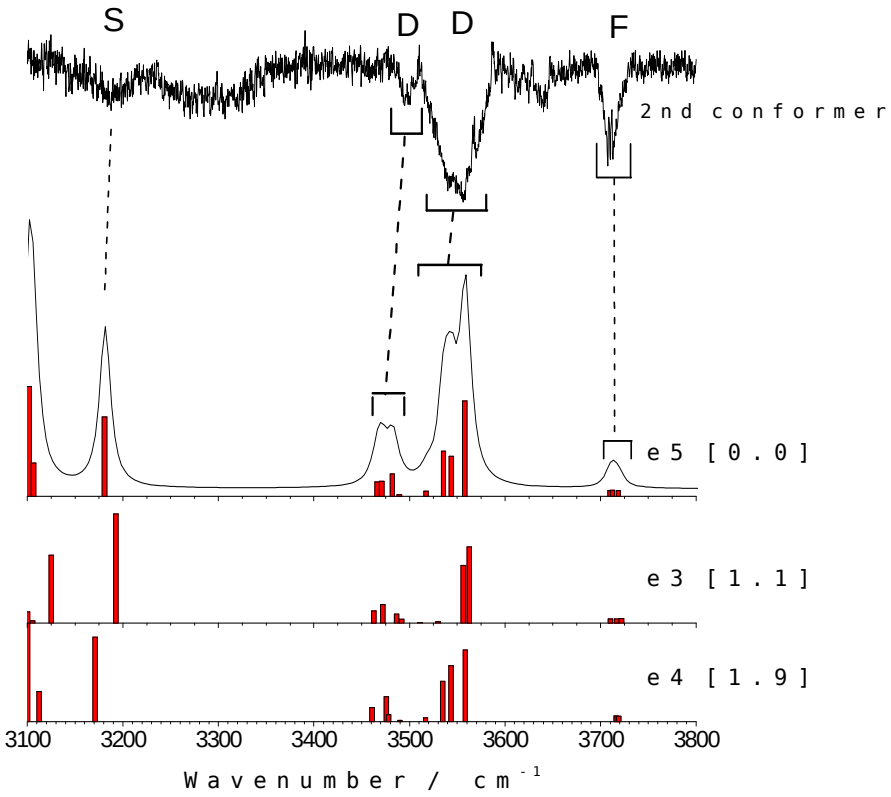

Figure 5.71. *Predicted spectra for the cubic-nearly-in-plane structure. The experimental results suggest a broad absorption between 3520 and 3580 cm^{-1} due to the convolution of some peaks.*

Regarding the first conformer, where the OH···π interaction takes place, structures *e1, e2 and e10* predicted spectra closely reproduce the experimental spectrum (Figure 5.72), and thus, the **first conformer** has a **cubic structure with an O-H···π interaction**.

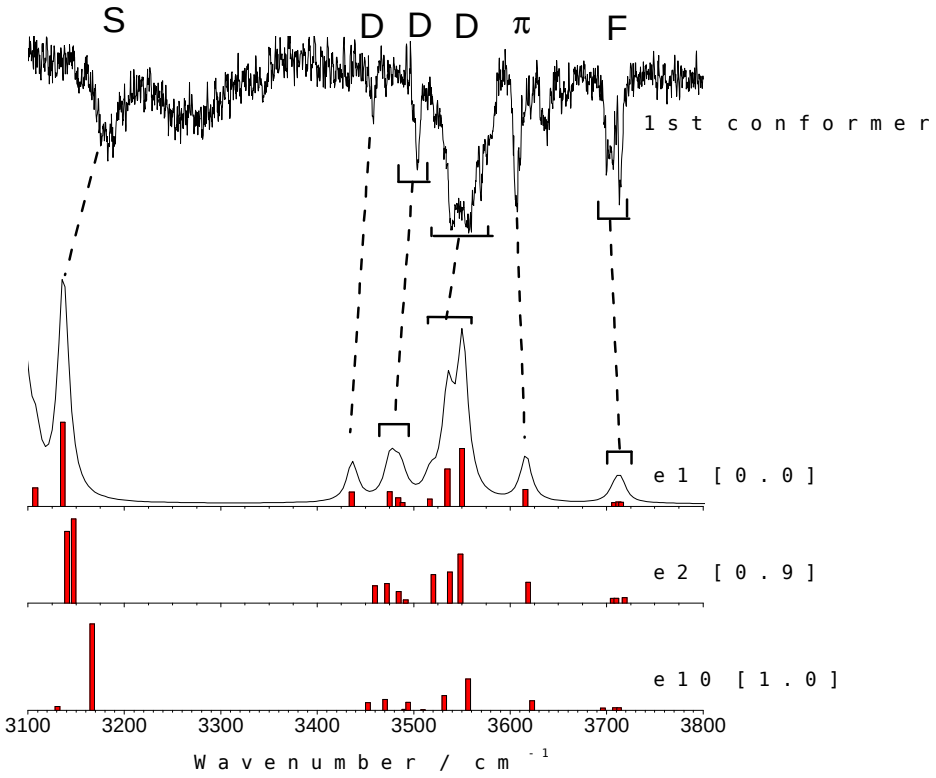

Figure 5.72. *Propofol's simulated spectra for the cubic structure with an OH interacts with the aromatic ring. The experimental trace presents a broad absorption due to the contribution of several peaks in the 3520 - 3580 cm^{-1} region, a strong peak located at c.a. 3500 cm^{-1} and another weak peak at c.a. 3450 cm^{-1}.*

Although a **complete distinction between S_4 and D_{2d} cannot be done**, due to the previously discussed small differences, it is clear that experimentally, at least a **cubic structure where the propofol's OH is part of the cube, and a cubic structure where a OH···π interaction** takes place, are found in the jet.

Finally, The OH stretching modes for each of the conformers are collected in Table 5.4 and compared with the structure *e1* for the first conformer and structure *e5* for the second conformer.

Table 5.4. *Experimental vibrational transitions in the IR traces of propofol·W_7 first and second conformers, with a tentative assignment based on a comparison with the calculated frequencies for structures e1 and e5.*

Experimental Peak (cm^{-1})	**structure *e1***		
	Frequency (cm^{-1})	Intensity	Vibrational type
-----	3016	387	σ_s^s (OH_w)
-----	3095	1140	σ_s^s (OH_w)
-----	3107	382	σ (OH_{ppf})
3181	3136	1738	σ_s^s (OH_w)
3458	3436	302	σ_s^d (OH_w)
3504 (x3 peaks)	3475	305	σ_s^d (OH_w)
	3484	178	σ_s^d (OH_w)
	3488	79	σ_s^d (OH_w)
3542 (x2 peaks)	3517	152	σ_{as}^d (OH_w)
	3535	774	σ_{as}^d (OH_w)
3560	3550	1195	σ_{as}^d (OH_w)
3607	3616	354	$\sigma^{O\text{-}H\cdots\pi}$ (OH_w)
3700	3708	81	σ^f (OH_w)
3707	3712	90	σ^f (OH_w)
3714	3715	85	σ^f (OH_w)

Experimental Peak (cm^{-1})	**structure *e5***		
	Frequency (cm^{-1})	Intensity	Vibrational type
-----	3058	52	σ_s^s (OH_w)
-----	3102	1671	σ_s^s (OH_w)
-----	3107	508	σ_s^s (OH_w)
3184	3181	1208	σ (OH_{ppf})
3495 (x4 peaks)	3466	219	σ_s^d (OH_w)
	3471	231	σ_s^d (OH_w)
	3482	342	σ_s^d (OH_w)
	3489	24	σ_s^d (OH_w)
3540 (x2 peaks)	3517	77	σ_{as}^d (OH_w)
	3536	684	σ_{as}^d (OH_w)
3556	3544	608	σ_{as}^d (OH_w)
3565	3558	1452	σ_{as}^d (OH_w)
3711 (x3 peaks)	3710	87	σ^f (OH_w)
	3713	89	σ^f (OH_w)
	3718	85	σ^f (OH_w)

5.2.8 – Propofol·W_8

As we explained in the previous section, the cubic water structure of propofol·W_7 is particularly stable. Using chemical intuition one should expect similar kinds of structures for propofol·W_8. Accordingly, despite that the number of conformers in the 20 kJ/mol window has grown exponentially with the addition of the eighth water molecule, those conformers with water cubes are particularly stable. Among all possibilities, we chose 90 structures in the above-mentioned 20 kJ/mol window and run full optimization at the M06-2x/6-311++G(d,p) level. Three kinds of structures clearly emerge (Figure 5.73): a cube of eight water molecules interacting with propofol's OH (structures *e4, e28, e19, e16, e38* for example), polyhedrons formed by the water molecules plus the propofol's OH (structures *e7, e35*) and the same type of structure but with a direct O-H···π interaction (structure *e23*). Such conformers present an energy difference bellow 6 kJ/mol and therefore, all of them could be found experimentally.

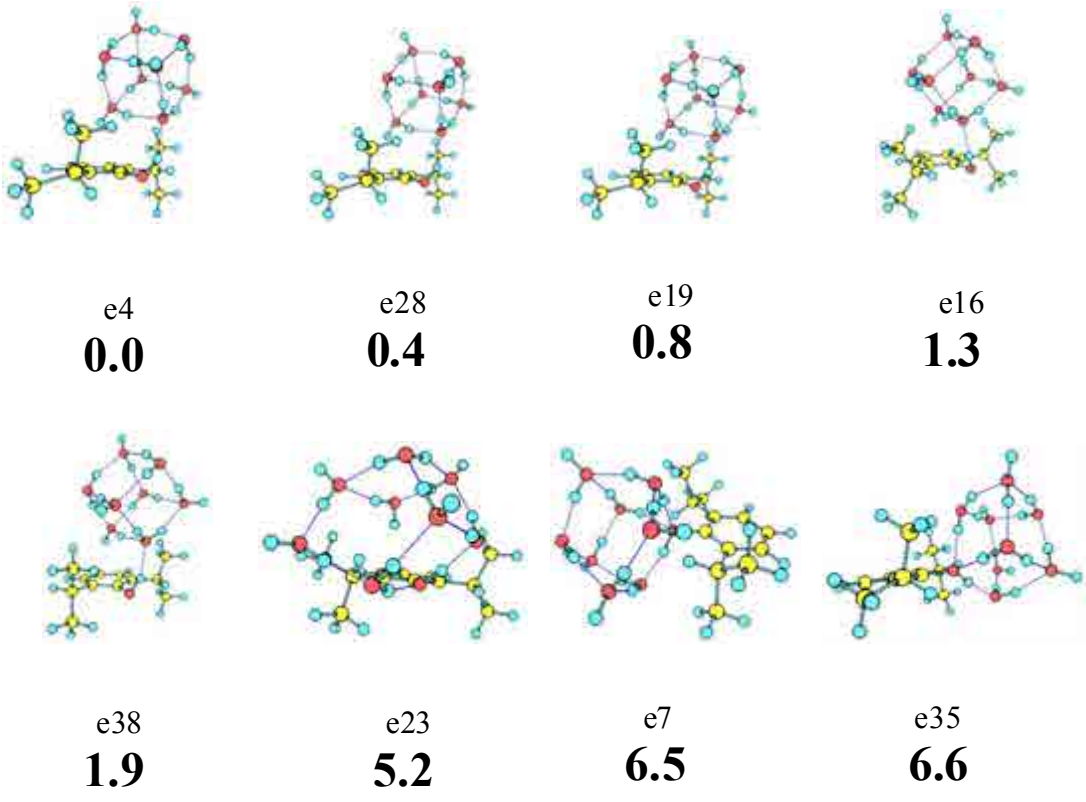

Figure 5.73. *Propofol·W_8 eight most stable conformers calculated at M06-2x/6-311++G(d,p) level, with their relative energies in bold. Energy values are in kJ/mol. The complete set of calculated structures can be found in appendix 7.1 (Figure 7.15).*

Figure 5.74 shows the *2c-REMPI* spectrum of propofol·W_8. The first noticeable aspect is the almost vanishing of the broad background present for propofol·W_n n=4-7. Some fragmentation from the propofol·W_9 cluster (Figure 5.65) is observed bellow 36000 cm^{-1}, but such features are considerably weaker than the transition at 36035 cm^{-1}, which is taken as the origin band.

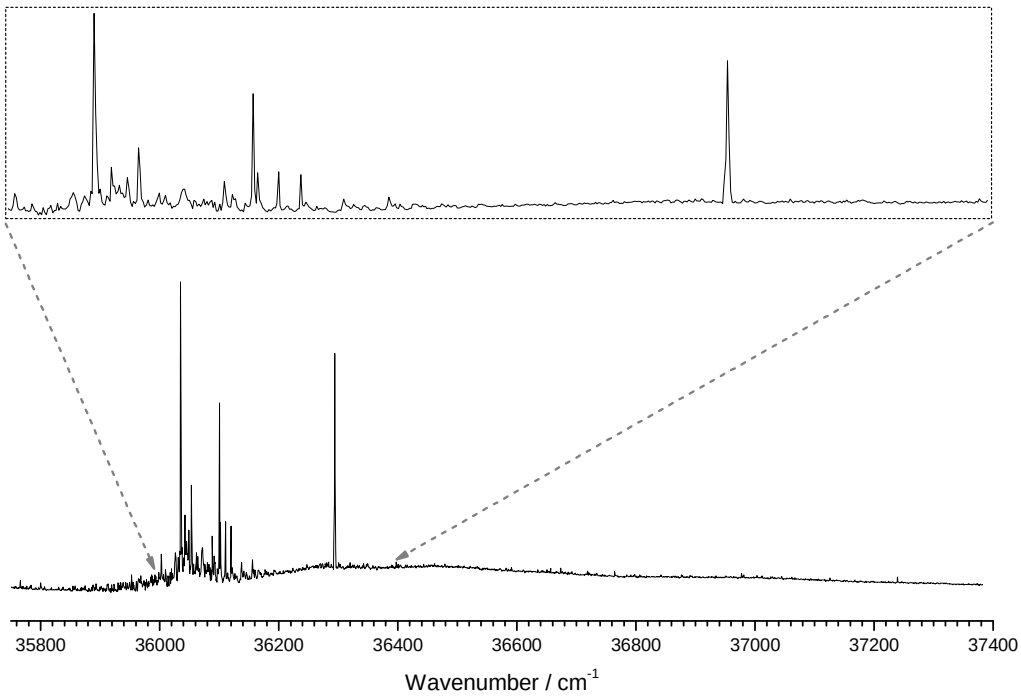

Figure 5.74. *2c-REMPI of propofol·W_7, in the 35750-37400 cm^{-1} region, recorded setting the probe laser at 27972 cm^{-1}. The insert shows a detailed view around the origin.*

Figure 5.75 shows the *hole burning* experiment of the 1:8 species, probing the origins at 36035, and 36295 cm^{-1}, together with propofol·W_8 *2c-REMPI* spectrum. As can be seen, at least two isomers are present and only a few transitions appear over the broad absorption for both conformers. Surprisingly, the spectrum of the second conformer appears to consist of a simple, intense feature.

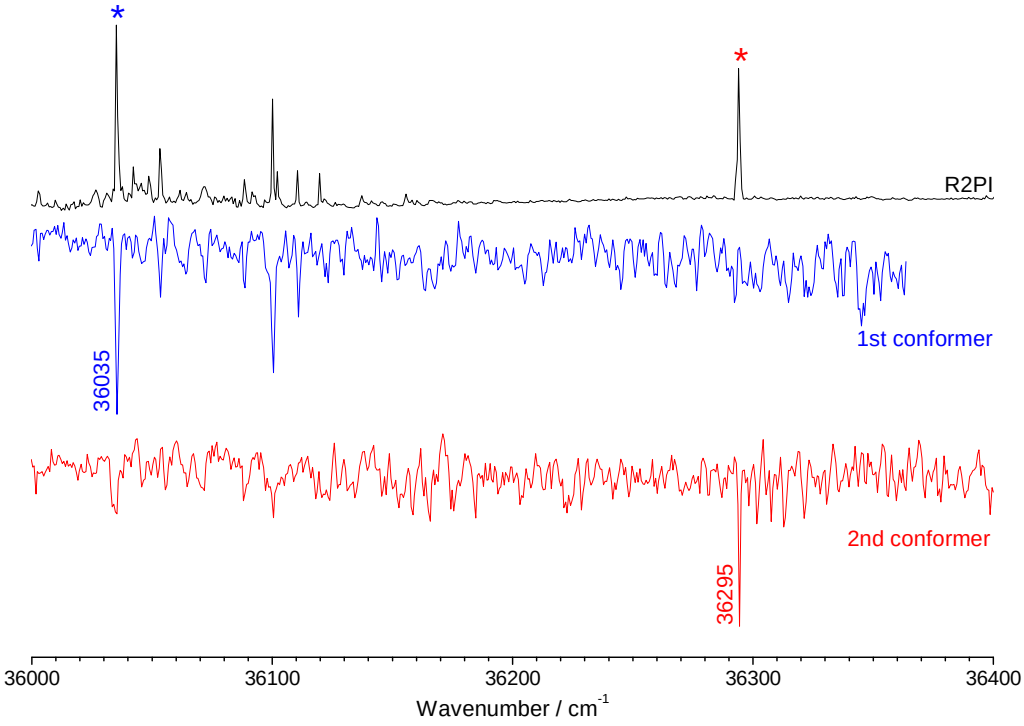

Figure 5.75. *Hole burning traces of propofol·W_8 recorded tuning the probe lasers (2-color detection) at 36035, and 36295 cm^{-1} respectively. The peaks notes with asterisks indicate the transitions employed for recording the hole burning spectra, as well as the IDIRS traces.*

In order to extract the maximum structural information to match the *2c-REMPI* spectra with the calculated structures, the IDIR spectra of the two conformers detected were recorded, both in the OH stretching and fingerprint regions (500-1700 cm^{-1}) using a free electron laser, and obtaining the spectra shown in Figure 5.76. The main differences between the IDIR spectra of the two conformers, is the peak at 3596 cm^{-1}, which is only present in the first conformer and, as mentioned in the propofol·W_7 section, is characteristic of an OH···π interaction. The peaks at higher frequencies, corresponds to the free OH stretching vibrations of the water molecules, while the peaks at mid frequencies (3450 – 3600 cm^{-1}) are due to antisymmetric and symmetric double-donor OH stretching modes. Finally, the peaks due to water single-donor OH stretching modes and/or phenolic OH stretching that take part in hydrogen bonds appear at lower frequencies. No enough tunable IR radiation was obtained to record the IR spectra

bellow 3100 cm^{-1} and therefore the predicted peaks bellow that wavenumber are missing in the experimental traces.

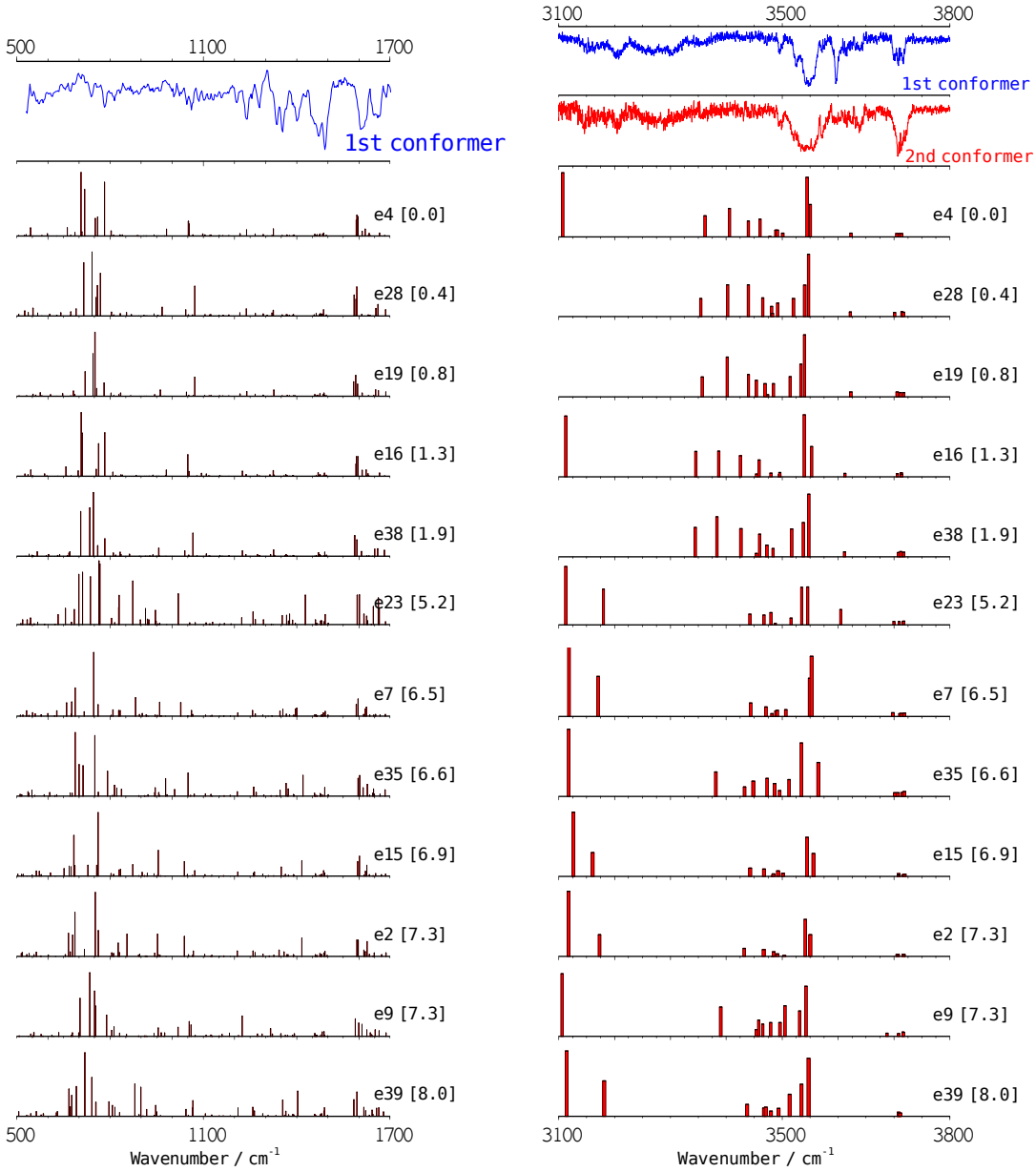

Figure 5.76. *IDIR spectra of propofol·W_8 recorded tuning the probe laser at 36035, and 36295 cm^{-1}. The predicted IR spectra for the 12 structures bellow 8 kJ/mol are also shown for comparison. The numbers in brackets are the relative energies of the calculated conformers, in kJ/mol. A correction factor of 0.938 was applied. The predicted IR spectra of all the calculated structures are recorded in appendix 7.1 (Figure 7.16).*

First conformer's S_1 IR spectrum was also recorded and is presented in Figure 5.77, together with the S_0 IDIR spectrum. As can be seen, in the S_1 state IDIR spectrum, the electronic excitation causes a decreasing in the OH stretching vibration of the water that is forming the O-H···π interaction (20 cm^{-1}) and also in the OH stretching vibration with hydrogen bonding of the same water (30 cm^{-1}). The first one points to an increasing in the strength of the O-H···π interaction due to electronic excitation, in agreement with the red shift in the 0-0 transition, respect to the second conformer. Such observation is in contradiction with what is normally accepted in the field: that O-H···π interaction leads to blue shifts in the electronic spectra.

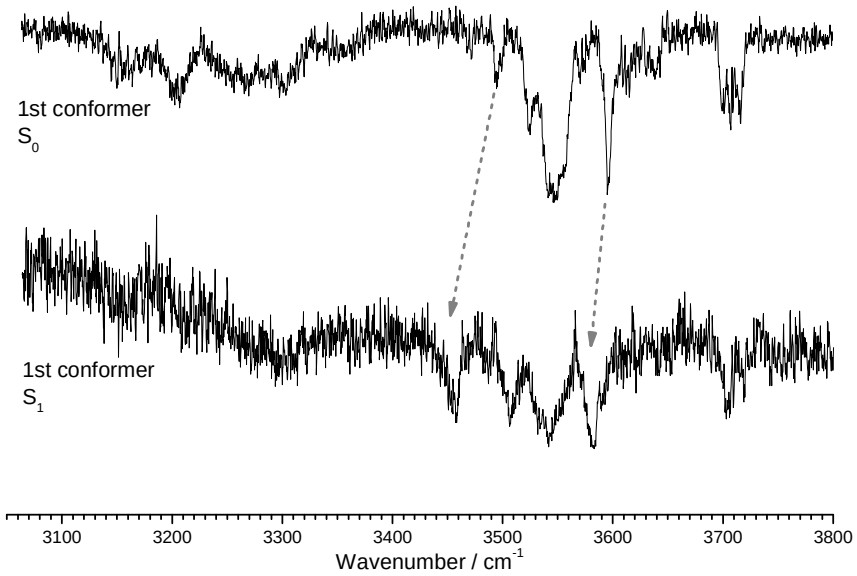

Figure 5.77. *Comparison between ground and excited state IRIDS of propofol·W_8 first isomer.*

Assignment

The main criterium to match the experimental spectra with calculated structures is the comparison between the IR data and the predicted spectra. As can be seen in Figure 5.78, **the first conformer** presents an isolated peak at 3596 cm^{-1}, which is the spectra signature of a OH···π interaction. The first six most stable structures present such type of interaction, but among them, only **structure *e23*** (Figure 5.79) fits reasonably well (Figure 5.78) because the predicted peaks between 3350 - 3440 cm^{-1} for the other structures are not present in the IDIR trace. Such assignment discards the presence of an eight water cube over the aromatic ring.

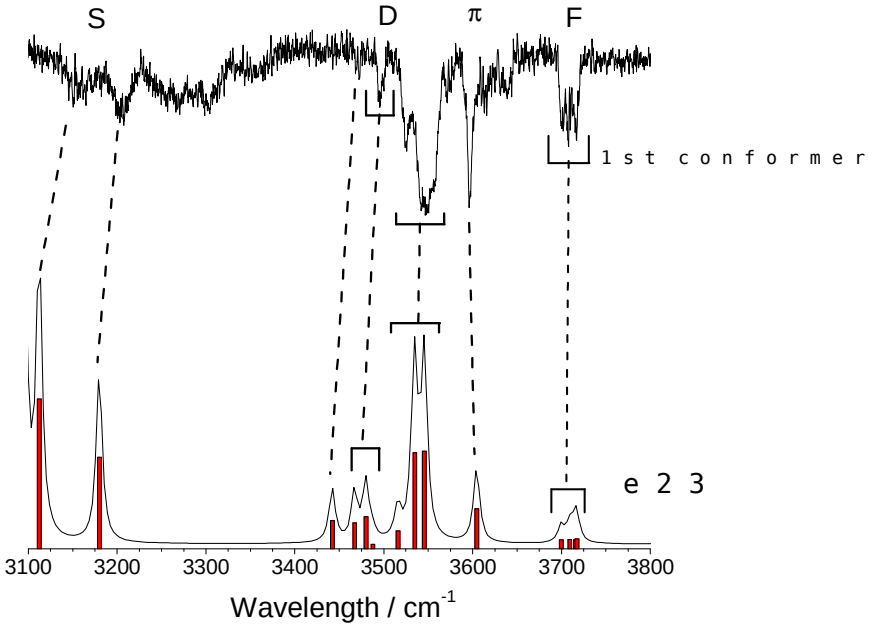

Figure 5.78. *A comparison of structure e23 with the experimental results for the first conformer. The good match between spectra confirms the assignment.*

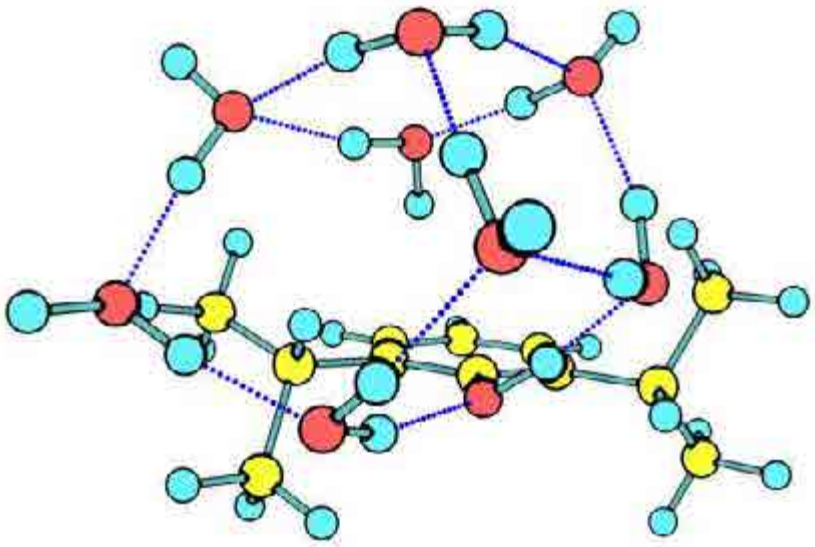

Figure 5.79. *Structure e23 reproduces the spectrum of the first conformer.*

For the second conformer, structures *e7*, *e15*, *e2* and *e39* (as well as other structures that are high in energy like *e32*, *e27*) reproduce reasonably well the experimental results, and although we cannot precisely assign to one of them only, they all have the same structure differing only in the position of the cube. Thus, **the second conformer is a cube formed by all the molecules** as shown in Figure 5.80, where the most stable structure of this group, structure *e7*, is shown. A comparison of this structure with the experimental results is given in Figure 5.81.

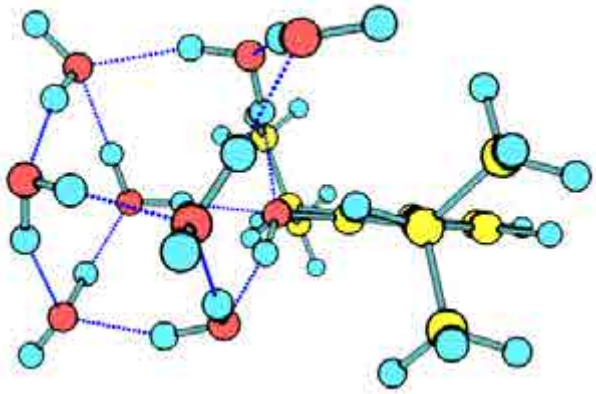

Figure 5.80. *Structure e7 reproduces the spectrum of the second conformer.*

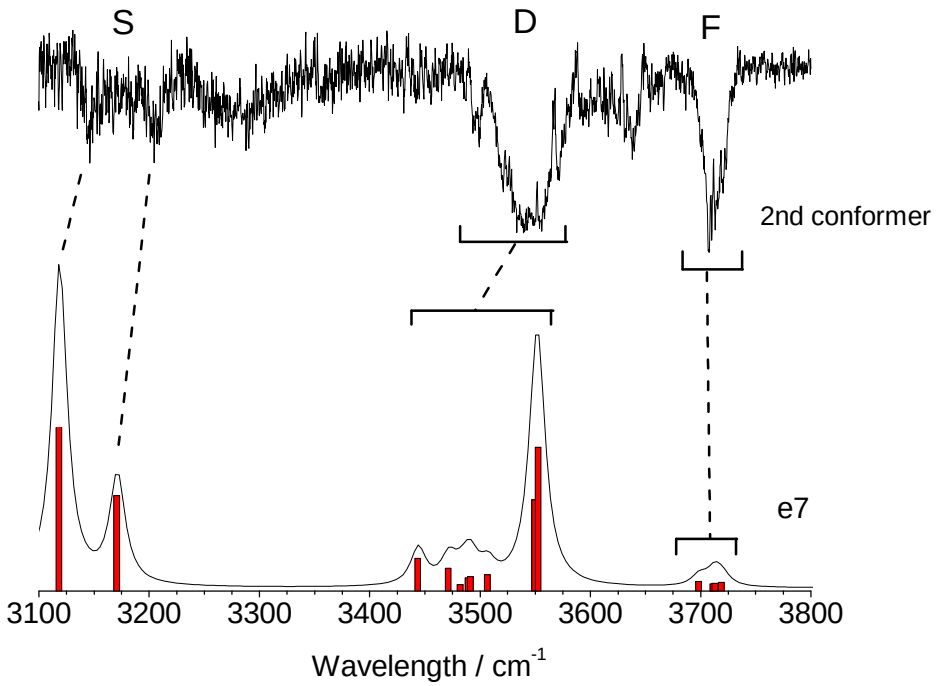

Figure 5.81. *A comparison of calculated IR spectrum for propofol's structure e7 with the experimental results for the second conformer. There is a very good agreement between them.*

The comparison between the structures of the assigned conformers (Figure 5.82) shows that both structures are identical, with the only difference being that the first one closes the cube in the aromatic ring, while the second one does it with propofol's OH.

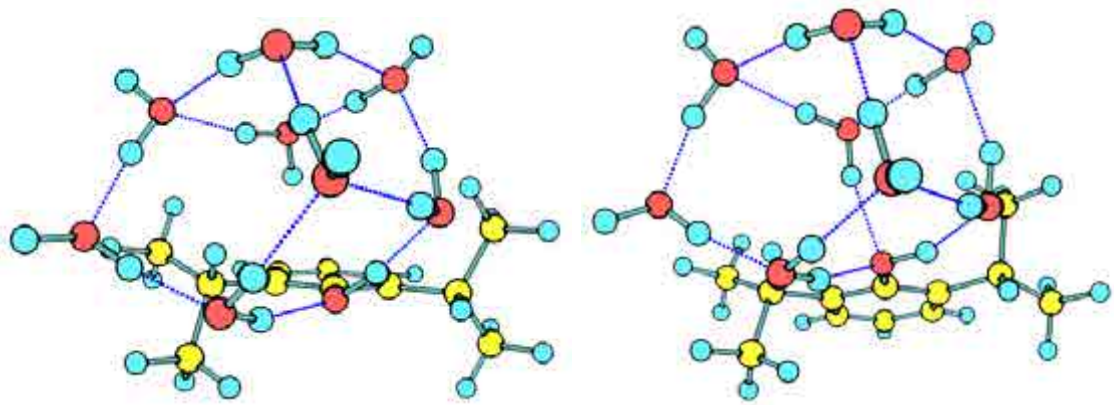

Figure 5.82. *e23 and e32 structures show the same pattern.*

A last question remains still open, which is the absence of the most stable structure for this stoichiometry, consisting of a water cube interacting with the propofol's OH moiety (Figure 5.83), which the calculations predict as a particularly

stable structure.[20] The answer may be a large change in geometry upon excitation or a lower robustness of the structure towards fragmentation, as the whole water cube is attached to the chromophore by a single hydrogen bond.

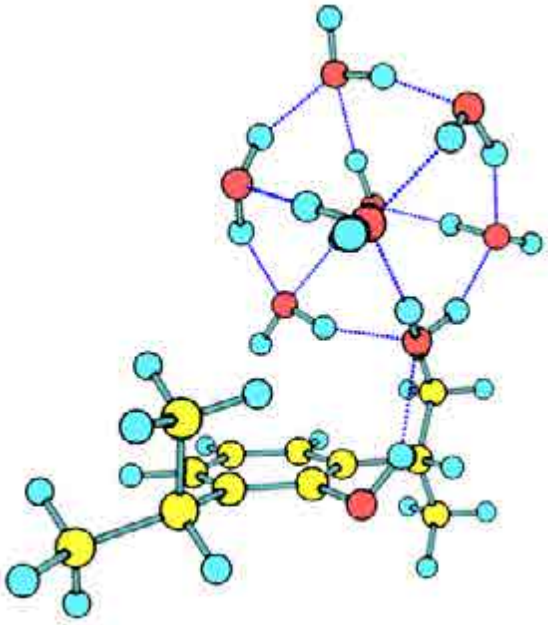

Figure 5.83. *Structure e4 is not found in the expansion, despite that one of the most stable isomers..*

Finally, The OH stretching modes for each of the conformers are collected in Table 5.5 and compared with the structure *e23* for the first conformer and structure *e7* for the second conformer.

Table 5.5. *Experimental vibrational transitions in the IR traces of propofol·W_8 first and second conformers, with a tentative assignment based on a comparison with the calculated frequencies for structures e23 and e7.*

Experimental Peak (cm^{-1})	**structure *e23***		
	Frequency (cm^{-1})	Intensity	Vibrational type
-----	3043	318	σ_s^s (OH_w)
-----	3058	596	σ (OH_{ppf})
-----	3096	1452	σ_s^s (OH_w)
3157	3113	1446	σ_s^s (OH_w)
3203	3180	885	σ_s^s (OH_w)
3469	3442	273	σ_s^d (OH_w)
3495	3467	249	σ_s^d (OH_w)
3526 (x3 peaks)	3480	307	σ_s^d (OH_w)
	3488	43	σ_s^d (OH_w)
	3516	170	σ_{as}^d (OH_w)
3542	3535	930	σ_{as}^d (OH_w)
3556	3546	944	σ_{as}^d (OH_w)
3596	3605	387	$\sigma^{O\text{-}H\cdots\pi}$ (OH_w)
3700	3700	87	σ^f (OH_w)
3708	3709	90	σ^f (OH_w)
3715	3716	84	σ^f (OH_w)
3717	3718	93	σ^f (OH_w)

Experimental Peak (cm^{-1})	**structure *e7***		
	Frequency (cm^{-1})	Intensity	Vibrational type
-----	2903	944	σ (OH_{ppf})
-----	3057	347	σ_s^s (OH_w)
-----	3065	83	σ_s^s (OH_w)
3146	3118	2933	σ_s^s (OH_w)
3207	3171	993	σ_s^s (OH_w)
3500	3443	339	σ_s^d (OH_w)
3537 (x5 peaks)	3471	238	σ_s^d (OH_w)
	3482	68	σ_s^d (OH_w)
	3489	137	σ_{as}^d (OH_w)
	3491	150	σ_s^d (OH_w)
	3507	168	σ_{as}^d (OH_w)
3556 (x2 peaks)	3549	952	σ_{as}^d (OH_w)
	3552	1492	σ_{as}^d (OH_w)
3710 (x4 peaks)	3698	99	σ^f (OH_w)
	3711	73	σ^f (OH_w)
	3713	78	σ^f (OH_w)
	3719	92	σ^f (OH_w)

5.2.9 – Propofol·W_9

The number of conformers in the 20 kJ/mol window for this cluster is even bigger than that for propofol·W_8, with some structures being particularly stable. Among the most stable structures (Figure 5.84) *open boxes* (structures *e29, e9*), *pentagonal prisms* (structure *e1, e10, e23, e7*) and cubes formed by all nine water molecules attached to propofol (structure *e38*) are found. All this kinds of structures are found bellow a relative energy of 6.5 kJ/mol. Contrarily to propofol·W_8 cluster, not only polyhedral structures are found in the stability window (structure *e35*).

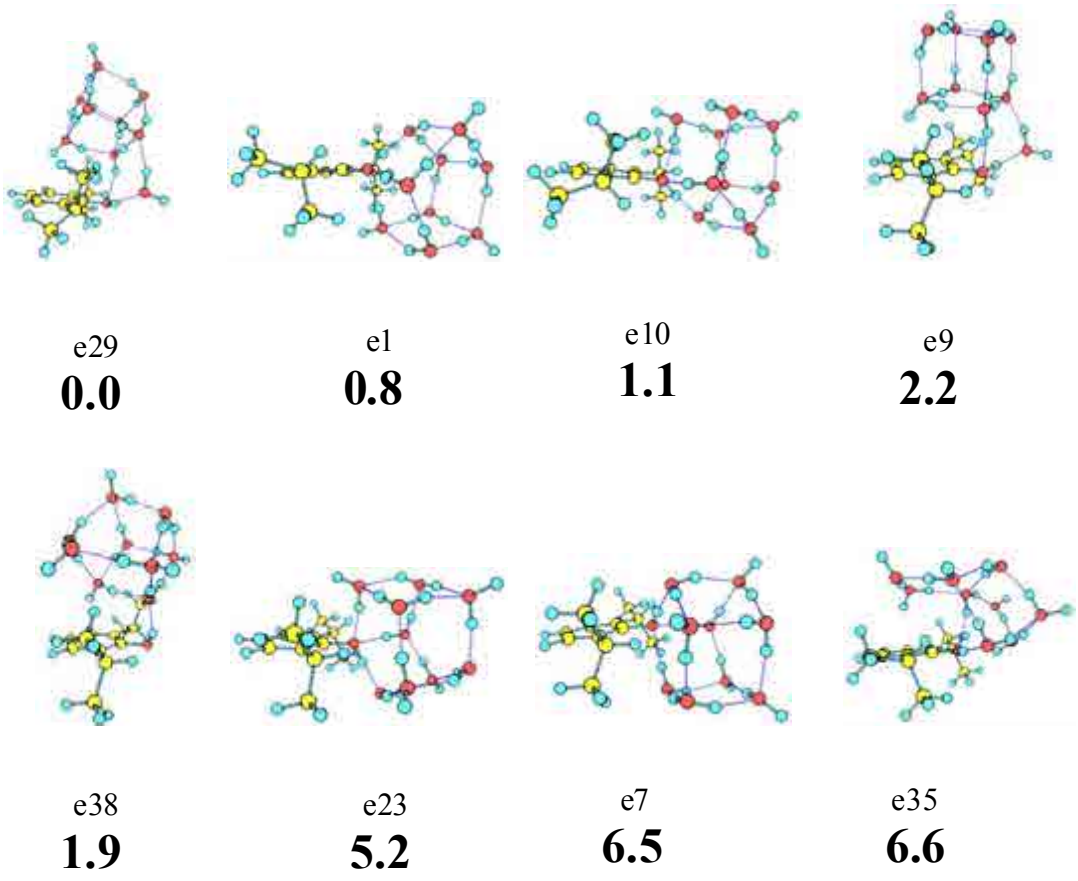

Figure 5.84. *Propofol·W_9 eight most stable conformers calculated at M06-2x/6-311++G(d,p) level, with their relative energies in bold. Energy values are in kJ/mol. The complete set of calculated structures can be found in appendix 7.1 (Figure 7.17).*

Figure 5.85 shows the *2c-REMPI* spectrum of propofol·W_9. Once more, the spectrum consists of discrete spectral features built over a broad absorption, although the latter is less intense than in propofol·W_n (n=4-7). The red-most band appears at 36002 cm^{-1} and therefore it is taken as the propofol·W_9 origin band, although fragmentation from higher order clusters cannot be traced back, due to the almost

coincidence of $propofol_2$ and propofol·W_{10} masses and the low signal intensity of the latter. Nevertheless, the IDIR spectrum will uncover any possible fragmentation.

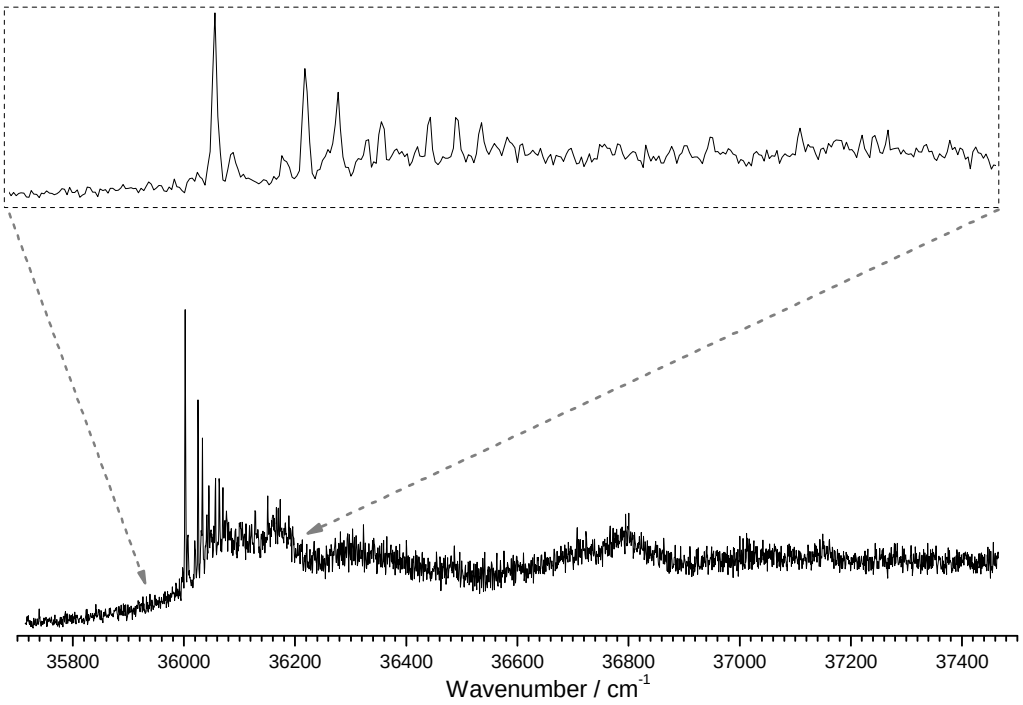

Figure 5.85. *2c-REMPI of propofol·W_7, in the 35700-37500 cm^{-1} region, recorded setting the probe laser at 27972 cm^{-1}. The insert shows a detailed view around the origin.*

To determine the number of isomers contributing to the spectrum of each stoichiometry, a *hole burning* experiment of the 1:9 species is done, shown in Figure 5.86, where a comparison between the propofol·W_9 *2c-REMPI* spectrum and the *hole burning* traces obtained probing the origin at 36002 cm^{-1} is offered. As can be seen, a single isomer is present with a few transitions in the first 100 cm^{-1}.

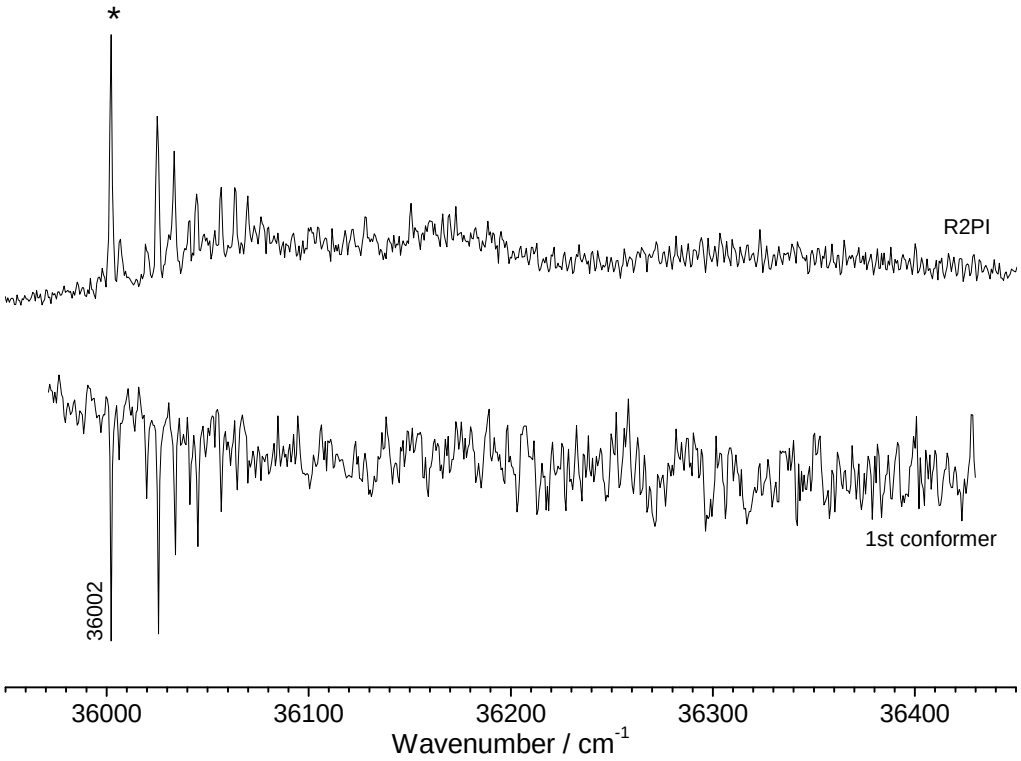

Figure 5.86. *Hole burning traces of propofol·W_9 recorded tuning the probe lasers (2-color detection) at 36002 cm^{-1}. The peak noted with an asterisk indicate the transition employed for recording the hole burning spectra, as well as the IDIRS trace.*

In order to extract the maximum structural information to match the *2c-REMPI* spectra with the calculated structures, the *IDIR* spectra of the detected conformer was recorded both, in the OH stretching region and in the fingerprint region (500-1700 cm^{-1}) using a free electron laser and, obtaining the spectra shown in Figure 5.87.

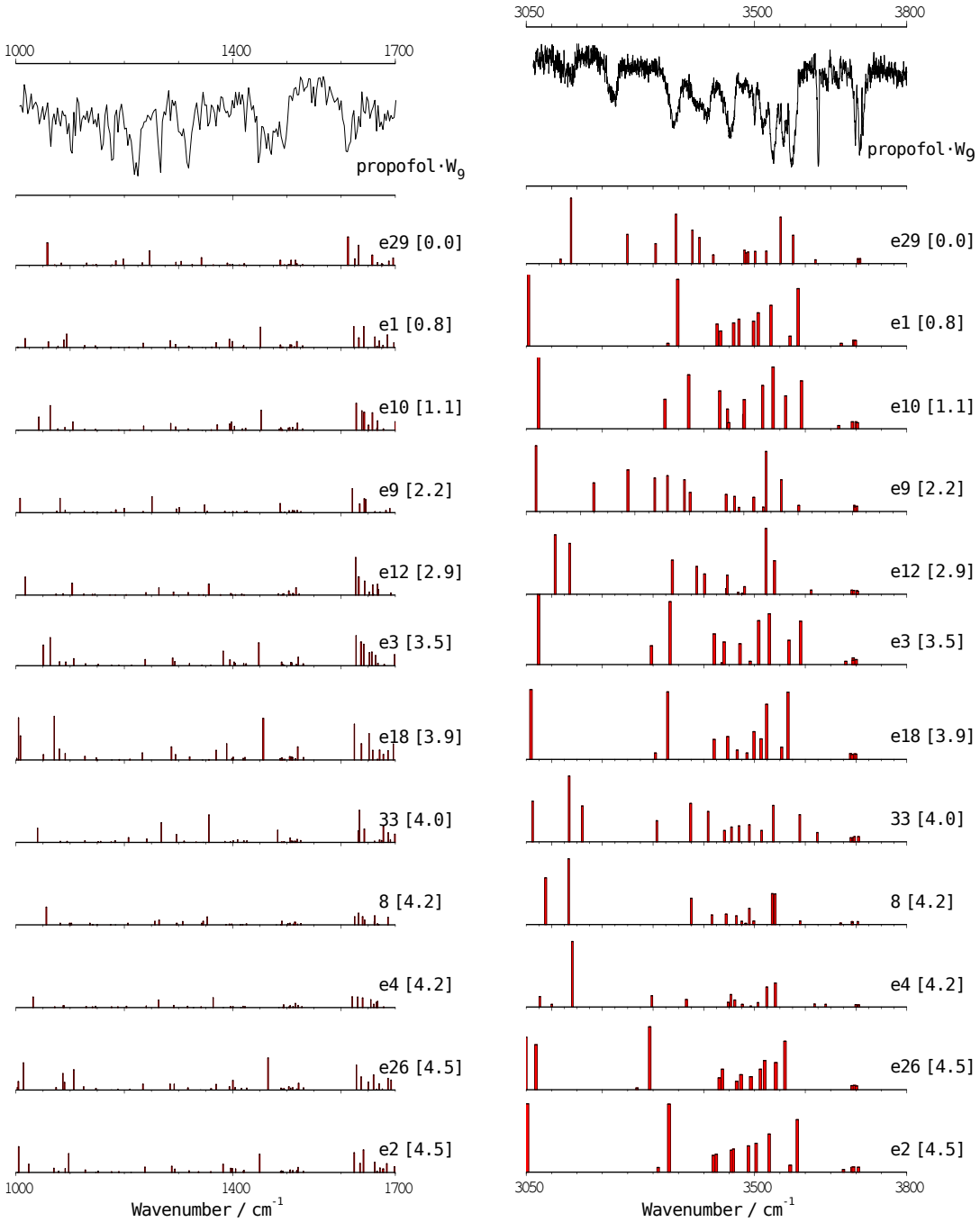

Figure 5.87. *IDIR spectra of propofol·W9 recorded tuning the probe laser at 36002 cm-1. The predicted IR spectra for the 12 structures bellow 4.5 kJ/mol of the calculated isomers are also shown for comparison. The numbers in brackets are the relative energies of the calculated conformers, in kJ/mol. A correction factor of 0.935 was applied. The predicted IR spectra of all the calculated structures are summarized in appendix 7.1 (Figure 7.18).*

A strong peak appears at 3625 cm^{-1}, which is characteristic of an OH···π interaction. Three peaks at higher frequencies can clearly be seen as shown in Figure 5.88, where a magnification of the c.a. 3700 cm^{-1} region is shown, corresponding to the free OH stretching vibrations of the water molecules. The central part of the spectrum is crowded with bands due to the double-donor waters (3480-3600 cm^{-1}) and due to single donor or double-donor waters in the 3320–3460 cm^{-1} region. The contribution of the latter will be discussed once the structure is assigned, as it presents a special case, because double donor stretching modes generally appear in the 3450-3600 cm^{-1} region. Two weak peaks are also found at 3130 and 3220 cm^{-1}.

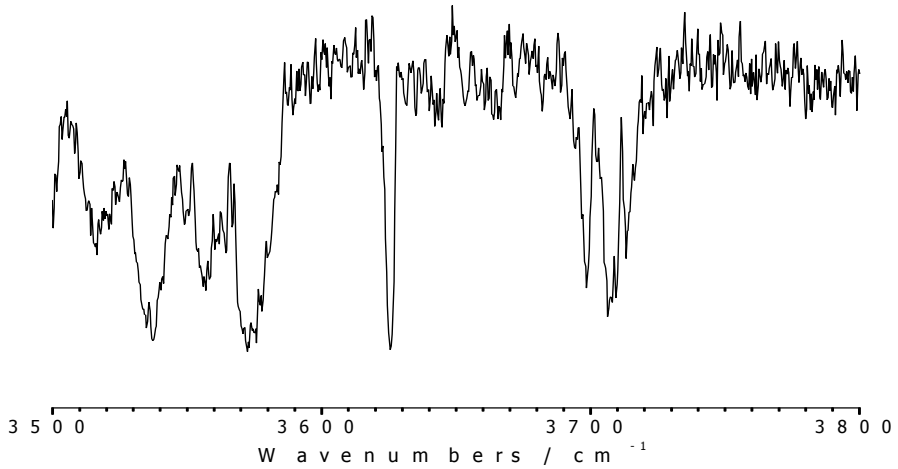

Figure 5.88. *A detailed view of the IDIRS spectrum in the 3500-3800 cm^{-1} region. Three peaks at c.a. 3700 cm^{-1} are observed.*

Assignment

As can be seen in Figure 5.87, only a few structures present the two mid-region intense groups: the characteristic OH···π peak and the two peaks at lower frequencies. Thus, only structures *e29* and *e9* reproduce the experimental results as can be seen in Figure 5.89. Consequently, we assign the experimental spectrum to a structure of the type of that depicted in Figure 5.90. This means that **the predicted most stable structure, is based on an open box type**.

One of the remarkable aspects is that compared to propofol·W_7 and propofol·W_8, the stretching due to the OH involved in the O-H···π interaction is nearly 30 cm^{-1} blue-shifted (3605 cm^{-1} for the 1:7 cluster and 3596 cm^{-1} for the 1:8 cluster), which seems to indicate that the interaction of the water's OH with the ring is not that strong, as it is closer to a free stretching.

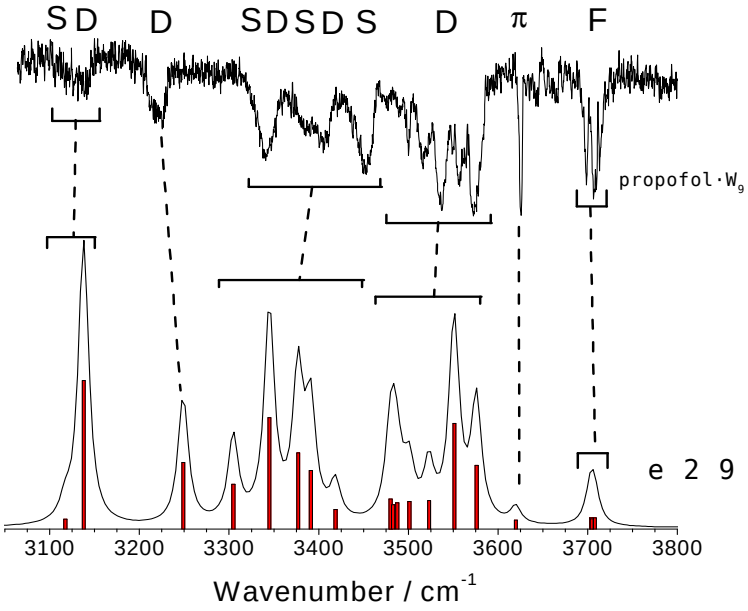

Figure 5.89. *Predicted IR spectrum for the structure e29. The experimental IDIR spectrum is also shown for comparison. As can be seen, the predicted spectrum for this structure is in good agreement with the experimental one for the first conformer.*

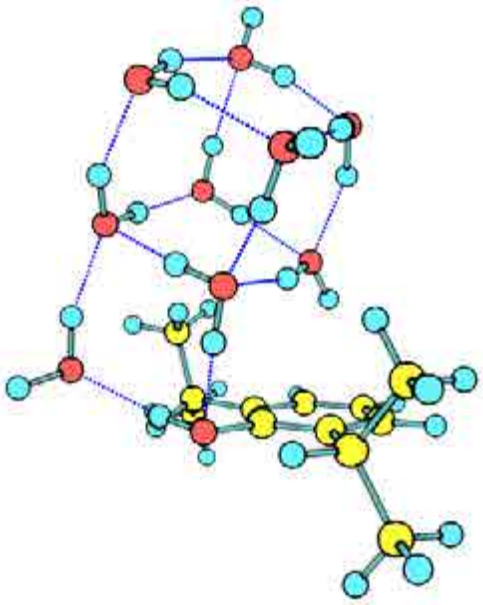

Figure 5.90. *Structure e29 is the theoretically predicted structure that better fits the experimental results. It is also the global minimum at M06-2x/6-311++G(d,p).*

Analyzing structure *e29*, the two peaks in the lower frequencies region are due to double donor stretching vibrations and they deserve special attention. The peak at 3220 cm^{-1} and the red-most peak are due to the tetracoordinated water molecule, which suffers a red shift from the expected 3450-3600 cm^{-1} region, where the double donor OH stretching modes typically appear.

Finally, the OH stretching modes for the experimental conformer are collected in Table 5.6 and compared with the structure *e29*.

Table 5.6. *Experimental vibrational transitions in the IR traces of propofol·W_9 conformer, with a tentative assignment based on a comparison with the calculated frequencies for structure e29.*

Experimental Peak (cm^{-1})	**structure *e29***		
	Frequency (cm^{-1})	Intensity	Vibrational type
3116	3117	90	σ_s^s (OH_w)
3139	3138	1336	σ_s^d (OH_w)*
3221	3249	599	σ_s^d (OH_w)
3341 (x2 peaks)	3305	403	σ_s^s (OH_w)
	3345	1002	σ_s^d (OH_w)
3385	3377	686	σ (OH_{ppf})
3406	3391	527	σ_s^d (OH_w)
3453	3419	174	σ_s^s (OH_w)
3489 (x2 peaks)	3480	269	σ_s^d (OH_w)
	3483	220	σ_s^d (OH_w)
3500	3487	237	σ_s^d (OH_w)
3516	3501	249	σ_s^d (OH_w)
3537	3523	255	σ_{as}^d (OH_w)
3557	3551	950	σ_{as}^d (OH_w)
3572	3576	573	σ_{as}^d (OH_w)
3626	3620	80	$\sigma^{O\text{-}H\cdots\pi}$ (OH_w)
3698	3704	100	σ^f (OH_w)
3706	3704	91	σ^f (OH_w)
3713	3708	101	σ^f (OH_w)

*This mode corresponds to the water that is interacting with the propofol's OH. The OH stretching modes of this molecule are coupled with a movement of the whole cube, thus, making one of its stretching modes to red-shift more than that expected.

5.2.10 – Propofol·W_n: Discussion

Propofol molecule and its hydrated clusters were studied in section 5.2, their electronic excited state were characterized by means of the *2c-REMPI* technique and the number of conformer present was determined using the double resonance *hole burning* technique. Another double resonance technique, *IDIRS,* was used to obtain reliable information of the structure types, as the O-H stretching modes are very sensitive to the type of hydrogen bond in which they are involved (length, angle, number of hydrogen types in the surrounding, strength, etc) as they vibrate directly against the hydrogen bond. All this work yields invaluable information regarding some important aspects:

- **Assigned structures**

When a water molecule interacts with propofol under supersonic expansions, the latter acts as a proton-donor to the water molecule that, due to the estheric effect imposed by the isopropyl groups, is forced to stay out of the aromatic plane and thus, it loses the optimum O-H···OH_2 angle and distance, although an interaction with the aromatic ring is introduced. The addition of a second water molecule results in the formation of a cycle between the OH moieties. The same trend is observed in propofol·W_3, although in this case, the water ring can adopt two different orientations: either in the same plane of the aromatic ring, or perpendicular to it. The latter is separated from a structure with a water chain between propofol's OH moiety and the aromatic ring by a shallow barrier and thus, there is a fragile equilibrium between both isomers.

Introduction of a fourth water molecule causes an important structural change: a cyclic structure in the same plane as the aromatic ring would experiment repulsive forces caused by the isopropyl groups and thus, such structure is no longer stable. Accordingly, the IDIR experiments clearly demonstrate that propofol·W_4 has a non-cyclic structure. Instead, waters form an eight-member ring, with the fourth water molecule interacting both with a water molecule and the π-cloud (Figure 5.93a).

For the subsequent systems only non-cyclic structures are found (Figure 5.93a): for **propofol·W_5** cluster a ***book*-type** structure was found for one of the conformers. **Propofol·W_6** gives two ***prism* structures**, one with and the other one without interaction with the aromatic ring. **Propofol·W_7** presents an interesting case as W_8 has

always been considered as an especially stable **cubic structure**. We found a **cubic structure for propofol·W_8** for one of the conformers, while the other one presents a similar structure, but closing the cube in the aromatic ring, i.e. with an OH···π interaction. **For propofol·W_9** cluster an ***open box* structure** is found.

Formation of other structures, such as a eight-water cube interacting with the propofol molecule in propofol·W_8, or a nine-water cube interacting with propofol in propofol·W_9 among others, cannot be ruled out as they can be present in the experiment but may not be detected due to fragmentation or to large changes in geometry upon excitation.

- **Reduction on the number of observed conformers**

One of the first surprising aspects of this study is that **the increase in cluster size results in a reduction on the number of observed conformers** (table 5.7). Four of propofol's five conformers (GG, Gg, EG and GE) were detected, being those with the isopropyl hydrogen atoms pointing *forward* the most stable ones, i.e. Gg and GG isomers. The introduction of a water molecule reduces the number of conformers to three (GE is no longer present), and the introduction of a second water molecule further reduces them to only two (presumably based on the GG conformer and differing only in the hydrogen atom positions). From this point, inclusion of water molecules does not increase the number of conformers and, the detected species differ in the orientation of the water molecules, maintaining the same chromophore structure. In most cases, one of the isopropyls rotate until the hydrogen atom is in the plane of the ring, eliminating the GG/Gg distinction.

Table 5.7. *Number of conformers observed experimentally for propofol·water$_n$. There is a reduction on the number of observed conformers as cluster size increases.*

Propofol·W_n	0	1	2	3	4	5	6	7	8	9
nº of detected isomers	4	3	2	2	1	2	2	2	2	1

- **Lifetimes**

Another important aspect is related to the (singlet) **propofol S_1 short lifetime,** which is similar to what is observed for phenol. For the bare molecule, the decay is due to internal conversion, even at the $S_1(v'=0)$ and, as it is reported in the literature,[32] the strong interaction between $n\pi^*$ and $\pi\pi^*$ states, disturb the S_1 potential surface and causes a strong overlap with the ground state vibrational levels. Thus, the decay of the S_1 state is through internal conversion to high-lying vibrational states of the S_0 manifold. The decay rates are greatly affected by the presence of a single hydrogen bond, demonstrated by the increase to nearly 20 ns for propofol·W_n (n=1-3). Such increase seem to correlate with the reduction on propofol's OH stretching vibrational frequency in the complex due to the formation of a propofol·OH···OH_2 hydrogen bond. Apparently, the hydrogen bond leads to smaller S_1-S_0 coupling for internal conversion.[33] Consecuently, in propofol·water complexes, the S_1 decay mainly goes through intersystem crossing where a decrease in the internal conversion rate is achieved. For propofol·W_n, where n>4, there is a general reduction in the excited state lifetime (Figure 5.91), pointing again to changes in the excited state's internal conversion rate, maybe related to a change in the energetic of the $^1\pi\sigma^*(S_1)$ state, or even to variations on the transition dipole moment.

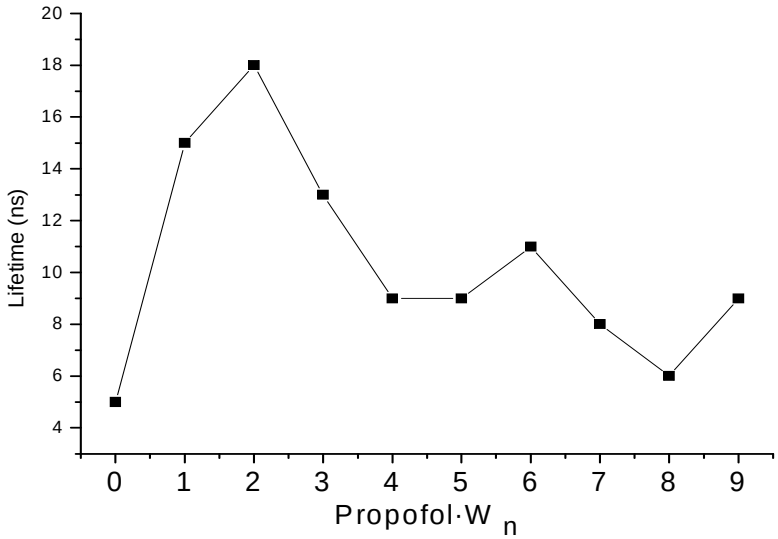

Figure 5.91. *Excited state lifetime for propofol·W_n clusters. It must be noted that there is a general reduction with the number of water molecules. The lifetimes of all the species is collected in appendix 7.2.*

- **General shape of the spectra:**

The spectra collected in Figure 5.92 show a significant change in the appearance with the degree of hydratation. While propofol$_n$, n=0-3, species exhibit discrete, although congested spectra with well-resolved structures, addition of a fourth water molecule results in a complete loss of structure. Surprisingly, with addition of more water molecules, the spectrum regains its resolved structure, although a background is always present. This broad absorption can be due to several processes: fragmentation from higher order clusters, accumulation of lines due to the presence of numerous, nearly identical conformers, which could possibly have almost identical $S_1 \leftarrow S_0$ transitions, preventing us of distinguishing between them in *hole burning* experiments, existence of dynamics in the excited state or even dramatic structural changes upon excitation.

Fragmentation can be discarded, as no changes were observed with variations in the probe laser fluency. On the other hand, if the broad absorption is due to accumulation of spectra due to conformational isomers, the IR spectra should also present broad or numerous absorptions, which is not the case. In addition, the measured S_1 lifetimes rule out the existence of fast, excited state dynamics, as the shortest lifetime was measured for the bare molecule, which presents a discrete spectrum. Therefore, the broad absorption may be due to conformational changes upon excitation. Indeed, the structure for propofol·W_4 is considerably floppy and, as it was demonstrated, experiments changes from S_0 to S_1. Consequently, its spectrum exhibits no discrete structure. The higher-order clusters studied in this work have more rigid structures, and therefore all present, at least, a discrete origin band. Thus, there may be some other floppy species which are responsible for the background and whose IR spectra were not found.

- **Stabilization upon ionization**

Table 5.8 shows the position of the origin band for each propofol·W_n, n=6-9, conformer, relative to the red-most one for bare molecule conformer (36222 cm^{-1}) and of propofol·W_1 red-most conformer (36030 cm^{-1}). On the other hand, Figure 5.92 shows the *2c-REMPI* spectra of all propofol·W_n clusters studied, together with a *ball and stick* representation of the structure of each conformer. Table 5.8 does not include the origin bands for propofol·W_4 and propofol·W_5 as their origins are not completely clear.

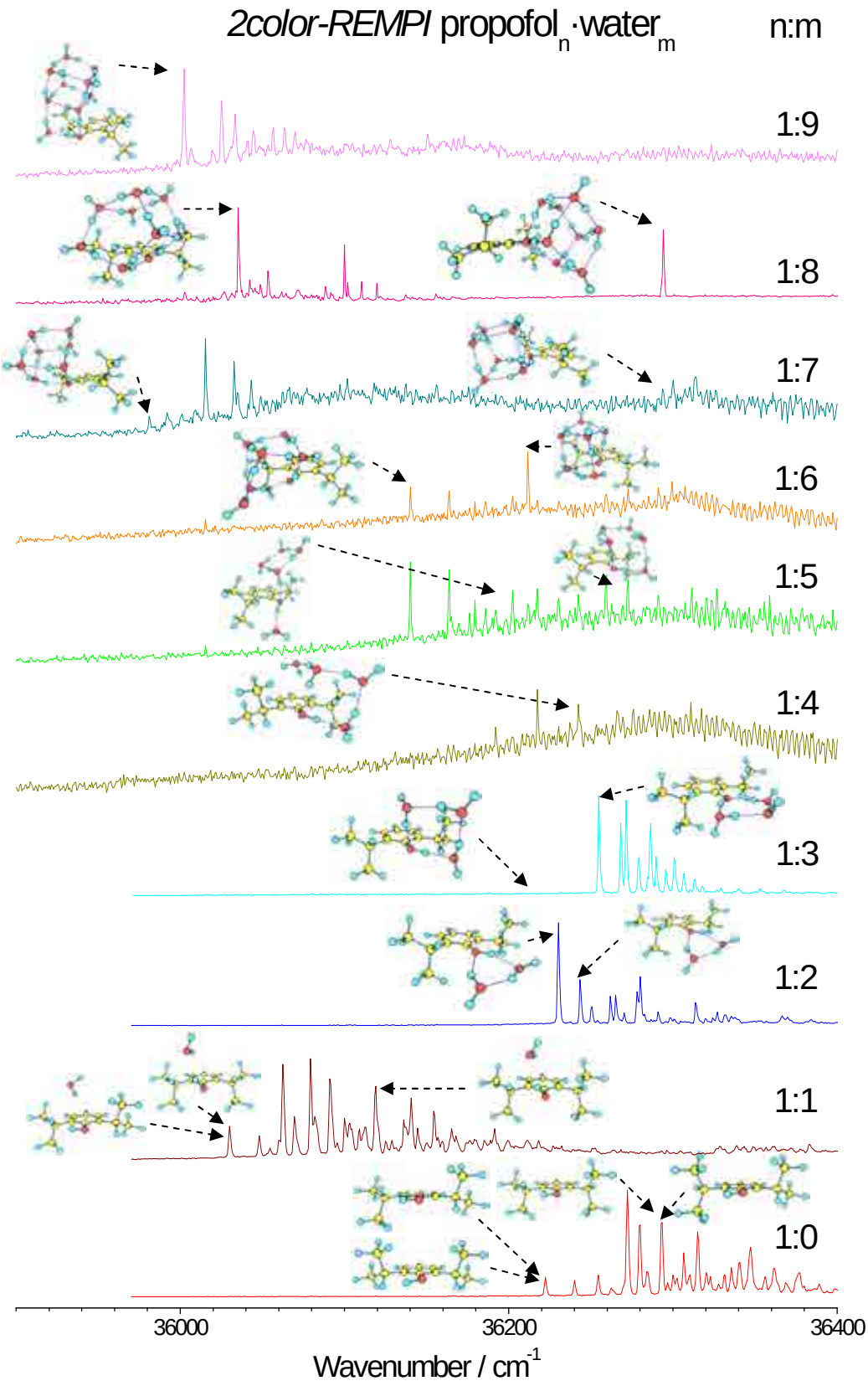

Figure 5.92. *2c-REMPI of propofol·W_n, n=0-9 in the 35700-37400 cm^{-1} region. The images show the structure assigned for each conformer.*

Table 5.8. *Position of the origin bands of propofol·W_n n=6-9 clusters, relative to propofol/propofol·W_1 0_0^0 transition. As can be seen, the origin band of the first conformer is always red-shifted from the bare molecule, while the second conformer exhibits a small shift, typically to the blue. Values are in cm^{-1}.*

Propofol·W_n	6	7	8	9
first conformer	-82 / +110	-241 / -49	-187 / +5	-220 / -28
second conformer	-10 / +182	+71 / +263	+73 / +265	-

As can be seen, the inclusion of the first water molecule, leads to a large red shift that can be attributed to the change in the inductive effect of the propofol's oxygen atom on the $\pi^*\leftarrow\pi$ transition, produced by the hydrogen bond. The $\pi^*\leftarrow\pi$ transition transfers electron density from the oxygen atom to the aromatic ring. Thus, cluster structures with an enlarged electron density on the oxygen atom will be more stabilized in the excited state than in the ground state, resulting in a red shift of the electronic origin relative to the monomer. Consequently, as propofol molecule acts as proton-donor (acid) the formation of a hydrogen bond leads to a red-shift. However, in propofol·W_2 the second water molecule acts as a proton-donor to the propofol's oxygen atom, reducing the inductive effect of the proton-acceptor water molecule and the red-shift is no longer observed, which is the typical signature of a ring formation. Propofol·W_3 follows the same trend: the water molecules also form a cyclic structure. For propofol·W_4 and propofol·W_5 such analysis may not be performed, as for the former no resolved transition was found, while for the latter, the experimental results point to an insufficient FCF window for direct access to the v'=0 level.

A close inspection of the **second conformer** of propofol·W_6, propofol·W_7 and propofol·W_8, shows that their origin bands appear very close to that of propofol bare molecule or they are slightly blue-shifted. This, a priori, suggests that **propofol's OH moiety forms part of a water-ring structure**. It is worthy to note that results for the **first conformer of propofol·W_n, n=6-9**, demonstrate that a **direct interaction between the water molecules and the aromatic ring** leads to a **red shift in the 0_0^0 transition**, against what is commonly accepted. Such red-shift is, in some cases, even greater than that found for propofol·W_1. In the excellent work by Kleinnerman's group on the solvation of phenol, they suggest that, for phenol·W_8 cluster,[24] one of the peaks located at 3619 cm^{-1} in the IR spectrum of one of the conformers is evidence of an O-H···π

interaction (Figure 5.93b), although they discarded such possibility, arguing that all the published electronic origins of benzene-water π-hydrogen bonded clusters are blue-shifted relative to the forbidden benzene origin.[19,21] In the light of the present results it is evident that the discarded possibility was the correct assignment.

The shift in the excitation energy is probably the most unpredictable property of non-covalent systems, as is the result of subtle changes in several weak interactions. The red-shift presented by the isomers to the red is, in these systems, due to a prevalence of the change in the importance of dispersive forces, caused by the increase of the size of the π cloud upon excitation.

Apart from the general aspect of the peak, intensity and being isolated for the rest of the double donor stretching bands, which are strong arguments supporting that this OH···π interaction is present, we successfully recorded propofol·W_8 red-shifted conformer's excited state IR spectrum (Figure 5.66). As it is clear, the electronic excitation causes a decreasing in the OH stretching vibration of the water forming the O-H···π interaction, pointing to an increasing in the strength of such interaction due to electronic excitation.

One last remarkable aspects concerning the O-H···π interaction is the shift experimented for this OH stretching vibration, as it is considerably more red-shifted than what is found for benzene·$water_8$ and benzene·$water_9$: c.a. 3640 - 3650 cm^{-1} (Zwier's group[19,30]). In our work, this band appears at 3624, 3610, 3596 and 3625 cm^{-1} for propofol·W_n, n=6-9 respectively. The main difference between benzene·W_8, phenol·W_8 and propofol·W_8 is the two isopropyl substituent of electron donor character, which increase the electron density of the aromatic ring, resulting in a reinforcement of the O-H···π interaction, and in a bigger red-shift.

- **Comparison with similar systems**

A comparison between the results obtained for propofol and those reported for phenol gives an estimation on the influence of the two isopropyl groups in the solvation process. Table 5.9 collects the most significant parameters determined for propofol, together with those reported for the equivalent phenol-containing species. The most evident difference between phenol and propofol is the appearance of four isomers in the latter, due to the relative orientations of the isopropyl groups. All four propofol

conformers present 0_0^0 transitions red-shifted respect to that of phenol, by 30-100 cm^{-1}. The influence of the isopropyl groups in the OH stretching vibration is small, as a mere ~ 6 cm^{-1} difference with the phenol homologue is observed. The difference between phenol and propofol OH stretching vibrations is not remarkable either, as it is bellow 10 cm^{-1}.

Complexation with one water molecule induces a red shift of ~ 350 cm^{-1} in the 0_0^0 transition. Phenol acts as proton donor, establishing a strong hydrogen bond, as demonstrated by the observed shift of ~ 130 cm^{-1} in the phenol OH stretching vibration. The water also enters as proton-acceptor in the propofol·W_1 complex. However, smaller shifts both in the 0_0^0 transition and in the OH stretching vibration are observed. The former points to a smaller change in the complex binding energy with excitation, while the latter indicates that the propofol-water hydrogen bond is weaker than in phenol. This is a consequence of the two hydrophobic isopropyl groups that interfere with the solvation process, due to out of plane of ring arrangement. The shift of the propofol OH stretching vibration is also smaller than in phenol, 3452/3540/3448 cm^{-1} for GG/Gg/EG isomers, compared to 3388 cm^{-1} for phenol. Thus, although the isopropyl groups debilitate the OH-water interaction, they fail in completely blocking the OH solvation site.

Table 5.9. *Comparison between propofol and phenol. The results for propofol·W_1 and propofol·W_2 with the phenol·W_1 and phenol·W_2 clusters are also included. All values are given in cm^{-1}.*

		Propofol·W conformer				Phenol
		1	2	3	4	
1:0						
	0_0^0	36224	36273	36315	36315[e]	36348[a,I,k], 36352[b,c], 36349[d]
	ν(OH), S_0	3652	3649	3645	3647	3657[a]
1:1						
	0_0^0	36029	36064	36120		35994[a], 35997[b], 35996[c,d], 36000[g], 35995.626(2)[i]
	ν(OH)					
	S_0	3557	3556	3556		3524[a,g,k], 3624[l]
	S_1	3452	3450	3448		3388[k,l]
	ν^{Free}(OH)	3740	3739	3740		3748[a,h]
1:2		3740	3740	3740		3748[h]
	0_0^0	36233	36246			36259[b,c], 36226[j]
	ν_1(OH)					
	S_0	3444	3448			3388[a]
	S_1	3334	3329			
	ν_2(OH)					
	S_0	3498	3506			3505 [a]
	S_1	3500[f]	3506			
	ν_3(OH)					
	S_0	3545	3546			3553 [a]
	S_1	3576	3577			
	ν_4(OH)					
	S_0	3717	3720			3722 [a]
	S_1	3718	3720			
	ν_5(OH)					
	S_0	3718	3720			3725 [a]
	S_1	3720	3726			

[a]Ref8
[b]Ref 9
[c]Ref 10
[d]Ref 11
[e]The difference between isomers 3 and 4 0_0^0 transition is less than 1 cm^{-1}.
[f]a new feature appears at 3369 cm^{-1}.
[g] Ref 12
[h]ν_1=3650 cm^{-1}, this vibration is too weak in propofol·W_1 to be detected,
[I] Ref 13
[j]Ref 14
[k]Ref 7
[l]Ref 15

Another remarkable aspect is the change in the excited state lifetime. While propofol S_1 state has a short lifetime, shorter than our nanosecond laser pulse's width, the introduction of a water molecule increases the S_1 lifetime to 15 ns. Assuming that dynamics of the excited state of propofol is not that different from phenol, its major pathway for decay from the S_1 state into the S_0 vibrational modes should be internal conversion along the OH coordinate. Complexation with water, should therefore lead to a decreasing on the internal conversion constant rate, resulting in an increasing of the S_1 state lifetime as it happens with phenol[5-7]. The results obtained here are in agreement with those obtained for the phenol molecule.

A comparison between the results obtained for propofol·W_2 and those reported for phenol·W_2[15] is also offered in table 5.9. Although phenol and propofol 1:2 complexes present similar cyclic structures, their spectroscopy is markedly different: while phenol 1:2 spectrum is a broad absorption, its propofol analogue shows well resolved vibrational bands. Also, the fast relaxation of phenol 1:2 precludes recording the IDIR spectrum in the excited state. Ebata et al. argued that, due to IVR process, there is a broadening of the OH stretching vibrational levels and therefore the IR laser was not effectively absorbed. Conversely, propofol·W_2 shows a discrete spectrum. Such observation may be related to the large differences observed in S_1 state lifetimes: c.a. 18 ns for propofol·W_2 and of a few ns for phenol·W_2. In the latter, this lifetime reduction may be due to a poor FCF to access the bottom of the potential well, as pointed out by Ebata et al,[15] which argue that there is a large conformational change from a ring-like to an open structure upon excitation. Such conformational change does not seem to take place in propofol·W_2 and that is why this system retains a larger lifetime. The voluminous isopropyl groups produce a general reduction in the strength of the hydrogen bonds, as demonstrated by the fact that all the ν(OH) vibrations observed are blue-shifted respect to their phenol·W_2 homologues, but they are not able to completely block the OH solvation site, and, as it was demonstrated above, the two 1:2 isomers detected present cyclic structures.

When compared to water,[31] benzene·W_n[19,26] and phenol·W_n,[8,14,24] some important differences can be appreciated. Due to the OH moiety phenol and propofol water clusters, can be envisioned as a water cluster in which one of the water molecules has a voluminous substituent. In phenol·W_n and benzene·W_{n+1} both, calculation and experiments, point to a change from cyclic to non-cyclic structures from six water

molecules onwards. In addition, for n=5 a single cyclic structure is considerably more stable than any other possibility. For phenol instead, such transition occurs at n=5. Despite that phenol·water is one of the most extensively studied systems, there is no general agreement on the structure of some clusters. For example, a single cyclic structure was reported by Watanabe et al.[8] for phenol·W_4. However, in a more recent work, Stanley and Castleman report a second isomer with a 3D hydrogen bond network. In subsequent works[36] it was demonstrated that such isomer was due to fragmentation from ph·W_5. Thus, **propofol·W_4 is the smallest of the four systems in adopting a non-cyclic structure**, due to the steric hindrance of the isopropyl groups.

For the **propofol·W_5** cluster a ***book*-type** structure was found for one of the conformers, which is one of the most stable conformers found for $water_6$ (*cyclic, book, cage* and *prism* types). Figure 5.93a collects the assigned propofol·W_n conformers and its equivalent W_{n+1} structure, while Figure 5.93b collects those for benzene·W_8 and benzene·W_9 and the most likely structures for phenol·W_5 and phenol·W_6. For the best of our knowledge, for benzene·W_6 the exact structure was determined so far, although it is clear from the IR spectrum that the water molecules adopt a 3D arrangement.[26] For phenol·W_5 there is not a ground assignment but the structure is either a *cage*- or a *book*-type isomer with the latter being more likely.[36]

Propofol·W_6 gives two ***prism* structures**, one with and the other one without interaction with the aromatic ring, in agreement with the predicted most stable water structure: W_7 gives rise to five stable families of structures denoted as *prism*, *cage*, *chair*, *bicyclic* and *hexamer+monomer* with the first being the most stable. Although benzene·W_7 and phenol·W_6 structures have, to our knowledge, yet not been identified, they also present non-cyclic structures as *no window* region is found.

Propofol·W_7 presents an interesting case, as W_8 has always been considered as an especially stable structure. As predicted by theoretical calculations and experimental results, the most stable conformers for W_8, benzene·W_8 and phenol·W_7 are almost isoenergetical cubics (S_4 and D_{2d}). Our results are in agreement with such findings, where one of the propofol·W_7 conformer is a **cubic structure** and the other one is similar but closing the cube in the aromatic ring instead of on the propofol's OH moiety.

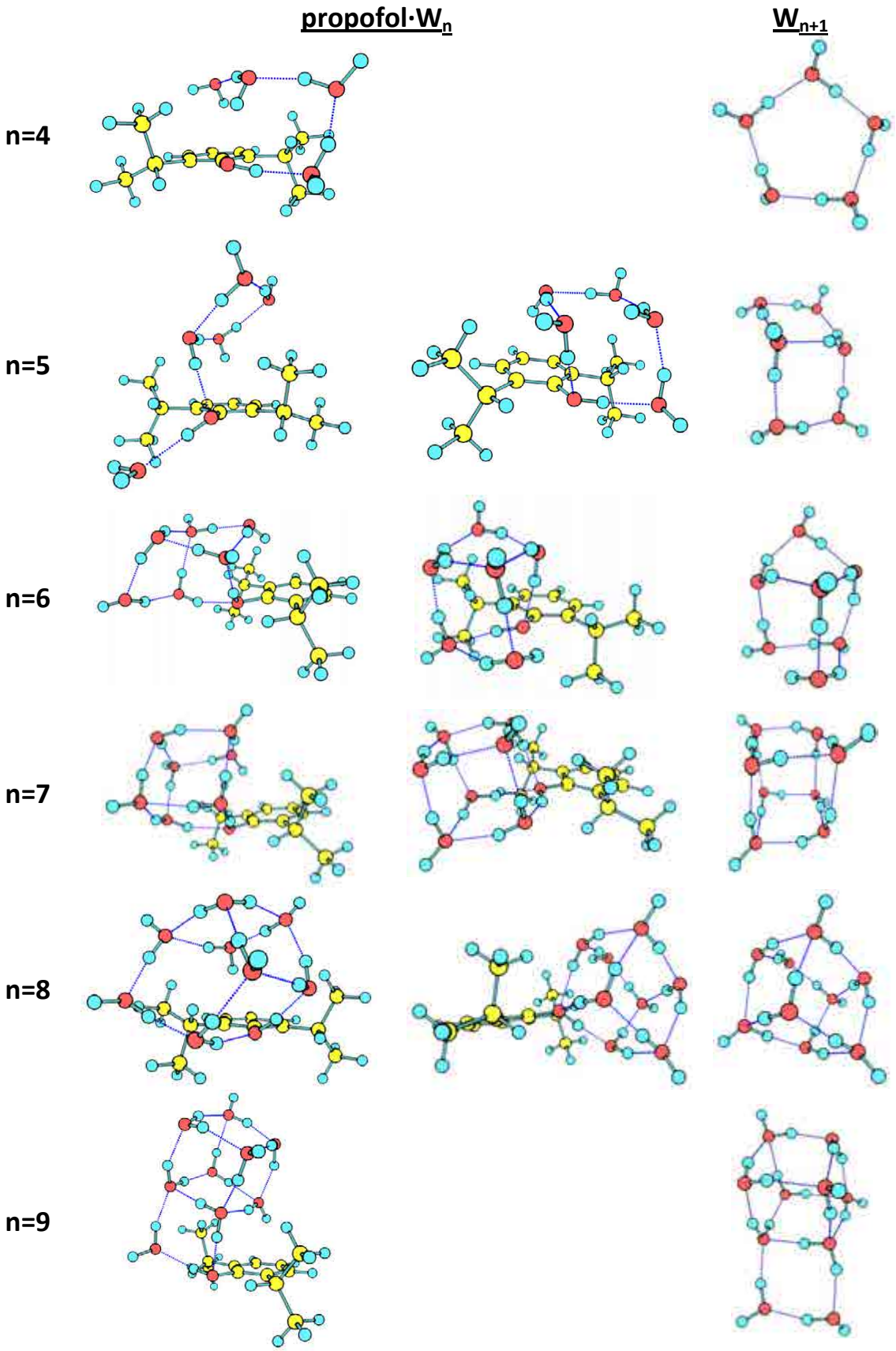

Figure 5.93a. *Assigned structures for the propofol·W_n conformers detected, together with their equivalent n+1 water complexes (right side).*

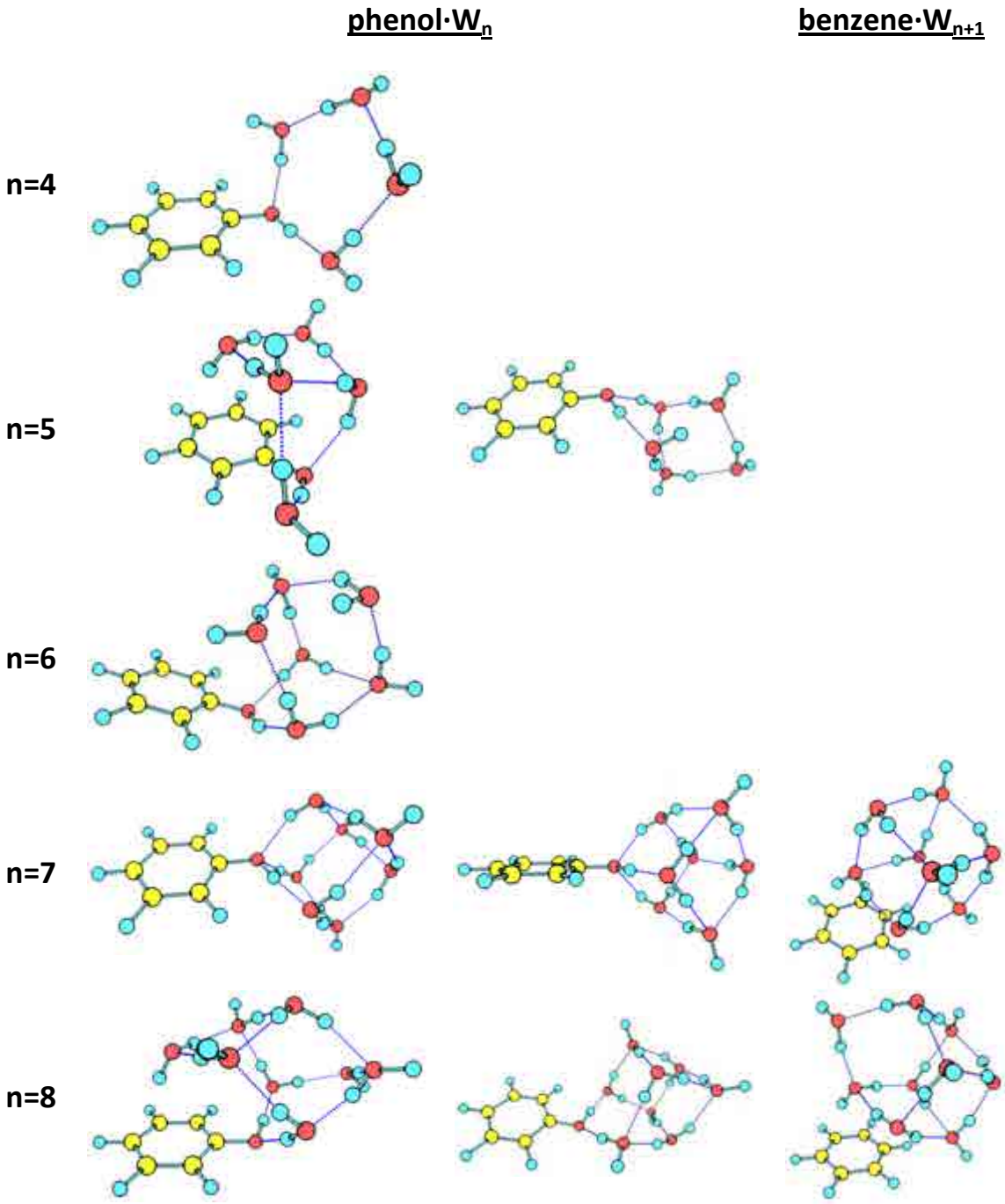

Figure 5.93b. *A comparison between phenol·W_n and benzene·W_{n+1} structures assigned by Kleinermanns' group[24] (the most likely for the phenol·W_5 and phenol·W_6 structures) and Zwier's group[19,30] respectively, conducted at M06-2x/6-311++G(d,p) level, and our results. In the light of the present work, we propose the phenol·W_8 structure where an O-H···π interaction is present for one of the structures.*

For W_9, **a stacked pentamer-tetramer** shape is predicted as the most stable conformer, and depending on the face of the cube where the new water molecule enters (homodromic or non-homodromic face, to a double-donor or donor-aceptor water molecule) different conformers are predicted: water adopts the same arrangement in benzene·W_9. We found the same type of structure **for propofol·W_8** second conformer, while the first conformer presents a similar structure, but with an OH···π interaction.

Finally, the predicted most stable W_{10} clusters are categorized into four main classes: *pentagonal prism*, *open box*, *distorted prism* and *cage* structures. Theoretical prediction **for propofol·W_9** clusters also point to this kind of structures and the only conformer found in our work is in agreement with the results as an ***open box*-type** is found, which is also the most stable structure predicted at M06-2x/6-311++G(d,p) level.

Thus, except for W_5 vs. propofol·W_4, propofol·W_n follows the structures predicted for W_{n+1}, leading to the conclusion that propofol molecule, despite the impediments introduced by the isopropyl groups, does not alter much the self auto-aggregation power of water, which is always able to accommodate in very similar ways to the structures observed for pure water clusters.

5.3 – Propofol $_2$

Propofol dimer is a specially complicated system, due to the existence of several stable configurations for the monomer, together with several possible interactions: stacked, O-H···π and O-H···O-H. Thus, the molecular mechanics calculations yield more than a thousand structures for this cluster in a 20 kJ/mol window. Figure 5.94 shows the eight more stable structures calculated at M06-2x/6-311++G(d,p) level. All of them point to an important contribution of π···π and C-H···π interactions in the cluster formation. In addition, the orientation of the OH groups indicates a dipole-dipole interaction, in most cases, that further stabilizes the cluster. Against, what is observed for propofol·water clusters, there is a considerably large energy difference (c.a. 7 kJ/mol) between the two most stable structures.

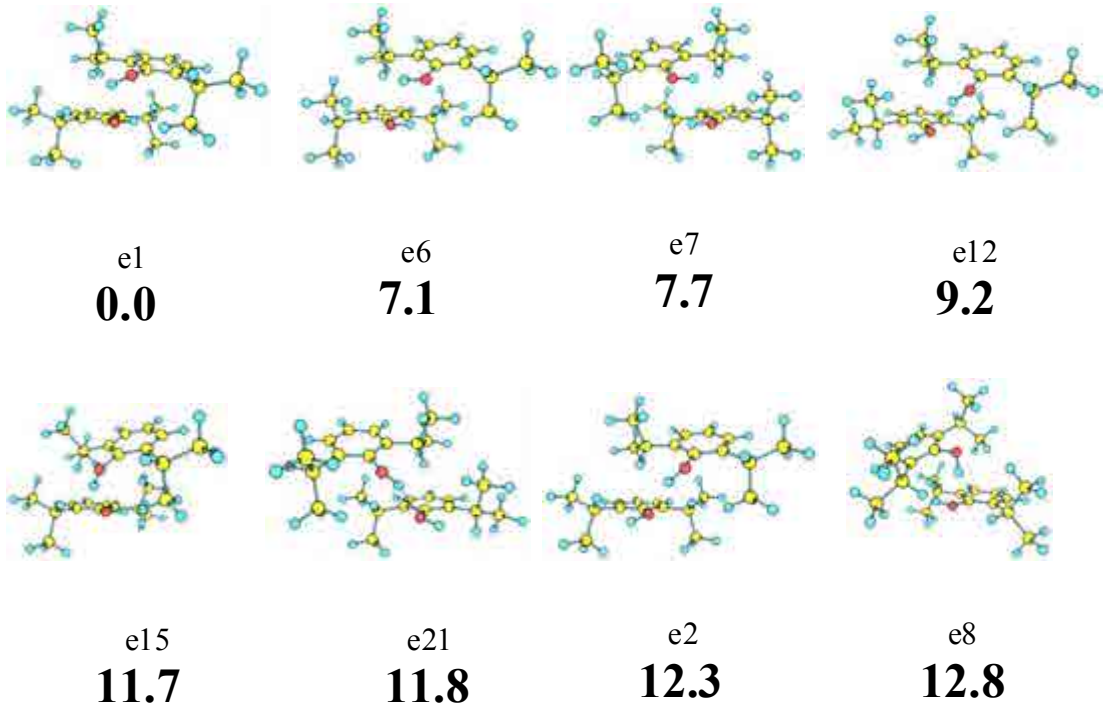

Figure 5.94. *Propofol$_2$ eight most stable conformers calculated at M06-2x/6-311++G(d,p) level, with their relative energies in bold. Energy values are in kJ/mol. All the calculated structures are presented in appendix 7.1 (Figure 7.19).*

Figure 5.95 shows the *2c-REMPI* spectrum of propofol$_2$ in the 35800 – 37400 cm^{-1} region, recorded with the probe laser at 27972 cm^{-1}. A large abundance of bands is observed, with the most intense peaks on the first 500 cm^{-1} and the origin band located at 36169 cm^{-1}. The overall spectrum resembles to that of the bare molecule, as the peaks

in the first 100 cm^{-1} are less intense than the system of bands at 36300 - 36400 cm^{-1}. Such observation leads to the assumption that a change in the geometry is taking place upon excitation, which results in an increase on the FCF with the excitation energy.

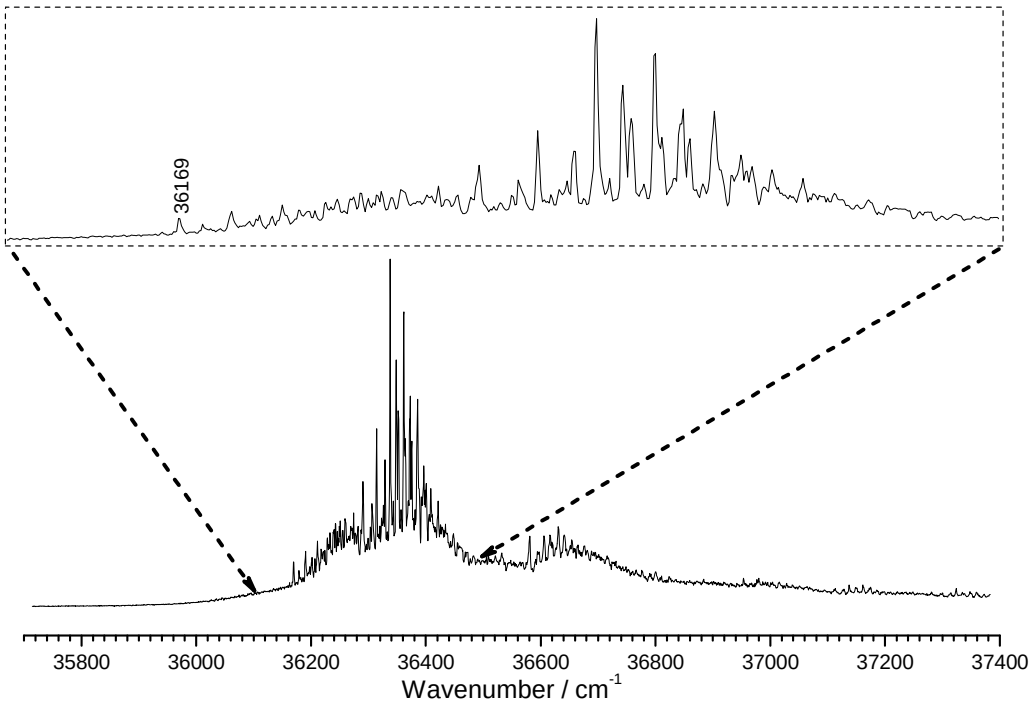

Figure 5.95. *2c-REMPI of propofol$_2$, in the 35700-37400 cm^{-1} region, recorded setting the probe laser at 27972 cm^{-1}. The insert shows a detailed view around the origin.*

To avoid fragmentation due to higher order clusters, a correct election of the second color is necessary. For propofol·W$_n$ clusters the third harmonic (355nm) of a Nd:YAG laser was used and in order to test if it is possible to use the same wavelength in this system, the photoionization efficiency curve was recorded, tunning the pump laser at the 0_0^0 transition (36169 cm^{-1}, Figure 5.96). The value obtained gives an ionization threshold of c.a. 63782 cm^{-1} (36169 cm^{-1} + 27613 cm^{-1}), which is similar to the value obtained for the bare molecule, and thus, 355 nm photons will be used for this system.

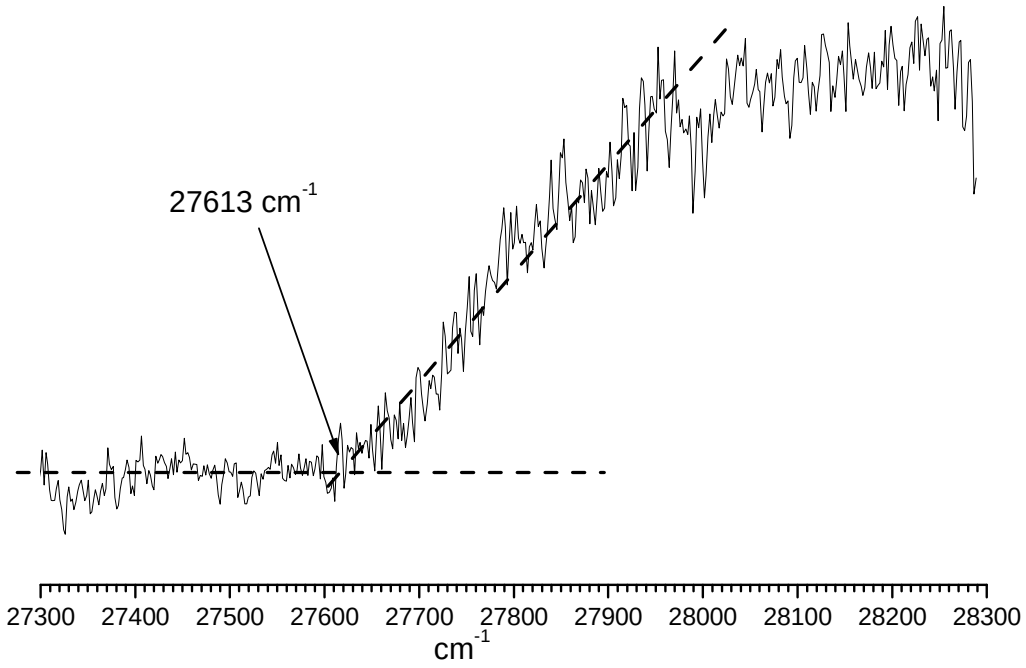

Figure 5.96. *Propofol$_2$ ionization threshold. The first color is tuned into the* 0_0^0 *transition, and the probe laser is scanned while the total ion current is collected.*

To determine the number of conformers, a *hole burning* experiment was carried out probing the transitions at 36355 and 36358 cm^{-1}, finding two isomers as can be seen in Figure 5.97. Both conformers present similar spectra and they show vibrational activity over an extension of 500 cm^{-1}. The position of the origin bands of the conformers is not clear, because both *hole burning* spectra seem to have a small deep in the red-most shifted peak located at 36176 cm^{-1}, which is also a very weak transition. Apparently, this peak is due to the first conformer and there is a crossed *hole burning* for the second conformer, as they present common transitions. Certainly, the overlap of transitions from both conformers is so important that it was difficult to find a transition for recording pure *hole burning* and IDIR spectra for each conformer. Luckily, the transitions at 36355 and 36358 cm^{-1} are characteristics for the first and second conformer respectively.

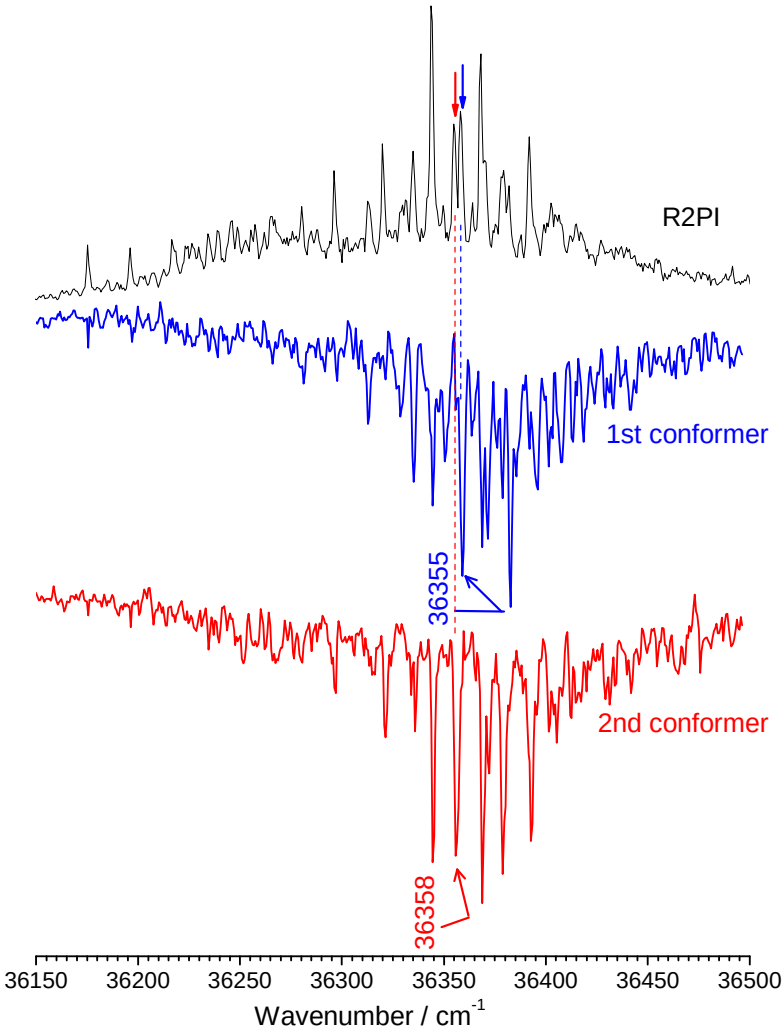

Figure 5.97. *Hole burning traces of propofol$_2$ recorded tuning the probe lasers (2-color detection) at 36355 and 36358 cm^{-1}. The peaks noted with arrows indicate the transitions employed for recording the hole burning spectra, as well as the IDIRS trace.*

Figure 5.98 shows the IDIR spectra of the detected conformers, recorded setting the probe laser at 36355 and 36358 cm^{-1}. While the first conformer clearly shows two transitions, the second one exhibits a single IR transition. The former points to a direct O-H···O-H interaction, which causes a shift in one of the OH stretching modes, while the latter points to an absence of hydrogen bond between the two molecules conforming the cluster.

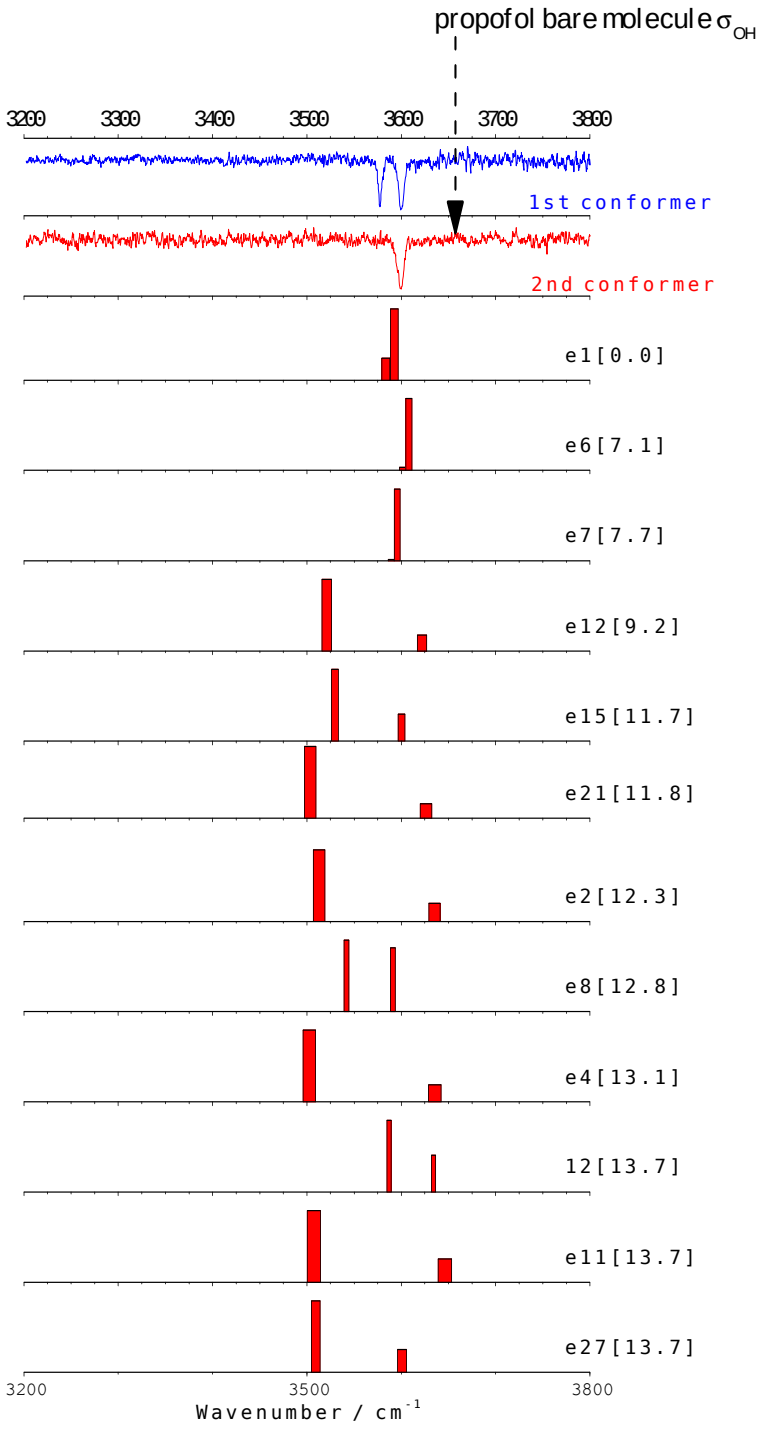

Figure 5.98. *IDIR spectra of propofol$_2$ recorded tuning the probe laser at 36355 and 36358 cm^{-1}. The predicted IR spectra for some of the calculated structures are also shown for comparison. The numbers in brackets are the relative energies of the calculated conformers, in kJ/mol. A correction factor of 0.93 has been applied. The predicted IR spectra of all the calculated structures are recorded in appendix 7.1 (Figure 7.20).*

The IR spectrum of the complex in the excited state is presented in Figure 5.99, together with the S_0 trace. As can be seen in the IDIRS spectra of the S_1 state, the electronic excitation causes a decreasing of c.a. 100 cm^{-1} in the OH stretching vibration. Surprisingly, two extra peaks appear in the S_1 state of the first conformer, which match those found for the second conformer, pointing to the existence of two conformers with overlapping transitions or an isomerization process in the excited state.

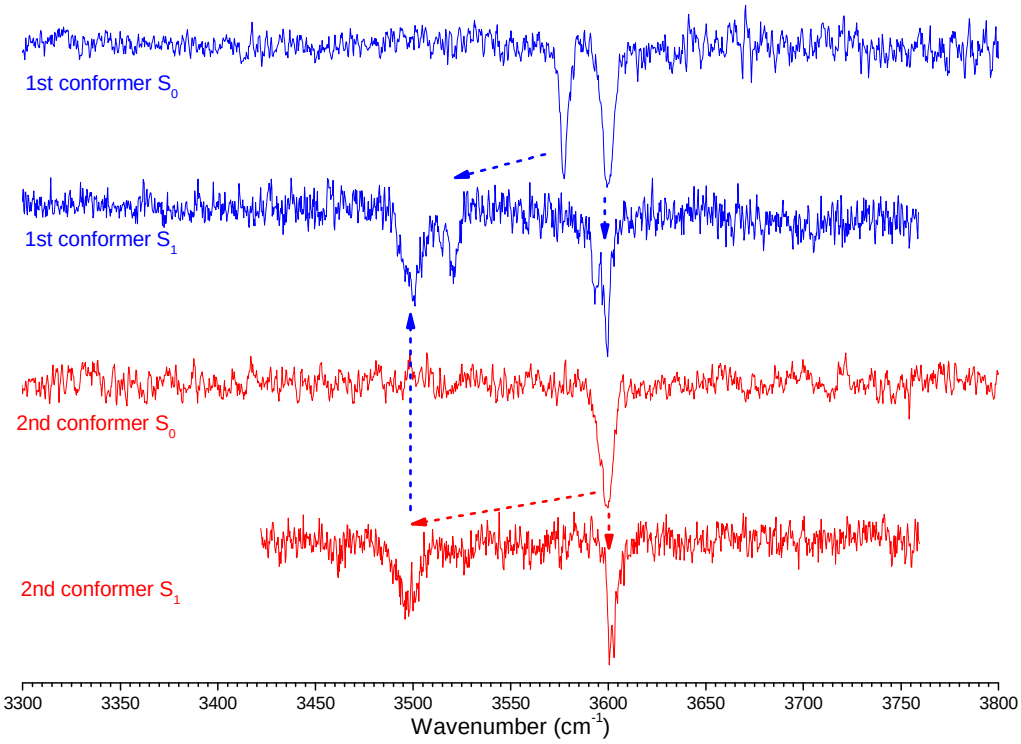

Figure 5.99. *Comparison between ground and excited state IRIDS of propofol$_2$ isomers.*

Discussion

As previously stated, propofol dimer is an interesting case, as there is a competition between hydrogen bond and dispersive forces. Phenol dimer[10,29] is the opposite example, as it is exclusively formed by a strong hydrogen bond between the two OH moieties. However, in the present system, the two voluminous isopropyl groups, on the one hand, create a more hostile environment for hydrogen-bond formation and, on the other hand, increase the importance of the interactions due to dispersive forces.

Molecular mechanics calculations predict a stacked-type structure as the most stable structure, with an additional stabilization due to the O-H···O-H interaction, which is of dipole-dipole nature in some of the structures, and a weak hydrogen bond in the others. The red shift in the origin bands of both isomers is in agreement with a stacked structure.[38] Besides, a small shift in the OH stretching is observed from the bare molecule (3650 cm^{-1}) to the cluster: the first conformer shows two inequivalent OH stretches at 3577 and 3600 cm^{-1}, while the second conformer IDIR spectrum presents a single feature at 3600 cm^{-1}.

Comparison between predicted and experimental IR spectra, shows that the spectrum of the **second conformer** is better reproduced by structures *e1, e6* (Figure 5.100) and *e7* among others, which present both OH stretching modes approximately at the same wavelength and slightly red-shifted with respect to that of the bare molecule. Such structures present a **dipole-dipole interaction** between the OH groups and thus, **the structure of second conformer is mainly formed by dispersive forces, with a small contribution of the dipole-dipole interaction between the two OH moieties**.

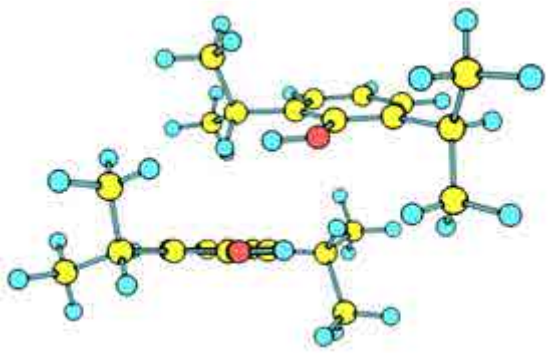

Figure 5.100. *Structure e6, in which the OH groups present a dipole-dipole interaction and whose IR spectrum matches that of the second conformer.*

A second type of structures are those where one of the propofol molecule's OH is a proton-donor to the other molecule's OH group, as shown for structures *e12* (Figure 5.101), *e21*, *e2, e4* and *e11* among others. The predicted IR spectra for this kind of structures do not match the experimental results, as the two OH stretching modes are too separated, due to the existence of relatively strong hydrogen bond.

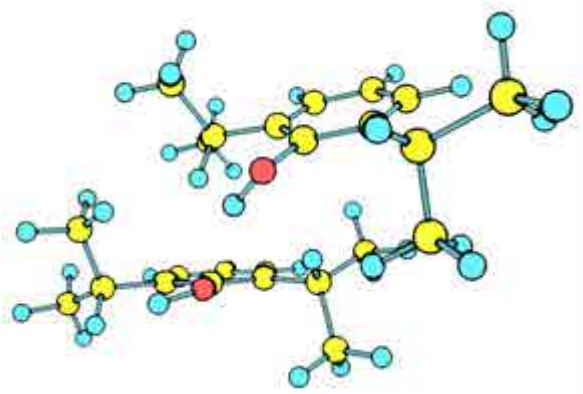

Figure 5.101. *Structure e12 where one of the propofol molecule's acts as an acid and the other OH moiety is not bonded.*

There is a third group of structures, which include structure *e1* among others, that present a slight variation respect to the ones of the previous group, as one of the molecules is shifted to one side, changing the relative position of the dipole-dipole interaction (Figure 5.102). Such structures reproduce the spectrum obtained for the **first conformer**.

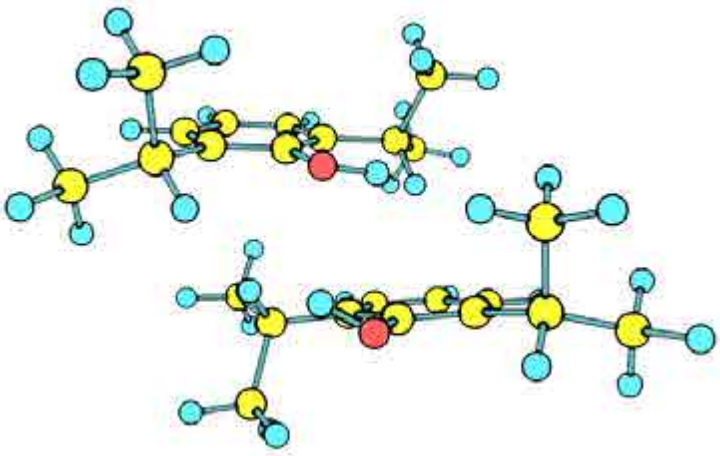

Figure 5.102. *Structure e1, where propofol molecule's present a slight variation from the other dipole-dipole interactions. These structures are in good agreement with the experimental results for the first conformer.*

There is a fourth group of structures, *e15, e8, e27*, *e19* among others, which are mid-way between second and third group: one of the molecules is shifted to one of the sides, favoring a weak O-H···π (dipole-polarizability) interaction, at a distance of c.a. 300 pm (Figure 5.102). Although weak, such interaction is strong enough to cause a 50 cm^{-1} shift in the OH stretching among such structures only structure *e8* (Figure 5.103) reproduces the spectrum obtained for the **first conformer**.

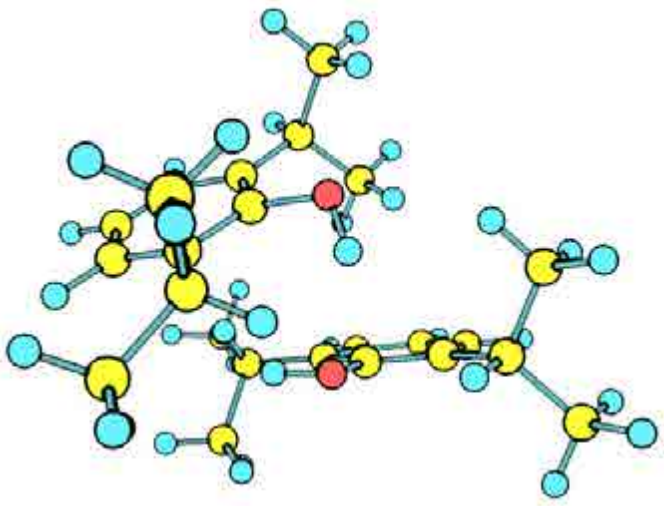

Figure 5.103. *Structure e8, where one of the propofol molecule's acts as an acid and the other has its OH moiety pointing towards the aromatic ring of the first. Its calculated IR spectrum explains the experimental results for the first conformer.*

These last two groups show some structural similarities and therefore, it is not surprising that there is a path with shallow barriers connecting their structures. Certainly, rotation of one of the isopropyl groups lead to a reposition of the other chromophore, that moves to one side. Such rotation may well be induced by excitation, leading to the appearance of new isomers in the excited state, as it will be demonstrated for propofol·phenol (see section 5.7.1). Such hypothesis is in agreement with the split observed in the S_1 IRID spectra of both conformers.

The rest of the structures, such as structures *12* or *9* (Figure 5.104), appear over 24 kJ/mol higher in energy than structure *e1*. In addition, there is a poor agreement between their predicted IR spectra and the observed ones.

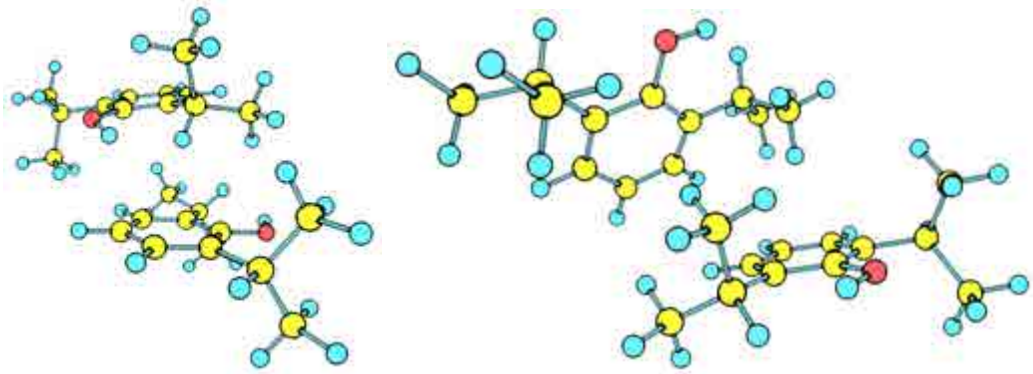

Figure 5.104. *Structures 12 or 9 where the molecules are mainly stabilized by dispersive forces do not reproduce the experimental results.*

5.4 – Propofol$_2$·W$_n$

Characterization of propofol$_2$·W$_n$ species is an important step in the understanding of the solvation process, which represents the transition from the pure substance to a mixture with the solvent. In propofol$_2$·W$_n$ complexes, it is possible to evaluate the competition between solute's self aggregation forces and solvent-solute interactions. In this section, we analyze propofol$_2$·W$_n$, n=1-7 clusters (Figure 5.105), following the same procedure as in previous sections. The inclusion of a second propofol molecule considerably increases the system's complexity, both experimental and theoretically, but still, some relevant conclusions can be extracted.

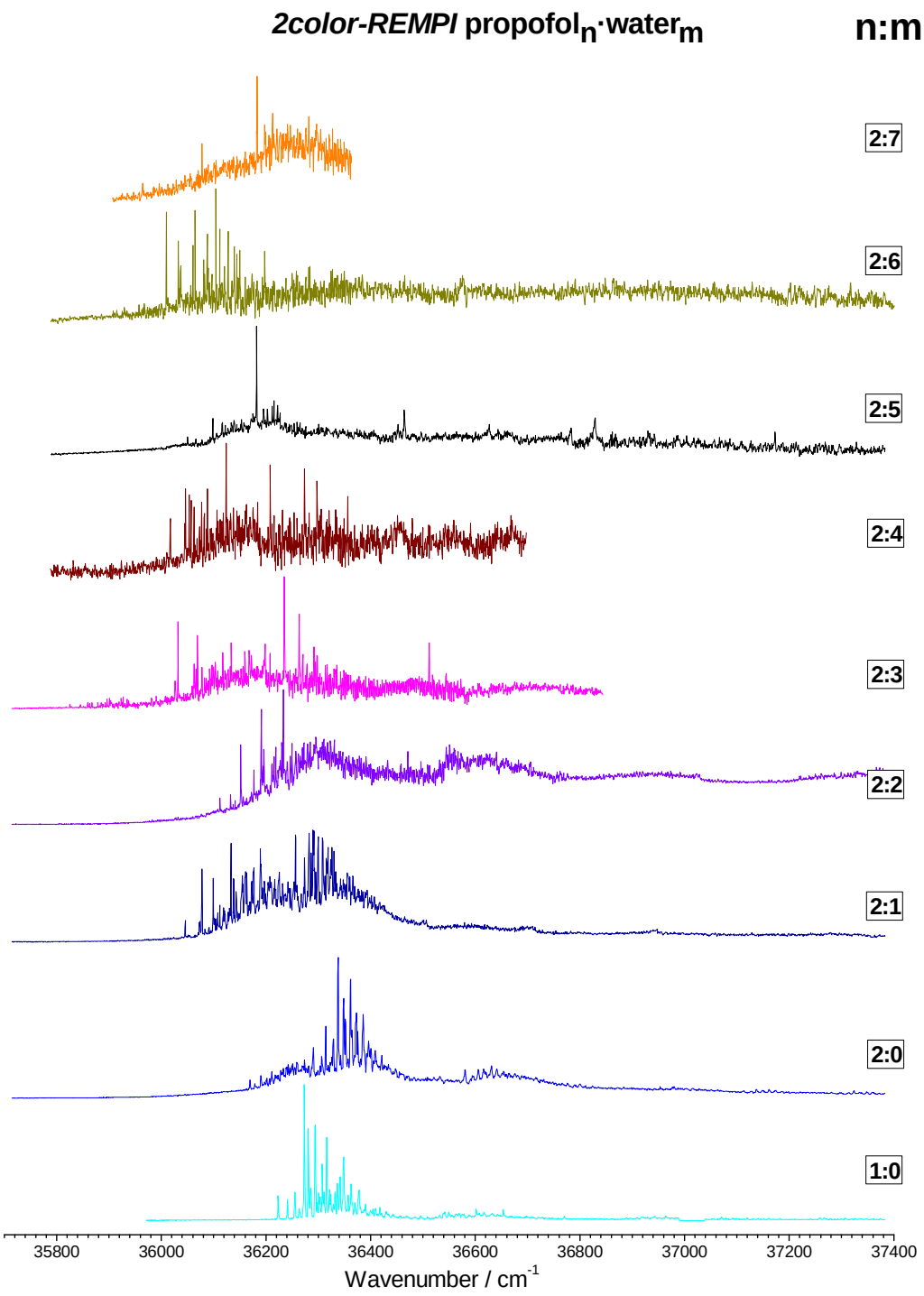

Figure 5.105. *2-color REMPI of propofol$_2$·W$_n$, n=0-7 in the 35700-37400 cm^{-1} region.*

5.4.1 – Propofol$_2$·W$_1$:

As it happens with the dimer, molecular mechanics calculation yields thousands of structures for this cluster in a 20 kJ/mol window, but only a few of them are found in a large number of occasions. According to the calculations at M06-2x/6-31+G(d) level, the most stable structures (structures *e15* and *e1*, Figure 5.106) have the two propofol molecules interacting by dispersive forces, through C-H···π interactions, while their OH moieties form a cyclic structure with the water molecule. The next four structures in Figure 5.106 (structures *e15, e1, e14, e22*) only differ slightly on the relative position of the molecules. A different type of structures is found above c.a. 7 kJ/mol, which present both O-H···OH and O-H···π interactions (structure *3, 6*). Clearly, the second type is energetically less favorable.

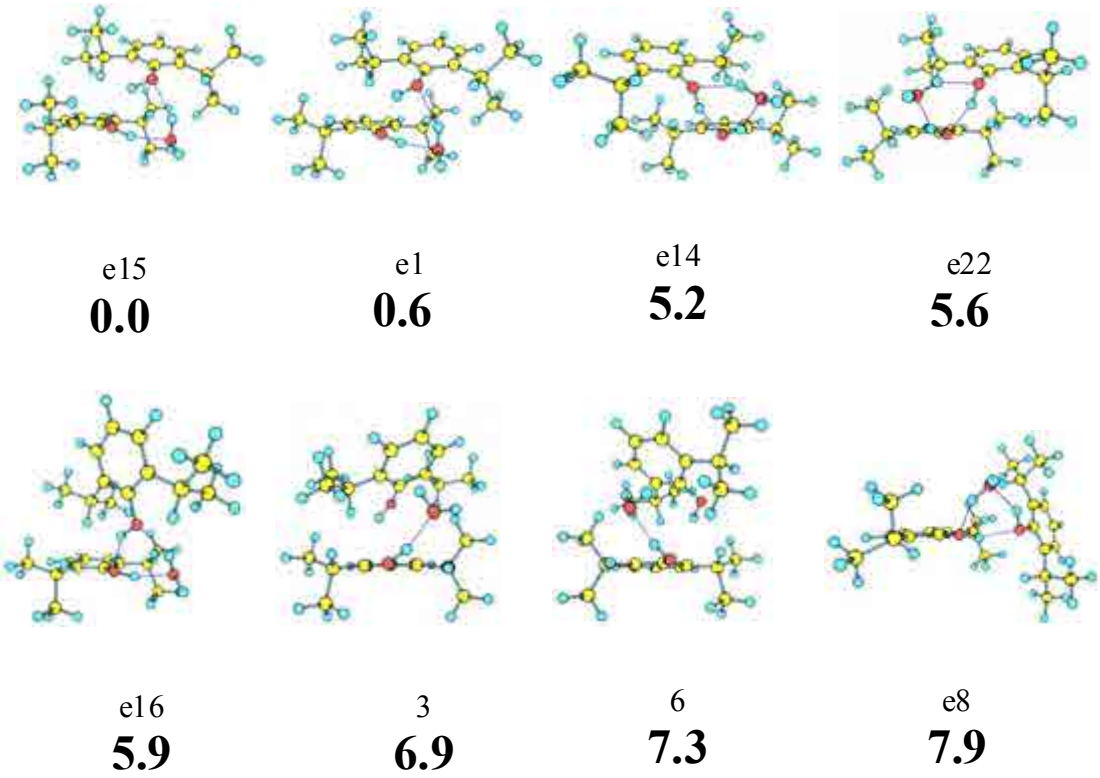

Figure 5.106. *Propofol$_2$·W$_1$ eight most stable conformers calculated at M06-2x/6-31+G(d) level, with their relative energies in bold. Energy values are in kJ/mol. All the calculated structures are presented in appendix 7.1 (Figure 7.21).*

Figure 5.107 shows the *2c-REMPI* spectrum of propofol$_2$·W$_1$, where the red-most peak is located at 36046 cm^{-1}. The spectrum is particularly congested, but it only extends for c.a. 400 cm^{-1}. In order to see if fragmentation is taking place, Figure

5.107 also offers a comparison with the *2c-REMPI* spectra of higher-order clusters. The coincidence of a few peaks from propofol$_2$·W$_2$ and propofol$_2$W$_3$ suggests that fragmentation is taking place, but such coincidences are due to the high density of spectral features, as the *hole burning* experiments demonstrates. The same experiment with almost no water present was carried out, to avoid formation of propofol$_2$·W$_2$ or higher order clusters and a similar propofol$_2$·W$_1$ spectrum was obtained, confirming the absence of fragmentation.

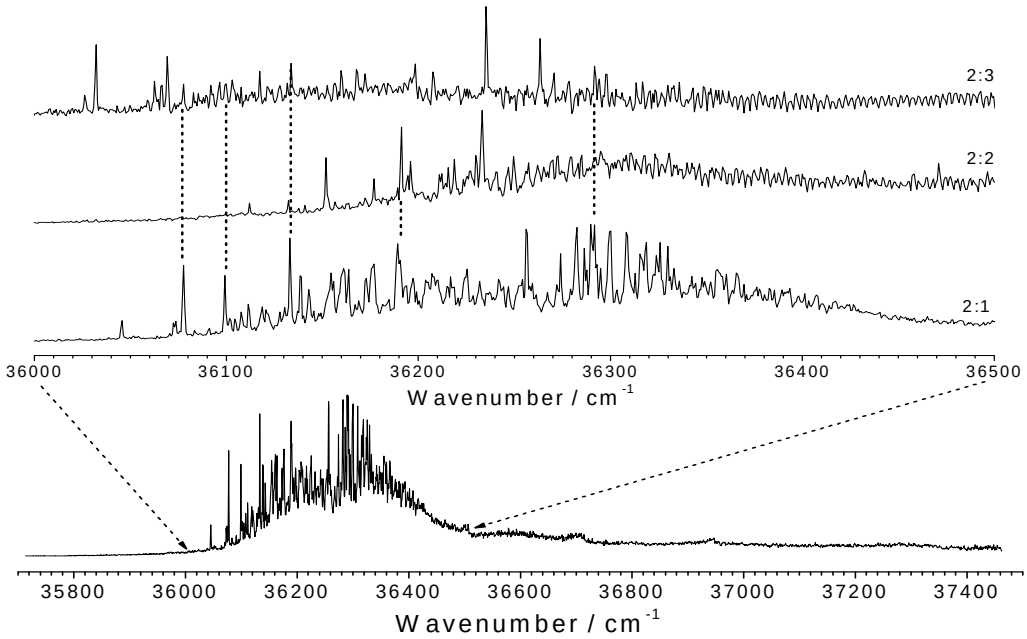

Figure 5.107. *2c-REMPI of propofol$_2$·W$_1$, in the 35700-37500 cm^{-1} region, recorded setting the probe laser at 27972 cm^{-1}. A detailed view of the propofol$_2$·W$_n$ (n=1-3) spectra, around the origin bands of propofol$_2$·W$_1$, is also shown for comparison. Although some of the peaks seem to come from fragmentation of higher-order cluster, no fragmentation is taking place.*

To determine the numbers of conformer present, *hole burning* experiments were carried out probing the transitions at 36046, 36078 and 36256 cm^{-1}, detecting three isomers, as can be seen in Figure 5.108. The first conformer's origin band is located at 36046 cm^{-1} and is red-shifted from the second conformer by only c.a. 30 cm^{-1}, which is located at 36078 cm^{-1}. The third conformer has an intense transition at 36256 cm^{-1}, that is, c.a. blue-shifted 200 cm^{-1} from the first conformer, but this does not seem to be the origin band. It is not clear where the true origin of the third conformer is, as there are

some weak transition that may be due either to a crossed *hole burning* or to weak transitions from the third conformer. The latter is not unusual as seen for propofol and propofol·W$_1$, where changes in geometry upon excitation lead to poor FCF to access the bottom of the potential energy well.

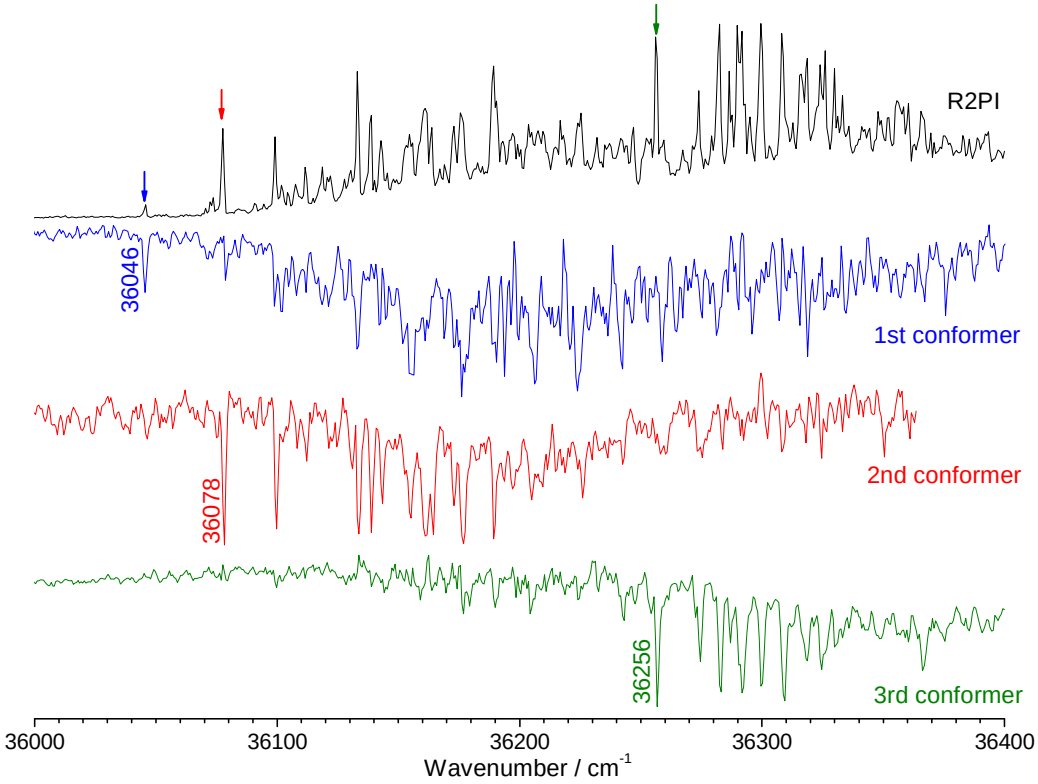

Figure 5.108. *Hole burning traces of propofol$_2$·W$_1$ recorded tuning the probe lasers (2-color detection) at 36046, 36078 and 36256 cm^{-1}. The peak noted with arrows indicate the transitions employed for recording the hole burning spectra, as well as the IDIRS trace.*

In order to extract further information from the system, IDIR spectra of the three conformers were recorded setting the probe laser at 36046, 36078 and 36256 cm^{-1} (Figure 5.109). As can be seen, the three conformers present similar spectra, composed of four strong features. The OH stretching located at 3710 cm^{-1} is due to the free OH stretching of the water molecule. The presence of the three peaks for the three conformers in the 3400 - 3550 region, due to the single OH stretching modes, with no other peak between them and the free OH stretching, can also be appreciated and

suggests a *window region* due to formation of a cyclic structure. The only difference between the IR spectra of the three molecules is a small variation on the position of the middle peak of this triad.

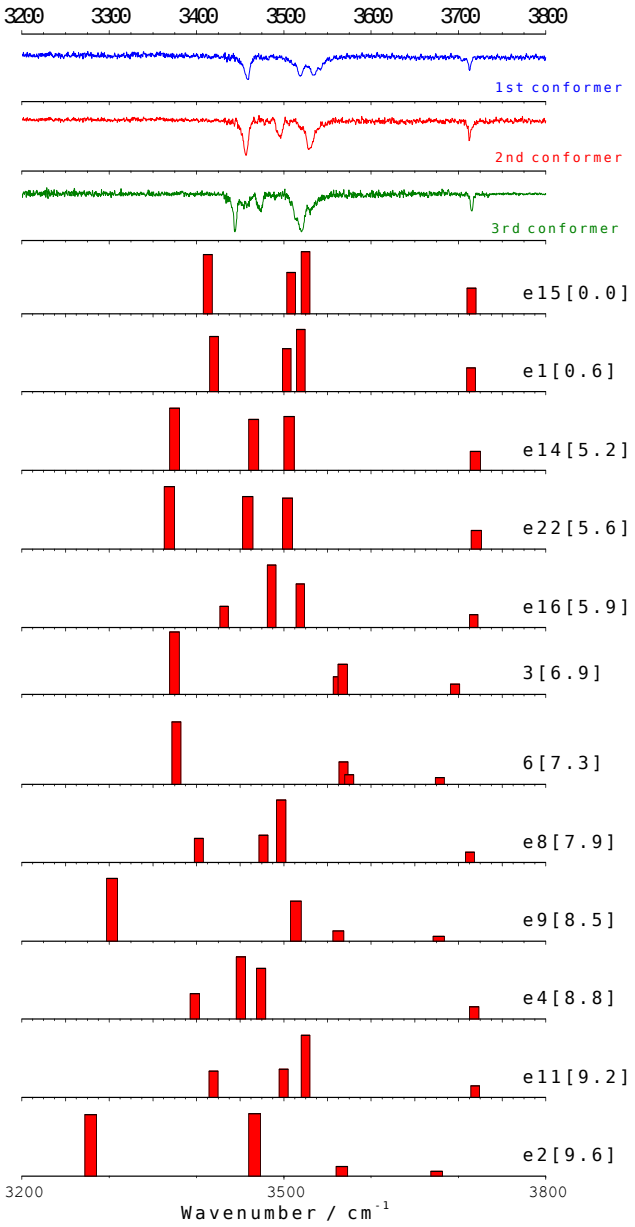

Figure 5.109. *IDIR spectra of propofol$_2$·W$_1$ recorded tuning the probe laser at 36046, 36078 and 36256 cm^{-1} respectively. The predicted IR spectra for some of the calculated structures are also shown for comparison. The numbers in brackets are the relative energies of the calculated conformers, in kJ/mol. A correction factor of 0.956 was applied. The predicted IR spectra of all the calculated structures are recorded in appendix (Figure 7.22).*

Assignment

Mass-resolved excitation spectroscopy of propofol$_2$·W$_1$ demonstrates the existence of at least three conformers with a congested spectra extending c.a. 400 cm^{-1}. IDIR spectra present similar features for all three conformers, and the formation of a cycle between the OH moieties is readily concluded, due to the absence of any peaks between the free OH stretching modes and the single bond OH stretching modes, i.e. the *window region*. The structural difference between the three conformers is expected to be very small, as the experimental IR spectra are almost identical and the most remarkable difference is the small shift of the middle peaks in the 3425-3550 cm^{-1} region. Although the exact assignation cannot be done because of the small variation in the OH stretching modes, that can perfectly be within the predicted structure's calculation error. The IR spectra predicted for structures *e15, e1, e8, e11* and *5* reproduces well that for any of the conformers, as shown in Figure 5.111, where only the first conformer's experimental spectrum is shown.

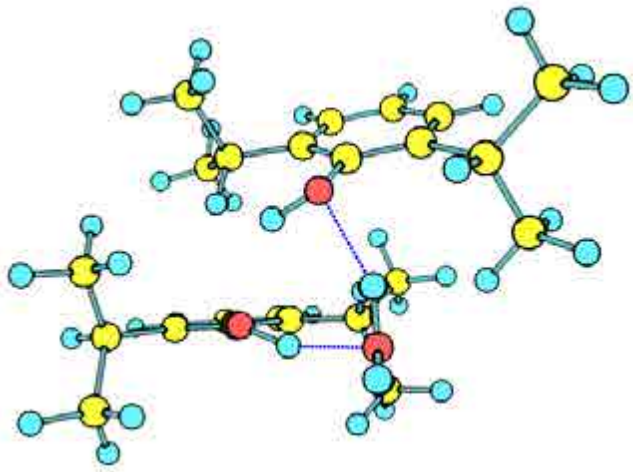

Figure 5.110. *Structure e15 reproduces the experimental results for any of the three conformers.*

There are also other types of structures that can match the experimental results for any of the conformers. Structure *e16* for instance, shown in Figure 5.112, and whose structure is similar to the previous group differing in one of the propofol molecule's orientation, reproduces well the experimental results as shown in Figure 5.111. In other structures, such as structure *e12* (Figure 5.112), there is a network between the OH moieties and an O-H···π interaction with the aromatic ring. These structures also

reproduce the experimental IR spectra as shown in Figure 5.111, although they appear at considerably high energy (> 11 kJ/mol).

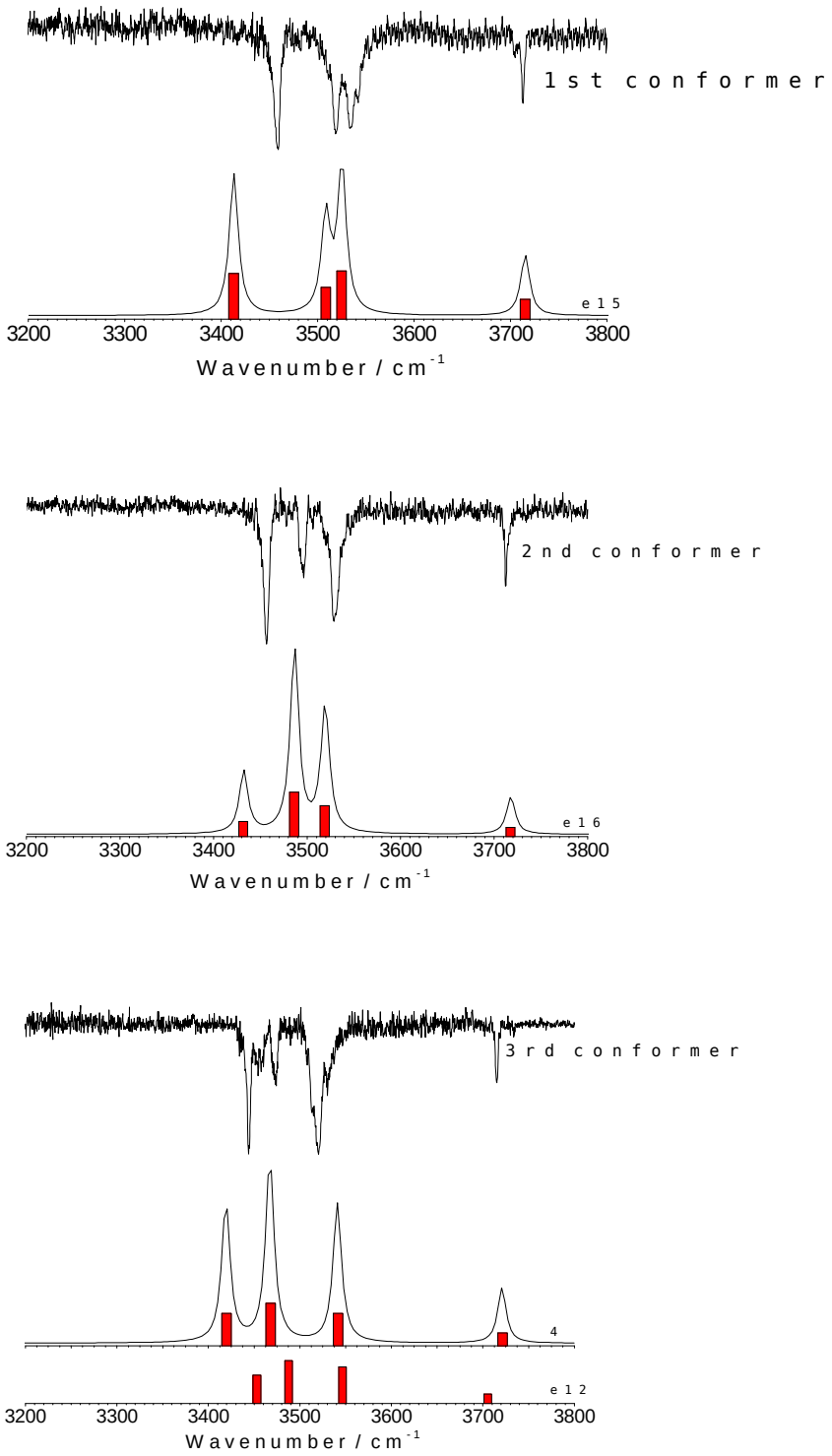

Figure 5.111. *Predicted IR spectra for some of the structures that match the experimental results.*

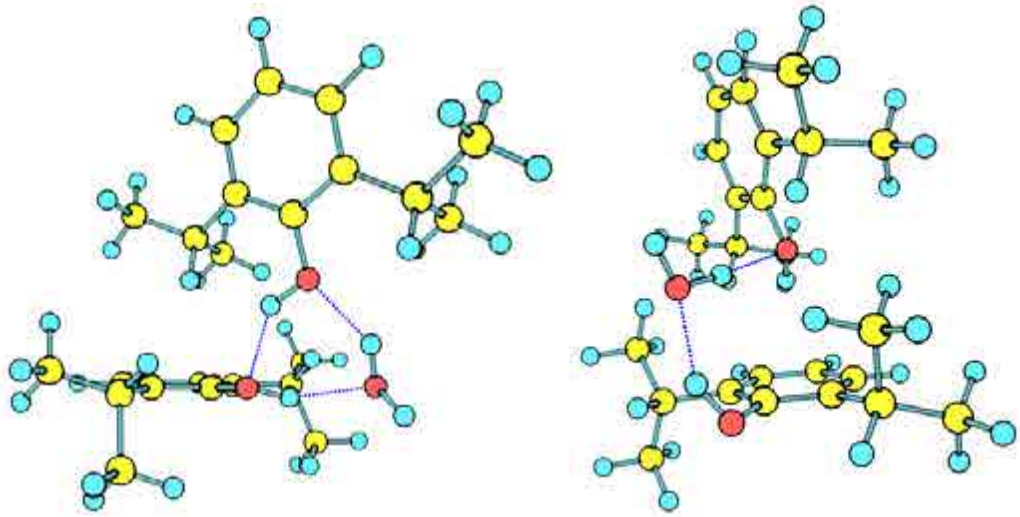

Figure 5.112. *Structures e16 and e12 which also reproduce the experimental results for any of the conformers.*

There are some arguments supporting the assignment to cyclic structures: first, as we will demonstrate, all the assigned structures for higher-order clusters and that made for the dimer, point to structures where both propofol molecules are stacked. Second, structures such as *e16* and *e12*, must suffer a large geometry change upon excitation, which probably makes impossible their experimental detection because of poor FCFs for accessing the excited state. Third, although it can be within calculation error, the IR spectra of the structures do not reproduce accurately the intensities of the experimental IR spectra, while that for the former does.

Finally, the excited state spectroscopy also supports this assignment: the origin of the first two conformers are located at 36046 cm^{-1} and 36078 cm^{-1} respectively, which accounts for a 180 cm^{-1} red-shift from the bare molecule´s 0_0^0 transition (36224 cm^{-1}) and a 40 cm^{-1} blue-shift from the propofol·W$_1$ cluster, which is the typical signature of a ring formation. Structure *e15*, as shown in Figure 5.110, has a weak hydrogen bond between both propofol molecules at an O-H··O distance of 204 pm and at an angle of 140º. Thus, there is not such a strong reduction in the inductive effect of the proton-acceptor water molecule causing a blue-shift smaller than expected.

5.4.2 – Propofol$_2$·W$_2$

The increase in the cluster size caused by the inclusion of a second water molecule has two effects. On the one hand, the number of possible structures continues growing, although in this case, there are some structures which are statistically more probable. On the other hand, the spectral congestion also increases, resulting in a broad absorption with only a few recognizable features. The second water molecule also increases the contribution of hydrogen bond interactions to the cluster stabilization energy. Accordingly, the most stable structures (Figure 5.113) present a cyclic hydrogen bond network formed by the two water molecules and the hydroxyl groups of the two propofol molecules. Apart from the relative orientation of the latter, the most remarkable difference between the structures is the position of the water molecules in the hydrogen bond network: either on one side (structures *e19, e1, e20*) or intercalated between the propofol molecules (structures *4, 9*).

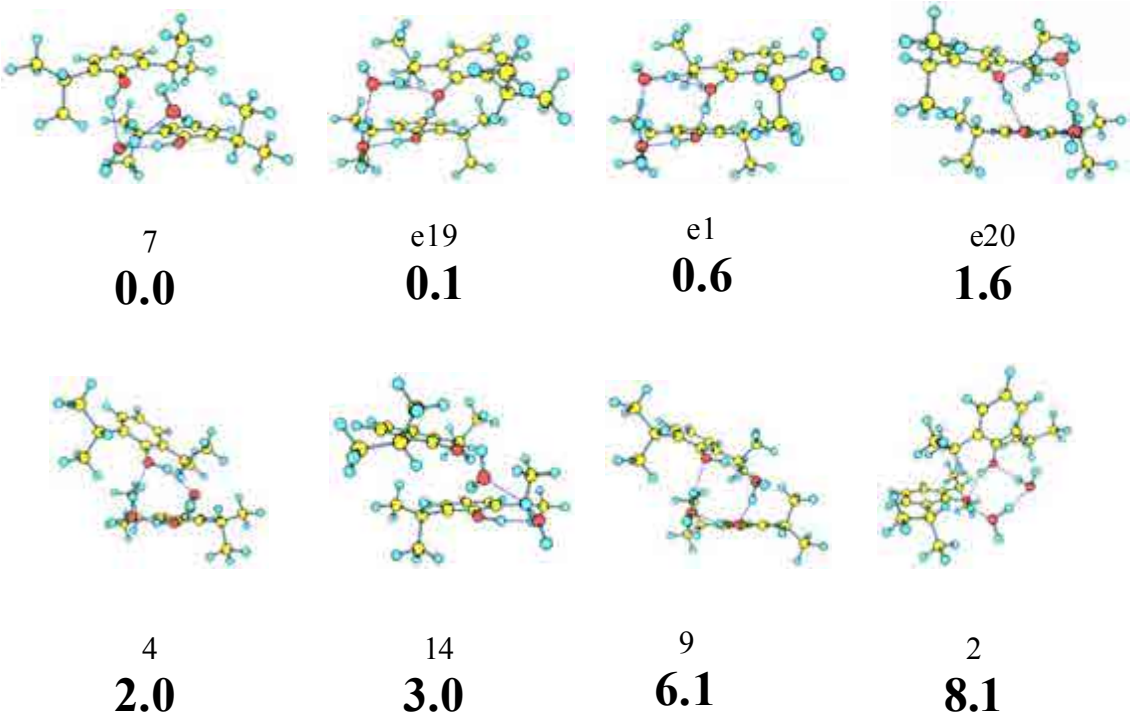

Figure 5.113. *Propofol$_2$·W$_2$ eight most stable conformers calculated at M06-2x/6-31+G(d) level, with their relative energies in bold. Energy values are in kJ/mol. All the calculated structures are presented in appendix 7.1 (Figure 7.23).*

Figure 5.114 shows the *2c-REMPI* spectrum of propofol$_2$·W$_2$ where a broad absorption, as happened with the propofol·W$_n$ (n>3) clusters, is present. Some peaks

protruding from the broad absorption can be seen, with the red-most band appearing at 36112 cm^{-1}. In order to see if there is fragmentation from higher-order clusters, Figure 5.135 also shows a comparison with propofol$_2$·W$_3$ and propofol$_2$·W$_4$ spectra. To the bare eye, the peaks marked with asterisks appear to form a fragmentation pattern. However, a careful examination shows a 2 cm^{-1} difference in their positions. No other suspicious feature was found and therefore we successfully avoided fragmentation thanks to a careful tune up of the experimental conditions.

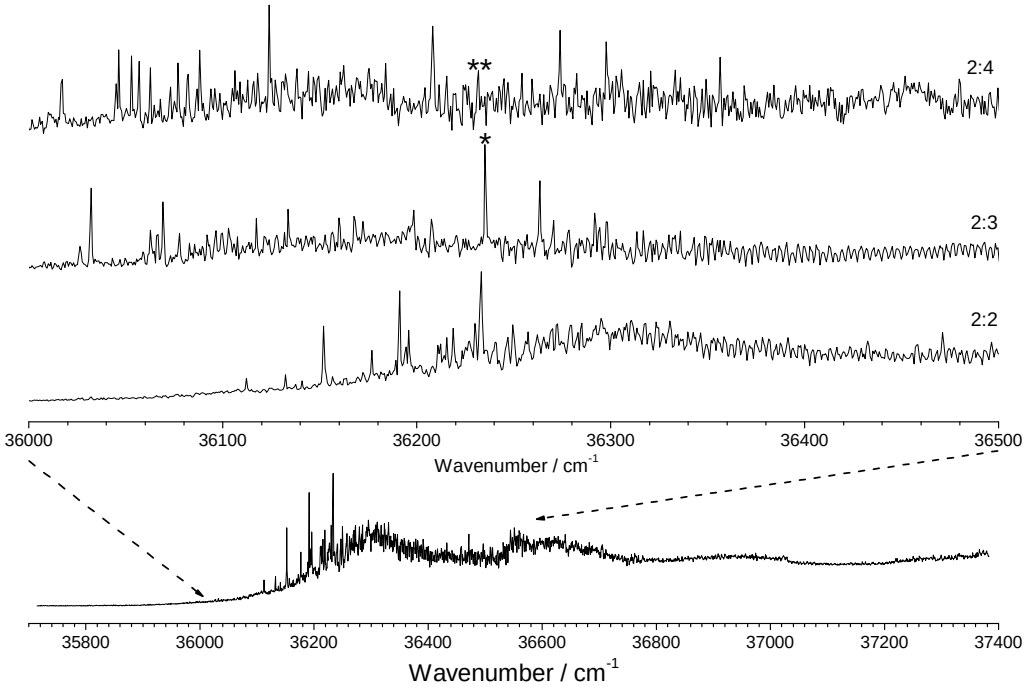

Figure 5.114. *2c-REMPI of propofol$_2$·W$_2$, in the 35700-37400 cm^{-1} region, recorded setting the probe laser at 27972 cm^{-1}. A detailed view of the propofol$_2$·W$_n$ (n=2-4) spectra, around the origin bands of propofol$_2$·W$_2$ conformer, is also shown. Appart from the peaks marked with asterisks, no other contribution due to fragmentation is observed.*

To determine the number of isomers, a *hole burning* experiment was done. The results are shown in Figure 5.115, where a comparison between the propofol$_2$·W$_2$ *2c-REMPI* spectrum and the *hole burning* traces obtained probing the origins at 36087 and 36152 cm^{-1} is offered. As can be seen, two isomers with origin bands separated by c.a. 65 cm^{-1} are present, with a few transitions that cover the first 150 cm^{-1}, from where a

broad absorption seems to take place. It is also worthy to note that none of the peaks disappear or change in intensity when He is replaced by Ne.

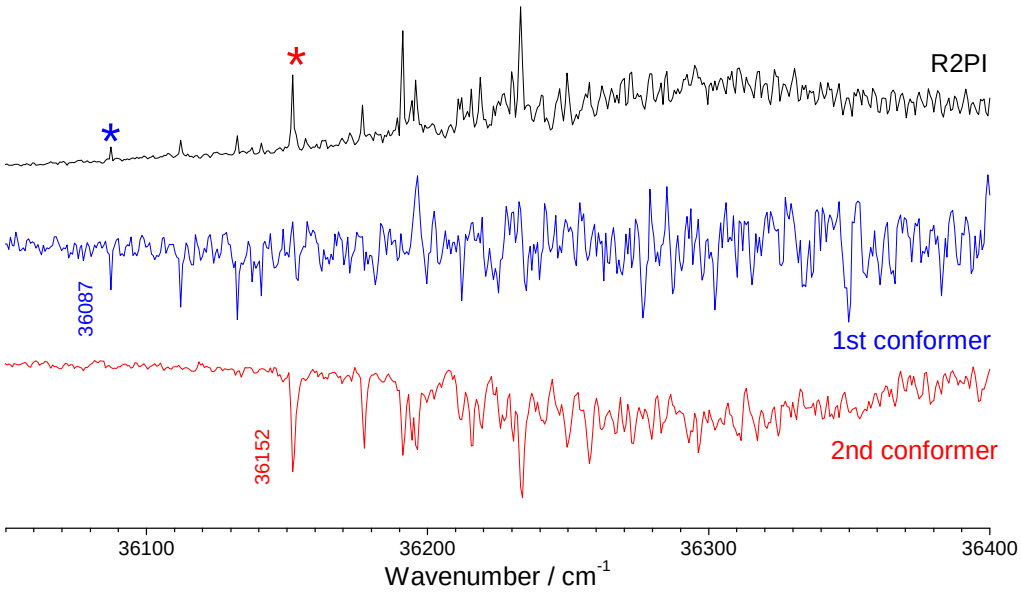

Figure 5.115. *Hole burning traces of propofol$_2$·W$_2$ recorded tuning the probe lasers (2-color detection) at 36087 and 36152 cm^{-1}. The peaks noted with asterisks indicate the transitions employed for recording the hole burning spectra, as well as the IDIRS trace.*

Figure 5.116 shows the IDIR spectra of both conformers recorded in the OH stretching region. Six peaks are clearly seen for the second conformer, while for the first conformer only five peaks are found, most surely due to peak overlapping. The bands are gathered in two groups: one of them consisting of four members, while the other one contains the two free OH stretching modes. There is a 200 cm^{-1} separation between both groups, indicating a structure of cyclic nature.

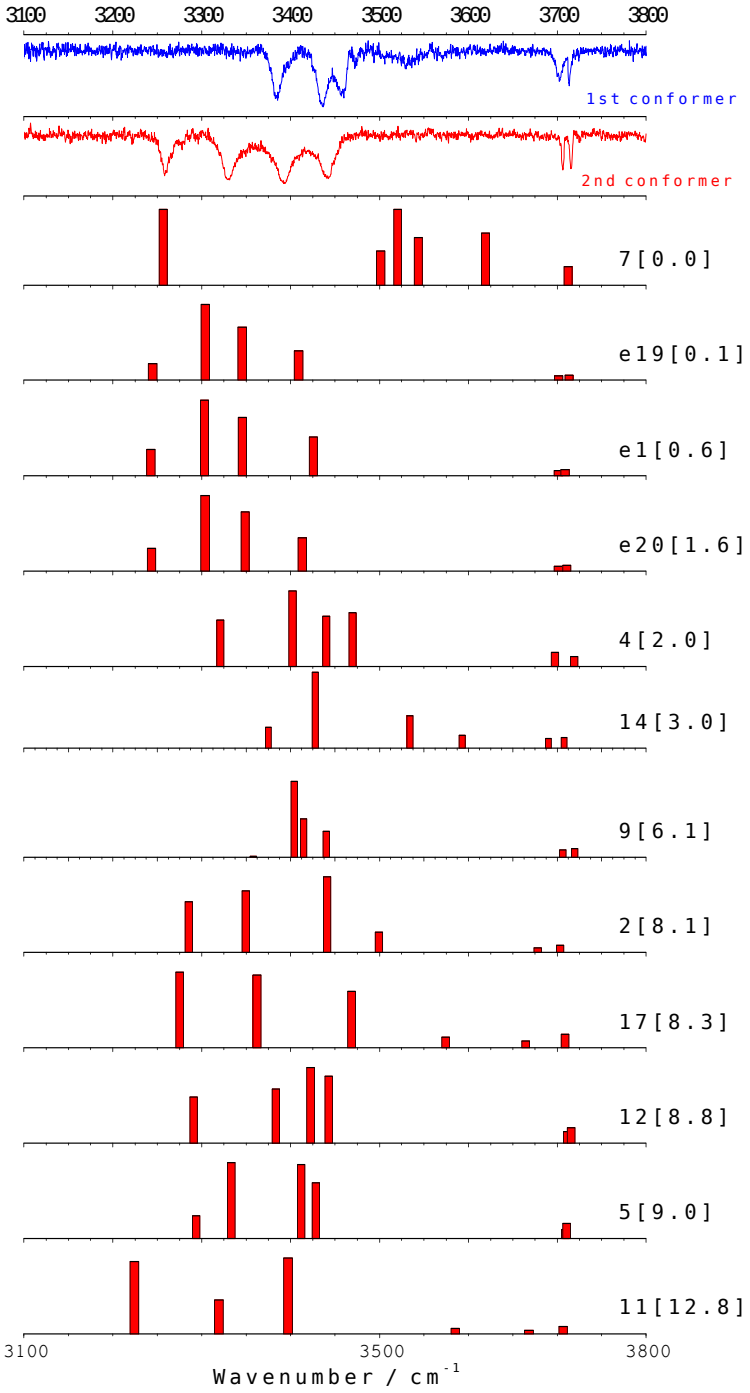

Figure 5.116. *IDIR spectra of propofol$_2$·W$_2$ recorded tuning the probe laser at 36087 and 36152 cm^{-1}. The predicted IR spectra for the 12 structures bellow 13 kJ/mol are also shown for comparison. The numbers in brackets are the relative energies of the calculated conformers, in kJ/mol. A correction factor of 0.955 was applied. The predicted IR spectra of all the calculated structures are recorded in appendix 7.1 (Figure 7.24).*

Assignment

Despite the experimental complexity of this system, the assignment of the propofol$_2$·W$_2$ species is in contrast, less confuse than those in the previous section, as only structures with an eight-member ring formed by the two water molecules and the two propofol hydroxyl groups can reproduce the experimental IR spectra. Still, several variations are observed between structures. Apart from slight changes in the orientation of the two chromophores, which are usually accompanied by variations on the angle formed by one (or more) of the isopropyl groups and the aromatic ring, the water molecules can interact one with the other, or they can alternate between the hydroxyl groups. The chromophores are mostly interacting with one of the isopropyl groups of the other molecule, instead of with the ring. Such variations result in modifications on the predicted IR spectra, allowing discrimination between structures.

Consequently, the only structure whose IR spectrum is able to reproduce the experimental results for the **first conformer is structure *9***, shown in Figure 5.117, where both propofol molecules are **stabilized by dispersive interactions** between one of the isopropyl groups with the other molecule's aromatic ring respectively, and where a **cycle between** the water molecules and the propofol's **OH moieties**, **alternating** the OH moieties (propofol-water-propofol-water) is formed. Figure 5.118 shows the comparison of the predicted IR with the experimental results for the first conformer.

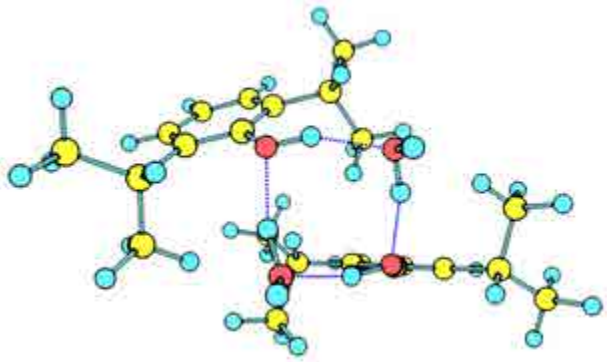

Figure 5.117. *Structure 9 is the theoretically predicted structure that better fits the experimental results for the first conformer.*

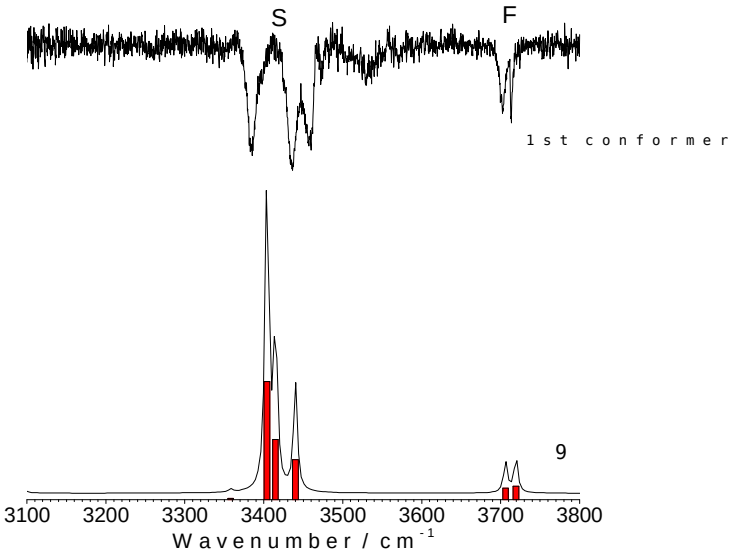

Figure 5.118. *Comparison of the predicted IR spectrum of structure 9 with the experimental results for the first conformer.*

The OH stretching vibrations of this structure are highly coupled, resulting in very symmetric vibrations, one of which (the most red-shifted OH stretching) is the result of the concerted motion of the four OH moieties in the same direction and therefore, it is forbidden. Consequently, it does not appear in the spectrum. Structure *4, 12* and *5*, are very similar to *e9*, but as there is a loss of symmetry the coupling is not that good and all four OH stretching vibrations should appear. Such effect is maximized in structure *6* (Figure 5.119). The predicted IR spectrum for this structure shows two very low-intense (forbidden) OH stretching modes helping us discarding it.

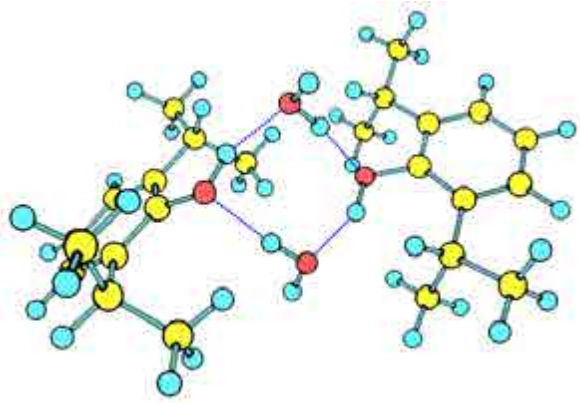

Figure 5.119. *structure 6 presents a high symmetry, which results in the loss of two peaks in the IR spectrum.*

Regarding the **second conformer**, **structures *e19* (Figure 5.120), *e1* and *e20***, are the structures that better reproduce the experimental results. Such structures only differ in the bare molecule conformation. One of the propofol molecules is placed above the other, stabilized by **dispersive forces** and **forming a hydrogen bond cyclic structure** with a propofol-OH···propofol-OH···water-OH···water-OH sequence. Figure 5.121 shows a comparison between the predicted IR spectrum for structure *9* and the experimental one. A good agreement is observed.

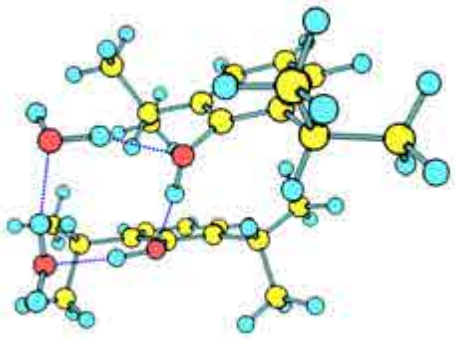

Figure 5.120. *structure e19 is one of the theoretically predicted structures that better fits the experimental results obtained for the second conformer.*

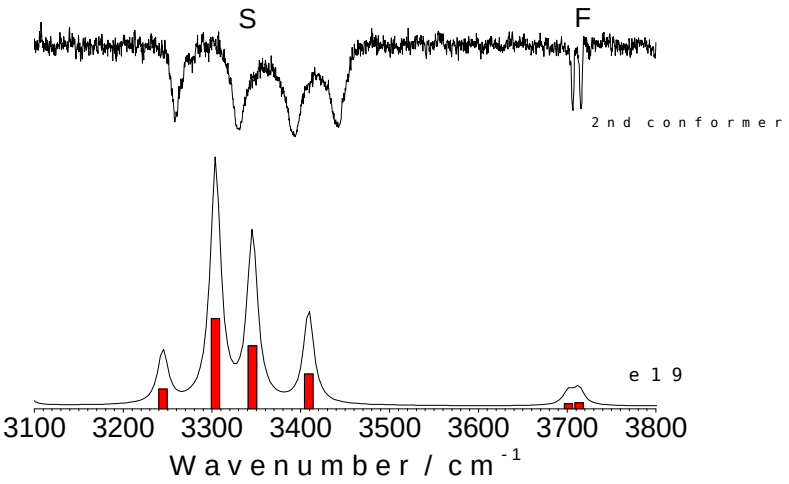

Figure 5.121. *Comparison of the predicted IR spectrum of structure e19 with the experimental results obtained for the second conformer.*

Structure *2*, which is similar to structure *e19* but with the propofol molecules perpendicular to each other, is also a good candidate for the second conformer, although the agreement with the experimental results is not as good as for the latter. In any case,

very likely, the barrier between all these structures is low and even at low temperatures, there may exists inter-conversion between all of them.

Thus, although it is difficult to univocally assign the exact structure, the interaction-type has been fully characterized, as in both conformers both propofol molecules are stabilized by dispersive forces and the four molecules are involved in a cyclic structure formed by the OH moieties, with the difference that in the first conformer the cycle is formed in propofol-water-propofol-water order and in propofol-propofol-water-water sequence in the second conformer. The fact that this two types of structures, only differing in the order in which the molecules are bonded, give remarkably different spectra in the OH region, allowing a ground assignment, supports that the IDIR spectroscopy is an invaluable tool for the assignment of such systems. The OH stretching modes for each of the conformers are collected in Table 5.10 assigned by comparison with structure *9* for the first conformer and with structure *e19* for the second one.

Table 5.10. *Experimental vibrational transitions in the IR traces of propofol$_2$·W$_2$ first and second conformers, with a tentative assignment based on a comparison with the calculated frequencies for structures e9 and e19.*

Experimental Peak (cm^{-1})	**structure *9***		
	Frequency (cm^{-1})	Intensity	Vibrational type
-----	3358	12	σ_s^s (stretches are coupled)
3383	3404	1232	σ_{as}^s (stretches are coupled)
3436	3415	627	σ_{as}^s (stretches are coupled)
3457	3440	416	σ_{as}^s (stretches are coupled)
3702	3706	119	σ^f (OH$_w$)
3714	3719	138	σ^f (OH$_w$)

Experimental Peak (cm^{-1})	**structure *e19***		
	Frequency (cm^{-1})	Intensity	Vibrational type
3258	3245	296	σ (OH$_{ppf}$)*
3328	3304	1356	σ_s^s (OH$_w$)*
3392	3346	947	σ (OH$_{ppf}$)*
3440	3409	522	σ_s^s (OH$_w$)*
3706	3702	78	σ^f (OH$_w$)
3716	3713	93	σ^f (OH$_w$)

* All this transitions are concerted movements of the four OH moieties involved in the ring, but the coupling is not that good as in the previous case and the modes have a preferential contribution from a single OH stretching mode.

5.4.2.2 - Special considerations

Regarding the study of this cluster, special attention must be paid to the optimization of the experimental conditions. The molecular weight of propofol is 178 g/mol, and that of the water is 18 g/mol. Thus, the molecular weight of the dimer is 178*2 = 256 g/mol and that of the propofol·W$_{10}$ cluster 178+18*10 = 258 g/mol. As the resolution of a time-of-flight mass spectrometer depends on the time/mass relationship, at higher delays, the temporal resolution is reduced, becoming harder to discriminate between two consecutive masses. Such discrimination can be improved by a carefully chosen of the time delay between the pulsed supersonic beam and the laser pulse, as the concentration of different aggregates varies along the supersonic beam.[25] As can be seen in Figure 5.122, carefully chosen the time delay can improve the signal of the desired cluster.

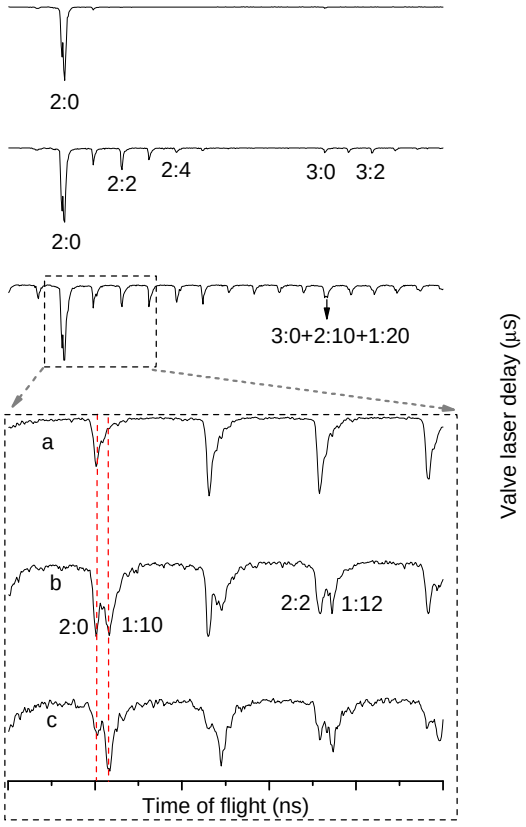

Figure 5.122. *Time of flight spectra of propofol$_m$·W$_n$ recorded at different delays of the valve with respect the excitation/ionization lasers. Changing the time delay between the valve and the laser, formation of different species can be favoured. This delay is critical when trying to optimize the signal of the clusters studied in this section.*

Thus, by changing the delay of the valve respect to the laser, formation of a given cluster can be favored, although a complete separation cannot be achieved. Besides, the delay values that allow a significant reduction on the signal from the propofol·W$_{10}$, allowing the study of pure propofol$_2$ species (Figure 5.122a) result in an unstructured *2c-REMPI* spectrum. Conditions such as in Figure 5.122c, on the other hand, lead to almost no formation of the desired specie. The best experimental conditions are those like in Figure 5.122b where signals due to both, the dimer·X$_n$ and monomer·X$_{n+10}$, are present, and that allow obtaining discrete spectra.

Finally, for some reason, experimental conditions seem to be more critical to obtain a good spectrum of **propofol$_2$·W$_2$ species,** which resulted to be **one of the most difficult systems to study,** even compared with those of higher order, such as, propofol$_2$·W$_6$ and propofol$_2$·W$_7$ or even propofol$_3$ or propofol$_4$.

5.4.3 – Propofol$_2$·W$_3$

The most evident effect of the introduction of a third water molecule is the rupture of the cyclic structure, to produce more complex structures. As for propofol$_2$·W$_2$, molecular mechanics calculations find thousands of structures in a 20 kJ/mol window, but a large number of them converge into considerably smaller number of geometries when running the *ab-initio* calculations. The most stable isomers (Figure 5.123) are those with the propofol molecules stabilized by dispersive forces and a cyclic hydrogen bond network connecting the water molecules and the two propofol OH groups (structures *e22, e18, e14*). There are also structures in which a propofol and the water molecules adopt a geometry, similar to that of propofol·W$_3$ isomer, with the second propofol molecule interacting with the ring of waters (structure 6) or with one of the isopropyl groups of the other (structure 8). Higher in energy are structures in which a ten-member ring involving all the water molecules and the two propofol is formed.

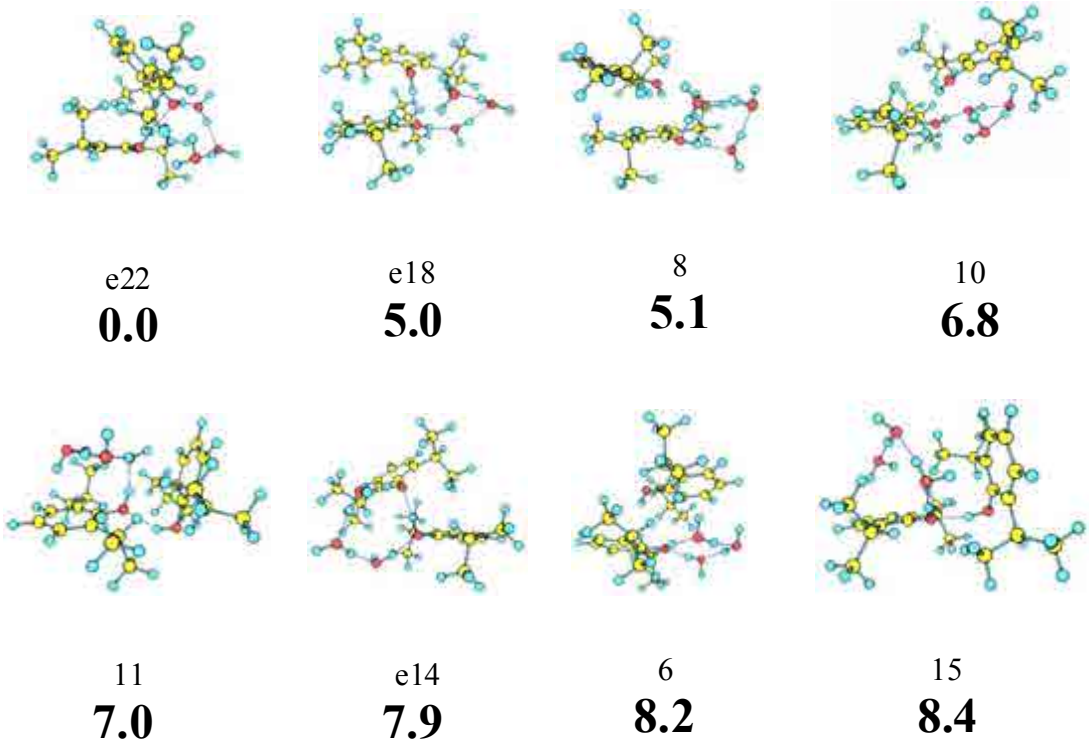

Figure 5.123. *Propofol$_2$·W$_3$ eight most stable conformers calculated at M06-2x/6-31+G(d) level, with their relative energies in bold. Energy values are in kJ/mol. All the calculated structures are presented in appendix 7.1 (Figure 7.25).*

Figure 5.124 shows the *2c-REMPI* spectrum of propofol$_2$·W$_3$ where the peak at 36026 cm^{-1} is taken as the 0_0^0 transition, although some very weak peaks appear at lower

frequencies. Such bands are not due to fragmentation as the comparison with the spectra of propofol$_2$·W$_4$ and propofol$_2$·W$_5$ demonstrates and most surely are due to a conformer with poor FCFs.

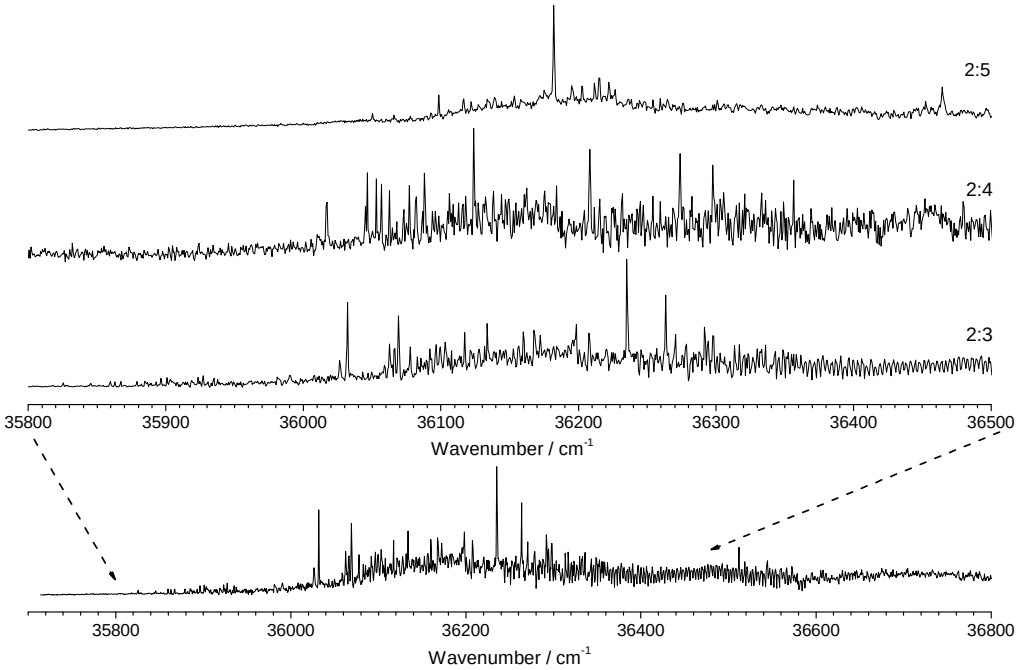

Figure 5.124. *2c-REMPI of propofol$_2$·W$_2$, in the 35700-36800 cm^{-1} region, recorded setting the probe laser at 27972 cm^{-1}. A detailed view of the propofol$_2$·W$_n$ (n=3-5) spectra, around the origin bands of propofol$_2$·W$_3$ conformer, is also shown. No fragmentation is observed in the mass-channel studied.*

To determine the number of isomers contributing to the spectrum, a *hole burning* experiment of the 2:3 species is performed. Figure 5.125 shows a comparison between the propofol$_2$·W$_3$ *2c-REMPI* spectrum and the *hole burning* traces obtained probing the transitions 36033 and 36235 cm^{-1}. As can be seen, two isomers are found.

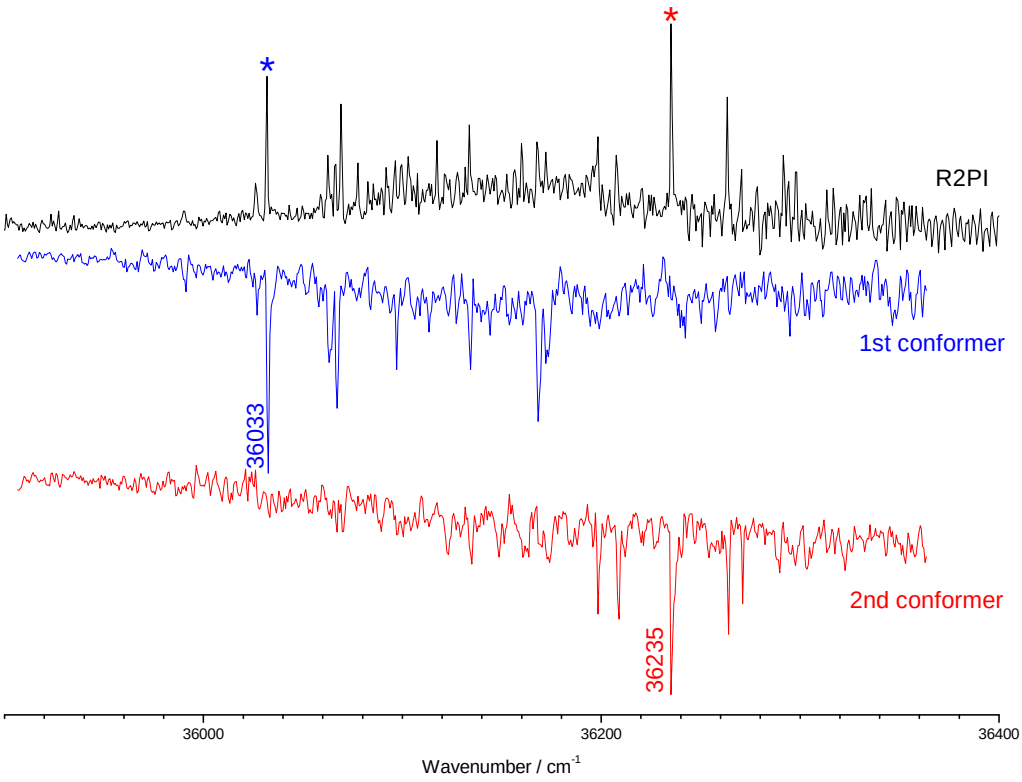

Figure 5.125. *Hole burning traces of propofol$_2$·W$_3$ recorded tuning the probe lasers (2-color detection) at 36033 and 36235 cm^{-1}. The peaks noted with asterisk indicate the transitions employed for recording the hole burning spectra, as well as the IDIRS traces.*

In order to extract the maximum structural information to match the REMPI spectra with the calculated structures, the IDIR spectra of both conformers were recorded in the OH stretching region, obtaining the spectra shown in Figure 5.126. The spectra indicate that the water molecules do not form a single cyclic structure, in agreement with the theoretical predictions for the most stable structures.

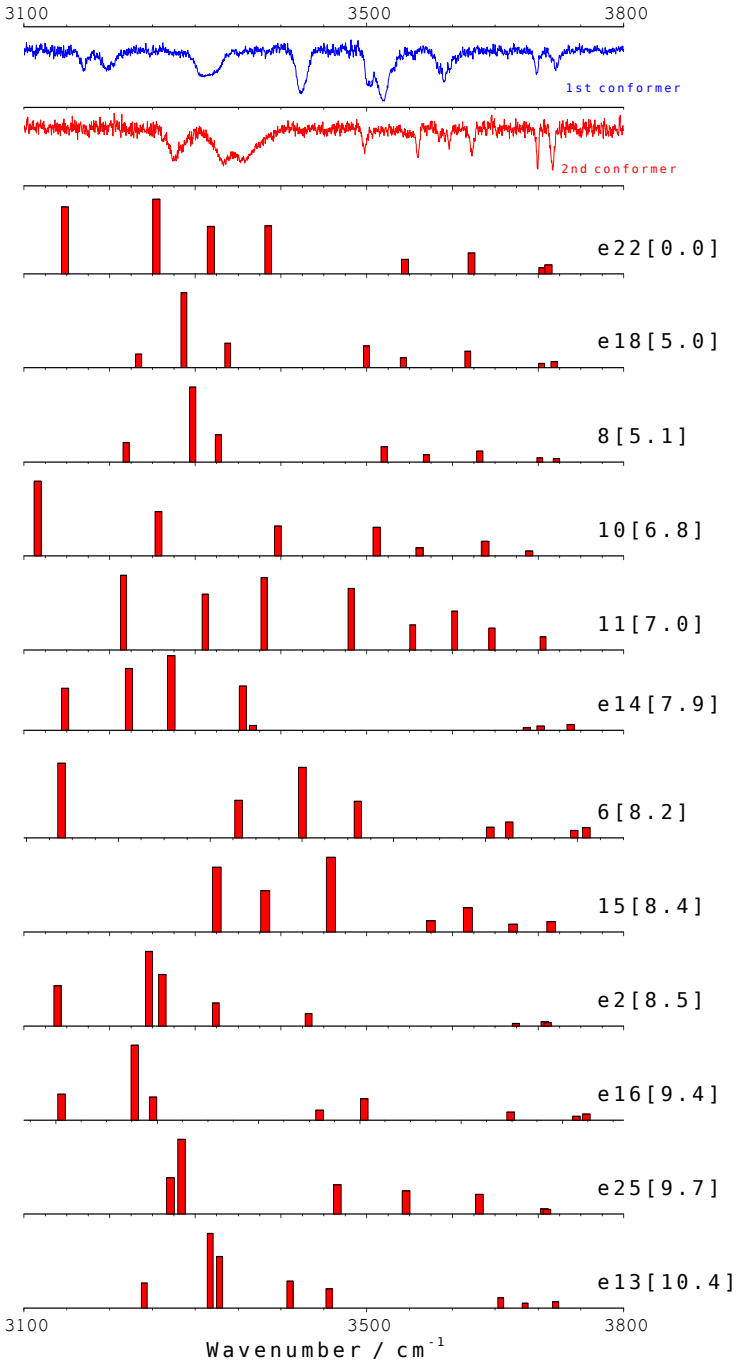

Figure 5.126. *IDIR spectra of propofol$_2$·W$_3$ recorded tuning the probe laser at 36033 and 36235 cm^{-1}. The predicted IR spectra for the twelve structures bellow 9 kJ/mol are also shown for comparison. The numbers in brackets are the relative energies of the calculated conformers, in kJ/mol. A correction factor is 0.956 was applied. The predicted IR spectra of all the calculated structures are recorded in appendix 7.1 (Figure 7.26).*

Assignment

Regarding the **first conformer**, one of the main characteristics of the IR spectrum, is that all the OH stretching modes are dispersed around the 3100-3750 cm^{-1} region, with the blue-most peaks, due to the free OH stretching modes, at c.a. 3700 cm^{-1}; the peaks at 3500-3600 cm^{-1} are double-donor stretching modes and the red-most peaks, in the 3100 - 3450 cm^{-1} region, are single-donor OH stretching vibrations. Structure *e22*, depicted in Figure 5.127, reproduces very well the experimental results, as shown in Figure 5.128. The propofol molecules are **stabilized by dispersive forces**, one of them acting as a proton-donor to the other, while one of the **water molecules** interacts with both as a **double donor**. This water molecule is the responsible for the two peaks at 3518 and 3590 cm^{-1}.

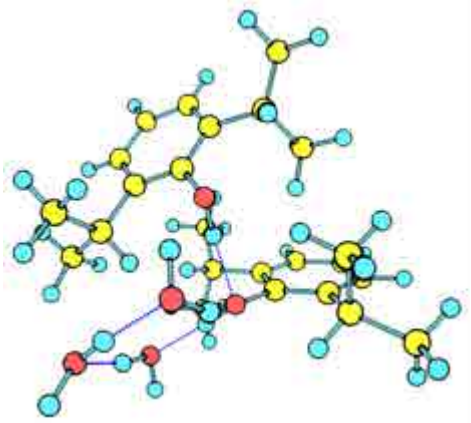

Figure 5.127. *Structure e22 is the theoretically predicted structure that better fits the experimental results for the first conformer.*

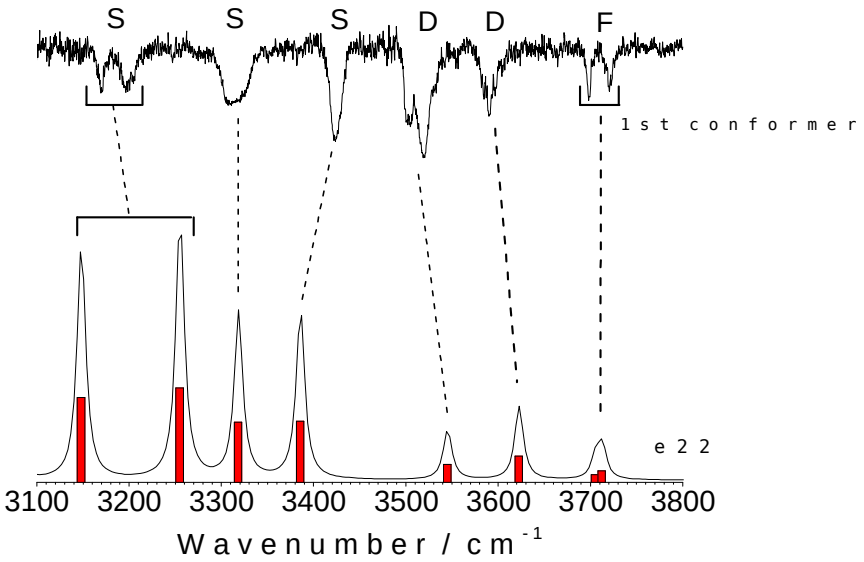

Figure 5.128. *Comparison of the predicted IR spectrum for structure e22 with the experimental results for the first conformer, as can be seen there is a good agreement between both spectra.*

For the **second conformer**, structures *e18* and *8* accurately reproduce the experimental spectrum, as shown in Figure 5.129. As can be seen in Figure 5.130, those structures are very similar to the structure *e22*, **with a slight difference on the relative position of the propofol molecules**. Such variation changes the distance of the OH bonding between the propofol acting as acid and the other propofol, from 166 to 173 pm, resulting in a shift on the OH stretching from 3500 to 3385 cm^{-1}, due to a reinforcement of the hydrogen bond. Similar effect is observed for the other propofol molecule's OH stretching mode.

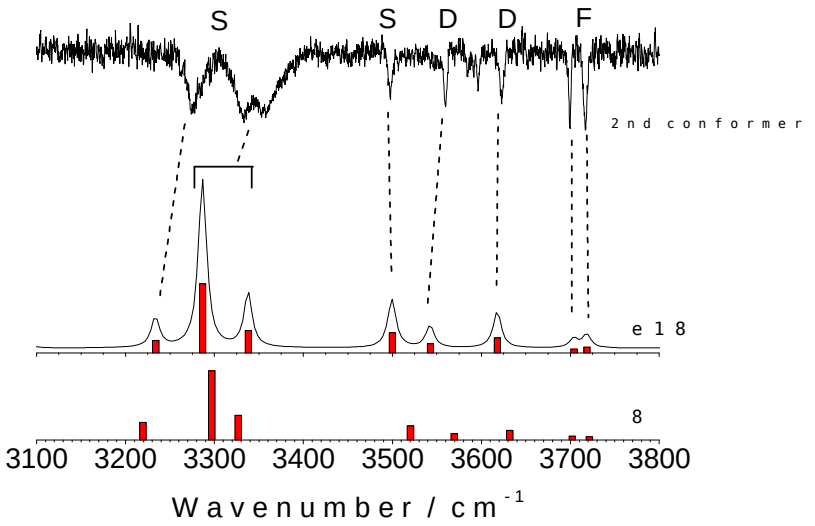

Figure 5.129. *Comparison of the predicted IR spectrum of structures e18 and 8 with the experimental results for the second conformer, as can be seen there is a good match between the spectra.*

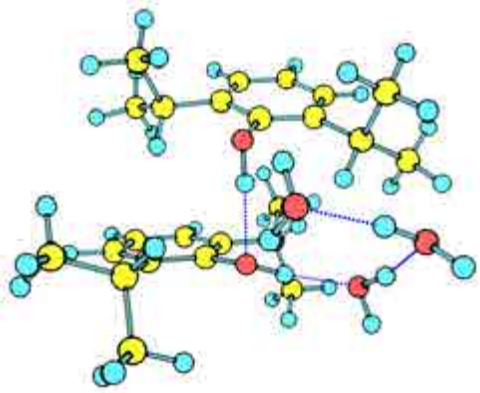

Figure 5.130. *Structure e18 reproduces very well the experimental results for the second conformer.*

The OH stretching modes for each of the conformers are collected in Table 5.11 and compared with the structure *e22* for the first conformer and structure *e18* for the second conformer.

Table 5.11. *Experimental vibrational transitions in the IR traces of propofol$_2$·W$_3$ first and second conformers, with a tentative assignment based on a comparison with the calculated frequencies for structures e22 and e18.*

Experimental Peak (cm^{-1})	**structure *e22***		
	Frequency (cm^{-1})	Intensity	Vibrational type
3169	3148	835	σ_s^{s*}
3196	3255	932	σ_s^{s*}
3310	3318	593	σ_s^{s*}
3422	3385	600	σ (OH$_{ppf}$)
3518	3545	177	σ_s^{d} (OH$_w$)
3590	3622	261	σ_{as}^{d} (OH$_w$)
3698	3705	76	σ^f (OH$_w$)
3721	3712	115	σ^f (OH$_w$)

Experimental Peak (cm^{-1})	**structure *e18***		
	Frequency (cm^{-1})	Intensity	Vibrational type
3274	3234	245	σ_s^{s*}
3332	3287	1382	σ_s^{s*}
3358	3338	447	σ_s^{s*}
3497	3500	399	σ (OH$_{ppf}$)
3560	3543	182	σ_s^{d} (OH$_w$)
3623	3618	298	σ_{as}^{d} (OH$_w$)
3700	3704	78	σ^f (OH$_w$)
3717	3719	110	σ^f (OH$_w$)

* All this OH stretching modes are coupled in such a way that it is difficult to make any distinction.

5.4.4 – Propofol$_2$·W$_4$

Propofol$_2$·W$_4$ presents a complicate landscape, with a considerably larger number of possible structures, as molecular mechanics calculations predict over ten thousand structures in a 20 kJ/mol window, which means a significant jump compared to propofol$_2$·W$_3$. The most stable isomers (Figure 5.131) present structures that resemble those found for W$_6$ systems[31]: *prisms* (structure *e33*), *book* (structures *e3, e4, e39, e77, e6, e2*) or *cage*-like structures (structure *4, e37*). *Monocyclic* types are also present at a relative energy of 17 kJ/mol and above.

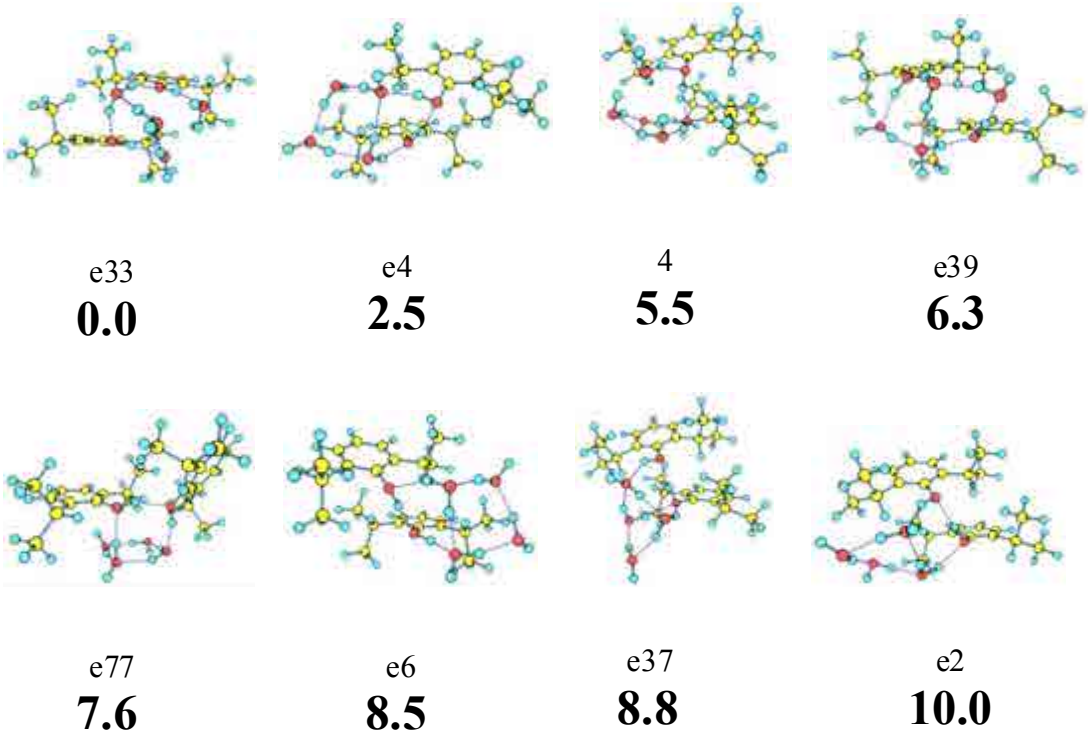

Figure 5.131. *Propofol$_2$·W$_4$ eight most stable conformers calculated at M06-2x/6-31+G(d) level, with their relative energies in bold. Energy values are in kJ/mol. All the calculated structures are presented in appendix 7.1 (Figure 7.27).*

Figure 5.132 shows the *2c-REMPI* spectrum of propofol$_2$·W$_4$ where the red-most peak appears at 36017 cm^{-1}, and extends for at least 400 cm^{-1}. In order to see if any fragmentation is taking place, Figure 5.132 also shows a comparison of the *2c-REMPI* spectra of propofol$_2$·W$_4$ with propofol$_2$·W$_5$ and propofol$_2$·W$_6$. As can be observed, only two peaks seem to be due to fragmentation.

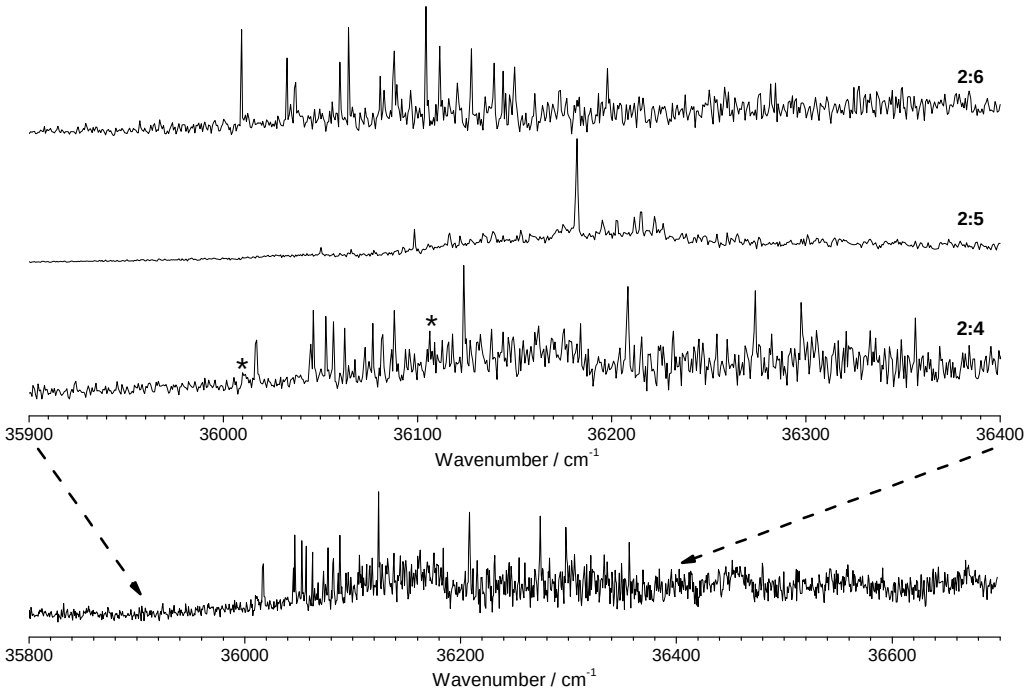

Figure 5.132. *2c-REMPI of propofol$_2$·W$_4$, in the 35800-36700 cm^{-1} region, recorded setting the probe laser at 27972 cm^{-1}. A detailed view of the propofol$_2$·W$_n$ (n=4-6) spectra, around the origin bands of propofol$_2$·W$_4$ conformer is also shown for comparison. The peaks marked with an asterisk are due to fragmentation.*

To determine the number of isomers contributing to the spectrum, a *hole burning* experiment is done. Figure 5.133, shows a comparison between propofol$_2$·W$_4$ *2c-REMPI* spectrum and the *hole burning* traces obtained probing the transitions 36018 and 36124 cm^{-1}. As can be seen, two isomers are present. The origin band of the first conformer is located at 36018 cm^{-1}, while that of the second conformer is at 36047 cm^{-1}. Both conformers are separated by only c.a. 40 cm^{-1}.

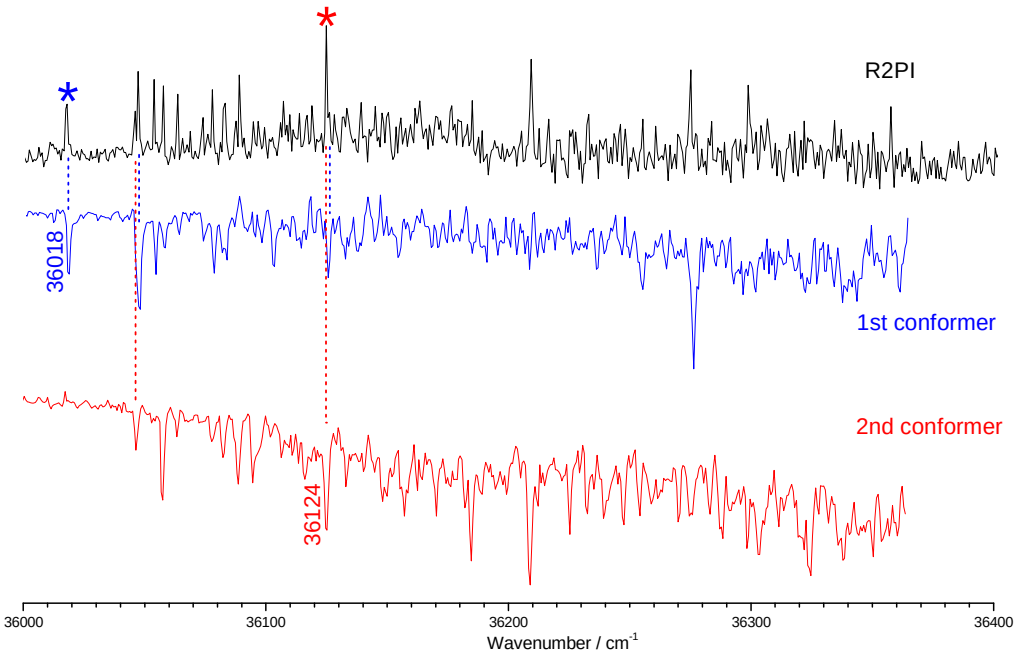

Figure 5.133. *Hole burning traces of propofol$_2$·W$_4$ recorded tuning the probe lasers (2-color detection) at 36018 and 36124 cm^{-1}. The asterisks indicate the transitions employed for recording the hole burning spectra, as well as the IDIRS traces. The dotted lines are eye guides to remark the difference between close transitions belonging to different isomers.*

Figure 5.134 shows the IDIR spectra recorded in the OH stretching region for both conformers. Both spectra are considerably different, pointing to the presence of two very different structures, one of them, the second conformer, with at least, one O-H···π interaction, not present for the first conformer.

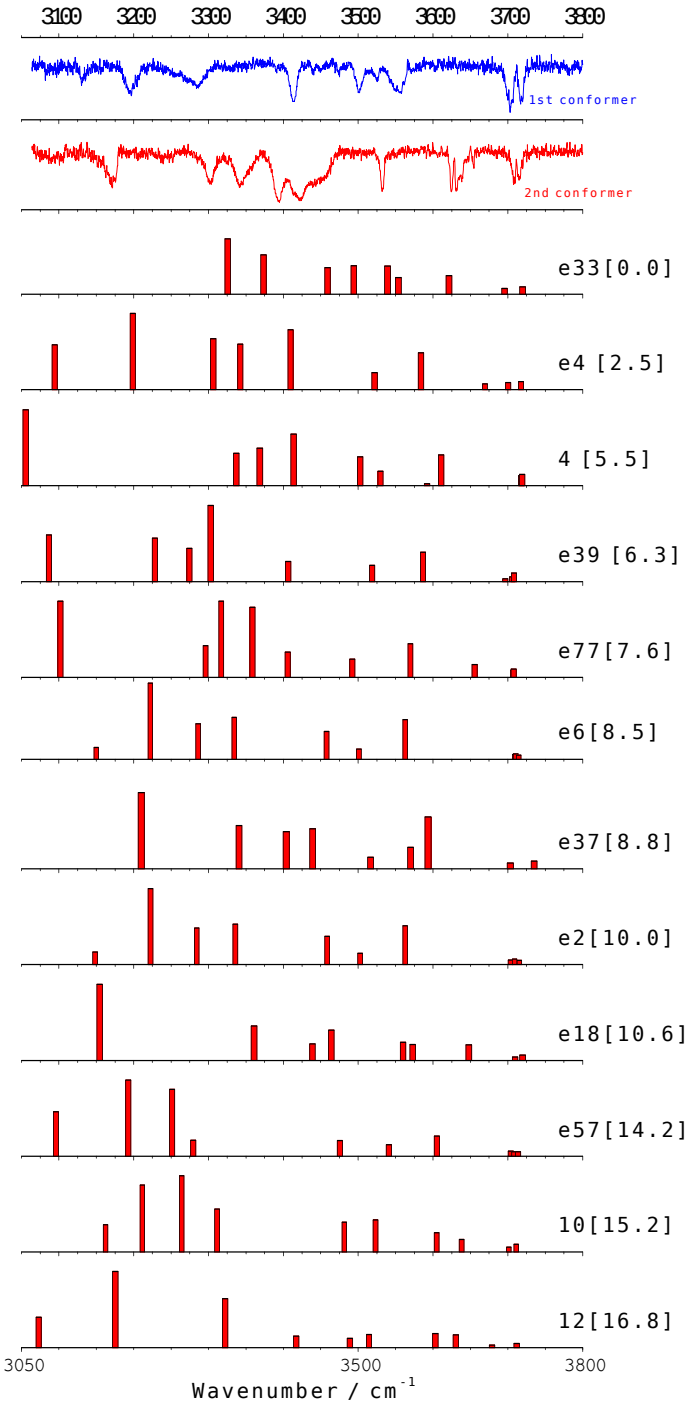

Figure 5.134. *IDIR spectra of propofol$_2$·W$_4$ recorded tuning the probe laser at 36018 and 36124 cm^{-1}. The predicted IR spectra for the twelve structures bellow 17 kJ/mol are also shown for comparison. The numbers in brackets are the relative energies of the calculated conformers, in kJ/mol. A correction factor of 0.956 was applied. The predicted IR spectra of all the calculated structures are collected in appendix 7.1 (Figure 7.28).*

Assignment

Propofol$_2$·W$_5$ cluster, as the mass spectrum suggest and as it will be discussed in the next section, constitutes a magic number and so, an especially stable stoichiometry. Thus, propofol$_2$·W$_4$ is expected to be on the verge of such stability isle.

Assignment of the IR spectrum of the **first conformer** is not difficult, as only structure *e4* reproduces the characteristics of the experimental spectrum, as shown in Figure 5.135: two free OH stretching vibrations, absences of any O-H···π interaction, and seven peaks distributed in the 3050-3600 cm^{-1} region. This structure (Figure 5.136) is a ***book*-type** structure.

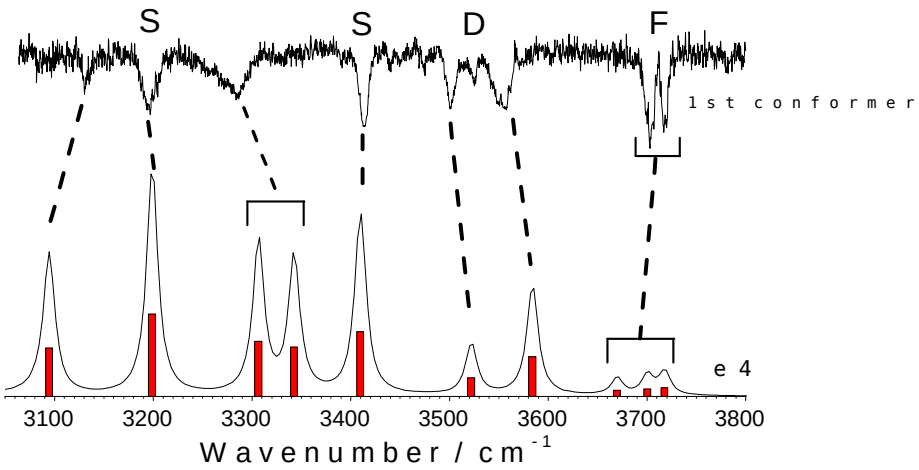

Figure 5.135. *Comparison of the IR spectrum predicted for structure e4 with the experimental results for the first conformer. As can be seen, there is a good match between the spectra.*

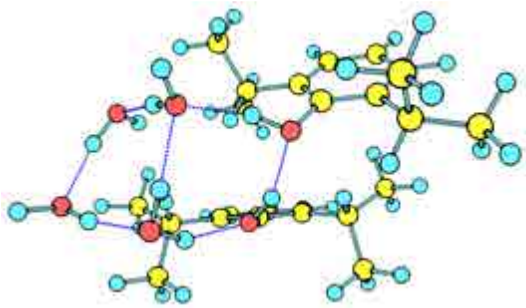

Figure 5.136. *Structure e4 is the theoretically predicted structure that better fits the experimental results for the first conformer.*

However, assignment of the **second conformer** is not that clear. In principle, some calculated structures, like structures *e77* and *18* (Figure 5.138), reproduce the general shape of the spectrum (Figure 5.137), although structure *e77* presents a single O-H···π interaction, while a doublet is found in the experimental spectrum at 3624 and 3632 cm^{-1}. On the other hand, structures *18* presents two O-H···π interactions, reproducing better this region, but it is considerably less stable: 28 kJ/mol above the global minimum, due to the lack of interaction between the two propofol molecules. Therefore, we conclude that structure *e77* is more likely to be the correct assignment for the second conformer and the extra peak may be due to overlapping of the spectrum with an additional conformer with nearly coincident electronic spectra. It must be noted that this structure is also a ***book*-type**.

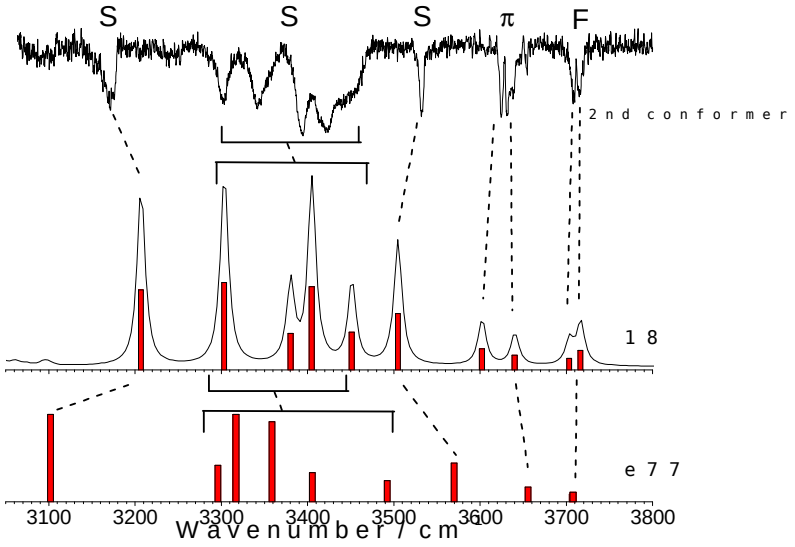

Figure 5.137. *Comparison between the IR spectrum predicted for structure 18 and the experimental results for the second conformer. As can be seen, there is a good match between the spectra.*

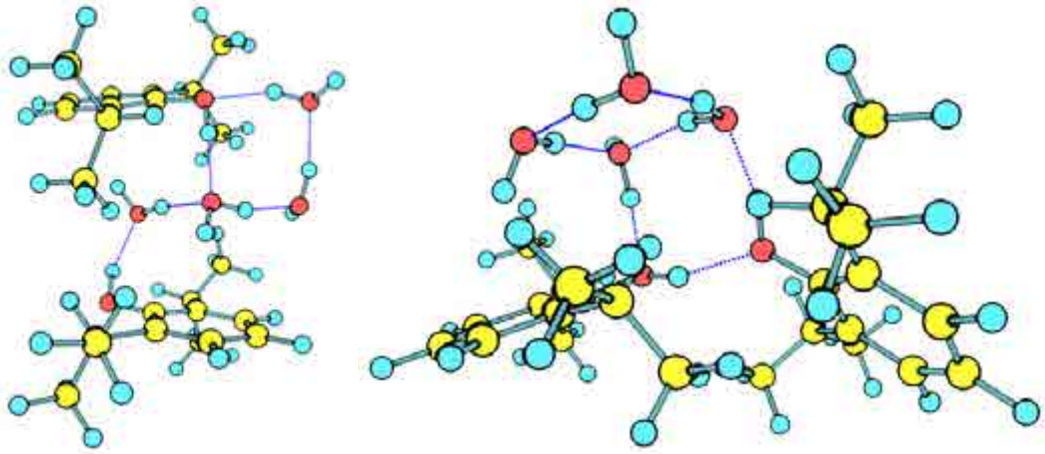

Figure 5.138. *Structures 18 and e77 are the theoretically predicted structures that better reproduce the experimental results for the second conformer, although the former is found at a relative high energy and thus, the latter is more likely.*

Finally, the absence of structure *e33*, being the most stable structure and also presenting a *book*-type conformation, is probably due to geometry changes upon excitation, which precludes accessing the excited state and thus its detection.

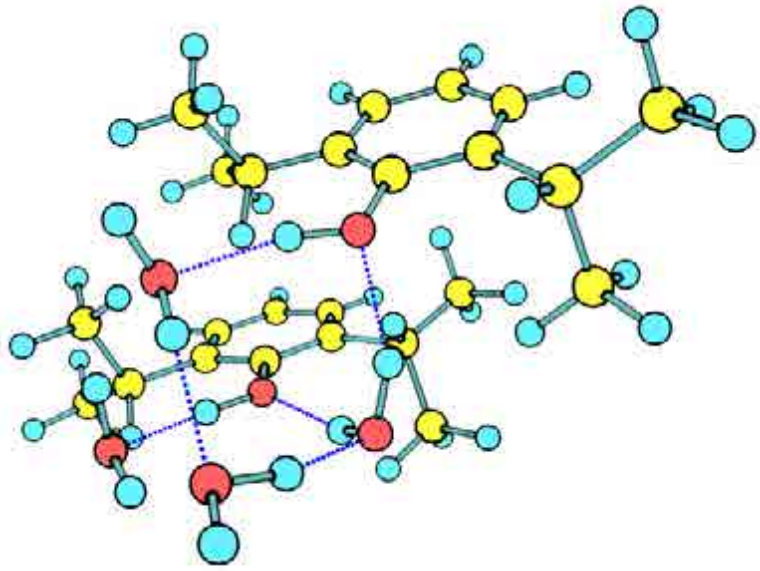

Figure 5.138. *Structure e33 is the predicted most stable structure. No experimental evidence of the presence of this structure was found.*

The OH stretching modes for each of the conformers are collected in Table 5.12 and compared with the structure *e4* for the first conformer and with structures *18* and *e77* for the second conformer.

Table 5.12. *Experimental vibrational transitions in the IR traces of propofol$_2$·W$_3$ first and second conformers, with a tentative assignment based on a comparison with the calculated frequencies for structures e4 for the first conformer and structures 18 and e77 for the second conformer.*

Experimental Peak (cm^{-1})	**structure *e4***		
	Frequency (cm^{-1})	Intensity	Vibrational type
3130	3094	572	σ_s^s (OH$_w$)
3195	3199	971	σ_s^s (OH$_w$)
3284 (x2 peaks)	3306	649	σ_s^s (OH$_w$)
	3342	581	σ (OH$_{ppf}$)
3413	3409	762	σ (OH$_{ppf}$)
3501	3522	219	σ_s^d (OH$_w$)
3557	3584	468	σ_{as}^d (OH$_w$)
3703 (x2 peaks)	3669	73	σ^f (OH$_w$)
	3700	86	σ^f (OH$_w$)
3717	3718	101	σ^f (OH$_w$)

Experimental Peak (cm^{-1})	**structure *18***		
	Frequency (cm^{-1})	Intensity	Vibrational type
3171	3207	664	σ_s^s (OH$_w$)
3303	3303	724	σ (OH$_{ppf}$)
3342	3380	301	σ (OH$_{ppf}$)
3394	3405	689	σ_s^s (OH$_w$)
3421	3451	313	σ_s^s (OH$_w$)
3532	3505	467	σ_s^s (OH$_w$)
3624	3602	173	σ$^{O\text{-}H\cdots\pi}$ (OH$_w$)
3632	3640	121	σ$^{O\text{-}H\cdots\pi}$ (OH$_w$)
3708	3703	95	σ^f (OH$_w$)
3716	3716	161	σ^f (OH$_w$)

Experimental Peak (cm^{-1})	**structure *e77***		
	Frequency (cm^{-1})	Intensity	Vibrational type
3171	3102	1018	σ (OH$_{ppf}$)
3303	3296	425	σ_s^s (OH$_w$)
3342	3317	1019	σ_s^s (OH$_w$)
3394	3359	933	σ (OH$_{ppf}$)
3421	3405	338	σ_s^d (OH$_w$)
3532	3492	244	σ_s^d (OH$_w$)
3624	3570	452	σ_s^d (OH$_w$)
3632	3656	172	σ$^{O\text{-}H\cdots\pi}$ (OH$_w$)
3708	3707	91	σ^f (OH$_w$)
3716	3708	110	σ^f (OH$_w$)

5.4.5 – Propofol$_2$·W$_5$

Accordingly to the mass spectrum (Figure 5.7), this is a particularly stable stoichiometry. Such stability isles are usually called "magic numbers", as their intensity is stronger than what one would expect from the sequence. All calculated most stable isomers (Figure 5.140) present tridimensional structures, in which nearly all the OH moieties participate in a hydrogen bond network. Remarkably, only three of the calculated structures are in the 10 kJ/mol window. two *cage*-type (structures *e2, e17*) and one *prism*-type (structure *e1*) structyures. The next predicted structures are *chair*-type, differing in the orientation of propofol molecules (structures *e4, e18, e3*), distorted *bi-cyclic* structures (structure *e5*) or *book*-like structures (structure *e36*). Part of the lower stability of such conformers is due to a reduced interaction between the two propofol molecules.

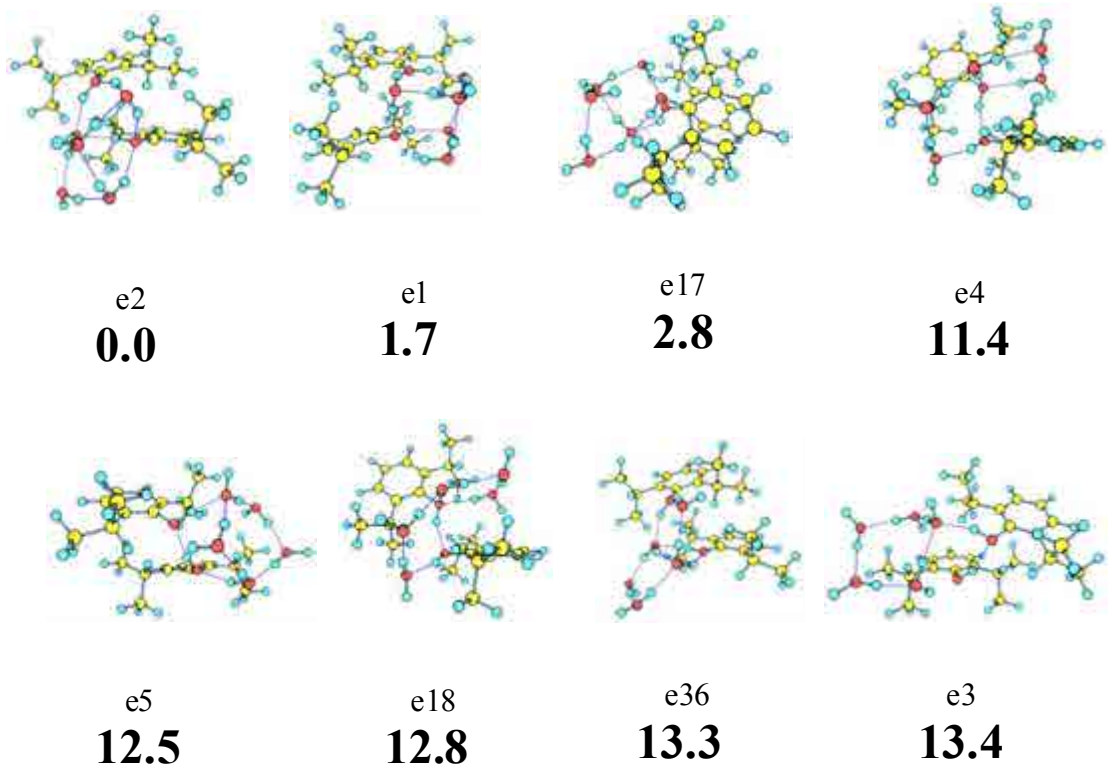

Figure 5.140. *Propofol$_2$·W$_5$ eight most stable conformers calculated at M06-2x/6-31+G(d) level, with their relative energies in bold. Energy values are in kJ/mol. All the calculated structures are presented in appendix 7.1 (Figure 7.29).*

Figure 5.141 shows the *2c-REMPI* of propofol$_2$·W$_5$ recorded between 35000-37400 cm^{-1}. As can be seen, the spectrum extends for, at least, 1400 cm^{-1}, with the red-

most band at 36050 cm^{-1}. The spectrum in Figure 5.141 resembles to that of propofol·W$_8$, as it is cleaner that those of the rest of propofol hydratated clusters containing more than three water molecules. Part of the features are due to fragmentation, especially in the red side of the spectrum.

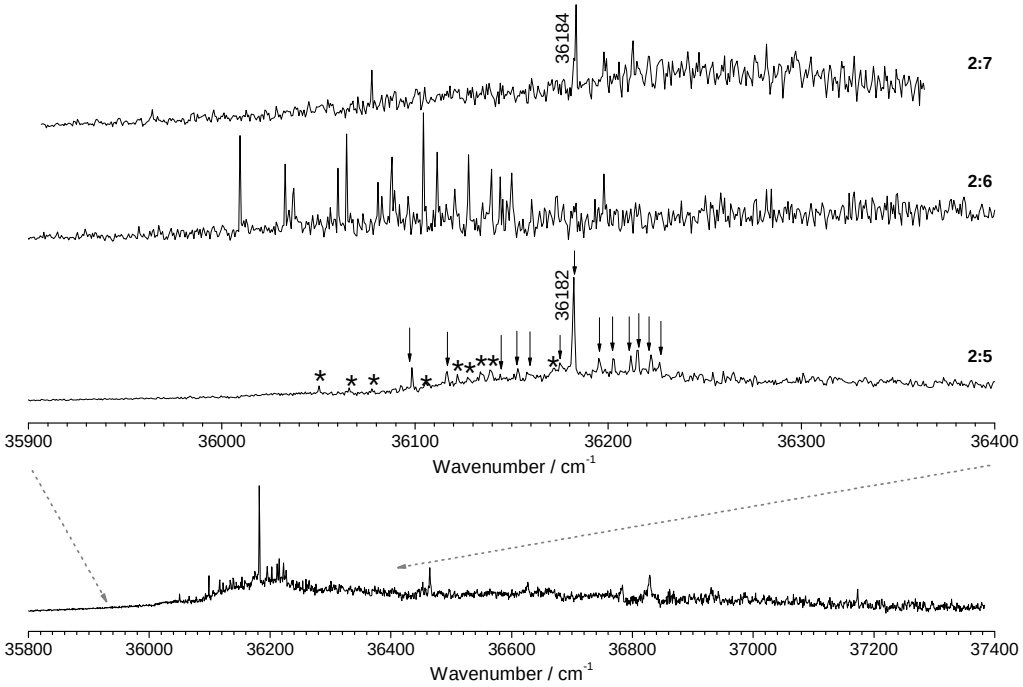

Figure 5.141. *2c-REMPI of propofol$_2$·W$_5$, in the 35800-37400 cm^{-1} region, recorded setting the probe laser at 27972 cm^{-1}. A detailed view of the propofol$_2$·W$_n$ (n=5-7) spectra, around the origin bands of propofol$_2$·W$_5$, is also shown for comparison. The peaks marked with asterisks are due to fragmentation. The arrows indicate the transitions belonging to propofol$_2$·W$_5$.*

Hole burning experiment (Figure 5.142) demonstrate the existence of at least three conformers. The 0_0^0 transition of the first conformer is located at 36098 cm^{-1}. However, the position of the origin band of second and third conformers is not that clear. Nevertheless, it must be noted that the peak located at 36182 cm^{-1} and, that belongs to the third conformer, is anomalously intense.

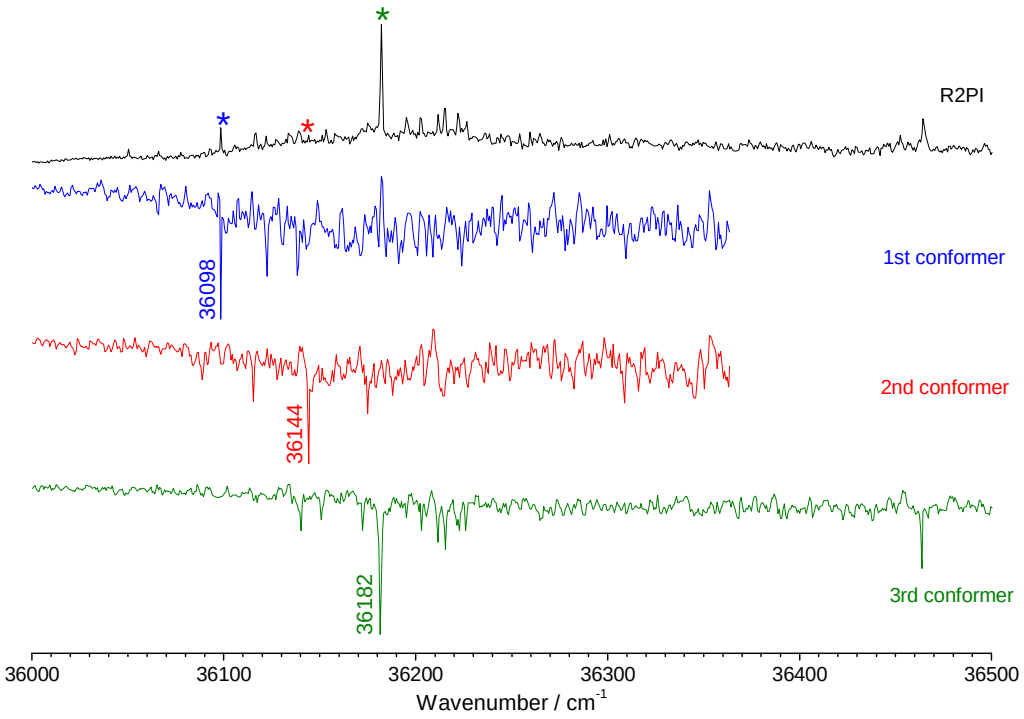

Figure 5.142. *Hole burning traces of propofol$_2$·W$_5$ recorded tuning the probe lasers (2-color detection) at 36098, 36144 and 36198 cm^{-1}. The peaks noted with asterisks indicate the transitions employed for recording the hole burning spectra, as well as the IDIRS traces.*

Finally, the IDIR spectra of the three conformers was recorded in the OH stretching region, obtaining the spectra shown in Figure 5.143. The spectrum for the second conformer is noisy due to the low signal intensity. The same applies to the first conformer but, in this case, a better resolved spectrum was obtained. For the third conformer, an improved s/n ratio was achieved, allowing resolving four peaks in the free OH stretching region. Regarding the first two conformers, it is difficult to extract any conclusion: the peak that appears for the first conformer at 3634 cm^{-1}, surely due to a O-H···π interaction, may also be present in the second conformer but due to the low signal intensity, a good depletion of the signal could not be performed. The same applies to the broad depletion observed for the second conformer in the 3500 – 3600 cm^{-1} region, being indicative of double-donor stretching modes. They also present a broad absorption in the 3250-3480 cm^{-1} region, which is surely due to the convolution of several OH stretching modes in that region. In addition, both present a peak at c.a. 3210 cm^{-1}. Such similarities point to resemblant structures.

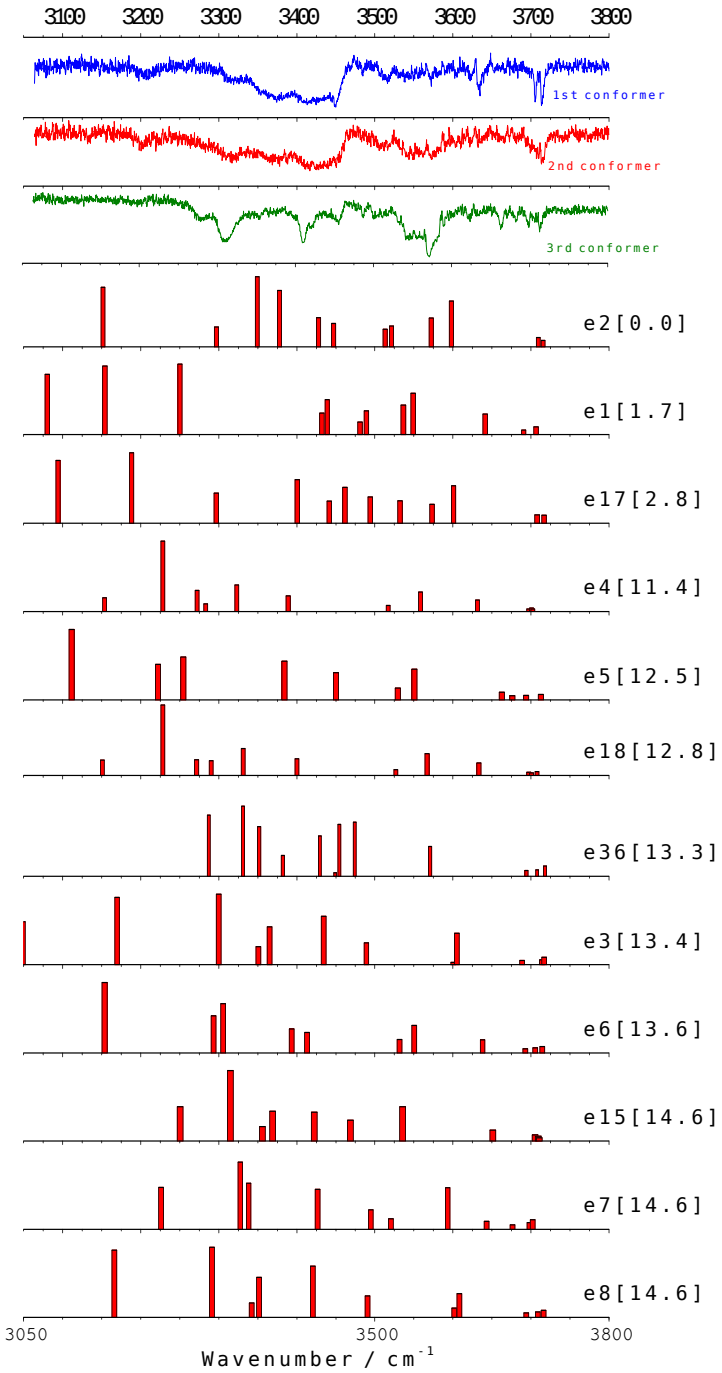

Figure 5.143. *IDIR spectra of propofol$_2$·W$_5$ recorded tuning the probe laser at 36098, 36144 and 36198 cm^{-1}. The predicted IR spectra for the twelve structures bellow 15 kJ/mol are also shown for comparison. The numbers in brackets are the relative energies of the calculated conformers, in kJ/mol. A correction factor of 0.954 was applied. The predicted IR spectra of all the calculated structures are recorded in appendix 7.1 (Figure 7.30).*

Assignment

As it happens with the monomer's high order water clusters, the large number of calculated structures makes difficult a univocal assignment. Therefore, the best choice is to group the structures into families with analogous spectra.

Structure *e2*, a ***cage*-type** structure (Figure 5.145), is a group on its own, being also the most stable structure. Despite that it presents a similar structure to *e17*, its predicted IR spectrum is the only one that reproduces that of the **second conformer** (Figure 5.144).

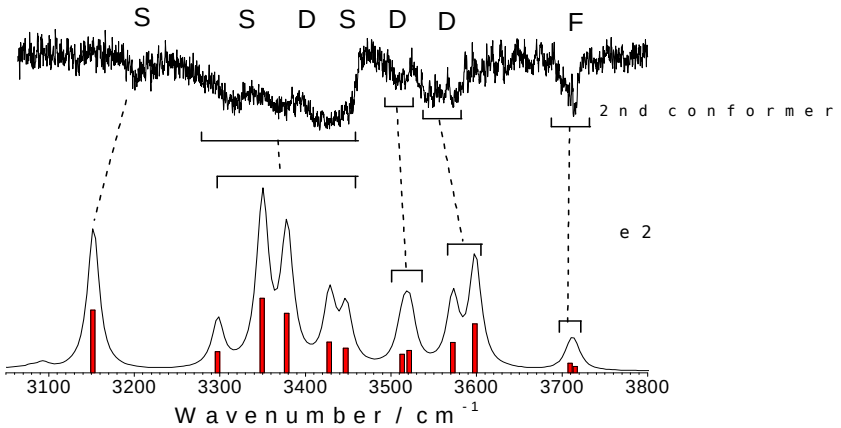

Figure 5.144. *Comparison between structure e2 calculated IR spectrum with the experimental results for the second conformer. As can be seen there is a good agreement between the spectra.*

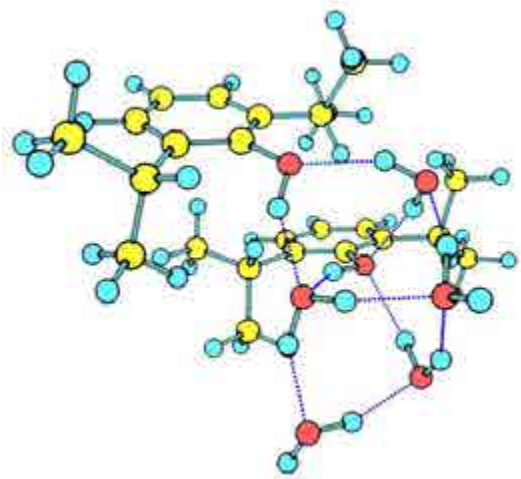

Figure 5.145. *Structure e2 is the theoretically predicted structure that better fits the experimental results for the second conformer.*

The **second group** is, again, formed by a single structure, *e1,* being also one of the most stable structures at a relative energy of only 1.7 kJ/mol. It presents a ***prism*-like** water arrangement (Figure 5.146). Its predicted IR spectrum does not match any of the experimental ones, as it presents a group of peaks in the 3420 - 3570 cm^{-1} region that are not present in any of the IR spectra. The experimental peaks in the 3250 - 3450 cm^{-1} region are missed as well.

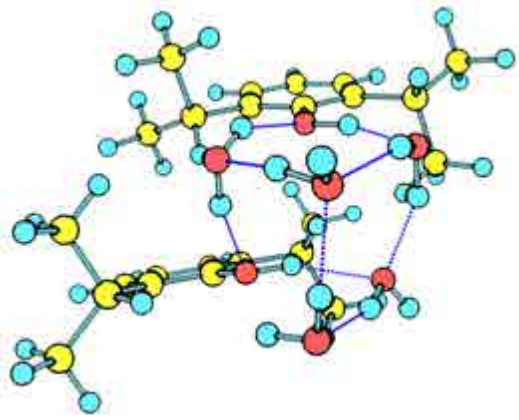

Figure 5.146. *Structure e1 is a prism type structure but does not reproduce correctly any of the experimental spectra.*

A **third group** is formed by structures *e5* and *e6*, whose structures are a combination of a water pentamer, hydrogen bonded to a propofol dimer (Figure 5.147). Figure 5.148 shows that the predicted spectra for such structures reproduce reasonably well the experimental results for the **third conformer**.

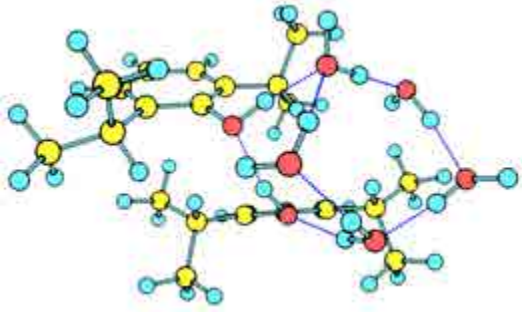

Figure 5.147. *Structure e5 where five water molecules are forming a ring and interact with the hydrogen-bonded propofol OH moieties. Such structure is a good candidate for the third conformer.*

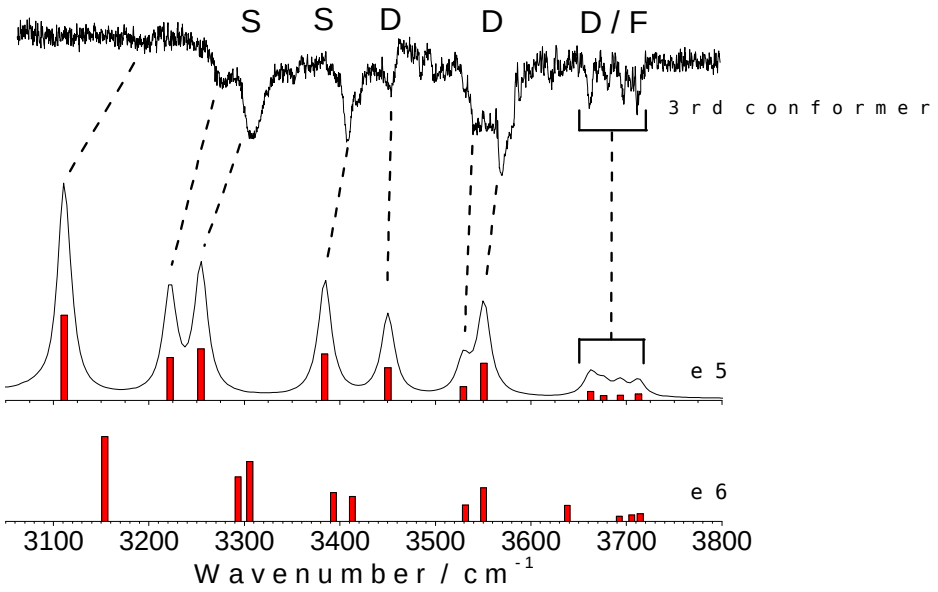

Figure 5.148. *Comparison between structures e5 and e6 calculated IR spectrum with the experimental results for the third conformer. As can be seen there is a good agreement between the spectra.*

***Chair*-like** structures constitute the fourth group. They are formed by two rings, one built by four OH moieties and the other one, built by five OH groups. Two types can be distinguished: one in which there is an O-H···π interaction (structures *e4, e18, e3, e8* and *e25*) and the other where such interaction is not present (structures *e15, e62, e11, e16, 4* and *e2352*). None of them are able to reproduce the experimental results, except structures *e3* and *e8,* which are slightly different as the closure of the ring is not complete, presenting an OH stretching midway between a free and a double donor stretching, matching the **first conformer** IR spectrum (Figure 5.149). Something similar happens with structure *e15*. Figure 5.150 shows structures *e3* and *e15,* which are able to reproduce accurately the experimental results for the **first conformer**.

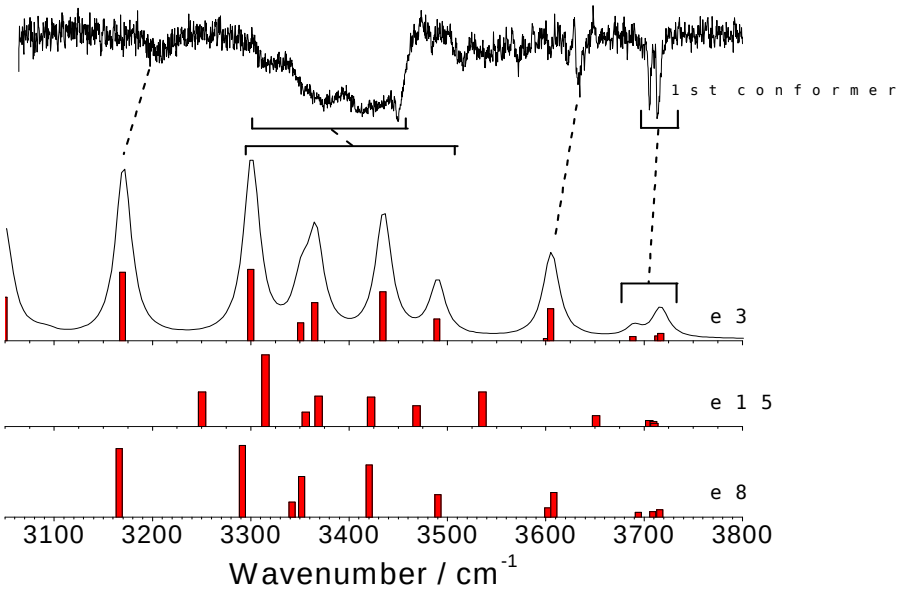

Figure 5.149. *Comparison between structures e3, e8 and e15 calculated IR spectrum with the experimental results for the first conformer. As can be seen there is a good agreement between the spectra.*

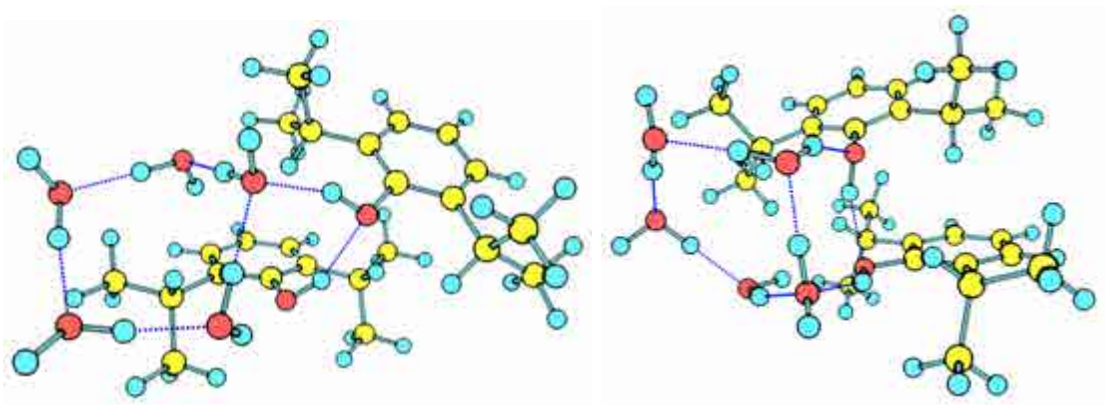

Figure 5.150. *Structures e3 and e15, where five water molecules are forming a ring and interact with the hydrogen-bonded propofol OH moieties. As it is discussed in the text, these structures are a good match for the first conformer.*

The fifth group includes structures *e36*, *8*, and *e5283,* where one of the propofol molecule's OH moiety and the water molecules form a ***book-like*** structure, with the other propofol molecule attached to it. Among the components of this group structure *8* presents a calculated spectrum that resembles the **first conformer** IR spectrum (Figure 5.151) One argument against its presence is that appears at 25 kJ/mol which is a

relatively high energy. This structure presents an O-H···π interaction (Figure 5.152) and therefore reproduces the feature at 3635 cm^{-1} in the experimental spectrum.

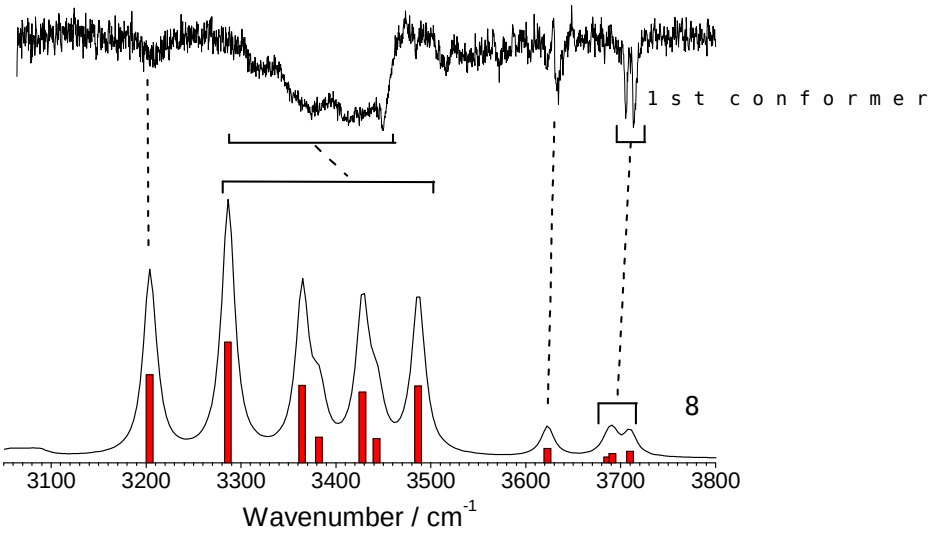

Figure 5.151. *Comparison of the IR spectrum predicted for structure 8 with the experimental results for the first conformer. There is a good agreement between both spectra.*

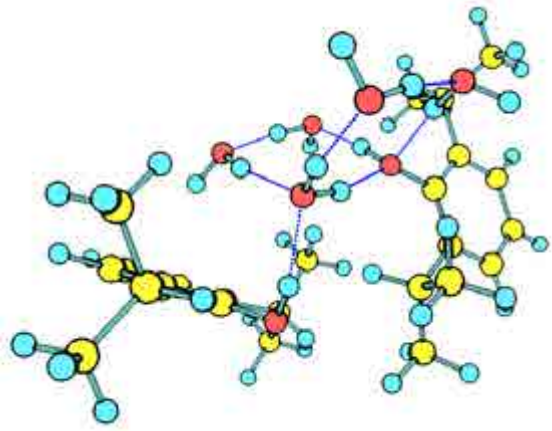

Figure 5.152. *Structure 8 is a book-type hydrogen bond network attached to a propofol's OH moiety. Among this type of structures, this is the only one that is able to reproduce the experimental results of the first conformer.*

The sixth group collects structures *7, 6* and *9*, that present ***bicyclic*** **structures** and, as can be seen in Figure 5.153, are also able to reproduce the experimental spectrum of the **first conformer**. Figure 5.154 shows structure *7*. Once more the

structures in this group appear at a relative high energy, in a 20-30 kJ/mol window, due to a reduced interaction between the two propofol molecules. Consequently, it is very unlikely to find such structures.

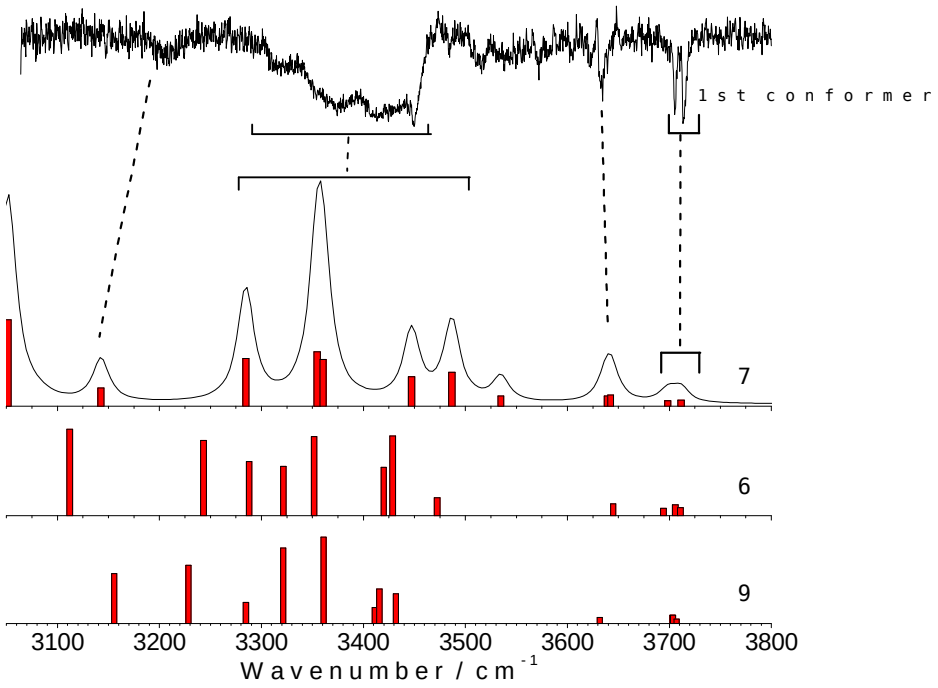

Figure 5.153. *Comparison of the IR spectrum predicted for structures 7, 6 and 9 with the experimental results for the first conformer. There is a good agreement between both spectra.*

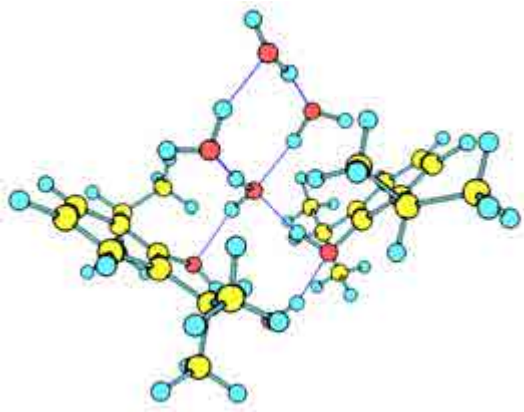

Figure 5.154. *Structure 7 is representative of the bicyclic-like structures. They are also able to reproduce the experimental results for the first conformer.*

Another family can be created with the structures in which the water molecules form a single cycle, including the two propofol's OH moieties (structure *e846*) or including only one of the propofol hydroxyl group (structure *2*), i.e. a ***monocyclic*** or the **hexamer-monomer** types respectively (Figure 5.155). **None** of these structures is able to reproduce the experimental results. Additionally, these structures appear at relative high energies (> 36 kJ/mol).

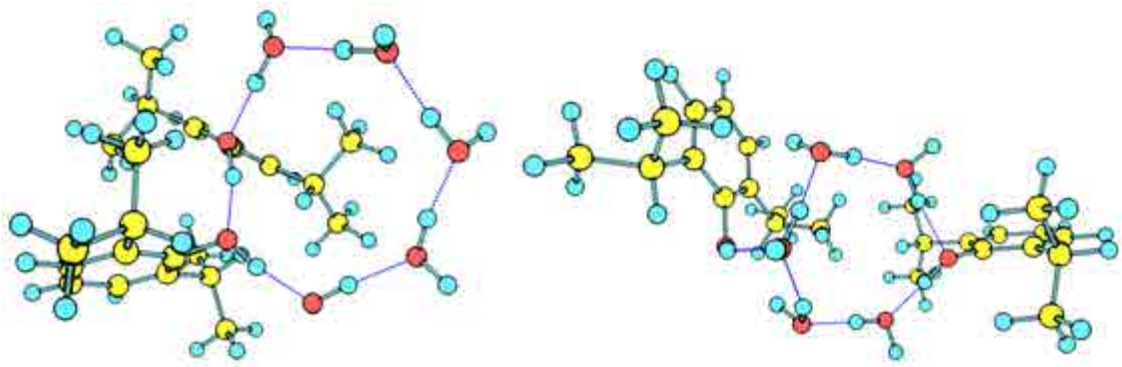

Figure 5.155. *Structures e846 and 2 are structures forming a seven or six OH member ring. They do not reproduce any of the experimental spectra.*

The rest of the structures, like four+three OH member ring, or five water molecules forming a ring between the propofol molecules, among others, do not reproduce the experimental results.

In summary, it is not clear if the structure of the first conformer is a *chair*-like, a *book*-like, or a *byciclic* structure; for the second conformer a *cage* structure is the best candidate and a structure where a ring of five-water molecules is attached to the propofol's hydroxyl group matches very well the spectrum of the third conformer. The OH stretching modes for each of the conformers are collected in Table 5.13 and compared with the structure *e2* for the second conformer and with structure *e5* for the third conformer. The first conformer is not assigned as the stretches vary depending on the interaction type.

Table 5.13. *Experimental vibrational transitions in the IR traces of propofol$_2$·W$_5$ second and third conformers, with a tentative assignment based on a comparison with the calculated frequencies for structures e2 and e5 respectively.*

Experimental Peak (cm^{-1})	**structure *e2***		
	Frequency (cm^{-1})	Intensity	Vibrational type
3200	3151	743	σ_s^s (OH$_w$)
3270-3460 (x5 peaks)	3297	250	σ_s^s (OH$_w$)
	3349	880	σ (OH$_{ppf}$)
	3378	706	σ_s^d (OH$_w$)*
	3428	366	σ_{as}^d (OH$_w$)*
	3447	294	σ (OH$_{ppf}$)
3495-3520 (x2 peaks)	3513	221	σ_s^d (OH$_w$)
	3521	264	σ_s^d (OH$_w$)
3530-3585 (x2 peaks)	3572	360	σ_{as}^d (OH$_w$)
	3598	577	σ_{as}^d (OH$_w$)
3705	3709	115	σ^f (OH$_w$)
3716	3715	78	σ^f (OH$_w$)

* This double donor stretching vibrations are more red-shifted than expected for this kind of vibrations as they are bound to the two propofol molecule's OH moieties.

Experimental Peak (cm^{-1})	**structure *e5***		
	Frequency (cm^{-1})	Intensity	Vibrational type
-----	2995	330	σ_s^s (OH$_w$)
3197	3111	1226	σ_s^s (OH$_w$)
3278	3222	618	σ_s^s (OH$_w$)
3309	3254	743	σ (OH$_{ppf}$)
3409	3384	670	σ (OH$_{ppf}$)
3456	3450	473	σ_s^d (OH$_w$)
3545	3529	199	σ_s^d (OH$_w$)
3572	3551	533	σ_{as}^d (OH$_w$)
3663	3662	132	$\sigma_{as}^{f,d}$ (OH$_w$)
3682	3676	72	σ^f (OH$_w$)
3700	3694	78	σ^f (OH$_w$)
3713	3713	93	σ^f (OH$_w$)

5.4.6 – Propofol$_2$·W$_6$

As demonstrated in the previous section, water clusters of this size tend to present polyhedral (predominantly cubic) structures. The study of propofol$_2$·W$_6$ will allow to calibrate the influence of the π···π interaction on such propensity. Most of the stable isomers found (Figure 5.156) present tridimensional structures in which most of the OH groups are tri- even tetra-coordinated, with the water molecules acting as double donors (structure *e29*). The existence of numerous conformers with the water molecules forming *book*-like structures (structure *e97*) instead of cubes is probably indicative of the influence of the interactions due to dispersive forces in the cluster conformation. Even in the complexes with cubic structures, such polyhedral is never completed (structures *e20*, *e9, e5, e25*).

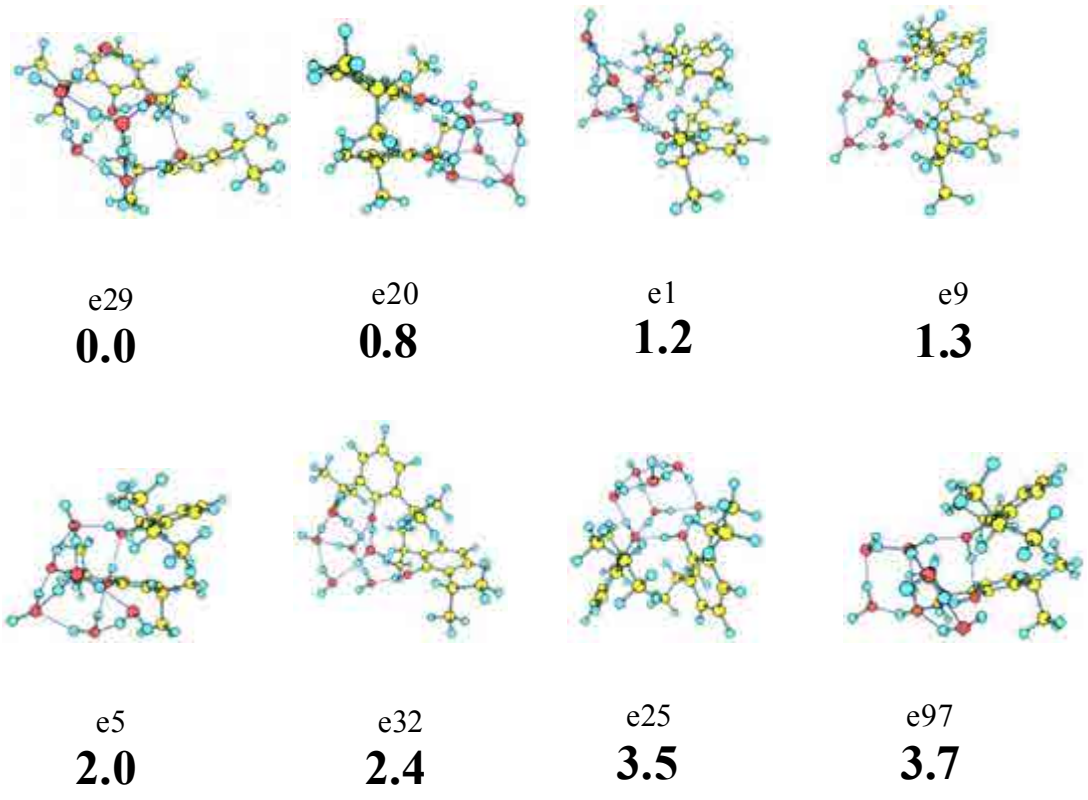

Figure 5.156. *Propofol$_2$·W$_6$ eight most stable conformers calculated at M06-2x/6-31+G(d) level, with their relative energies in bold. Energy values are in kJ/mol. All the calculated structures are presented in appendix 7.1 (Figure 7.31).*

Figure 5.157 shows the *2c-REMPI* spectrum of propofol$_2$·W$_6$ between 35800-37400 cm^{-1}. The red-most peak appears at 36009 cm^{-1}, and clear features are observed

for no more than 600 cm^{-1}. As can be seen, only two of those peaks are demonstrated to be due to fragmentation from propofol$_2$·W$_7$.

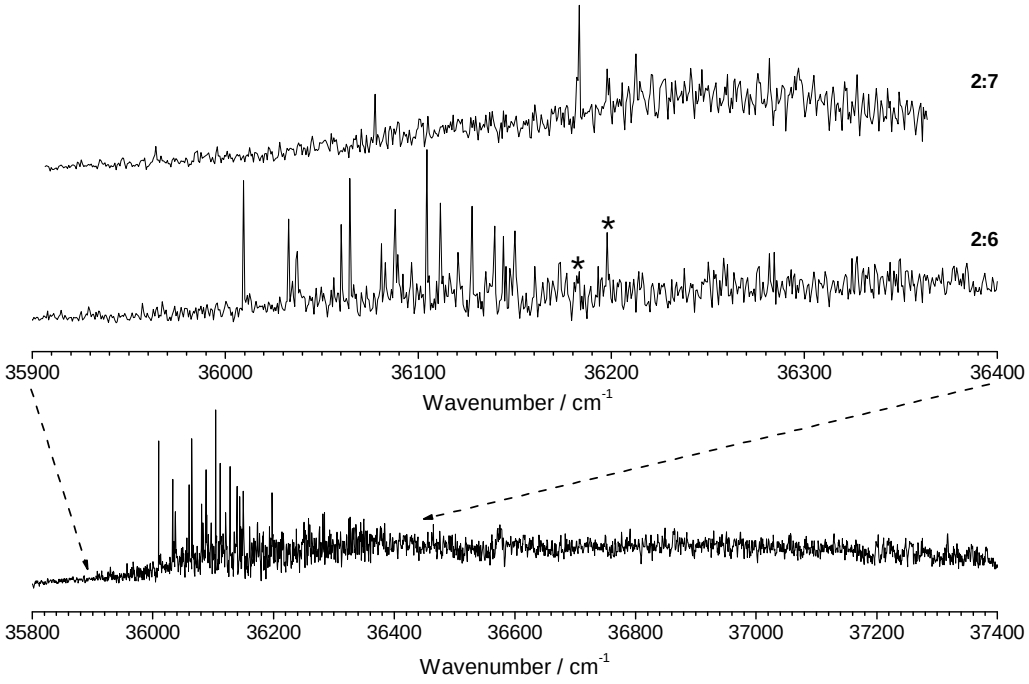

Figure 5.157. *2-color REMPI of propofol$_2$·W$_6$, in the 35800-37400 cm^{-1} region, recorded setting the probe laser at 27972 cm^{-1}. A detailed view of propofol$_2$·W$_n$ (n=6-7) spectra around the origin bands of propofol$_2$·W$_6$, is also shown. The peaks marked with asterisks are due to fragmentation.*

The *hole burning* experiment (Figure 5.158) demonstrates that all the bands are due to a single conformer, whose origin band is located at 36009 cm^{-1}.

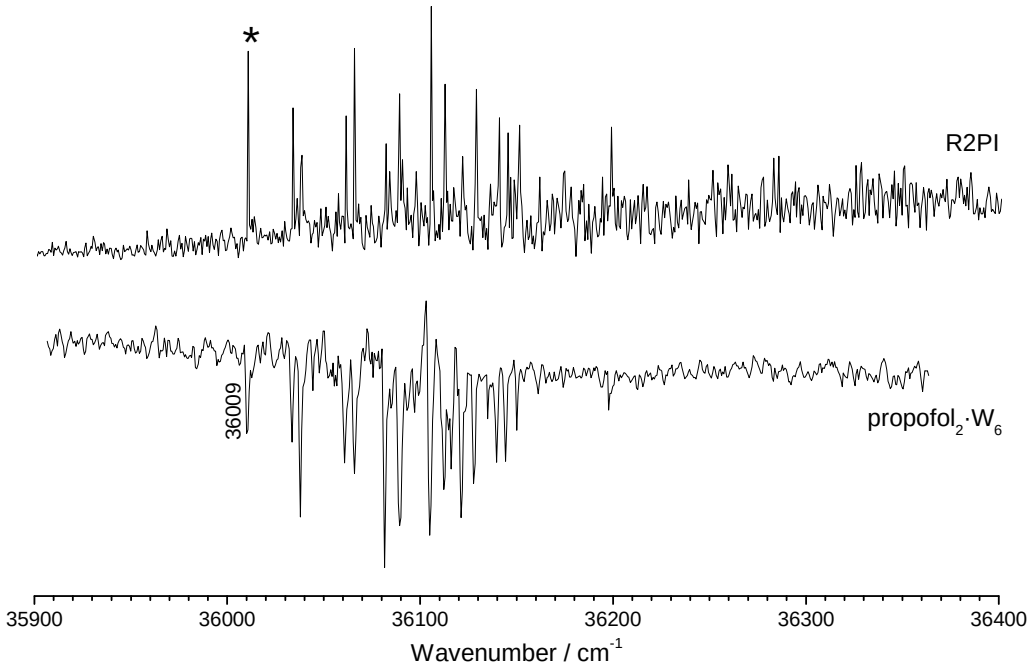

Figure 5.158. *Hole burning spectrum of propofol$_2$·W$_6$ recorded tuning the probe laser (2-color detection) at 36009 cm^{-1}. The peak noted with an asterisk is the transition employed for recording the hole burning spectrum, as well as the IDIRS trace.*

Taking into account the large size of this cluster, a well-resolved IDIR experiment was obtained (Figure 5.159). The most important observation is that no O-H···π interaction seems to be present, giving an important clue on the cluster's structure.

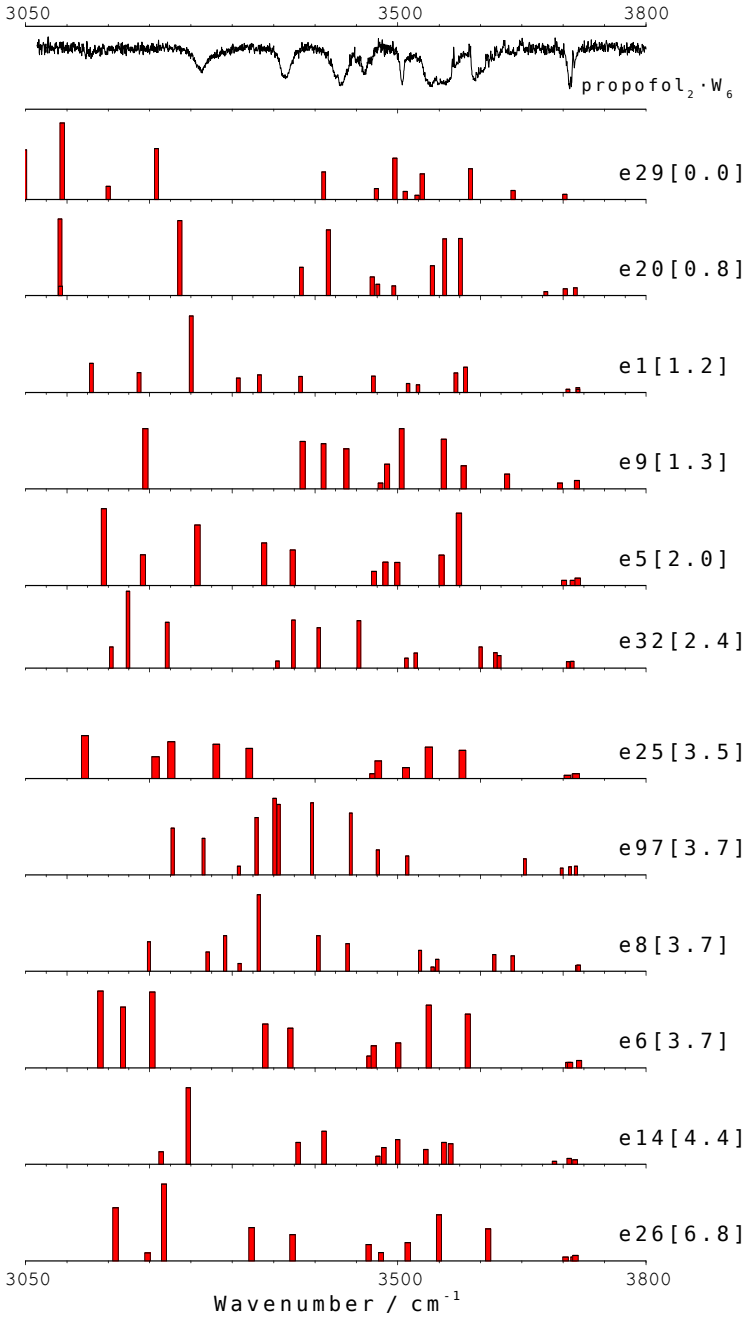

Figure 5.159. *IDIR spectra of propofol$_2$·W$_6$ recorded tuning the probe laser at 36009 cm^{-1}. The predicted IR spectra for the twelve structures bellow 7 kJ/mol are also shown for comparison. The numbers in brackets are the relative energies of the calculated conformers, in kJ/mol. A correction factor of 0.955 was applied. The predicted IR spectra of all the calculated structures are recorded in appendix 7.1 (Figure 7.32).*

Assignment

Two families of structures can reproduce the experimental spectrum: those with water cubes (structures *e20, e9, e5, e25, e14, e26* and *e3899*) and mixed *book-cage* structures (structures *e1, e60, e39* and *e24*), although with a water acting as a double donor. In both cases, the two propofol molecules present a direct interaction, exposing their hydroxyl groups to the water cluster. Figures 5.160 and 5.161 show a comparison between the experimental spectrum with the predicted spectra for structures *e24* and *e20*, while Figure 5.162 shows *ball and stick* models of representative members of those families. The prediction for structure *e24* reproduces slightly better the separation between the free OH stretching modes, but presents a frequency at c.a. 3050 cm^{-1} that is not found in the experimental trace. Furthermore, the structure *e20* spectrum offers a better description of the broad absorption at the 3550 cm^{-1}. Taking into account that such structure, *e20*, is considerably more stable we assign the **detected conformer** to a **cubic structure**.

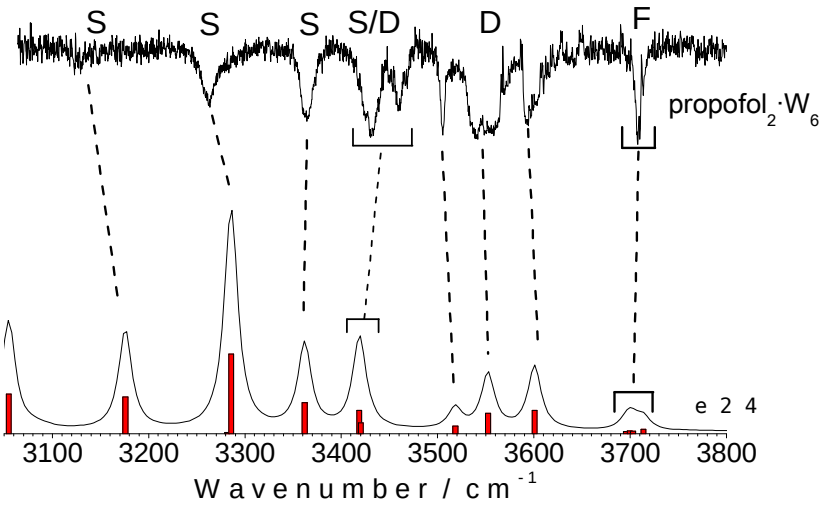

Figure 5.160. *Comparison of the predicted IR spectrum of structure e24 with the experimental results for the experimental conformer, as can be seen there is a reasonably agreement between predicted and experimental spectra.*

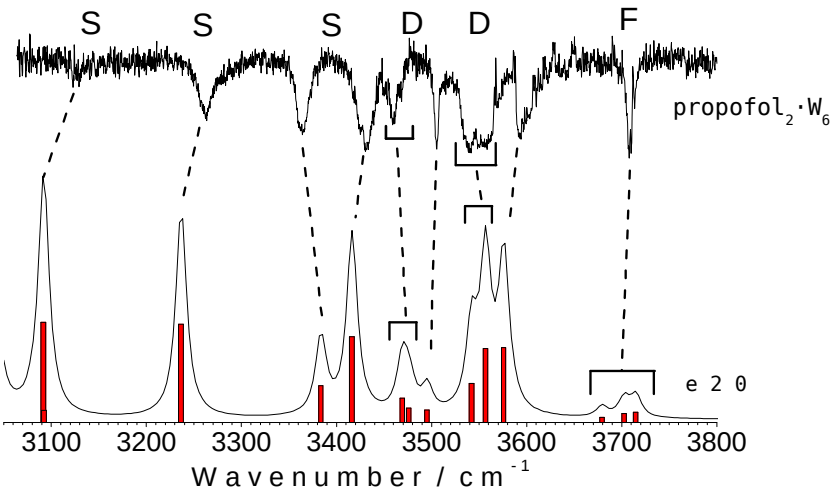

Figure 5.161. *Comparison of the predicted IR spectrum of structure e20 with the experimental results for the experimental conformer, as can be seen there is a good agreement between predicted and experimental spectra.*

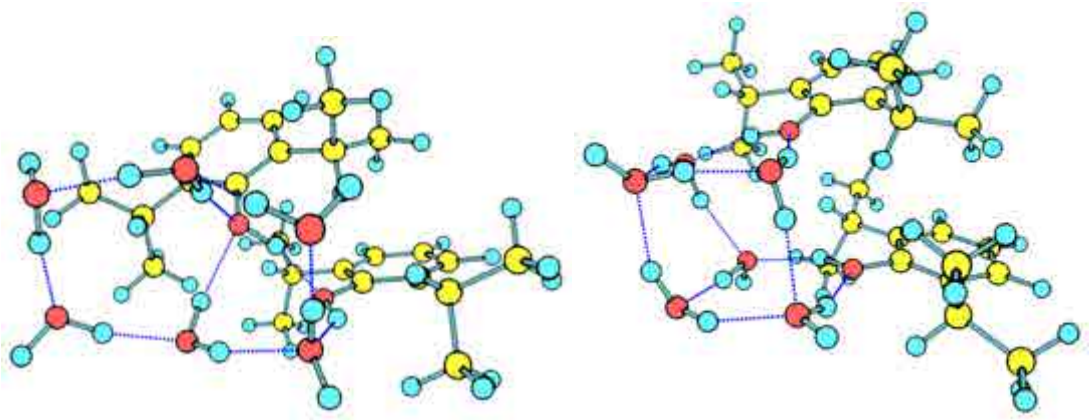

Figure 5.162. *Structures e24 and e20 are the theoretically predicted structures that fit the experimental spectrum. The second structure is more likely to be present.*

It is worthy to note that, for these cubic structures, if both propofol molecules act as a proton-donor to the water molecules, the cube can never close and, on the other hand, if one of the propofol molecules' hydrogen bonds one other each, one of the water molecules encounters steric hindrances and thus the cube can never close completely. This observation is shown in Figure 5.163.

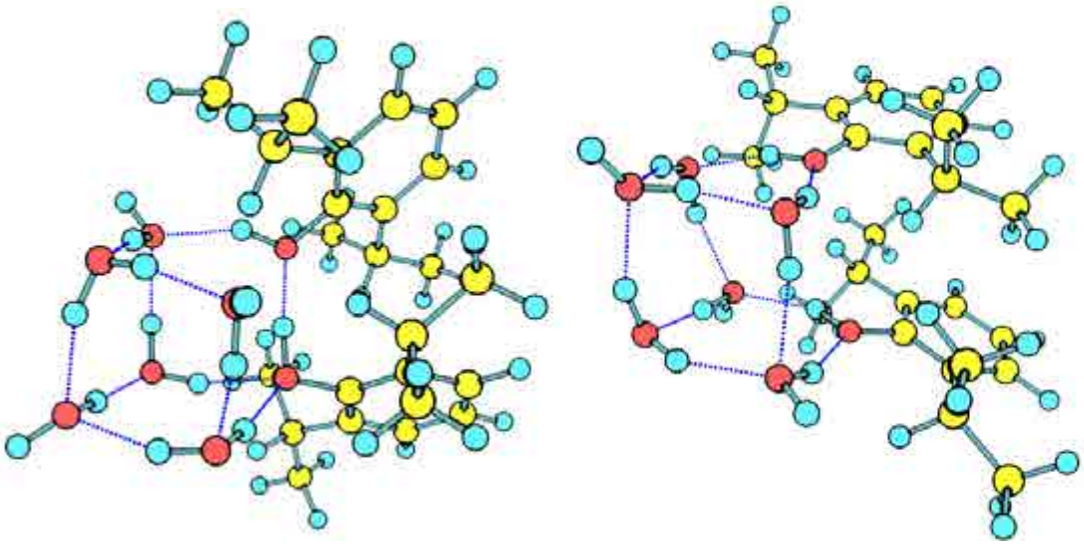

Figure 5.163. *Structures e5 and e20 are cube-like structures although they cannot be completely closed.*

The rest of the structures present different type of interactions such as *cage*-like structures (*e29, e1, e5, e32, e97, e8, e6, e60, e38, e12, e22 e100, e39, e18*), *book*-like structures (*e33, e10, e2, e28, e48, e19, e23, e11* and *e7*), *chair*-like structures (*e30, e103, 8, 11* and *e120)* or other heterogeneous groups as shown in Figure 5.164. Their predicted IR spectra do not reproduce the experimental results.

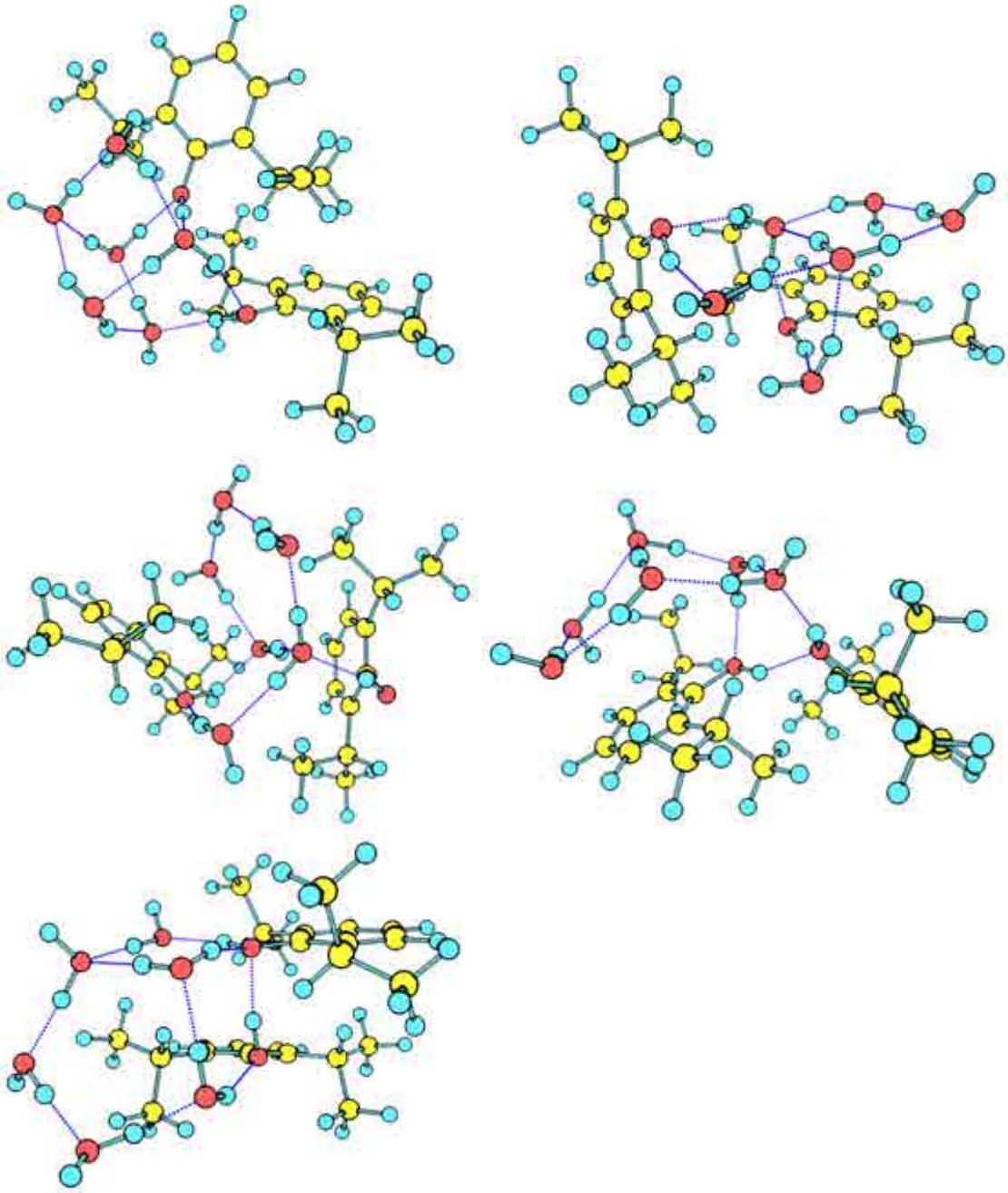

Figure 5.164. *Structures e29, e33, 8, e34 and e21 are examples of the theoretically predicted double-book structures. None of them reproduce the experimental results.*

Assignment of the IR spectrum using conformers *e24* and *e20* as a guide is offered in Table 5.14.

Table 5.14. *Experimental vibrational transitions in the IR traces of propofol$_2$·W$_6$ conformer, with a tentative assignment based on two different type of interactions with the calculated frequencies for structures e24 and e20 respectively.*

Experimental Peak (cm^{-1})	**structure *e24***		
	Frequency (cm^{-1})	Intensity	Vibrational type
-----	3055	939	σ_s^s (OH$_w$)
3130	3176	869	σ_s^s (OH$_w$)
3264 (x2 peaks)	3282	37	σ_s^s (OH$_w$)
	3286	1890	σ (OH$_{ppf}$)
3365	3362	738	σ_s^s (OH$_w$)
3430	3418	552	σ (OH$_{ppf}$)
3445-3470	3420	263	σ_s^d (OH$_w$)
3505	3518	185	σ_s^d (OH$_w$)
3525-3575	3552	485	σ_{as}^d (OH$_w$)
3593	3601	554	σ_{as}^d (OH$_w$)
3708 (x4 peaks)	3695	53	σ^f (OH$_w$)
	3699	72	σ^f (OH$_w$)
	3703	63	σ^f (OH$_w$)
	3714	107	σ^f (OH$_w$)

Experimental Peak (cm^{-1})	**structure *e20***		
	Frequency (cm^{-1})	Intensity	Vibrational type
3130 (x2 peaks)	3092	1023	σ_s^s (OH$_w$)
	3092	125	σ_s^s (OH$_w$)
3264	3236	1002	σ (OH$_{ppf}$)
3365	3383	377	σ (OH$_{ppf}$)
3430	3416	875	σ_s^s (OH$_w$)
3445-3470 (x2 peaks)	3469	251	σ_s^d (OH$_w$)
	3476	150	σ_s^d (OH$_w$)
3505	3495	128	σ_s^d (OH$_w$)
3525-3575 (x2 peaks)	3542	401	σ_{as}^d (OH$_w$)
	3557	757	σ_{as}^d (OH$_w$)
3593	3576	764	σ_{as}^d (OH$_w$)
3708	3679	52	σ^f (OH$_w$)
	3702	91	σ^f (OH$_w$)
	3715	104	σ^f (OH$_w$)

Curiosities

Structure *e25* presents a peculiar OH stretching that deserves special attention. The propofol molecule that acts as a proton acceptor of the other propofol is also coordinated with another two water molecules, establishing a particularly strong hydrogen bond with one of them. Its OH stretching mode is predicted to be at c.a. 2610 cm^{-1}, i.e. at lower frequencies than the C-H stretching modes. Note that structure *e25* belongs to cube-like structures, which are the ones assigned to the experimental conformer.

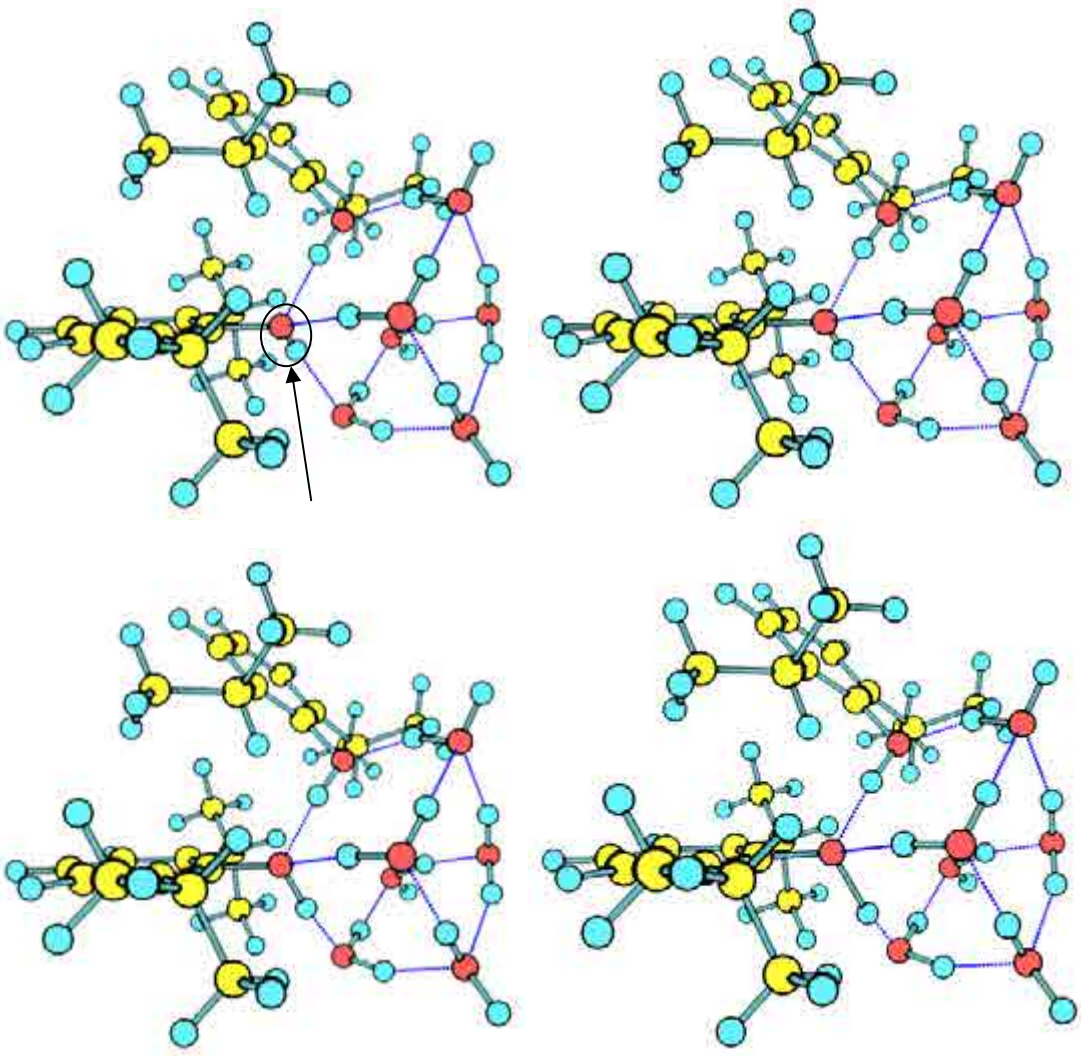

Figure 5.165. *Structure e25 presents a propofol molecule very strong bonded. A sequence of the stretching is showed from left to right.*

5.4.7 – Propofol$_2$·W$_7$

On the light of the results shown in previous sections, it is not surprising to find formation of water polyhedrons, mainly cubic structures, among the most stable propofol$_2$·W$_7$ species (Figure 5.166). As in lower-order clusters, the two propofol molecules hold together through dispersive forces, either sharing the hydroxyl groups with the water cube (structures *e7, e1, e14*) or one of the propofol's is integrated in a water cube, attached to the other propofol molecule (structure *e26*).

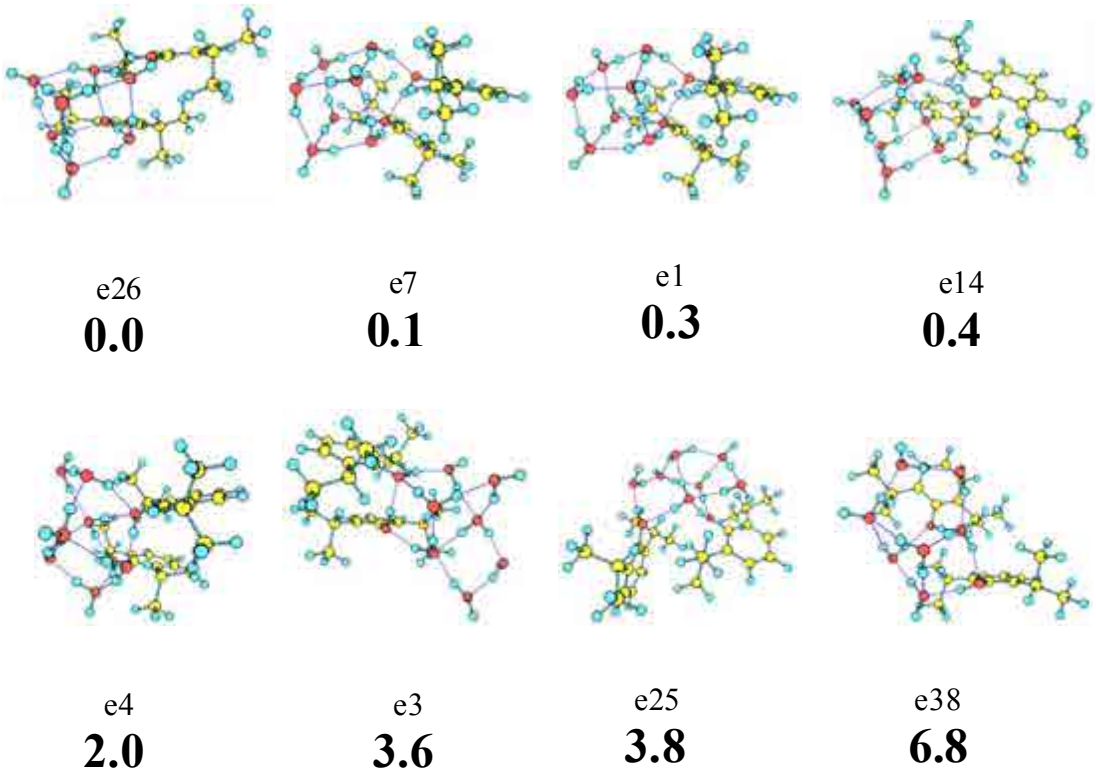

Figure 5.166. *Propofol$_2$·W$_7$ eight most stable conformers calculated at M06-2x/6-31+G(d) level, with their relative energies in bold. Energy values are in kJ/mol. All the calculated structures are presented in appendix 7.1 (Figure 7.33).*

The *2c-REMPI* spectrum of the propofol$_2$·W$_7$ (Figure 5.167), presents only a few well-resolved bands, built over a continuum background. As the comparison with the *2c-REMPI* spectra of propofol$_2$·W$_8$ and propofol$_2$·W$_9$ shows, this is the largest propofol$_2$·W$_n$ cluster for which discrete features could be resolved. Also the comparison points to fragmentation as a possible origin for the broad absorption.

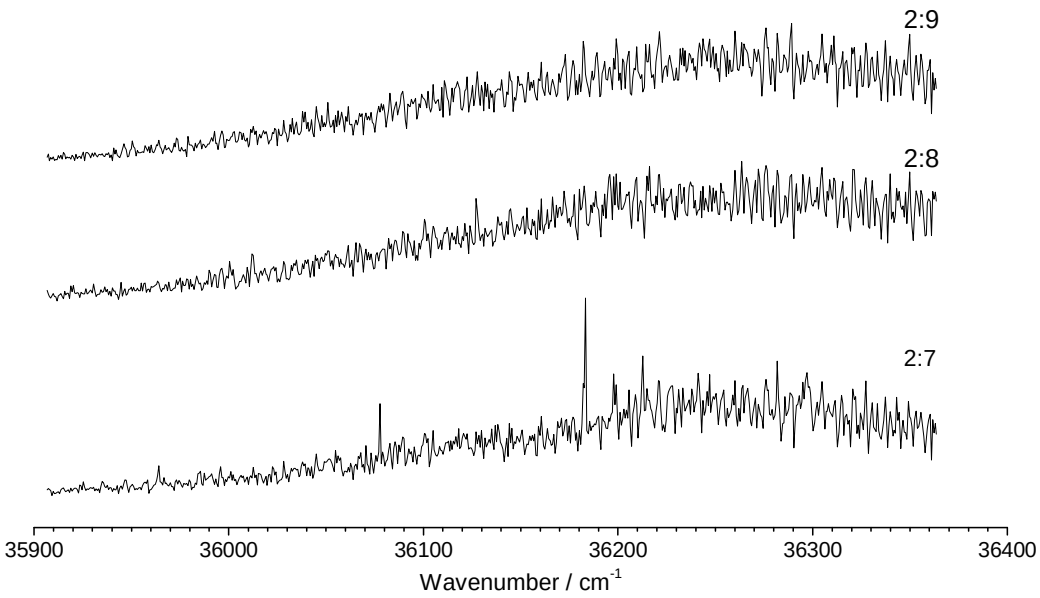

Figure 5.167. *2-color REMPI of propofol$_2$·W$_7$, in the 35900-36400 cm^{-1} region, recorded setting the probe laser at 27972 cm^{-1}, together with a comparison of propofol$_2$·W$_n$ (n=7-9) spectra. No fragmentation seems to be taken place, apart from the broad background.*

A correct adjustment of the experimental conditions is critical to record the 2c-REMPI, due to the extremely low ion signal. Nevertheless, it was possible to run *hole burning* experiments probing the origins at 36078 and 36184 cm^{-1} (Figure 5.168), demonstrating the existence of, at least, two conformers with same resolved bands and a broad absorption associated to each origin. The analysis of the *hole burning* spectra point to an overcongested spectrum as the origin of the spectral background. The general aspect of the *hole burning* spectra also indicate the presence of large geometry changes upon excitation.

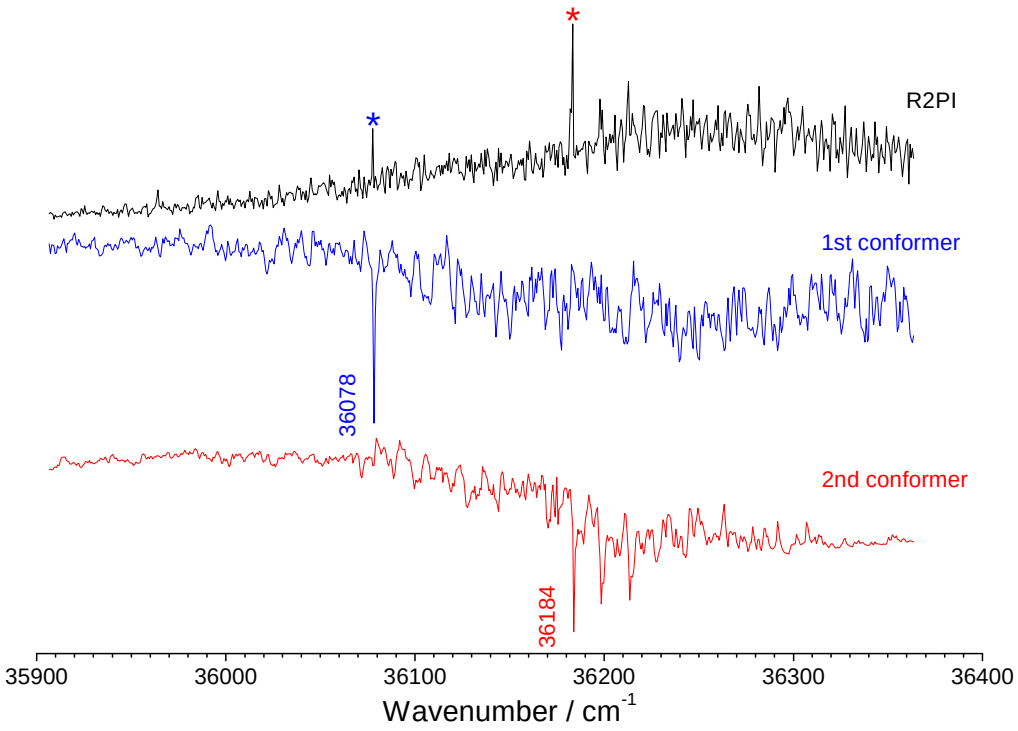

Figure 5.168. *Hole burning traces of propofol$_2$·W$_7$, recorded tuning the probe laser (2-color detection) at 36078 and 36184 cm^{-1}. The peaks noted with asterisks are the transitions employed for recording the hole burning spectra, as well as the IDIRS traces.*

As in previously studied systems, IDIR experiments yield invaluable information for the assignment of the *2c-REMPI* spectrum (Figure 5.169). IDIR spectra show some clear differences between the detected isomers as, for example, the characteristic feature at 3670 cm^{-1} in the first conformer, or the different spacing of the bands between 3500-3600 cm^{-1}. Such differences will guide the assignment in the next section.

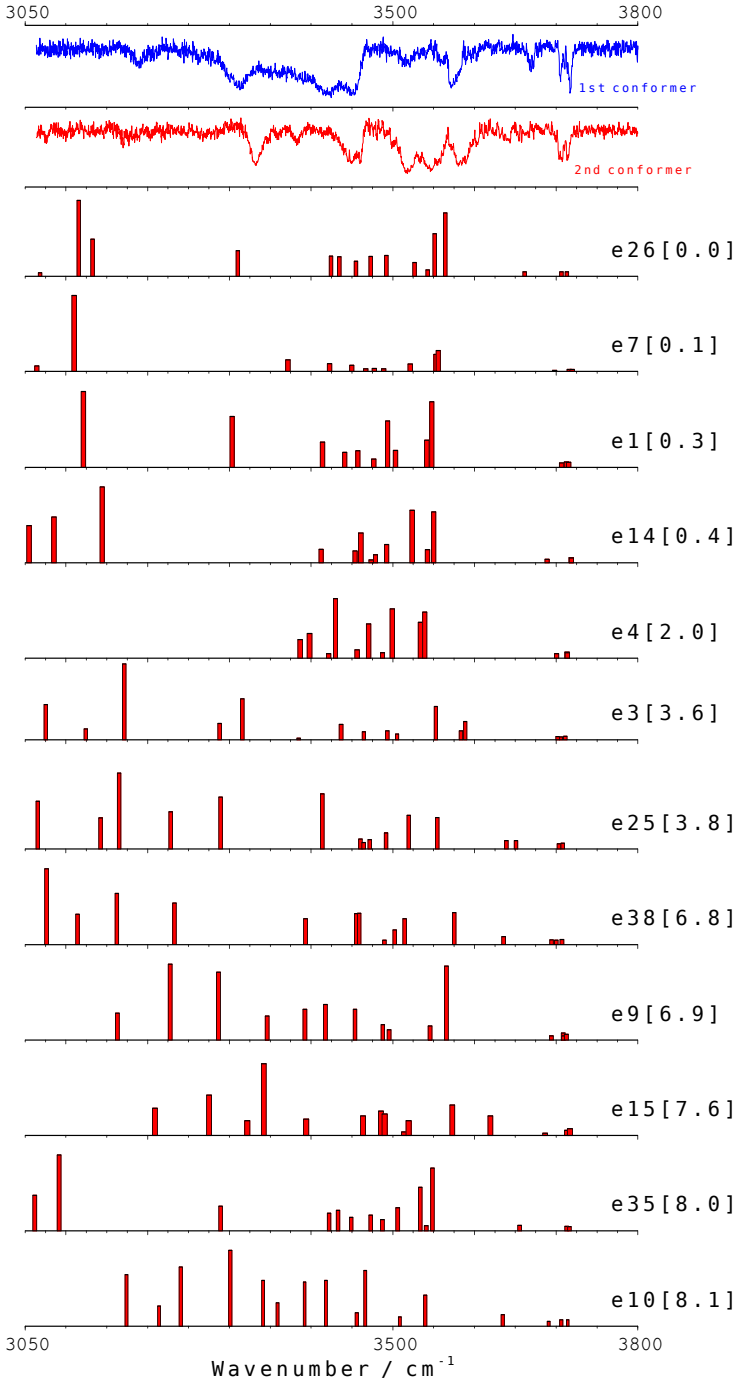

Figure 5.169. *IDIR spectra of propofol$_2$·W$_7$ recorded tuning the probe laser at 36078 and 36184 cm^{-1}. The predicted IR spectra for the twelve structures bellow 8 kJ/mol are also shown for comparison. The numbers in brackets are the relative energies of the calculated conformers, in kJ/mol. A correction factor of 0.955 was applied. The predicted IR spectra of all the calculated structures are collected in appendix 7.1 (Figure 7.34).*

Assignment

There are not many structures whose predicted spectra reproduce the experimental results and, among them, the predicted most stable structures deserve special attention. For the first conformer, structures *e26 and e35* match very well the experimental results (Figure 5.171) while structure *e1* does it for the second conformer (Figure 5.172). A picture of these structures is shown in Figure 5.170. Note that both conformers have water cubes of S_4 symmetry, although the contribution of clusters with water cubes of both, S_4 and D_{2d} symmetry, cannot be discarded if both molecules share the same excited state transition, as their IR spectra are very similar. For example, structures *e7* and *e1* are the same structure differing only in that their water cubes are D_{2d} and S_4 symmetry respectively. Thus the **first conformer** is assigned as a **cubic** structure **attached to a propofol** molecule, while the **second conformer** is assigned to a **cubic** structure formed by **all the water molecules and the two propofol hydroxyl groups**.

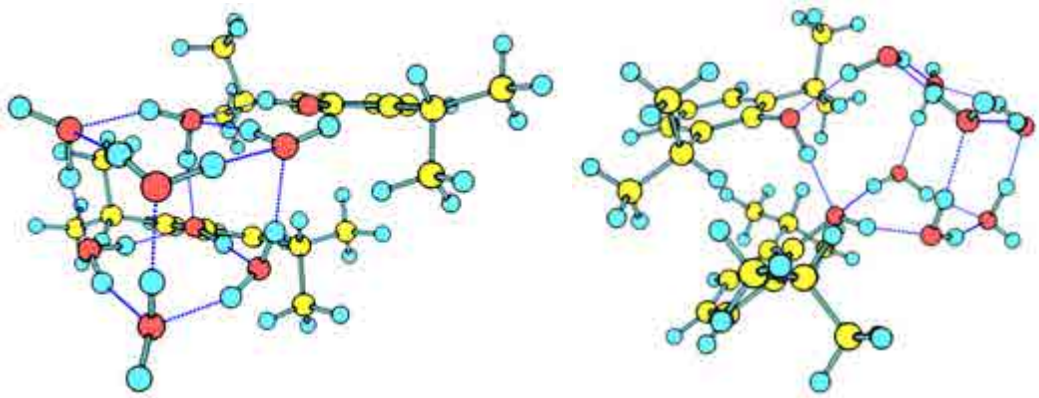

Figure 5.170. *Structures e26 and e1 are some of the few theoretically predicted structures that reproduce the experimental results for first and second conformers respectively.*

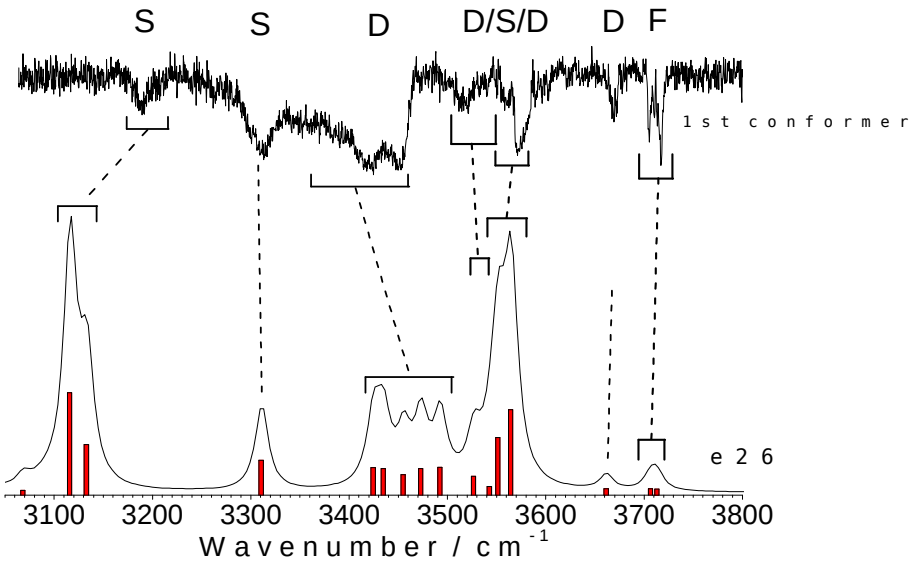

Figure 5.171. *Comparison of the predicted IR spectrum of structures e26 with the experimental results for the experimental first conformer, as can be seen there is a reasonable agreement between predicted and experimental spectra.*

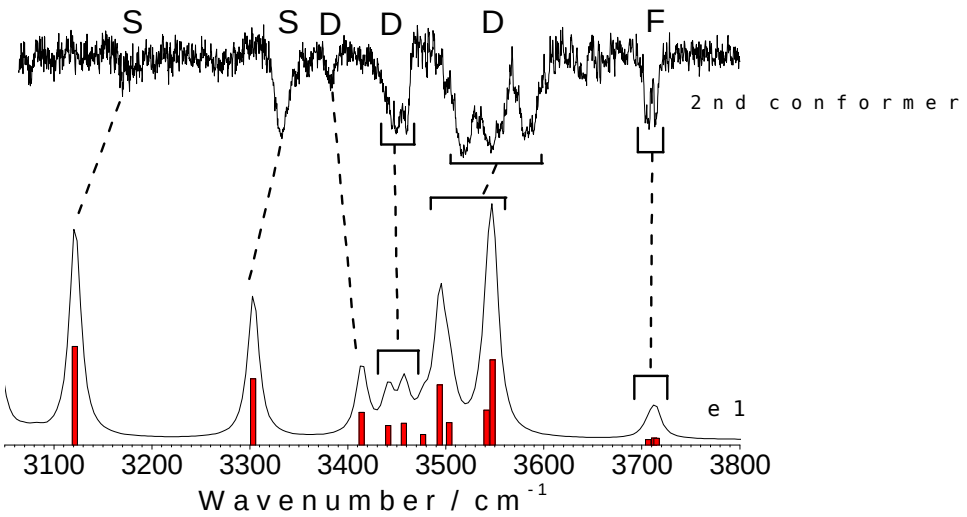

Figure 5.172. *Comparison of the predicted IR spectrum of structures e1 with the experimental results for the experimental second conformer, as can be seen there is a reasonable agreement between predicted and experimental spectra.*

Another important aspect is the great variation in the relative energy, introduced by the bare molecule conformation. Structure *e26* (Figure 5.170) is GG/GG-based, while structure *e35 is* Gg/Gg-based being the latter 8 kJ/mol less stable.

Other structures whose predicted IR spectra reproduce the experimental results are structures *e31* and *2* for the first conformer and structure *3* (Figure 5.173) for the second conformer, although the fact that they all are at a relative high energy (over 20 kJ/mol for the formers and over 31 kJ/mol for the latter) is a strong argument against their presence. Note the similarities between structures *2* and *3*.

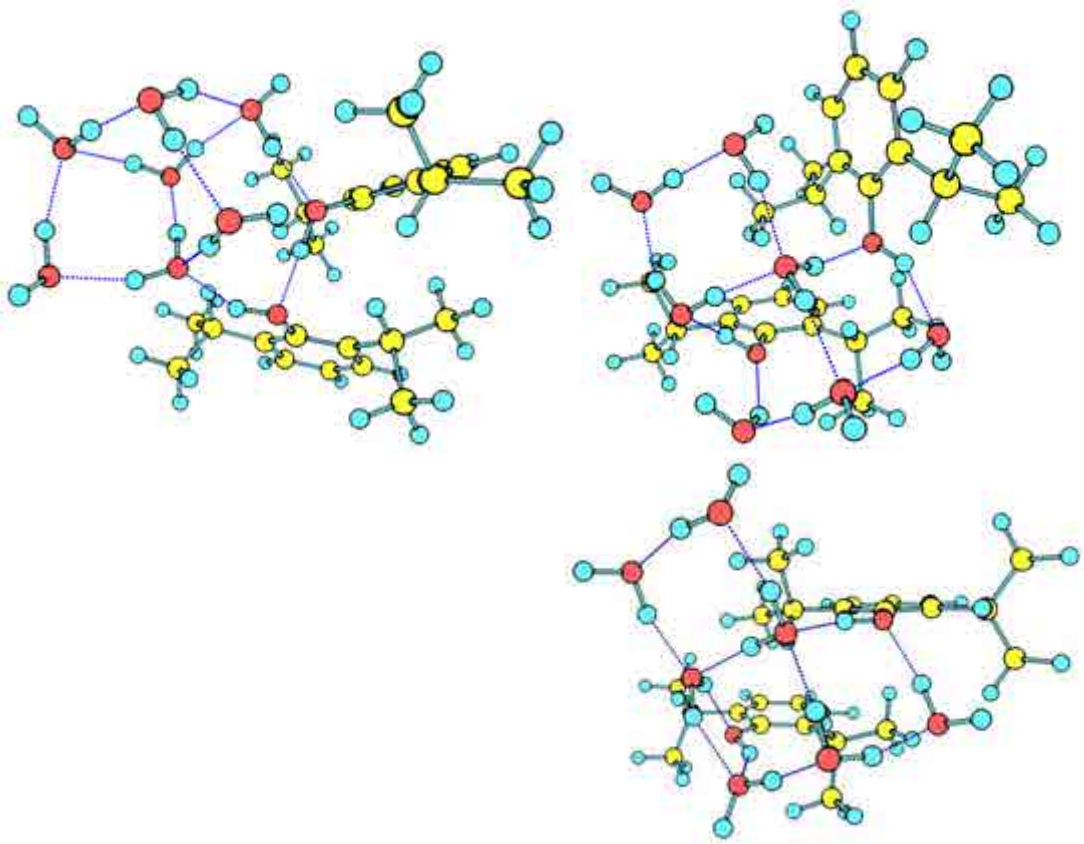

Figure 5.173. *Structures e31, 2 and 3 are some structures that also reproduce the experimental IR spectra. However, they appear at a relative high energy to be found in the expansion.*

Finally, The OH stretching modes for each of the conformers are collected in Table 5.15 and compared with the structure *e26* for the first conformer and with structure *e1* for the second conformer.

Table 5.15. *Experimental vibrational transitions in the IR traces of propofol$_2$·W$_7$ first and second conformers, with a tentative assignment based on a comparison with the calculated frequencies for structures e26 and e1.*

Experimental Peak (cm^{-1})	**structure *e26***		
	Frequency (cm^{-1})	Intensity	Vibrational type
(not observed)	3068	70	σ_s^s (OH$_w$)
3189 (x2 peaks)	3116	1517	σ_s^s (OH$_w$)
	3133	750	σ (OH$_{ppf}$)
3310	3311	515	σ_s^s (OH$_w$)
3360-3460 (x5 peaks)	3424	411	σ_s^d (OH$_w$)
	3435	393	σ_s^d (OH$_w$)
	3455	302	σ_s^d (OH$_w$)
	3473	398	σ_s^d (OH$_w$)+σ_{as}^d (OH$_w$) (coupled)
	3492	415	
3516 (x2 peaks)	3527	279	σ_{as}^d (OH$_w$)
	3543	130	σ (OH$_{ppf}$)
3573 (x2 peaks)	3551	855	σ_{as}^d (OH$_w$)
	3564	1270	σ_{as}^d (OH$_w$)
3669	3661	94	$\sigma_{as}^{f,d}$ (OH$_w$)*
3705	3706	94	σ^f (OH$_w$)
3717	3713	89	σ^f (OH$_w$)

*This stretching mode corresponds to the water's OH that is not completely free as it slightly perturbed by propofol's OH moiety.

Experimental Peak (cm^{-1})	**structure *e1***		
	Frequency (cm^{-1})	Intensity	Vibrational type
(not observed)	2907	1199	σ (OH$_{ppf}$)
(not observed)	3003	1162	σ_s^s (OH$_w$)
(not observed)	3044	408	σ_s^s (OH$_w$)
3172	3121	1300	σ_s^s (OH$_w$)
3331	3303	872	σ (OH$_{ppf}$)
3450 (x4 peaks)	3414	426	σ_s^d (OH$_w$)
	3441	257	σ_s^d (OH$_w$)
	3457	285	σ_s^d (OH$_w$)
	3477	136	σ_s^d (OH$_w$)
3518	3494	790	σ_{as}^d (OH$_w$)
3547 (x2 peaks)	3503	291	σ_{as}^d (OH$_w$)
	3542	460	σ_{as}^d (OH$_w$)
3585	3548	1120	σ_{as}^d (OH$_w$)
3706 (x2 peaks)	3707	71	σ^f (OH$_w$)
	3713	91	σ^f (OH$_w$)
3714	3715	87	σ^f (OH$_w$)

5.4.8 – Propofol$_2$·W$_n$: Discussion

In section 5.2, a complete study of the effects of microsolvation of propofol was carried out, demonstrating the strong self-aggregation power of water. The dimer and its complexation with water is an important step forward in the understanding of the solvation process, understood as the transit between the bare substance and the propofol molecules immersed in the solvent. In sections 5.3 and 5.4, propofol dimer and its hydrated clusters were studied, using mass-resolved excitation spectroscopy, obtaining invaluable information on the structure of each species.

- **Assigned structures**

Complexation of propofol dimer with a water molecule is a particularly interesting system, because the interaction due to dispersive forces is in the dimer, at least, of the same importance as the hydrogen bonds between OH moieties. Therefore, it is not clear a priori what the effect of the addition of water will have. In general, we demonstrate that the introduction of water into the dimer leads to structures where the two propofol molecules retain the interaction by dispersive forces between both molecules and where the water molecules form hydrogen bond networks with the propofol's OH moieties.

As can be seen in Figure 5.174a, in **propofol$_2$·W$_1$ and propofol$_2$·W$_2$**, all the OH moieties are involved in a **cyclic structure** as happens with the equivalent monomer systems. One particularity of propofol$_2$·W$_2$ is the existence of two conformers with the only difference of the bonding sequence: propofolOH·waterOH·propofolOH·waterOH in one of them and propofolOH·waterOH·waterOH·propofolOH in the other one.

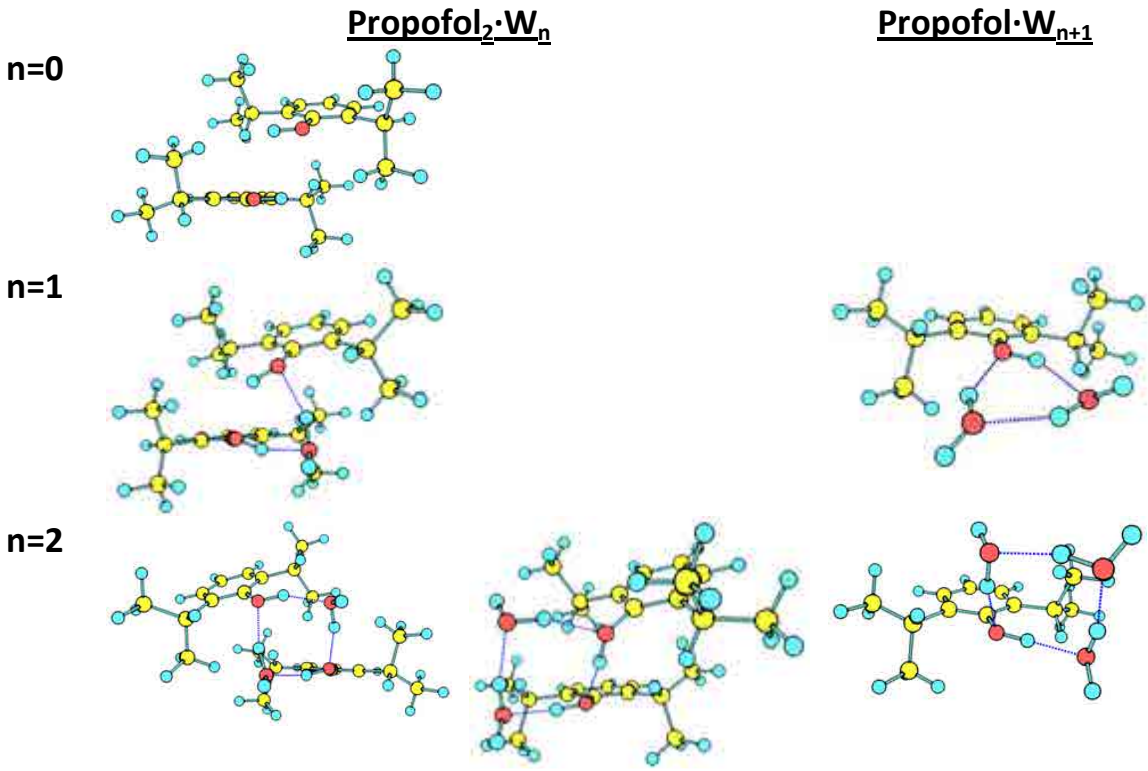

Figure 5.174a. *Assigned structures for the propofol$_2$·W$_n$ conformers detected and its comparison with propofol·W$_{n+1}$.*

Propofol$_2$·W$_3$ presents a similar structure to propofol·W$_4$ but with one of the hydrogens of the water molecule that interacts with the aromatic ring, replaced by a voluminous ·ph(i$_{pr}$)$_2$ substituent (see Figure 5.174b). As theoretical calculations predict, there are only a few cyclic structures due to the impediments introduced by the voluminous isopropyl groups. In good agreement the two isomers detected for propofol$_2$·W$_3$ cluster present a non-cyclic structure: introduction of the fourth water molecule in the dimer cluster triggers the transition from cyclic to non-cyclic structures. Similarly, propofol·W$_4$ does not present a cyclic water arrangement and, as we will demonstrate, the same applies for propofol$_4$·W$_1$. Taking all the results into account, it is surprising that, for the clusters studied during this work, a general rule can be extracted: **for propofol$_m$·W$_n$ clusters the changeover from cyclic to non-cyclic cluster structures occurs at n=5-m, i.e. propofol·W$_4$, propofol$_2$·W$_3$ and propofol$_4$·W$_1$.**

Propofol$_2$·W$_4$ has two conformers with ***book* type** structures, which is the same kind of structure found for the equivalent propofol·W$_5$ system. **Propofol$_2$·W$_5$** represents a special case, as the water arrangement is considerably different from that found in propofol·W$_6$: *cage*-like structures in the former and *prism*-like structures in the latter.

Propofol$_2$·W$_6$ demonstrates the robustness of the ***cubic*** **structures**. Again what one would expect, the water molecules are able to form such structure, while the two propofol molecules maintain their C-H···π interactions. The final structure is not that different from what is found in propofol·W$_7$. The same applies for **propofol$_2$·W$_7$** as the two conformers found for this system, present water **cubic structures** with the two propofol molecules interacting as previously described, i.e. a **stacked pentamer-tetramer structure**.

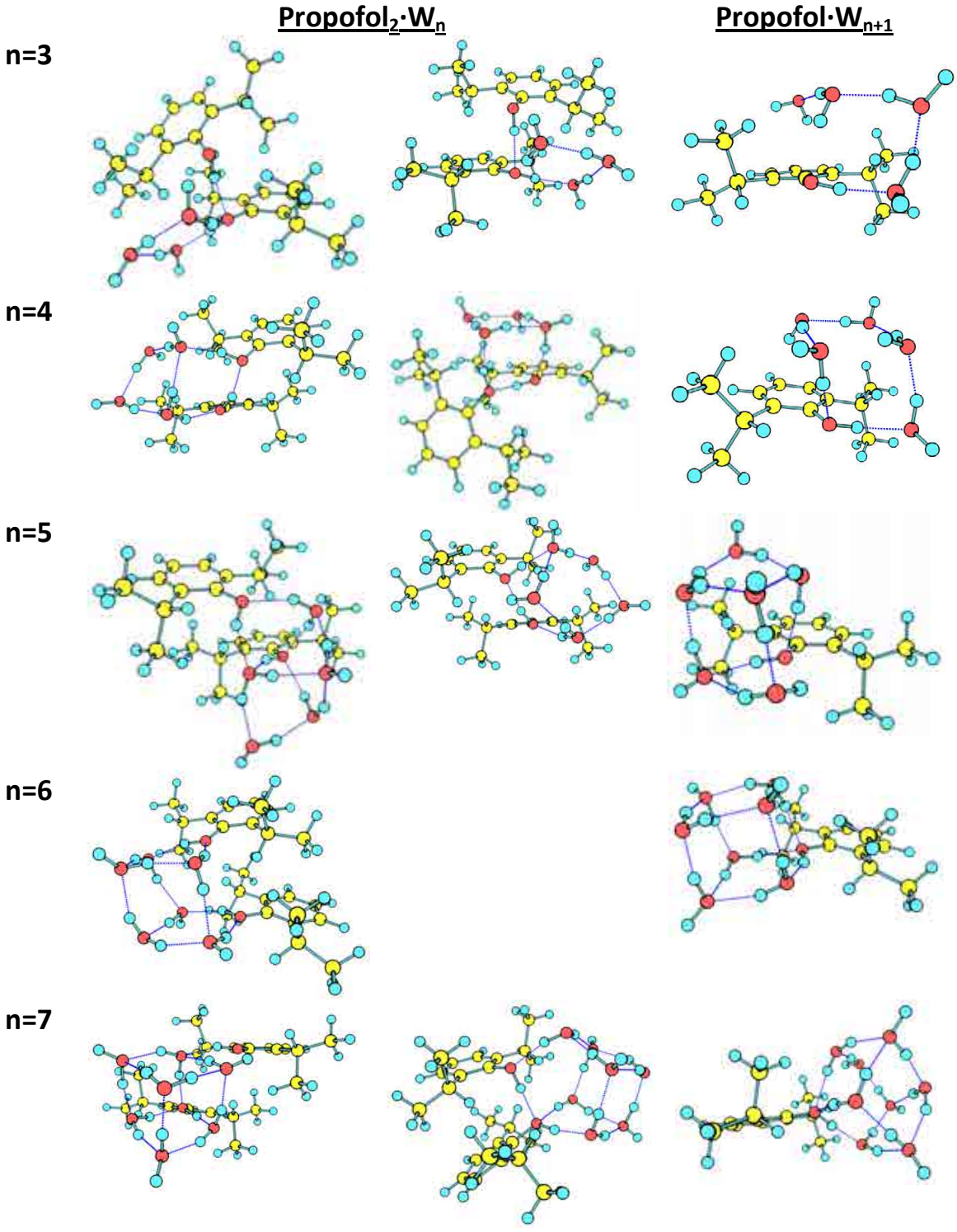

Figure 5.174b. *Assigned structures for the propofol$_2$·W$_n$ conformers detected and its comparison with propofol·W$_{n+1}$.*

- **Magic number**

One of the most amazing results comes for the **propofol$_2$·W$_5$** cluster as there are various facts that point to the **existence of a magic number** for this structure. First, the theoretical finding of only three structures, among the large quantity of structures studied, at a relative energy of less than 3kJ/mol while the next structure is at 11.4 kJ/mol is probably related to the existence of a magic number. Second, the first experimental results drops some light into the matter, as the time of flight mass spectrum shown in Figure 5.11, shows that there is a special stability in the formation of this cluster. The study of the excited state of propofol$_2$·W$_5$ in Figure 5.141, shows an extension of at least 1400 cm^{-1}, which is not found for the rest of the dimer·water clusters. Third, the spectral intensity of the transition located at 36182 cm^{-1} is extremely high. When talking overall about all the clusters studied in this work, and dividing them into five groups, *very intense*, *intense*, *normal*, *low* and *very low* (nearly counting the ions reaching the detector), **considering the systems studied in this work, i.e. propofol$_m$·W$_n$, and except for that of propofol$_1$·W$_n$ for n=1-3, this molecule is the only cluster with an *intense* signal**. It has to be remarked, that the stability of propofol$_2$·W$_5$ seems to be equal or even greater than that for propofol·W$_8$.

The presence of a magic number of this cluster in the mass spectrum, the *jump* in the predicted most stable conformers where only three conformers are within the first 10 kJ/mol of relative intensity, and the anomalous high intensity of some of the peaks, seem to indicate a *special* behavior for this cluster. If this reasons are not enough, and as evidenced from the *hole burning* experiments, **three conformers** are present, which is against all the results obtained for the propofol hydratated cluster, as more than two conformers based on different type of interactions has not been observed for none of the rest of structures (note that for propofol·W$_1$ the three detected conformers are based in the same type of interaction differing only in the bare molecule's conformation).

The theoretical prediction of a special stability for water clusters consisting of a ring with four water molecules (n=4,8,…) was reported by Lee[27] et al. For phenol this observation also seems to match.[24] Conversely, for the propofol dimer system, this seems not to be the case: propofol$_2$W$_5$ can be envisioned as a water cluster with 7 monomers because propofol molecules can be part of the ring, and thus, this should not lead to any special magic number and thus, the inspective stability of this cluster needs

to be explained. A look to the structure of the propofol$_2$·W$_5$ third conformer, which is responsible of the anomalous intense transition (Figure 5.175), shows that the two propofol molecules are stacked while a monocyclic-pentamer formed by the five water molecules is attached to the dimer. Comparison with the water clusters[31] shows that the most stable structure for W$_5$ is that where the water molecules form a (monocyclic) pentamer, while the rest of possibilities are considerably higher in energy. Conversely, for W$_4$ a tetramer and a *prism* structure are within 5 kJ/mol while for W$_6$ *book*, *cage* and *prism* structures can be found at nearly the same relative energy. In summary: such conformer is formed by a **stable water structure pentamer, interacting with propofol dimer, resulting in a specially robust species.**

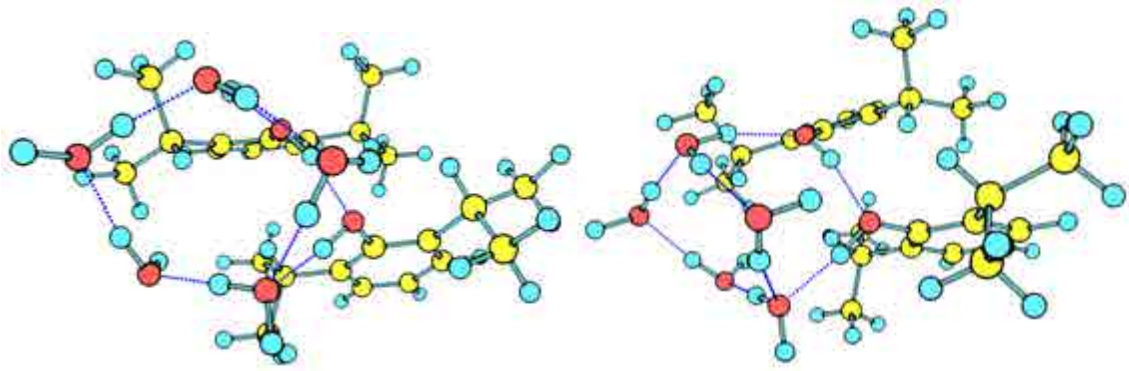

Figure 5.175. *Assigned structure for propofol$_2$·W$_5$ third conformer. Two different views are showed.*

- **Conformer selectivity**

As happened with the hydratation of the bare molecule, there seem to be a general reduction on the number of conformers with the number of water molecules. Table 5.16 shows the number of conformer found for propofol and propofol$_2$ systems, as a function of the number of water molecules. As can be seen, in most cases, there is an important tendency to the decrease of the number of conformers as the number of water molecules increases, probably due to the self-aggregation propensity of water.

Table 5.16. *Number of conformers observed experimentally for the propofol monomer·water$_n$ and dimer·water$_n$ systems .*

W	0	1	2	3	4	5	6	7	8	9
Propofol	4	3	2	2	1	2	2	2	2	1
Propofol$_2$	2	3	2	2	2	3	1	2	-	-

- **Lifetimes**

For the bare molecule, the S_1 decay process (< 5 ns) proceeds through internal conversion to the high-lying vibrational states in the S_0 manifold and is highly affected by the presence of a single hydrogen bond as it increases to nearly 20 ns for the propofol·W_n clusters (n=1-3). Accordingly, the same line applies to the dimer as its lifetime is of c.a. 15 ns. On the other hand and against what is observed in the microsolvation of the bare molecule, the S_1 lifetime seems to remain stable with the number of water molecules (Figure 5.176).

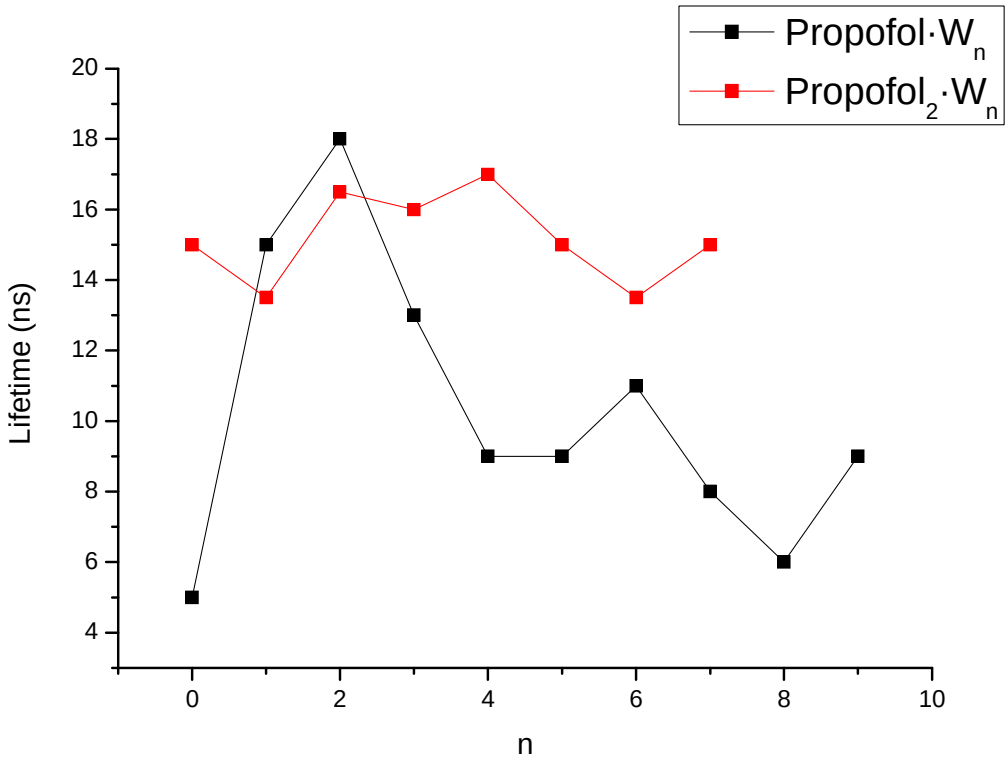

Figure 5.176. *Excited state lifetime for propofol·W_n and propofol$_2$·W_n clusters. While for the formers there is a general reduction tendency as the number of water molecules is increased, for the latter it remains constant. The lifetimes of all the species is collected in appendix 7.2.*

- **Comparison with similar systems**

Toluene dimer, preset a stacked conformation because the dipole-dipole attractive interaction overwhelms the repulsive quadrupole-quadropole one, which is maximized (repulsive) for parallel aromatic rings, but that normally become an attractive force for the *T-shaped* structures. On the other hand, the main stabilizing interaction in propofol dimer is the intermolecular hydrogen bond, although the π-π interaction still plays a significant role leading the cluster to adopt neither a stacked nor a face-to-face conformation. For the latter it is also important to note that one of the phenol molecules acts as an acid while the other molecule acts as a base. The nature of the propofol dimer is a combination of dispersive forces, C-H···π, and hydrogen bond interactions, O-H···O-H. Only the latter is a directional interaction and therefore, it is responsible for the orientation of the two propofol molecules: both with their OH

moieties in close contact. The dispersive forces are less exigent and therefore they accommodate the two rings as to maximize the C-H···π interactions..

Finally, Figure 5.177 shows the *2c-REMPI* spectra of all the propofol$_2$·W$_n$ clusters (n=0-7) with each assigned structure. The arrows indicate the (possible) origin band of each conformer.

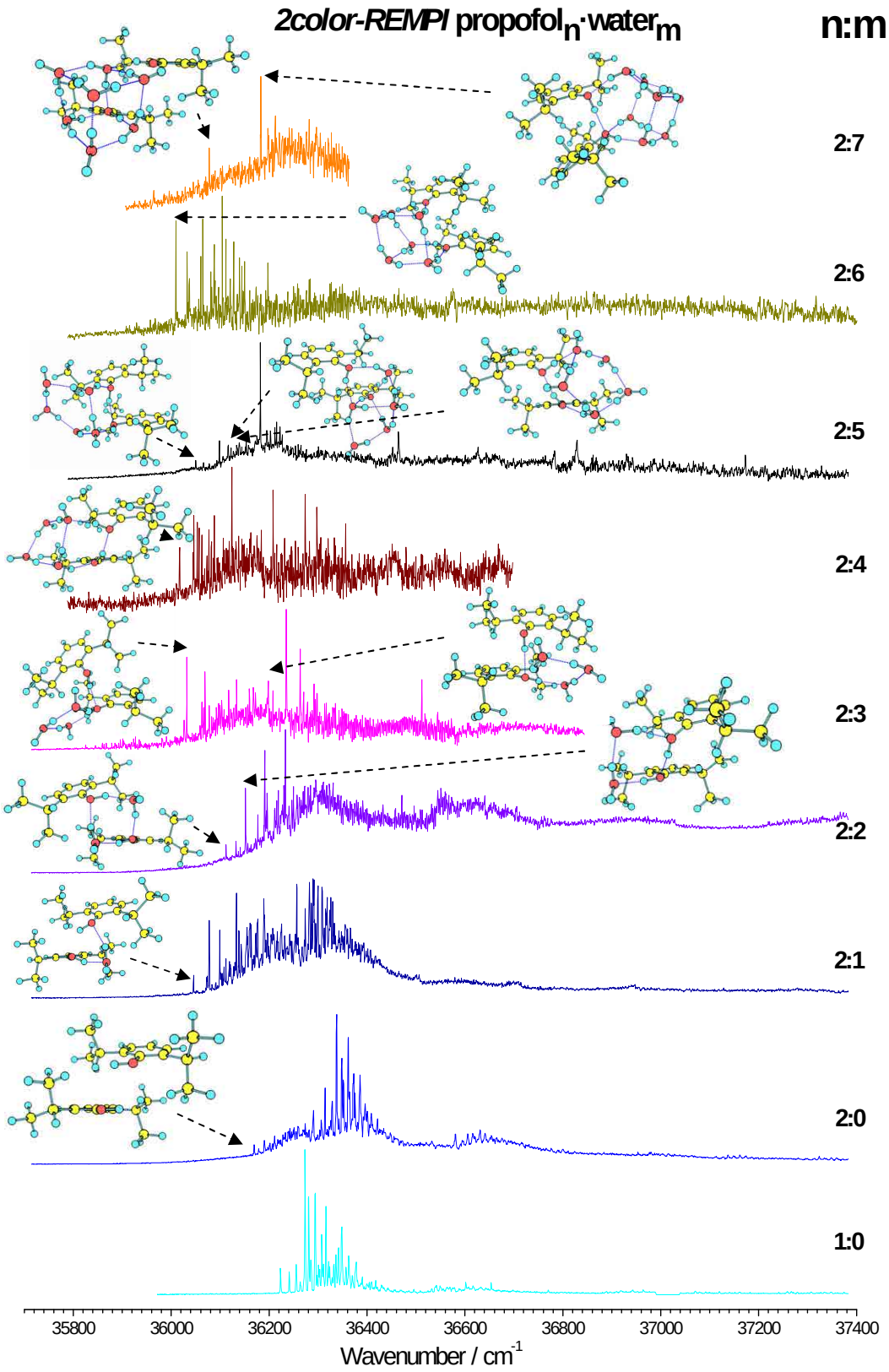

Figure 5.177. *2c-REMPI of propofol$_n$·W$_m$, m=0-9 in the 35700-37400 cm^{-1} region. The images show the structure assigned for each conformer of each cluster.*

5.5 – Propofol$_n$

Up to know hydratation of propofol and propofol$_2$ has been studied using mass-resolved electronic spectroscopy. The subject of this section is the characterization of the homomers with up to six propofol molecules, whose *2c-REMPI* spectra are collected in Figure 5.178.

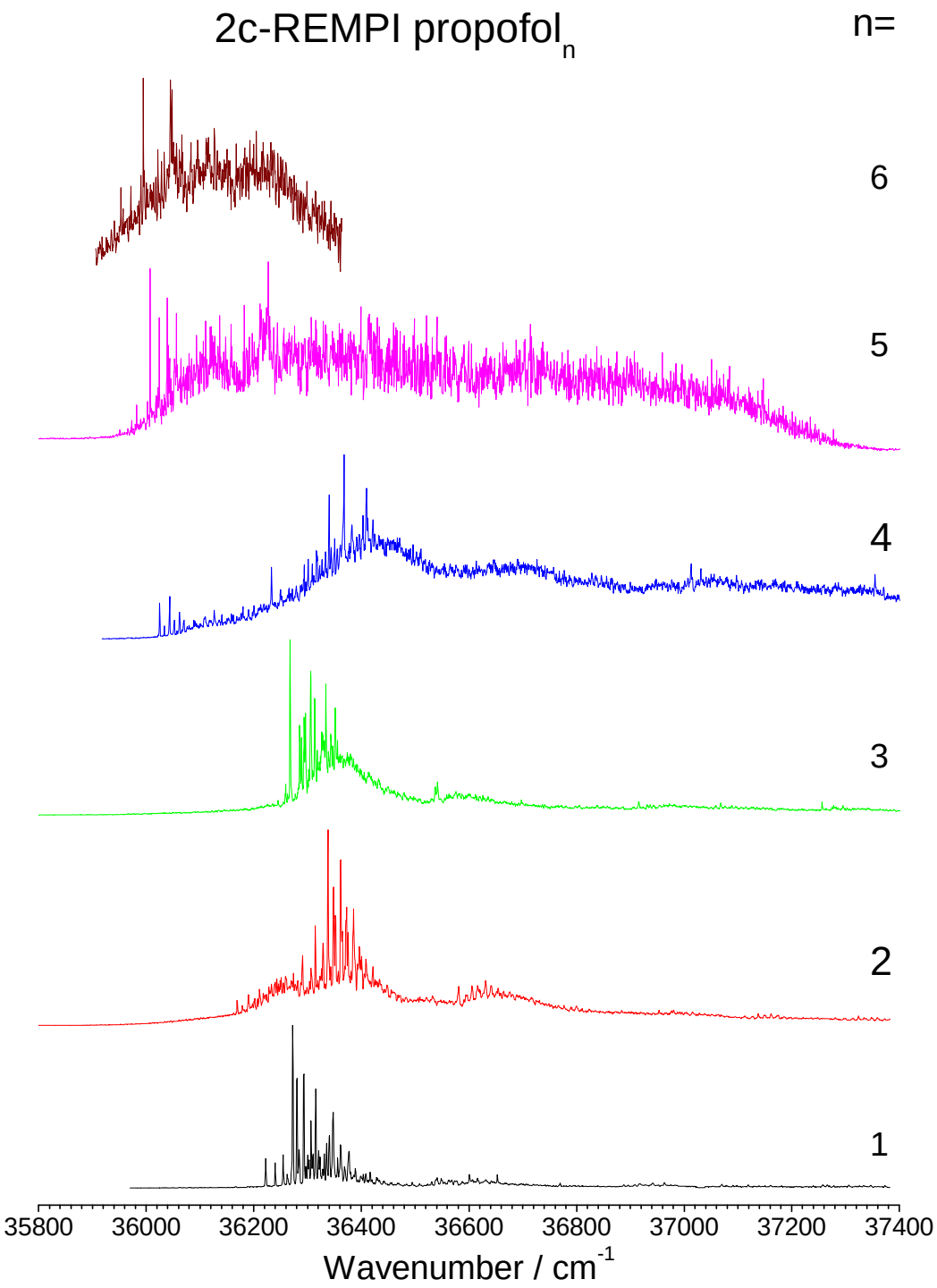

Figure 5.178. *2c-REMPI of propofol$_n$, n=1-6 in the 35800-37400 cm^{-1} region.*

5.5.1 – Propofol$_3$

Molecular mechanics predict hundreds of structures in a 20 kJ/mol window. Most of them are statistically meaningful, being divided in two main types of structures (Figure 5.179): either a chain of O-H···O-H···O-H···π interactions (structures *e11, e6, e7*) or an O-H···O-H···O-H cycle (structures *e1, e3, e15, 2, 3*). In both types there are extensive interactions between the isopropyl and the aromatic ring of different molecules. Most of the propofol molecules are in GG/Gg conformations, although eventually one of them may adopt an EG conformation in the complex.

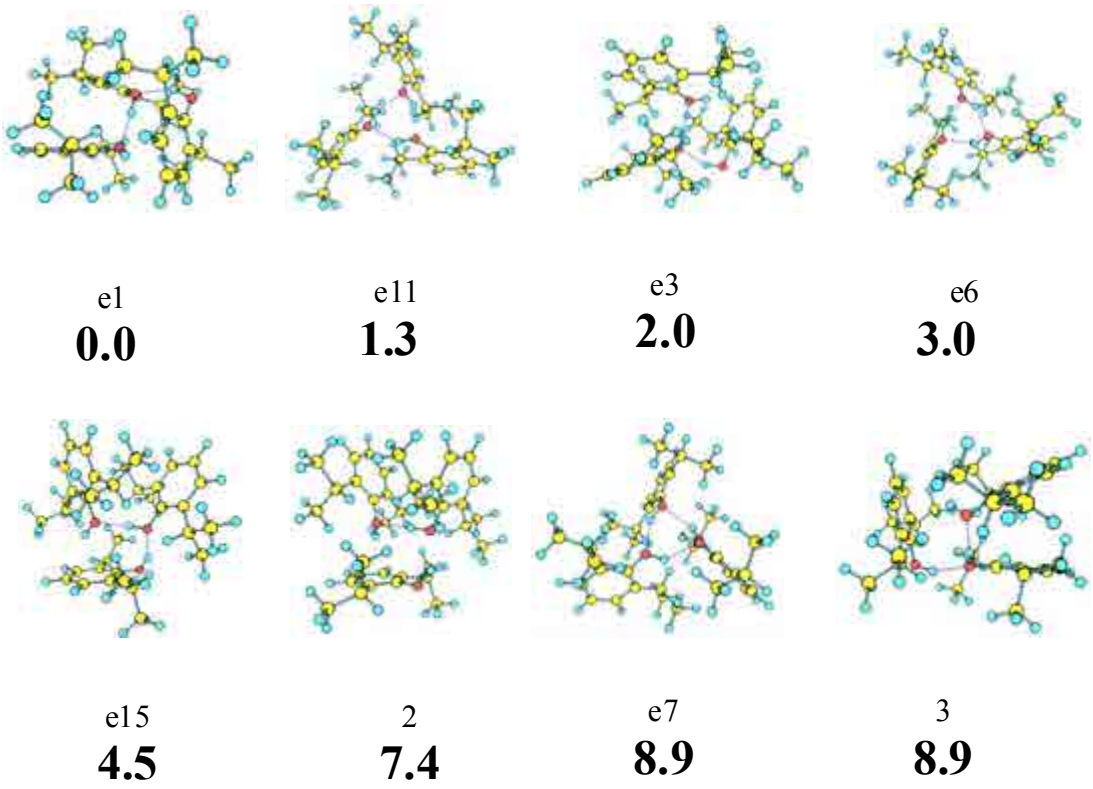

Figure 5.179. *Propofol$_3$ eight most stable conformers calculated at M06-2x/6-31+G(d) level, with their relative energies in bold. Energy values are in kJ/mol. The complete set of calculated structures can be found in appendix 7.1 (Figure 7.35).*

Figure 5.180 shows the *2c-REMPI* spectrum of propofol$_3$. The spectrum shows the red-most peak at 36267 cm^{-1} and some intense peaks in a small region of only c.a. 150 cm^{-1}, although some weak transitions can be seen for at least c.a. 1000 cm^{-1}.

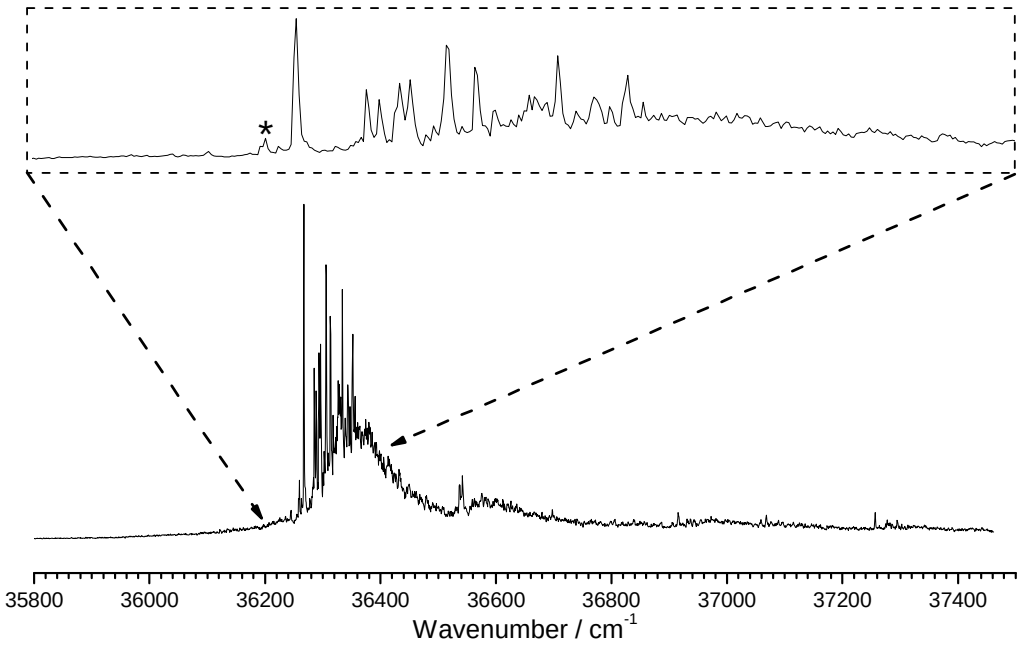

Figure 5.180. *2c-REMPI of propofol$_3$, in the 35800-37500 cm^{-1} region, recorded setting the probe laser at 27972 cm^{-1}. The insert shows a detailed view around the origin. The peak marked with an asterisk is due to fragmentation from propofol$_3$·W$_1$ cluster.*

To determine the number of isomers of propofol$_3$, a *hole burning* experiment is done, finding a single isomer as can be seen in Figure 5.181. The origin band for this conformer is located at 36267 cm^{-1}.

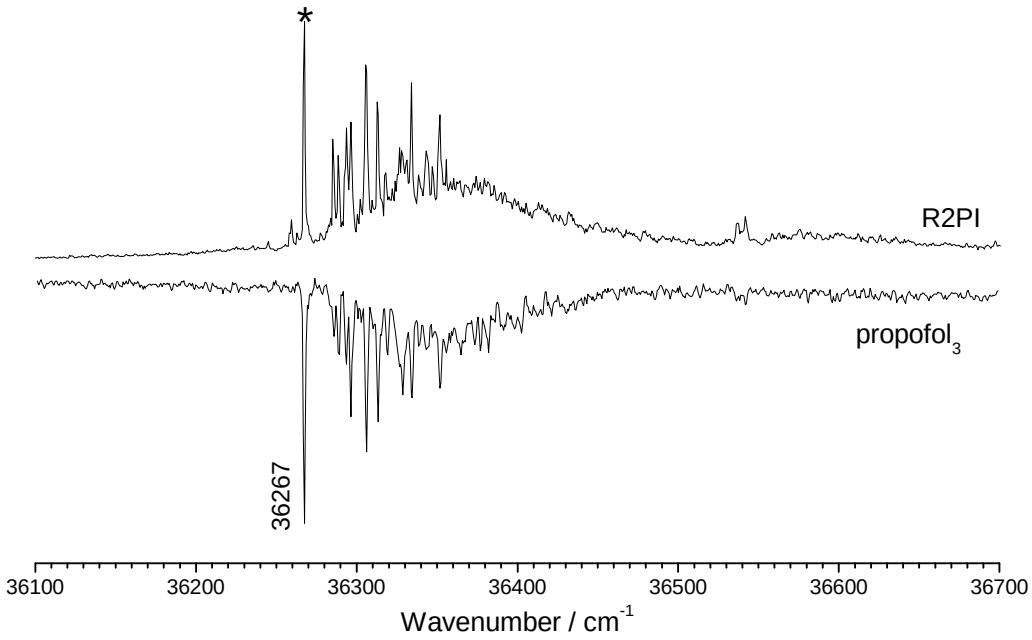

Figure 5.181. *Hole burning trace of propofol$_3$ recorded tuning the probe lasers (2-color detection) at 36267 cm^{-1}. The peak noted with asterisk indicates the transition employed for recording the hole burning spectrum, as well as the IDIRS trace for this conformer.*

Figure 5.182 shows the IDIR spectrum of the single conformer found for propofol$_3$ and, as can be seen, all the peaks are grouped in a narrow region around c.a. 3500 cm^{-1}, clearly indicating that the three OH moieties are involved in a similar interaction and, that they must present the same type of environment: a cyclic structure comes quickly into mind. A closer inspection of the experimental spectrum shows that the peaks are doublets, probably due to the existence of at least two conformers with overlapping $S_1 \leftarrow S_0$ transitions.

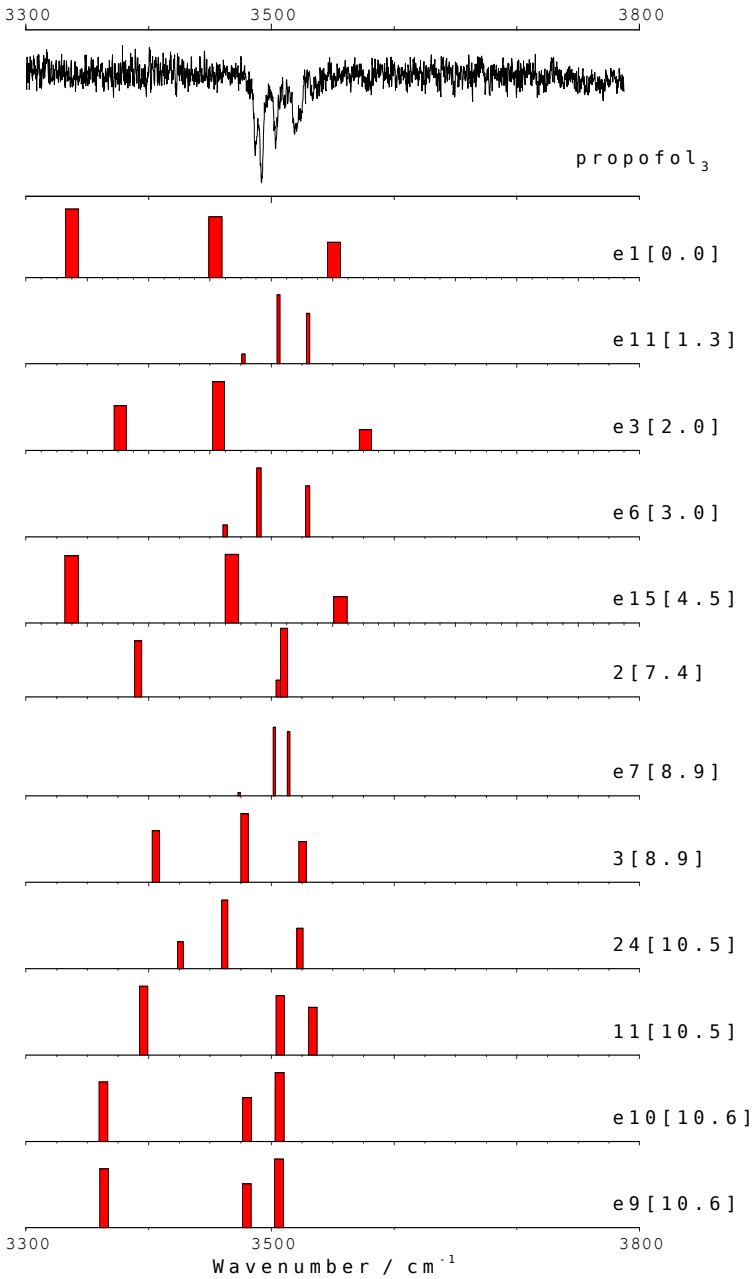

Figure 5.182. *IDIR spectra of propofol$_3$ recorded tuning the probe laser at 36267 cm^{-1}. The predicted IR spectra for the most stable calculated structures are also shown for comparison. The numbers in brackets are the relative energies of the calculated conformers, in kJ/mol. A correction factor of 0.953 was applied. The predicted IR spectra for the complete set are recorded in appendix 7.1 (Figure 7.36).*

The excited state spectrum has also been recorded and it is presented in Figure 5.183 together with the S_0 IDIR spectrum. As can be seen, the electronic excitation causes a small blue-shift in the OH stretching vibration of one of the propofol's molecules but, a large red-shift of c.a. 135 cm^{-1} is also produced in another OH stretching, indicating that this OH is more strongly bound in the excited state. It is also worthy to note that the excited state IDIR spectrum, like the S_0, shows more than three peaks, maybe due to the contribution of different conformers that cannot be separated using the *hole burning* technique.

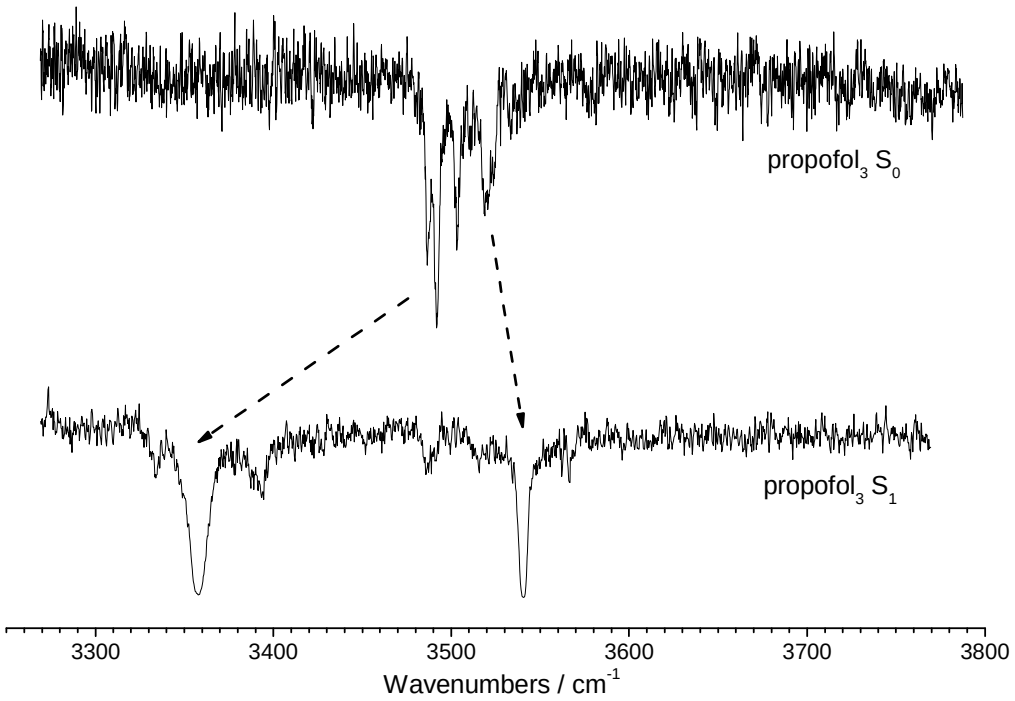

Figure 5.183. *Comparison between ground and excited state IDIRS of propofol$_3$.*

Assignment

The assignment of the experimental structure is not difficult, as the IDIR spectrum clearly indicates that the three hydroxyl groups are involved in a cyclic structure. A comparison between the structures with this kind of interaction (structures *e11, e6, e7*) clearly confirms such assumption, as can be seen in Figure 5.184.

The intensity predicted for the red-most OH stretching is weaker than what it is observed. This stretching is predicted to be a coupled vibration of the three OH moieties. Very likely, such coupling is not that strong, due to slight differences in the positions of the isopropyl groups. Another remarkable aspect is the presence of a doublet for each of the peaks, probably related to the presence of at least two conformers differing only in the orientation of the isopropyl groups and, whose electronic spectra are similar, as for example observed for the bare molecule (section 5.1). Such conformers usually share the excited state and therefore, if their stability is very similar (almost equal) it is not possible to separate their spectra. In consequence, their IDIR traces appear intermixed. This way, well be another source of discrepancy in the intensity pattern between experimental and simulated spectra.

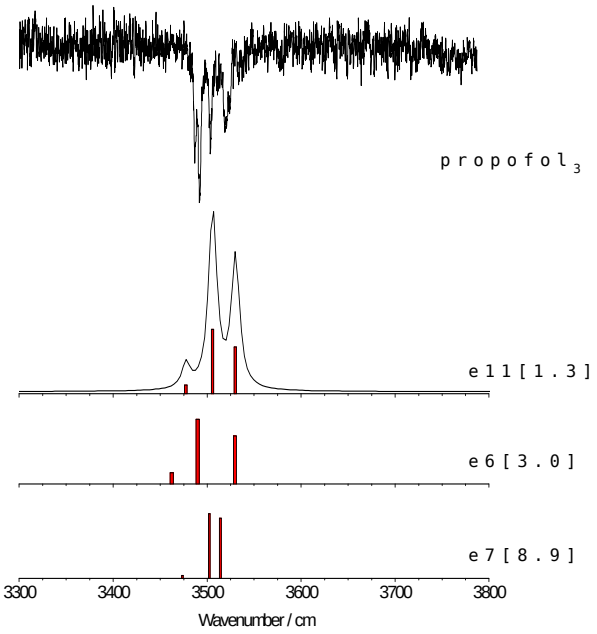

Figure 5.184. *Comparison of the predicted IR spectrum of structures e11, e6 and e7 with the experimental results for the experimental conformer. As can be seen there is a good agreement with the experimental spectrum.*

A remarkable aspect of this system is the large energy difference observed between the assigned structures (structures *e11, e6* and *e7*) and another group of conformers, also forming an O-H cycle, like structures *8* (Figure 5.185) and *6*, which are c.a. 24 kJ/mol higher in energy. Such energy difference arises from a less optimum interaction between the isopropyl groups and the aromatic rings. Clearly the general shape of the cluster is determined by the directionality of the hydrogen bonds, but the dispersive interactions are by no means a secondary and less important source of stabilization.

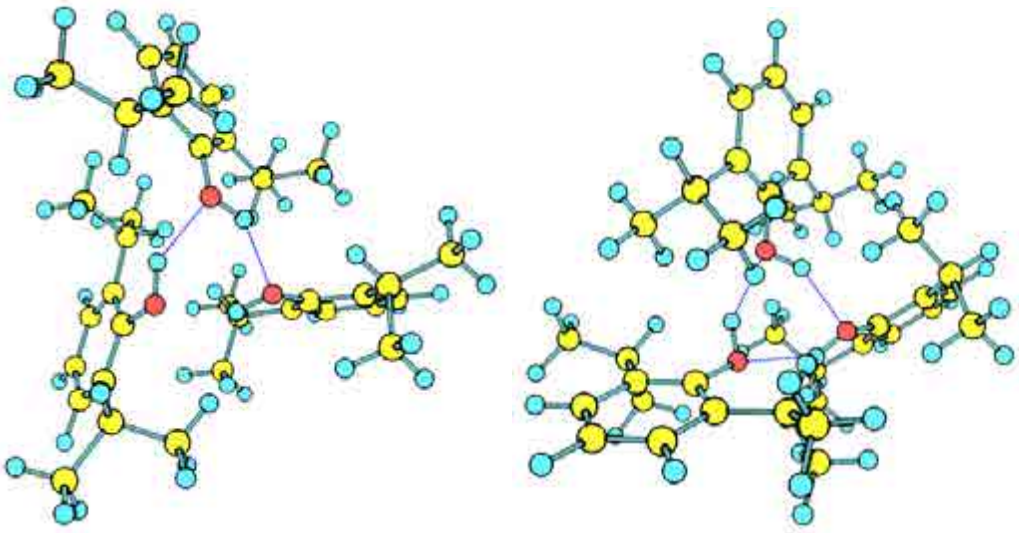

Figure 5.185. *Structures e11 (left) and 8 (right) are those where the OH moieties are involved in a cycle, but the apparent minor differences in the relative position of the molecules, result in a great difference in their stabilization.*

Figure 5.186 collects other types of structures that are not observed experimentally: structures with an O-H···O-H···O-H···π (structure *e1*) interaction, being also among the most stable ones; structures where two of the propofol molecules are stabilized by an OH···π interaction (structure *13*) which are found above 14 kJ/mol; structures with an O-H···O-H···O-H interaction (structure *18*) having the last OH free which causes an increase in the energy to 17 kJ/mol; or structures where the propofol molecules are stacked (structure *5*) and that are found over 21 kJ/mol higher in energy.

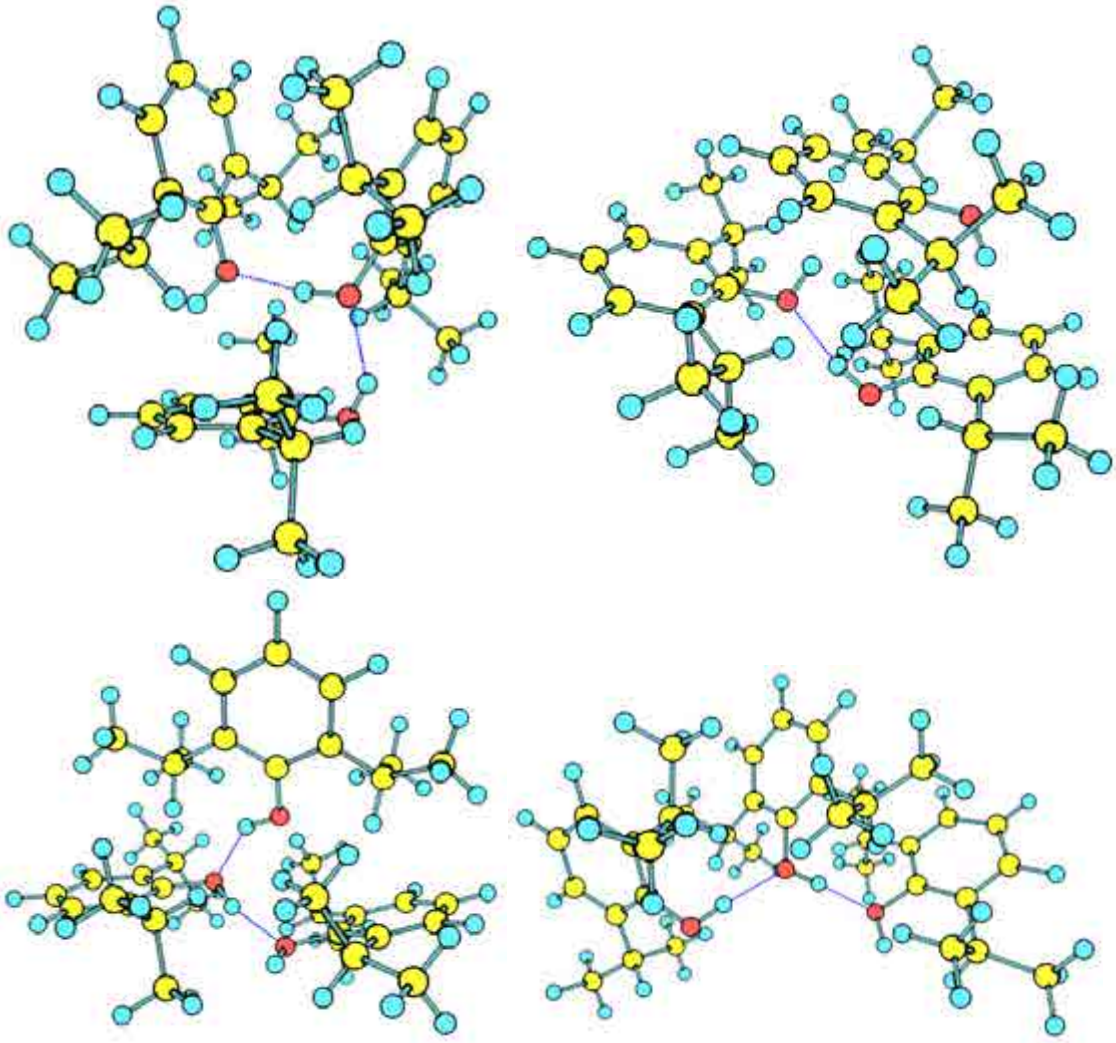

Figure 5.186. *Structures e1, 13, 18 and 5 are structures where there is no OH cyclic structure. These structures are not found experimentally.*

5.5.2 – Propofol$_4$

Conversely to what one would expect, the considerably increase in the system's size from propofol$_3$ to propofol$_4$ leads to a simplification on the assignment, due to formation of very symmetric structures, which are notably more stable than the rest. Figure 5.187 show the eight most stable propofol$_4$ structures. All of them are micelle-like structures, with the hydroxyl groups forming an eight-member cycle and with C-H···π interactions. Thus, the micelle hides the propofol's hydrophilic side and exposes the hydrophobic side of the molecules. The difference among these structures lies in the propofol molecule's relative position and orientation.

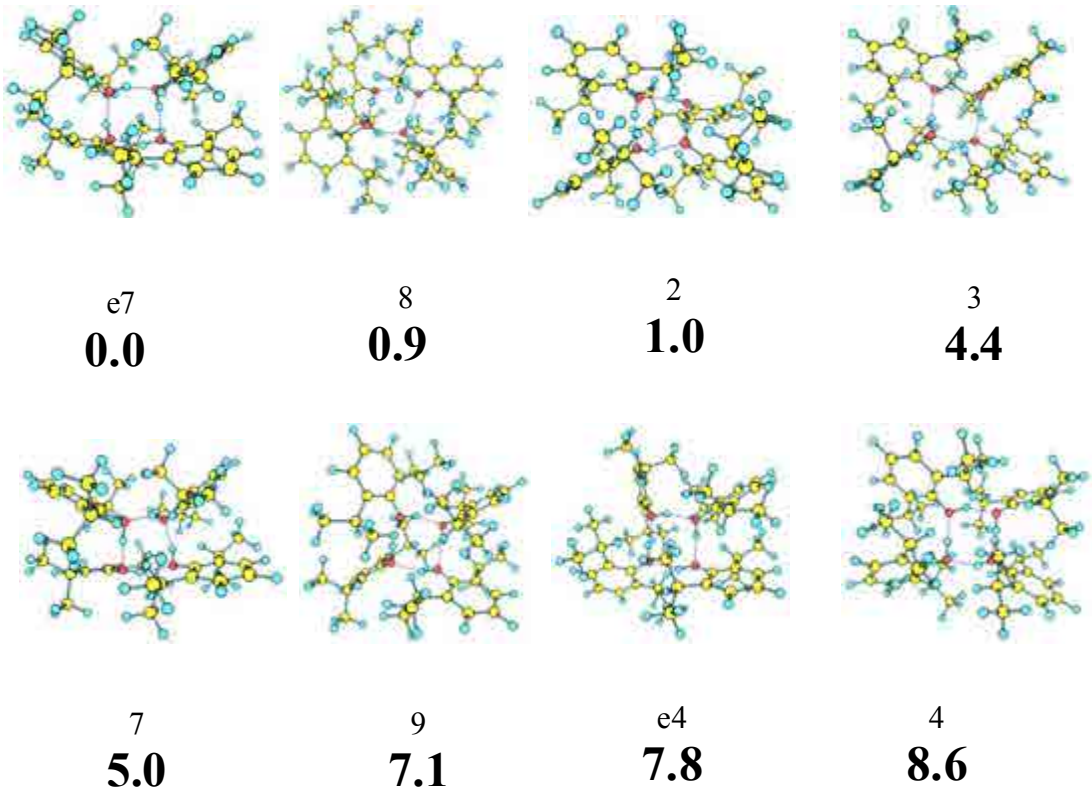

Figure 5.187. *Propofol$_4$ eight most stable conformers calculated at M06-2x/6-31+G(d) level, with their relative energies in bold. Energy values are in kJ/mol. The whole set of calculated structures is collected in appendix 7.1 (Figure 7.37).*

Figure 5.188 shows the *2c-REMPI* spectrum of propofol$_4$. The origin band appears at 36024 cm^{-1} and some intense peaks are found in the first c.a. 500 cm^{-1}, although the spectrum extends for more than 1500 cm^{-1}. Another noticeable aspect is the broad background observed that covers the whole scanned region.

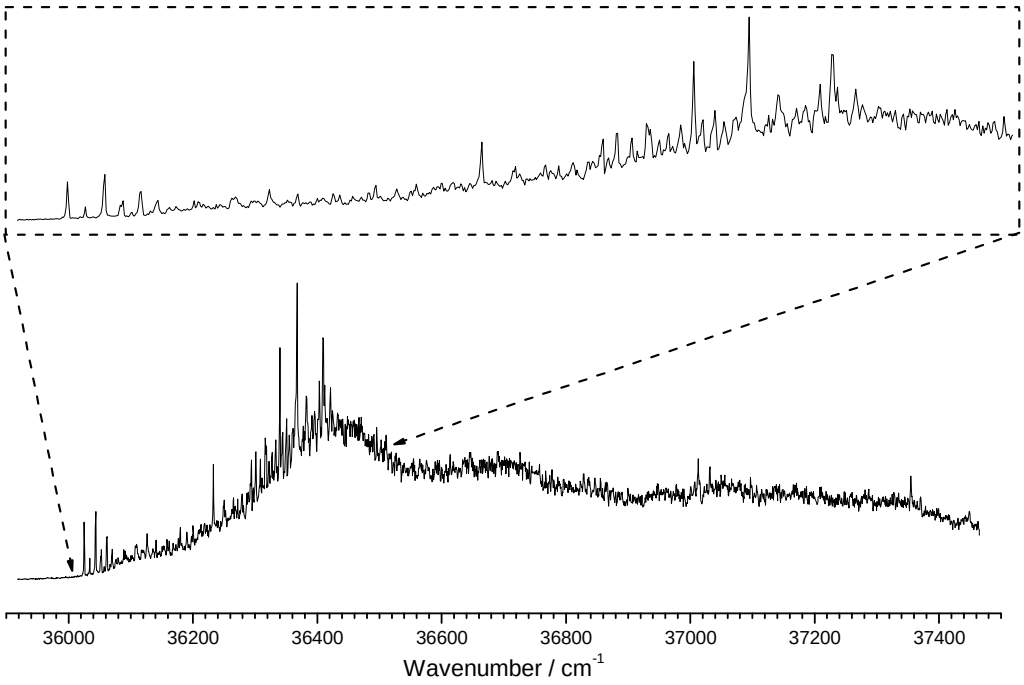

Figure 5.188. *2c-REMPI of propofol$_4$, in the 35900-37500 cm^{-1} region, recorded setting the probe laser at 27972 cm^{-1}. The insert shows a detailed view around the origin.*

In order to test the existence of fragmentation, Figure 5.189 shows a comparison of the *2c-REMPI* spectra of propofol$_4$ with propofol$_5$ and propofol$_6$, demonstrating the absence of fragmentation in propofol$_4$ channel.

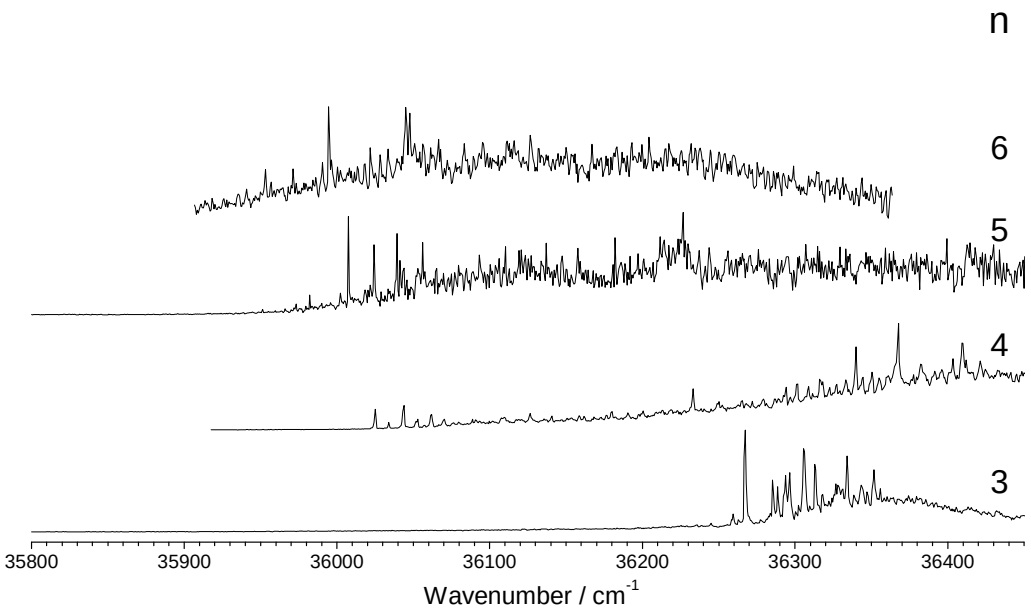

Figure 5.189. *2c-REMPI comparison of propofol$_n$ n=3-6. No other contribution due to fragmentation is observed in the studied mass-channel.*

To determine the number of isomers, a *hole burning* experiment on the tetramer is done, shown in Figure 5.190, together with propofol$_4$ *2c-REMPI* spectrum. Two isomers are present: the origin band of the first conformer is located at 36024 cm^{-1}; while the position of the origin band of the second conformer is not clear although the c.a. 320 cm^{-1} blue-shifted peak at 36341 cm^{-1} seems to be the first discrete feature. Extrapolating what we have learnt from the previous systems, like propofol, propofol·W$_1$... such spectral pattern indicates geometry changes upon excitation.

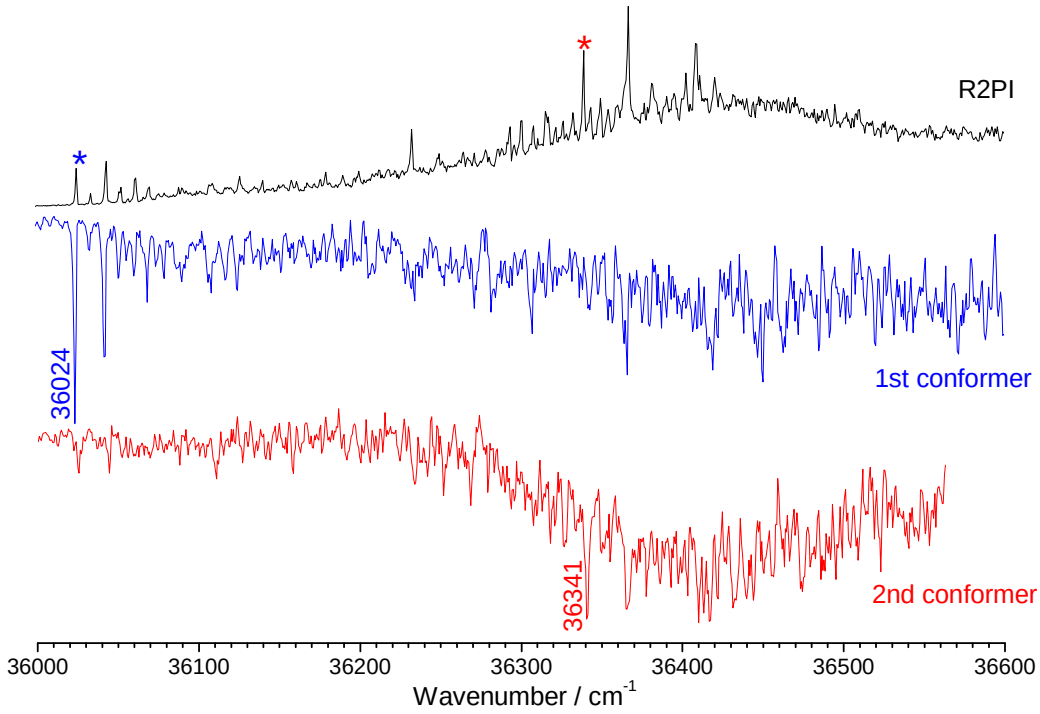

Figure 5.190. *Hole burning trace of propofol$_4$ recorded tuning the probe lasers (2-color detection) at 36024 and 36341 cm^{-1}. The peaks noted with asterisk indicate the transitions employed for recording the hole burning spectra, as well as the IDIRS traces.*

The IDIR spectra of both conformers were recorded in the OH stretching region, obtaining the spectra shown in Figure 5.191. Apart from the reduced s/n ratio of the second conformer's spectrum, it is clear that both conformers have similar structures with all the OH moieties bonded, as all the features are red-shifted respect to the propofol's free OH stretching (c.a. 3650 cm^{-1}). Both conformers present very similar spectra, apart from the position of the central peak: at c.a. 3385 cm^{-1} for the first conformer and at 3360 cm^{-1} in the second conformer's IR spectrum.

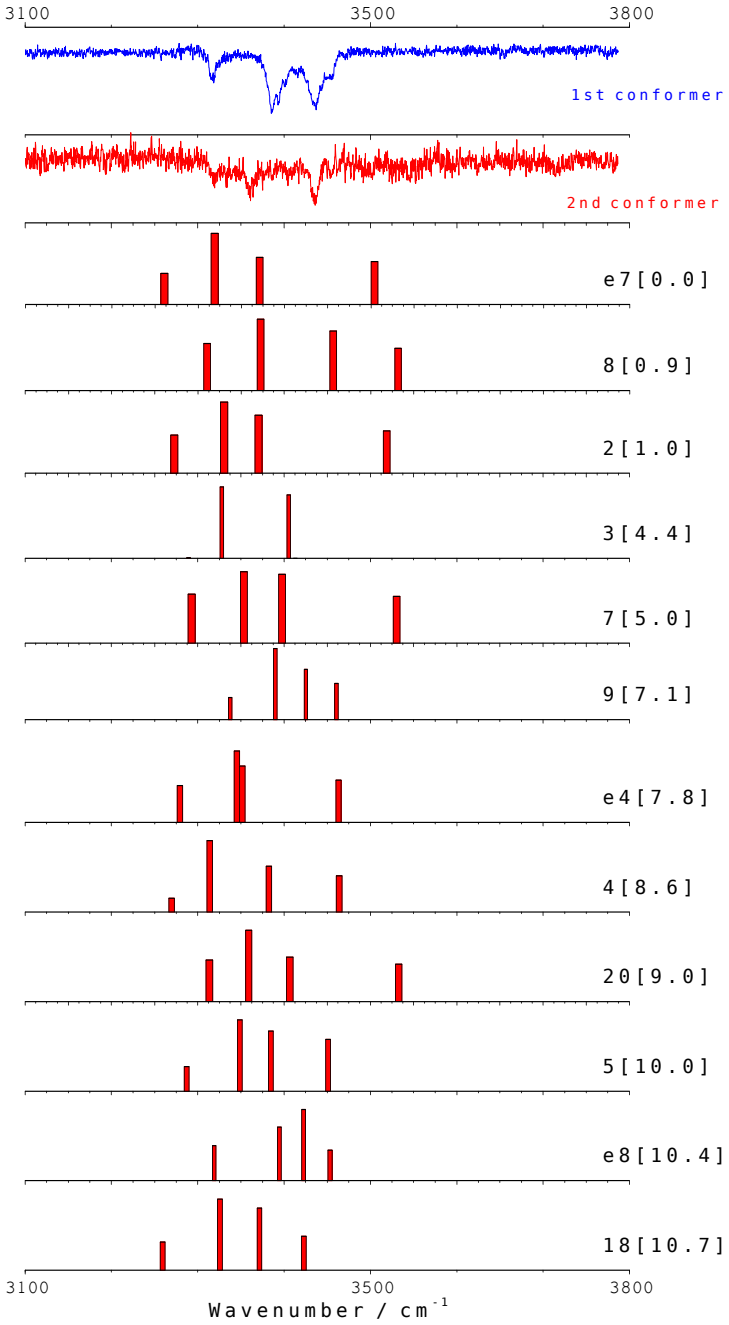

Figure 5.191. *IDIR spectra of propofol$_4$ recorded tuning the probe laser at 36024 and 36341 cm^{-1}. The predicted IR spectra for the most stable calculated structures are also shown for comparison. The numbers in brackets are the relative energies of the calculated conformers, in kJ/mol. A correction factor of 0.956 was applied. The predicted IR spectra of all the calculated structures are recorded in appendix 7.1 (Figure 7.38).*

Assignment

The first important aspect concerning propofol$_4$ is that nearly all the calculated species yield structures where the molecules are hydrogen-bonded together forming a cyclic structure. We only found a single structure where this cycle is not present, structure *14*, but this type of structures can be easily discarded as they present two OH stretching modes in the 3500-3600 cm^{-1} region, which are not found experimentally.

Concerning the cyclic structures, it is difficult to make any particular assignment as slight modifications on the orientation of the propofol molecules result in small shifts in the predicted spectra. In any case, very likely most of the structures collapse into the global minimum during the cooling process.

Most important differences between the sets of structures are related to the spacing between the propofol molecules in the micelle: from almost equi-spaced (structure *3*) to two pairs of molecules closer and separated from one another (structures *e7*, *2*, *7*, *4*, *20*, *11*, *16* and *21*), but never breaking the ring. Figure 5.192 shows this kinds of structures. Their predicted spectra do not reproduce correctly the experimental results.

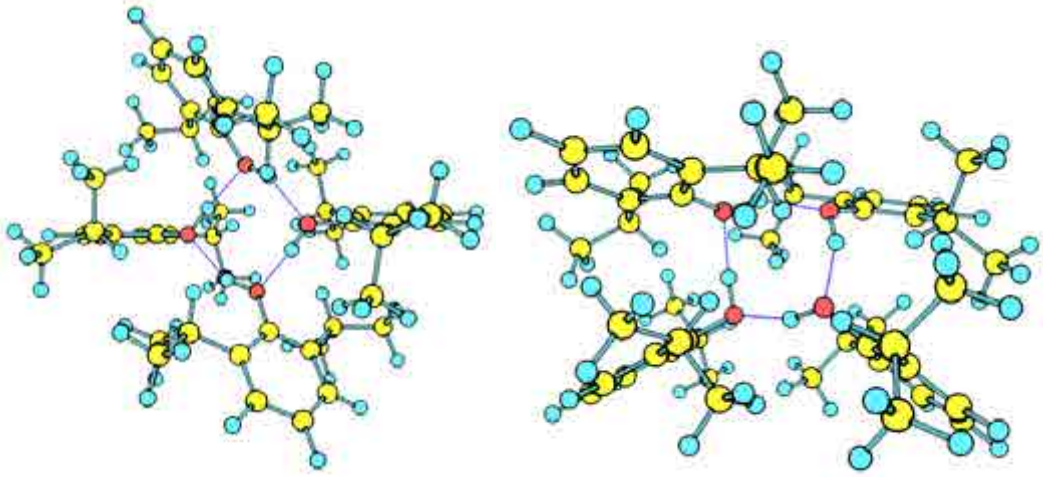

Figure 5.192. *Structures 3 and e7.*

Finally, Figure 5.193 shows a comparison between the experimental trace for the first conformer and the calculated spectrum of structure *9* (Figure 5.194), which is one of the structures (among others such as *e4*, *5*, *e8*, *18*, *10* or *19*) that better reproduce the experimental spectrum and it is only at 7 kJ/mol above the global minimum. As can be seen, there is a remarkable agreement between both traces. In these structures, three

propofol molecules are stacked and the last propofol molecule remains slightly separated. This type of arrangement takes advantage of the propofol positions to establish stronger hydrogen bonds while the isopropyl groups have more space to rotate and adjust to an optimum position giving more flexibility to the system.

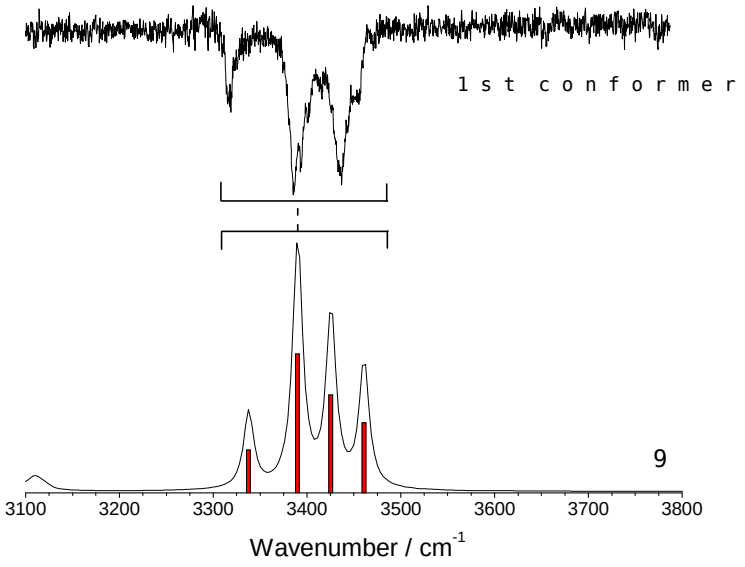

Figure 5.193. *Comparison of the predicted IR spectrum of structure 9 with the experimental results. As can be seen, there is a good agreement between the spectra.*

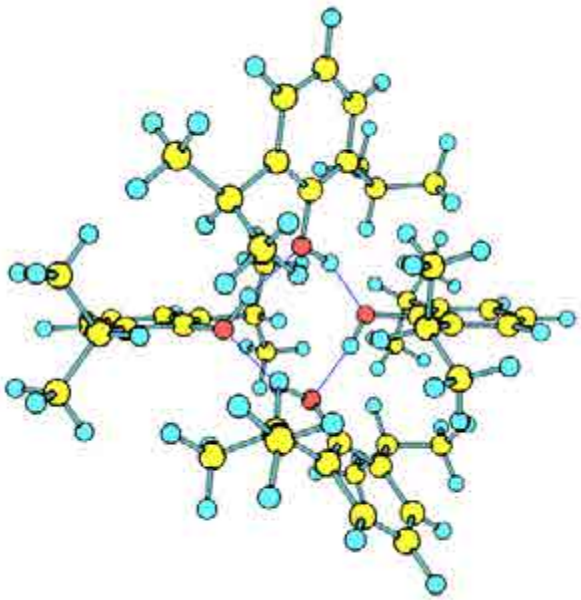

Figure 5.194. *Structure 9. This particular structure is in good agreement with the experimental results.*

5.5.3 – Propofol$_5$

As it happens with propofol$_4$, the most stable structures are those where the OH moieties are hydrogen-bonded, forming a cyclic structure, i.e. a micelle, as can be seen in Figure 5.195 (structures *1, 5, 2*). Non-cyclic structures appear above 16 kJ/mol, remarking the special stability of these micelles. Among this non-cyclic structures, those where four propofol molecules are in a cyclic structure and the fifth propofol molecule is either interacting with the ring of OH moieties (structure *6*), with one propofol's aromatic ring (structure *13*), or stabilized by dispersive forces (structure *7*) are the most stable types. Finally, there are other structures where the OH moieties form an O-H···O-H···O-H···O-H···O-H···π network (structure *3* and *4*), but they are > 20kJ/mol less stable than the global minimum.

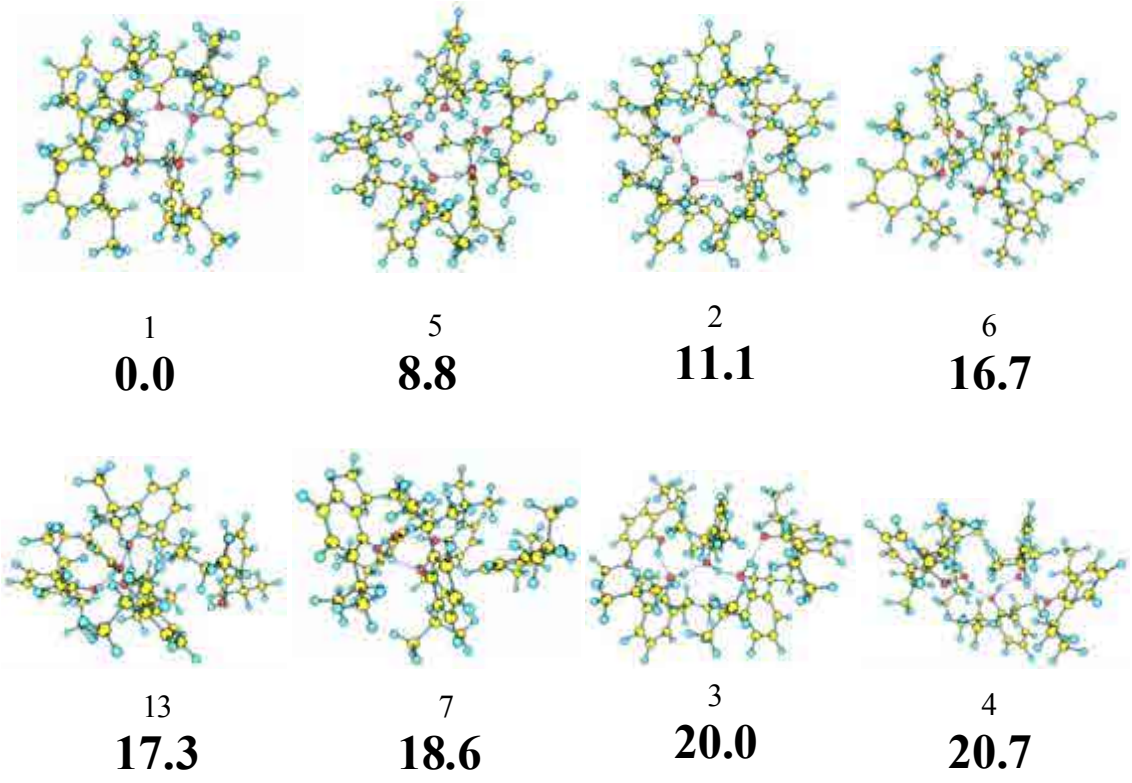

Figure 5.195. *Propofol$_5$ eight most stable conformers calculated at M06-2x/6-31+G(d) level, with their relative energies in bold. Energy values are in kJ/mol. The whole set of calculated structures are collected in appendix 7.1 (Figure 7.39).*

Figure 5.196 shows the *2c-REMPI* spectrum of propofol$_5$. The red-most peak is likely to be the very weak feature at 35951 cm^{-1} and, in the first 200 cm^{-1} some peaks

can be seen appearing from a broad background that extends for c.a. 1200 cm^{-1}. The aspect of the excitation spectrum clearly reflects the high complexity of the system.

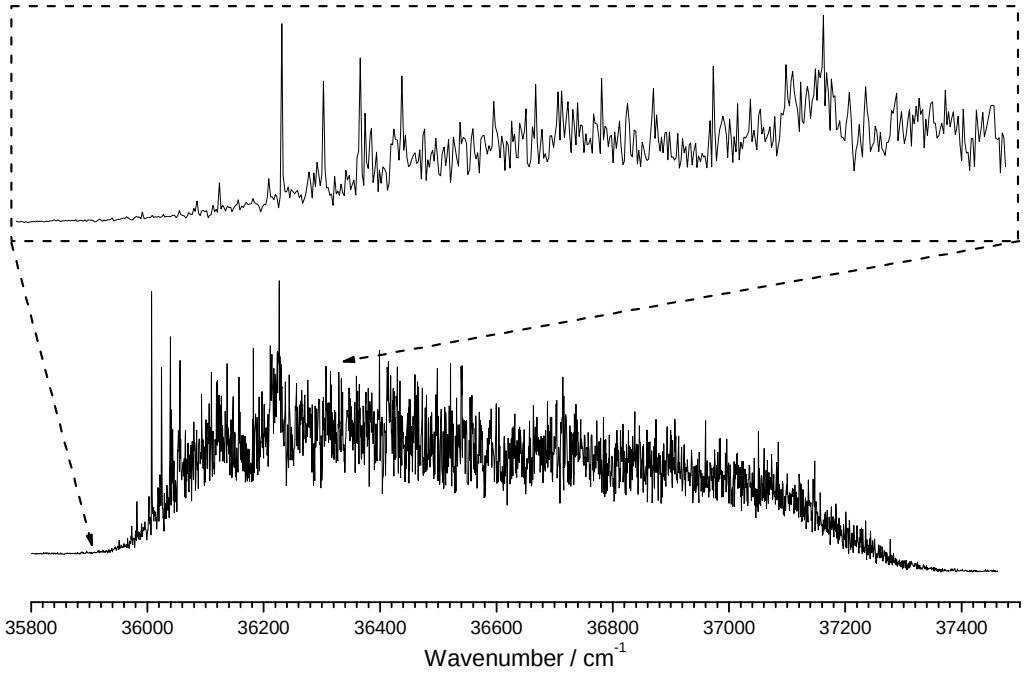

Figure 5.196. *2c-REMPI of propofol$_5$, in the 35800-37500 cm^{-1} region, recorded setting the probe laser at 27972 cm^{-1}. The insert shows a detailed view around the origin.*

Figure 5.189, shown in the previous section, indicates that no fragmentation from propofol$_6$ seems to be present.

To determine the number of isomers contributing to the spectrum of each stoichiometry, a *hole burning* experiment of the tetramer is done. Figure 5.197 shows where a comparison between the propofol$_5$ *2c-REMPI* spectrum and the *hole burning* traces obtained probing the transitions 35951 and 36007 cm^{-1}. Two isomers are present: the origin band for the first conformer is very weak, which largely complicates exploring the spectroscopy of this conformer, with its 0_0^0 transition located at 35951 cm^{-1}, while the origin band for the second conformer is blue-shifted c.a. 50 cm^{-1}, i.e. located at 36007 cm^{-1}, being an intense peak compared to the previous one.

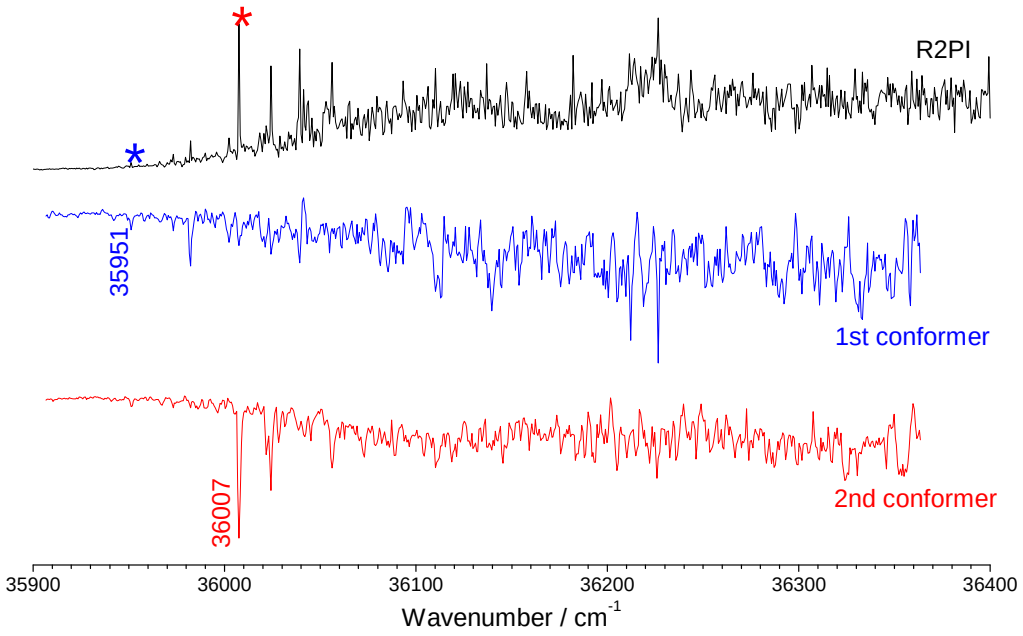

Figure 5.197. *Hole burning trace of propofol$_5$ recorded tuning the probe lasers (2-color detection) at 35951 and 36007 cm^{-1}. The peaks noted with asterisk indicate the transitions employed for recording the hole burning spectra, as well as the IDIRS traces.*

In order to extract the maximum structural information to match the *2c-REMPI* spectra with the calculated structures, the IDIR spectra of both conformers was recorded in the OH stretching region, obtaining the spectra shown in Figure 5.198. The IDIR spectra show that all the OH stretching vibrations are in the 3150-3450 cm^{-1} region for both conformers. It must be said that the s/n ratio for the first conformer is not very good, due to the weak signal and, despite several transitions were probed looking for an improvement on the S/N ratio, it was not possible to record a better spectrum. On the other hand, the obtained spectrum is sufficient to conclude that this conformer seems to be similar to the second conformer's structure, as only slight shifts in the OH stretching modes can be appreciated.

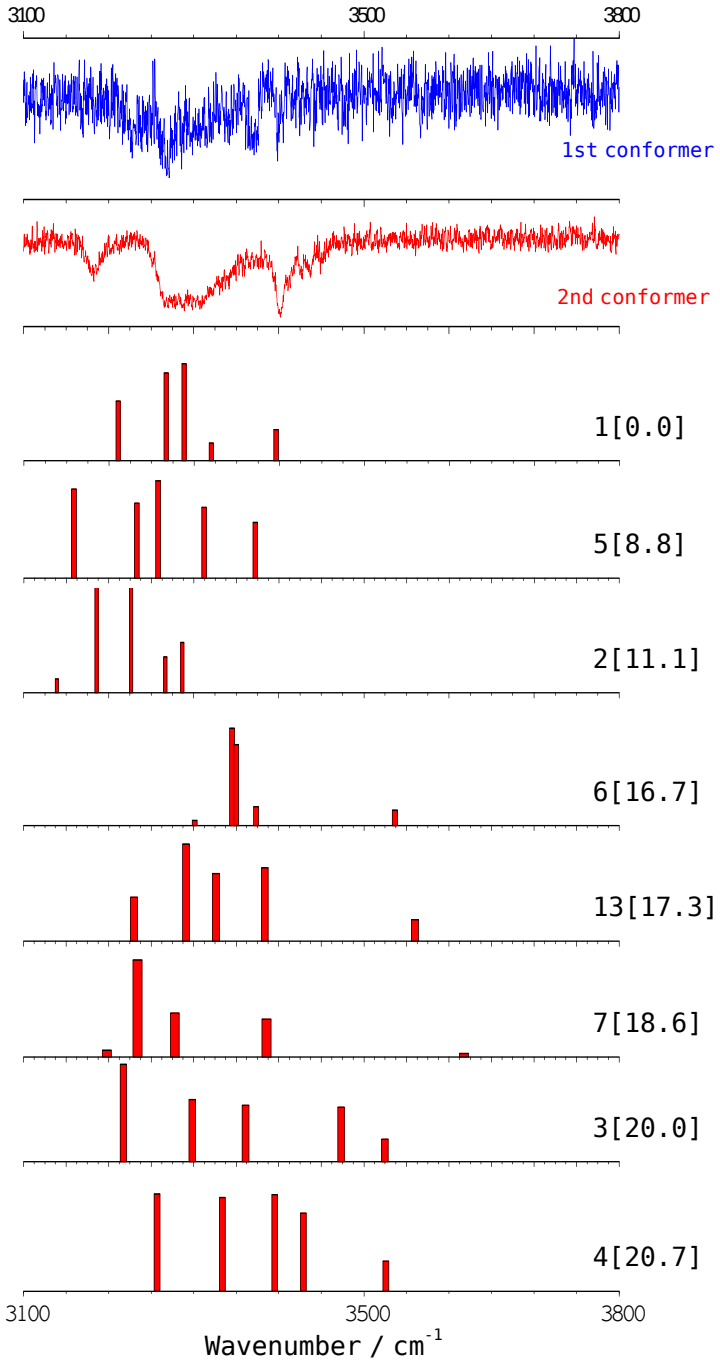

Figure 5.198. *IDIR spectra of propofol$_5$ recorded tuning the probe laser at 35951 and 36007 cm^{-1}. The predicted IR spectra for the most stable calculated structures are also shown for comparison. The numbers in brackets are the relative energies of the calculated conformers, in kJ/mol. A correction factor of 0.942 was applied. The predicted IR spectra of all the calculated structures are collected in appendix 7.1 (Figure 7.40).*

Assignment

As the predicted IR of the calculated structures show, it is clear that only those structures in which the molecules are forming a **pentameric micelle** can reproduce the experimental results. Among them, only the calculated structures *1* and *5* (Figure 5.200) present a spectra remarkably similar to the experimental ones (Figure 5.199). The difference between such structures and other cyclic structures (for example structure *2* shown in Figure 5.201) is that, for the latter, the OH moieties are in the same plane, while for the formers the OH moieties present an ***envelope*** arrangement which seems to be **our experimental structure**.

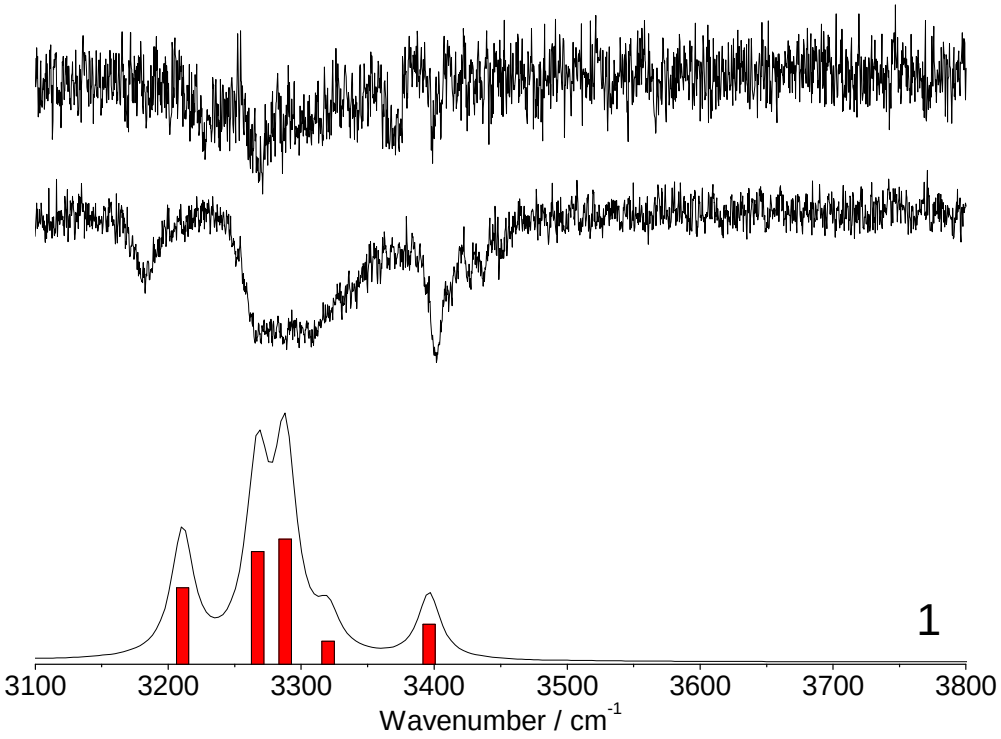

Figure 5.199. *Comparison of structure 1 predicted IR spectrum with the experimental results for both conformers. A good agreement between the spectra is achieved.*

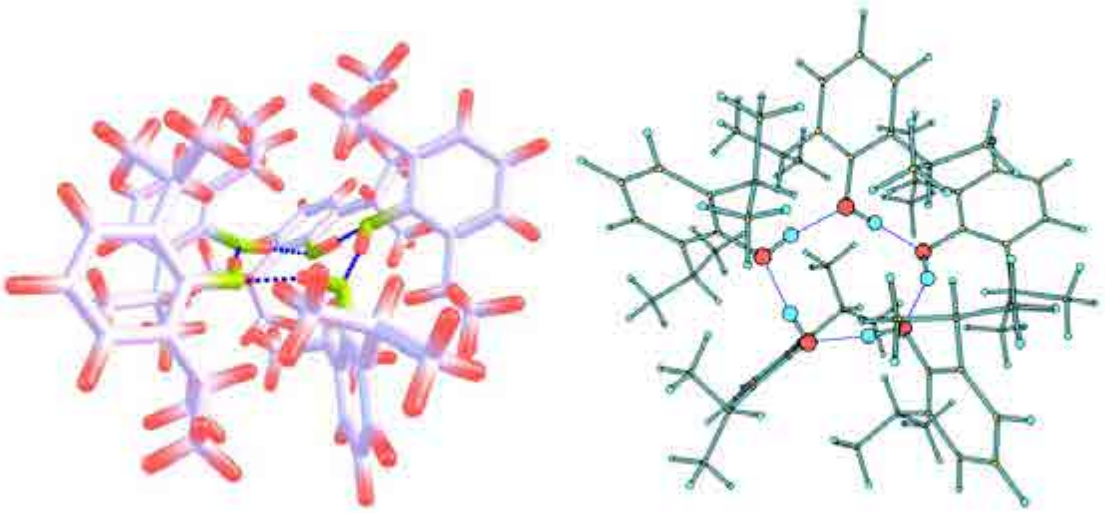

Figure 5.200. *Structure 1 is the theoretically predicted structure that better fits the experimental results for the first conformer. Note that the cyclic OH moieties present an envelope shape. A side view (sticks) and an upper view (the OH are in their original size, but the rest of the atom's sizes have been modified in order to offer a better view) is offered.*

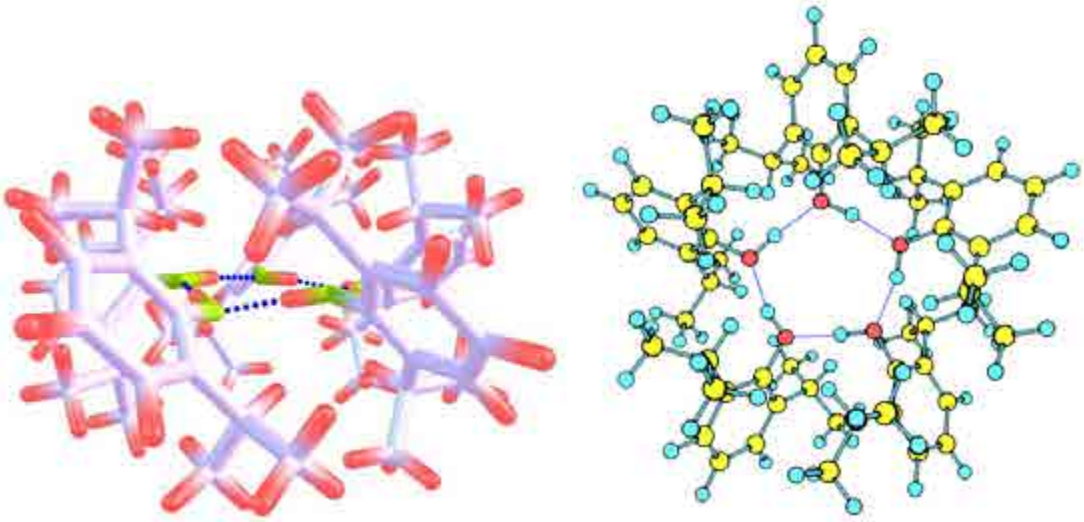

Figure 5.201. *Structure 2 is another structure where the OH moieties form a cyclic structure although, in this case, the OH-cycle is planar. This type of structures does not reproduce the experimental results. A side view (sticks) and an upper view of is offered.*

5.5.4 – Propofol$_6$

Contrary to the results obtained for propofol$_4$ and propofol$_5$, where molecular mechanics calculations predict basically formation of cyclic structures, for propofol$_6$ very stable non-cyclic structures are also found, although the size of the system precludes an exhaustive exploration of the conformational landscape. Figure 5.202 shows the most relevant structures found by molecular mechanics. As can be seen, cyclic structures are still present (structure *e1*) but, in this case, other non-cyclic structures such as an OH network (structure *e4*), an almost cyclic structure but with a OH moiety interacting with an aromatic ring (structure *e12*), four propofol molecules forming a cyclic structure while the other two propofol molecules interact together with this macrostructure (structure *e37*) or a supramolecular structure formed by five propofol molecules and the sixth molecule interacting with the former (structure *e45*) are also present.

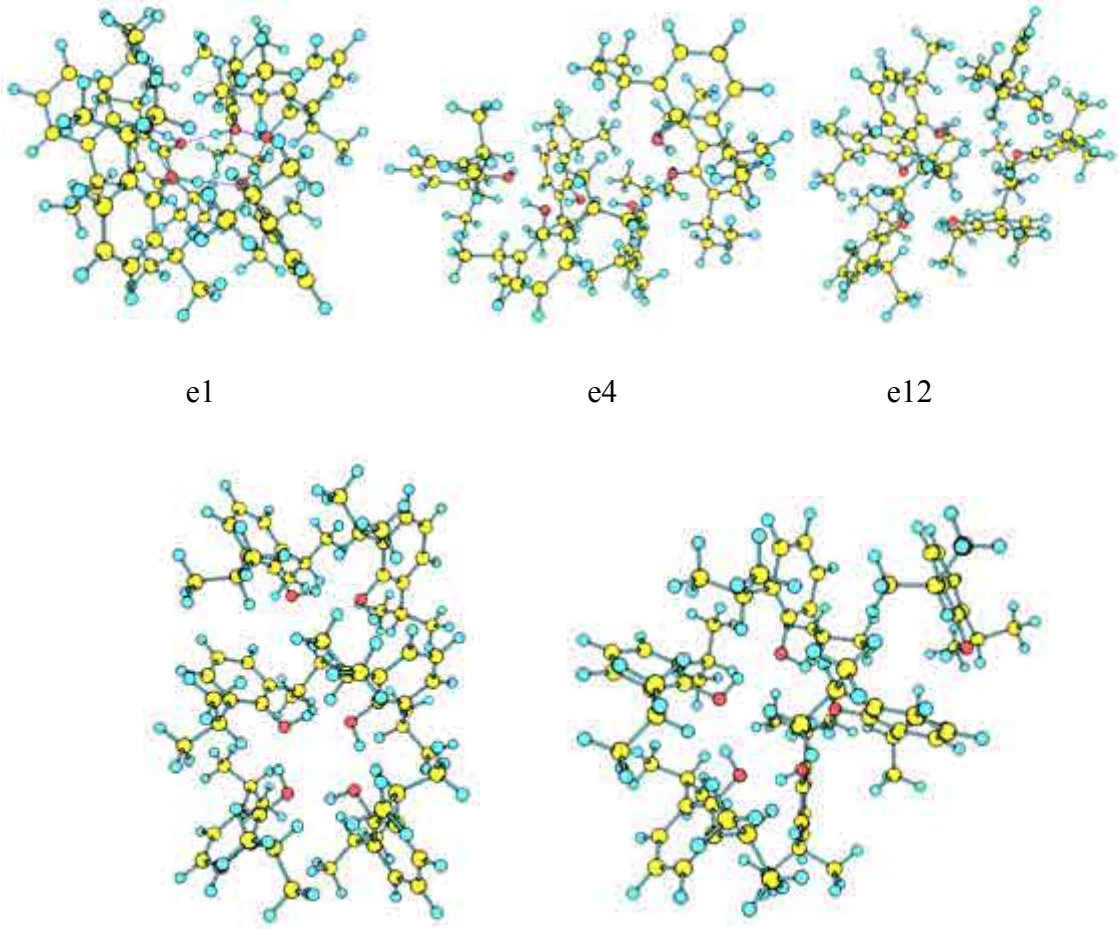

Figure 5.202. *Propofol$_6$ most stable types predicted by molecular mechanics.*

Figure 5.203 shows the *2c-REMPI* spectrum of propofol$_6$. Clearly, it is a broad absorption, with some discrete features, the first of which appears at 35953 cm^{-1}: that is, only 2 cm^{-1} to the blue of the pentamer's first conformer 0_0^0 transition. As can be seen, there is a broad background all over the spectrum, due to the complexity of the system, which also precluded obtaining a *hole burning* spectrum with acceptable s/n ratio.

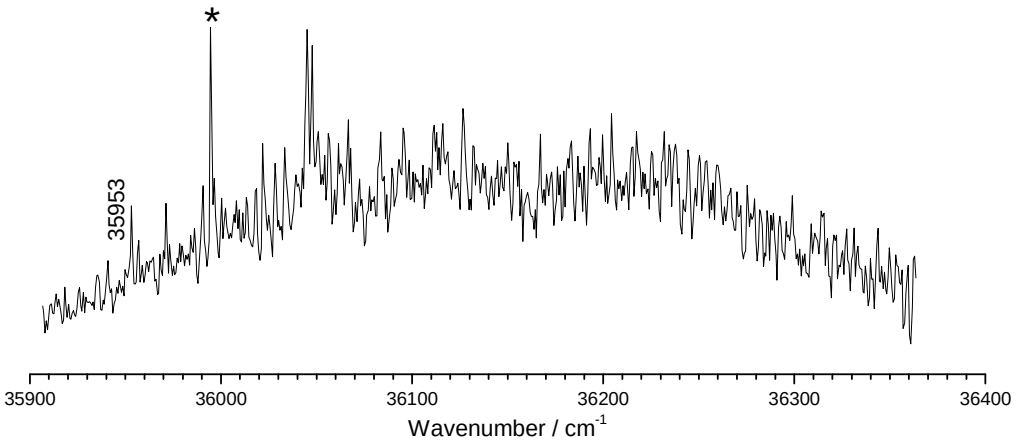

Figure 5.203. *2c-REMPI of propofol$_6$, in the 35900-36400 cm^{-1} region, recorded setting the probe laser at 27972 cm^{-1}.*

Several wavelengths on the continuum were used to record the IR spectrum always obtaining the spectrum in Figure 5.204, in which all the OH stretching vibrations are grouped in a narrow spectral region (3125-3325 cm^{-1}), which is the signature of an OH cyclic structure.

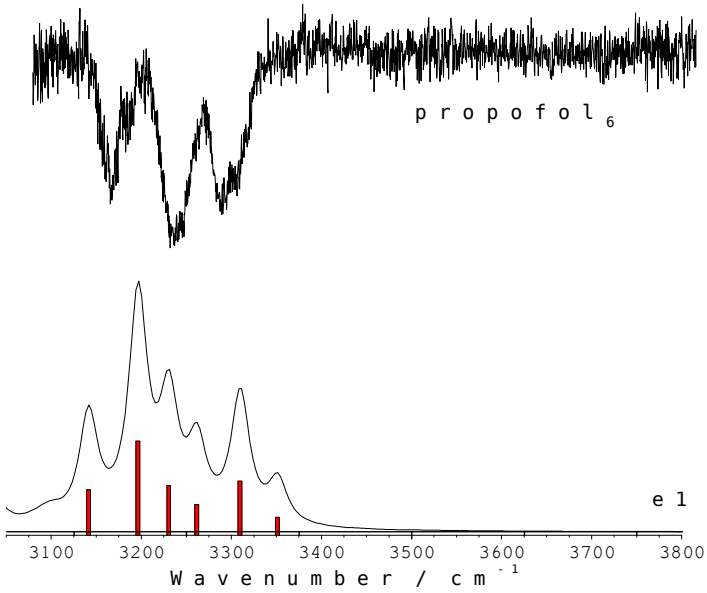

Figure 5.204. *IDIR spectrum of propofol$_6$ recorded tuning the probe laser at 35995 cm^{-1}. The predicted IR spectrum for one of the calculated cyclic structures is also shown for comparison. A correction factor of 0.96 was applied. The binding energy of this structure is 267 kJ/mol (BSSE corrected).*

Assignment

Due to the expensive computational cost of propofol$_6$ (see appendix 7.3 for details), only one structure was calculated so far (structure *e1*), which corresponds to a **micelle with all the hydroxyl groups forming a twelve-member ring** that resemble a ***boat* conformation**. Nevertheless, its computed spectrum accurately reproduces the main features of the experimental trace (Figure 5.204) and the small differences found may be due to small discrepancies in the relative orientations of the propofol molecules. As can be seen in Figure 5.205 where structure *e1* is shown, this OH-*boat* configuration maximizes the hydrogen bond interactions as they all are in an O-H···O angle of c.a. 165-180º and distances of 167-175 pm.

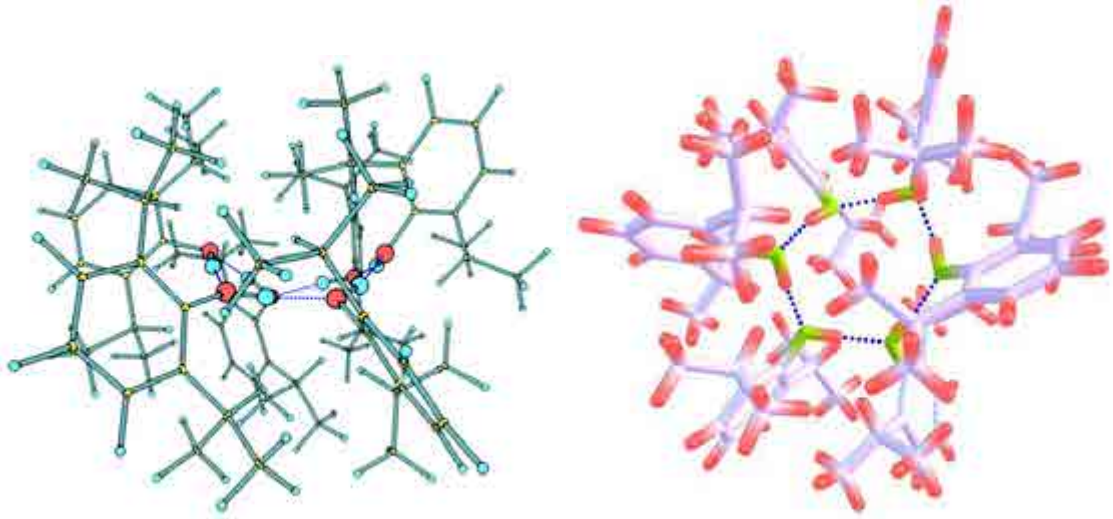

Figure 5.205. *Structure e1 predicted IR spectrum reproduces accurately the experimental results for the obtained conformer. Note that the cyclic OH moieties present a boat conformation. A side view (the OH are in their original size, but the rest of the atom's sizes have been modified in order to offer a better view) and an upper view (sticks) is offered.*

We are still working in the calculations of non-cyclic structures that will allow definitely rule out other possibilities but the one used in the assignment.

5.5.5 – Propofol$_n$: Discussion

In this section we have studied the intermolecular forces at play in the formation of propofol homomers. As the study of the dimer already showed and, although the hydrogen bond still plays an important role, propofol molecules are mainly stabilized by dispersive forces. The increase in the number of molecules is an important step in the understanding of how both types of interaction combine to give the clusters their final shape. The study presents the additional interest of being one of the largest systems ever solved by spectroscopy in supersonic expansions.

One of the most remarkable aspects is the counter intuitive observation that the voluminous isopropyl groups are the responsible of the *perfect* stacking of propofol molecules. As the width of the aromatic ring is c.a. 250 pm, and the average diameter for the isopropyl group is of 300 pm, the ratio between the two parameters, together with the flexibility of the propofol's isopropyl angle allow the molecules to accommodate to maximize the C-H···π interaction. The results are the cyclic structures found for all the homomers. Figure 5.206 shows the *2c-R2PI* spectra of the homomers together with their assigned structures.

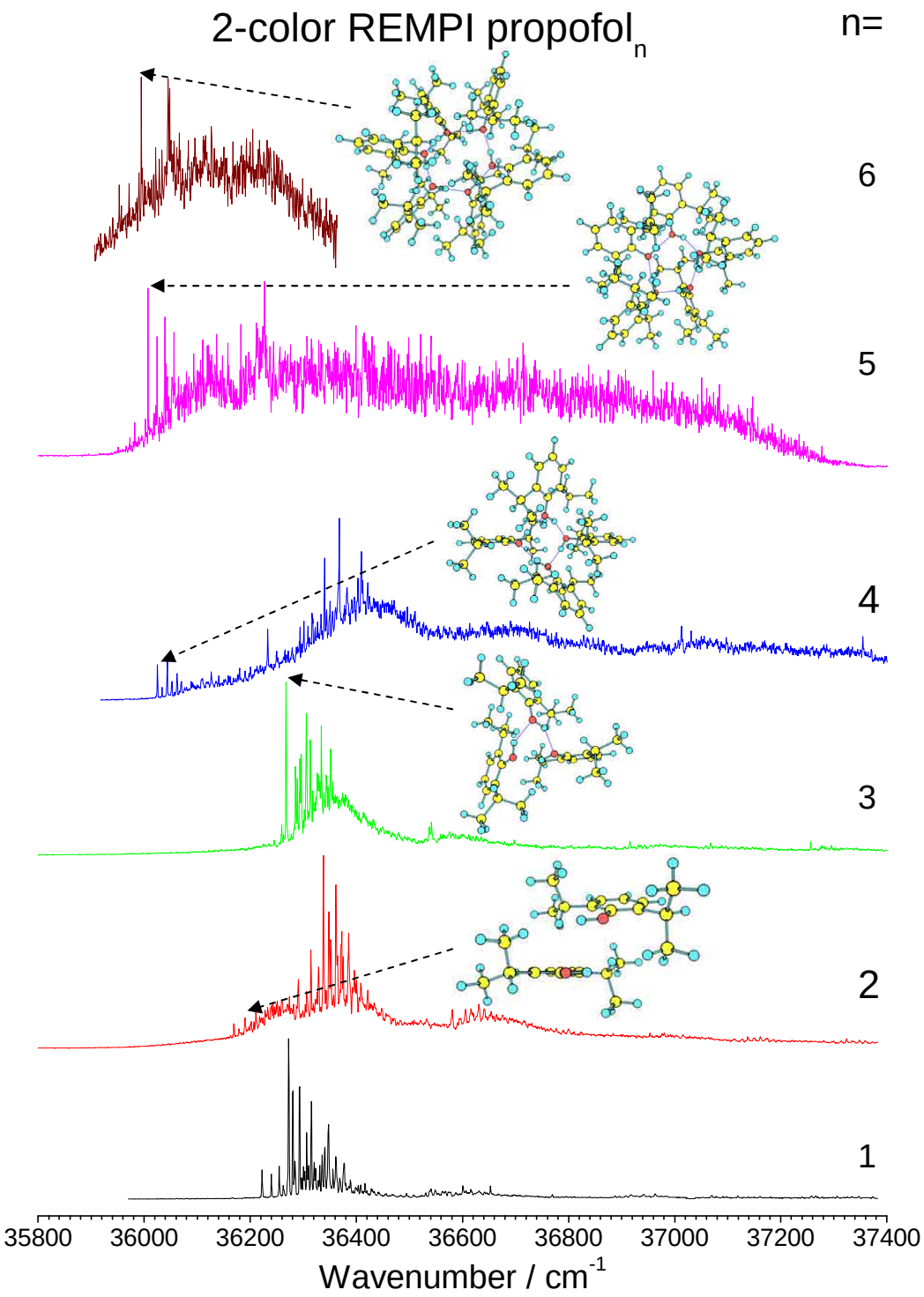

Figure 5.206. *2c-REMPI of propofol$_n$, n=1-6 in the 35800-37400 cm^{-1} region. The images show the structure assigned for each conformer of each cluster.*

We cannot conclude the discussion without representing in the same Figure the structures which represent the steps in the formation of a globular aggregate (Figure 5.207).

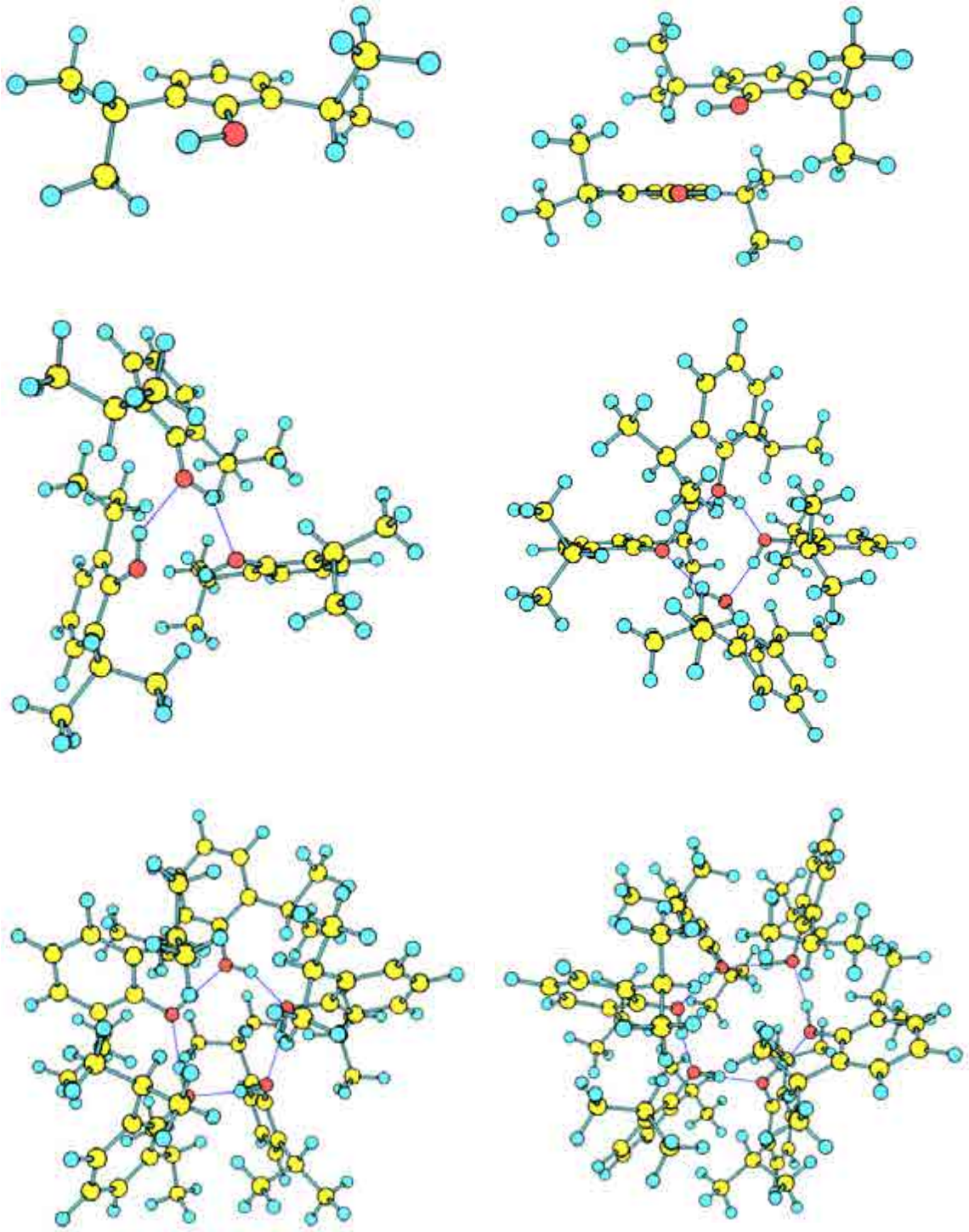

Figure 5.207. *Assigned structures for propofol$_n$, n=1-6.*

5.6 – Propofol$_{3\text{-}4}$·W$_1$

Up to now, a complete study on the micro-solvation of propofol and propofol$_2$ was done. The first study focuses on the spectroscopy of the bare molecule and how water molecules try to form similar structures to those in pure water clusters and how they are perturbed by the chromophore. On the other hand, the second study is an important step in the understanding of the solvation process, defined as the transition between the pure solute to a situation in which the solute is surrounded by solvent molecules. The pure solute phase was characterize in the study of propofol homomers, finding the formation of micellar aggregates for the largest clusters. An important conclusion of the study is the subtle interplay between dispersive forces and hydrogen bond. In this section, we focus on the effect a single water molecule produces in the behavior of the homomers. Thus, this section deals with the electronic spectroscopy of propofol$_3$·W$_1$ and propofol$_4$·W$_1$ clusters.

5.6.1 – Propofol$_3$·W$_1$

Heterogeneous clusters always present a more complicated conformation landscape than the equivalent homogeneous ones. Consistently, molecular mechanics calculations find more than a thousand structures in a 20 kJ/mol window, although some of them are statistically more probable. Among the most stable conformers (Figure 5.208), two type of structures with similar stability are found: in one of them, being also the global minimum, the three propofols and the water molecule form a cyclic structure through the interaction of their OH moieties, with the propofol molecules also interacting by dispersive forces (structures *e10, e2, e23, e17, e26, e8*). In the other one, the hydrogen bond network forms a tetrahedral structure (structures *3, 5*), being at only 3 kJ/mol of relative energy.

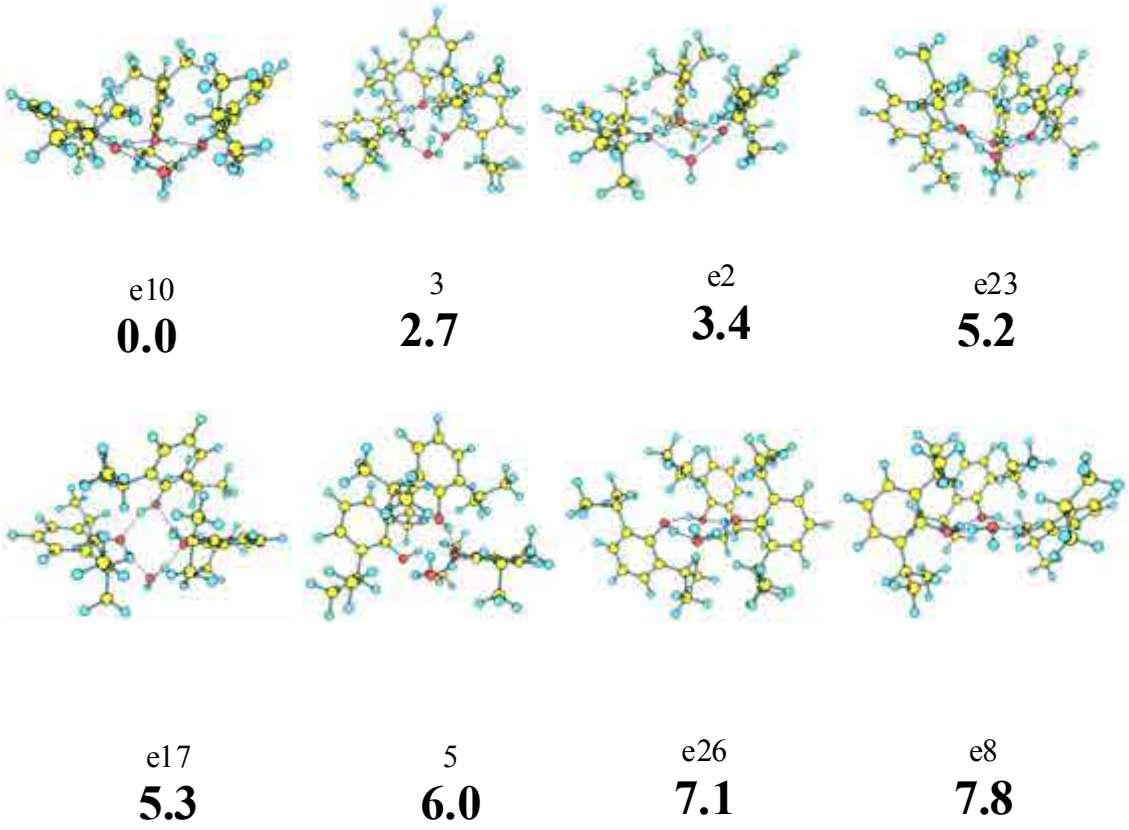

Figure 5.208. *Propofol$_3$·W$_1$ eight most stable conformers calculated at M06-2x/6-31+G(d) level, with their relative energies in bold. Energy values are in kJ/mol. The whole set of calculated structures is collected in appendix 7.1 (Figure 7.41).*

Figure 5.209 shows the *2c-REMPI* spectrum of propofol$_3$·W$_1$. The red-most peak is located at 35976 cm^{-1} and there is a rich spectroscopy extending for more than 500 cm^{-1}. A broad background is observed covering the whole scanned region.

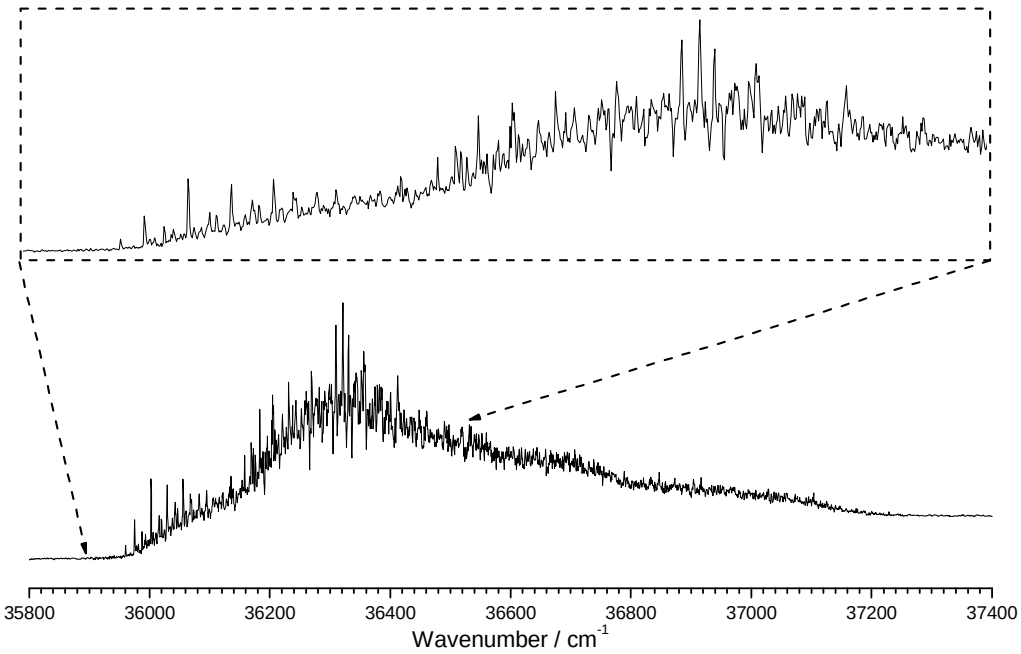

Figure 5.209. *2c-REMPI of propofol$_3$·W$_1$, in the 35800-37400 cm^{-1} region, recorded setting the probe laser at 27972 cm^{-1}. The insert shows a detailed view around the origin.*

To determine the number of isomers contributing to the spectrum, a *hole burning* experiment of propofol$_3$·W$_1$ is done, shown in Figure 5.210, together with propofol$_3$·W$_1$ *2c-REMPI*. Two isomers are found probably overlapping transitions like the one at 35976 cm^{-1}.

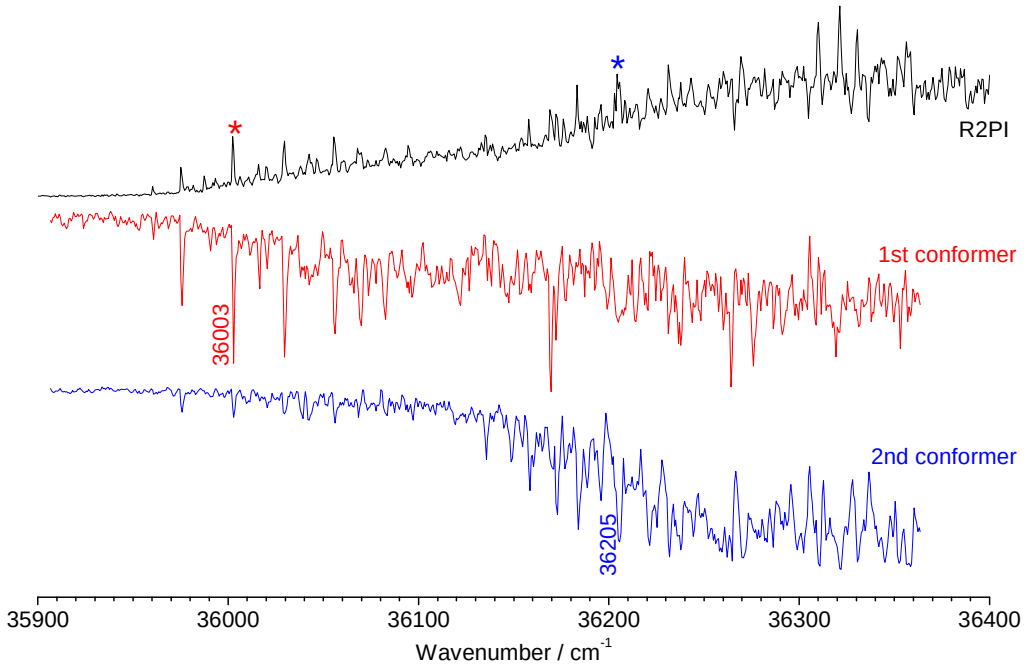

Figure 5.210. *Hole burning trace of propofol$_3$·W$_1$ recorded tuning the probe lasers (2-color detection) at 36003 and 36205 cm^{-1}. The peaks noted with asterisk indicate the transitions employed for recording the hole burning spectra, as well as the IDIRS traces.*

In order to extract the maximum structural information, the IDIR spectra of both conformers were recorded in the OH stretching region, obtaining the results shown in Figure 5.211. Both conformers present similar spectra with a peak located at c.a. 3705 cm^{-1} and four peaks in the 3200-3475 cm^{-1} region. The main difference between both conformers is the peak located at c.a. 3410 cm^{-1} for the first conformer and at c.a. 3450 cm^{-1} for the second one.

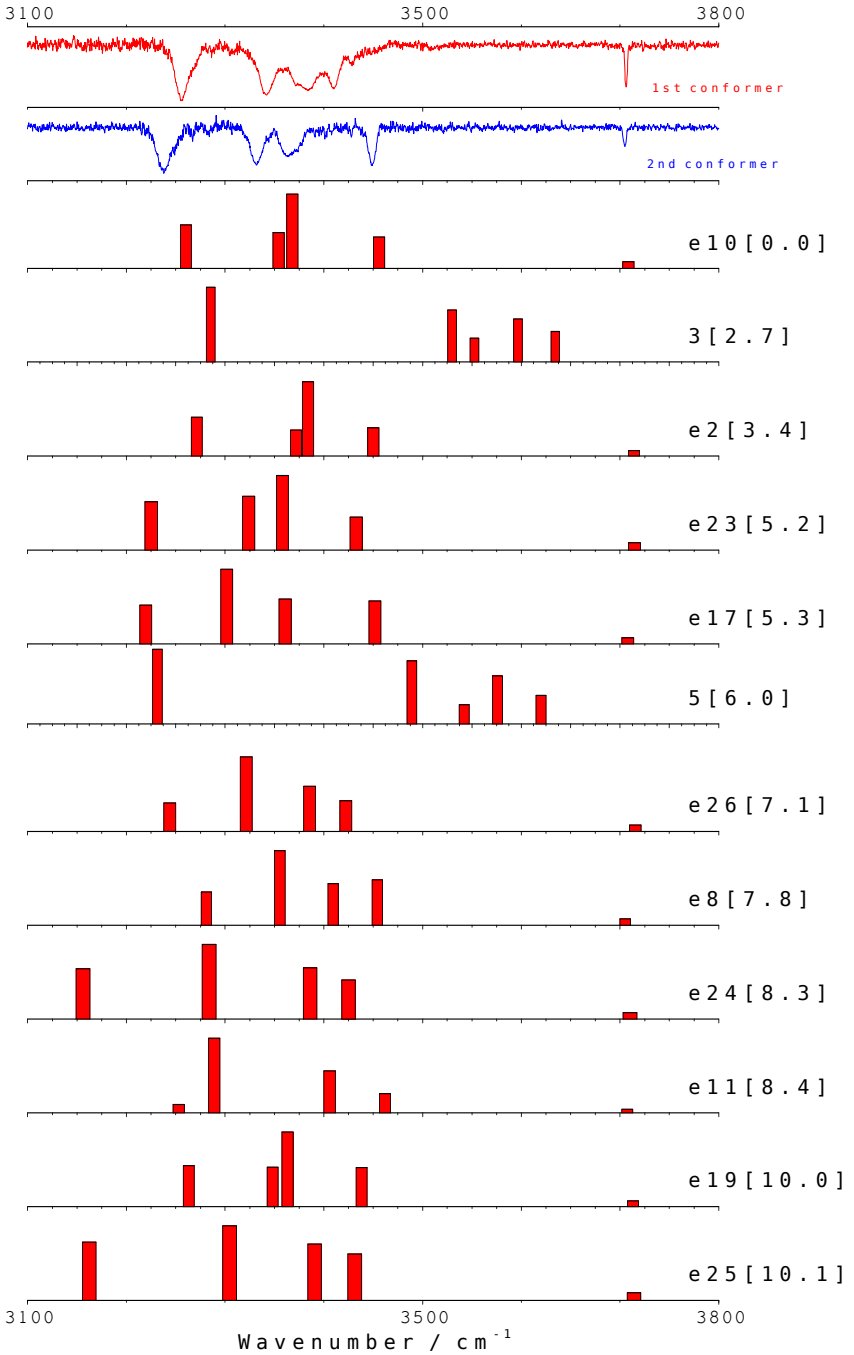

Figure 5.211. *IDIR spectra of propofol$_3$·W$_1$ recorded tuning the probe laser at 36003 and 36205 cm^{-1}. The predicted IR spectra for the most stable calculated structures are also shown for comparison. The numbers in brackets are the relative energies of the calculated conformers, in kJ/mol. A correction factor of 0.958 was applied. The predicted IR spectra of all the calculated structures are recorded in appendix 7.1 (Figure 7.42).*

Assignment

The experimental IR spectra in Figure 5.211 point to **cyclic structures** as no peak is observed between the single OH stretching modes and the water molecule's free OH stretching. Moreover, propofol$_3$·W$_1$ *2c-REMPI* spectrum resembles to that of propofol$_4$ (Figure 5.212), which, as demonstrated in section 5.5.2, also presents a cyclic structure.

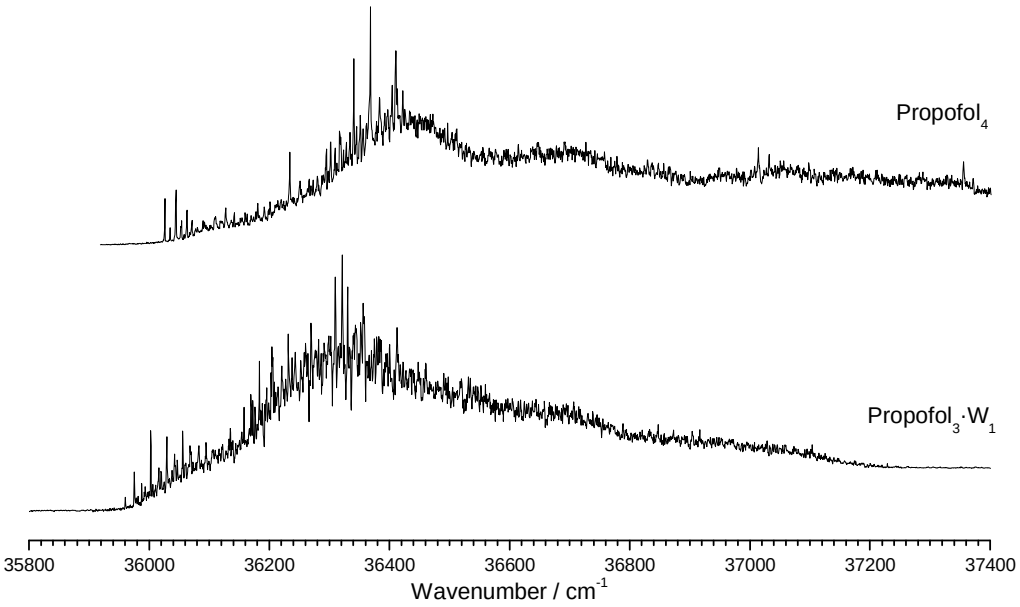

Figure 5.212. *Comparison of the 2c-REMPI spectra of propofol$_3$·W$_1$ and propofol$_4$.*

The direct comparison between the experimental and predicted IR spectra shows, without any doubt, that the only structures that match the experimental results are those where propofol and water molecules are forming a cyclic structure. Figure 5.213 shows a comparison of the predicted IR spectrum of the most stable conformers forming a cyclic structure with the experimental spectra. Although structures such as *e10* and *e23* fit better the experimental spectrum of the second conformer and structure *e26* that for the first conformer, there is a good agreement between all of them and such distinction can be within the theoretical error. The main difference between both types of structures is the position of the propofol molecules (Figure 5.214): for structures like *e10*, all the propofol molecules take part in a C-H···π interaction, while in those like

structure *e26*, one of the propofol molecules is at a larger distance, lacking therefore, of such interaction.

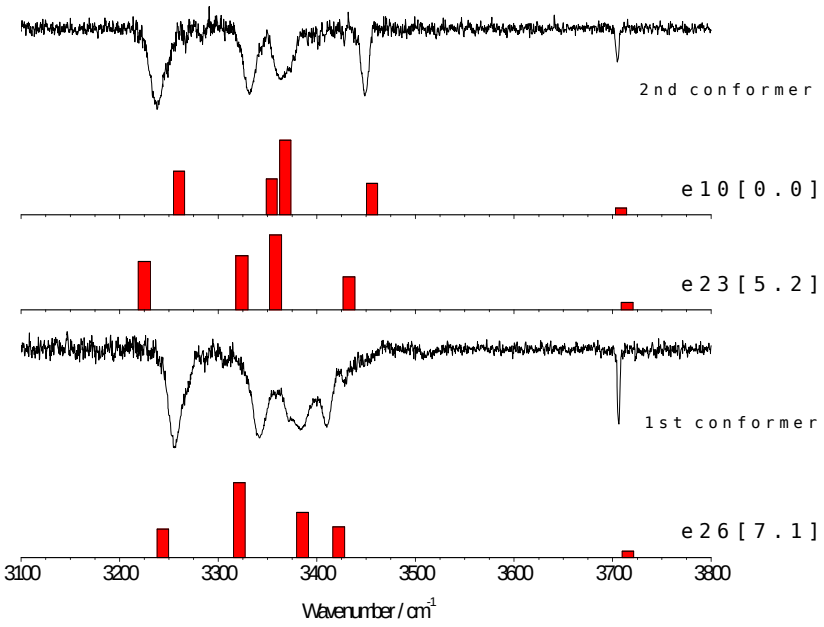

Figure 5.213. *Comparison of the predicted IR spectrum of structures e10, 23 and e26 with the experimental results for the two experimental conformers, as can be seen, there is a good agreement between the spectra.*

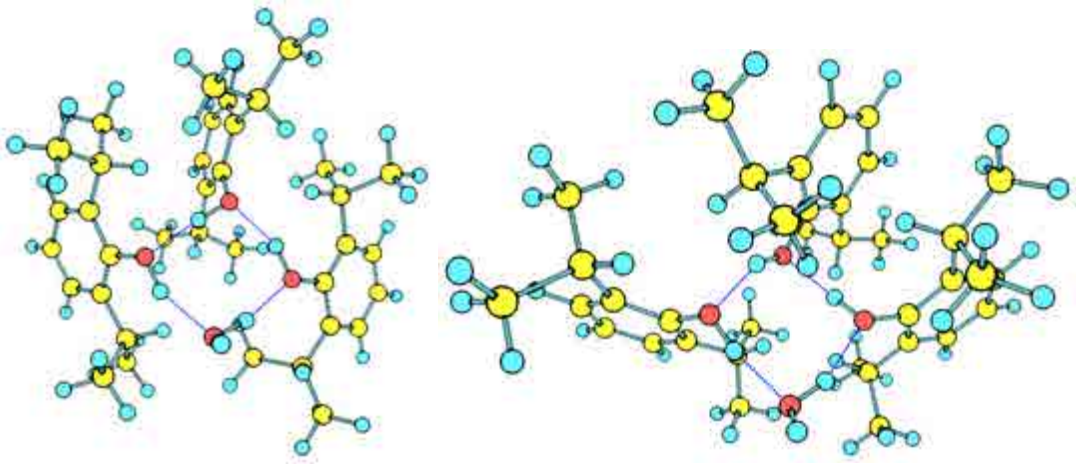

Figure 5.214. *Comparison of structures e10 and e26.*

On the other hand, tetrahedral structures like structure *3* (Figure 5.215), are also found among the most stable structures but they do not reproduce the experimental results. Other type of structures are those where the propofol molecules form an OH

network with the water molecule, which also interacts with the aromatic ring of one of the propofol molecule, as shown in Figure 5.215 for structure *12*. This type of structures can also be discarded as they do not reproduce the experimental results.

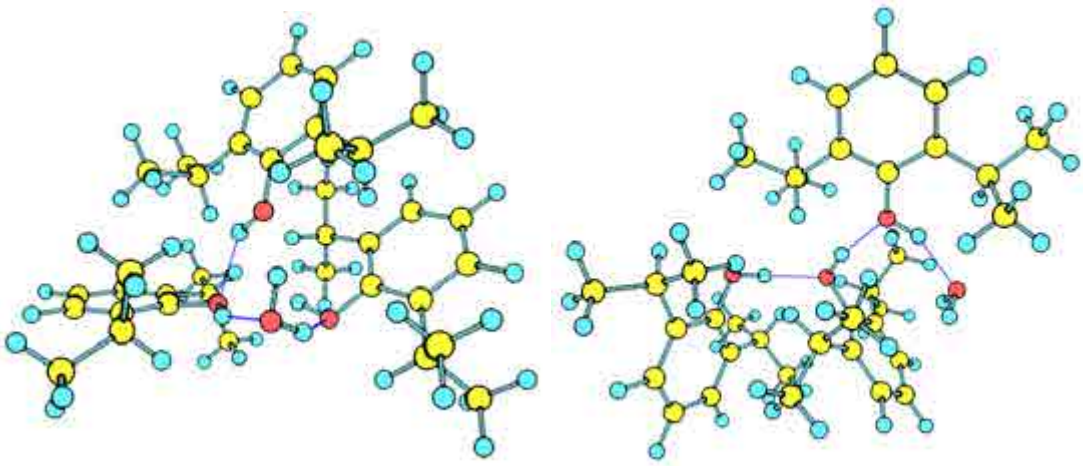

Figure 5.215. *Structures 3 and 12 are other type of interactions. None of them reproduce the experimental results.*

Finally, it is worthy to note that not all the cyclic structures reproduce the experimental results. Structures such as *e24* or *25* (Figure 5.216) show an IR spectra with an OH stretching of a considerably lower frequency than those in the experimental spectrum. This means that this OH moiety presents a stronger hydrogen bond, due to an arrangement in which two OH moieties are nearly perpendicular to their aromatic ring, resulting in a decrease in the stability as shown in Figure 5.217.

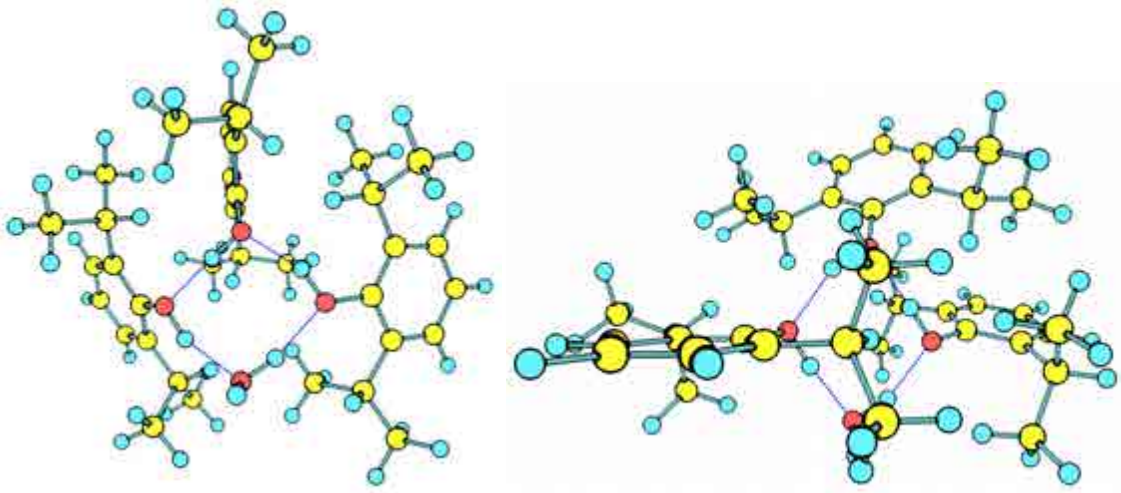

Figure 5.216. *Comparison of structures e10 and e24. Due to the orientation of the OH groups of the propofol molecules, the latter is found 8.3 kJ/mol higher.*

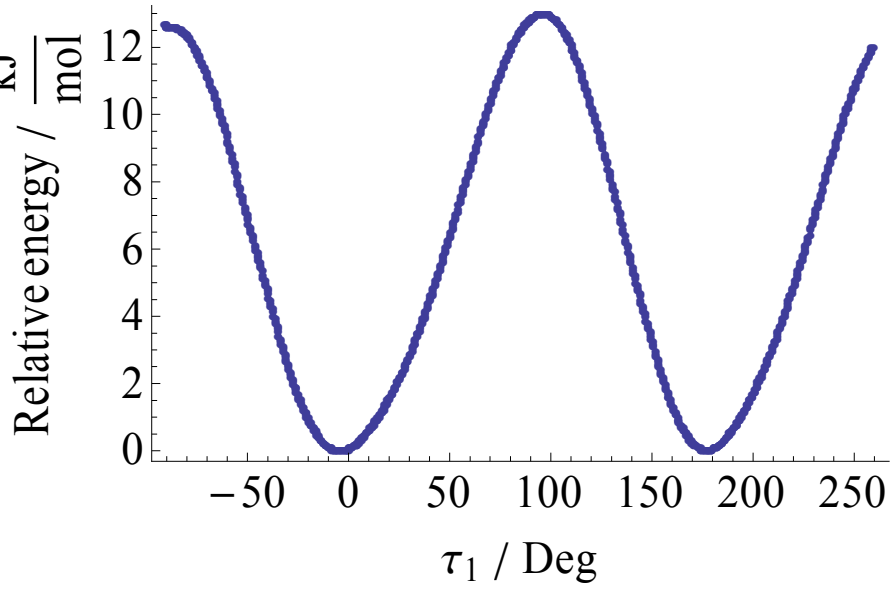

Figure 5.217. *Theoretical calculations for the bare molecule (Gg) rotating the OH dihedral angle with respect the aromatic ring each 10º. The calculations are conducted at B3LYP/6-31G++(d,p). As the OH moiety rotates out of the aromatic ring plane (0 and 180º), a decrease in the stability is found which is maximum when the OH group is perpendicular to the ring (90º and 270º).*

5.6.2 – Propofol$_4$·W$_1$

Molecular mechanics calculations yield of the order of thousand of structures in a 20 kJ/mol window, which means a considerable increase in the complexity of the system compared with propofol$_4$, for which an order of magnitude less structures were found. Such increase is mainly due to the appearance of new non-cyclic structures, although the most stable ones contain hydroxyl rings (Figure 5.218), following the same trend observed for the propofol$_3$·W$_1$ cluster.

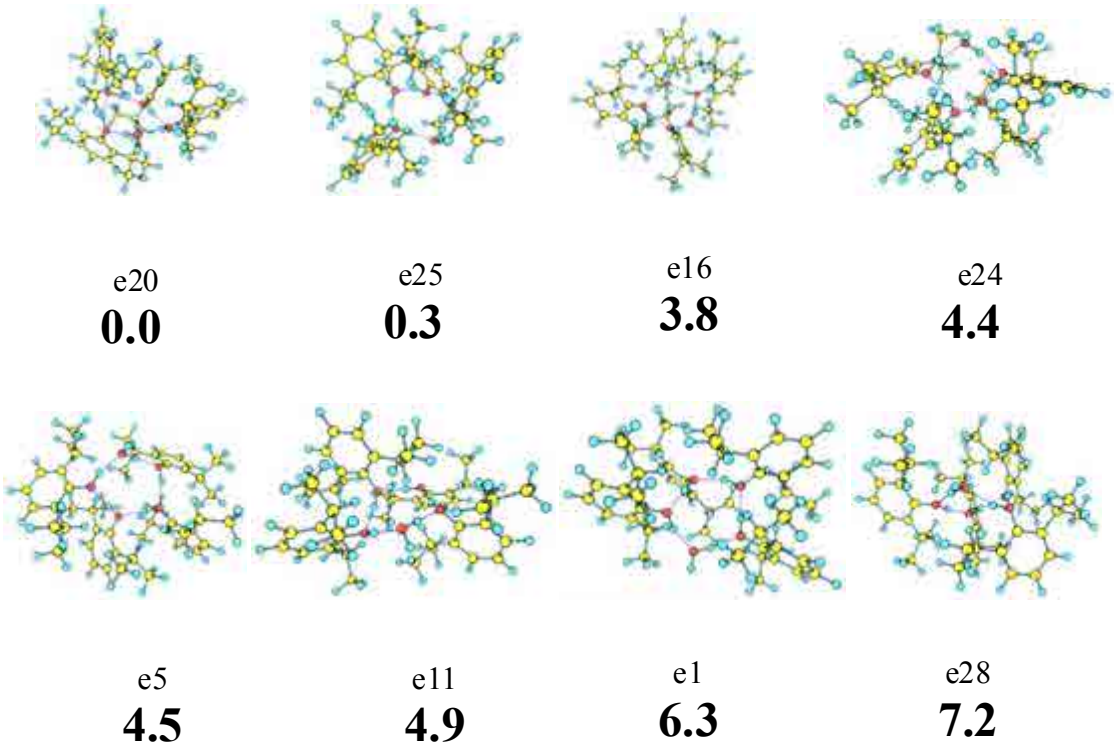

Figure 5.218. *Propofol$_4$·W$_1$ eight most stable conformers calculated at M06-2x/6-31+G(d) level, with their relative energies in bold. Energy values are in kJ/mol. The whole set of calculated structures is collected in appendix 7.1 (Figure 7.43).*

Figure 5.219 shows the *2c-REMPI* spectrum of propofol$_4$·W$_1$. There is a clear loss of structure from propofol$_3$·W$_1$ and/or propofol$_4$ spectra. The experimental conditions for recording the propofol$_4$·W$_1$ spectrum probed to be particularly critical: slight modifications of such conditions to increase signal intensity results also in a complete loss of spectral structure, may be due to an increase in fragmentation or in the number of species.

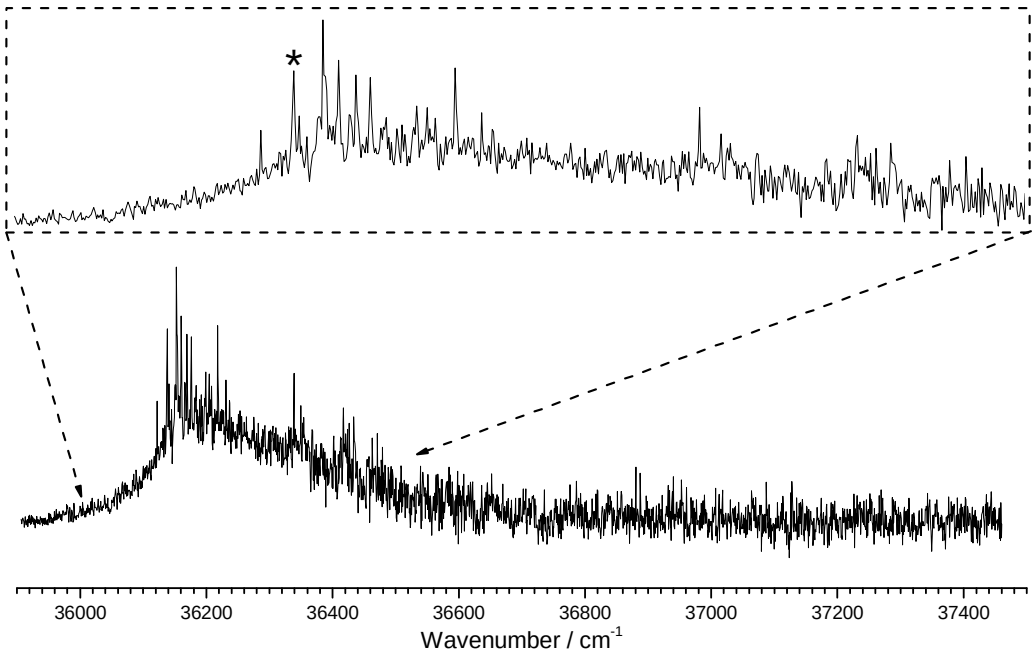

Figure 5.219. *2c-REMPI of propofol$_4$·W$_1$, in the 35800-37400 cm^{-1} region, recorded setting the probe laser at 27972 cm^{-1}. The insert shows a detailed view around the origin. The peak noted with an asterisk indicates the transition employed for recording the IDIRS trace.*

A collateral effect of the weak signal is the inability to record a *hole burning* spectrum. Fortunately, IDIR experiments were successful, yielding to the spectrum in Figure 5.220. The spectrum present some discrete peaks located at 3605, 3595, 3530, 3465, 3238 and 3168 cm^{-1}, although it seems that there are some weak peaks between the 3450-3600 cm^{-1} region and a broad absorption in the 3230-3360 cm^{-1} region, most probably due to the contribution of more than one conformer. Nevertheless, the spectrum clearly demonstrates the presence of non-cyclic structures, as there are some peaks in the double-donor or/and OH···π stretching region. Furthermore, no peak due to the water free OH stretching (c.a. 3710 cm^{-1}) was found.

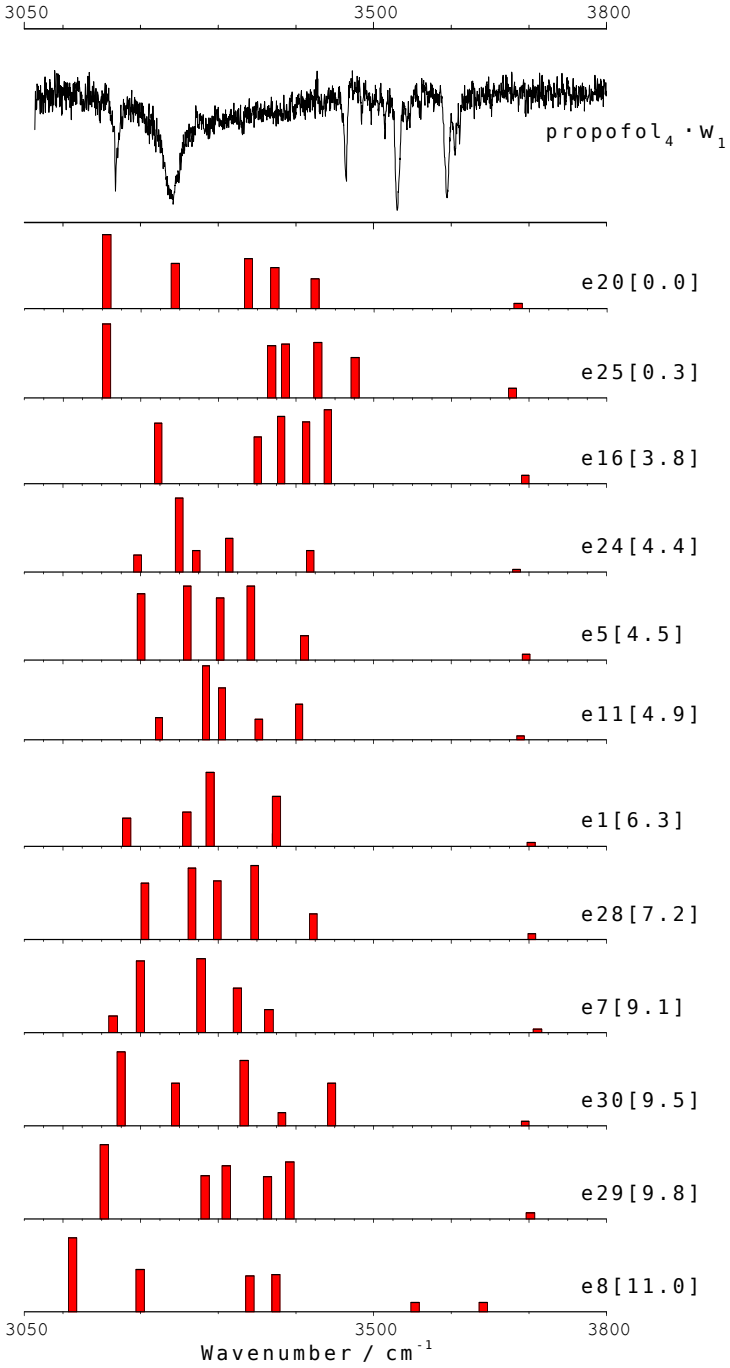

Figure 5.220. *IDIR spectrum of propofol$_4$·W$_1$ recorded tuning the probe laser at 36138 cm^{-1}. The predicted IR spectra for the most stable calculated structures are also shown for comparison. The numbers in brackets are the relative energies of the calculated conformers, in kJ/mol. A correction factor of 0.955 was applied. The predicted IR spectra of all the calculated structures are recorded in appendix 7.1 (Figure 7.44).*

Assignment

The **most relevant** aspect of the experimental IDIR spectrum is that **no cyclic structure** can reproduce the experimental results. Among the more than sixty calculated structures, only structures *4* and *5* (Figure 5.221) were found to present calculated spectra that resemble the experimental one. Although the former is too high in energy (34 kJ/mol), the latter is at an acceptable relative energy of c.a. 12 kJ/mol. The large diversity of structures found for this system makes almost impossible to explore all the possibilities and therefore, we cannot rule out the existence of other structure similar to *5*, but of higher stability. Nevertheless, as can be seen in Figure 5.222, the predicted spectrum of structure *5*, considering the level employed for the calculations, M06-2x/6-31+G(d), matches reasonably well the one obtained for the experimental conformer. In this structure, the OH moieties of three propofol molecules and the water molecule form an eight-member ring, while the other propofol molecule, is located in one of the sides, interacting both with the water and the π-cloud of other propofol molecule. For structure *4*, the conditions are similar but, in this case, the propofol molecule is interacting with the other propofol molecule's aromatic ring instead of its OH moiety. It is very important to note that these structures are **a propofol molecule attached to** the structure assigned for **propofol$_3$·W$_1$** in the previous section.

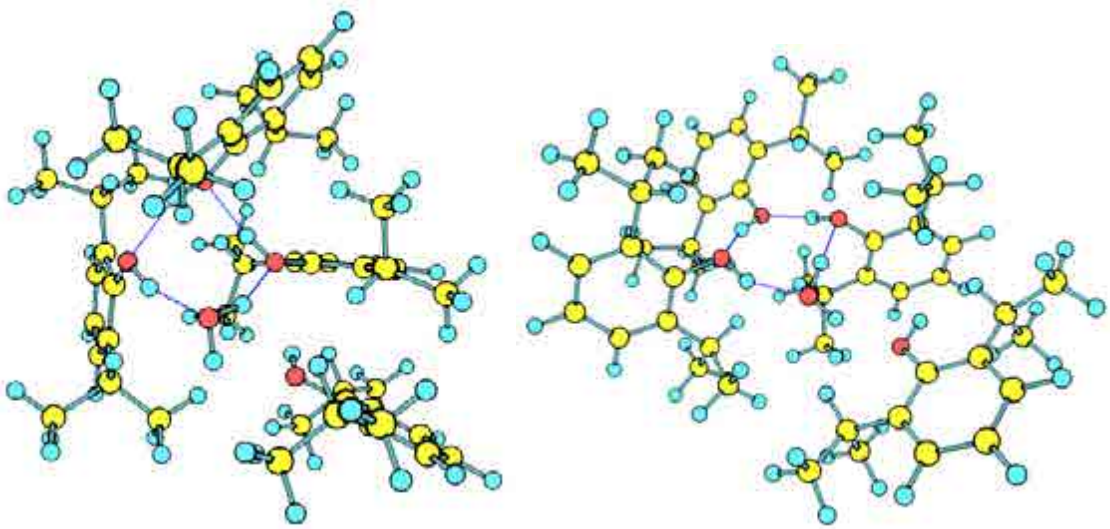

Figure 5.221. *Structures 5 and 4 are the theoretically predicted structure that better fits the experimental results.*

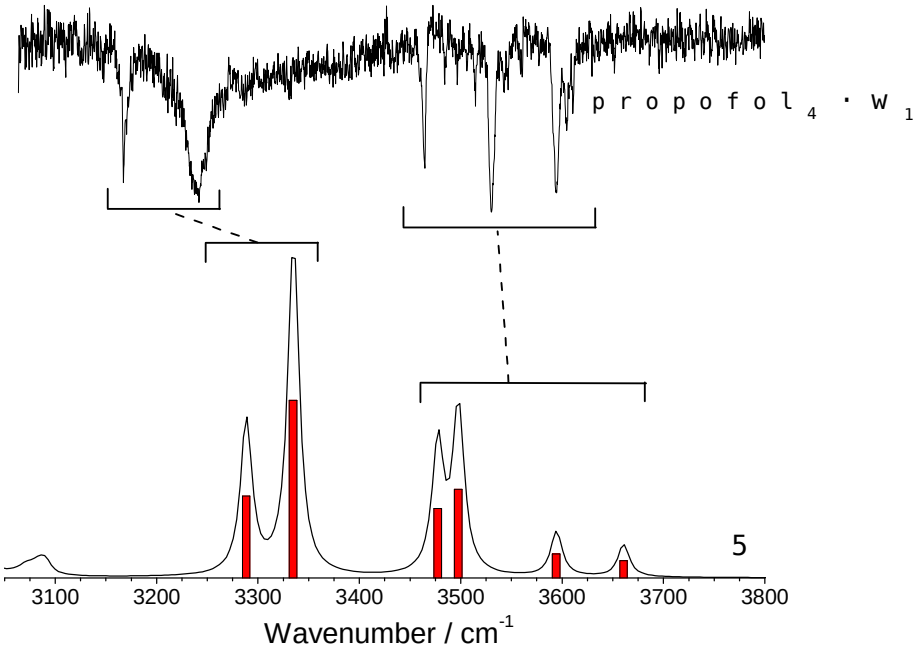

Figure 5.222. *Comparison of the predicted IR spectrum of structure 5 with the experimental results, as can be seen the predicted spectrum matches reasonably well.*

A good prediction of the experimental spectrum is also obtained, if one assumes that it is the combination of the spectra of two isomers (Figure 5.223). As no *hole burning* spectrum was obtained, one cannot rule out such possibility. In this case, the red part of the spectrum would be due to a cyclic structure like *e8* (Figure 5.224) while the blue part would be due to an isomer with the hydroxyl groups forming two six-member rings linked by a tetra-coordinated water molecule, like in structure *17*.

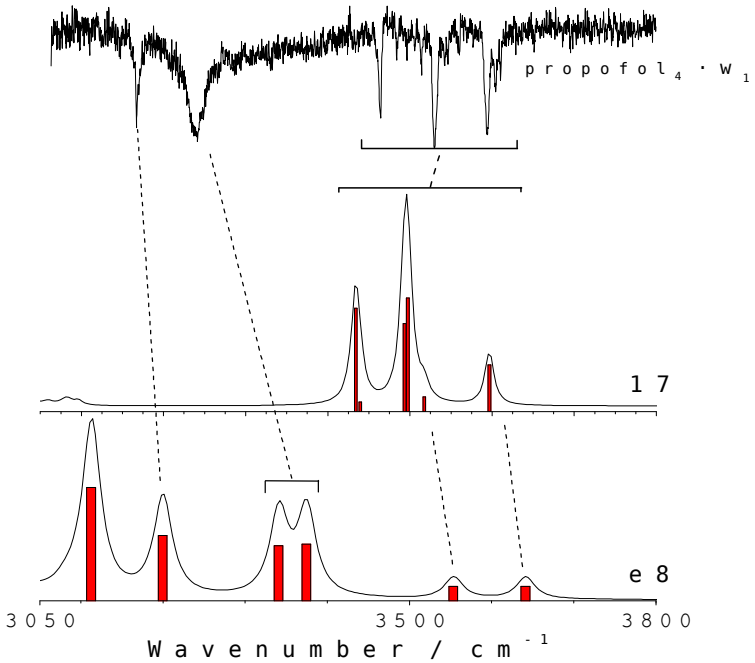

Figure 5.223. *Comparison of the predicted IR spectrum of structures 17 and e8 with the experimental results. As can be seen, the sum reproduces reasonably well the experimental spectrum.*

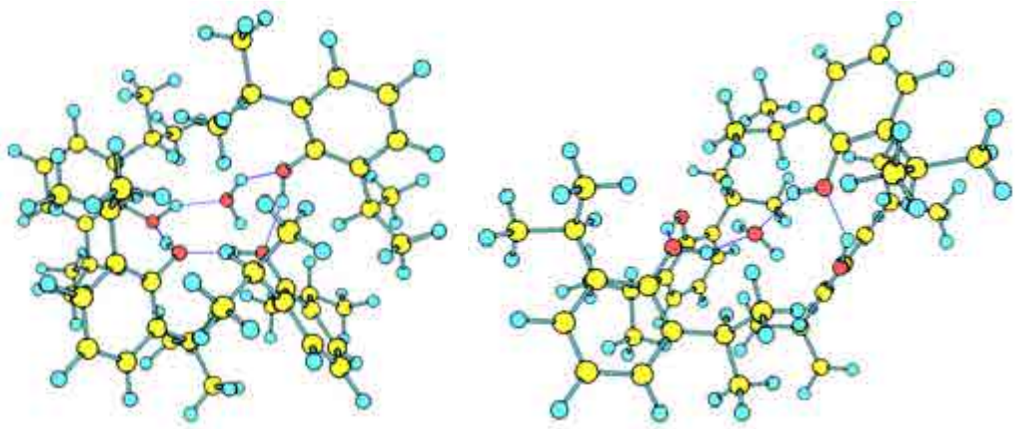

Figure 5.224. *Structures e8 and 17 are two of the structures whose combination also reproduces the experimental results.*

It is difficult to make a complete assignment for this system due to the huge number of conformations that the molecules can adopt, although the most important aspect has been achieved: the water molecule competes with the propofol molecule's OH moieties and forces them to break **the cyclic structure,** which **is no longer present**.

5.6.3 – $\underline{\textbf{Propofol}_{3\text{-}4}\cdot\textbf{W}_1\textbf{: Discussion}}$

It is worthy to note the unexpected observation that **a single water molecule is able to perturb the micellar structure formed by propofol$_4$** deeply transforming the cluster's structures, displacing a propofol molecule from the hydrogen cyclic structure. It would be interesting to continue the work with the study of species such as propofol$_4$·W$_4$ or even with larger contents of water, to test if a water core is formed with the propofol molecules forming an outer layer, or if the tendency is to form water aggregates with all the propofol molecules sticking together by dispersive interactions.

5.7 – Propofol·amino acids residues

As previously stated, the docking process of propofol into the channel's active site can be contemplated as a competition between the solvation of the anaesthetic by water and by the active site's environment. In the previous sections, the study of the microsolvation of propofol was carried out and in this section, the interaction between propofol and tyrosine/treonine aminoacid residues is analyzed though the spectroscopic study of propofol·phenol and propofol·2-propanol clusters.

5.7.1 – Propofol·phenol

Despite the reduced size of the system, compared with previously analyzed complexes, the molecular mechanics search finds over a hundred structures in a 20 kJ/mol window. Most stable isomers (Figure 5.225) present structures with a dipole-dipole interaction between the OH moieties (structures *e15*, *e4*), structures governated by dispersive forces (structures *e13*, *e20*), or by weak hydrogen bonds either with phenol (structures *e3*, *e18*) or propofol (structures *e7*, *e8*), acting as a proton donor to the other molecule.

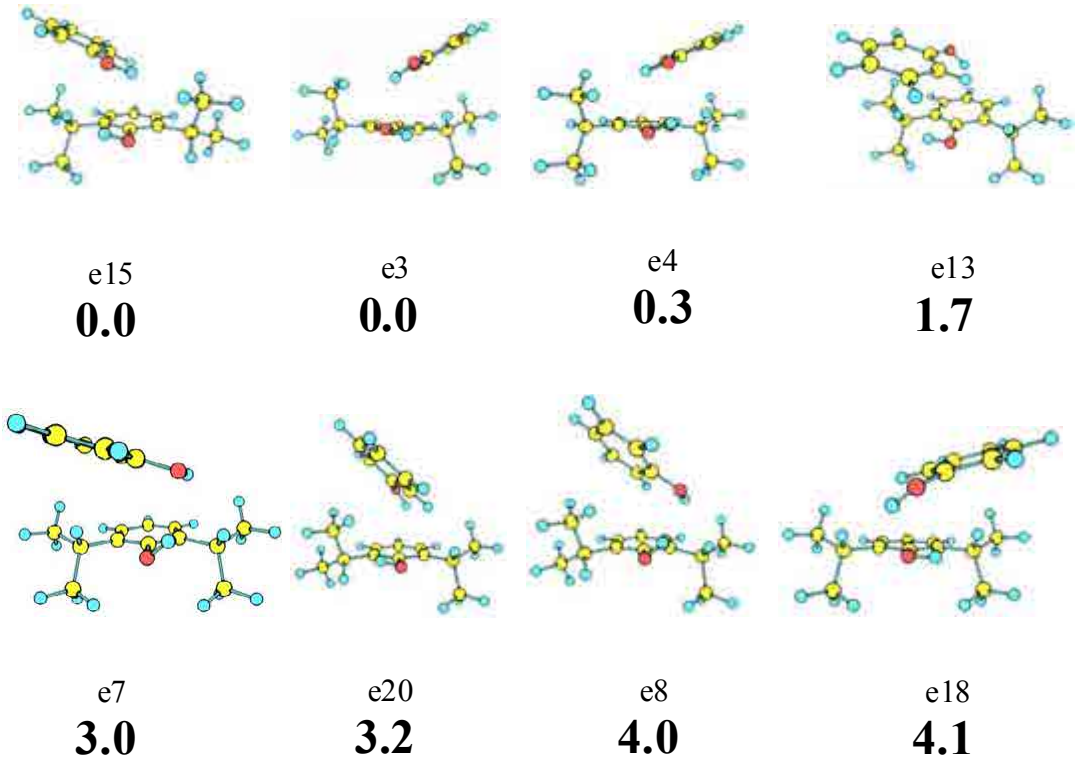

Figure 5.225. *Propofol·phenol eight most stable conformers calculated at M06-2x/6-31+G(d) level, with their relative energies in bold. Energy values are in kJ/mol. The whole set of calculated structures is collected in appendix 7.1 (Figure 7.45).*

Figure 5.226 shows the *2c-REMPI* of propofol·phenol, covering at least an extension of 1200 cm^{-1}. The red-most peak appears at 36050 cm^{-1}. Some weak bands are found in the first part of the spectrum, presumably due to some conformers. The spectrum gains considerably intensity in the 36160 – 36400 cm^{-1} region, partly due to the abundance of conformers, as it will be shown.

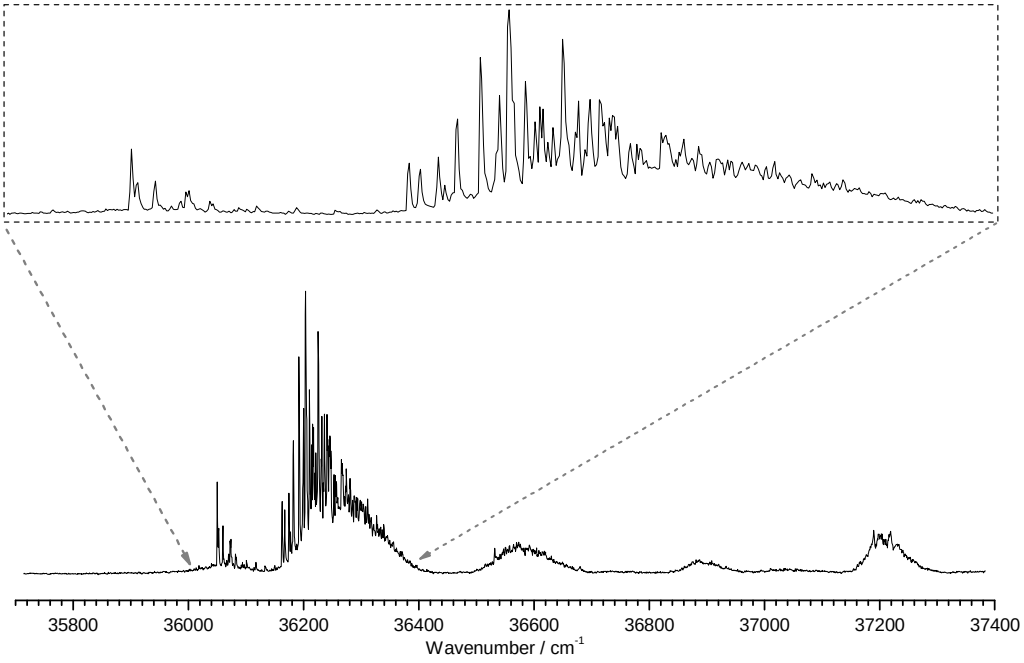

Figure 5.226. *2c-REMPI of propofol·phenol, in the 35700-37400 cm^{-1} region, recorded setting the probe laser at 27972 cm^{-1}. The insert shows a detailed view around the origin.*

To determine the number of isomers, a *hole burning* experiment was done. Figure 5.227 shows a comparison between the propofol·phenol *2c-REMPI* spectrum and *the hole burning* traces obtained probing the transitions at 36050, 36101, 36192, 36200 and 36231 cm^{-1}. At least five isomers are present and, although the origin band for the first (36050 cm^{-1}) and second conformers (36101 cm^{-1}) are clearly found, the position of the origin band for the rest of the conformers is not clear. Furthermore, the last three conformers seem to share some transition, like for example the band at 36162 cm^{-1}. Based on the conclusions reached in the study of the bare molecule, such effect may be related to the excited state isomerization of some of the conformers, which may converge to the same structure. The *hole burning* spectrum also demonstrates that all the isomers contribute to built a broad absorption in the 36160 – 36400 cm^{-1} region. Another important aspect is that, at least another conformer is present and although we were not able to isolate its transitions using *hole burning*, its presence will be confirmed in the IDIR spectrum.

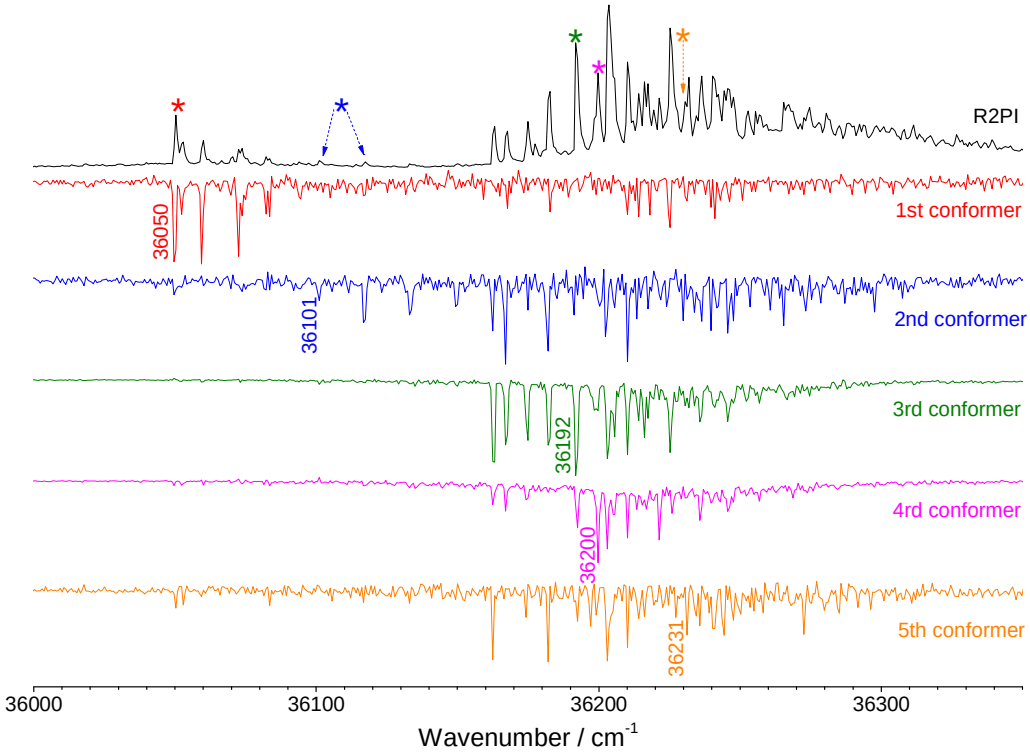

Figure 5.227. *Hole burning traces of propofol·phenol recorded tuning the probe laser (2-color detection) at 36050, 36101, 36192, 36200 and 36231 cm^{-1}. The asterisks denote the transitions employed for recording the hole burning spectra, as well as the IDIRS trace for the observed conformers.*

Another evidence of the existence of isomerization processes is obtained replacing He by Ne or Ar as buffer gas. Figure 5.228 shows a comparison of the *2c-REMPI* spectrum using each of the three noble gases. Clearly, the transitions due to the first and second conformers completely disappear, and the first and intense peaks near 36160 cm^{-1} almost completely vanish. The rest of the spectra loses part of the vibrational structure, may be due to formation of new, less stable species, or even Ar clusters.

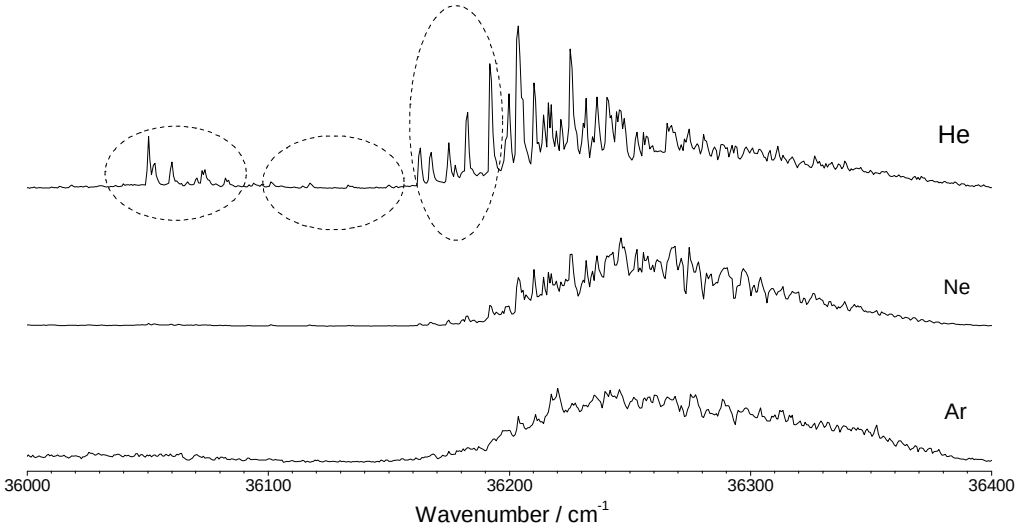

Figure 5.228. *2c-REMPI of propofol·phenol, in the 36000-36400 cm^{-1} region, recorded using helium (upper trace), neon (middle trace) and argon (lower trace). The dashed lines highlight the groups of transitions depleted.*

In order to extract the maximum structural information to assign the *2c-REMPI* spectra to the calculated structures, the IDIR spectra for all conformers were recorded in the OH stretching region, obtaining the spectra shown in Figure 5.229a. As can be seen, for some of the selected transitions, the IR spectrum shows more than two bands, probably due to the presence of different conformers sharing the probed transition. Such interference may be eluded in an IR-IR-UV triple resonance experiment as demonstrated in Figure 5.229b.

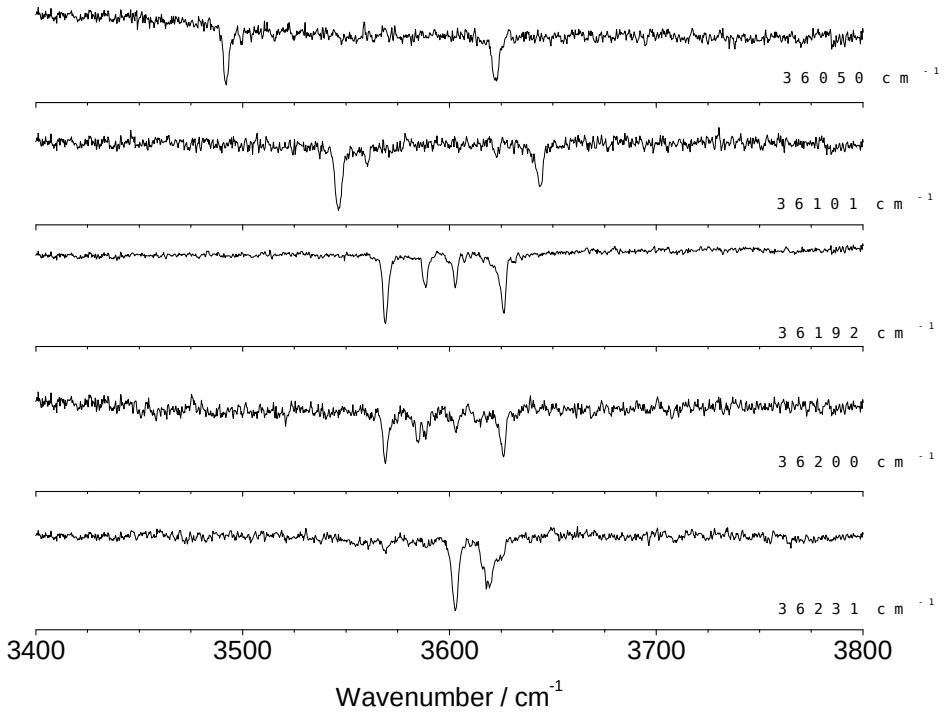

Figure 5.229a. *IDIR spectra of propofol·phenol recorded tuning the probe laser at 36050, 36101, 36192, 36200 and 36231 cm^{-1}. As can be seen, some of the electronic transitions share more than one conformer.*

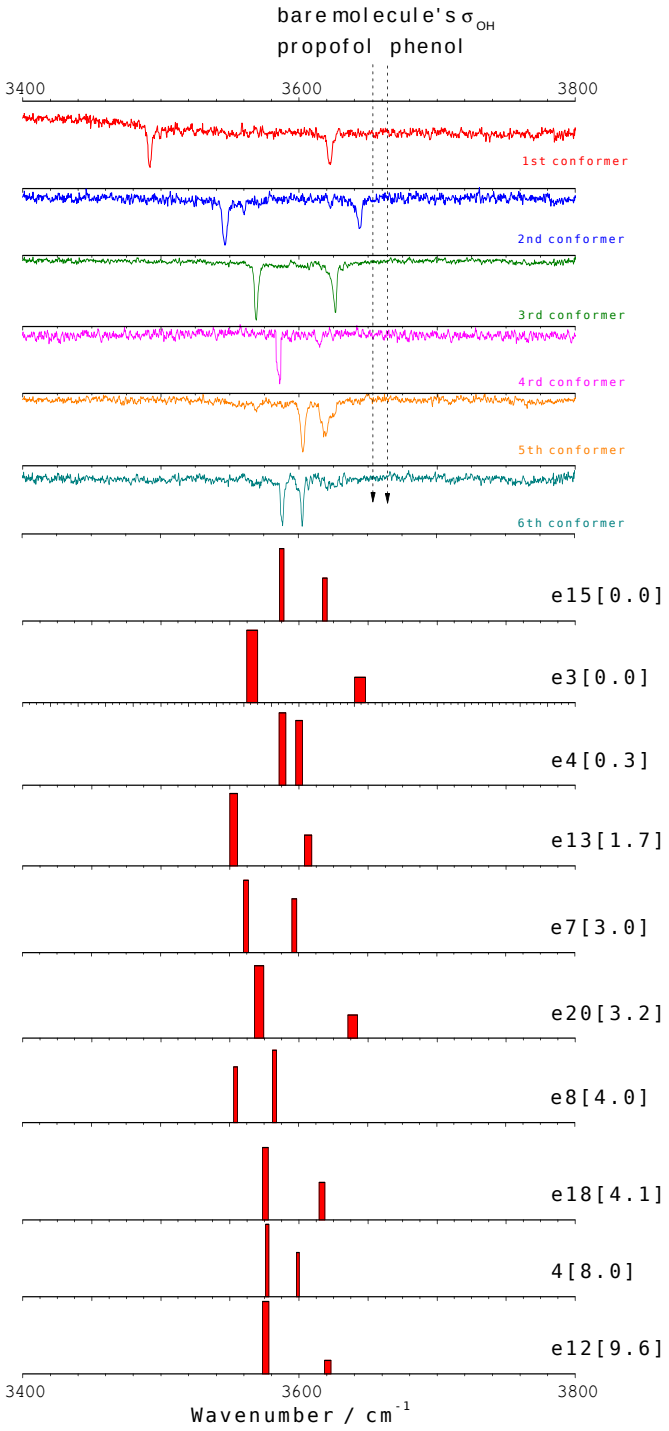

Figure 5.229b. *IDIR spectra of propofol·phenol recorded tuning the probe laser at 36050, 36101, 36192, 36200 and 36231 cm^{-1}. The predicted IR spectra for the most stable calculated structures are also shown for comparison. The numbers in brackets are the relative energies of the calculated conformers, in kJ/mol. A correction factor of 0.952 was applied. The predicted IR spectra of all the calculated structures are recorded in appendix 7.1 (Figure 7.46).*

Discussion

There is a great interest behind the study of this cluster, as it reproduces the interaction between propofol and phenol, the tyrosine's residue. It also has an intrinsic interest, as the interaction between these two monomers give rise to some interesting questions: both monomers are acids so, which molecule is more acidic? Is this system governed by dispersive interactions or by hydrogen bonds? This questions become more interesting when comparing to phenol dimer.[10,28-29] In the experimental structure found for this complex, one of the phenols is placed perpendicular to the other, acting as a proton donor. In contrast, in the propofol dimer, the voluminous isopropyl groups preclude formation of such structure. Consequently, propofol$_2$ adopts a stacking geometry with an additional dipole-dipole interaction between both OHs. Thus, such notable differences in their structures make interesting the mixed cluster.

One would expect propofol·phenol heterodimer to present a less complicated conformational landscape than propofol$_2$, as phenol has a single conformer. Conversely, the intermolecular PES exhibits a large number of minima. The smaller size of phenol compared to propofol results in an increasing on the number of relative orientations available. Furthermore, according to the calculations, when there is a hydrogen bonds interaction, from the energetic point of view it is almost indifferent which molecule acts as proton donor, as there is as low as 3 kJ/mol energy difference between both possibilities, which is well within the calculation error. Such observation answers one of our two previous questions: the isopropyl groups do not have a significant influence on the acid character of the molecule.

The study of the excitation spectrum shows that the first conformer's origin band is located at 36050 cm^{-1}. The second conformer's origin is blue shifted by c.a. 50 cm^{-1}, and the last three isomers seem to have a common transition at 36161 cm^{-1}. Propofol's origin band is located at 36222 cm^{-1} and that of phenol is at 36350 cm^{-1}, thus, it suggests a strong hydrogen bond between the molecules for the first and second conformers, and a weaker for the latter. Similarly to what it is observed for other systems, depletion of the first three conformers is observed when He is replaced by Ne or Ar, probably due to isomerization to the rest of the species.

It is clear from Figure 5.229 that a complete assignment is not possible due to the similarity of several of the calculated spectra and therefore, it is important to classify

the structures into families, taking the similarity between the calculated spectra as a guide. Thus, structures *e2, e10 and e6* present spectra that reproduce the IR spectrum of the first conformer. Following the same criteria, the structure of the second conformer must be that of structures *e11 or e14*. A large number of structures reproduce the spectrum of the third conformer: *e3, e13, e20, e12, e16* and *e19*. Finally, it is highly speculative to establish a separated assignment for isomers third to sixth, due to the similarity of their spectra (their OH stretching modes are within only 15 and 20 cm^{-1} difference). Therefore, their structure must be considerably similar and close to structures *e15, e4, e7, e8, e18* and *4*.

In the **first group** (Figure 5.230) the **phenol acts as a proton donor** at a bond distance of 186 pm, which means that a **strong hydrogen bond** is formed and the O-H···O angle, 170º, also confirms such assumption. The predicted spectra for this type of structures are in agreement with that of the **first conformer**. Furthermore, the observed **red shift**, 0_0^0 transitions located at 36050 cm^{-1}, is also in agreement with the proposed assignment. For example, a red shift of 354 cm^{-1} is observed in phenol·W_1 (0_0^0 is at 36350 cm^{-1} for phenol[8-11,13] and at 35996 cm^{-1} for phenol·W_1[12-13]). Although considerably larger than in the present system, due to a stronger hydrogen bond, in both systems phenol acts as a proton donor. If the observed shift is mainly due to changes in the strength of the hydrogen bond, this means that phenol is acting as chromophore. However, there is also a clear interaction between both rings and the change in its strength upon excitation may account also for a large part of the shift. In such case, it may even compensate for a blue shift due to the weakening of the hydrogen bond upon excitation, implicating that it is propofol the cluster's chromophore.

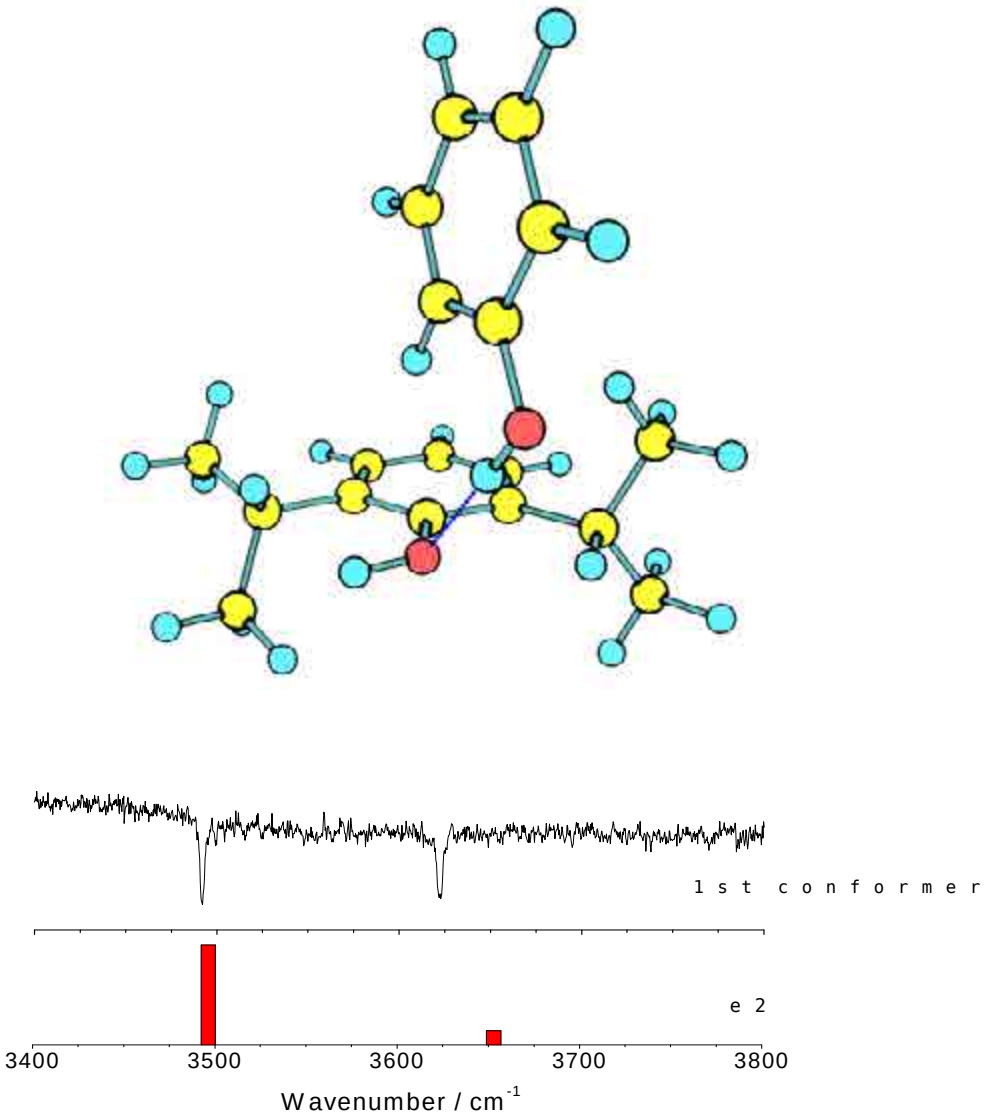

Figure 5.230. *A detailed view of structure e2 that is representative of the first group. The structures in this group are stabilized by a phenolic strong hydrogen bond. The predicted spectra for this type of structures match that of the first conformer.*

A close look to the **second group** shows that in all the structures **propofol acts as a proton donor**. As figure 5.231 shows, the phenol molecule can be both perpendicular and facing propofol's aromatic ring (structure *e7*) or almost parallel and opposing it (structure *e11*). Only the spectrum of the latter matches the experimental IR results of the **second conformer**. In this case, the hydrogen bond distance is of c.a. 190 pm and the angle is of c.a. 160º indicating a slight reduced strength respect to the previous family, but still a **moderate hydrogen bond**. A **red shift** is also found for this structure, although smaller than in the case of the first conformer, as in this case the

origin band is located at 36101 cm^{-1}. Such observation suggests that propofol is acting as chromophore in this cluster, while phenol is the chromophore in the first conformer.

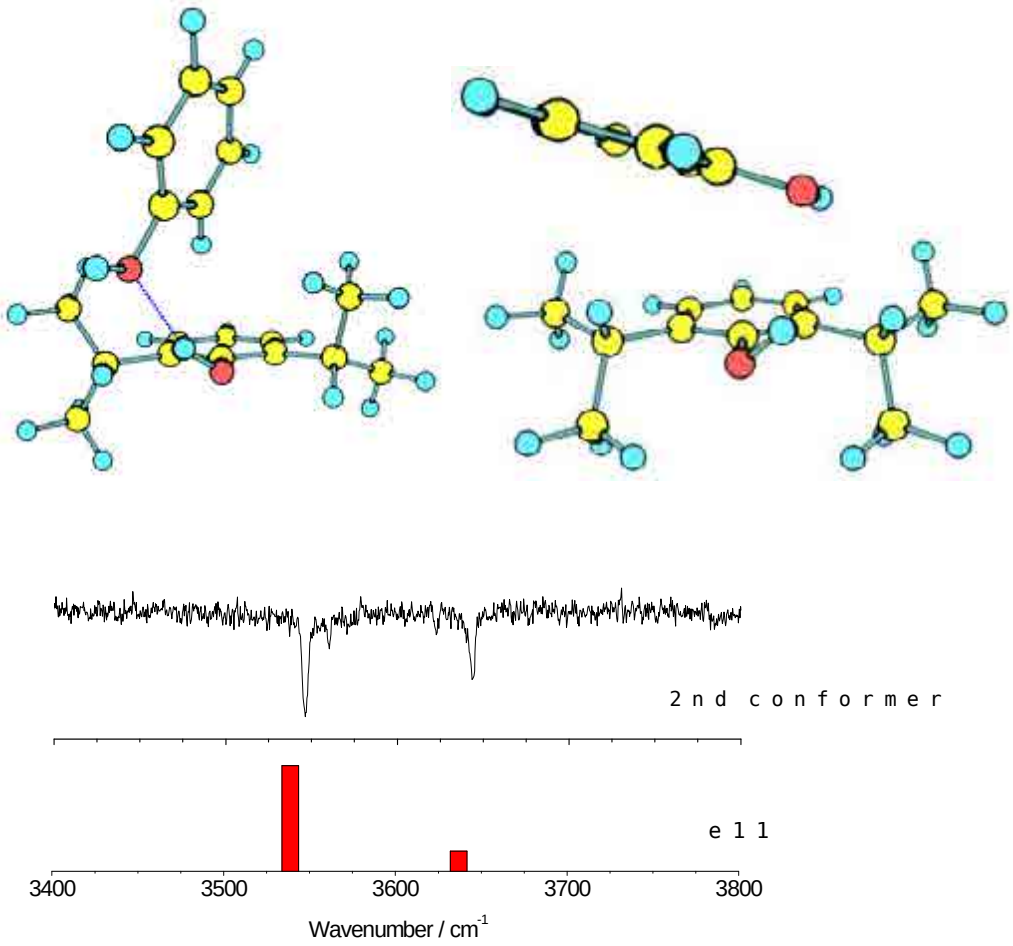

Figure 5.231. *A detailed view of structures e11 and e7. The structures in this group are stabilized by a propofol's strong hydrogen bond. The former is representative of the second group and, as can be seen, its spectrum matches the experimental one for the second conformer.*

A **third group** can be formed by those structures in which phenol's ring is **stabilized by dispersive forces** as it interacts with one of the isopropyl groups and, at the same time, the two OH moieties present an angle of c.a. 135º, indicating an **interaction mid-way between a dipole-dipole and hydrogen bond** (structure *e3* in Figure 5.232). Such interaction is weaker than the hydrogen bond in the previous groups and therefore results in a smaller shift in the OH stretching in the IR spectrum, reproducing the spectrum obtained for the **third conformer**.

The remaining spectra are very similar, presenting all of them small shifts in the OH stretching modes respect to the bare molecules (3650 cm^{-1} for propofol and 3660 cm^{-1} for phenol[8]). Accordingly, such spectra are assigned to structures in which there is a weak **dipole-dipole interaction** between the two OH moieties. The **fourth, fifth and sixth conformers** belongs to this group. An example of such conformers is presented in Figure 5.208, where a comparison between structure *e3*, assigned to the third group and *e4* (assigned to the fourth group) is offered. As can be seen, the only difference lies in the position of the propofol's OH moiety with respect to that of phenol's OH group.

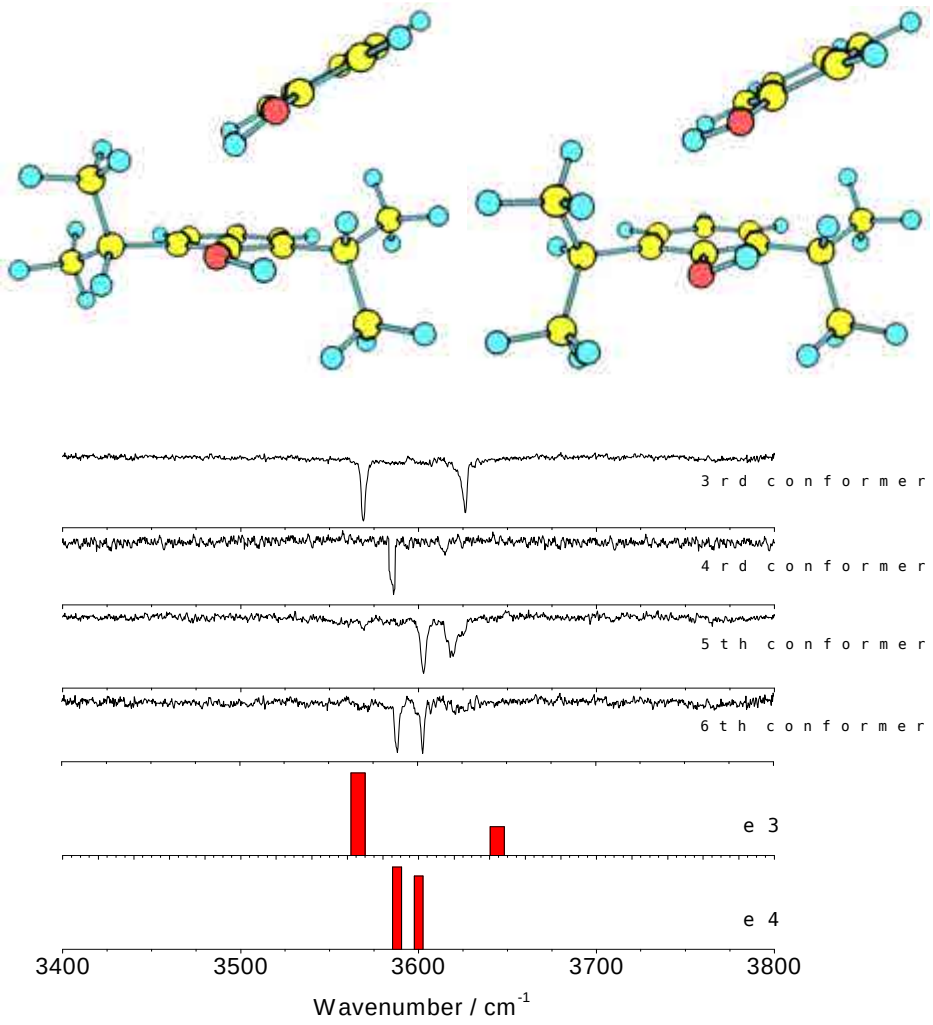

Figure 5.232. *A detailed view of structures e3 (upper panel - left) and e4 (upper panel - right). The difference lies in a weak hydrogen bond for the former and a dipole-dipole interaction for the latter. The former belongs to the third group and matches the experimental results for the third conformer, while the latter matches the rest of the experimental conformers: fourth, fifth and sixth conformers.*

Figure 5.233 summarizes the assignments, remarking that a wide range of interactions, from strong hydrogen bond to weak dipole-dipole, were found. Furthermore, both molecules alternate their donor-acceptor roles.

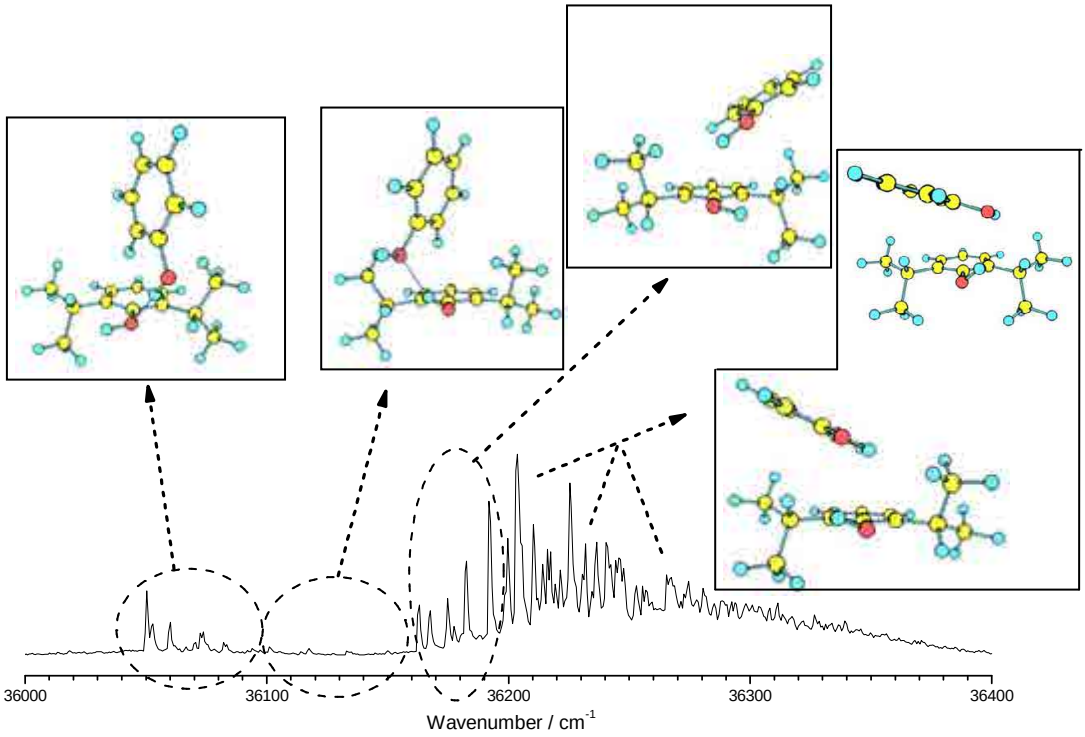

Figure 5.233. *2c-REMPI spectrum of the propofol.phenol cluster in the 36000 – 36400cm^{-1} region with the assigned structures. A wide range of interactions between the two molecules is observed experimentally.*

The proposed assignment also correlates with the S_1 lifetimes found for the detected conformers (see appendix 7.2, Figure 7.55, for further details). The lifetimes of the first and second conformers are of c.a. 12 ns, while those of the rest of the conformers are c.a. 5 ns. Apparently, the formation of a propofol-OH···OH-Phenol hydrogen bond lowers propofol's OH stretching vibration, resulting in a smaller S_1-S_0 coupling for internal conversion, as demonstrated for the propofol·W_1 complex (see section 5.2). The rest of the conformers, third to sixth conformers, present weaker O-H···O-H interactions and the lifetime is shorter due to a weaker $S_1 \leftarrow S_0$ coupling. Consequently, the result is a faster internal conversion rate.

Assignment in Figure 5.233 can also explain the population transfer observed when Ne or Ar are used instead of He. Figure 5.234 shows the SEP, calculated at

M06-2x/6-31G++(d,p), obtained for structures *e3* (upper panels) and *e11* (lower panels), rotating the isopropyl groups in 30º steps. All the detected species are located in such surfaces (Figures 5.235 and 5.236), demonstrating that it is propofol's conformation which ultimately affects the position of phenol. The barriers between minima in the SEP built taken structure *e3* as starting point are too high to explain the observed depopulation effect. However, those found in the structure *e11* surface will allow it. The main difference between the surfaces is phenol's OH orientation: pointing towards propofol's ring in structure *e3* and away from it in structure *e11*. If one takes into account that both types of structures may be connected by proton tunneling and that several other degrees of freedom may be at play in the isomerization process, one may expect low-enough barriers to allow population transfer due to collisions with Ne and/or Ar.

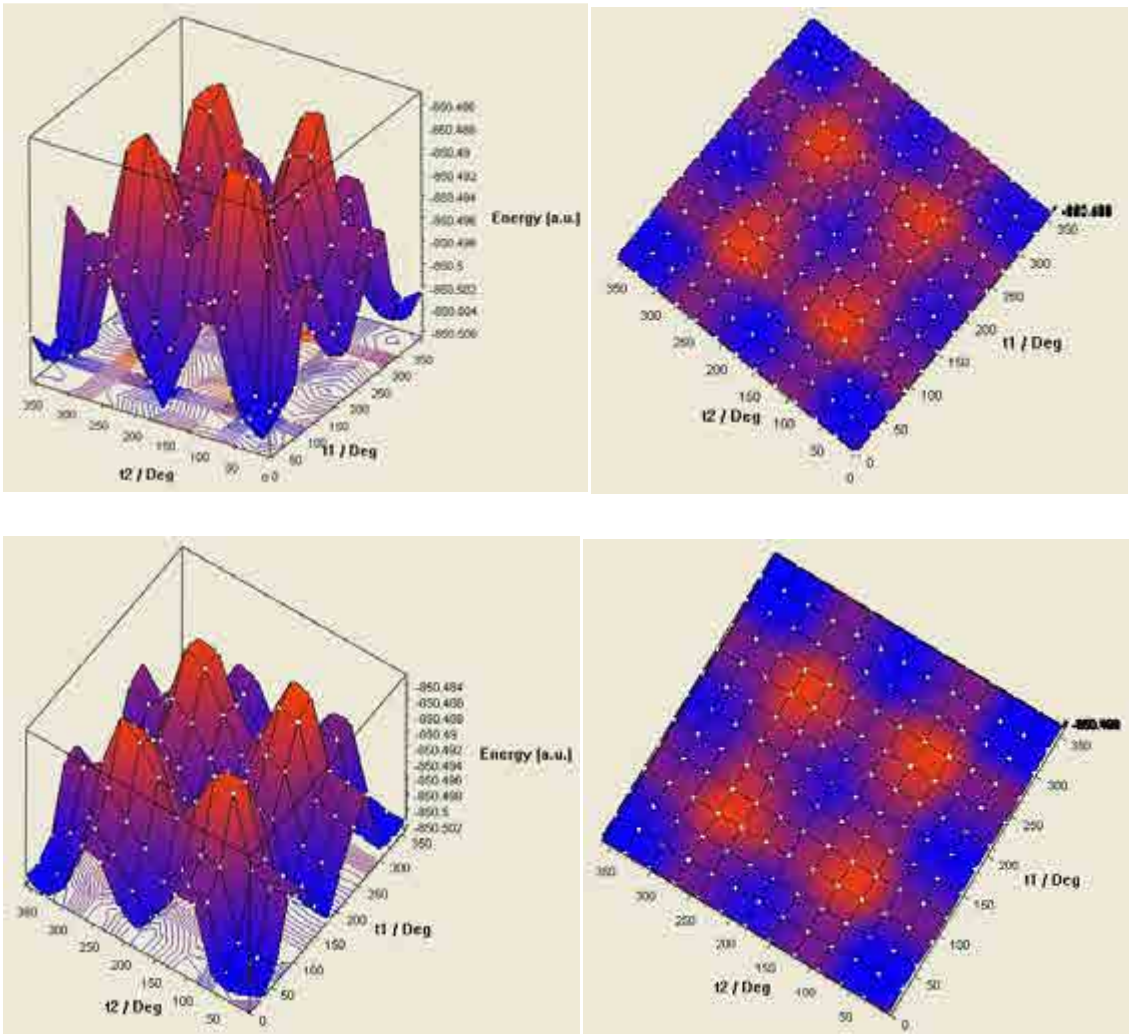

Figure 5.234. *SEP of structures e3 (upper panels) and e11 (lower panels).*

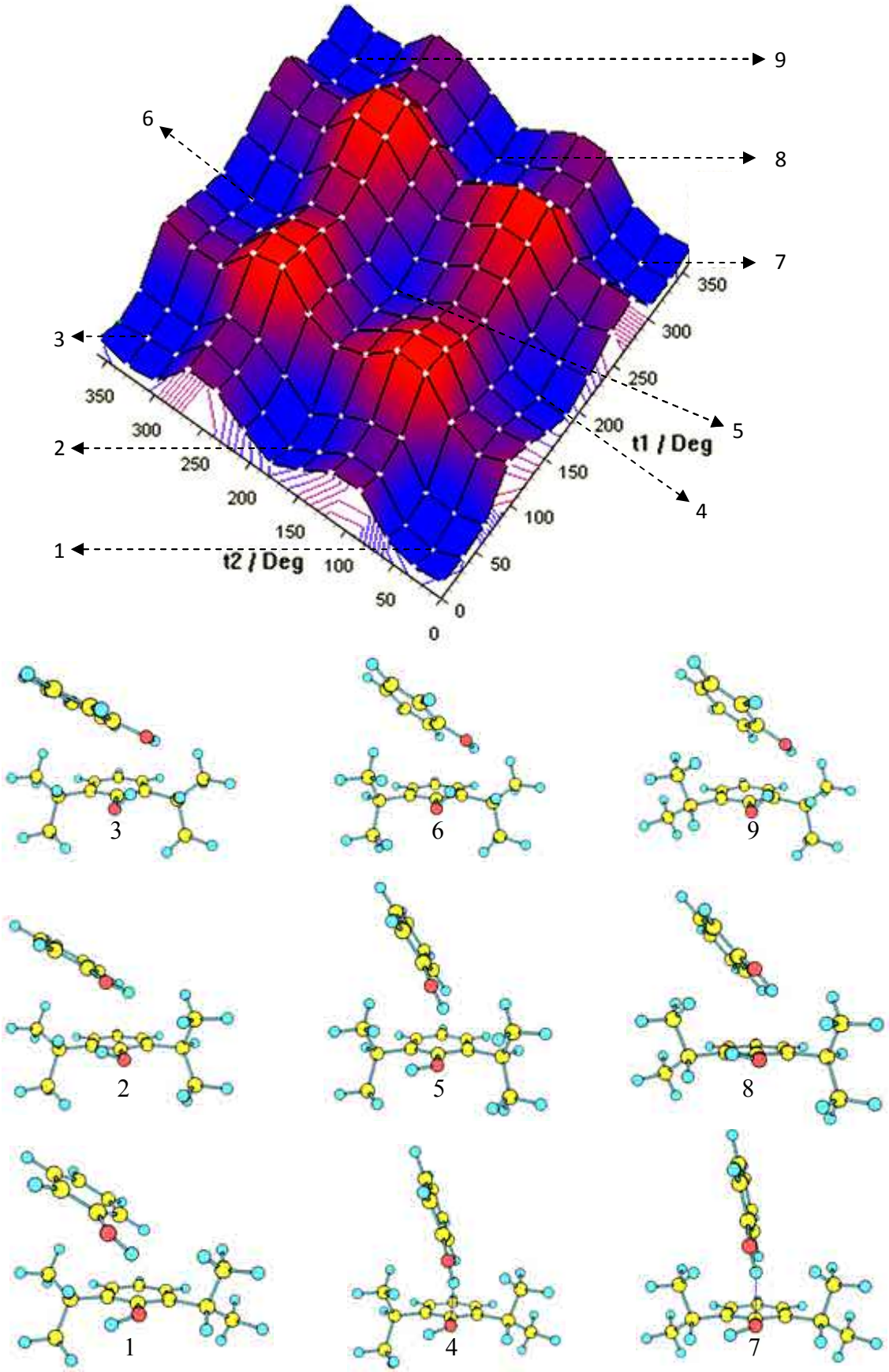

Figure 5.235. *SEP of structure e3.*

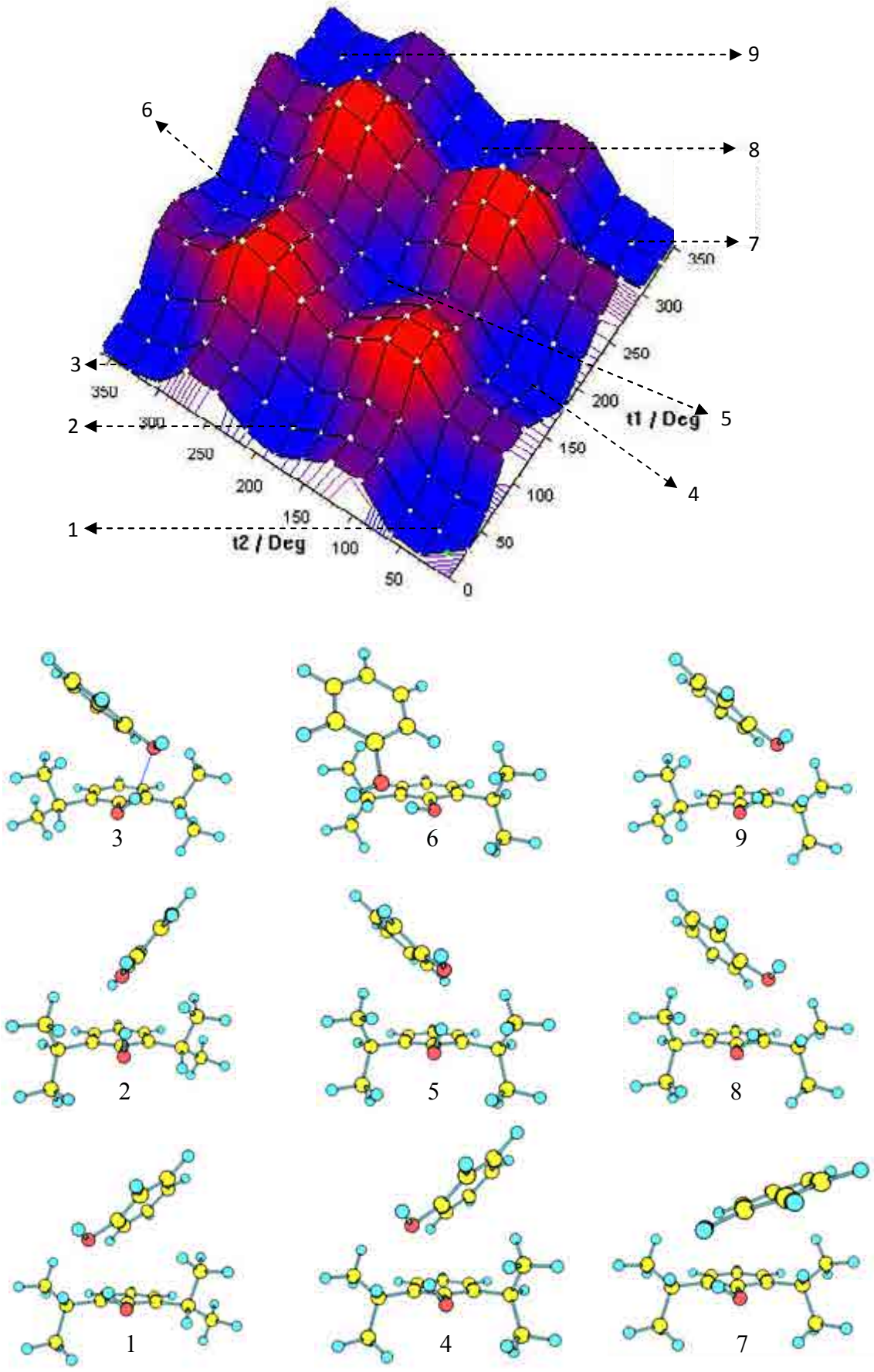

Figure 5.236. *SEP of structure e11.*

Moreover, taking into account the conformational changes observed in propofol upon excitation, one would expect such changes to also take place in propofol·phenol, resulting in several species sharing a common excited state, as observed for propofol·W_1. Such observation explains the similarity of the vibrational spectra of some of the detected conformers. Hints on the existence of such excited state conformational change are also found when the S_1 IDIR spectrum is recorded for the first and second conformers (the short S_1 lifetime of the rest of the conformers hampers obtaining their S_1 IR spectra). The spectra for the first conformer, shown in Figure 5.237, clearly show four peaks in the spectrum of the first conformer's S_1 state, separated by less than 10 cm^{-1}. That the two additional bands are due to a new conformer and not to Fermi resonances or combination bands is demonstrated by the IR-IR-UV triple resonance experiment: probing the band at 3616 cm^{-1}, only two bands are detected. Therefore, the bands at 3335 and 3616 cm^{-1} are due to the probed conformer, while the bands at 3326 and 3623 cm^{-1} may be due to another isomer formed upon excitation, may be due to tunneling effect in S_1 or to FCF that allow promoting the probed isomer into two different minima of the S_1 state.

The same effect was observed for propofol$_2$: the two peaks of the first conformer split into four peaks in the S_1 state (section 5.3, Figure 5.99). Comparison between the structure of the first conformer of the dimer and propofol·phenol first conformer shows very close structures, indicating a common mechanism for the peak splitting.

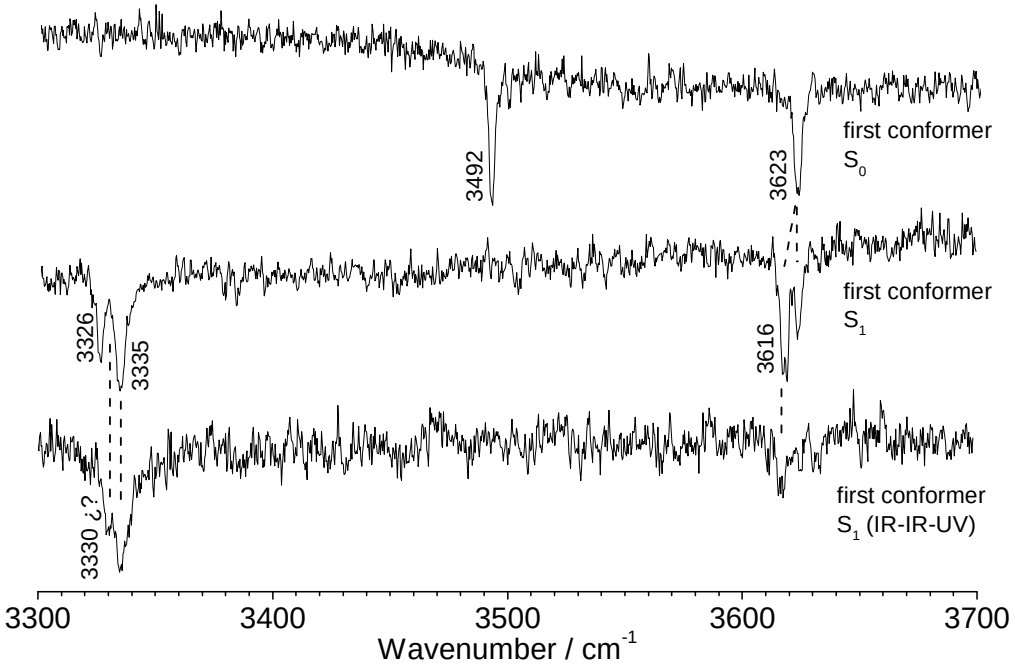

Figure 5.237. *S_1 IDIR spectrum for the first conformer. The experiment points to the existence of two conformers which is confirmed with an IR-IR-UV experiment. A new OH stretching at 3330 cm^{-1} could point to the presence of a third conformer.*

An IDIR in the excited state of the second conformer was also done as shown in Figure 5.238, however the S/N ratio is not as good as for the first conformer, and therefore the data are not conclusive.

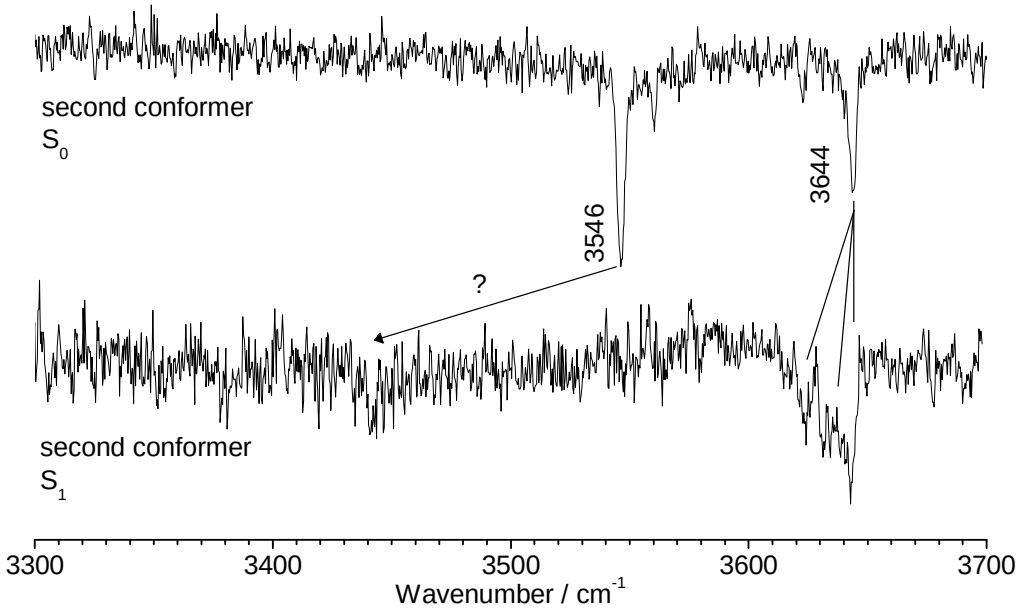

Figure 5.238. *S_1 IDIR spectrum for the second conformer. The experiment points to the existence of more than one conformer.*

Finally, the relative orientation of the aromatic rings also deserves some attention. While in the first and second groups (and hence the first and second conformers) phenol's aromatic ring is more perpendicular to propofol molecule's aromatic ring, and thus the excited state electronic transitions are due only to one of the chromophores, in the third-to-six conformers, it lies nearly-parallel, and thus when a transition occurs, an excitation transfer from one of the aromatic rings to the other could follow, further stabilizing the cluster. Furthermore, when two identical molecules come in close proximity, their transition dipole moments interact during the electronic excitation. This is the, so-called, excitonic coupling, which produces a splitting inversely proportional to the distance and that depends on the angle between the two rings. In our system, the ring-ring distance is very small, which should result in a shift of the order of hundreds of cm^{-1} but as the rings are at an angle close to the magic angle $\theta = 54.7^{o}$, the dipoles should appear as almost non-interacting, which fits very well with the 2.6 cm^{-1} splitting observed for the first conformer's 0_0^0 transition, reinforcing the assignment made.

Another observation is related to the theoretical calculations, for this is a good system to test the functionality and limitations of the most used level of theory during this work: the **M06-2x level of theory**. All the results obtained for this cluster are in good agreement with the predicted structures. The **relative energy** of the different **interactions** observed are predicted **with high accuracy** which, thanks to the He/Ne/Ar *2c-REMPI* experiment, we have been able to confirm, as the most stable structures are does predicted by M06-2x. Also, the less stable structures predicted by calculations were not observed experimentally. This can be corroborated, as the less stable structures (such as structure *2*) present no OH interaction of any type, being the cluster stabilized only by dispersive forces. These structures, found at a relative energy of 15.6 kJ/mol, present both OH moieties free and thus, their IR spectra do not match the experimental results for any of the conformers. Additionally, this level of theory **also** reproduces accurately the experimental **IR spectra**.

5.7.2 – Propofol·isopropanol

According to the calculations at M06-2x/6-31+G(d) level, the most stable structures (Figure 5.239a) are those where the propofol acts as acid, hydrogen bonded to the isopropyl´s hydroxyl group. There are other contact points between the two molecules, but the distances and angles of such interactions seem to indicate that the hydrogen bond is the main interaction. Against what is found in all the previously studied systems, isopropanol has three different conformers, due to the two different orientations the OH moiety can adopt (Figure 5.239b). Nevertheless, due to the reduced size of the alcohol, the number of conformers found using molecular mechanics is not larger than in propofol·phenol. Thus, the main differences between calculated structures are the conformation adopted by phenol and if the alcohol is in the plane of propofol (structures *e9, e3, 14* and *e20*) or out of plane (structures *e7, e10, e21* and *e11*) as observed for propofol·W_1. Structures where the isopropanol molecule acts as proton donor appear over 7 kJ/mol higher in energy, and those with a dipole-dipole interaction over 12 kJ/mol.

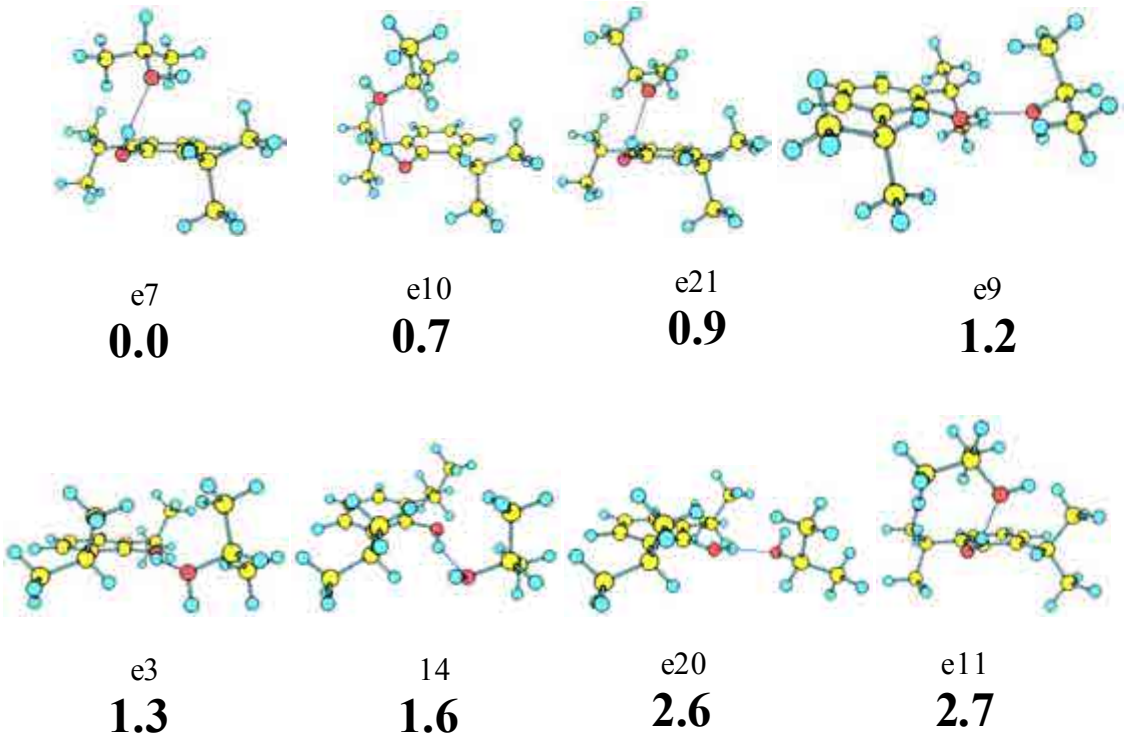

Figure 5.239a. *Propofol·isopronanol eight most stable conformers, calculated at M06-2x/6-31+G(d) level, with their relative energies in bold. Energy values are in kJ/mol. The whole set of calculated structures is collected in appendix 7.1(Figure 7.47).*

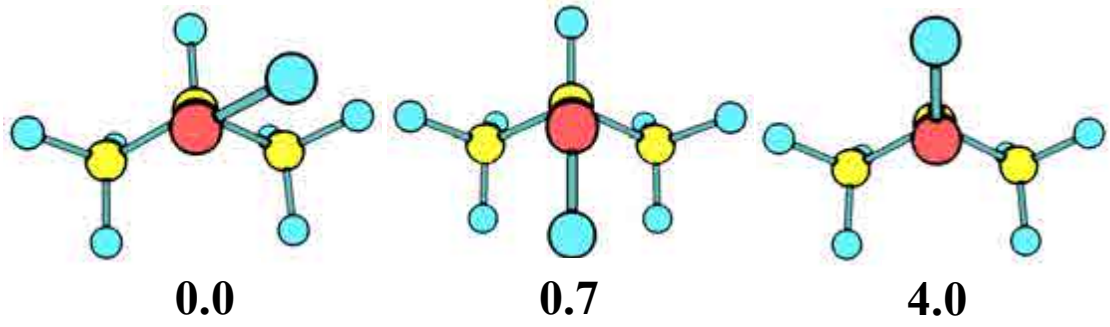

Figure 5.239b. *Isopropanol conformers calculated at M06-2x/6-31+G(d). Energy values are in kJ/mol. As can be seen, three conformers are found: staggered, opposed (trans) and eclipsed.*

Figure 5.240 shows the *2c-REMPI* spectrum of propofol·isopropanol. It is not easy to locate the 0_0^0 transition, due to the strong background and the spectral congestion, although it seems to be near 36000 cm^{-1}. Most of the intensity is accumulated in the first 100 cm^{-1}, of a spectrum that extends for more than 1500 cm^{-1}. The spectrum presents a background that is characteristic of molecules having CH_3 groups. If we compare this spectrum with the one obtained for the bare molecule, some common characteristics are found: the first transitions (the red-most ones) are very weak, and they start gaining in intensity in a few wavenumber, which for the bare molecule is due to a common transition in the excited state for different bare molecule isomers (GG and Gg). In order to test if a similar situation takes place in this system, a heavier gas was employed in the supersonic expansion and *2c-REMPI* spectra were recorded in different conditions, as shown in Figure 5.241. It can be clearly seen, that the peaks around 36000 - 36040 cm^{-1} disappear using neon instead of helium and, when it is replaced by argon, the peaks in the 36040-36054 cm^{-1} region also disappear.

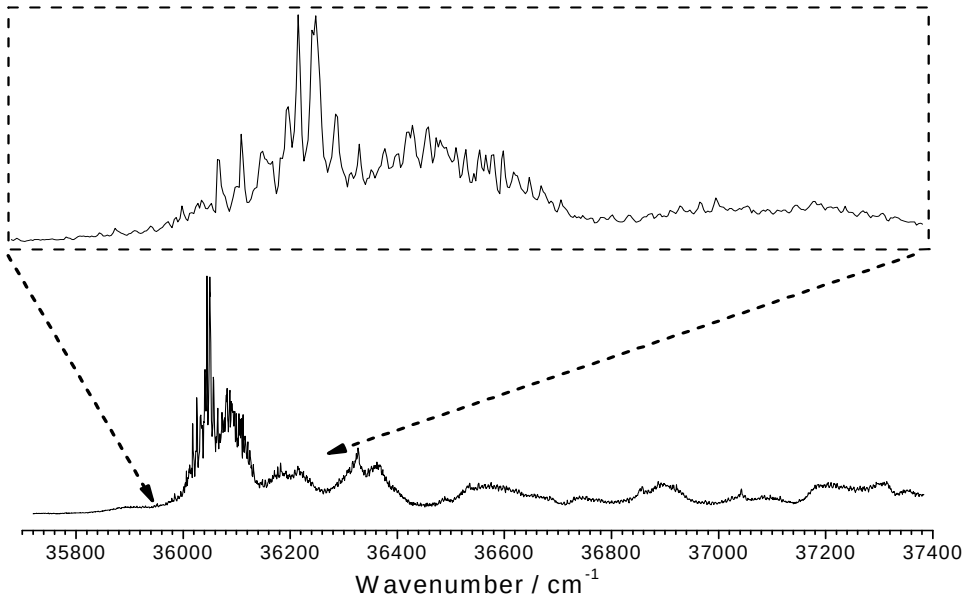

Figure 5.240. *2c-REMPI of propofol·isopropanol, in the 35700-37400 cm^{-1} region, recorded setting the probe laser at 27972 cm^{-1}. The insert shows a detailed view around the origin.*

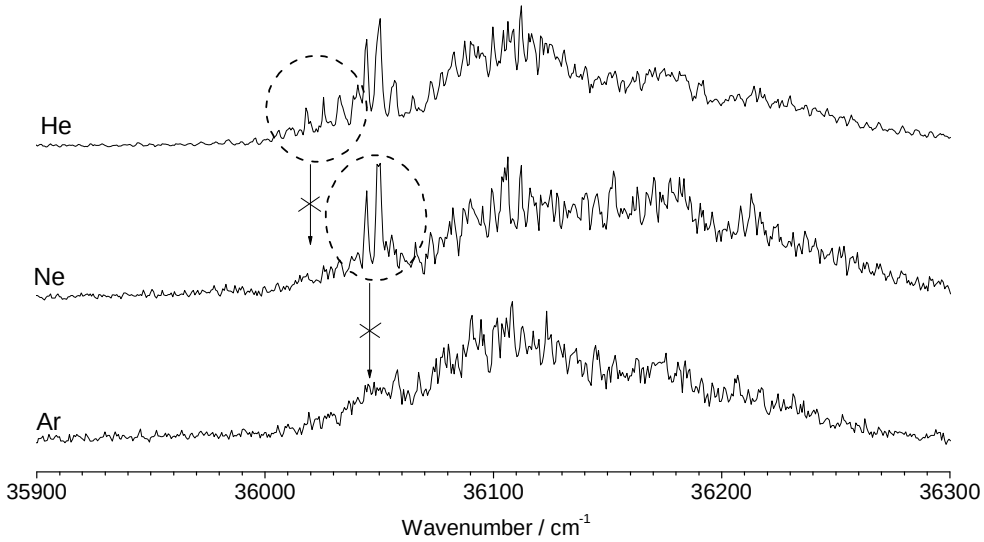

Figure 5.241. *2c-REMPI of propofol·isopropanol, in the 35900-36300 cm^{-1} region, recorded using helium (upper trace), neon (middle trace) and argon (lower trace). The circles highlight the transitions that experiment a change with the buffer gas.*

To determine the number of conformers, *hole burning* experiments were carried out probing the transitions at 36018, 36044 and 36109 cm^{-1}, finding three isomers, as can be seen in Figure 5.242. It is not clear where the origin band of the first conformer is, but it seems to be the weak peak located at 36001 cm^{-1}. The origin for the second conformer seems to be the intense peak at 36044 cm^{-1}, as when using neon as the buffer gas, the rest of the red-shifted peaks nearly disappear while this peak remains with the same intensity. Regarding the third conformer, it is not possible to ensure where its origin band is, but its main activity seems to be in the 36075-36115 cm^{-1} region, being the peaks that remain unaffected by the buffer gas employed.

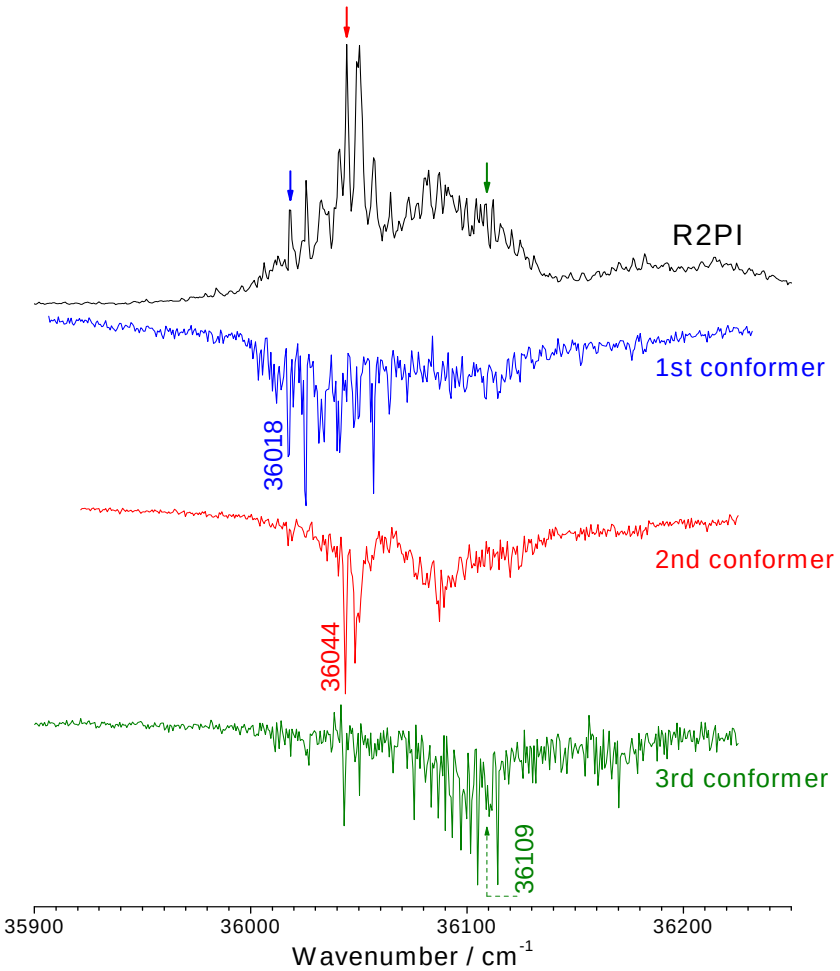

Figure 5.242. *Hole burning traces of propofol·isopropanol recorded tuning the probe lasers (2-color detection) at 36018, 36044 and 36109 cm^{-1}. The peaks noted with arrows indicate the transitions employed for recording the hole burning spectra, as well as the IDIRS trace for the corresponding conformer.*

In this system, IDIRS is not able to isolate the IR spectrum of each conformer, as shown in Figure 5.243, where the transition at 36044 cm^{-1} was probed. The spectrum obtained shows four OH stretching modes, due to the contribution of two conformers. Discriminating the contribution of conformer requires of an IR/IR/UV experiment, with two-colour detection. In this way, the three spectra in Figure 5.244 are obtained. The predicted IR spectra of some of the calculated structures are also shown. As can be seen, the spectra of the three conformers are very similar. The two OH stretching modes can be clearly appreciated at 3457 and 3641 cm^{-1} for the first conformer, 3471 and 3645 cm^{-1} for the second isomer, and at 3465 and 3643 cm^{-1} for the third one.

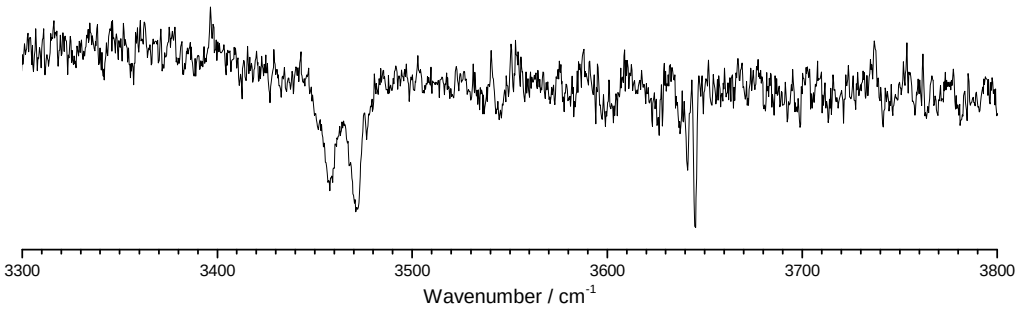

Figure 5.243. *IDIR spectrum of propofol·isopropanol recorded tuning the probe laser at 36044 cm^{-1}. The four peaks in the spectrum indicate contribution of two different conformers with overlapping transitions. In order to isolate each spectrum, a triple resonance experiment, IR/IR/UV, is necessary.*

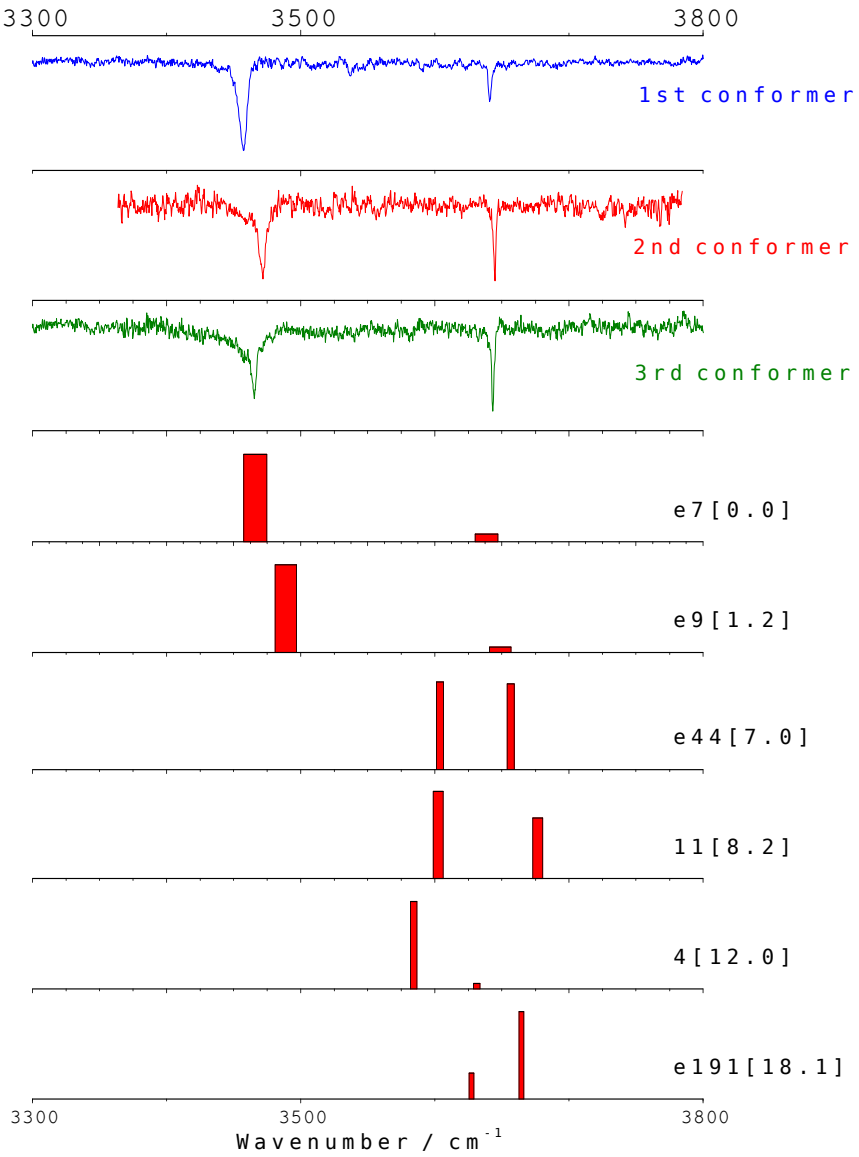

Figure 5.244. *IR-IR-UV spectra of propofol·isopropanol recorded tuning the probe laser at 36018, 36044 and 36109 cm^{-1}. The predicted IR spectra for the calculated structures for each of the interaction types are also shown for comparison. The numbers in brackets are the relative energies of the calculated conformers, in kJ/mol. A correction factor of 0.956 was applied. The predicted IR spectra of all the calculated structures are recorded in appendix 7.1 (Figure 7.48).*

Discussion

As demonstrate using the *hole burning* experiments, at least three conformers are present with 0_0^0 transitions very close to those found in propofol·W_1: 36000 cm^{-1} compared with the 36029 cm^{-1} for propofol·W_1 first conformer, pointing to a similar interaction in both cases. The additional shift found in propofol·isopropanol maybe due either to the additional stabilization supplied by the interactions due to dispersive forces, to a stronger hydrogen bond than that for propofol·water. This suggests that the propofol molecule is acting as a proton donor to the isopropanol molecule. An example of such possibility is illustrated in Figure 5.245 where structure *e7* is shown.

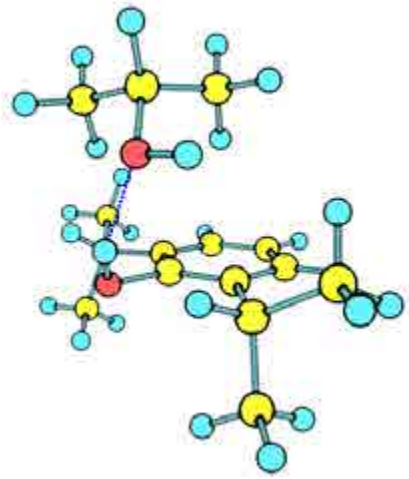

Figure 5.245. *Predicted most stable structure, e7, where propofol acts as acid in a hydrogen bond with isopropanol molecule. An additional H···π interaction stabilizes the system. This structure explains a larger red shift in the* 0_0^0 *transition than in propofol·*W_1.

In order to go further in the assignment, IR-IR-UV experiments were done for the three conformers, finding very similar IR spectra with two peaks: one at c.a. 3455 - 3470 and the other one around 3640-3646 cm^{-1}. The calculations (Figure 5.244) show six possibilities: a hydrogen bond with propofol acting as a donor and phenol out of the molecular plane interacting with the aromatic ring (structures *e7, e10, e21, e11, e1, e4, e5* and *e15*), the same structure but with isopropanol in plane, and therefore without the CH_3···π interaction (structures *e9, e3, 14, e20, e19, e6, e13, e22*, *e18, 5* and *6*), isopropanol acting as proton-donor (structures *e44, e47* and *8*), isopropanol acting as proton donor to the aromatic ring in an O-H···π interaction (structures *11, 15* and *13*), a

dipole-dipole interaction between both OH moieties (structures *4, 9, 2, 7, 10* and *3*) and the two molecules attached by dispersive forces only (structures *e191* and *12*). Figure 5.246 shows one structure of each type.

From an energetically point of view, the propofol acting as acid either *in-plane* or *out-of-plane*, are the most favorable ones, followed by the phenol acting as acid, which is 7 kJ/mol less stable, isopropanol stabilized by a O-H···π with the aromatic ring of the propofol molecule at 8 kJ/mol over the global minimum, dipole-dipole interactions at 12 kJ/mol and the dispersive forces, which are, at least, 18 kJ/mol above the global minimum.

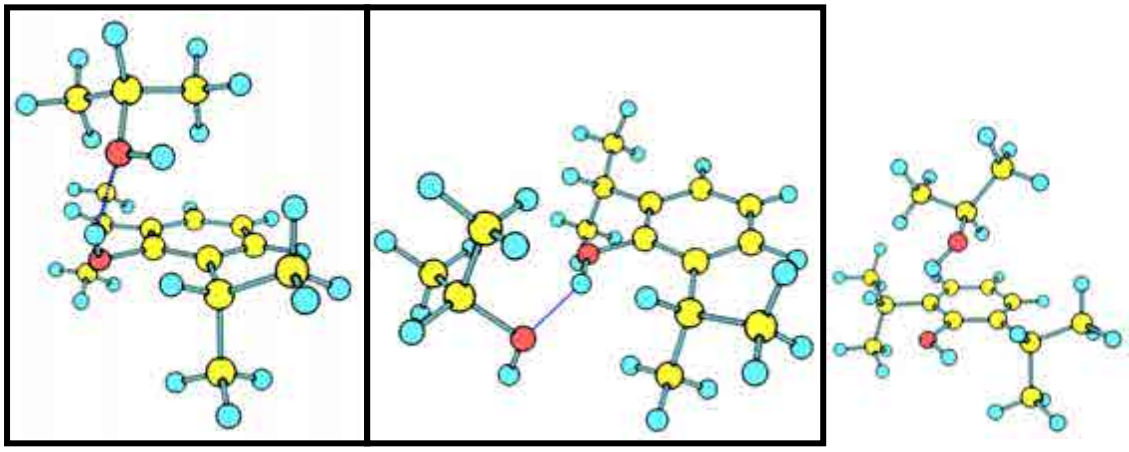

structure e7 ***structure e9*** ***structure e44***

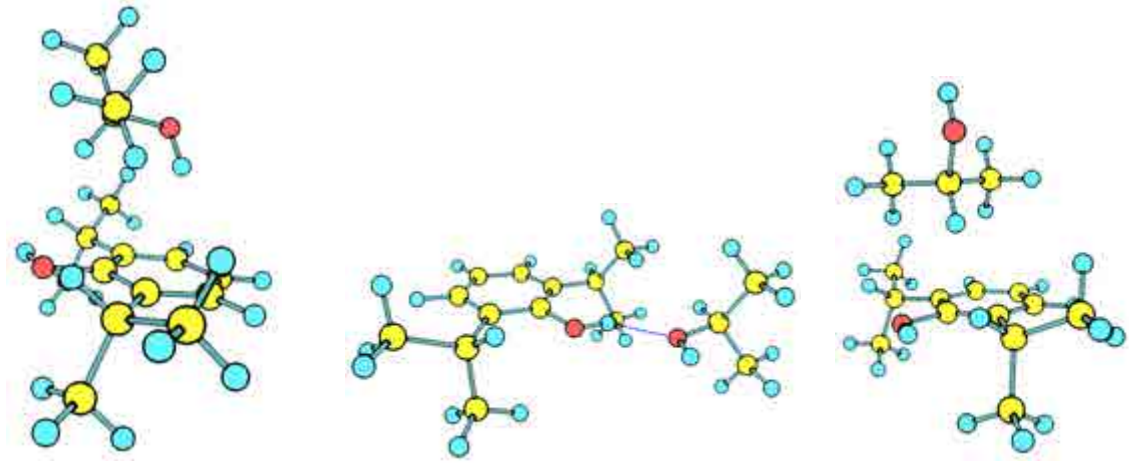

structure 11 ***structure 4*** ***structure e191***

Figure 5.246. *Representative structures for each of the interaction types found in the exploration of the conformational landscape: from left to right, structures e7, e9, e44, 11, 4 and e191. The structures in boxes are those whose calculated spectra reproduce the experimental ones.*

The comparison between the experimental results and the predicted IR spectra clearly shows that the detected conformers present a hydrogen bond, with propofol acting as proton donor, although it is not possible to distinguish whether there is a $CH_3\cdots\pi$ or not, as the predicted spectra for both interaction types are almost identical.

Surprisingly, a comparison between propofol·isopropanol and propofol·W_1 structures show that the former presents a stronger hydrogen bond, as indicated by the structural parameters: it presents a shorter O-H···O-H distance and a wider O-H···O angle. Figure 5.247 shows a comparison between the two possible propofol·isopropanol structures: *in-plane* and *out-of-plane* and the propofol·W_1 homologues.

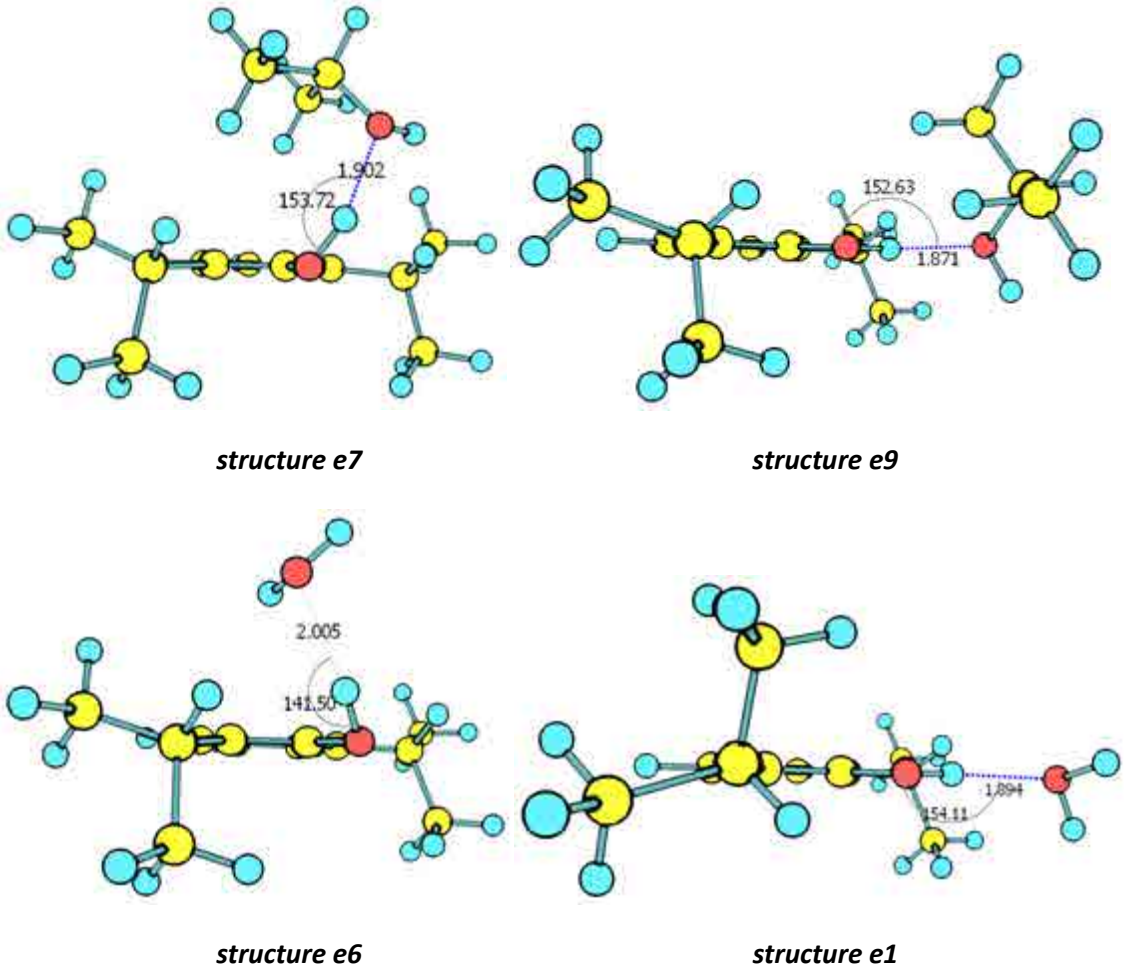

Figure 5.247. *Comparison between the two possible propofol·isopropanol structures (upper panels) and the propofol·W_1 homologues (lower panels). The structures to the left are those with an out-of-plane configuration while those to the right show an in-plane configuration.*

5.7.3 – Propofol·phenol and propofol·2-propanol: Discussion

In this work we demonstrate that for propofol·phenol complex, there are at least six conformers. All of them present O-H···O-H interactions with the only difference in the type of interaction: phenol acting as a proton donor, propofol acting as a proton donor, or both molecules taking part in a dipole-dipole interaction. We have also probed that these conformers are connected by a complex potential energy surface that implicates the rotating of the isopropyl and OH groups and the phenol's aromatic ring position with respect the propofol's ring. Such character may explain the mobility propofol presents inside the cavity as the results obtained by X-ray diffraction suggest.

We also demonstrate that for the propofol·isopropanol system several conformers are present, where the propofol molecule always acts as acid to the isopropanol molecule, with the latter being either in an *in-plane* or an *out-of-plane* configuration, while stabilized by dispersive forces with the propofol's aromatic ring. The binding energy of propofol·phenol and propofol·2-propanol systems is similar, as it is around 30-35 kJ/mol. Thus, there must be a competence between both residues for the hydrogen of propofol's OH moiety, and the shape of the cavity will discriminate between the two possible interactions.

5.8 – References

1. A. Lesarri, S. T. Shipman, J. L. Neill, G. G. Brown, R. D. Suenram, L. Kang, W. Caminati, B. H. Pate, "Interplay of Phenol and Isopropyl Isomerism in Propofol from Broadband Chirped-Pulse Microwave Spectroscopy." *Journal of the American Chemical Society,* **132**, 13417-13424 (2010).

2. S. F. Boys, F. Bernardi, "Calculation of Small Molecular Interactions by Differences of Separate Total Energies - Some Procedures with Reduced Errors." *Molecular Physics*, **19**, 553-566 (1970).

3. S. F. Boys, F. Bernardi, "The calculation of small molecular interactions by the differences of separate total energies. Some procedures with reduced errors (Reprinted from Molecular Physics, vol 19, pg 553-566, 1970)." *Molecular Physics*, **100**, 65-73 (2002).

4. A. Lesarri, S. T. Shipman, J. L. Neill, G. G. Brown, R. D. Suenram, L. Kang, W. Caminati, B. H. Pate, "Interplay of Phenol and Isopropyl Isomerism in Propofol from Broadband Chirped-Pulse Microwave Spectroscopy." *Journal of the American Chemical Society*, **132**, 13417-13424 (2010).

5. A. Sur, P. M. Johnson, "Radiationless Transitions in Gas-Phase Phenol and the Effects of Hydrogen-Bonding." *Journal of Chemical Physics*, **84**, 1206-1209 (1986).

6. R. J. Lipert, G. Bermudez, S. D. Colson, "Pathways of S1 Decay in Phenol, Indoles, and Water Complexes of Phenol and Indole in A Free Jet Expansion." *Journal of Physical Chemistry*, **92**, 3801-3805 (1988).

7. T. Ebata, N. Mizuochi, T. Watanabe, N. Mikami, "OH stretching vibrations of phenol-(H2O)(1) and phenol-(H2O)(3) in the S-1 state." *Journal of Physical Chemistry*, **100**, 546-550 (1996).

8. T. Watanabe, T. Ebata, S. Tanabe, N. Mikami, "Size-selected vibrational spectra of phenol-(H2O)(n) (n=1-4) clusters observed by IR-UV double resonance and stimulated Raman-UV double resonance spectroscopies." *Journal of Chemical Physics*, **105**, 408-419 (1996).

9. A. Oikawa, H. Abe, N. Mikami, M. Ito, "Solvated phenol studied by supersonic jet spectroscopy." *The Journal of Physical Chemistry*, **87**, 5083-5090 (1983).

10. K. Fuke, K. Kaya, "Electronic absorption spectra of phenol---(H2O)n and (phenol)n as studied by the MS MPI method." *Chemical Physics Letters*, **94**, 97-101 (1983).

11. O. Dopfer, K. Mullerdethlefs, "S-1 Excitation and Zero Kinetic-Energy Spectra of Partly Deuterated 1/1 Phenol-Water Complexes." *Journal of Chemical Physics*, **101** , 8508-8516 (1994).

12. T. Ebata, A. Iwasaki, N. Mikami, "Vibrational relaxation of OH and OD stretching vibrations of phenol and its clusters studied by IR-UV pump-probe spectroscopy." *Journal of Physical Chemistry A*, **104**, 7974-7979 (2000).

13. R. M. Helm, H. J. Neusser, "Highly resolved UV spectroscopy of clusters: isotope substitution studies of hydrogen-bonded phenol-water." *Chemical Physics*, **239**, 33-47 (1998).

14. C. Jacoby, W. Roth, M. Schmitt, C. Janzen, D. Spangenberg, K. Kleinermanns, "Intermolecular vibrations of phenol(H2O)(2-5) and phenol(D2O)(2-5)-d(1) studied by

UV double-resonance spectroscopy and ab initio theory." *Journal of Physical Chemistry A*, **102**, 4471-4480X (1998).

15. T. Ebata, A. Fujii, N. Mikami, "Structures of size-selected hydrogen-bonded phenol-(H2O)(n) clusters in S-0, S-1 and ion." *International Journal of Mass Spectrometry and Ion Processes*, **159**, 111-124 (1996).

16. H. Nury, C. Van Renterghem, Y. Weng, A. Tran, M. Baaden, V. Dufresne, J. P. Changeux, J. M. Sonner, M. Delarue, P. J. Corringer, "X-ray structures of general anaesthetics bound to a pentameric ligand-gated ion channel." *Nature,* **469** (7330) 428-431 (2011).

17. T. Ebata, "Study on the Structure and Vibrational Dynamics of Functional Molecules and Molecular Clusters by Double Resonance Vibrational Spectroscopy." *Bulletin of the Chemical Society of Japan*, **82**, 127-151 (2009).

18. M. N. R. Ashfold; B. Cronin; A. L. Devine; R. N. Dixon; M. G. D. Nix, *Science*, **312** (5780) 1637-1640 (2006)

19. C. J. Gruenloh, J. R. Carney, C. A. Arrington, T. S. Zwier, S. Y. Fredericks, K. D. Jordan, "Infrared spectrum of a molecular ice cube: The S-4 and D-2d water octamers in benzene-(water)(8)." *Science*, **276** (5319), 1678-1681 (1997).

20. C. J. Chai, K. D. Jordan, *J. Chem. Phys.* **95**, 3850 (1991).

21. T. Zwier, K. D. Jordan, *Science,* **276**, 1678 (1997).

22. C. J. Chai, K. D. Jordan, *J. Phys. Chem.* **97**, 5208 (1993).

23. R. J. Lipert, S. D. Colson, *J. Phys. Chem.,* **94**, 2358 (1990).

24. Ch. Janzen, D. Spangenberg, W. Roth, K. Kleinermanns, *J. Chem. Phys.*, **110**, 9898 (1999).

25. M. Dey and J. Grotemeyer, *Eur. Mass. Spectrom.*, **1**, 95 (1995).

26. R.N. Pribble, T. Zwier; *Science.*, **265**, 75 (1994).

27. C. Lee, H. Chen, and G. Fizgerald; *J. Chem. Phys.*, **102**, 1266 (1995).

28. L. Connel, S. Ohline, P. Joireman, T. Corcoran, P. Felker, *J. Chem. Phys.* **96**, 2585 (1992).

29. M. Schmitt, M. Böhm, C. Ratzer, D. Krügler, K. Kleinermanns, I. Kalkman, G. Berden, L. Meerts; *Chem. Phys. Chem.*, **7**, 1241 (2006).

30. C. J. Gruenloh, J. R. Carney, F. C. Hagemeister and T. S. Zwier, *J. Chem. Phys.*, **113**, 2290 (2000).

31. R. M. Shields, B. Temelso, K. A. Archer, E. T. Morrell, and G. C. Shields, *J. Phys. Chem.*, **114**, 11725 (2010).

32. Y. H. Li and E.C. Lim, *Chem Phys.*, **9**, 279 (1971)

33. R. J. Liert, G. Bermudez, S.D. Coloson, *J. Phys. Chem.*, **92**, 3801 (1988)

34. E. A. Meyer, R.K. Castellano, F. Driederich, *Angew. Chem. Int. Ed.*, **42**, 1210 (2003)

35. F. L. Gervasio, R. Chelli, P. Procacci, V. Schettino, *J. Phys. Chem*, **106**, 2945 (2002)

36. A. Lüchow, D. Spangenberg, C. Janzen, A. Jansen, M. Gerhards, K. Kleinermanns, *Phys. Chem. Chem. Phys.*, **3**, 2771 (2001).

37. J. M. Ugalde, I. Alkorta, J. Elguero, *Angew. Chem. Int. Ed.*, **39**, 717 (2000).

38. Himansu S. Biswal, E. Gloaguen, M. Mons, *J. Phys. Chem. A* (**DOI:** 10.1021/jp1119684, Publication Date (Web): March 17, 2011)

CHAPTER 6

CONCLUSIONS AND PERSPECTIVES

6 – Conclusions and perspectives

- **Solvation of propofol**

Examination of the whole hydration of the propofol molecule lead to the conclusion that **solvation of propofol is dominated by water self-aggregation**. Despite the two voluminous isopropyl groups that protect propofol's OH moiety from establishing strong hydrogen bonds, the water molecules are able to accommodate between the hydrophobic methyl groups an adopt geometries very similar to those of the pure water clusters. Such process requires propofol to renounce to four of its five conformational isomers, as only the isomer in which propofol's OH moiety is less shielded from the water molecules survives the solvation process. On the other hand, the isopropyl groups are an obstacle and thus there is a change in the energetic order of the predicted most stable structures, with compact structures staying behind. This also explains the **weak solubility of propofol**.

- **Stabilization forces: hydrogen bond vs. dispersive forces**

Propofol dimer presents a structure where one of the propofol molecules is always stacked above the other, so that one molecule's isopropyl group interacts with the other's aromatic ring by dispersive forces, while there is a dipole-dipole interaction between the OH moieties. The hydrophobity of the propofol is reflected in that **all** the **dimer·water** complexes studied **present a stacked-dimer** cluster, **exposing their OH** moieties to the water molecules, trying to adopt the most stable water geometry. This feature remarks the importance of both stabilization forces, and **remarks** that a complete understanding of **the π-π stacking is fundamental** to explain many supramolecular organization and recognition processes, as base pairing in the DNA supramolecular structure, side-chain interactions in proteins and intercalation of certain drugs with the DNA.

Following the tendency of the bare molecule hydratated species, only those isomers in which propofol's OH moiety is less shielded from the water molecules survives the solvation process.

- **Formation of micelles**

The stacking structures encountered in all the homomers further remarks the importance of both, hydrogen bonds and dispersive interactions and, it can explain many supramolecular organization and recognition processes, as DNA-base pairing in the DNA supramolecular structure or side-chain interactions in proteins. This study suggests that in this particular system, the **OH moieties guide** the molecules towards a ring formation, while **dispersive forces give** the cluster **its final shape**. Such observation is in agreement with the directional nature of the hydrogen bond and the lack of such directionality of dispersive forces. So the process can be envisioned as if the OH moieties give the direction of a vector, and the dispersive forces the orientation in the 3-dimensional space. In biological systems, as for example the three dimensional organization of DNA structures, the origin of the vectors is fixed due to the covalent interactions of the molecules inside each of the chains and thus, the orientation of the molecules is suggested to be mainly due to **the combination of this two interactions**, **producing the arrangement of supramolecular structures and thus the helicoidal structure**.

Finally, it is interesting how **propofol homomers** resemble the structure of reverse **micelles** (in non-polar solvents), like the water-in-oil system, which has its hydrophilic part in the core, while the hydrophobic part remains outside. Furthermore, **propofol homomers** probably are the **first case of nano-micellar** systems fully resolved using mass-selective laser spectroscopy.

- **Solvation of micelles**

It is interesting how the addition of a **single water molecule to propofol$_4$** is able to perturb these micelles as they interact with the monomer's OH moieties, **solvating** the propofol molecules. The results obtained clearly demonstrate that water can only attach to propofol$_n$ globular structures if they lose their micellar shape.

- **Biological implication**

The data obtained in this work complement those obtained by X-ray diffraction from the crystallized structures of propofol inside the active site of the $GABA_A$ receptor: comparing both sets of data, it is very likely that the isopropyl groups orientation in the X-ray structure is not correct. This is a striking observation as the structure presented in ref16 shows propofol in a conformation that is neither Gg nor GG, as one of the isopropyl groups is in a position that is a transition state in gas phase. Very likely, the resolution of the structure (3.3 Å) is not high enough to accurately determine the orientation of the isopropyl groups.

The authors also demonstrate, using molecular dynamic simulations, that propofol is not strongly attached to any of the interacting residue and that exhibits a significant mobility inside the cavity. This mobility observed for propofol inside the $GABA_A$ receptor cavity may be explained in the light of the present data: the **isopropyl groups do not allow the formation of a strong propofol-tyrosine hydrogen bond**, in the same way that they block the propofol-water interaction. Thus as we demonstrate in this work, for the solvation of propofol, the isopropyl group shield the OH group from hydrogen bond formations. Similarly, our studies between propofol and the amino acid residues also suggest that propofol molecule's isopropyl groups shield the OH moiety, although they are not able to block completely the interaction, they prevent propofol for establishing a strong hydrogen bond with Y254. **At room temperature**, their rotation must produce a continuous change in the interaction type forcing the phenol's OH moiety to change its role from acid to base, passing through a dipole-dipole interaction. The competence for the propofol's OH moiety between phenol and 2-propanol molecules makes the whole system to be quite enthropic and, as a result, the position of propofol inside the $GABA_A$ receptor cavity is not well defined at room temperature, and the anaesthetic molecule encounters many weak interactions that compete with the hydrogen bond formation explaining the **mobility of the propofol molecule in the cavity**.

Besides, the X-ray studies clearly show that propofol apart from interacting with the lateral chain of a tyrosine (Y254) and with a threonine residue establishing a hydrogen bond, the rest of interactions, are mainly established with non-polar groups which must interact with the aromatic ring of the propofol molecule.

- **Theoretical calculations**

Regarding the theoretical calculations, it is worthy to note that, as it is well known, MP2 level of theory overestimates the dispersive forces. Formation of the 1:1 complex is a competition between the ring and the OH solvation sites, although in all the detected species, water acts as proton-acceptor, in an *out of plane* configuration, as demonstrated by the comparison between predicted IR spectra and the IDIR traces. Calculations conducted at **MP2 level of theory, systematically fails** to predict correctly the energetic order of the 1:1 isomers, as they predict that those structures with *in plane* proton-acceptor water are more stable, and thus, **overestimate the importance of the HO-H···π interaction**, as they point to such structures as the most stable ones, while they are not observed experimentally.

For propofol·W_2 clusters, such effect is reinforced. While the MP2 calculations always predict the OH···π water-chain structures to be the most stable ones, experimentally we have detected only ring-like structures, although in this case, the chain-like structures are very dynamic and therefore, they may well experience such a geometry change upon excitation that there is no Frank-Condon window for the excitation. Therefore, the formation of such complexes in the expansion cannot be ruled out.

Because of the complexity of the potential surface for propofol·W_n bigger clusters, which arise from the large number of degrees of freedom, DFT calculation yield many possible structures and thus, for bigger systems, another level of theory more suitable was employed: **M06-2x**. It is worthy to note that this level of theory **yields excellent good results in both energetic order** of the structures **and** the predicted **IR spectrum** at a really **low computational cost**, even for the bigger clusters studied. It has shown outstanding results, and in most of the cases, the **experimental structures are** found to be those **within the predicted most stable ones** (see appendix 7.3 for more details). Note that for all the calculated species, the assigned structures are, at least, predicted among the first 80 structures given by molecular mechanics (a structure between *e1-e80* has been assigned) and in most of the cases within the first 30 structures.

- **Perspectives**

In future works it is likely to carry propofol studies in several directions:

- Higher homomers must be explored in order to investigate if bigger micelles are obtained.

- Solvation of such micelles has proven to be very interesting and thus, water molecules would be introduced in bigger systems, which leads to some interesting questions: propofol$_4$·W$_4$ must be a really interesting case, would it conform a cubic structure between the OH moieties? would a water molecule solvate the propofol pentamer and hexamer? if not, how many water molecule would be necessary?

- In parallel, the introduction of a non-polar solvent should also be interesting in order to test if they are able to reach the core of these micelles or if they remain interacting, due to dispersive forces, with the aromatic rings of these aggregates, confirming a water-in-oil system.

- Finally, the interaction between propofol and size-increasing residues of tyrosine and threonine must be explored in order to reproduce more accurately the interactions that take place in the active site. Thus, an ablation system is being prepared in our lab to produce these amino acids in supersonic expansions.

CHAPTER 7

APPENDIX

7 – APPENDIX

7.1 – Figures and tables for all the calculations.

All the figures and tables with the binding energies for the calculated structures are presented in the following pages. A comparison of the experimental IR spectra of the detected species with the predicted IR spectra for the calculated structures is also shown.

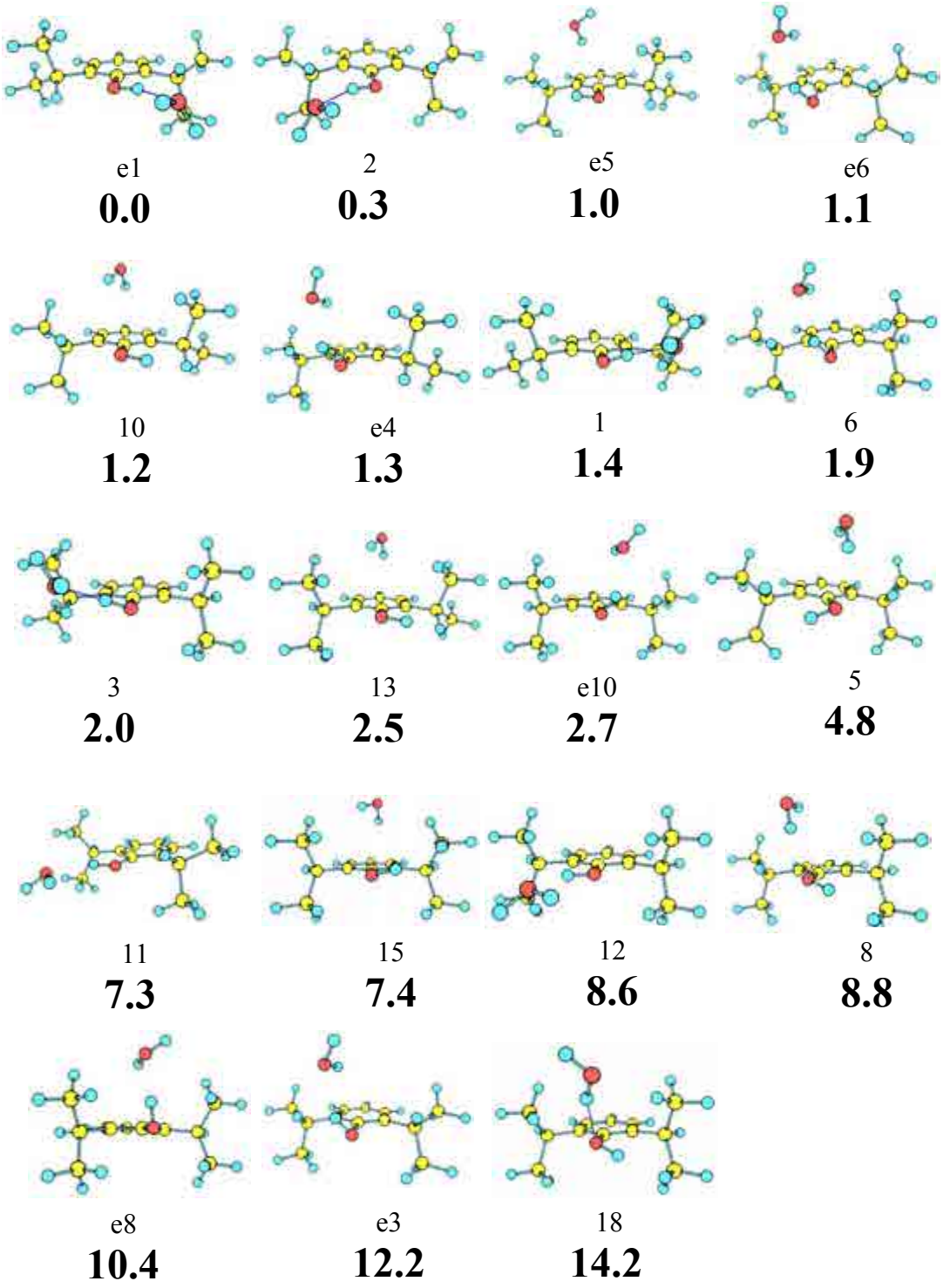

Figure 7.1. *Propofol·W_1 calculated structures at MP2/6-311++G(d,p).*

Table 7.1. *Propofol·W_1 structures with their relative energies and binding energies calculated at MP2/6-311++G(d,p).*

Structure	*ΔE (kJ/mol)*	*ΔE_{ZPE} (kJ/mol)*	*D_0 (kJ/mol)*	*BSSE (kJ/mol)*
e1	0.20	0.00	-13.35	11.37
2	0.00	0.30	-13.21	11.80
e5	3.11	1.02	-11.67	12.34
e6	1.55	1.12	-11.94	11.97
10	4.22	1.24	-9.78	13.73
e4	1.93	1.32	-11.22	12.18
1	0.85	1.37	-11.97	11.70
6	2.41	1.94	-11.40	12.50
3	2.20	2.02	-11.89	11.92
13	5.87	2.53	-9.79	13.52
e10	4.41	2.67	-10.94	12.23
5	4.96	4.81	-7.84	12.38
11	9.18	7.31	-11.15	11.11
15	10.23	7.40	-10.20	13.52
12	11.20	8.65	-11.23	11.25
8	8.85	8.77	-7.58	13.23
e8	11.91	10.40	-7.63	13.10
e3	12.55	12.23	-10.91	11.88
18	14.06	14.22	-6.09	10.82

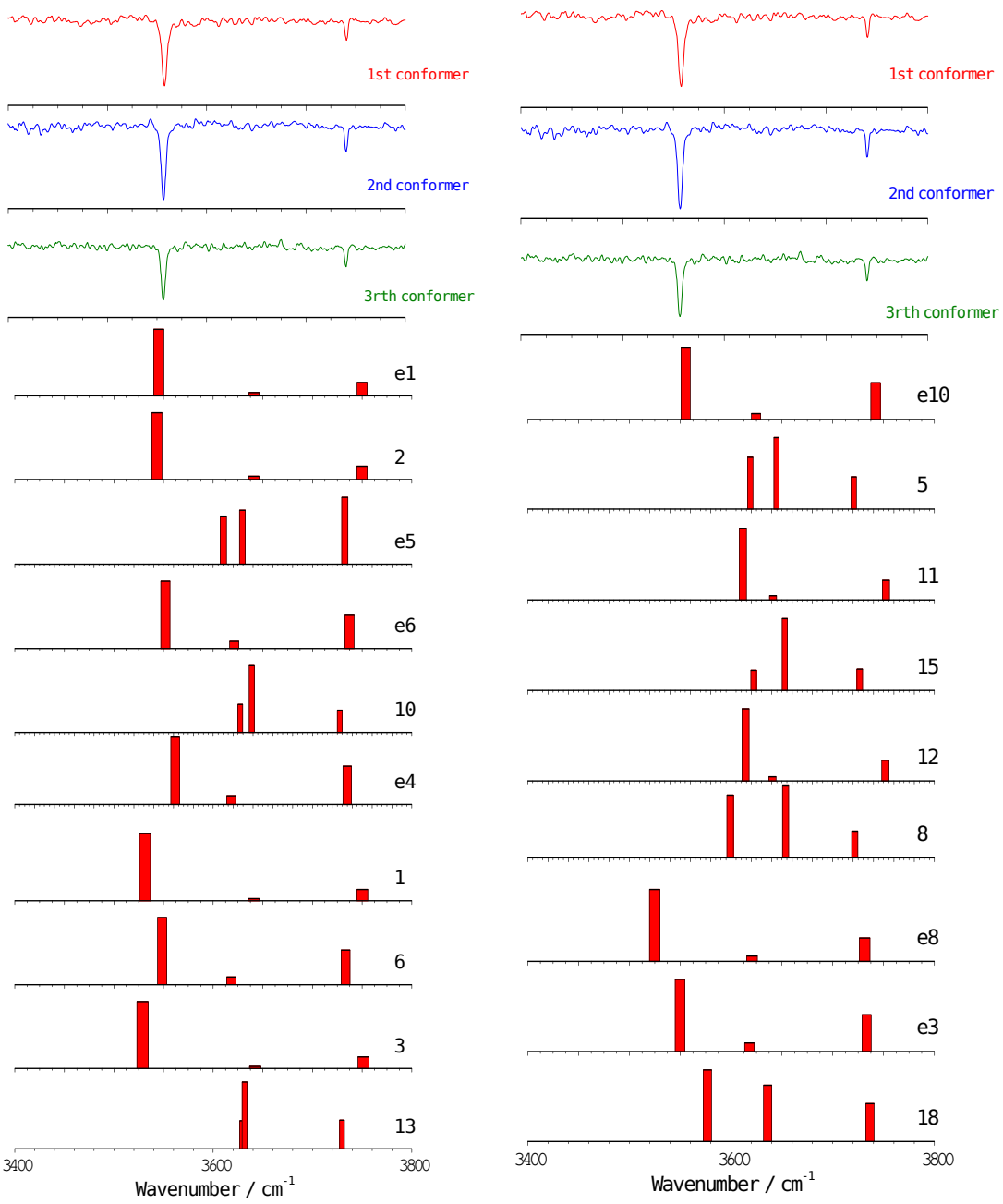

Figure 7.2. *Experimental IDIRS for propofol·W_1 (upper traces) together with the predicted frequencies for each calculated structure. A correction factor of 0.943 was employed.*

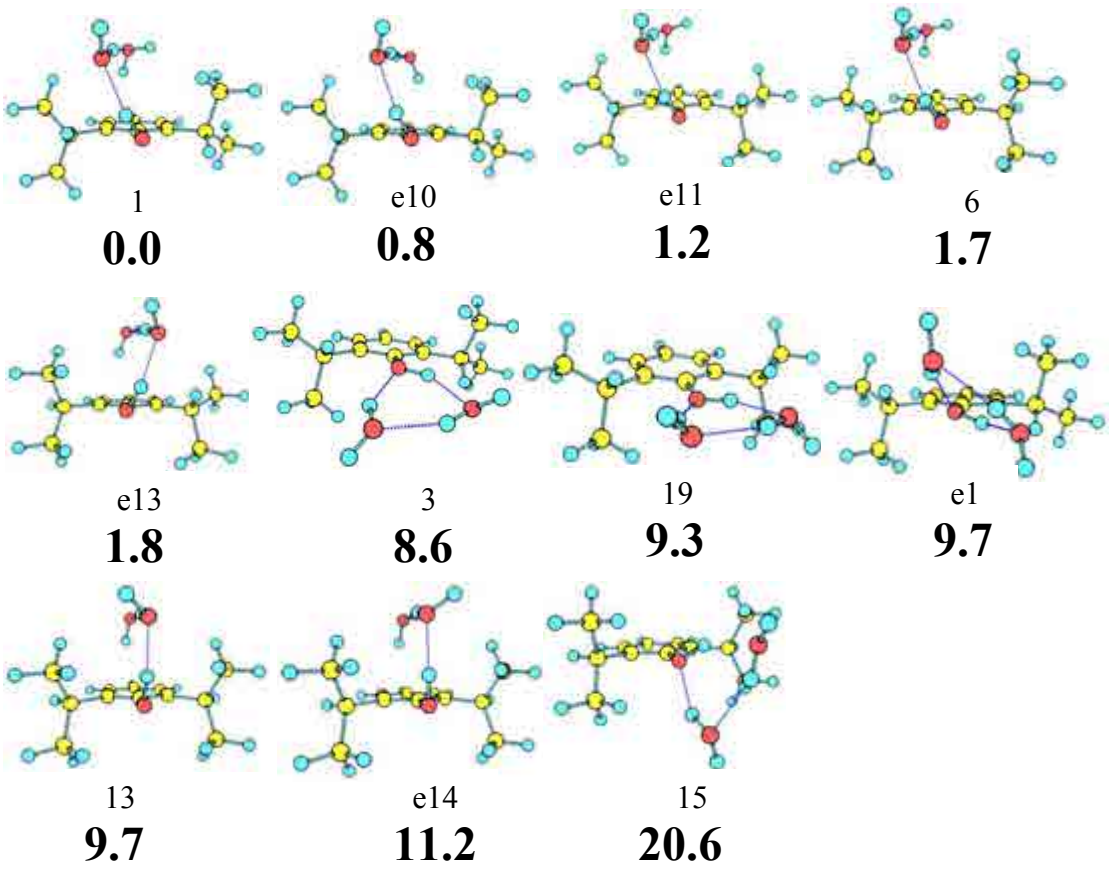

Figure 7.3. *Propofol·W_2 calculated structures at MP2/6-311++G(d,p).*

Table 7.2. *Propofol·W_2 structures with their relative energies and binding energies calculated at MP2/6-311++G(d,p)..*

Structure	*ΔE (kJ/mol)*	*ΔE_{ZPE} (kJ/mol)*	*D_0 (kJ/mol)*	*BSSE (kJ/mol)*
1	0.00	0.00	-40.30	31.25
e10	0.21	0.83	-39.16	31.56
e11	0.45	1.16	-39.95	30.82
6	1.40	1.75	-40.00	30.94
e13	0.67	1.77	-39.71	31.22
3	7.07	8.56	-38.99	24.00
19	7.66	9.29	-38.34	24.30
e1	8.09	9.71	-37.94	23.90
13	9.05	9.71	-36.40	31.88
e14	11.04	11.15	-35.43	31.41
15	20.04	20.64	-31.86	25.48

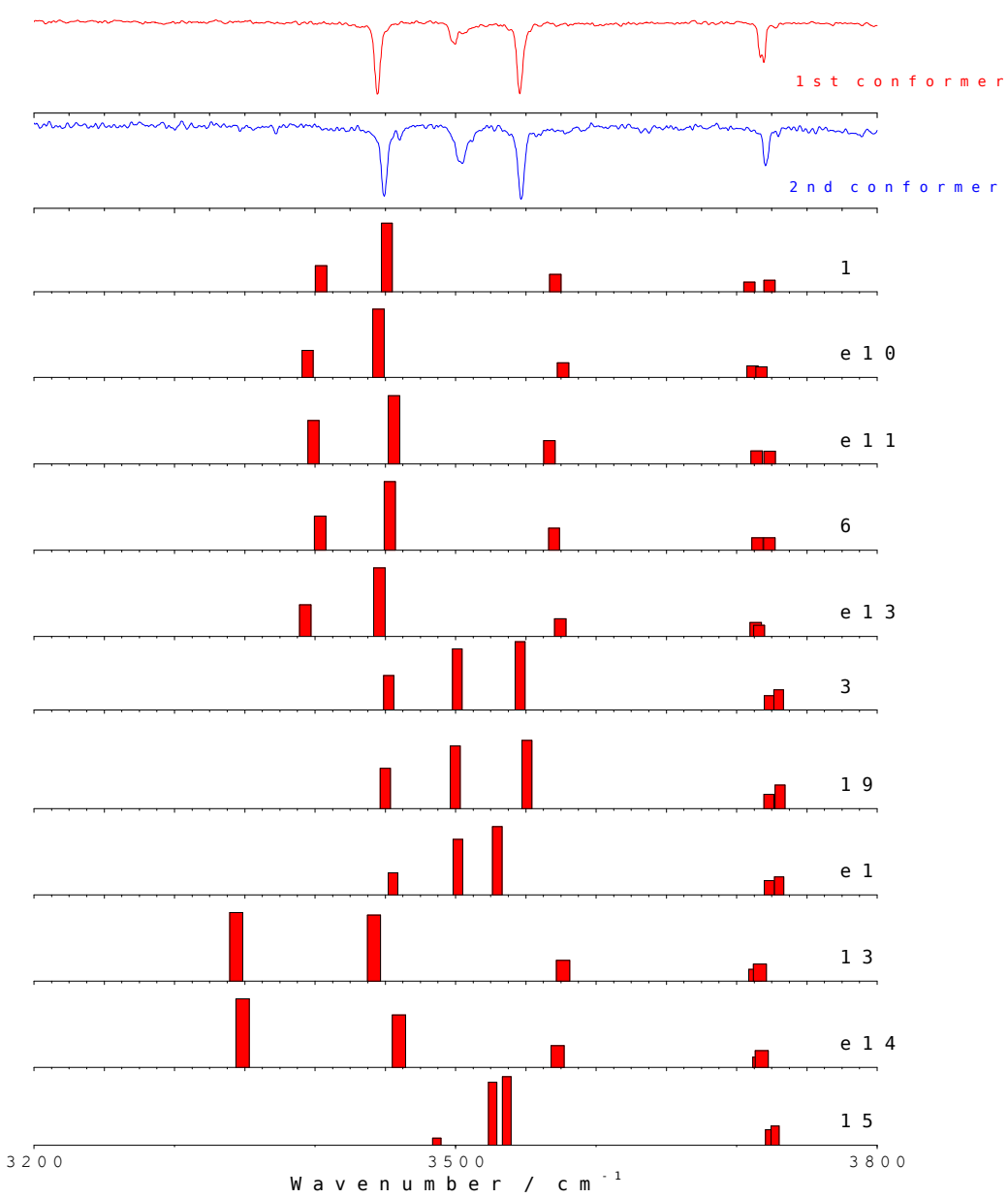

Figure 7.4. *Experimental IDIRS for propofol·W_2 (upper traces) together with the predicted frequencies for each calculated structure. A correction factor of 0.943 was employed.*

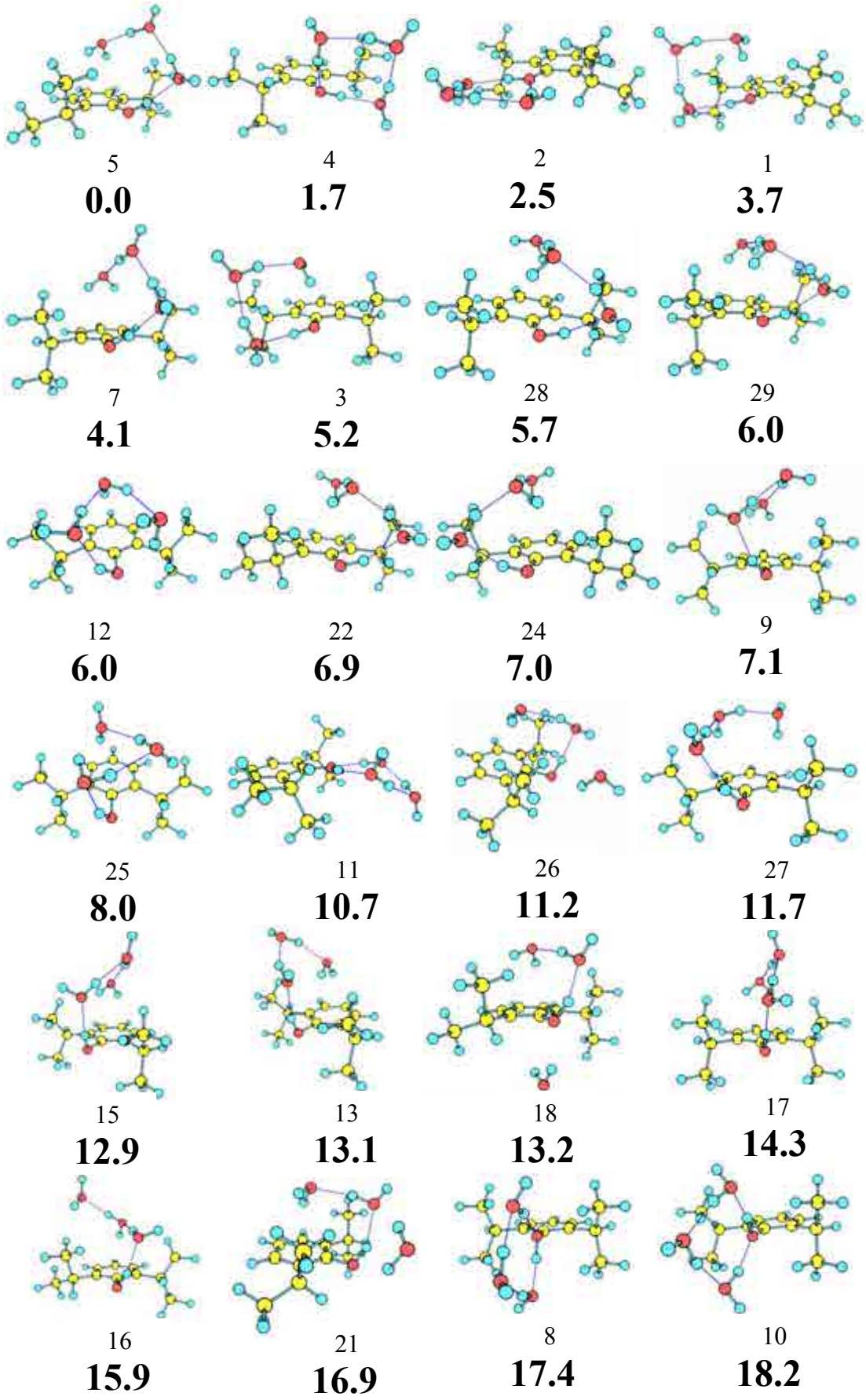

Figure 7.5. *Propofol·W_3 calculated structures at M06-2x/6-311++G(d,p).*

Table 7.3. *Propofol·W_3 structures with their relative energies and binding energies calculated at M06-2x/6-311++G(d,p).*

Structure	*ΔE (kJ/mol)*	*ΔE_{ZPE} (kJ/mol)*	*D_0 (kJ/mol)*	*BSSE (kJ/mol)*
5	0.	0.	-95.19	16.89
4	-0.05	1.68	-93.66	16.74
2	0.01	2.46	-93.83	15.79
1	2.08	3.71	-91.65	16.71
7	4.88	4.10	-94.87	16.92
3	4.29	5.22	-93.79	16.86
28	4.97	5.67	-93.76	16.45
29	4.36	6.03	-93.15	16.70
12	3.10	6.04	-89.31	16.73
22	6.07	6.94	-88.63	16.50
24	6.07	6.99	-88.58	16.51
9	5.75	7.09	-92.33	16.46
25	7.91	8.02	-87.44	16.76
11	9.21	10.73	-89.70	15.44
26	10.65	11.23	-85.46	15.38
27	12.62	11.68	-87.32	16.88
15	12.83	12.89	-91.61	15.96
13	12.67	13.09	-91.51	15.87
18	16.32	13.20	-82.45	16.43
17	16.66	14.30	-88.95	17.22
16	16.07	15.86	-80.42	15.80
21	17.39	16.88	-79.12	16.08
8	18.64	17.38	-86.64	16.45
10	18.46	18.20	-85.83	16.44

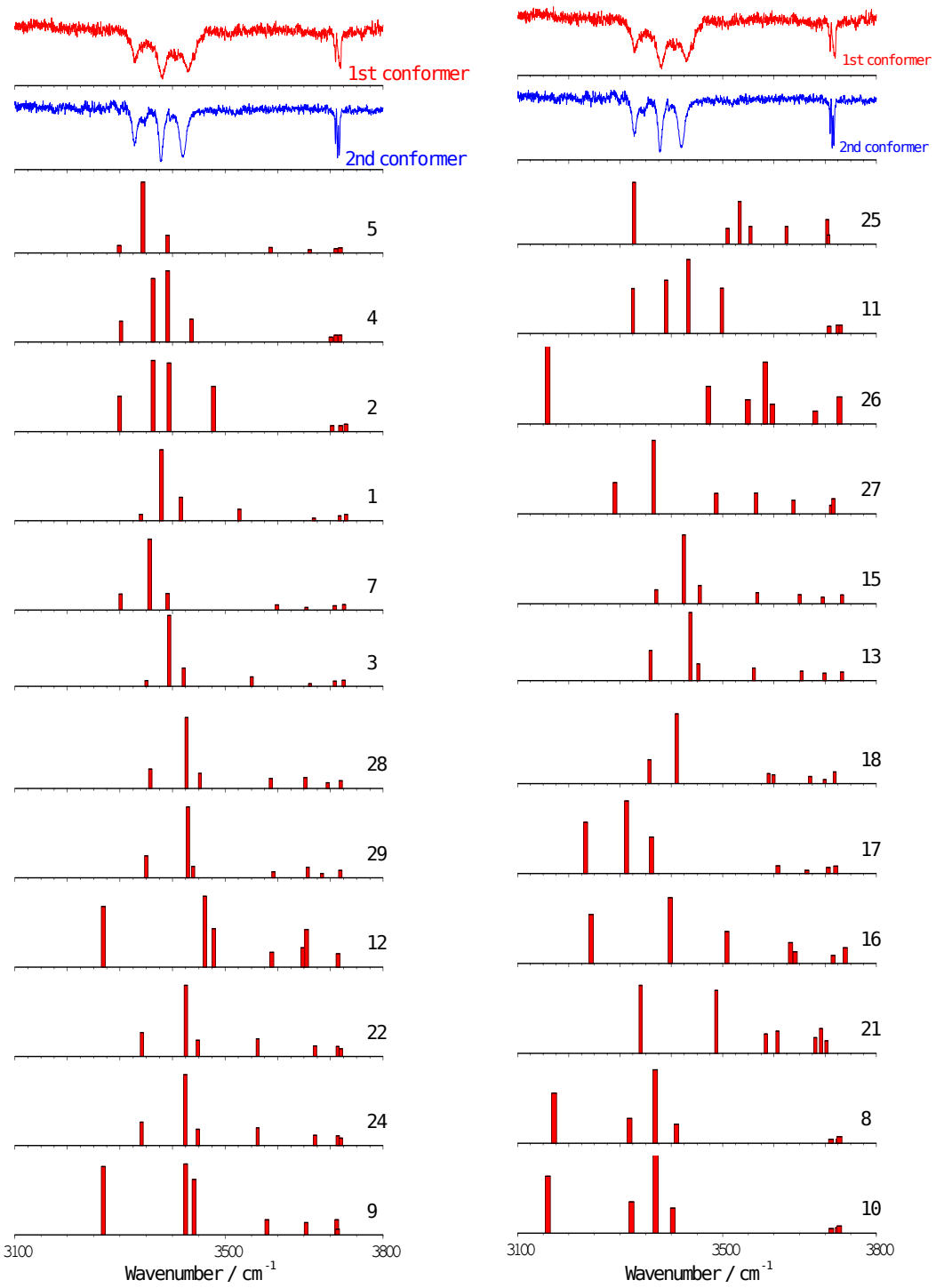

Figure 7.6. *Experimental IDIRS for propofol·W_3 (upper traces) together with the predicted frequencies for each calculated structure. A correction factor of 0.938 was employed.*

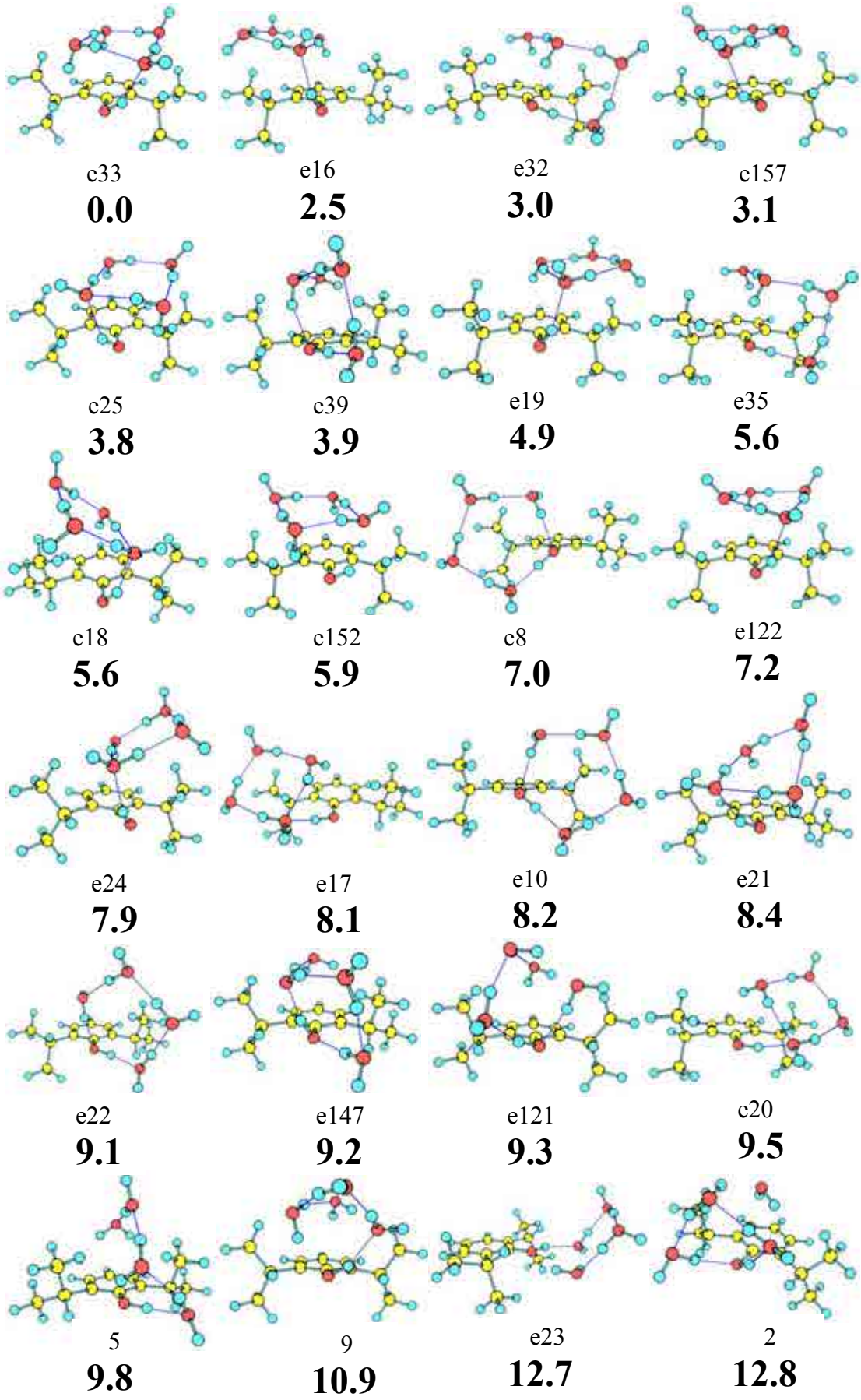

Figure 7.7a. *Propofol·W_4 calculated structures at M06-2x/6-311++G(d,p).*

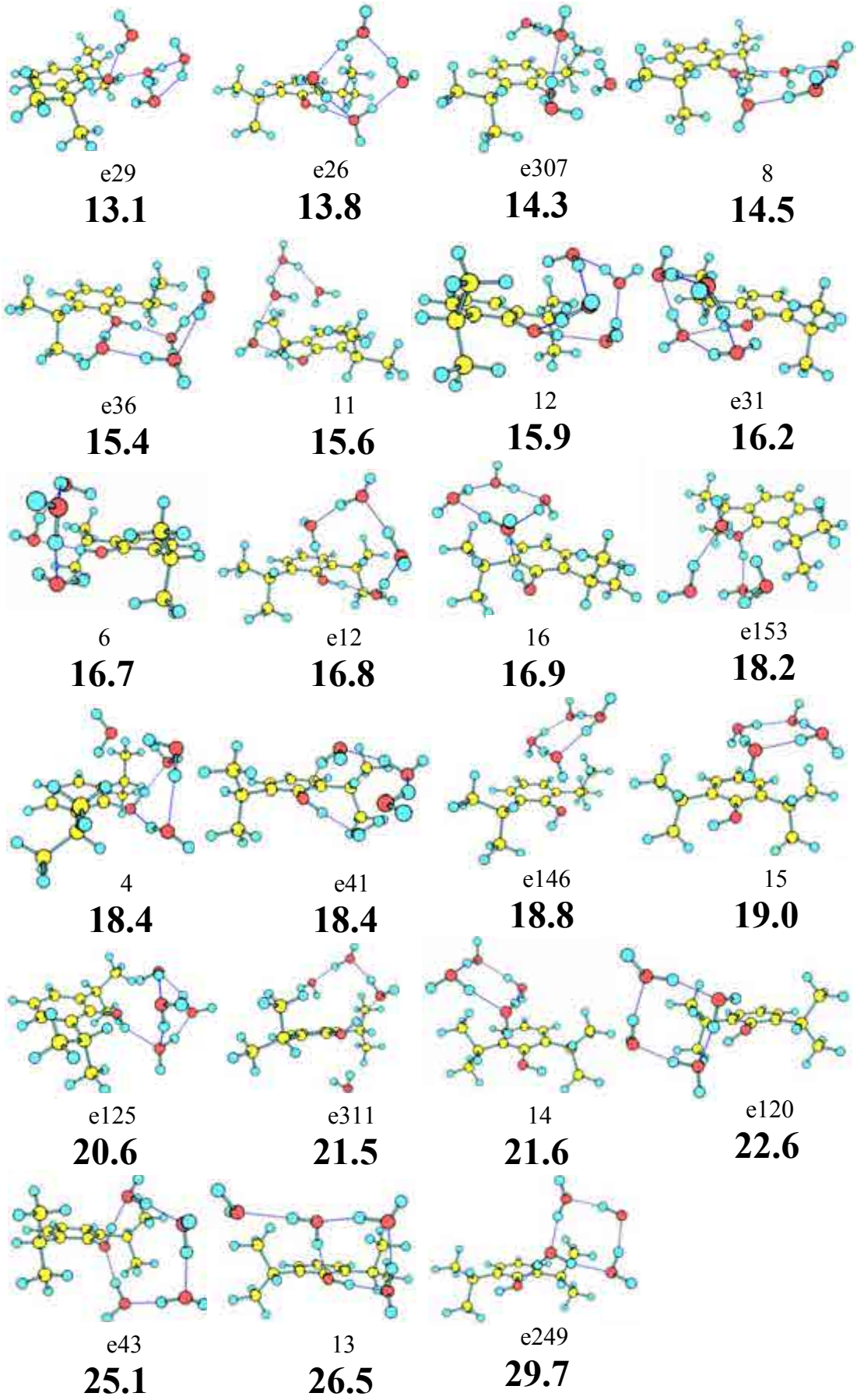

Figure 7.7b. *Propofol·W_4 calculated structures at M06-2x/6-311++G(d,p).*

Table 7.4. *Propofol·W_4 structures with their relative energies and binding energies calculated at M06-2x/6-311++G(d,p).*

Structure	*ΔE (kJ/mol)*	*ΔE_{ZPE} (kJ/mol)*	*D_0 (kJ/mol)*	*BSSE (kJ/mol)*
e33	0.00	0	-133.19	24.31
e16	2.16	2.47	-131.09	23.94
e32	4.92	3.04	-131.54	22.92
e157	3.44	3.07	-130.44	24.13
e25	3.01	3.84	-130.22	23.43
e39	3.64	3.85	-130.30	23.34
e19	5.14	4.87	-132.36	24.07
e35	8.76	5.58	-132.72	22.99
e18	5.89	5.63	-128.86	23.00
e152	3.71	5.91	-128.03	23.70
e8	8.18	6.99	-127.09	23.41
e122	7.31	7.23	-126.81	23.6
e24	9.24	7.93	-130.37	22.99
e17	8.02	8.14	-126.30	23.06
e10	11.18	8.25	-129.61	23.43
e21	8.57	8.37	-127.16	21.96
e22	10.56	9.06	-125.65	22.78
e147	10.70	9.20	-126.37	21.93
e121	9.68	9.30	-125.04	23.15
e20	10.73	9.54	-128.65	23.10
5	11.79	9.77	-126.60	21.26
9	11.69	10.88	-123.44	23.17
e23	12.77	12.69	-123.69	21.26
2	13.19	12.76	-122.63	22.11
e29	13.71	13.15	-122.83	21.65
e26	13.43	13.82	-122.34	21.33
e307	14.49	14.28	-121.19	22.03
8	17.09	14.52	-122.67	20.45
e36	14.55	15.43	-122.01	20.06
11	18.29	15.59	-120.57	21.33
12	15.39	15.89	-123.72	21.68
e31	16.28	16.21	-123.48	21.61
6	17.50	16.69	-123.87	20.74
e12	19.49	16.78	-119.54	21.31
16	19.26	16.89	-118.19	22.41
e153	17.63	18.23	-122.19	20.87
4	19.89	18.39	-117.73	21.37
e41	18.93	18.44	-122.66	20.19
e146	19.47	18.83	-116.63	22.04
15	18.54	19.02	-116.00	22.62
e125	21.10	20.65	-119.46	21.18
e311	27.53	21.49	-113.59	22.42
14	22.30	21.61	-114.27	21.62
e120	24.34	22.60	-118.86	21.68
e43	28.75	25.10	-118.36	22.43
13	28.62	26.50	-109.52	21.47
e249	30.80	29.69	-107.01	20.80

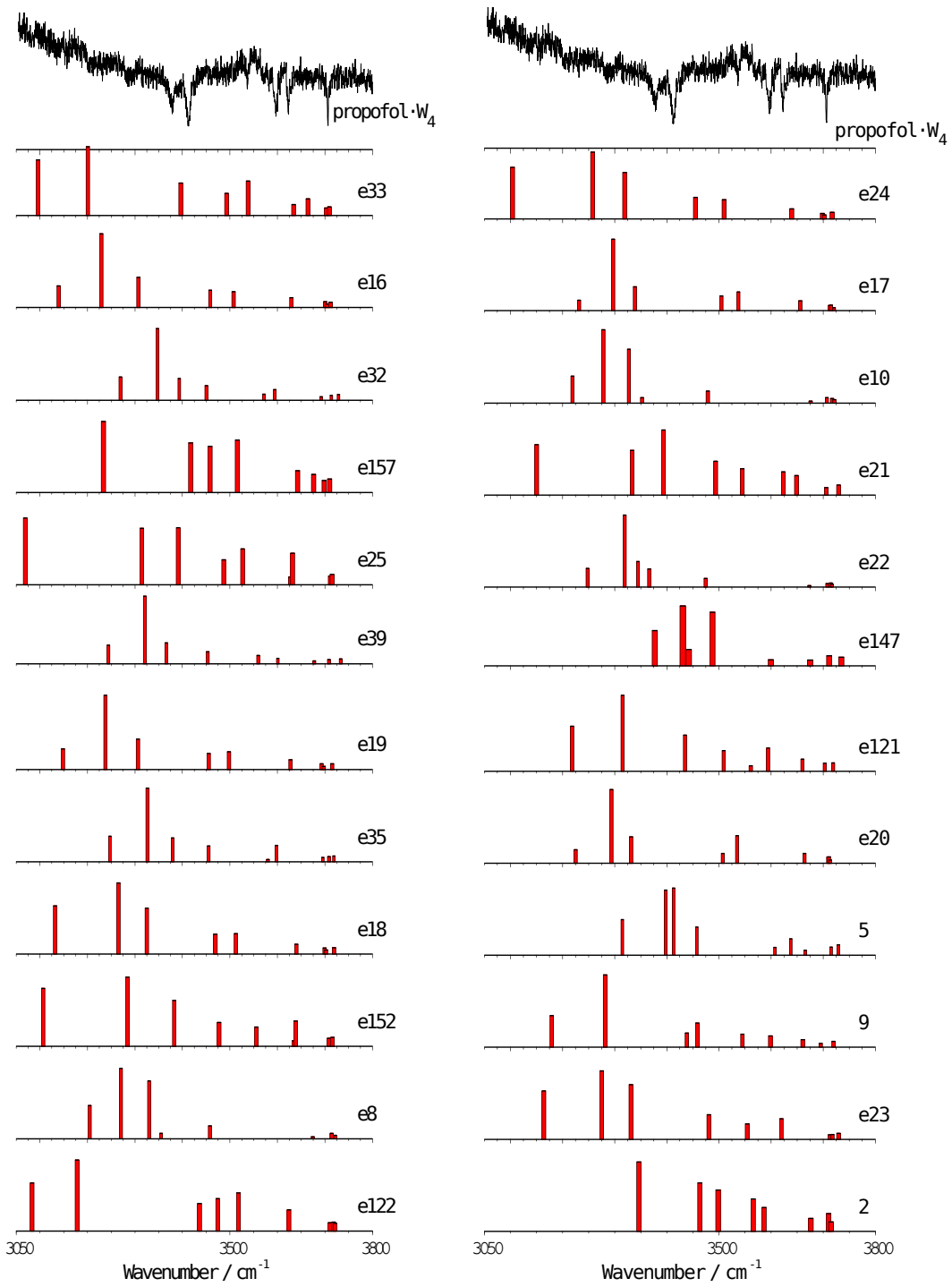

Figure 7.8a. *Experimental IDIRS for propofol·W_4 (upper trace) together with the predicted frequencies for each calculated structure. A correction factor of 0.938 was employed.*

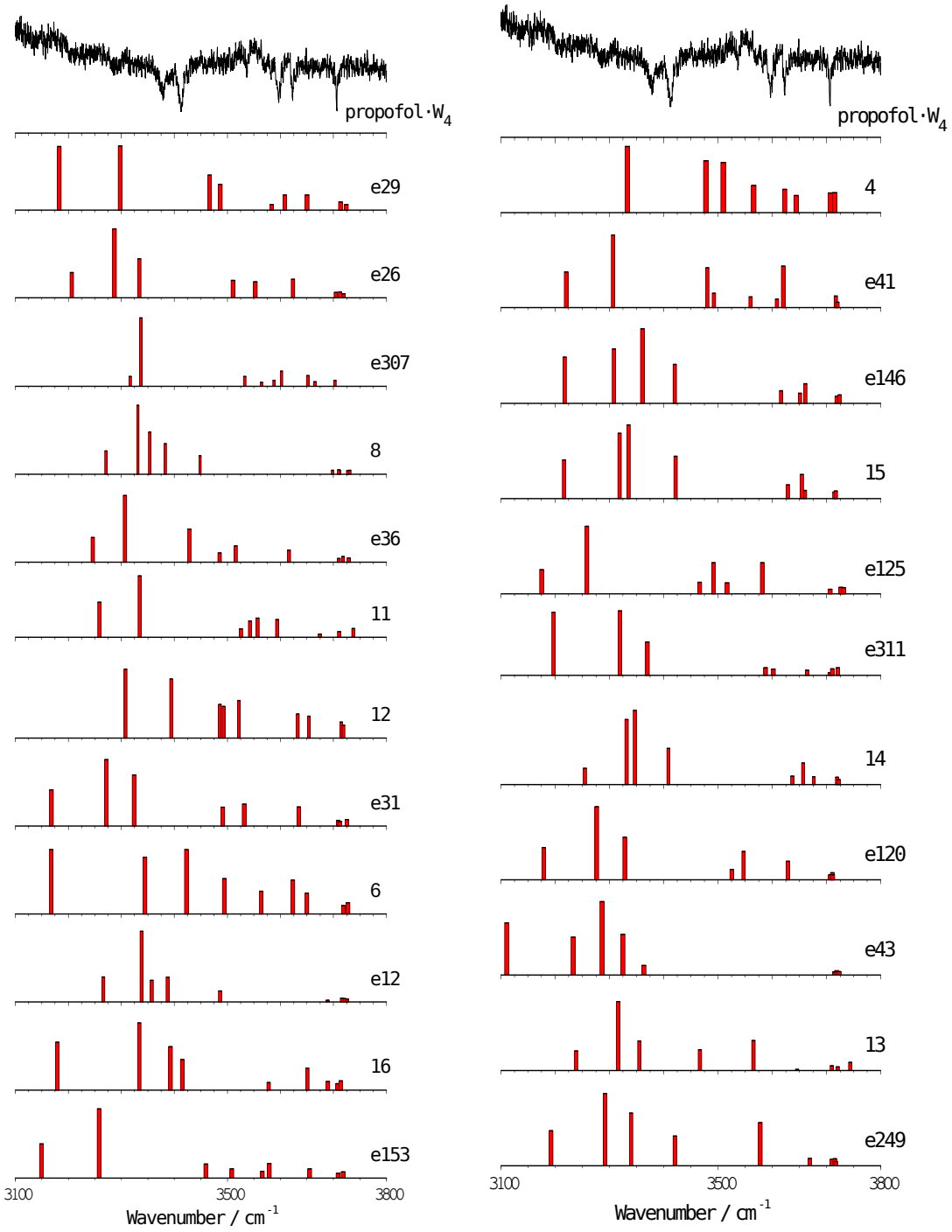

Figure 7.8b. *Experimental IDIRS for propofol·W_4 (upper trace) together with the predicted frequencies for each calculated structure. A correction factor of 0.938 was employed.*

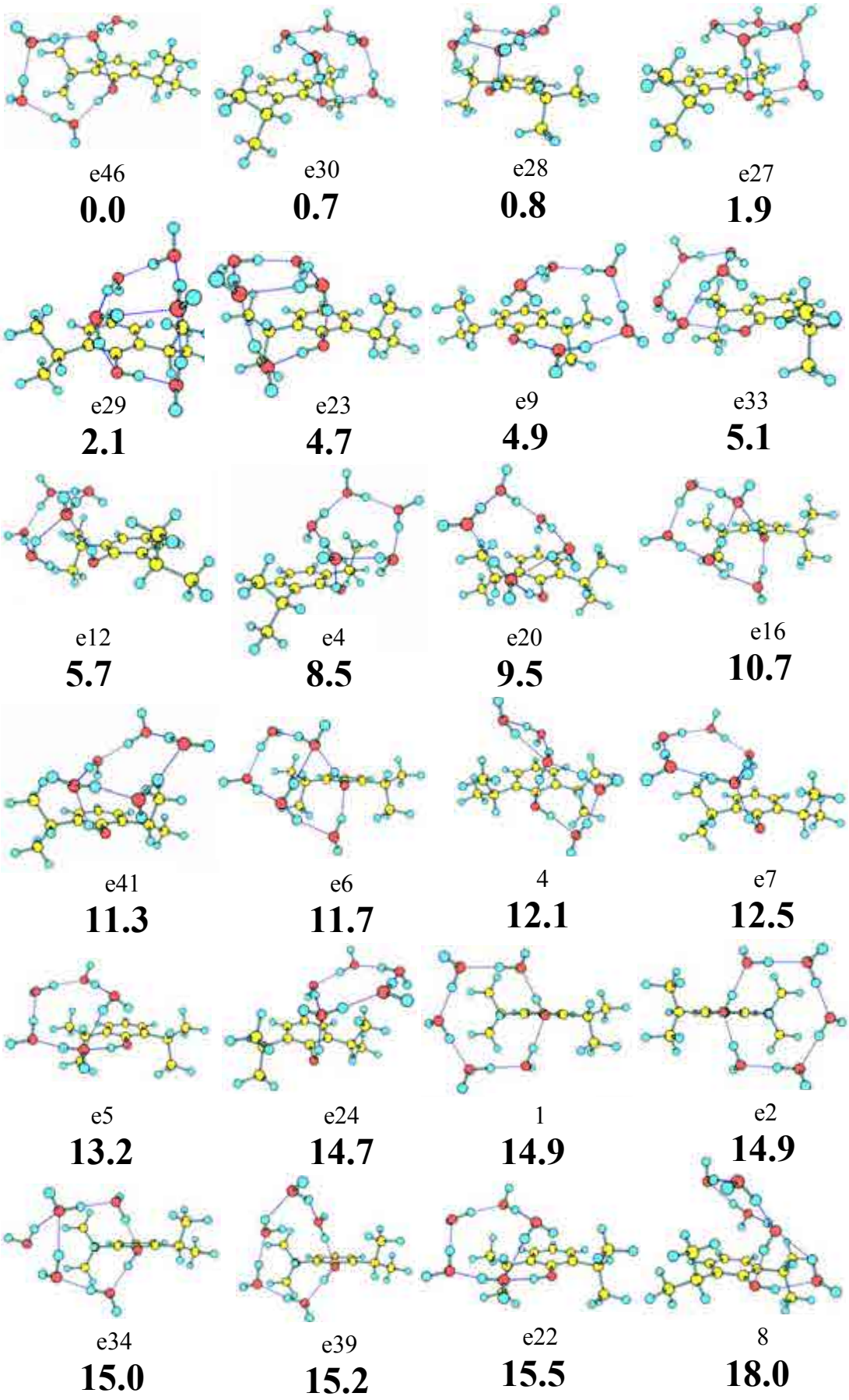

Figure 7.9a. *Propofol·W_5 calculated structures at M06-2x/6-311++G(d,p).*

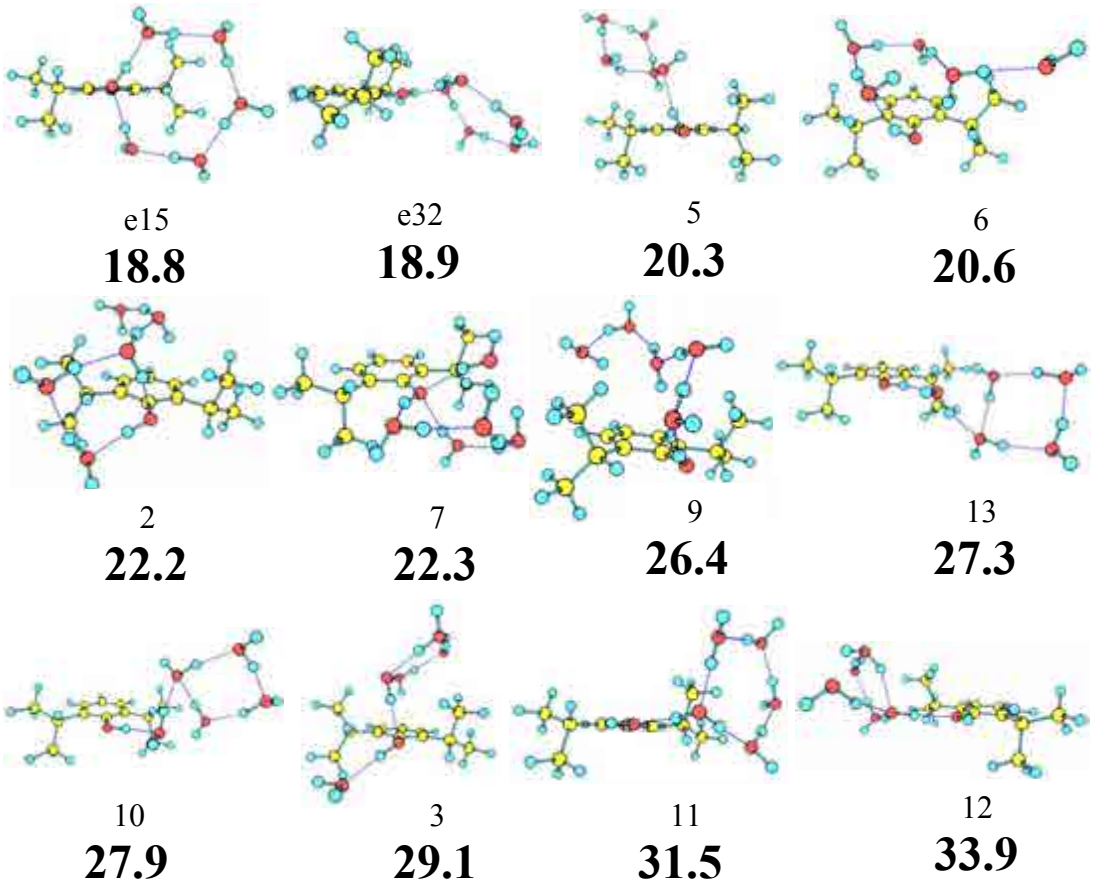

Figure 7.9b. *Propofol·W_5 calculated structures at M06-2x/6-311++G(d,p).*

Table 7.5. *Propofol·W_5 with their relative energies and binding energies calculated at M06-2x/6-311++G(d,p).*

Structure	*ΔE (kJ/mol)*	*ΔE_{ZPE} (kJ/mol)*	*D_0 (kJ/mol)*	*BSSE (kJ/mol)*
e46	0.00	0.00	-168.95	29.89
e30	-2.98	0.66	-167.41	30.77
e28	-1.07	0.83	-167.76	30.39
e27	-2.01	1.90	-166.50	30.43
e29	-2.02	2.14	-167.33	29.37
e23	0.93	4.69	-164.33	29.82
e9	2.57	4.91	-164.31	29.62
e33	2.26	5.10	-167.51	30.02
e12	3.90	5.67	-163.77	29.40
e4	7.09	8.54	-162.03	28.27
e20	8.33	9.53	-159.95	29.35
e16	10.34	10.66	-163.58	28.40
e41	8.80	11.28	-158.99	28.56
e6	7.68	11.68	-158.86	28.43
4	10.70	12.11	-159.41	27.32
e7	12.16	12.55	-158.01	28.27
e5	11.36	13.19	-156.50	29.29
e24	14.05	14.68	-159.55	28.41
1	15.81	14.87	-155.33	28.63
e2	18.09	14.92	-158.99	28.72
e34	12.95	14.99	-154.90	28.94
e39	13.92	15.23	-155.76	27.85
e22	12.97	15.51	-157.63	29.49
8	16.01	17.99	-154.20	26.64
e15	18.20	18.77	-151.47	28.59
e32	17.61	18.9	-153.69	26.39
5	17.80	20.33	-155.29	27.01
6	17.21	20.58	-149.96	28.29
2	20.00	22.22	-148.77	27.84
7	19.94	22.26	-149.21	27.36
9	27.97	26.43	-146.41	25.99
13	26.03	27.31	-146.51	25.16
10	26.00	27.93	-145.18	25.87
3	29.61	29.15	-142.43	27.25
11	30.96	31.51	-141.55	25.77
12	31.26	33.91	-140.82	24.10

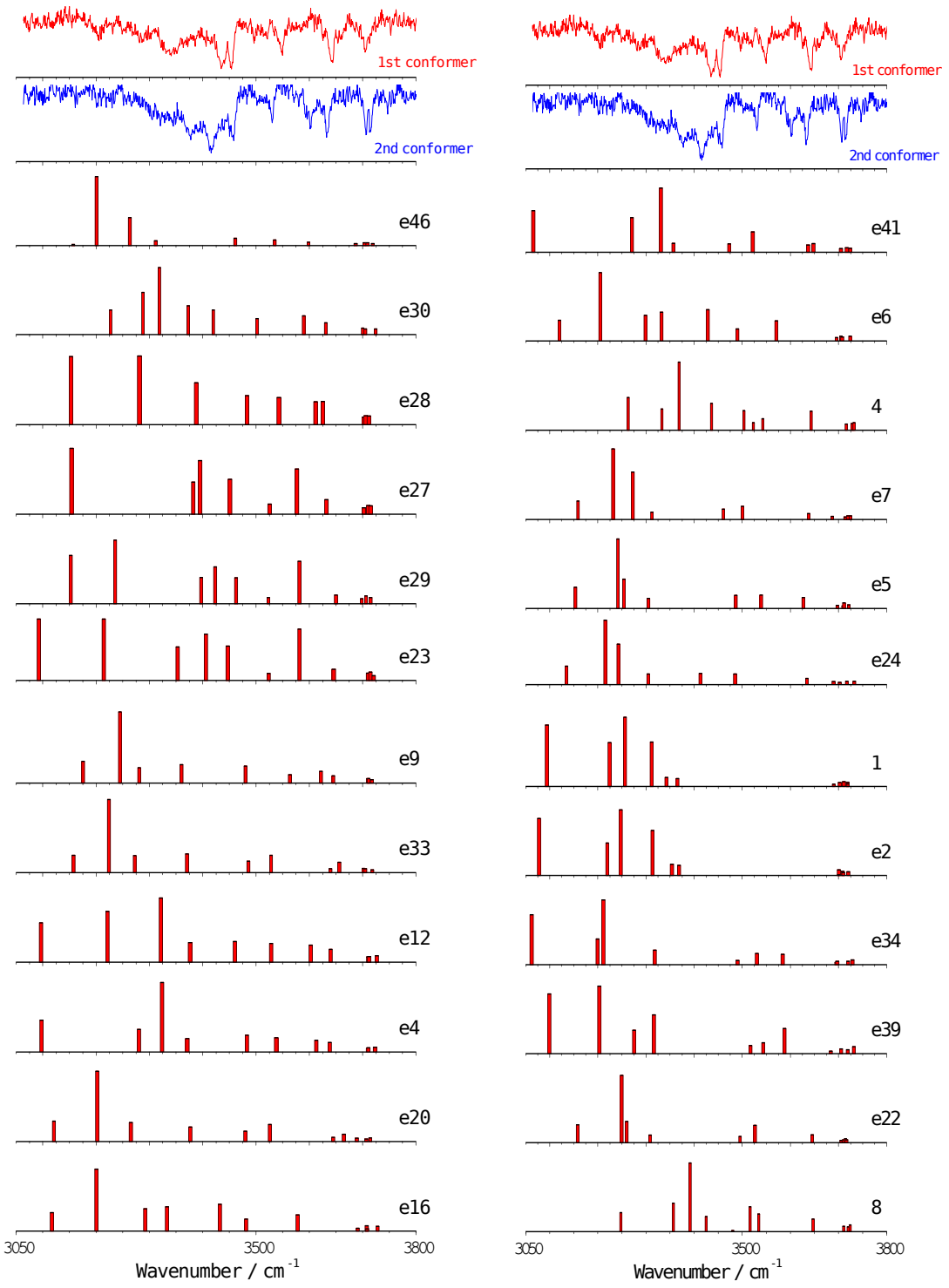

Figure 7.10a. *Experimental IDIRS for propofol·W_5 (upper traces) together with the predicted frequencies for each calculated structure. A correction factor of 0.938 was employed.*

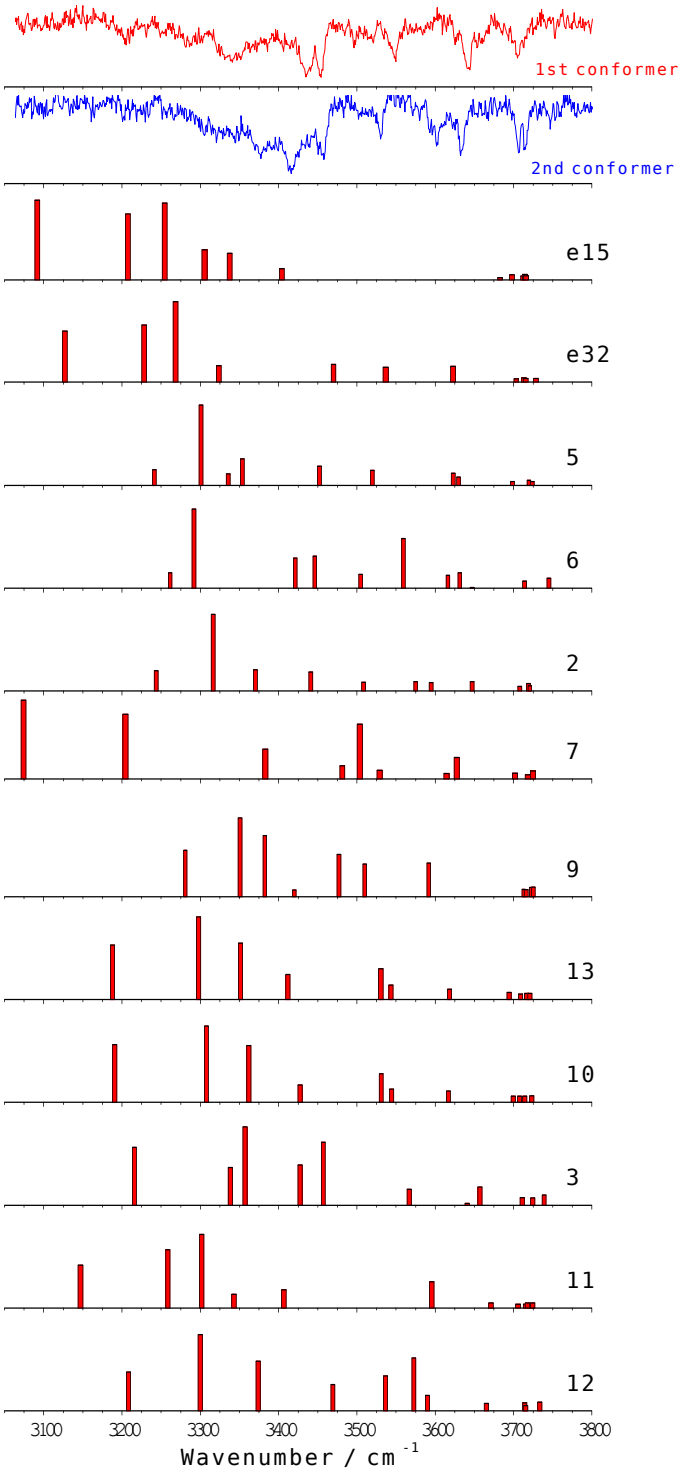

Figure 7.10b. *Experimental IDIRS for propofol·W_5 (upper traces) together with the predicted frequencies for each calculated structure. A correction factor of 0.938 was employed.*

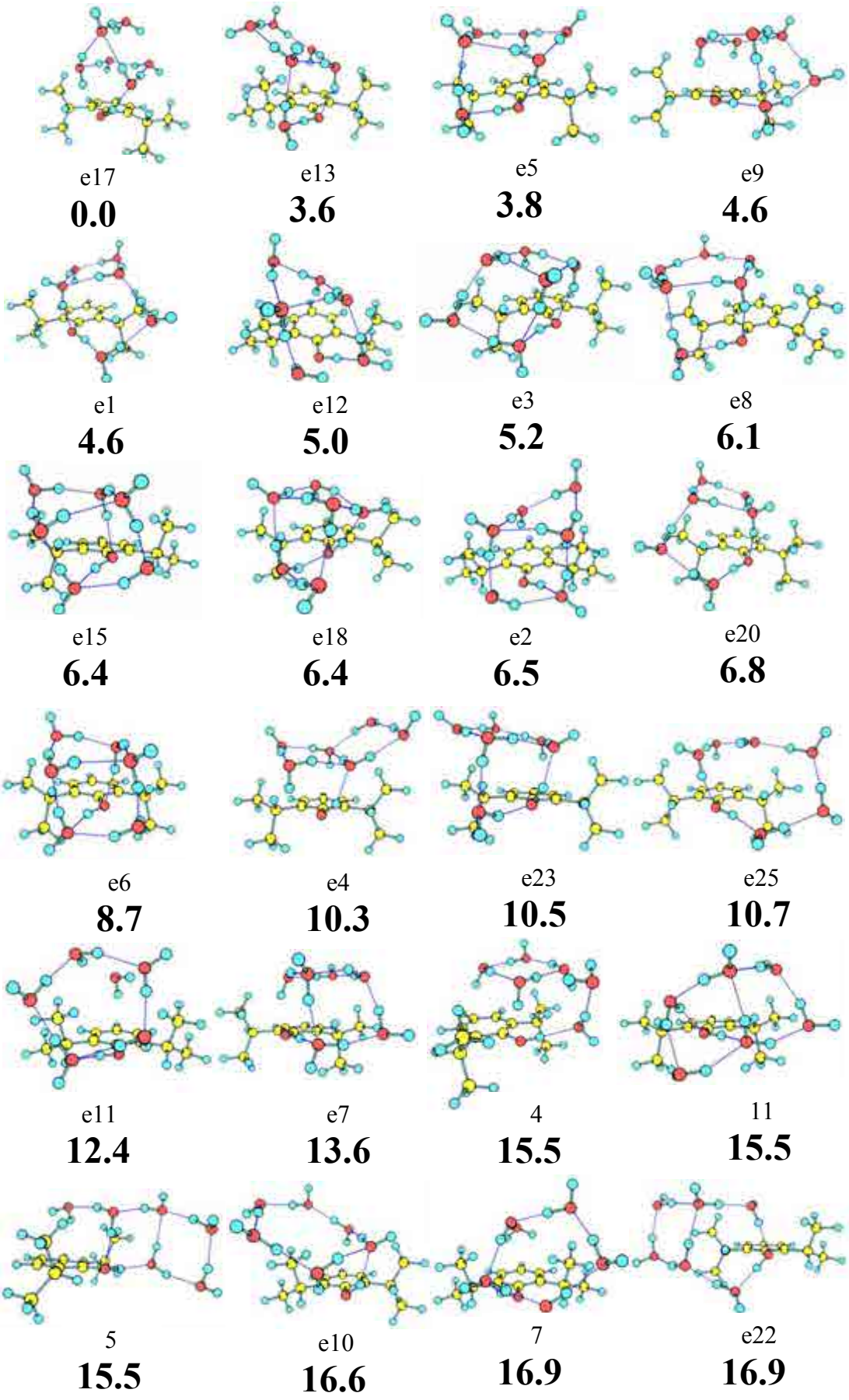

Figure 7.11a. *Propofol·W_6 calculated structures at M06-2x/6-311++G(d,p).*

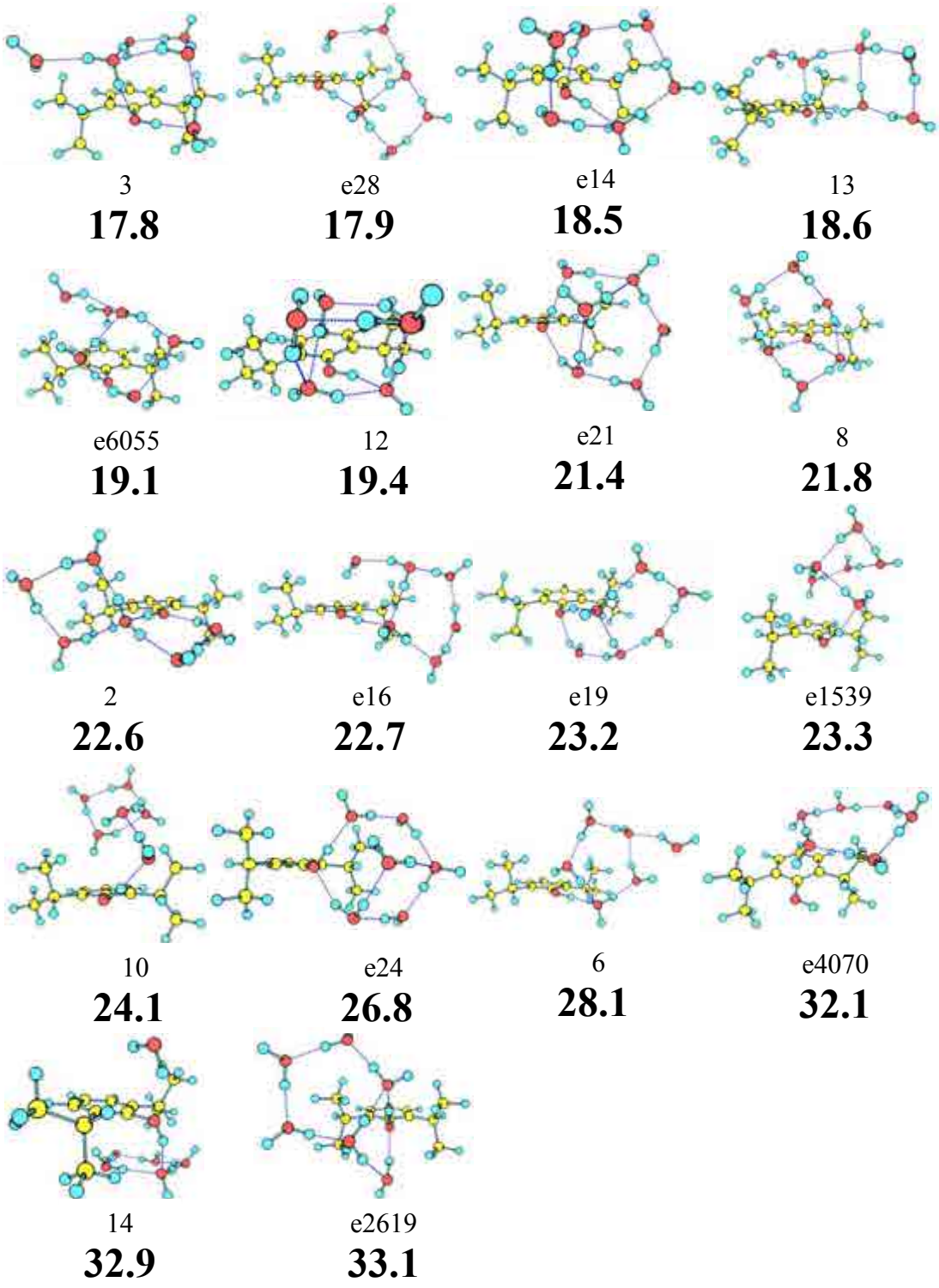

Figure 7.11b. *Propofol·W_6 calculated structures at M06-2x/6-311++G(d,p).*

Table 7.6. *Propofol·W_6 structures with their relative energies and binding energies calculated at M06-2x/6-311++G(d,p).*

Structure	*ΔE (kJ/mol)*	*ΔE_{ZPE} (kJ/mol)*	*D_0 (kJ/mol)*	*BSSE (kJ/mol)*
e17	0.00	0.00	-206.74	36.46
e13	7.56	3.59	-203.30	36.31
e5	8.78	3.80	-202.65	36.89
e9	7.21	4.65	-202.13	36.41
e1	9.89	4.94	-201.37	36.88
e12	8.25	4.98	-203.45	34.78
e3	8.81	5.17	-201.88	36.14
e8	10.89	6.10	-200.10	36.99
e15	10.13	6.42	-201.82	34.96
e18	7.67	6.42	-201.87	34.90
e2	9.20	6.47	-201.97	34.91
e20	11.01	6.80	-203.64	36.56
e6	10.24	8.75	-199.18	35.41
e4	12.58	10.28	-199.16	33.76
e23	18.01	10.52	-197.31	35.36
e25	17.20	10.67	-197.04	35.48
e11	16.71	12.36	-196.09	34.89
e7	18.97	13.57	-198.12	35.31
4	17.04	15.48	-196.28	35.23
11	17.28	15.49	-194.07	33.78
5	20.89	15.53	-194.35	33.31
e10	22.85	16.56	-192.52	34.12
7	23.40	16.86	-192.56	33.92
e22	22.81	16.95	-191.77	34.48
3	22.84	17.79	-190.68	34.87
e28	24.44	17.87	-191.99	33.33
e14	23.48	18.50	-190.21	34.63
13	25.66	18.59	-191.76	32.85
e6055	24.18	19.06	-194.47	33.47
12	21.73	19.36	-190.83	33.16
e21	28.90	21.45	-186.59	35.16
8	28.69	21.80	-188.95	32.45
2	26.93	22.58	-188.76	31.87
e16	29.40	22.69	-186.85	33.65
e19	29.51	23.22	-186.71	33.27
e1539	28.14	23.35	-190.08	33.56
10	29.72	24.08	-186.42	32.70
e24	32.03	26.78	-186.26	33.96
6	33.70	28.06	-183.01	32.27
e4070	39.36	32.15	-181.39	33.46
14	41.61	32.91	-175.71	34.58
e2619	42.19	33.10	-184.32	34.17

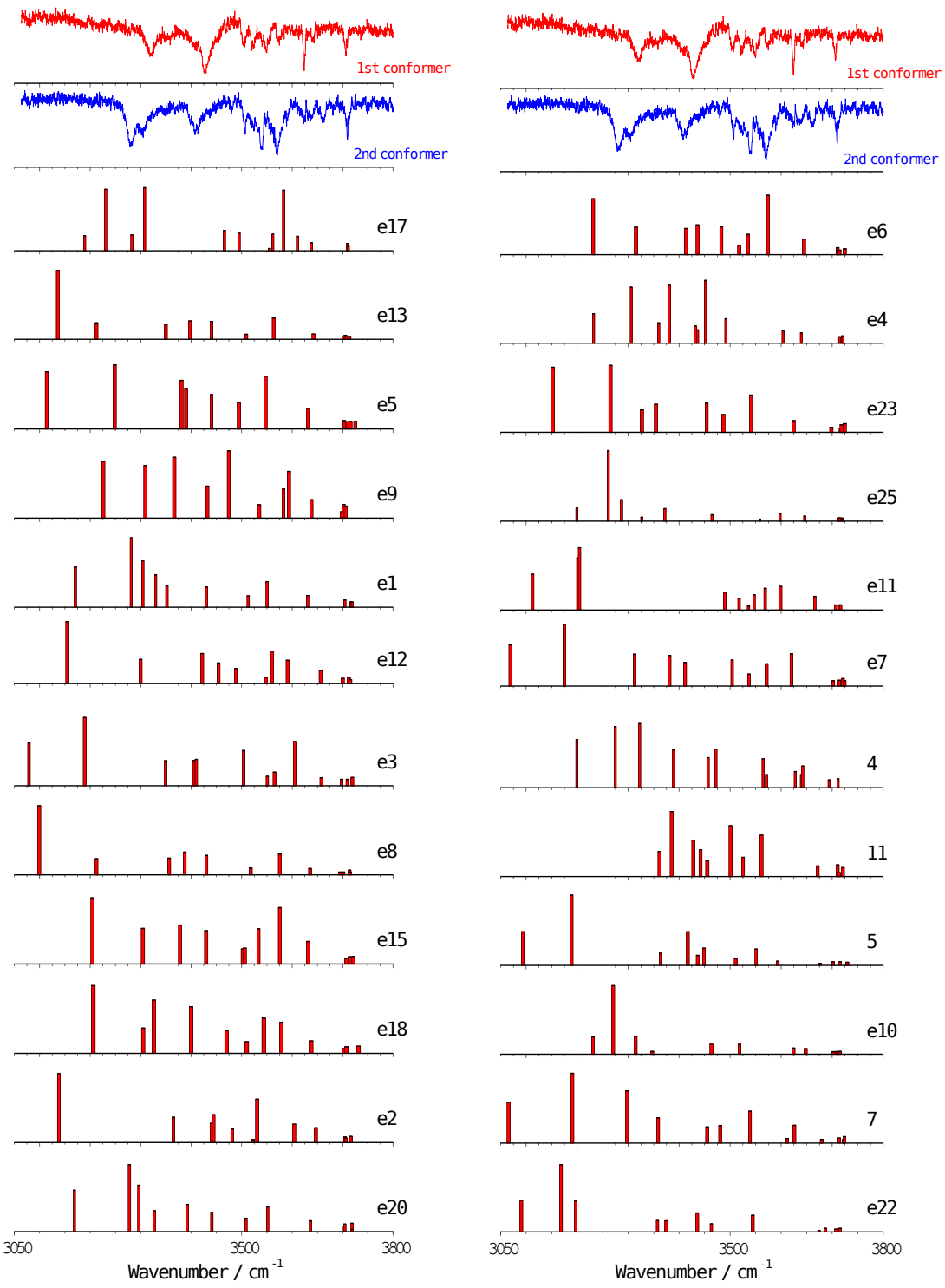

Figure 7.12a. *Experimental IDIRS for propofol·W_6 (upper traces) together with the predicted frequencies for each calculated structure. A correction factor of 0.938 was employed.*

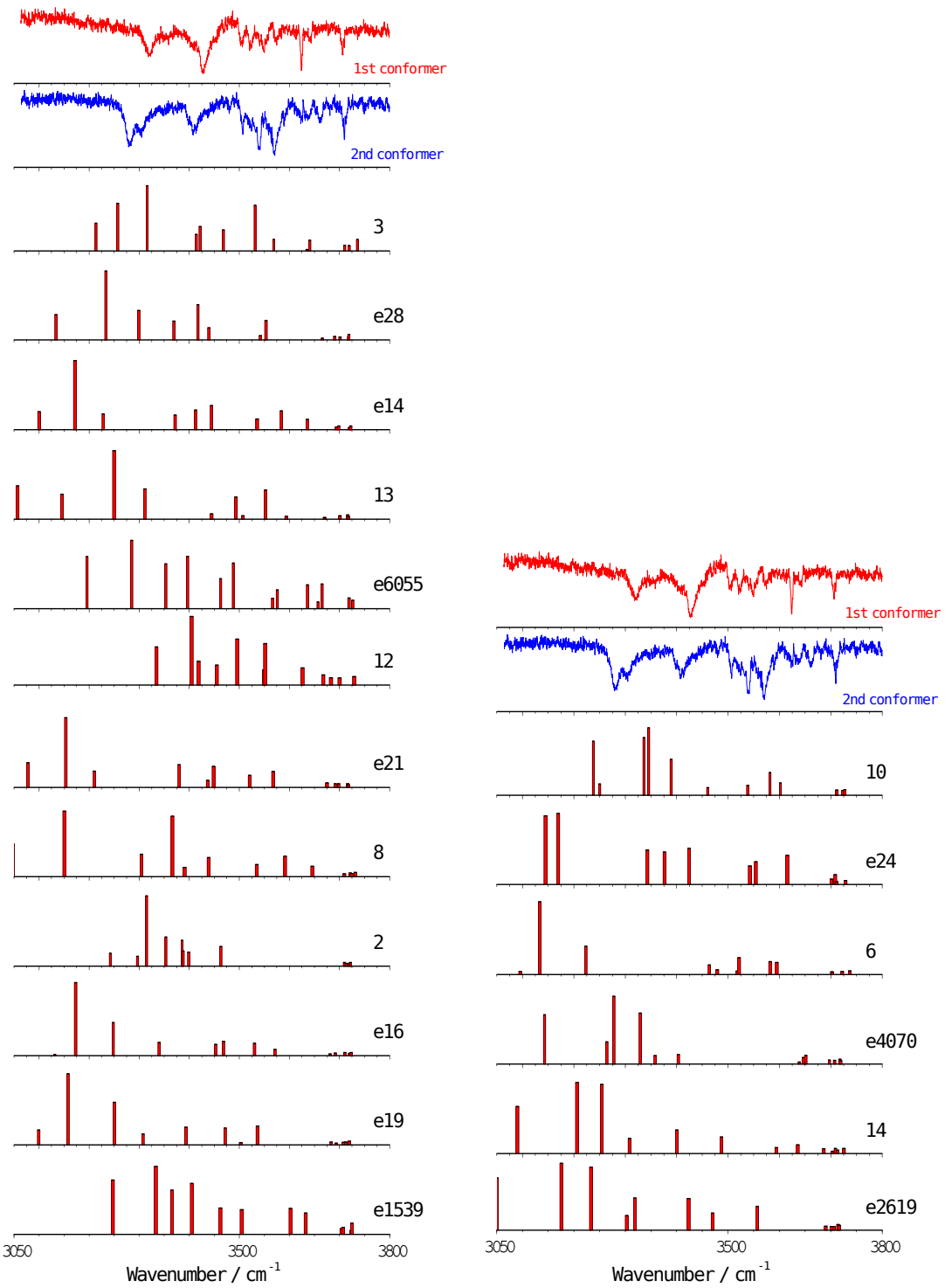

Figure 7.12b. *Experimental IDIRS for propofol·W_6 (upper traces) together with the predicted frequencies for each calculated structure. A correction factor of 0.938 was employed.*

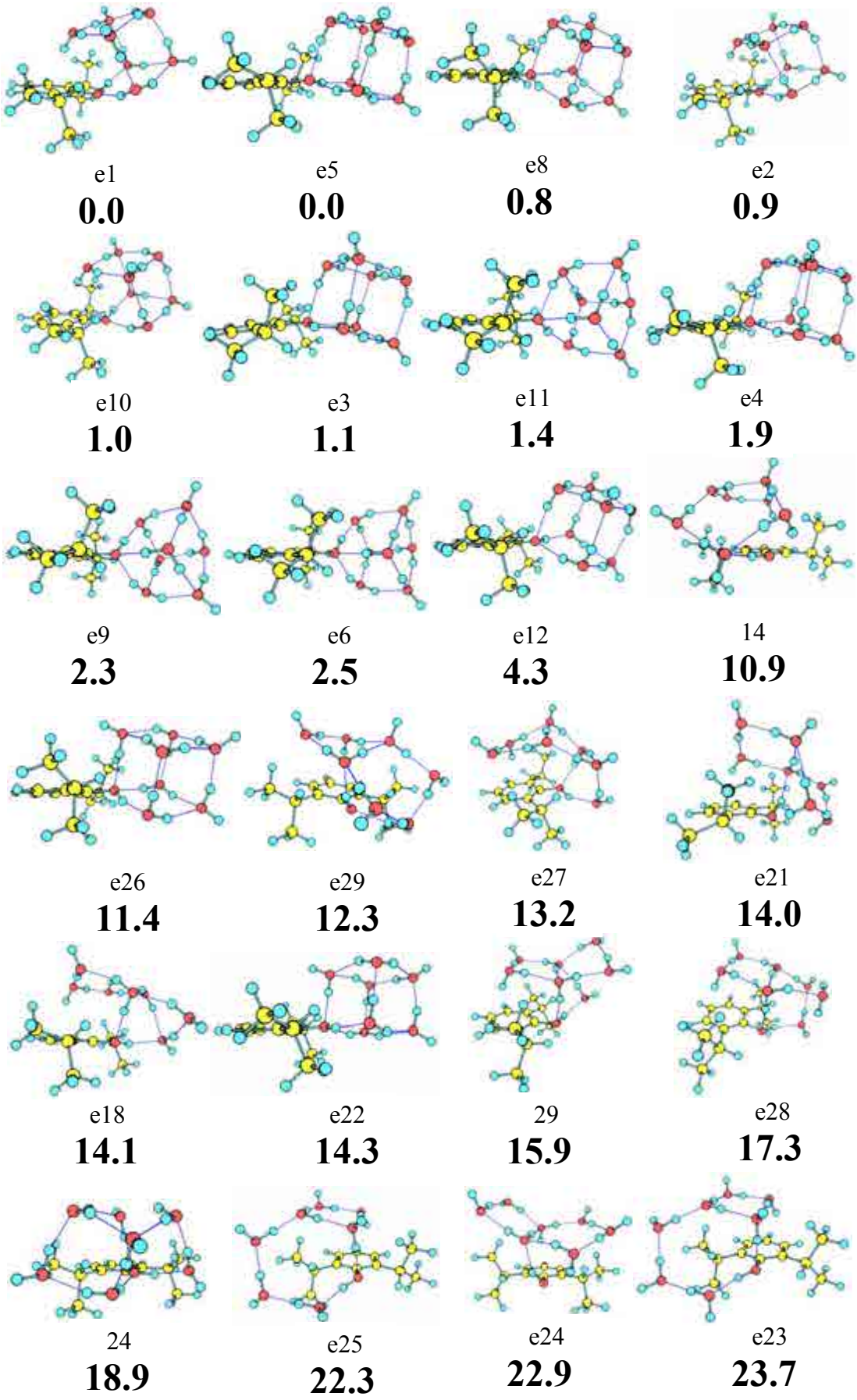

Figure 7.13a. *Propofol·W_7 calculated structures at M06-2x/6-311++G(d,p).*

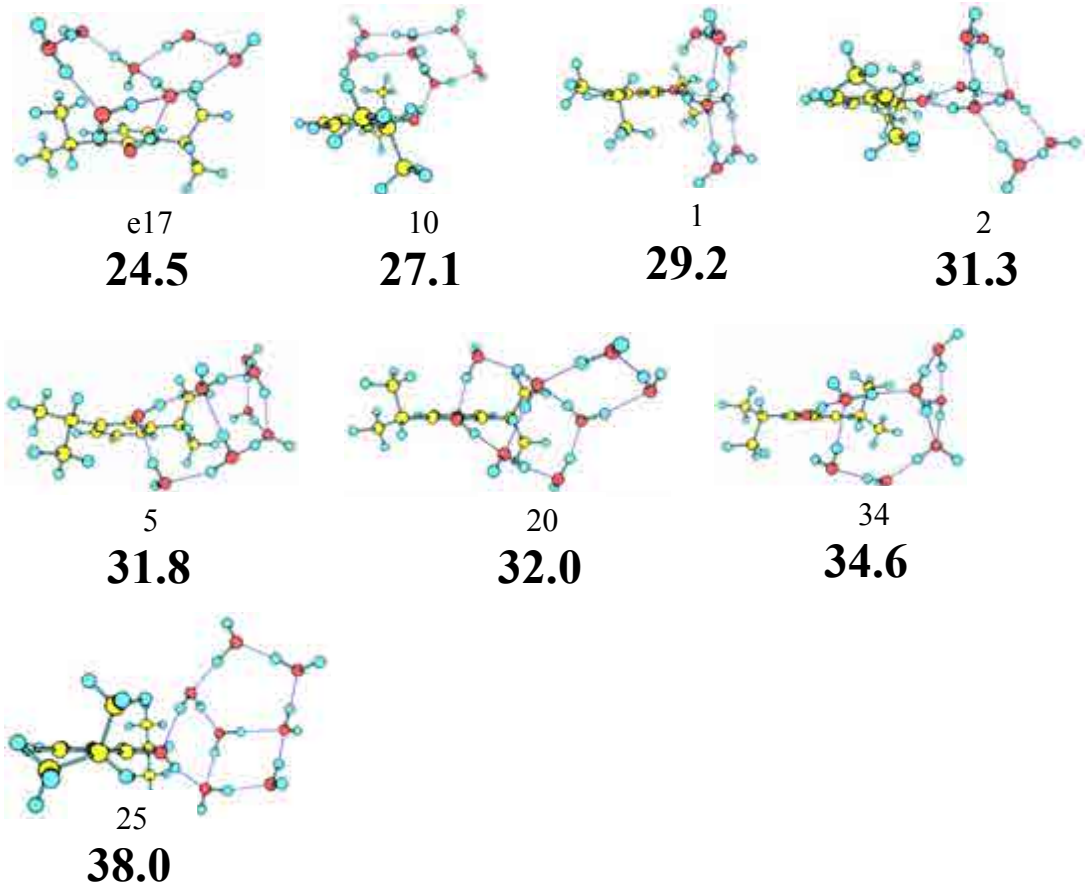

Figure 7.13b. *Propofol·W_7 calculated structures at M06-2x/6-311++G(d,p).*

Table 7.7. *Propofol·W_7 structures with their relative energies and binding energies calculated at M06-2x/6-311++G(d,p).*

Structure	*ΔE (kJ/mol)*	*ΔE_{ZPE} (kJ/mol)*	*D_0 (kJ/mol)*	*BSSE (kJ/mol)*
e1	0	0	-251.93	41.96
e5	-1.15	0.05	-252.75	41.09
e8	1.19	0.84	-252.18	40.87
e2	0.27	0.90	-251.14	41.86
e10	0.19	1.03	-250.86	42.0
e3	-0.76	1.11	-252.03	40.76
e11	1.38	1.40	-251.98	40.51
e4	-0.26	1.91	-250.88	41.11
e9	1.68	2.35	-250.85	40.70
e6	2.18	2.51	-250.68	40.71
e12	2.67	4.28	-248.68	41.08
14	13.04	10.95	-240.15	42.79
e26	12.86	11.43	-241.71	40.76
e29	16.83	12.28	-240.18	41.58
e27	16.03	13.19	-238.40	42.29
e21	18.33	13.99	-238.54	41.37
e18	16.42	14.14	-238.26	41.63
e22	14.24	14.28	-238.36	41.40
29	15.48	15.86	-237.61	40.42
e28	18.21	17.28	-234.85	41.77
24	19.89	18.86	-233.86	41.32
e25	27.27	22.28	-229.81	41.80
e24	27.38	22.91	-230.98	40.01
e23	30.25	23.68	-227.53	42.68
e17	29.34	24.50	-230.14	39.26
10	31.37	27.11	-228.84	37.93
1	33.57	29.20	-227.47	37.36
2	33.16	31.34	-225.72	36.84
5	35.13	31.77	-222.97	39.16
20	36.98	31.96	-223.21	38.72
34	39.75	34.61	-219.54	39.73
25	44.10	38.01	-217.26	38.62

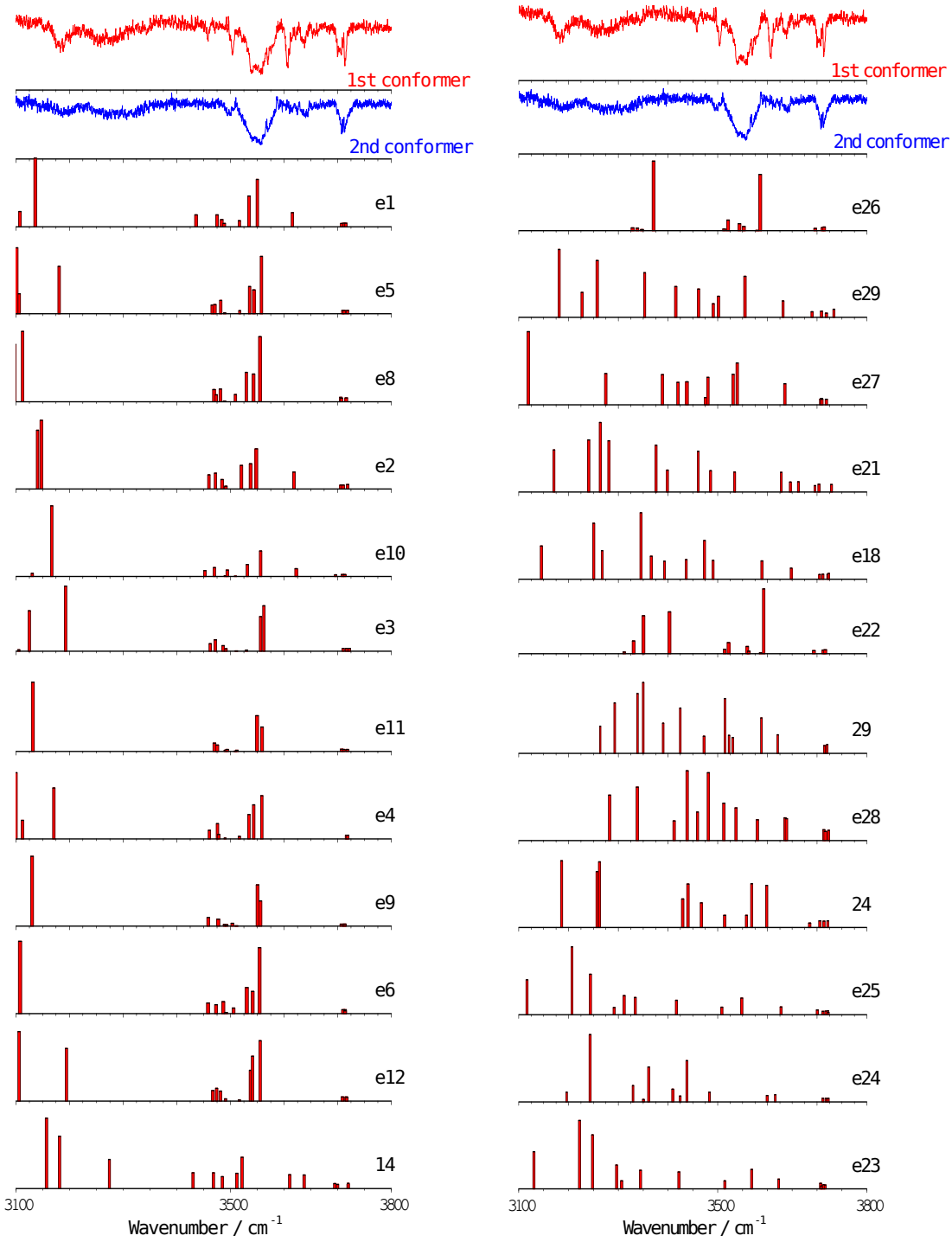

Figure 7.14a. *Experimental IDIRS for propofol·W_7 (upper traces) together with the predicted frequencies for each calculated structure. A correction factor of 0.938 was employed.*

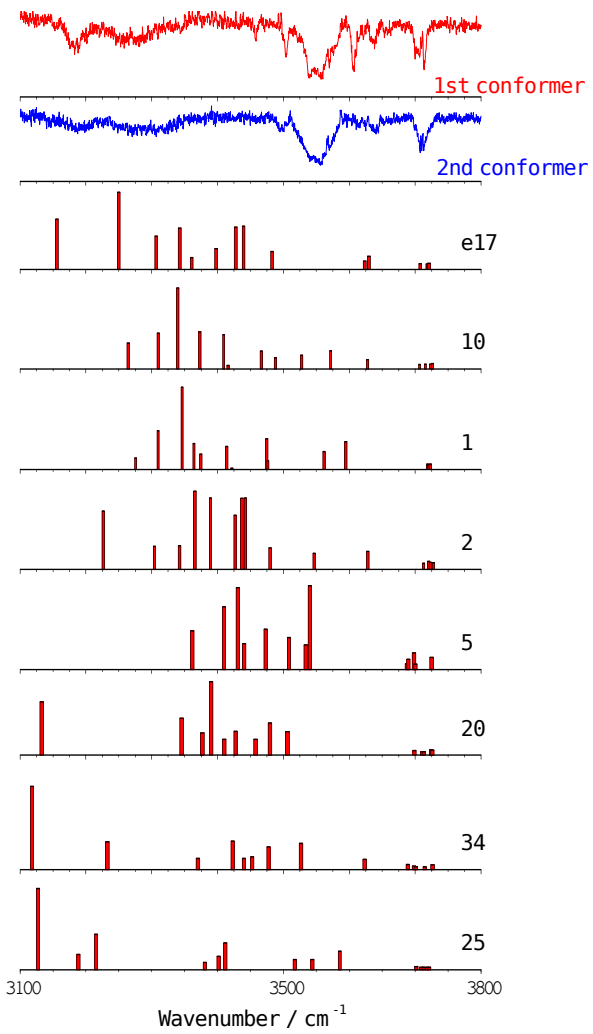

Figure 7.14b. *Experimental IDIRS for propofol·W_7 (upper traces) together with the predicted frequencies for each calculated structure. A correction factor of 0.938 was employed.*

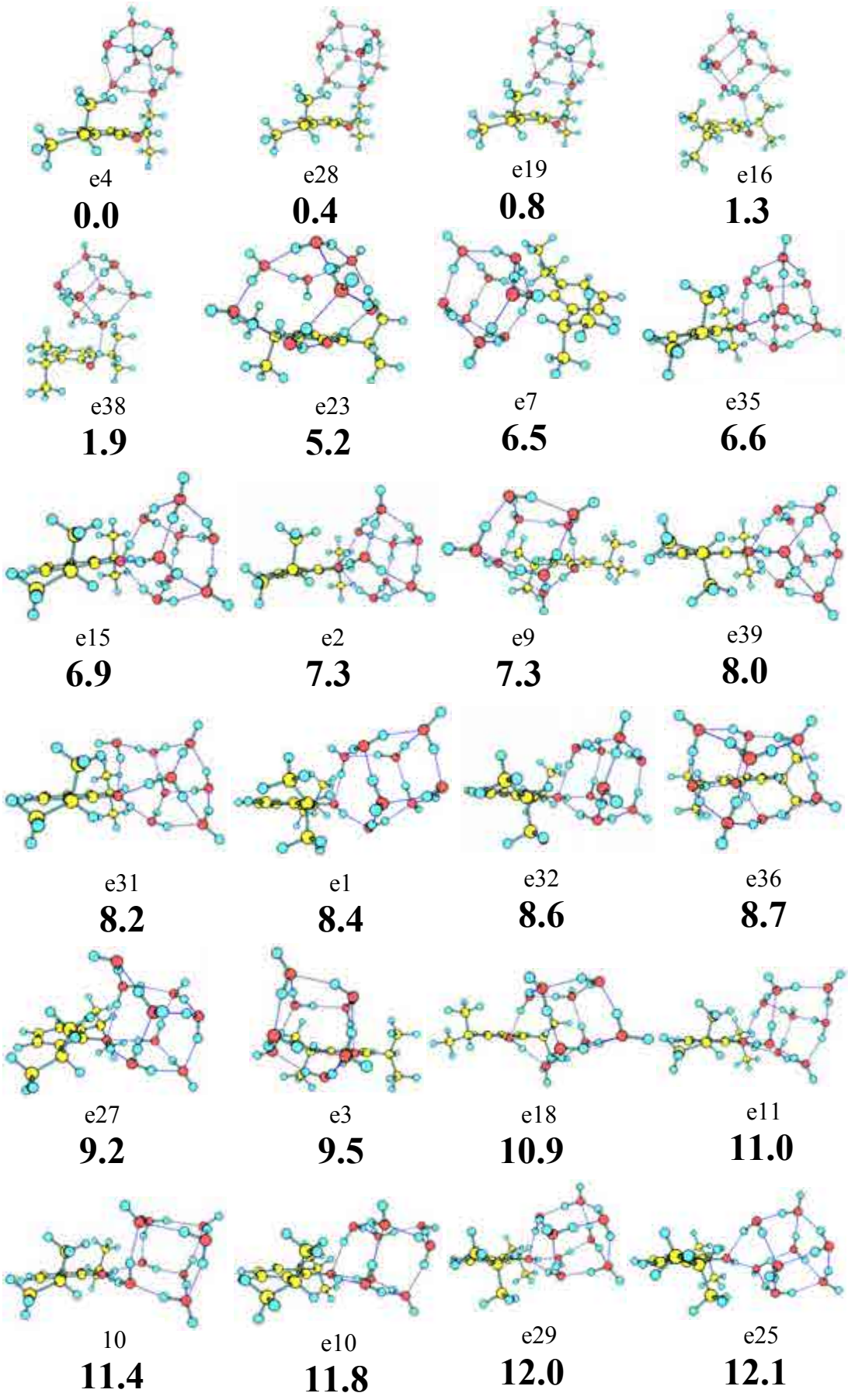

Figure 7.15a. *Propofol·W_8 calculated structures at M06-2x/6-311++G(d,p).*

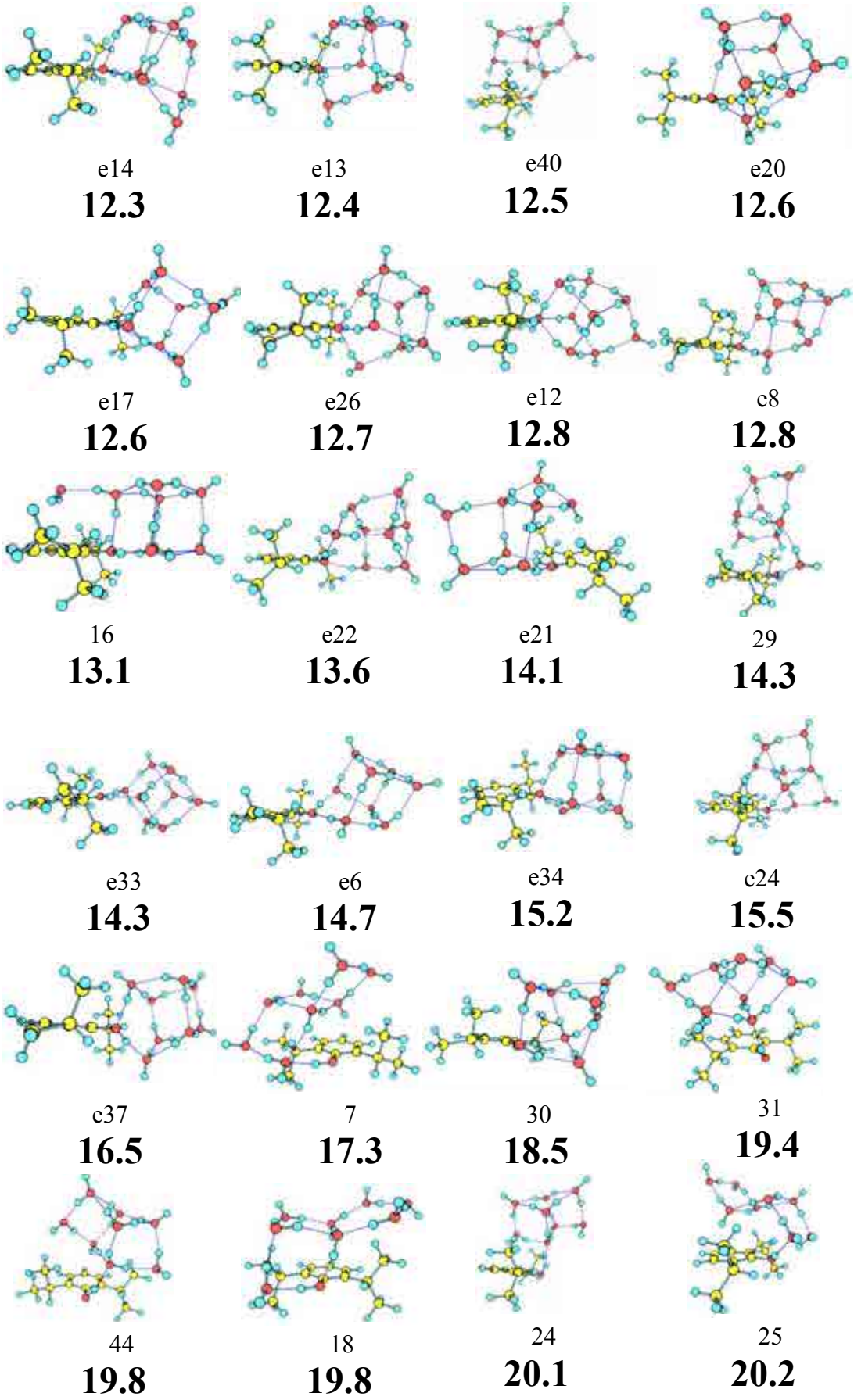

Figure 7.15b. *Propofol·W_8 calculated structures at M06-2x/6-311++G(d,p).*

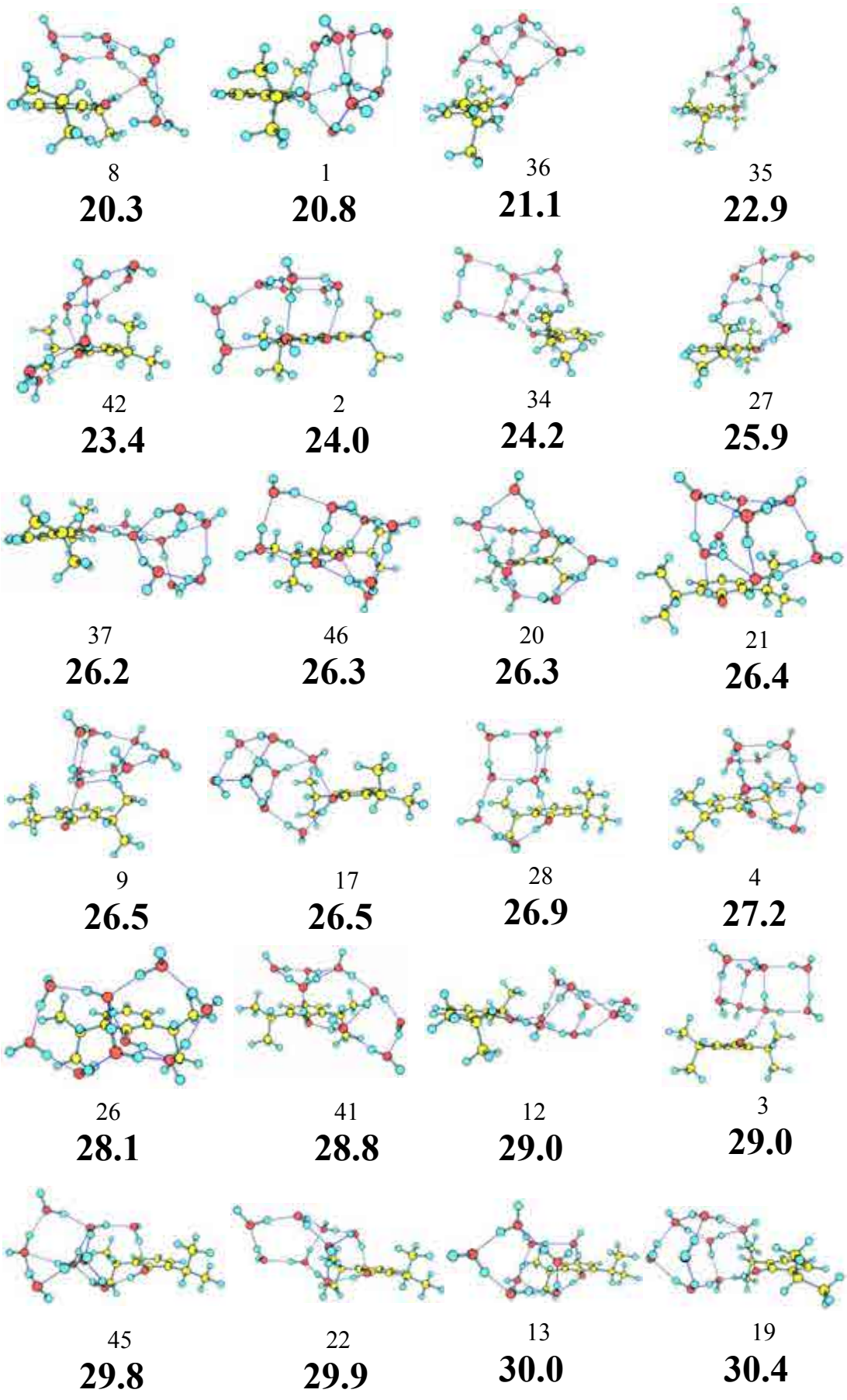

Figure 7.15c. *Propofol·W_8 calculated structures at M06-2x/6-311++G(d,p).*

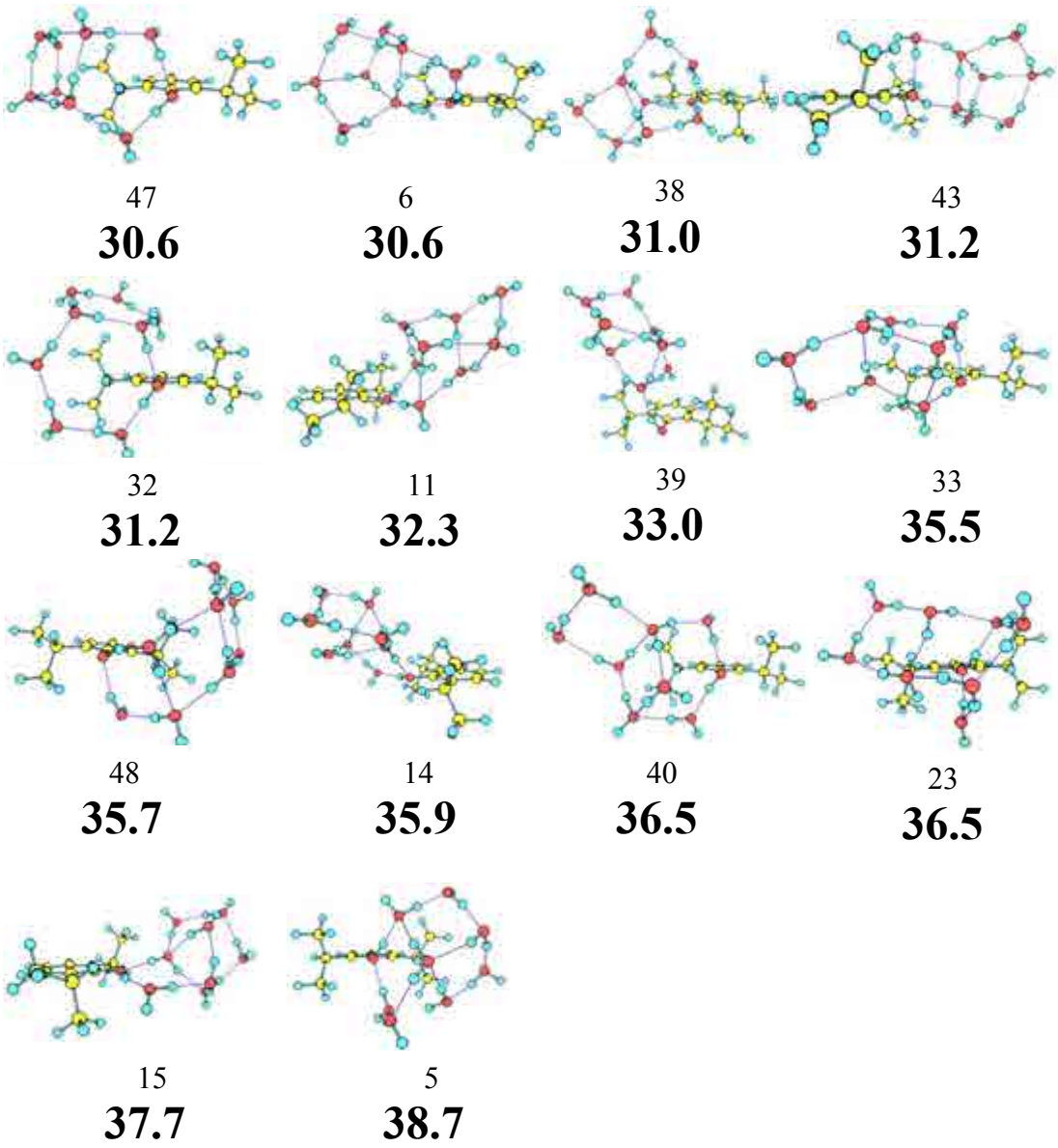

Figure 7.15d. *Propofol·W_8 calculated structures at M06-2x/6-311++G(d,p).*

Table 7.8a. *Propofol·W_8 structures with their relative energies and binding energies calculated at M06-2x/6-311++G(d,p).*

Structure	*ΔE (kJ/mol)*	*ΔE_{ZPE} (kJ/mol)*	*D_0 (kJ/mol)*	*BSSE (kJ/mol)*
e4	0.00	0.00	-290.84	47.19
e28	1.10	0.39	-290.26	47.38
e19	0.45	0.82	-289.64	47.58
e16	3.74	1.34	-293.55	46.94
e38	4.34	1.88	-292.61	47.34
e23	7.40	5.23	-284.11	48.69
e7	9.96	6.49	-283.50	48.05
e35	10.29	6.60	-283.20	48.23
e15	10.66	6.90	-282.75	48.38
e2	11.29	7.28	-282.36	48.39
e9	8.55	7.35	-282.90	47.78
e39	13.04	7.99	-282.38	47.66
e31	12.92	8.16	-282.12	47.75
e1	10.23	8.36	-282.39	47.27
e32	11.40	8.61	-281.42	48.00
e36	13.45	8.70	-281.39	47.94
e27	10.83	9.23	-281.27	47.53
e3	12.54	9.46	-284.85	47.52
e18	11.20	10.89	-280.21	46.93
e11	14.54	11.04	-280.26	46.73
10	13.28	11.37	-281.75	45.05
e10	12.05	11.84	-279.18	47.01
e29	15.11	11.97	-279.15	47.06
e25	14.77	12.12	-278.94	47.11
e14	14.53	12.30	-278.78	46.95
e13	15.63	12.37	-278.43	47.23
e40	17.57	12.46	-279.02	46.55
e20	14.70	12.56	-282.43	46.84
e17	16.37	12.57	-278.34	47.26
e26	15.55	12.72	-277.97	47.33
e12	16.54	12.78	-278.70	46.55
e8	15.78	12.83	-278.73	46.46
16	16.88	13.08	-277.55	47.55
e22	16.70	13.62	-278.64	45.76
e21	18.91	14.11	-277.67	46.40
29	17.10	14.34	-277.05	46.64
e33	15.59	14.34	-279.03	44.66
e6	15.53	14.73	-277.51	45.79
e34	19.22	15.25	-276.20	46.57
e24	22.70	15.49	-276.72	45.82
e37	20.17	16.52	-273.64	47.87
7	23.42	17.25	-273.87	46.90
30	18.98	18.49	-274.32	45.37
31	24.28	19.44	-275.72	46.67
44	23.34	19.76	-271.80	46.48
18	28.21	19.76	-270.73	47.54

Table 7.8b. *Propofol·W_8 structures with their relative energies and binding energies calculated at M06-2x/6-311++G(d,p).*

Structure	*ΔE (kJ/mol)*	*ΔE_{ZPE} (kJ/mol)*	*D_0 (kJ/mol)*	*BSSE (kJ/mol)*
24	24.91	20.10	-271.52	46.41
25	25.18	20.25	-270.90	46.88
8	26.00	20.34	-270.99	46.84
1	25.51	20.80	-270.02	47.20
36	27.15	21.07	-270.06	46.89
35	27.88	22.91	-269.58	45.54
42	31.63	23.38	-267.36	47.29
2	30.85	24.04	-265.12	48.87
34	30.97	24.23	-269.25	44.54
27	32.00	25.94	-265.65	46.43
37	29.94	26.21	-268.31	43.51
46	33.11	26.32	-266.49	45.21
20	32.79	26.34	-269.37	46.11
21	29.90	26.37	-265.91	45.74
9	30.21	26.48	-264.78	46.76
17	28.73	26.50	-265.34	46.18
28	35.42	26.87	-265.83	45.34
4	34.51	27.22	-266.76	47.85
26	33.81	28.06	-262.96	47.15
41	35.49	28.79	-263.56	45.82
12	33.49	28.96	-264.95	44.12
3	33.94	28.98	-263.97	45.07
45	34.74	29.76	-263.28	44.99
22	36.04	29.88	-263.08	45.07
13	35.24	29.98	-262.43	45.62
19	34.47	30.42	-262.99	44.61
47	34.99	30.58	-261.25	46.19
6	33.30	30.61	-264.76	42.80
38	35.34	30.97	-263.8	43.26
43	36.00	31.20	-262.94	43.89
32	41.10	31.22	-259.83	46.98
11	37.56	32.33	-260.98	44.72
39	39.45	33.01	-261.43	43.58
33	39.55	35.51	-257.95	44.57
48	43.08	35.73	-256.20	46.09
14	41.98	35.91	-258.98	43.14
40	43.56	36.51	-256.18	45.34
23	45.10	36.53	-255.17	46.32
15	40.31	37.70	-257.43	42.90
5	47.13	38.67	-257.89	45.27

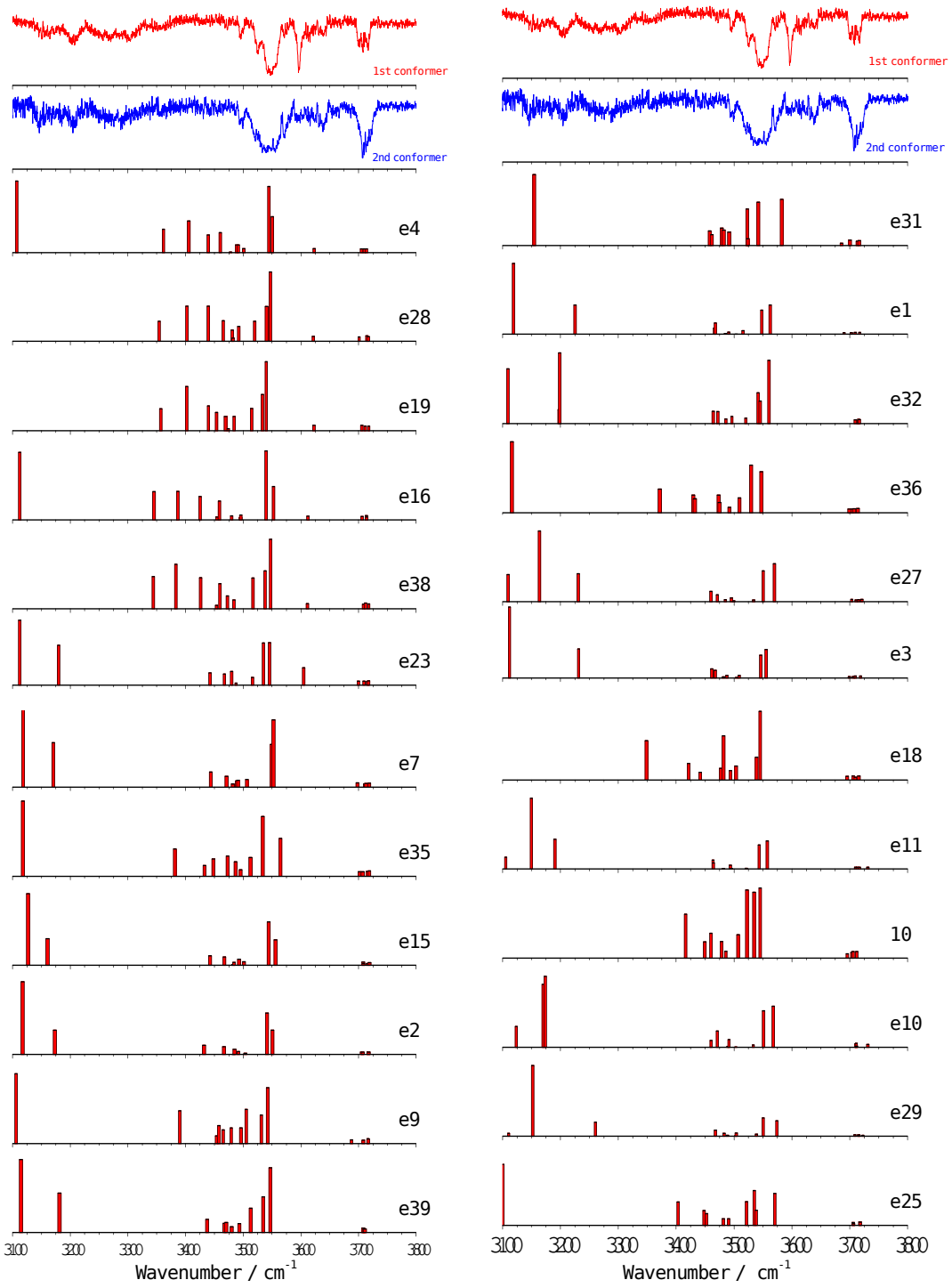

Figure 7.16a. *Experimental IDIRS for propofol·W_8 (upper traces) together with the predicted frequencies for each calculated structure. A correction factor of 0.938 was employed.*

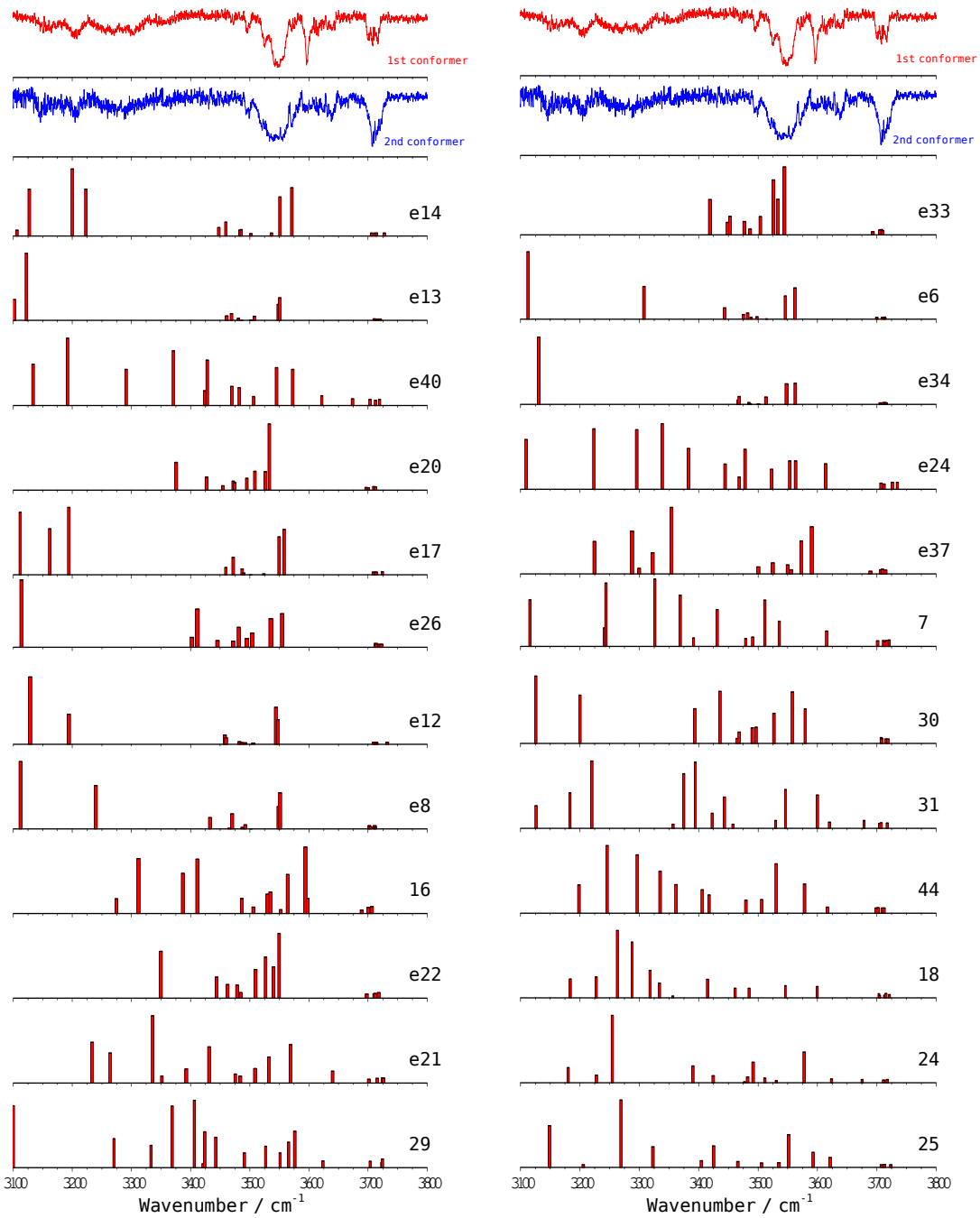

Figure 7.16b. *Experimental IDIRS for propofol·W_8 (upper traces) together with the predicted frequencies for each calculated structure. A correction factor of 0.938 was employed.*

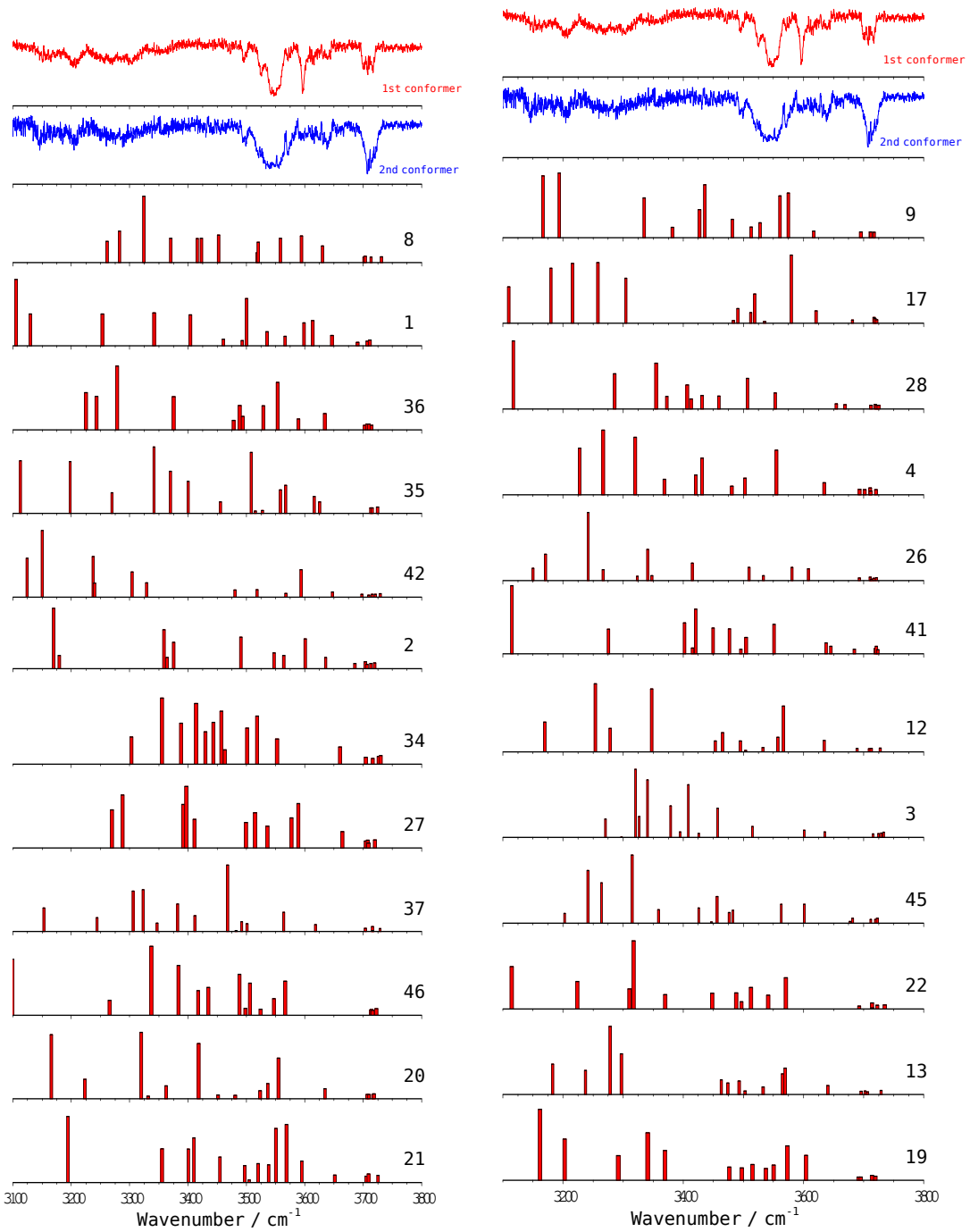

Figure 7.16c. *Experimental IDIRS for propofol·W_8 (upper traces) together with the predicted frequencies for each calculated structure. A correction factor of 0.938 was employed.*

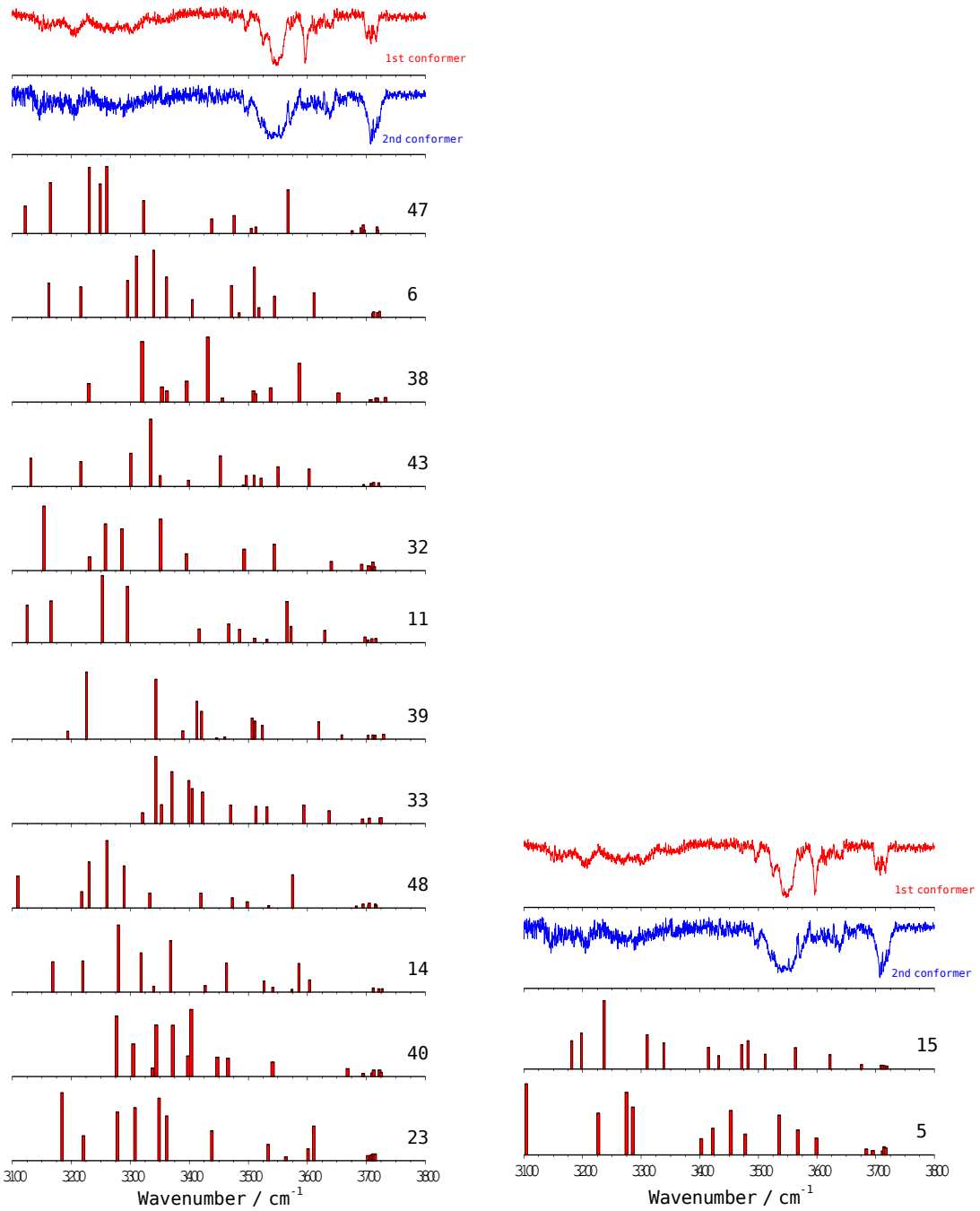

Figure 7.16d. *Experimental IDIRS for propofol·W_8 (upper traces) together with the predicted frequencies for each calculated structure. A correction factor of 0.938 was employed.*

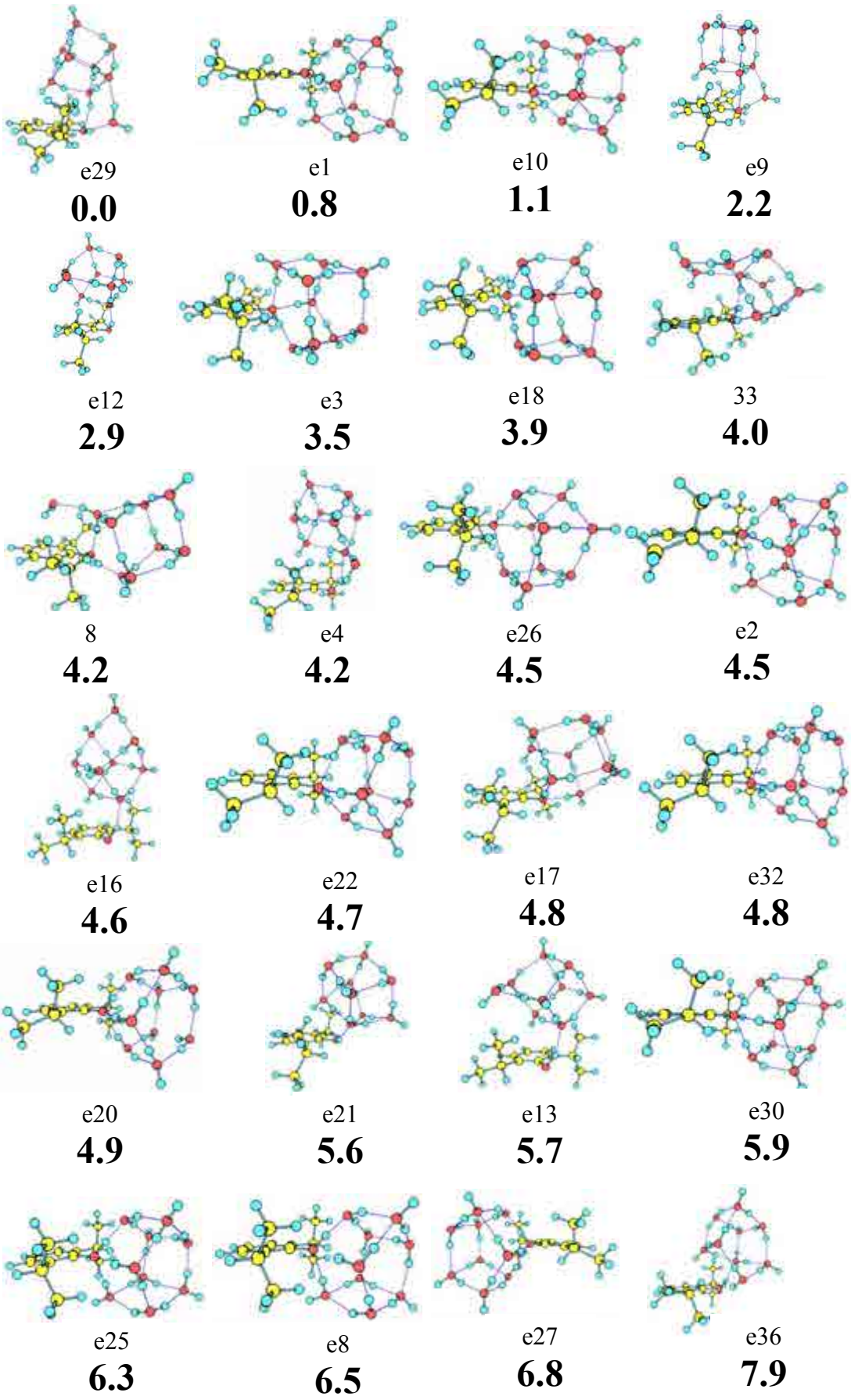

Figure 7.17a. *Propofol·W_9 calculated structures at M06-2x/6-311++G(d,p).*

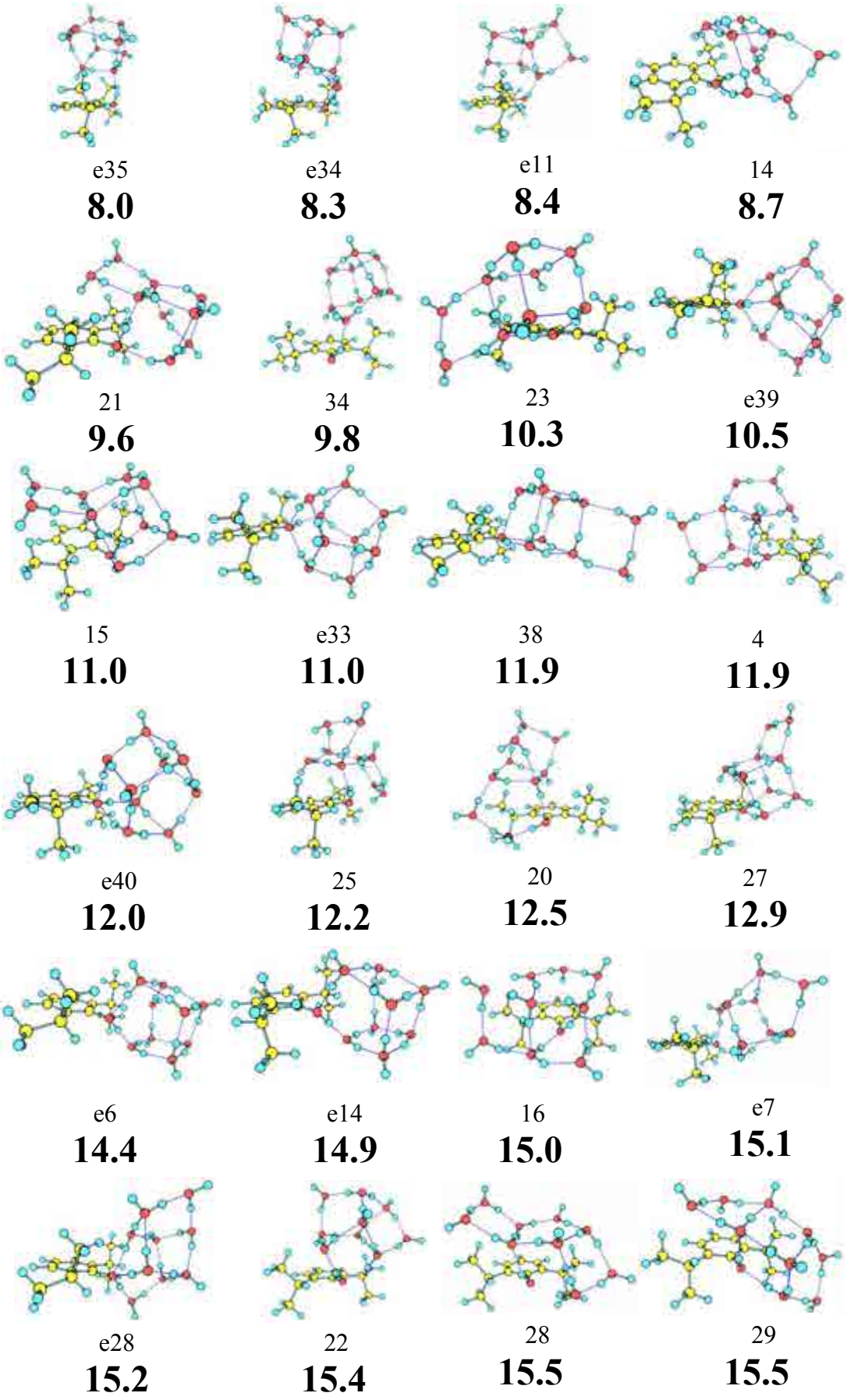

Figure 7.17b. *Propofol·W_9 calculated structures at M06-2x/6-311++G(d,p).*

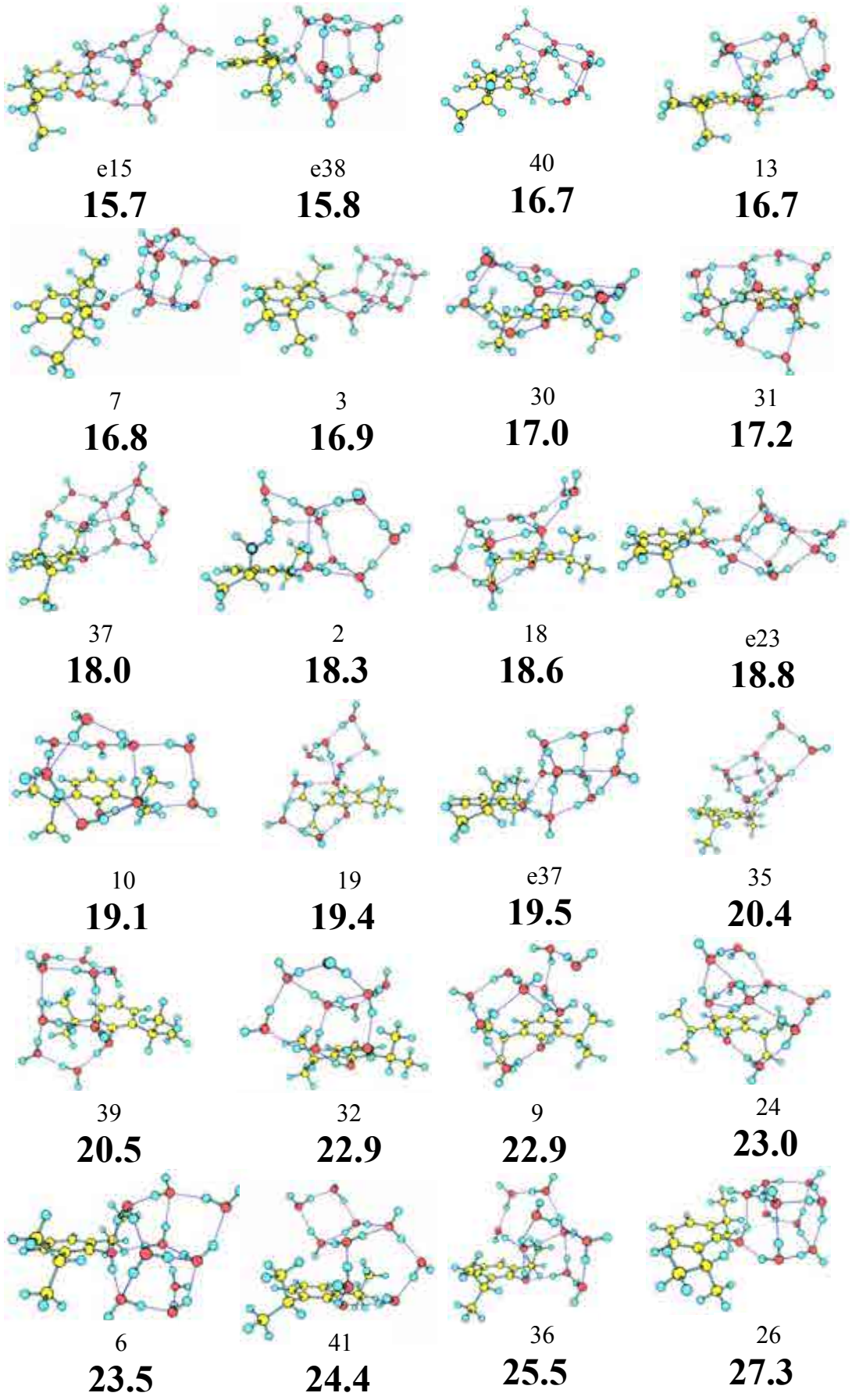

Figure 7.17c. *Propofol·W_9 calculated structures at M06-2x/6-311++G(d,p).*

11 **27.4** 5 **27.6** 17 **30.2**

Figure 7.17d. *Propofol·W_9 calculated structures at M06-2x/6-311++G(d,p).*

Table 7.9a. *Propofol·W_9 structures with their relative energies and binding energies calculated at M06-2x/6-311++G(d,p).*

Structure	*ΔE (kJ/mol)*	*ΔE_{ZPE} (kJ/mol)*	*D_0 (kJ/mol)*	*BSSE (kJ/mol)*
e29	0.00	0	-325.95	53.36
e1	3.21	0.85	-323.68	54.79
e10	2.58	1.12	-323.24	54.94
e5	2.58	1.14	-323.24	54.93
e9	0.81	2.23	-323.41	53.67
e12	5.73	2.88	-322.42	54.01
e3	5.01	3.55	-321.08	54.68
e18	6.44	3.89	-320.68	54.74
33	5.71	3.96	-319.80	55.55
8	6.49	4.18	-325.17	53.76
e4	4.63	4.21	-321.03	54.06
e26	6.32	4.50	-320.12	54.68
1	6.31	4.52	-320.11	54.68
e2	5.68	4.53	-320.17	54.61
e16	7.81	4.64	-321.58	53.09
e22	6.90	4.74	-319.74	54.83
e17	7.41	4.77	-320.58	53.96
e32	6.90	4.83	-319.66	54.82
e20	8.81	4.90	-319.69	54.72
e21	5.97	5.59	-319.33	54.38
e13	6.07	5.65	-319.65	54.01
e30	8.23	5.85	-318.94	54.51
e31	8.23	5.86	-318.94	54.51
e25	8.46	6.34	-322.00	54.77
e8	8.54	6.48	-321.69	54.93
e27	8.45	6.83	-317.85	54.63
e24	8.45	6.83	-317.83	54.65
e36	6.51	7.92	-317.52	53.86
e35	9.00	7.96	-321.07	54.08
e34	7.35	8.25	-316.97	54.08
e11	8.89	8.44	-316.95	54.06
14	10.07	8.75	-317.16	53.40
21	14.20	9.56	-315.96	53.79
34	10.12	9.78	-316.66	53.01
23	12.43	10.33	-316.11	52.87
e39	12.30	10.50	-314.25	54.56
15	12.11	10.96	-314.74	53.76
e33	12.30	11.04	-313.85	54.42
38	12.84	11.89	-316.32	51.10
4	17.21	11.93	-314.83	52.70
e40	12.93	12.01	-313.24	54.20
25	12.25	12.20	-313.55	53.71
20	15.58	12.46	-313.62	53.22
27	14.12	12.87	-314.48	51.96
e6	17.69	14.45	-311.13	53.73
e14	19.99	14.94	-314.30	53.87

Table 7.9b. *Propofol·W_9 structures with their relative energies and binding energies calculated at M06-2x/6-311++G(d,p).*

Structure	*ΔE (kJ/mol)*	*ΔE_{ZPE} (kJ/mol)*	*D_0 (kJ/mol)*	*BSSE (kJ/mol)*
16	21.36	14.96	-312.95	51.40
e7	19.22	15.09	-310.96	53.40
e19	19.22	15.11	-310.95	53.40
e28	20.59	15.20	-309.83	54.28
22	18.61	15.39	-311.01	52.91
28	18.37	15.47	-310.60	53.24
29	21.93	15.48	-309.90	53.93
e15	20.60	15.72	-313.80	53.59
e38	19.40	15.83	-310.31	53.17
40	19.69	16.70	-309.49	53.12
13	18.92	16.70	-310.74	51.87
7	18.54	16.86	-311.94	50.65
3	15.94	16.91	-312.32	50.08
30	22.19	16.98	-309.84	52.63
31	22.07	17.20	-309.33	52.78
37	21.20	18.04	-309.26	52.01
2	21.78	18.35	-308.56	52.55
18	26.32	18.58	-307.69	53.18
e23	21.14	18.80	-308.61	51.90
10	24.59	19.06	-307.36	52.89
19	23.44	19.36	-307.43	52.51
e37	23.37	19.51	-307.29	52.51
35	20.38	20.41	-306.72	52.18
39	29.53	20.46	-304.79	54.06
32	27.11	22.91	-306.48	50.07
9	24.00	22.91	-305.73	50.67
24	24.37	22.97	-305.13	51.21
6	26.25	23.49	-304.67	51.15
41	30.21	24.45	-303.44	51.56
36	28.53	25.49	-302.24	51.58
26	29.74	27.33	-300.10	51.88
11	33.25	27.38	-301.69	50.23
5	34.16	27.60	-299.51	52.19
17	34.45	30.21	-296.74	52.50

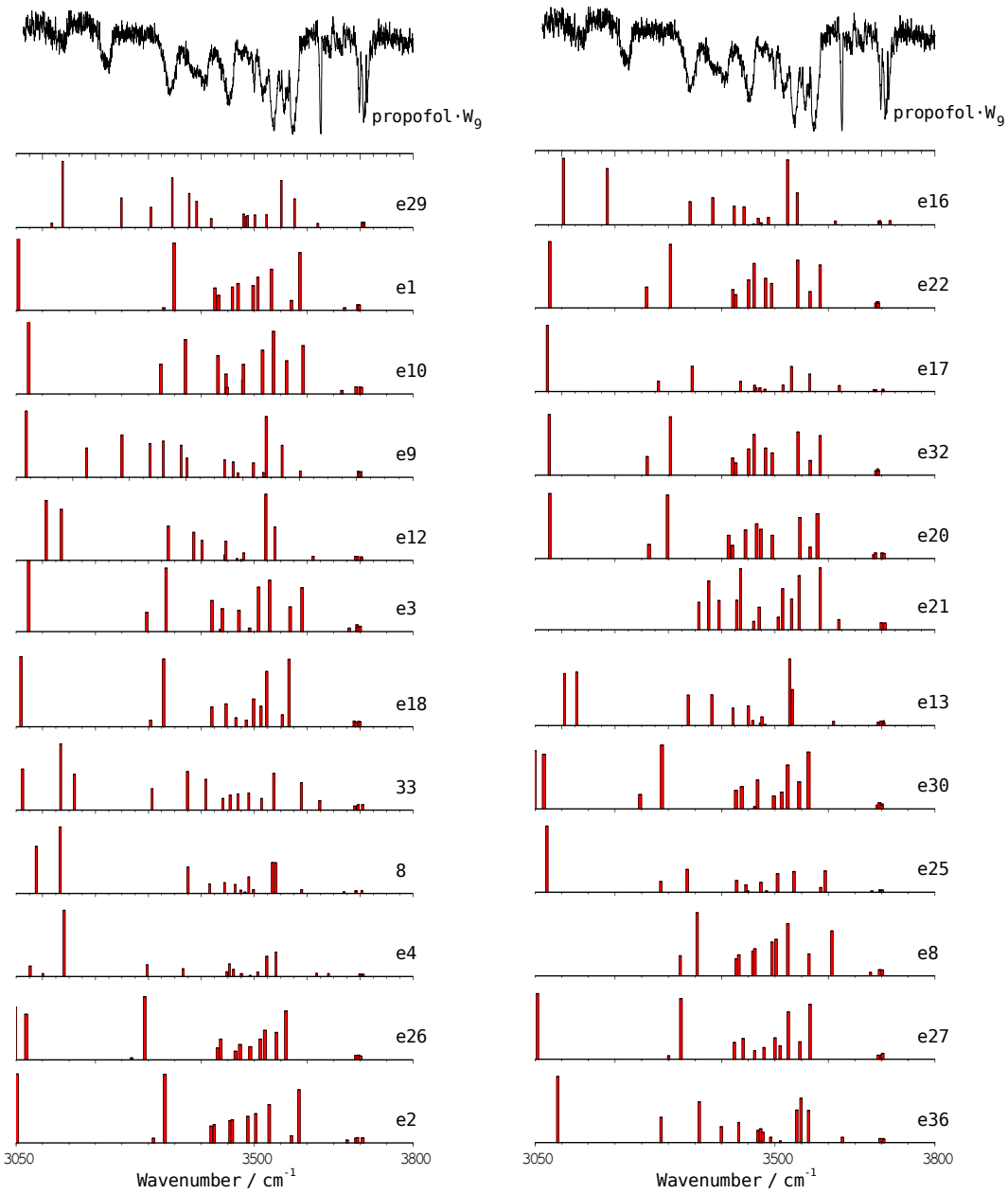

Figure 7.18a. *Experimental IDIRS for propofol·W_9 (upper traces) together with the predicted frequencies for each calculated structure. A correction factor of 0.935 was employed.*

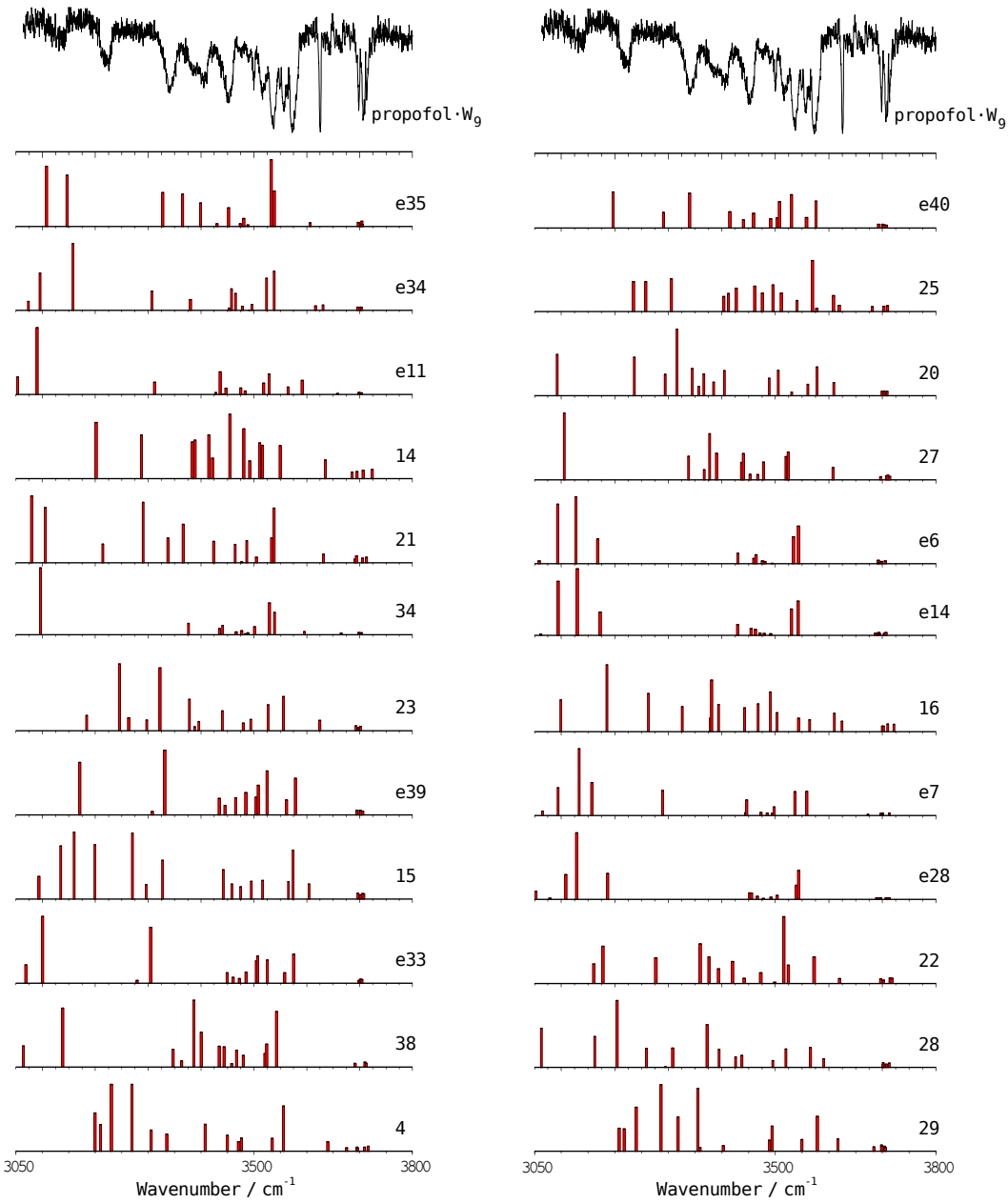

Figure 7.18b. *Experimental IDIRS for propofol·W_9 (upper traces) together with the predicted frequencies for each calculated structure. A correction factor of 0.935 was employed.*

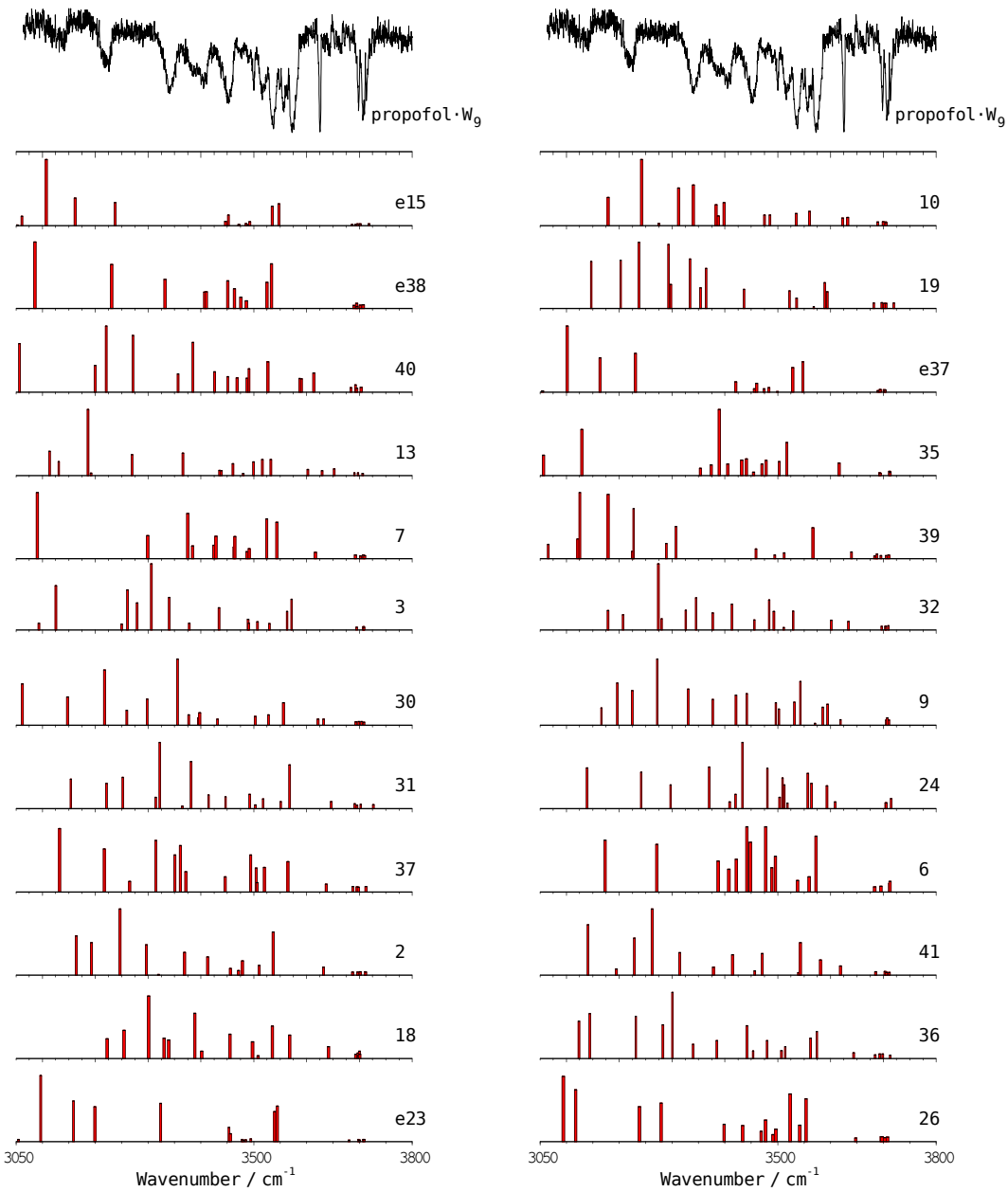

Figure 7.18c. *Experimental IDIRS for propofol·W_9 (upper traces) together with the predicted frequencies for each calculated structure. A correction factor of 0.935 was employed.*

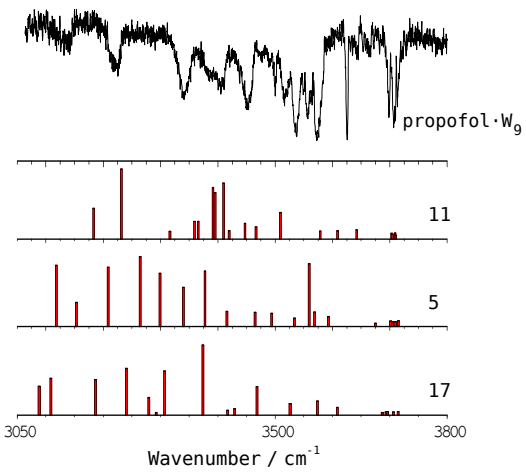

Figure 7.18d. *Experimental IDIRS for propofol·W_9 (upper traces) together with the predicted frequencies for each calculated structure. A correction factor of 0.935 was employed.*

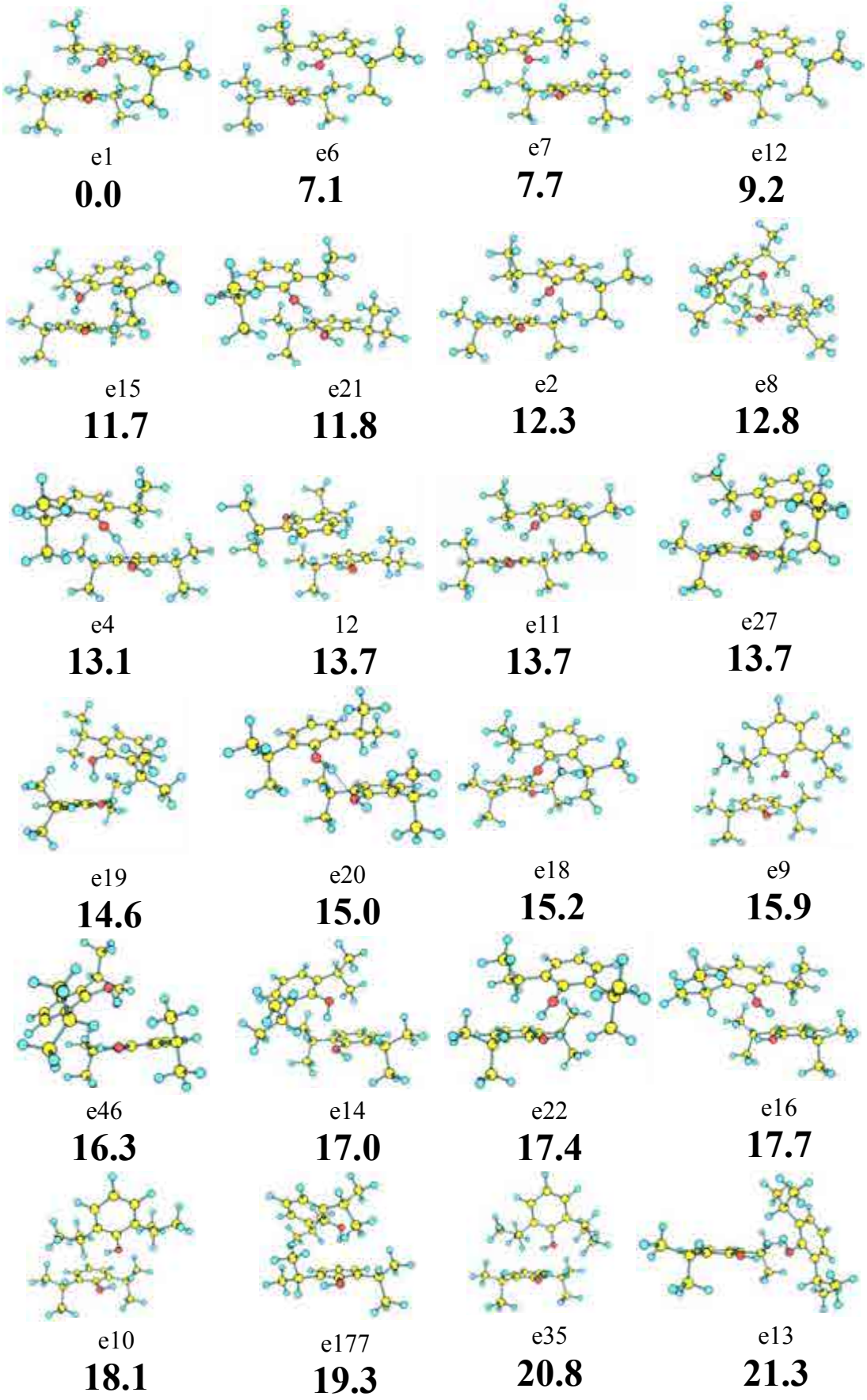

Figure 7.19a. *Propofol$_2$ calculated structures at M06-2x/6-311++G(d,p).*

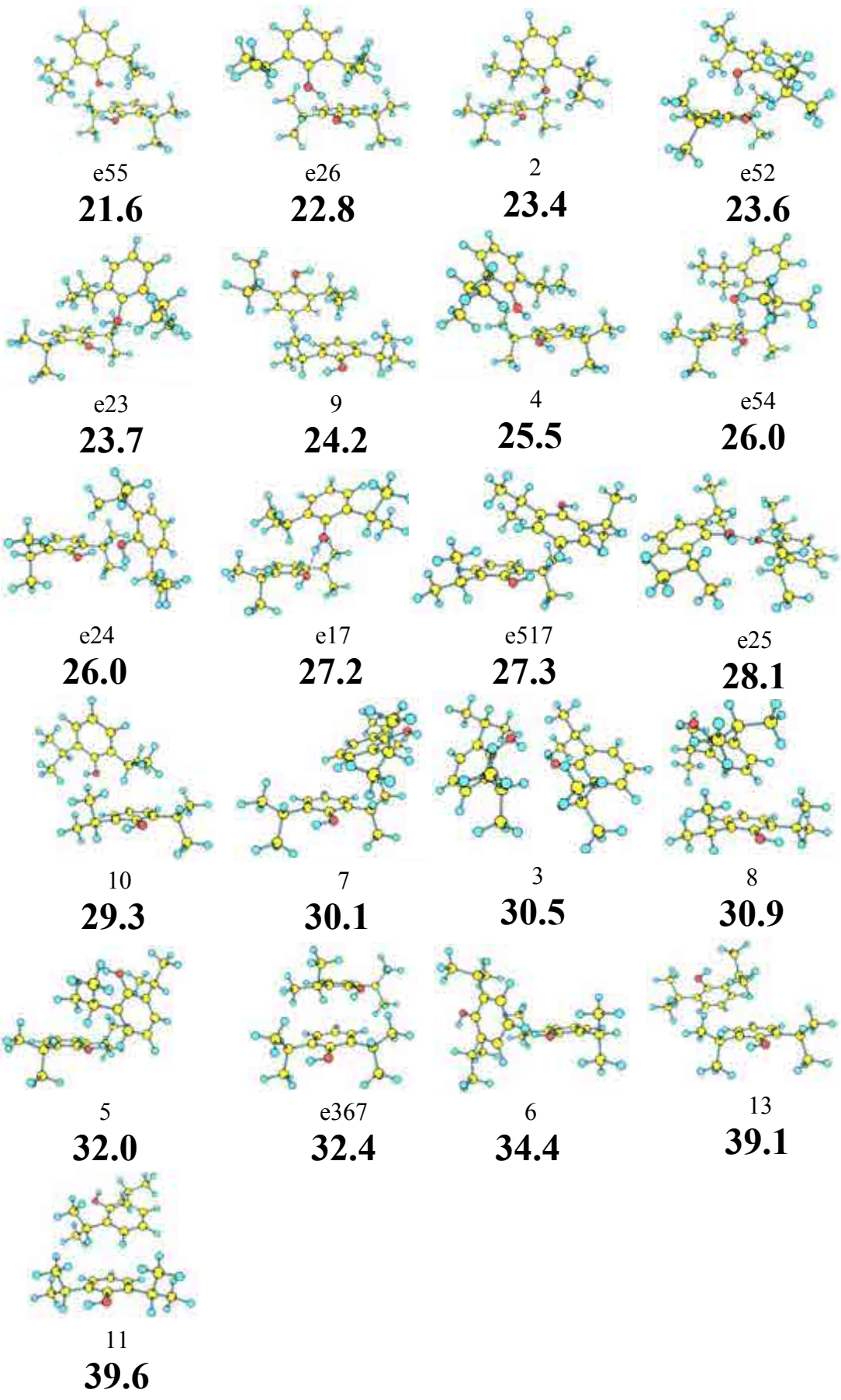

Figure 7.19b. *Propofol$_2$ calculated structures at M06-2x/6-311++G(d,p).*

Table 7.10. *Propofol$_2$ structures with their relative energies and binding energies calculated at M06-2x/6-311++G(d,p).*

Structure	*ΔE (kJ/mol)*	*ΔE_{ZPE} (kJ/mol)*	*D_0 (kJ/mol)*	*BSSE (kJ/mol)*
e1	0.00	0.00	-49.69	7.92
e6	6.80	7.06	-46.66	7.55
e7	8.56	7.73	-50.08	7.26
e12	9.97	9.17	-40.30	7.99
e15	12.57	11.69	-38.26	7.51
e21	11.59	11.77	-41.51	7.99
e2	12.01	12.26	-37.52	7.83
e8	13.31	12.78	-40.89	7.60
e4	13.26	13.14	-40.50	7.77
12	13.37	13.66	-40.94	6.67
e11	14.41	13.69	-41.63	7.79
e27	14.61	13.70	-40.19	7.37
e19	16.85	14.59	-35.83	7.04
e20	15.82	15.03	-44.00	7.88
e18	16.40	15.23	-40.54	7.35
e9	18.99	15.89	-35.63	6.09
e46	15.07	16.29	-41.64	7.14
e14	18.63	17.02	-37.16	7.23
e22	19.14	17.39	-42.43	7.010
e16	18.41	17.74	-38.63	6.89
e10	19.50	18.08	-33.65	6.03
e177	18.92	19.29	-35.38	6.59
e35	21.85	20.82	-34.70	5.75
e13	21.04	21.28	-30.52	5.96
e55	22.42	21.60	-35.65	6.01
e26	23.36	22.84	-27.76	7.01
2	23.02	23.42	-31.87	6.11
e52	24.77	23.58	-36.52	6.82
e23	24.14	23.72	-31.64	5.91
9	27.21	24.24	-31.82	5.35
4	24.87	25.54	-33.31	6.21
e54	28.09	25.98	-32.77	6.31
e24	25.26	26.05	-32.80	6.22
e17	28.10	27.22	-27.26	6.78
e517	27.97	27.28	-29.59	6.25
e25	27.28	28.11	-24.16	5.34
10	29.87	29.34	-22.21	5.92
7	31.56	30.11	-22.24	5.26
3	31.23	30.49	-28.42	4.20
8	33.50	30.91	-21.91	4.80
5	33.28	31.99	-24.14	5.14
e367	34.42	32.41	-28.92	5.58
6	35.80	34.41	-26.33	4.32
13	42.44	39.14	-22.26	4.61
11	42.05	39.57	-17.79	4.05

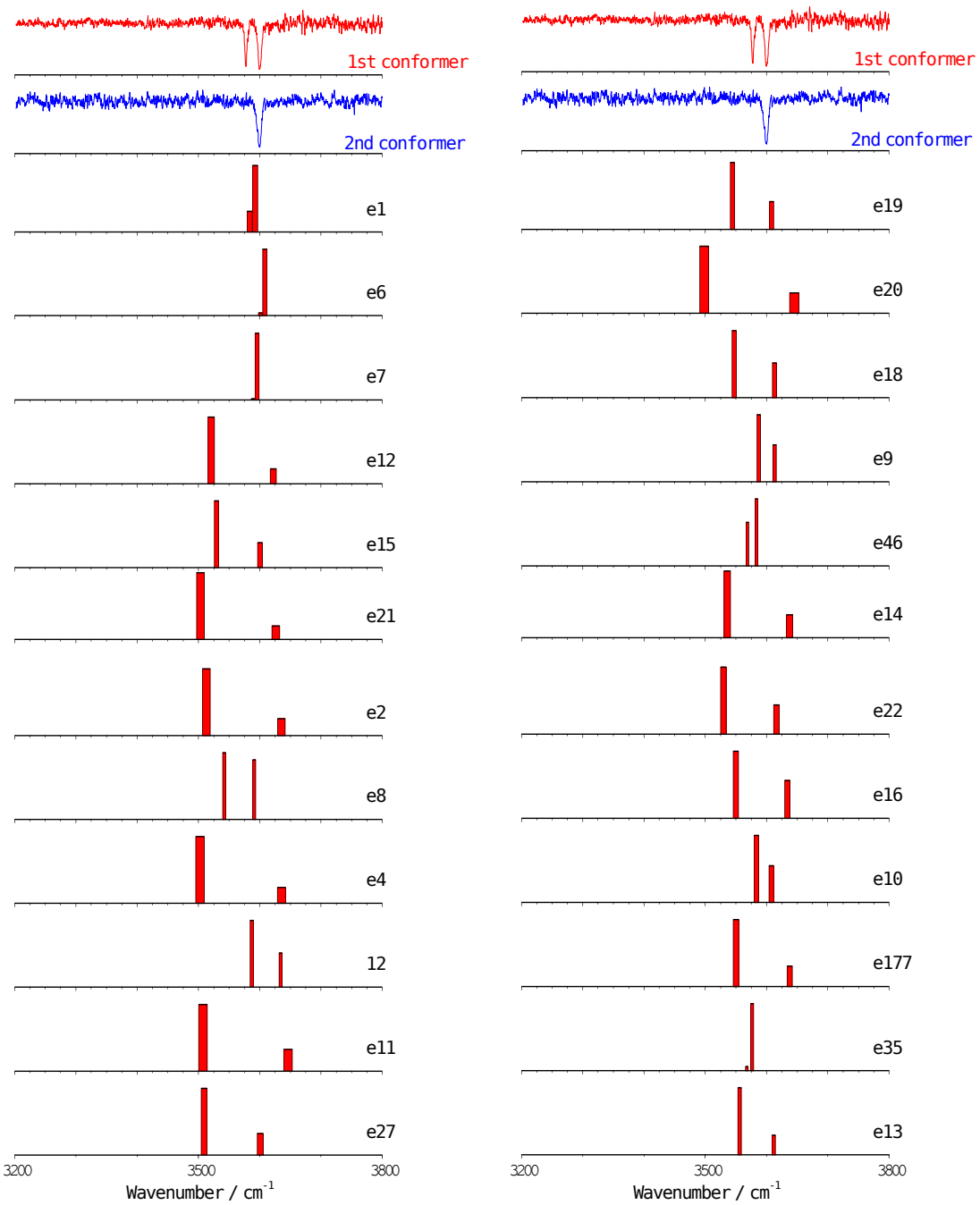

Figure 7.20a. *Experimental IDIRS for propofol$_2$ (upper traces) together with the predicted frequencies for each calculated structure. A correction factor of 0.93 was employed.*

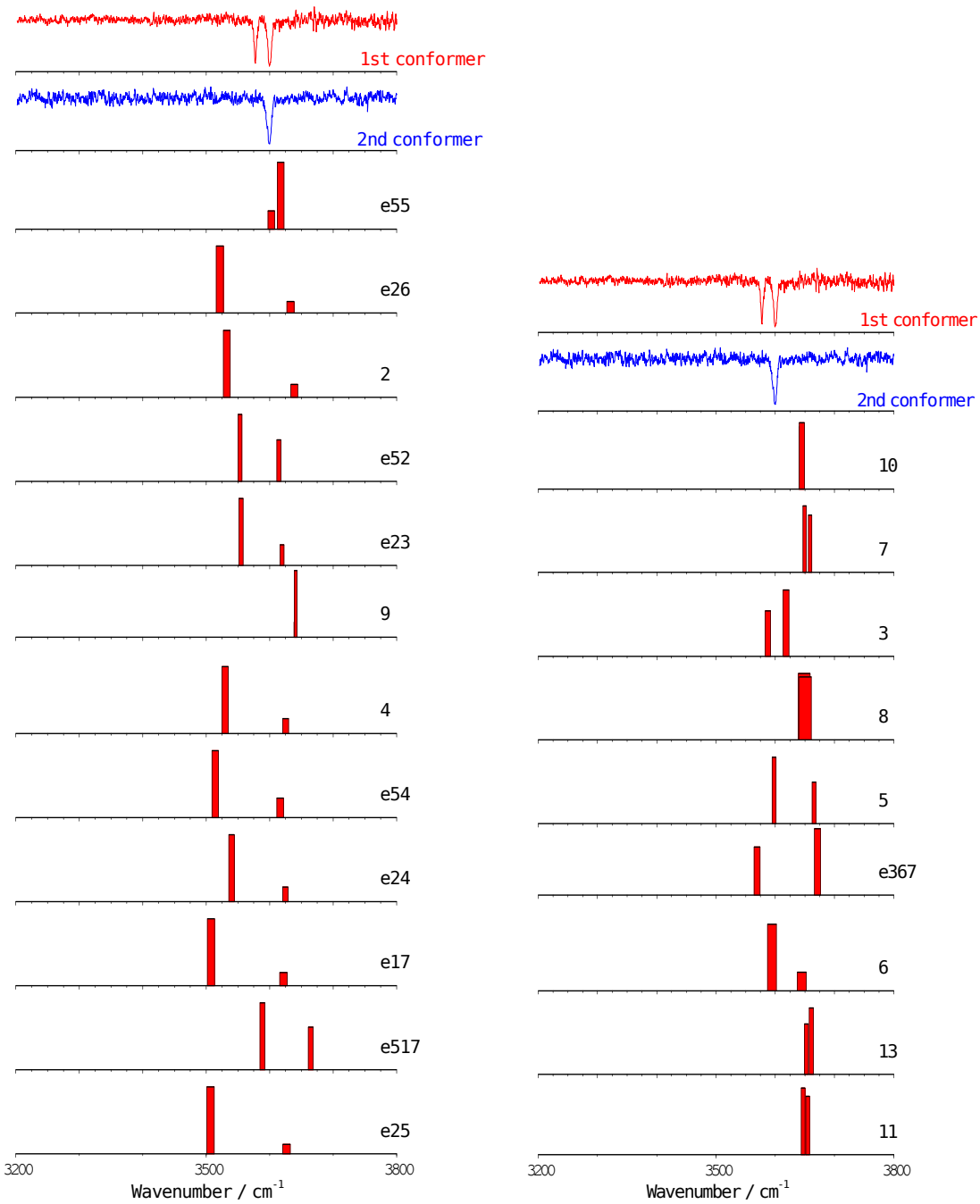

Figure 7.20b. *Experimental IDIRS for propofol$_2$ (upper traces) together with the predicted frequencies for each calculated structure. A correction factor of 0.93 was employed.*

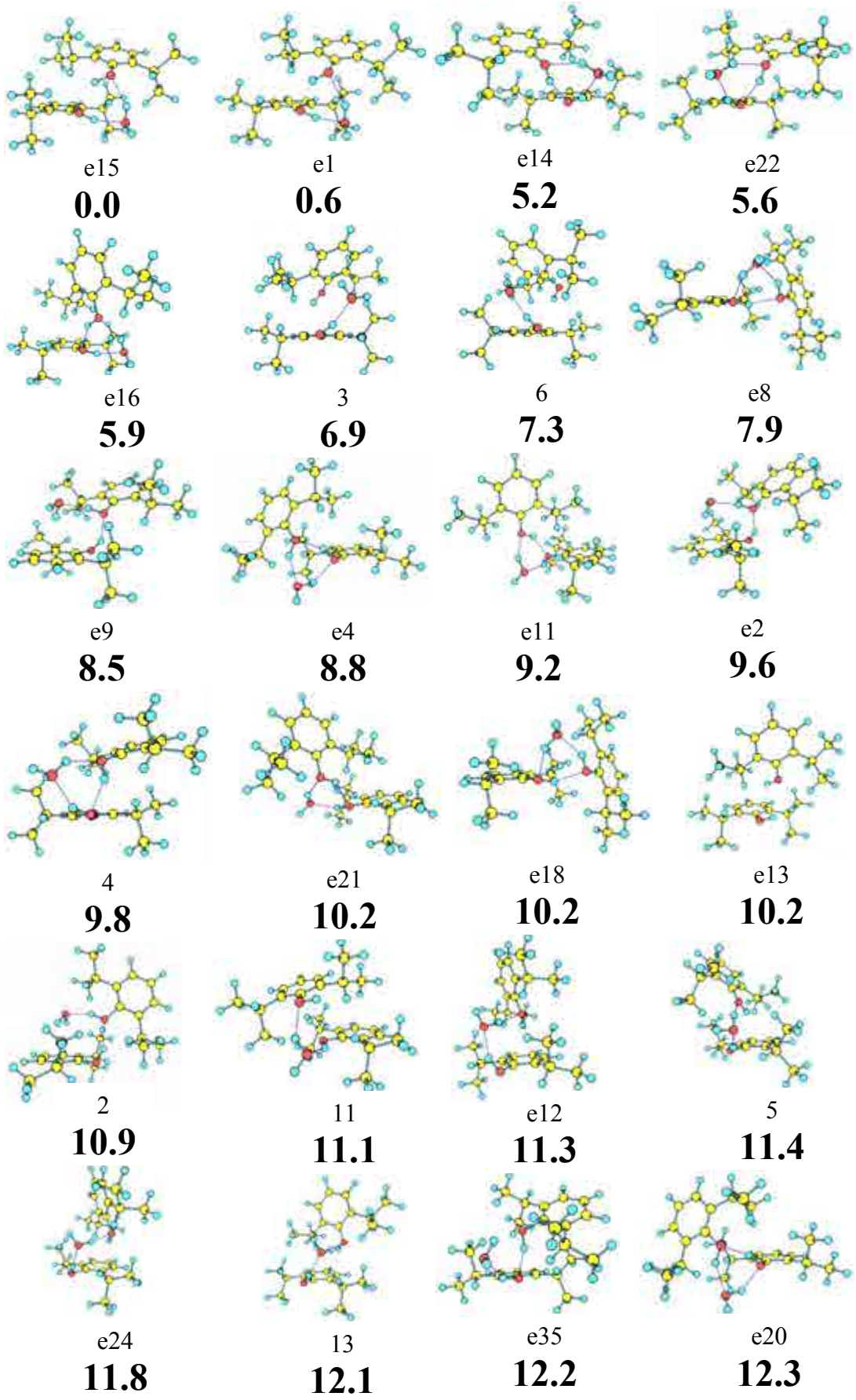

Figure 7.21a. *Propofol$_2$·W$_1$ calculated structures at M06-2x/6-31+G(d).*

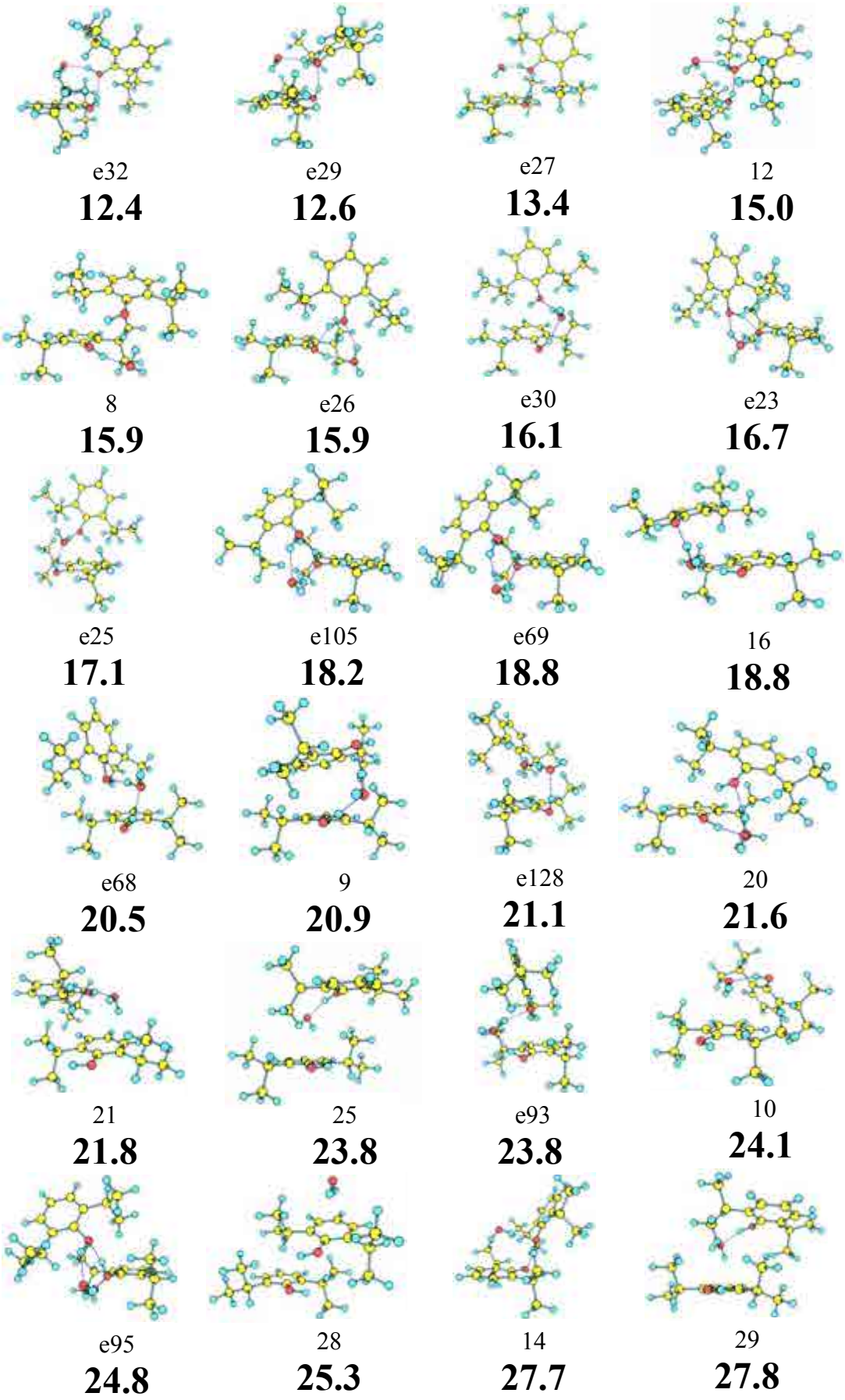

Figure 7.21b. *Propofol$_2$·W$_1$ calculated structures at M06-2x/6-31+G(d).*

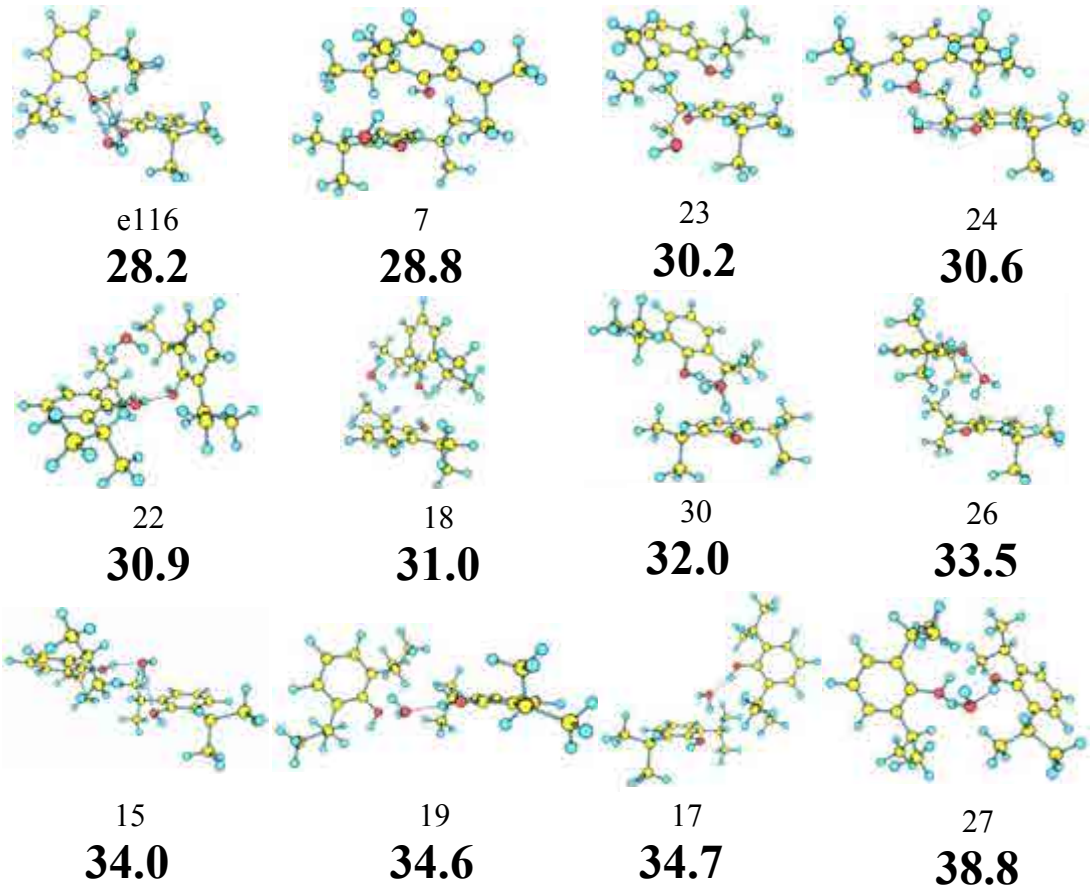

Figure 7.21c. *Propofol$_2$·W$_1$ calculated structures at M06-2x/6-31+G(d).*

Table 7.11a. *Propofol$_2$·W$_1$ structures with their relative energies and binding energies calculated at M06-2x/6-31+G(d).*

Structure	*ΔE (kJ/mol)*	*ΔE_{ZPE} (kJ/mol)*	*D_0 (kJ/mol)*	*BSSE (kJ/mol)*
e15	0.00	0.00	-86.00	16.96
e1	-0.79	0.63	-81.79	17.24
e14	4.58	5.16	-77.35	16.74
e22	5.47	5.64	-80.61	16.71
e16	4.29	5.94	-79.08	15.05
3	11.18	6.91	-76.48	16.27
6	6.92	7.31	-76.31	15.63
e8	7.80	7.94	-76.17	15.56
e9	9.09	8.46	-73.55	17.65
e4	8.57	8.78	-73.96	16.52
e11	7.37	9.20	-75.14	15.73
e2	9.81	9.58	-72.01	17.66
4	10.55	9.80	-74.32	15.53
e21	10.02	10.16	-77.52	15.69
e18	10.02	10.19	-77.08	15.69
e13	11.14	10.21	-76.79	15.96
2	11.39	10.93	-71.91	16.41
11	11.36	11.07	-71.23	17.36
e12	14.78	11.26	-72.46	15.94
5	12.11	11.41	-74.27	17.27
e24	11.37	11.78	-71.39	16.49
13	13.52	12.12	-71.41	16.13
e35	13.90	12.18	-74.54	16.23
e20	14.27	12.21	-74.84	15.90
e32	14.05	12.37	-72.79	17.81
e29	13.33	12.57	-72.43	17.96
e27	15.24	13.37	-69.56	16.32
12	14.41	15.03	-72.31	16.02
8	13.93	15.86	-70.13	17.38
e26	15.18	15.92	-72.40	15.05
e30	16.94	16.09	-67.99	15.58
e23	18.06	16.67	-75.07	14.93
e25	17.86	17.11	-70.59	15.67
e105	18.36	18.24	-72.17	16.25
e69	20.90	18.83	-71.84	16.00
16	17.04	18.84	-68.09	13.14
e68	24.16	20.54	-69.10	15.79
9	21.29	20.87	-63.78	14.61
e128	23.98	21.07	-71.22	15.72
20	21.26	21.63	-69.90	14.32
21	23.56	21.75	-62.33	15.17
25	26.40	23.78	-61.02	14.46
e93	24.56	23.84	-67.08	15.75
10	28.17	24.12	-60.25	15.29
e95	25.84	24.83	-71.18	15.69
28	30.29	25.25	-63.71	13.99

Table 7.11b. *Propofol$_2$·W$_1$ structures with their relative energies and binding energies calculated at M06-2x/6-31+G(d).*

Structure	*ΔE (kJ/mol)*	*ΔE_{ZPE} (kJ/mol)*	*D_0 (kJ/mol)*	*BSSE (kJ/mol)*
14	29.77	27.66	-58.07	13.93
29	30.13	27.76	-57.90	14.00
e116	31.11	28.22	-65.02	14.76
7	31.82	28.83	-54.40	16.03
23	33.28	30.18	-57.51	15.27
24	29.09	30.58	-54.46	14.62
22	33.14	30.86	-54.57	14.64
18	35.13	31.03	-55.89	13.15
30	34.37	31.99	-52.49	15.59
26	36.05	33.52	-55.01	16.91
15	34.15	34.02	-50.54	15.51
19	37.34	34.61	-48.48	16.58
17	37.34	34.66	-49.98	15.02
27	36.35	38.84	-56.78	13.53
e116	31.11	28.22	-65.02	14.76
7	31.82	28.83	-54.40	16.03
23	33.28	30.18	-57.51	15.27
24	29.09	30.58	-54.46	14.62
22	33.14	30.86	-54.57	14.64
18	35.13	31.03	-55.89	13.15
30	34.37	31.99	-52.49	15.59
26	36.05	33.52	-55.01	16.91
15	34.15	34.02	-50.54	15.51
19	37.34	34.61	-48.48	16.58
17	37.34	34.66	-49.98	15.02
27	36.35	38.84	-56.78	13.53

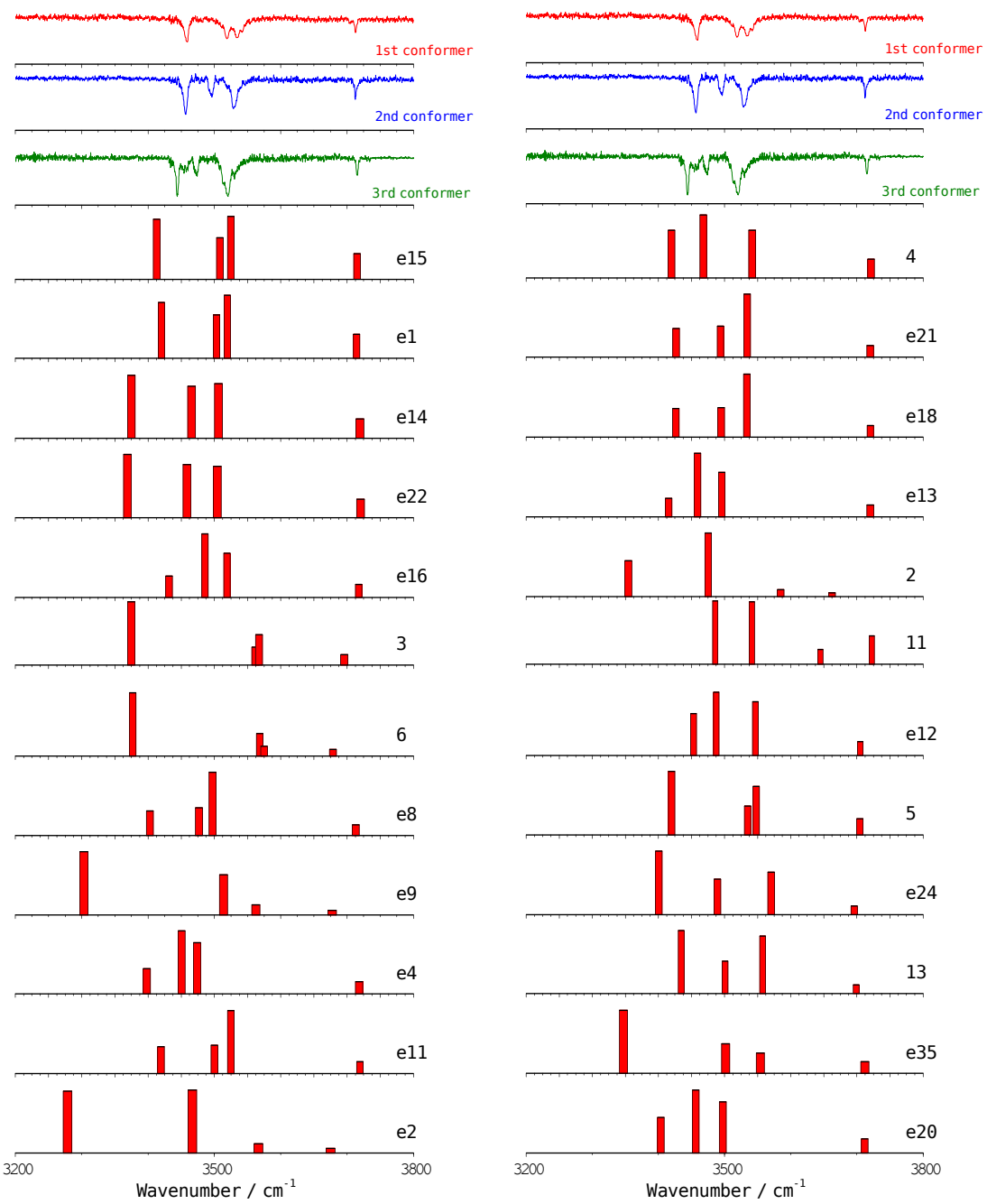

Figure 7.22a. *Experimental IDIRS for propofol$_2$·W_1 (upper traces) together with the predicted frequencies for each calculated structure. A correction factor of 0.956 was employed.*

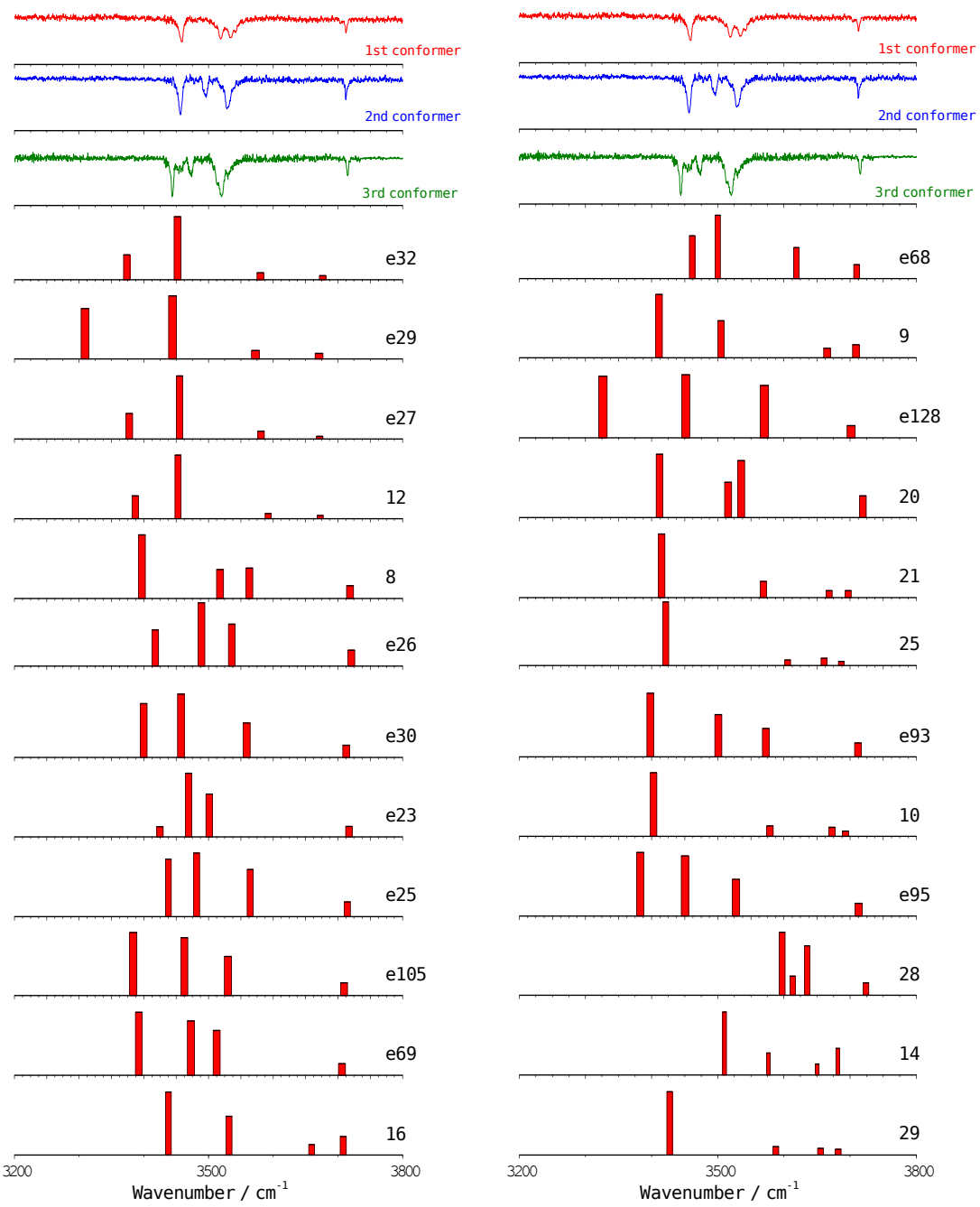

Figure 7.22b. *Experimental IDIRS for propofol$_2$·W$_1$ (upper traces) together with the predicted frequencies for each calculated structure. A correction factor of 0.956 was employed.*

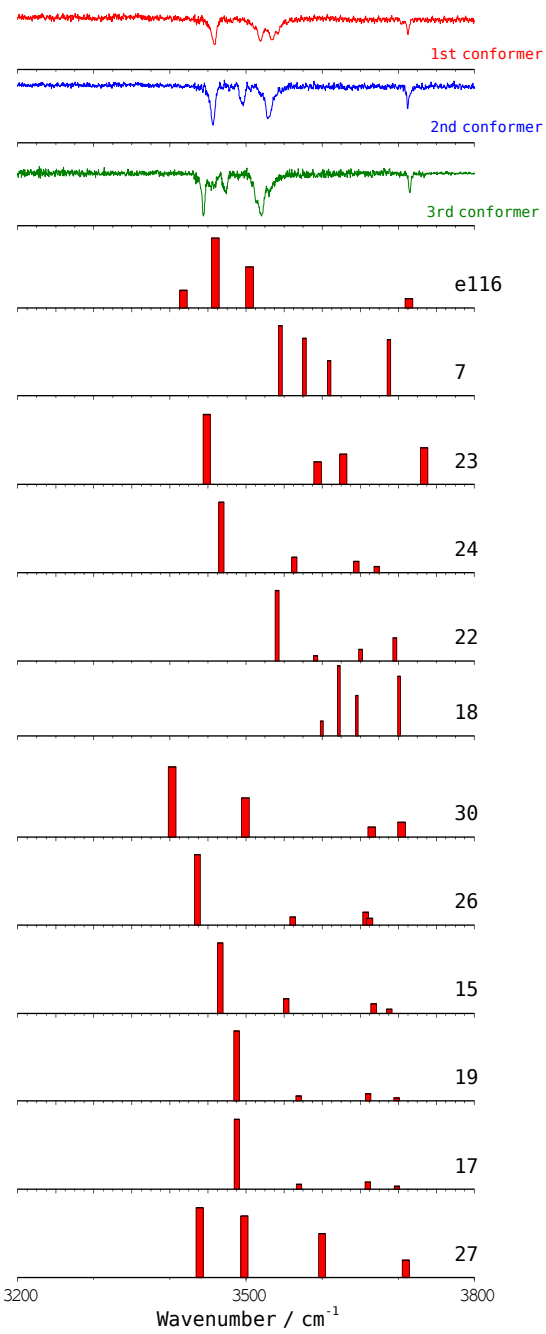

Figure 7.22c. *Experimental IDIRS for propofol$_2$·W_1 (upper traces) together with the predicted frequencies for each calculated structure. A correction factor of 0.956 was employed.*

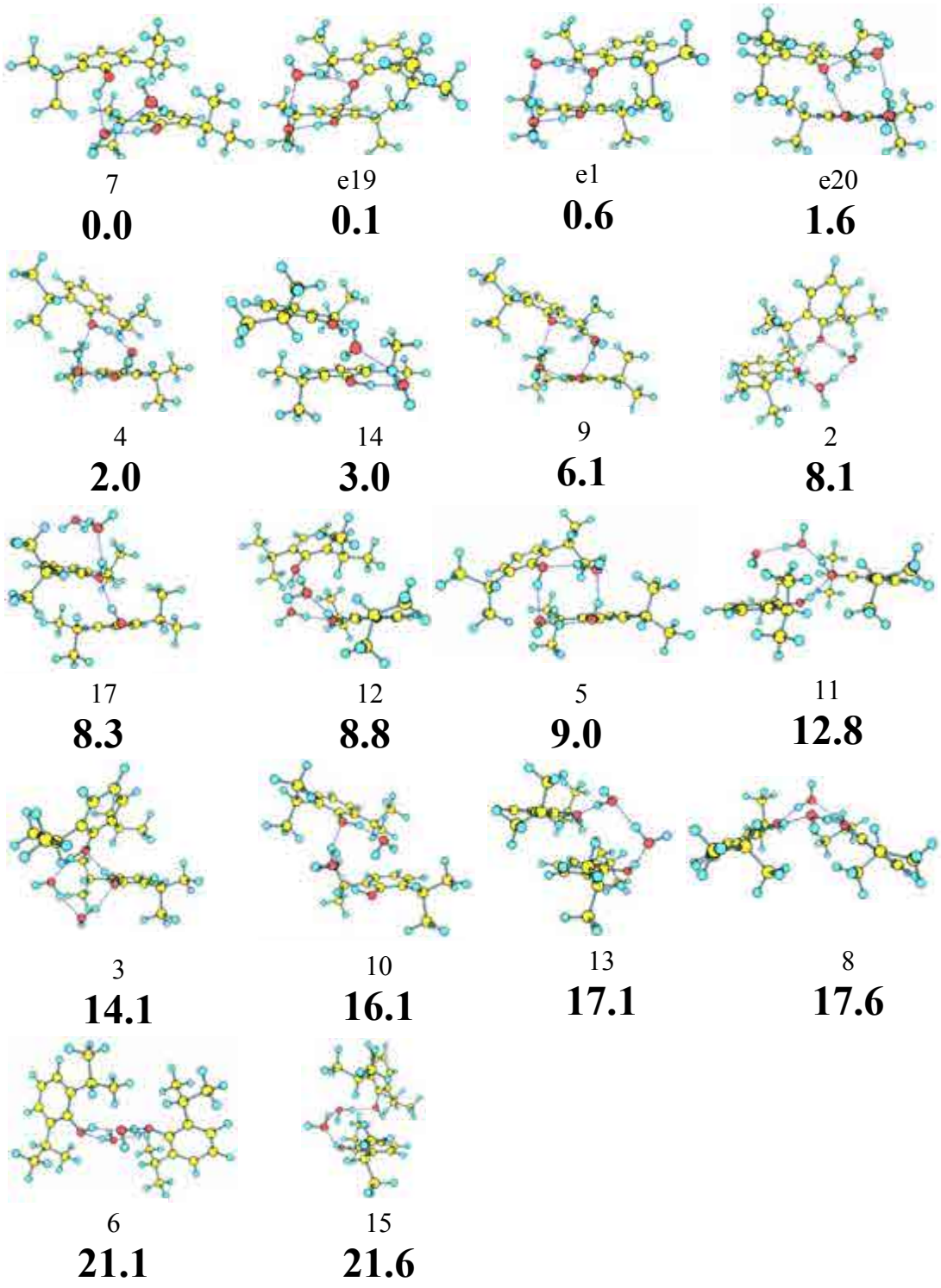

Figure 7.23. *Propofol$_2$·W$_2$ calculated structures at M06-2x/6-31+G(d).*

Table 7.12. *Propofol$_2$·W$_2$ structures with their relative energies and binding energies calculated at M06-2x/6-31+G(d).*

Structure	*ΔE (kJ/mol)*	*ΔE_{ZPE} (kJ/mol)*	*D_0 (kJ/mol)*	*BSSE (kJ/mol)*
7	0.00	0.00	-120.41	24.77
e19	1.96	0.14	-118.13	27.72
e1	1.93	0.57	-117.50	27.52
e20	3.01	1.61	-120.07	27.63
4	2.96	1.97	-116.60	26.62
14	3.13	3.05	-117.79	24.76
9	5.86	6.09	-112.27	27.24
2	8.81	8.12	-111.47	26.41
17	11.71	8.30	-111.11	25.78
12	10.42	8.81	-111.41	24.97
5	12.24	8.997	-111.32	25.28
11	17.49	12.79	-107.43	25.38
3	15.30	14.08	-104.96	26.55
10	19.26	16.12	-108.26	24.92
13	22.14	17.13	-103.80	25.08
8	16.96	17.58	-104.13	23.89
6	21.65	21.06	-102.87	24.96
15	23.34	21.60	-98.21	26.20

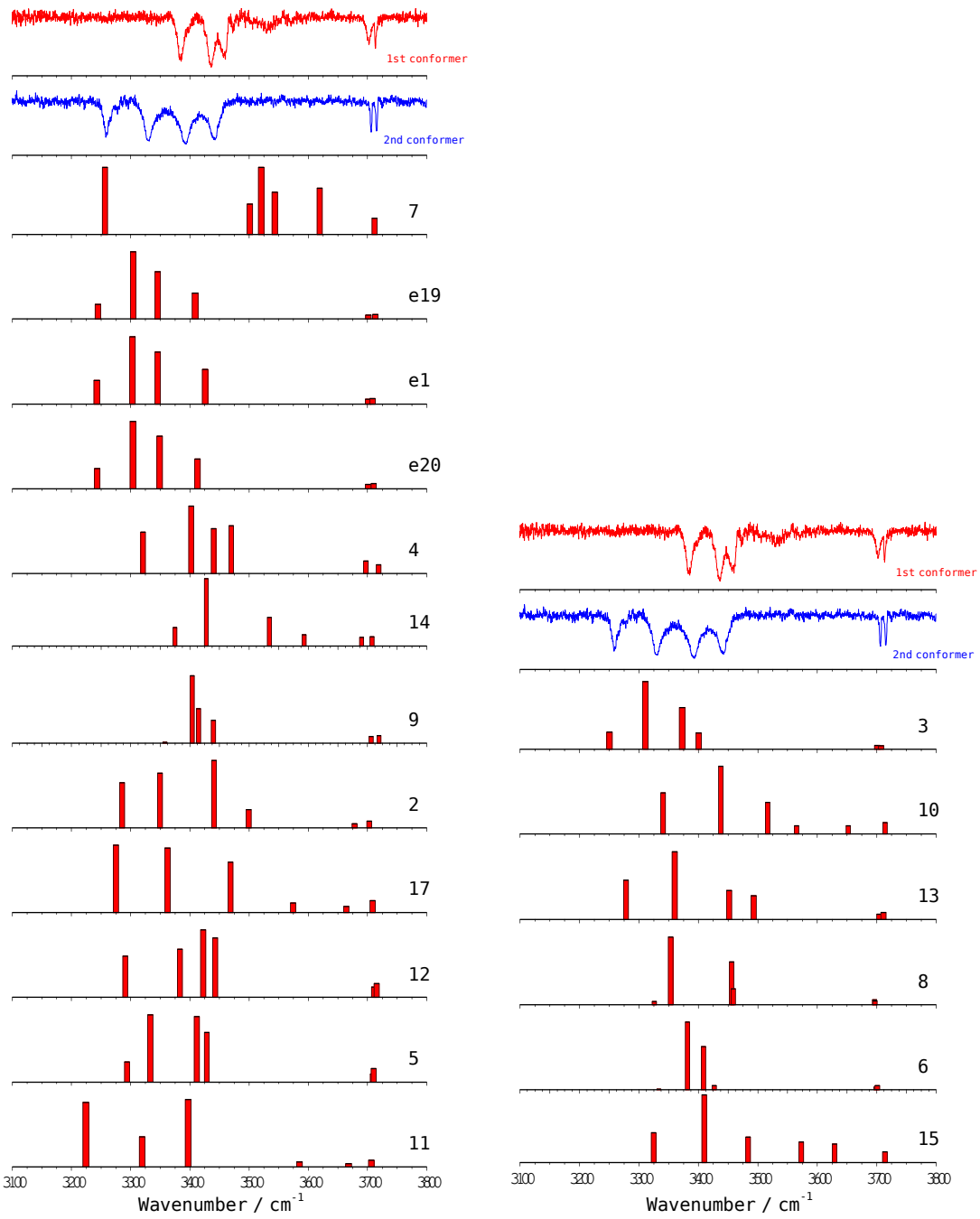

Figure 7.24. *Experimental IDIRS for propofol$_2$·W$_2$ (upper traces) together with the predicted frequencies for each calculated structure. A correction factor of 0.955 was employed.*

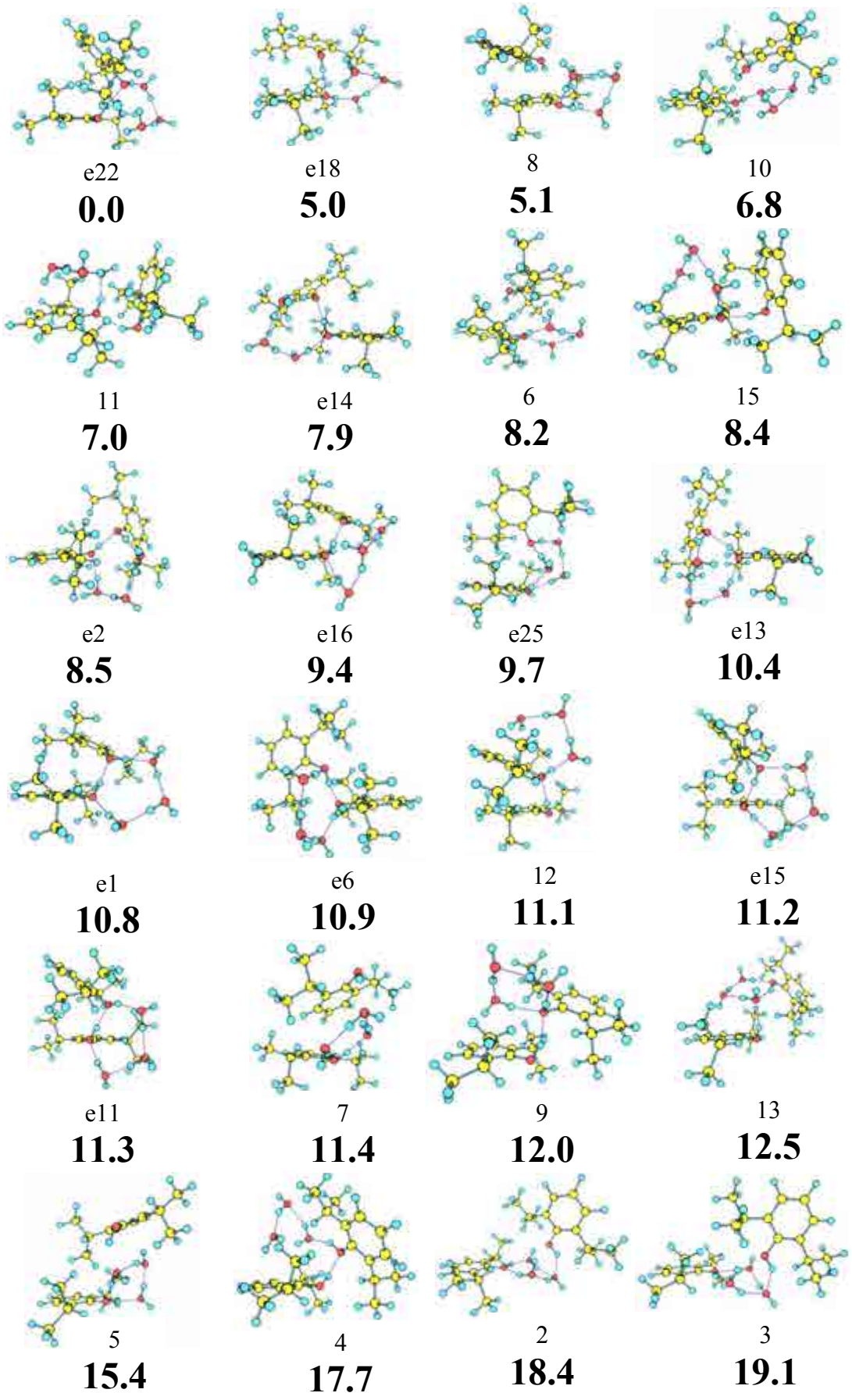

Figure 7.25. *Propofol$_2$·W$_3$ calculated structures at M06-2x/6-31+G(d).*

Table 7.13. *Propofol$_2$·W$_3$ structures with their relative energies and binding energies calculated at M06-2x/6-31+G(d).*

Structure	*ΔE (kJ/mol)*	*ΔE_{ZPE} (kJ/mol)*	*D_0 (kJ/mol)*	*BSSE (kJ/mol)*
e22	0.00	0.00	-153.31	37.53
e18	4.40	5.02	-149.55	37.07
8	1.97	5.15	-151.80	34.30
10	2.08	6.76	-144.81	39.26
11	6.45	6.96	-147.35	36.52
e14	9.07	7.87	-149.64	37.45
6	4.68	8.19	-147.05	36.00
15	9.93	8.45	-146.27	36.13
e2	6.76	8.55	-148.56	37.44
e16	10.45	9.39	-147.58	34.28
e25	8.44	9.67	-144.89	36.69
e13	9.15	10.40	-144.26	36.59
e1	11.90	10.82	-145.79	35.04
e6	12.78	10.96	-150.13	37.17
12	13.94	11.14	-145.03	34.67
e15	12.24	11.16	-146.70	36.69
e11	11.77	11.34	-142.85	37.06
7	9.01	11.44	-144.58	35.22
9	10.41	11.97	-141.87	37.00
13	11.01	12.52	-142.46	35.86
5	13.95	15.43	-140.14	35.27
4	17.65	17.74	-137.80	35.30
2	15.54	18.42	-140.67	32.15
3	15.65	19.05	-140.55	31.64

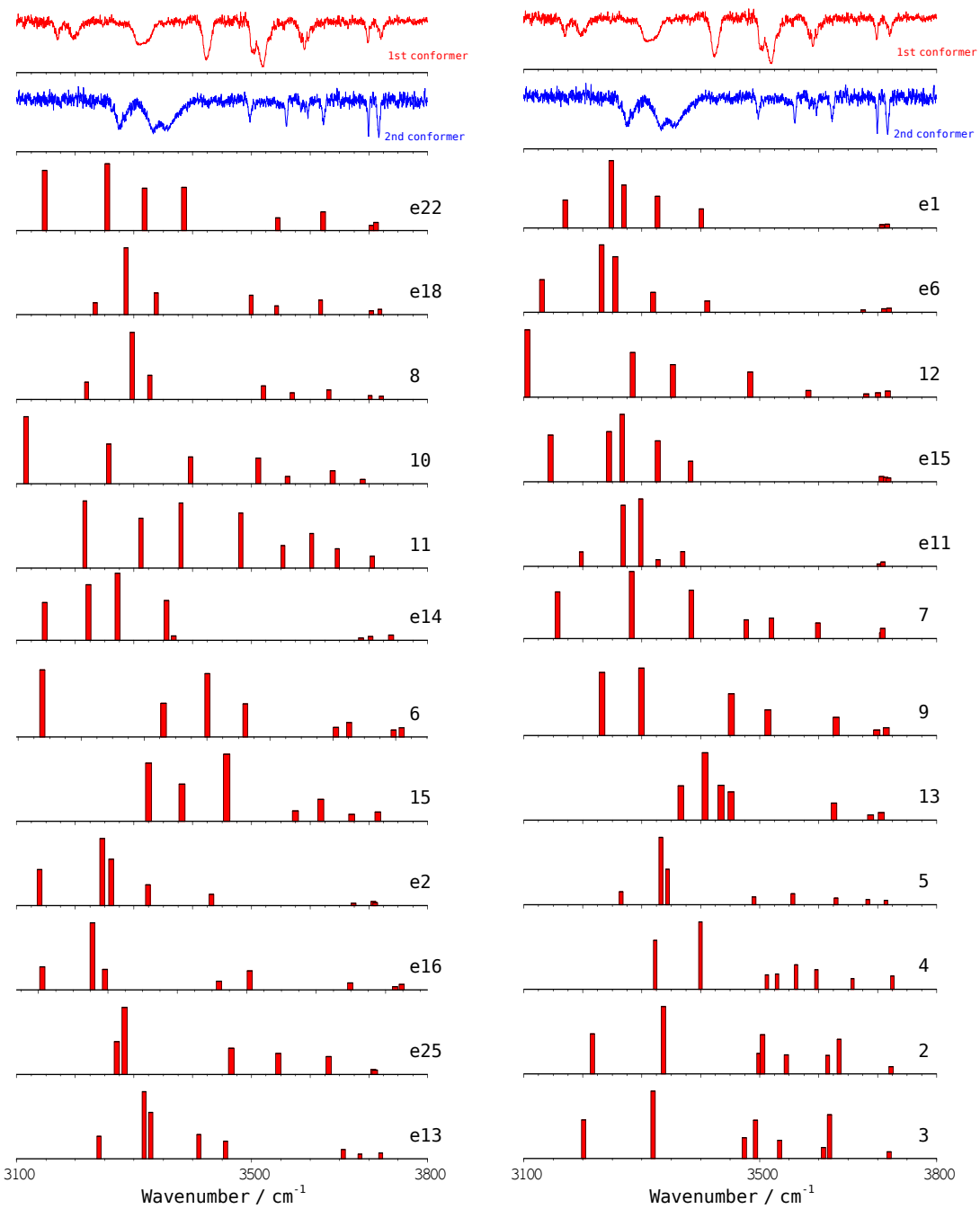

Figure 7.26. *Experimental IDIRS for propofol$_2$·W$_3$ (upper traces) together with the predicted frequencies for each calculated structure. A correction factor of 0.956 was employed.*

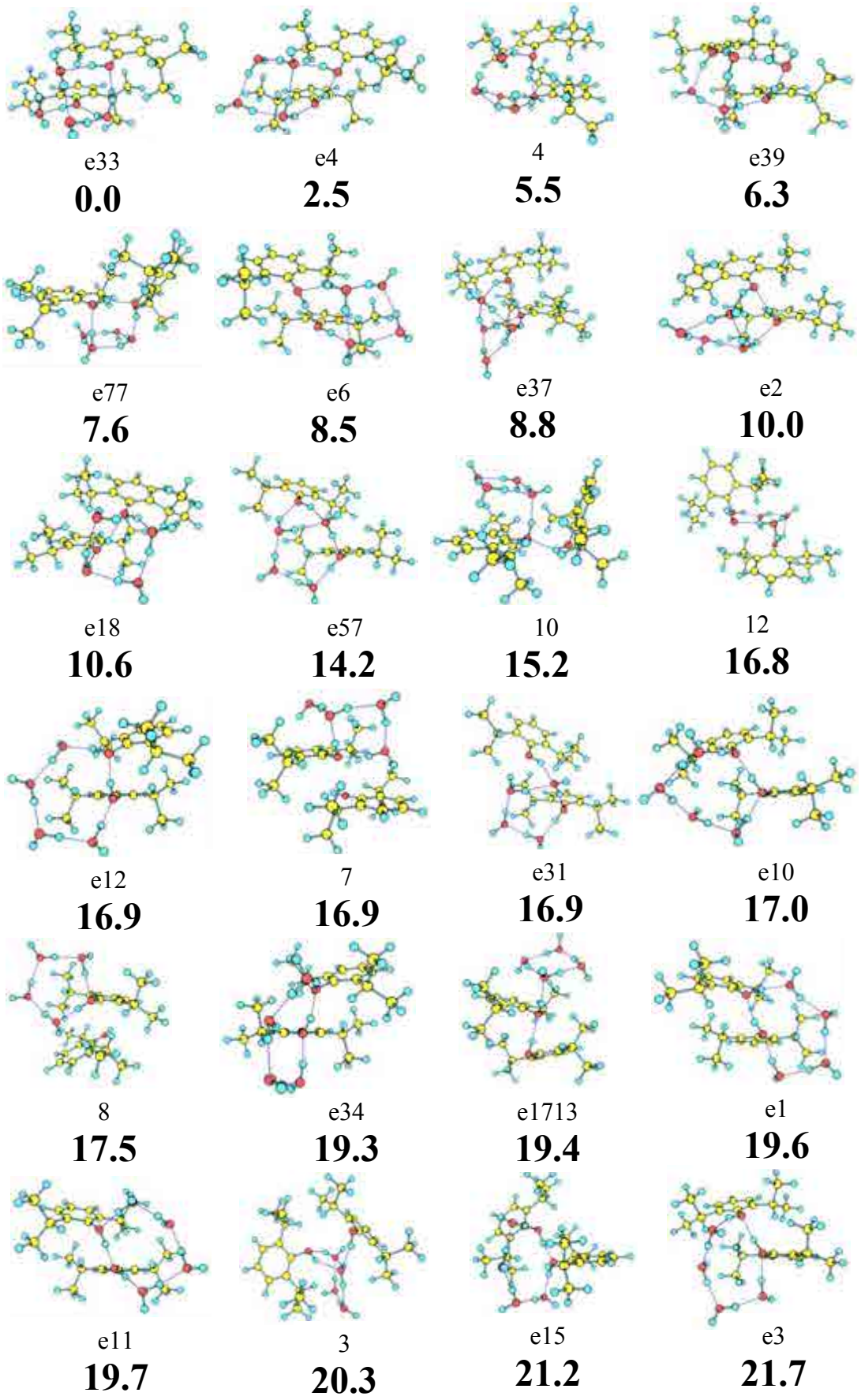

Figure 7.27a. *Propofol$_2$·W$_4$ calculated structures at M06-2x/6-31+G(d).*

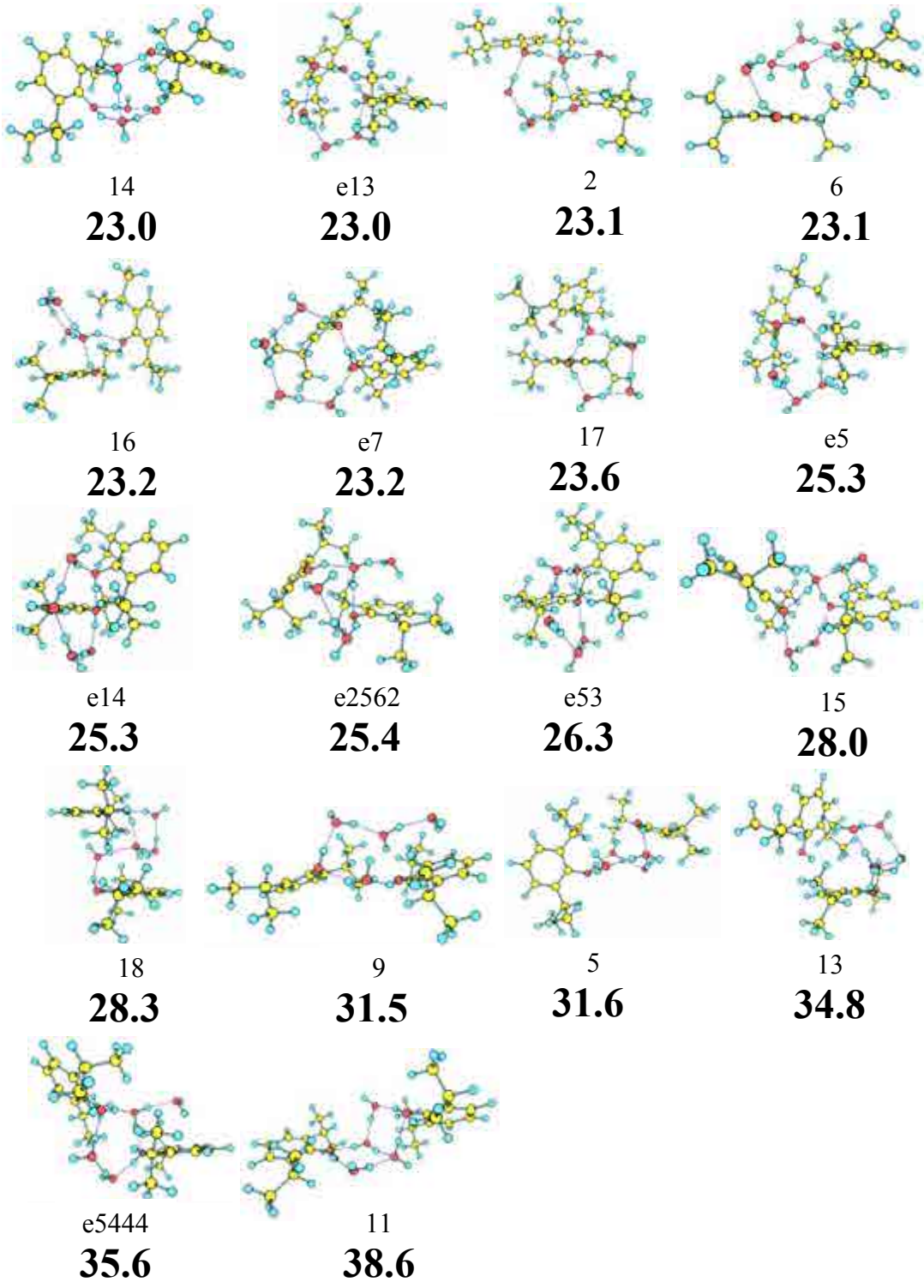

Figure 7.27b. *Propofol$_2$·W$_4$ calculated structures at M06-2x/6-31+G(d).*

Table 7.14. *Propofol$_2$·W$_4$ structures with their relative energies and binding energies calculated at M06-2x/6-31+G(d).*

Structure	*ΔE (kJ/mol)*	*ΔE_{ZPE} (kJ/mol)*	*D_0 (kJ/mol)*	*BSSE (kJ/mol)*
e33	0.00	0.00	-197.84	44.37
e4	5.88	2.52	-194.63	45.88
4	10.31	5.52	-190.67	46.44
e39	11.12	6.36	-191.04	44.81
e77	12.58	7.55	-187.60	47.07
e6	15.75	8.52	-192.57	45.24
e37	11.35	8.80	-189.28	44.54
e2	14.69	9.96	-187.39	45.27
e18	17.15	10.57	-188.15	43.9
e57	22.54	14.21	-183.45	44.55
10	20.72	15.24	-186.34	44.74
12	20.86	16.76	-178.31	47.55
e12	25.76	16.85	-181.56	44.61
7	24.83	16.87	-179.65	46.10
e31	25.48	16.92	-180.87	44.42
e10	27.39	17.03	-181.04	44.96
8	27.49	17.50	-180.33	44.79
e34	27.30	19.26	-179.68	43.68
e1713	29.44	19.40	-178.44	44.38
e1	28.41	19.67	-179.36	43.59
e11	28.90	19.69	-178.33	44.60
3	23.15	20.32	-179.99	42.71
e15	33.26	21.15	-175.98	45.08
e3	31.41	21.66	-177.35	43.61
14	30.22	23.00	-177.75	45.17
e13	33.77	23.05	-177.70	45.18
2	31.09	23.11	-177.33	45.89
6	28.57	23.14	-175.18	43.89
16	30.13	23.19	-176.44	42.58
e7	33.45	23.24	-175.38	43.59
17	33.16	23.64	-174.54	44.03
e5	34.92	25.28	-179.33	45.01
e14	35.02	25.31	-175.34	45.27
e2562	31.48	25.35	-178.80	44.66
e53	33.58	26.35	-168.65	47.21
15	38.53	28.03	-167.50	46.69
18	34.74	28.32	-174.02	43.58
9	39.13	31.46	-168.95	41.81
5	38.37	31.61	-165.56	45.04
13	42.48	34.82	-165.79	42.01
e5444	43.73	35.63	-174.74	44.30
11	45.91	38.63	-166.86	40.43

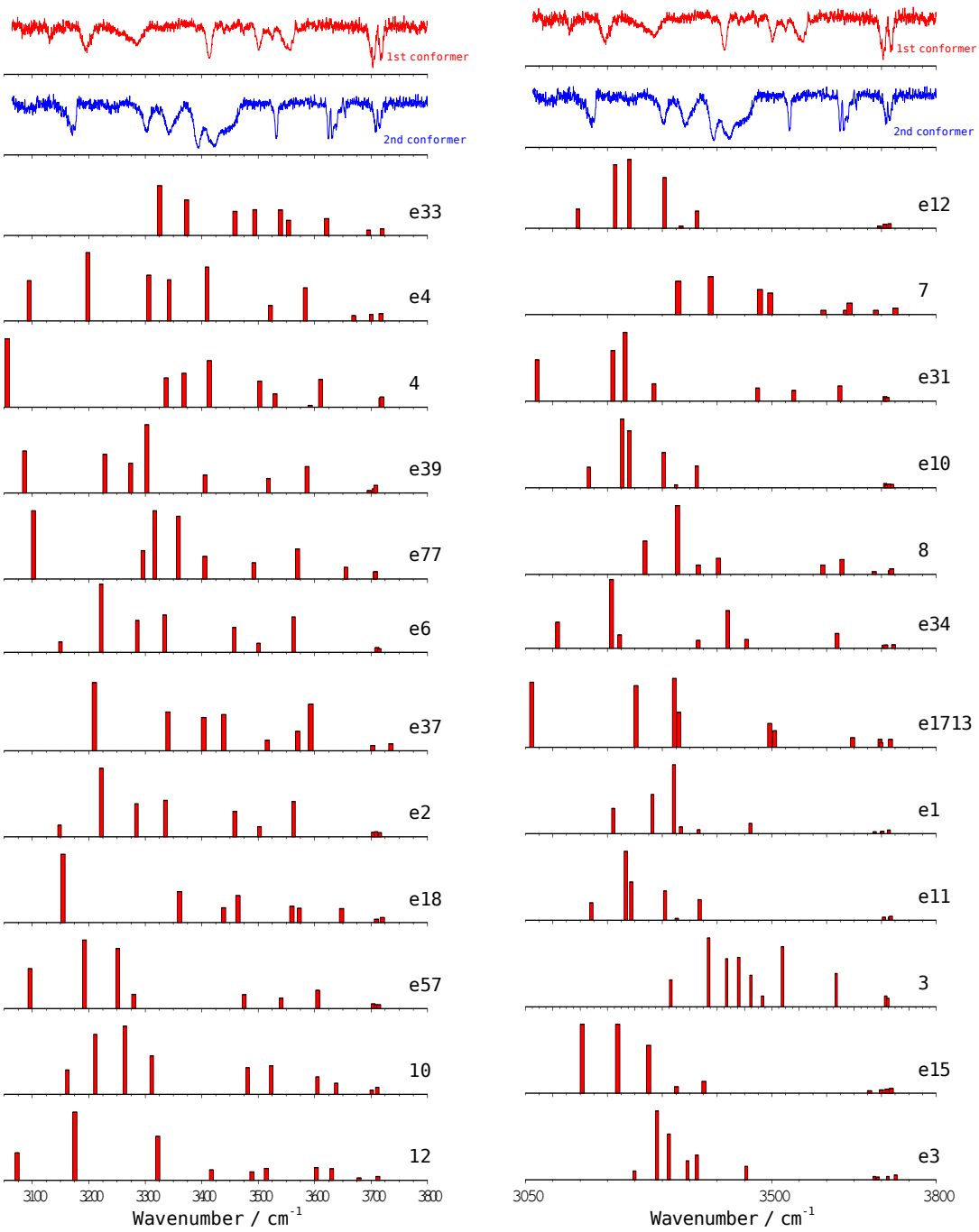

Figure 7.28a. *Experimental IDIRS for propofol$_2$·W$_4$ (upper traces) together with the predicted frequencies for each calculated structure. A correction factor of 0.956 was employed.*

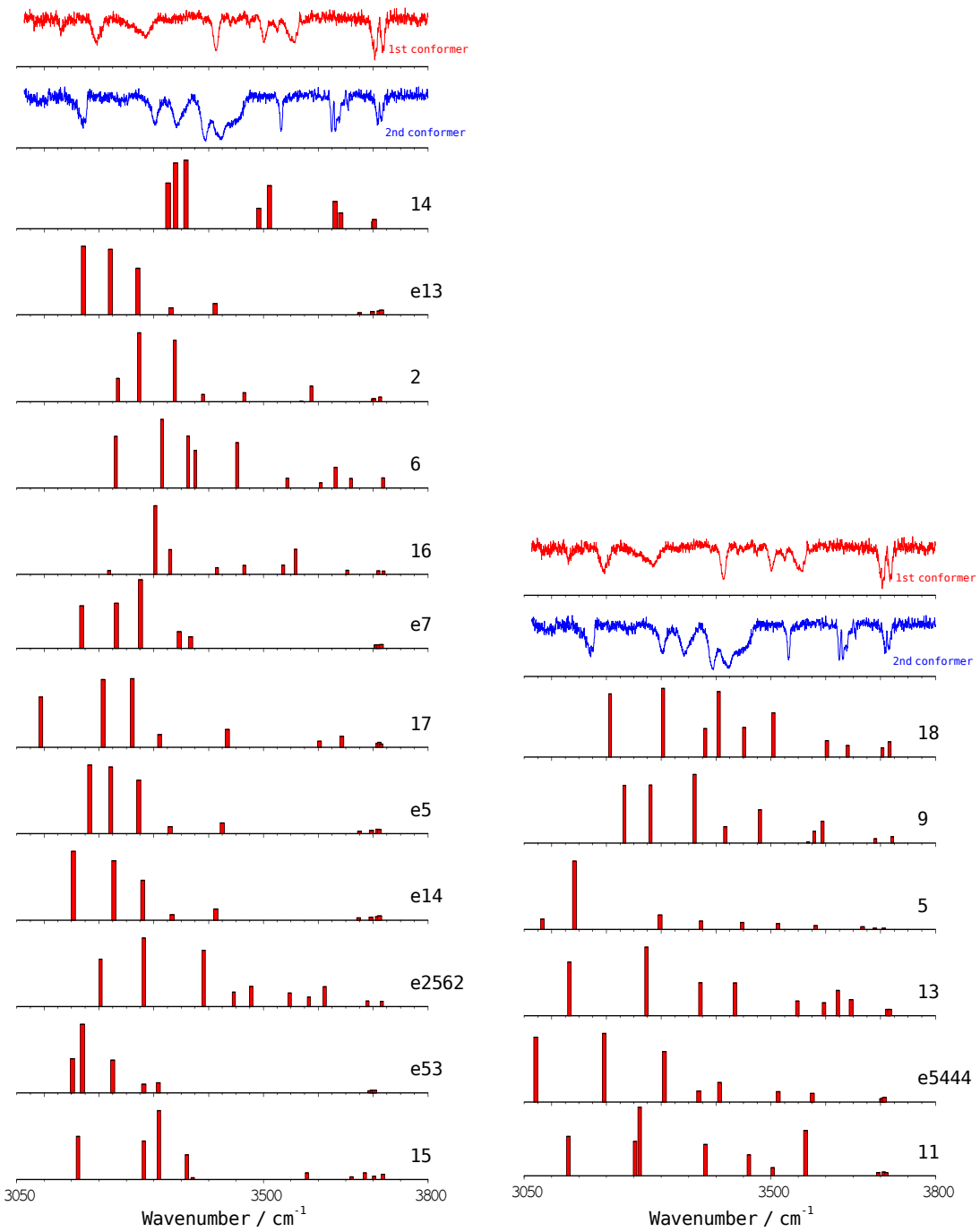

Figure 7.28b. *Experimental IDIRS for propofol$_2$·W$_4$ (upper traces) together with the predicted frequencies for each calculated structure. A correction factor of 0.956 was employed.*

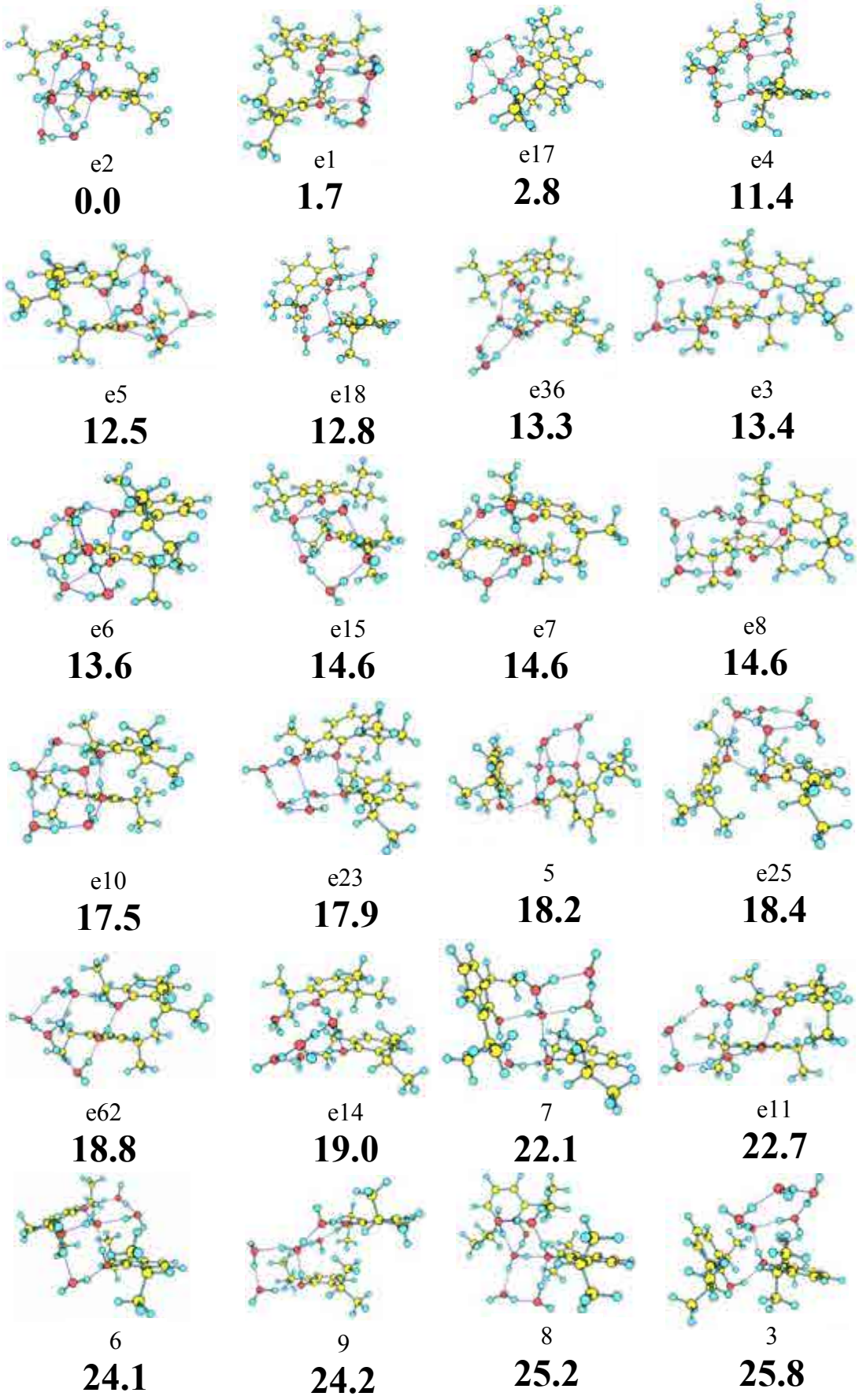

Figure 7.29a. *Propofol$_2$·W$_5$ calculated structures at M06-2x/6-31+G(d).*

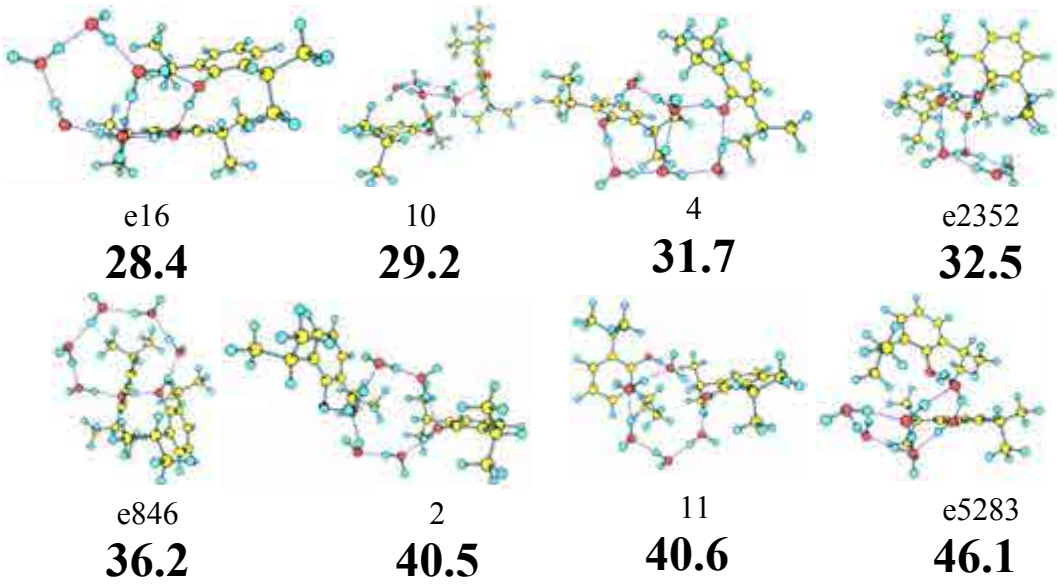

Figure 7.29b. *Propofol$_2$·W$_5$ calculated structures at M06-2x/6-31+G(d).*

Table 7.15. *Propofol$_2$·W$_5$ structures with their relative energies and binding energies calculated at M06-2x/6-31+G(d).*

Structure	*ΔE (kJ/mol)*	*ΔE_{ZPE} (kJ/mol)*	*D_0 (kJ/mol)*	*BSSE (kJ/mol)*
e2	0.00	0.00	-239.45	54.02
e1	0.08	1.71	-236.35	55.41
e17	1.10	2.81	-235.09	55.57
e4	13.30	11.40	-224.84	57.64
e5	18.56	12.49	-224.96	56.83
e18	14.55	12.81	-223.93	57.54
e36	16.38	13.30	-230.37	49.81
e3	15.86	13.40	-225.01	55.87
e6	20.34	13.62	-223.98	56.28
e15	18.86	14.58	-223.49	55.80
e7	16.41	14.59	-223.60	55.69
e8	17.49	14.60	-227.46	55.51
e10	22.04	17.47	-221.40	55.41
e23	21.90	17.87	-219.35	56.26
5	20.75	18.16	-219.72	56.00
e25	19.41	18.41	-217.50	57.55
e62	22.38	18.77	-220.33	55.18
e14	20.37	18.96	-222.72	51.79
7	28.88	22.07	-220.22	54.89
e11	29.74	22.68	-221.51	53.40
6	28.61	24.10	-220.66	52.42
9	29.40	24.24	-218.58	51.06
8	31.27	25.16	-214.82	53.49
3	32.95	25.84	-214.81	53.22
e16	33.68	28.45	-213.82	51.62
10	36.20	29.20	-210.74	53.53
4	37.99	31.73	-208.07	53.68
e2352	41.00	32.49	-213.92	54.48
e846	45.81	36.17	-211.88	49.12
2	46.79	40.51	-204.35	52.32
11	48.87	40.65	-199.85	52.97
e5283	49.53	46.05	-199.38	52.15

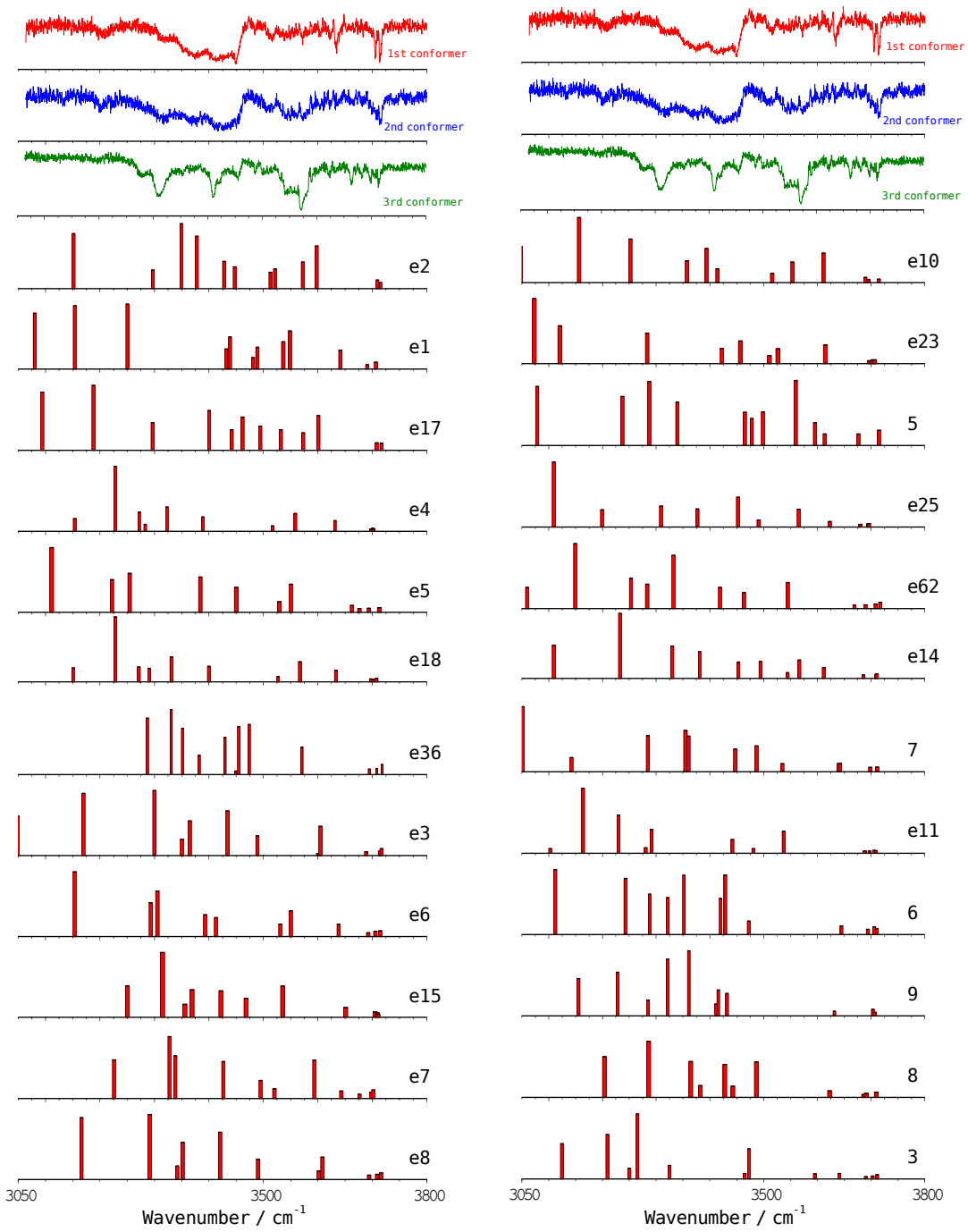

Figure 7.30a. *Experimental IDIRS for propofol$_2$·W$_5$ (upper traces) together with the predicted frequencies for each calculated structure. A correction factor of 0.954 was employed.*

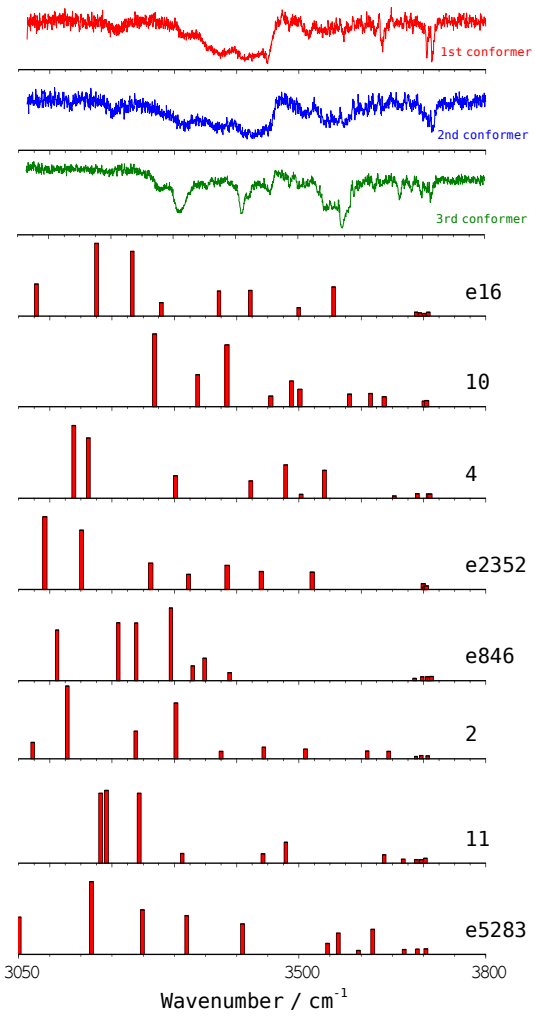

Figure 7.30b. *Experimental IDIRS for propofol$_2$·W$_5$ (upper traces) together with the predicted frequencies for each calculated structure. A correction factor of 0.954 was employed.*

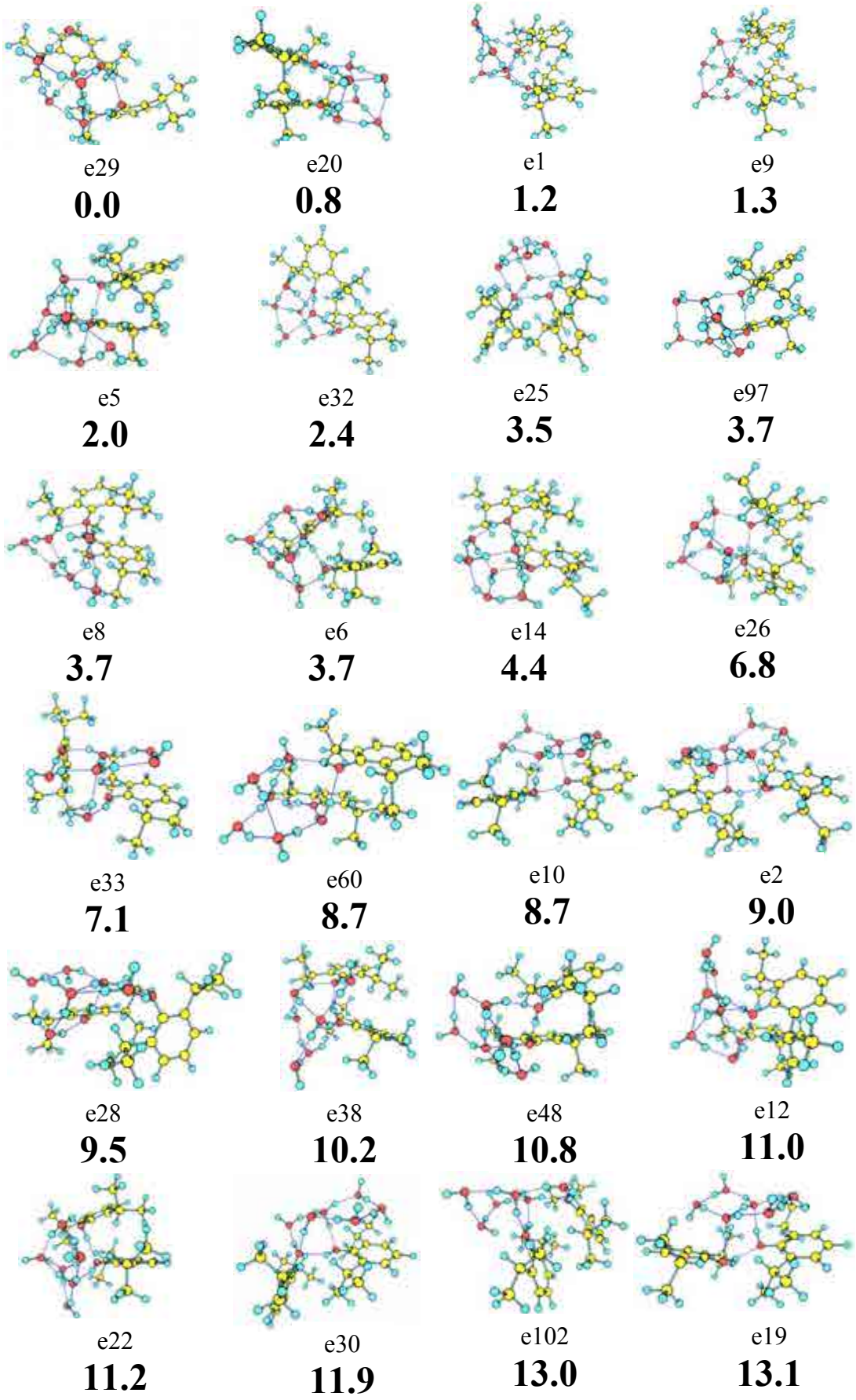

Figure 7.31a. *Propofol$_2$·W$_6$ calculated structures at M06-2x/6-31+G(d).*

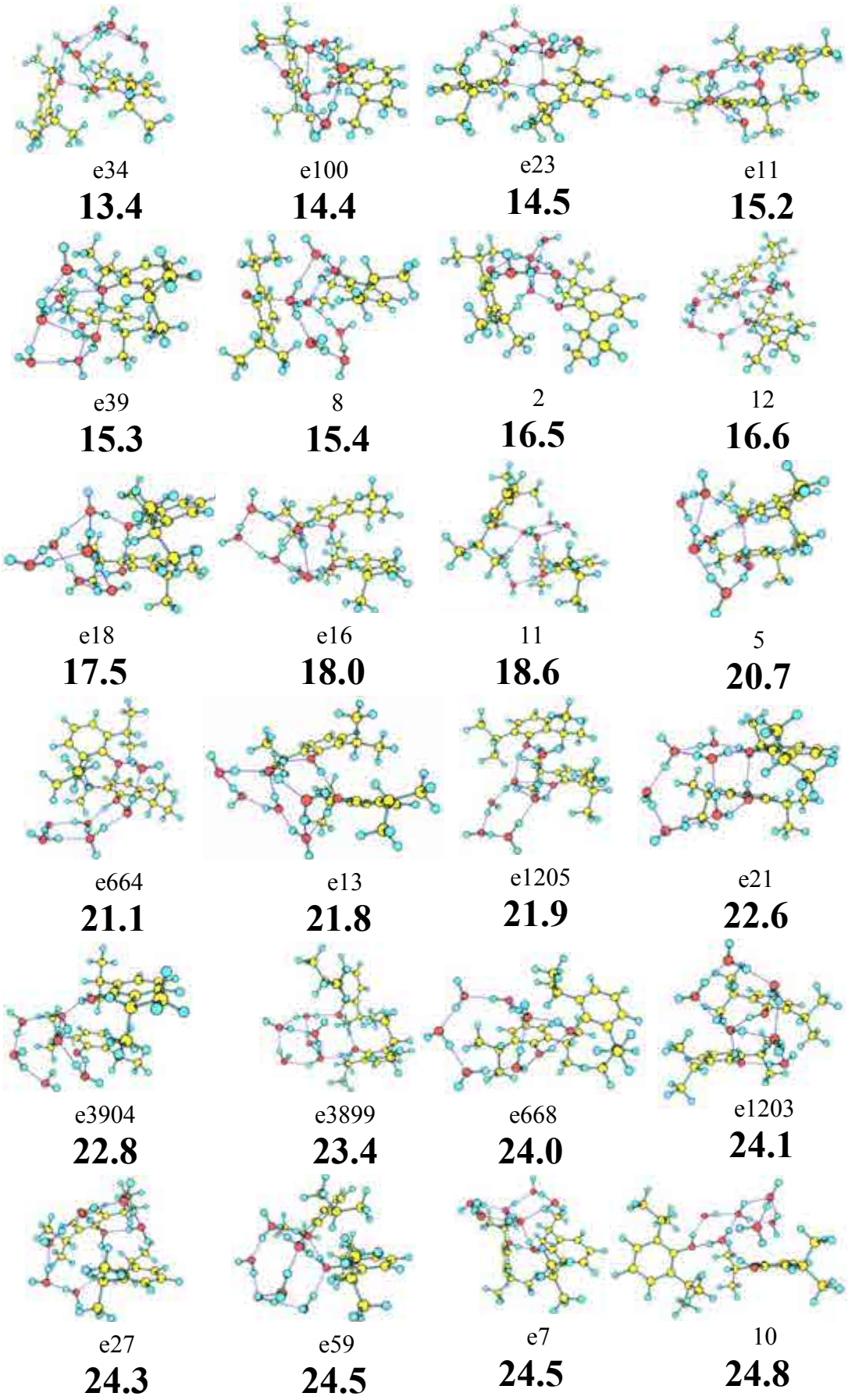

Figure 7.31b. *Propofol$_2$·W$_6$ calculated structures at M06-2x/6-31+G(d).*

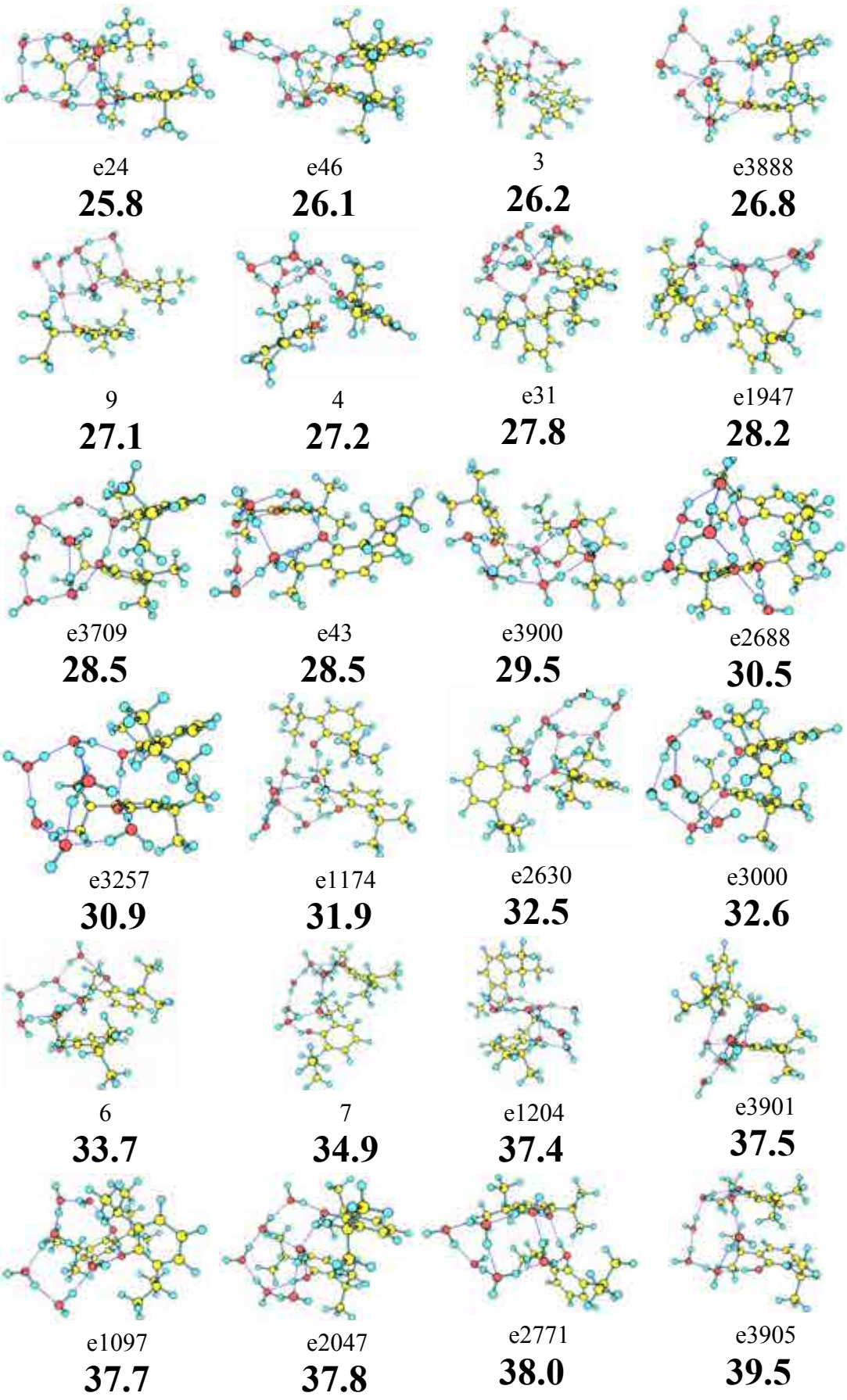

Figure 7.31c. *Propofol$_2$·W$_6$ calculated structures at M06-2x/6-31+G(d).*

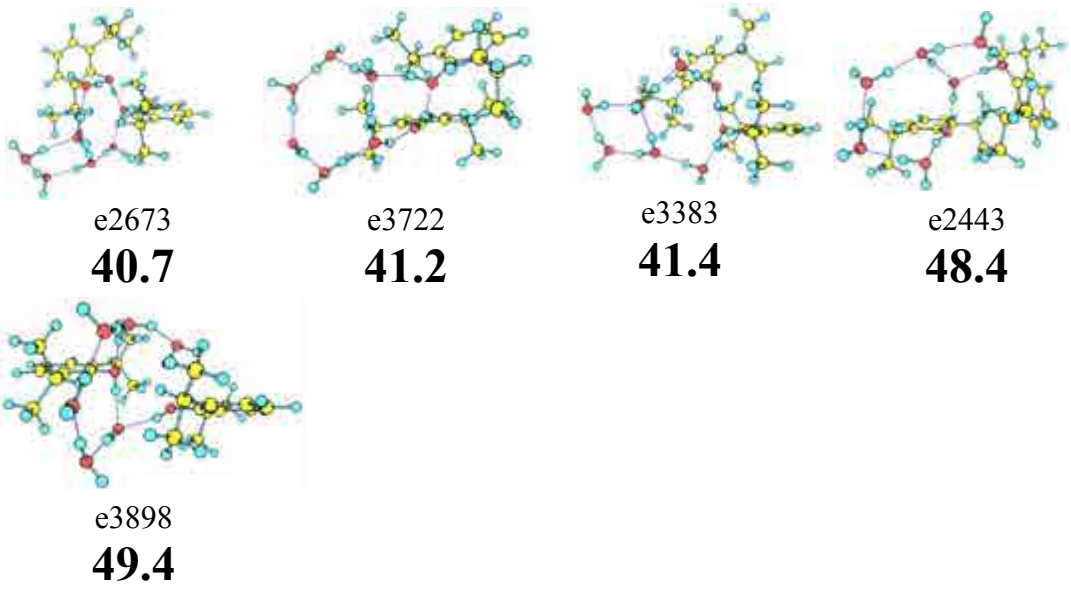

Figure 7.31d. *Propofol$_2$·W$_6$ calculated structures at M06-2x/6-31+G(d).*

Table 7.16a. *$Propofol_2{\cdot}W_6$ structures with their relative energies and binding energies calculated at M06-2x/6-31+G(d).*

Structure	*ΔE (kJ/mol)*	*ΔE_{ZPE} (kJ/mol)*	*D_0 (kJ/mol)*	*BSSE (kJ/mol)*
e29	0.00	0.00	-275.38	66.40
e20	-4.55	0.78	-277.09	63.51
e1	0.93	1.23	-276.34	63.81
e9	-2.15	1.33	-273.66	66.39
e5	2.17	1.98	-272.48	67.33
e32	3.33	2.43	-272.52	66.84
e25	4.38	3.48	-270.74	67.98
e97	6.46	3.67	-273.54	64.58
e8	3.43	3.73	-270.93	67.53
e6	4.06	3.74	-270.67	67.79
e14	3.99	4.38	-273.55	63.45
e26	7.77	6.77	-271.39	67.34
e33	6.60	7.13	-266.69	67.55
e60	7.17	8.69	-271.65	61.04
e10	9.95	8.71	-265.74	66.94
e2	10.48	9.05	-264.56	67.77
e28	10.07	9.50	-267.26	65.02
e38	15.18	10.24	-267.15	64.80
e48	15.27	10.77	-271.30	63.42
e12	11.80	11.03	-266.80	63.95
e22	14.41	11.20	-265.24	65.34
e30	13.25	11.90	-262.99	67.29
e102	12.63	13.05	-267.21	61.12
e19	12.94	13.11	-263.58	65.09
e34	16.33	13.38	-262.36	65.64
e100	16.46	14.40	-263.49	63.90
e23	14.63	14.50	-263.88	66.71
e11	12.77	15.24	-265.37	60.76
e39	16.47	15.35	-263.63	62.40
8	16.78	15.43	-260.15	65.80
2	18.46	16.51	-259.43	65.84
12	22.16	16.63	-262.43	63.13
e18	20.31	17.48	-259.70	64.61
e16	18.98	17.99	-262.07	62.13
11	19.70	18.63	-260.22	66.23
5	23.74	20.69	-259.20	61.49
e664	25.25	21.05	-258.12	62.21
e13	26.05	21.80	-258.14	62.25
e1205	26.25	21.93	-265.59	57.57
e21	26.63	22.62	-254.90	64.67
e3904	22.53	22.81	-254.71	64.27
e3899	22.95	23.43	-257.41	64.25
e668	29.99	24.00	-258.83	62.67
e1203	28.24	24.09	-259.58	63.90
e27	32.85	24.25	-251.74	65.80
e59	29.22	24.49	-254.52	62.77

Table 7.16b. *Propofol$_2$·W$_6$ structures with their relative energies and binding energies calculated at M06-2x/6-31+G(d).*

Structure	*ΔE (kJ/mol)*	*ΔE_{ZPE} (kJ/mol)*	*D_0 (kJ/mol)*	*BSSE (kJ/mol)*
e7	26.23	24.54	-255.88	60.96
10	24.10	24.80	-253.87	62.70
e24	31.81	25.82	-252.34	63.62
e46	31.74	26.08	-255.89	59.82
3	30.30	26.20	-256.18	63.11
e3888	31.27	26.81	-256.70	61.98
9	30.49	27.14	-253.77	60.88
4	31.48	27.16	-253.41	61.62
e31	32.18	27.77	-246.29	67.72
e1947	32.81	28.15	-260.43	60.21
e3709	31.99	28.45	-256.50	63.84
e43	31.53	28.54	-251.94	61.30
e3900	35.39	29.47	-252.08	60.24
e2688	33.63	30.47	-253.53	64.79
e3257	34.45	30.93	-251.36	63.21
e1174	36.10	31.93	-253.63	59.93
e2630	37.10	32.46	-252.91	63.42
e3000	38.48	32.61	-251.42	61.46
6	38.86	33.67	-247.12	61.00
7	38.97	34.90	-245.19	61.29
e1204	39.55	37.37	-249.65	61.77
e3901	43.89	37.50	-247.81	60.18
e1097	45.41	37.66	-249.12	62.01
e2047	41.42	37.8	-249.01	61.99
e2771	40.62	38.04	-250.58	60.18
e3905	44.25	39.51	-246.29	59.68
e2673	47.98	40.71	-245.68	62.41
e3722	47.44	41.22	-249.72	57.85
e3383	50.09	41.44	-242.10	61.55
e2443	55.26	48.36	-233.74	59.69
e3898	58.07	49.45	-232.81	63.23

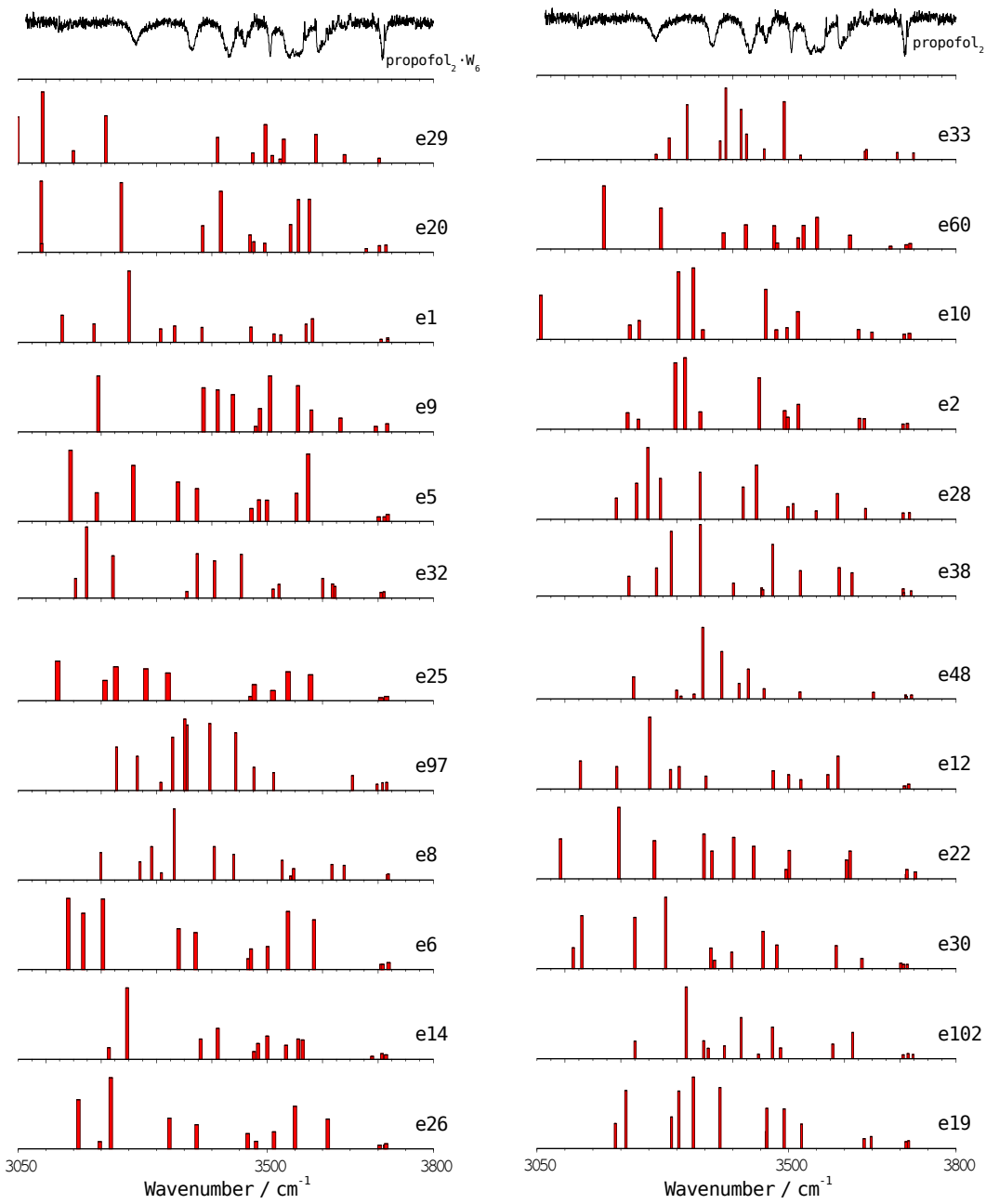

Figure 7.32a. *Experimental IDIRS for propofol$_2$·W$_6$ (upper trace) together with the predicted frequencies for each calculated structure. A correction factor of 0.955 was employed.*

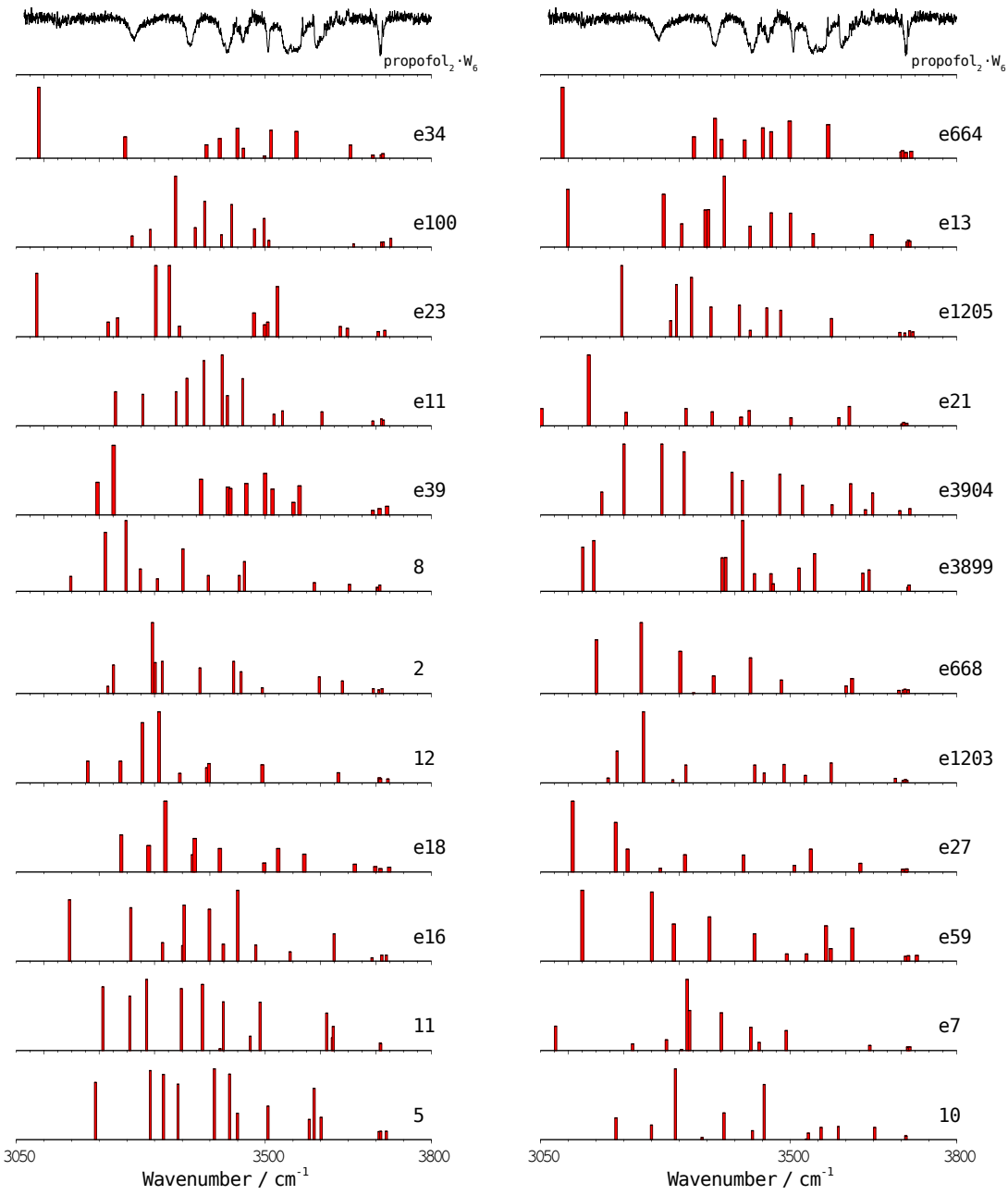

Figure 7.32b. *Experimental IDIRS for propofol$_2$·W_6 (upper trace) together with the predicted frequencies for each calculated structure. A correction factor of 0.955 was employed.*

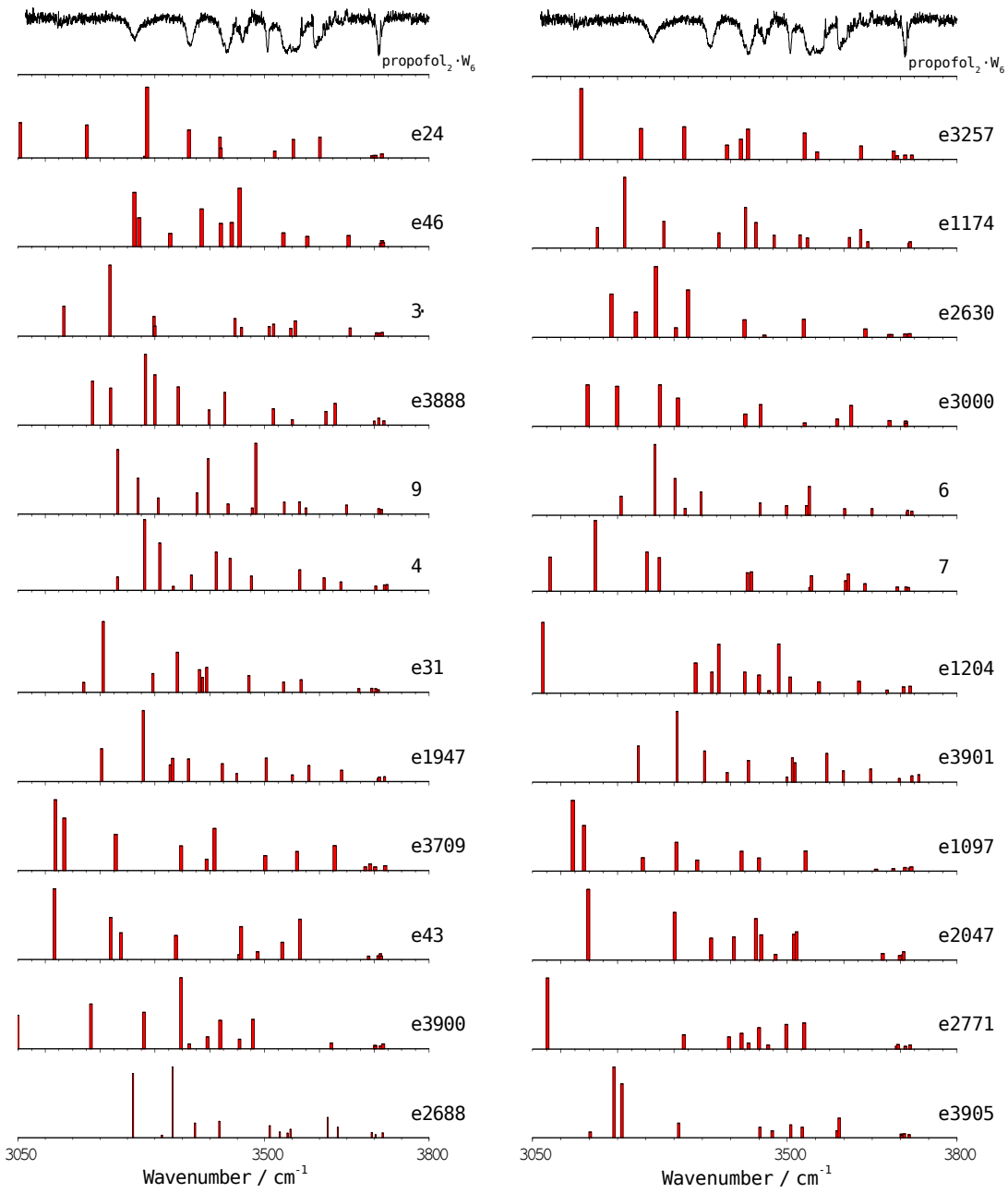

Figure 7.32c. *Experimental IDIRS for propofol$_2$·W$_6$ (upper trace) together with the predicted frequencies for each calculated structure. A correction factor of 0.955 was employed.*

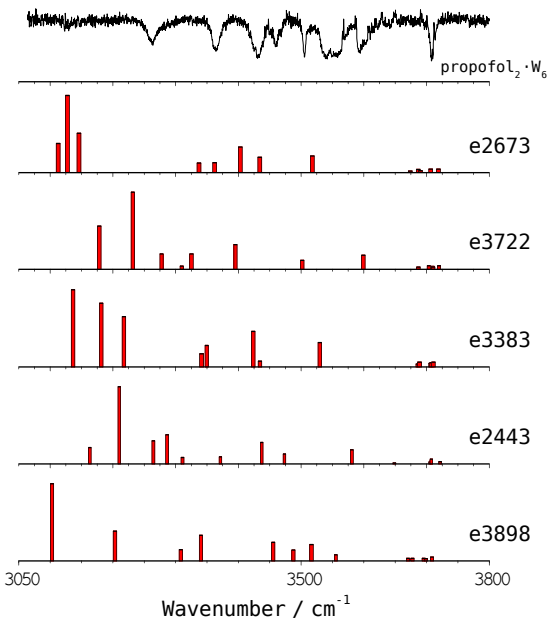

Figure 7.32d. *Experimental IDIRS for propofol$_2$·W$_6$ (upper trace) together with the predicted frequencies for each calculated structure. A correction factor of 0.955 was employed.*

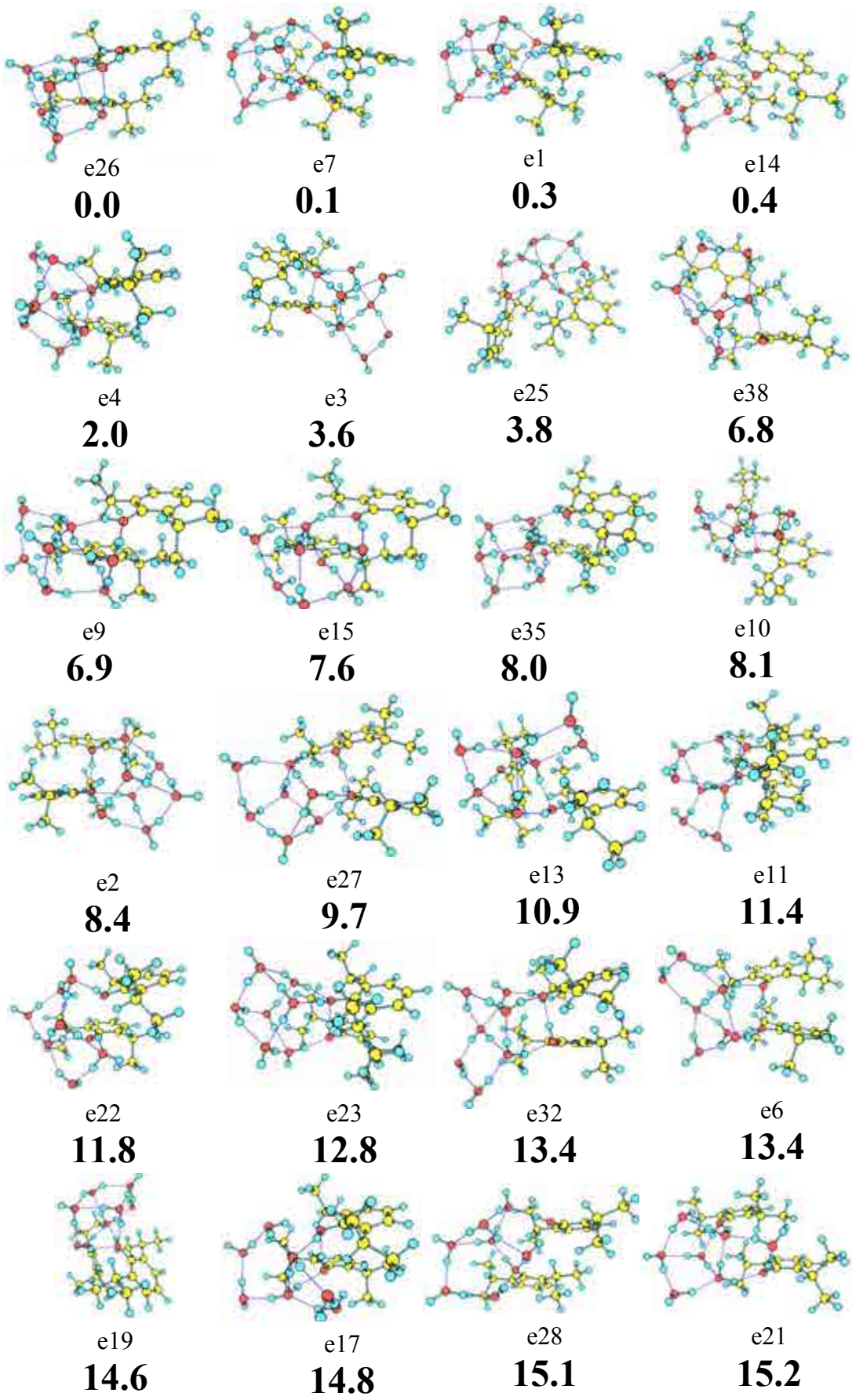

Figure 7.33a. *Propofol$_2$·W$_7$ calculated structures at M06-2x/6-31+G(d).*

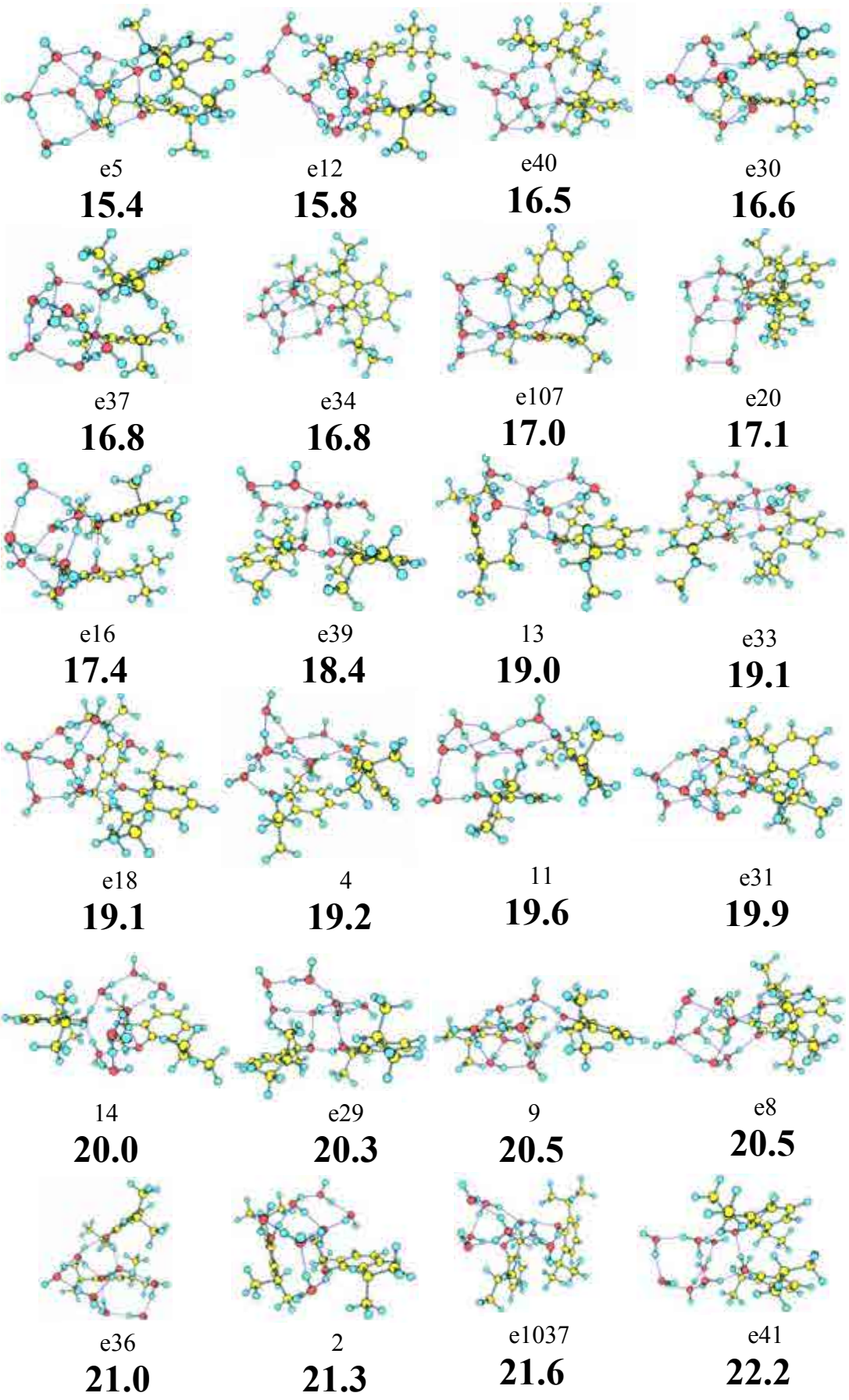

Figure 7.33b. *Propofol$_2$·W$_7$ calculated structures at M06-2x/6-31+G(d).*

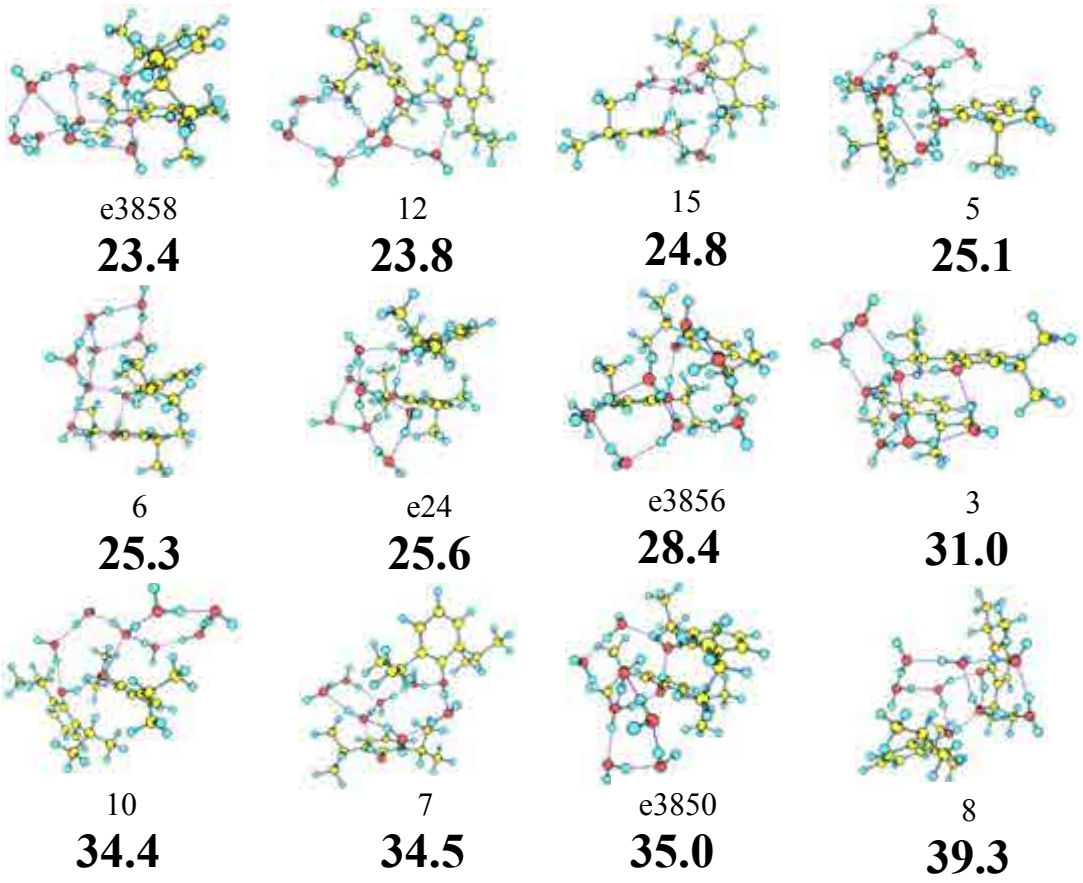

Figure 7.33c. *Propofol$_2$·W$_7$ calculated structures at M06-2x/6-31+G(d).*

Table 7.17a. *$Propofol_2 \cdot W_7$ structures with their relative energies and binding energies calculated at M06-2x/6-31+G(d).*

Structure	*ΔE (kJ/mol)*	*ΔE_{ZPE} (kJ/mol)*	*D_0 (kJ/mol)*	*BSSE (kJ/mol)*
e26	0.00	0	-319.51	74.69
e7	4.01	0.09	-319.22	75.71
e1	5.34	0.29	-318.74	75.98
e14	2.20	0.37	-318.47	75.35
e4	3.67	1.96	-316.24	75.99
e3	7.58	3.59	-316.42	74.18
e25	7.79	3.79	-315.14	75.68
e38	12.94	6.79	-310.59	76.82
e9	11.83	6.92	-314.28	73.00
e15	10.20	7.64	-311.13	75.42
e35	7.87	8.00	-312.86	74.15
e10	12.25	8.05	-309.67	76.47
e2	14.83	8.45	-311.03	75.54
e27	15.57	9.69	-311.81	73.50
e13	16.36	10.92	-308.95	74.33
e11	16.08	11.39	-309.21	73.60
e22	20.02	11.81	-308.53	74.67
e23	19.65	12.81	-306.49	75.71
e32	18.60	13.37	-308.06	73.58
e6	18.60	13.38	-308.05	73.58
e19	20.84	14.64	-306.17	73.80
e17	22.67	14.82	-304.92	75.27
e28	20.85	15.07	-304.69	74.43
e21	19.75	15.18	-305.82	73.19
e5	20.87	15.40	-303.82	75.80
e12	22.72	15.79	-305.90	73.33
e40	25.14	16.52	-304.59	73.90
e30	23.94	16.60	-302.12	75.88
e37	25.58	16.81	-302.20	75.60
e34	23.74	16.83	-303.24	74.94
e107	20.15	17.02	-303.25	73.92
e20	22.00	17.10	-307.86	69.24
e16	24.88	17.44	-303.62	73.95
e39	25.55	18.39	-301.86	74.35
13	25.75	18.99	-301.22	74.39
e33	29.67	19.08	-298.70	76.41
e18	26.37	19.08	-301.49	74.03
4	25.85	19.20	-301.31	73.68
11	22.37	19.55	-300.12	74.93
e31	23.63	19.94	-301.13	73.95
14	26.54	20.01	-296.24	77.94
e29	28.77	20.33	-299.01	74.86
9	23.24	20.49	-303.07	74.74
e8	23.22	20.51	-299.64	74.45
e36	29.78	20.97	-299.45	74.19
2	30.69	21.32	-299.76	73.12

Table 7.17b. *Propofol$_2$·W$_7$ structures with their relative energies and binding energies calculated at M06-2x/6-31+G(d).*

Structure	*ΔE (kJ/mol)*	*ΔE_{ZPE} (kJ/mol)*	*D_0 (kJ/mol)*	*BSSE (kJ/mol)*
e1037	26.26	21.62	-301.16	71.82
e41	28.88	22.24	-299.25	73.52
e3858	29.92	23.38	-299.96	71.66
12	33.72	23.78	-298.24	72.98
15	35.67	24.81	-294.25	75.14
5	32.59	25.12	-297.14	72.35
6	33.94	25.27	-297.95	71.39
e24	33.46	25.62	-295.55	73.43
e3856	37.19	28.38	-296.55	72.97
3	37.27	30.96	-292.57	71.07
10	46.91	34.34	-290.72	69.53
7	45.34	34.49	-287.26	72.45
e3850	42.32	34.99	-290.01	73.30
8	45.85	39.33	-287.89	71.09

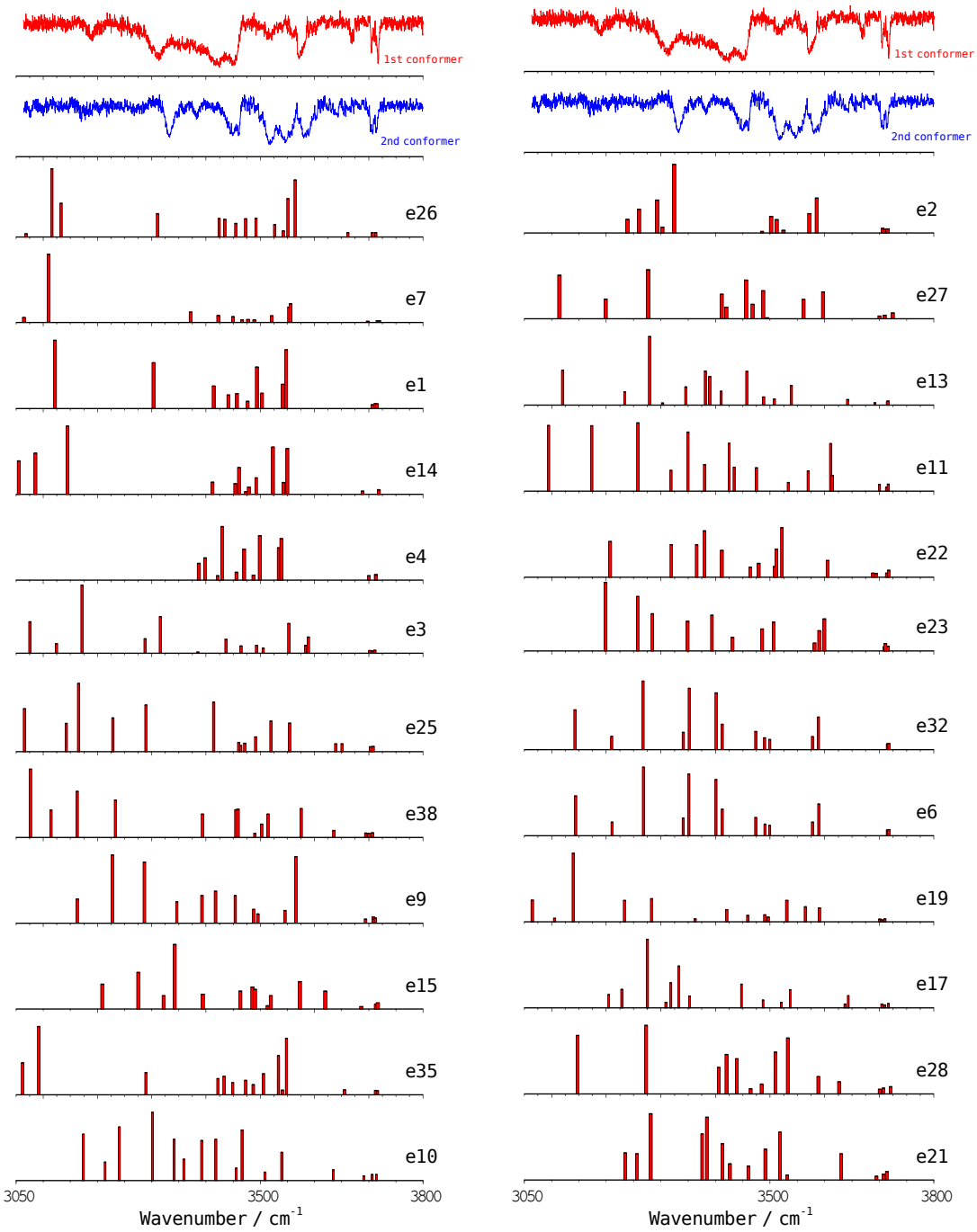

Figure 7.34a. *Experimental IDIRS for propofol$_2$·W$_7$ (upper traces) together with the predicted frequencies for each calculated structure. A correction factor of 0.955 was employed.*

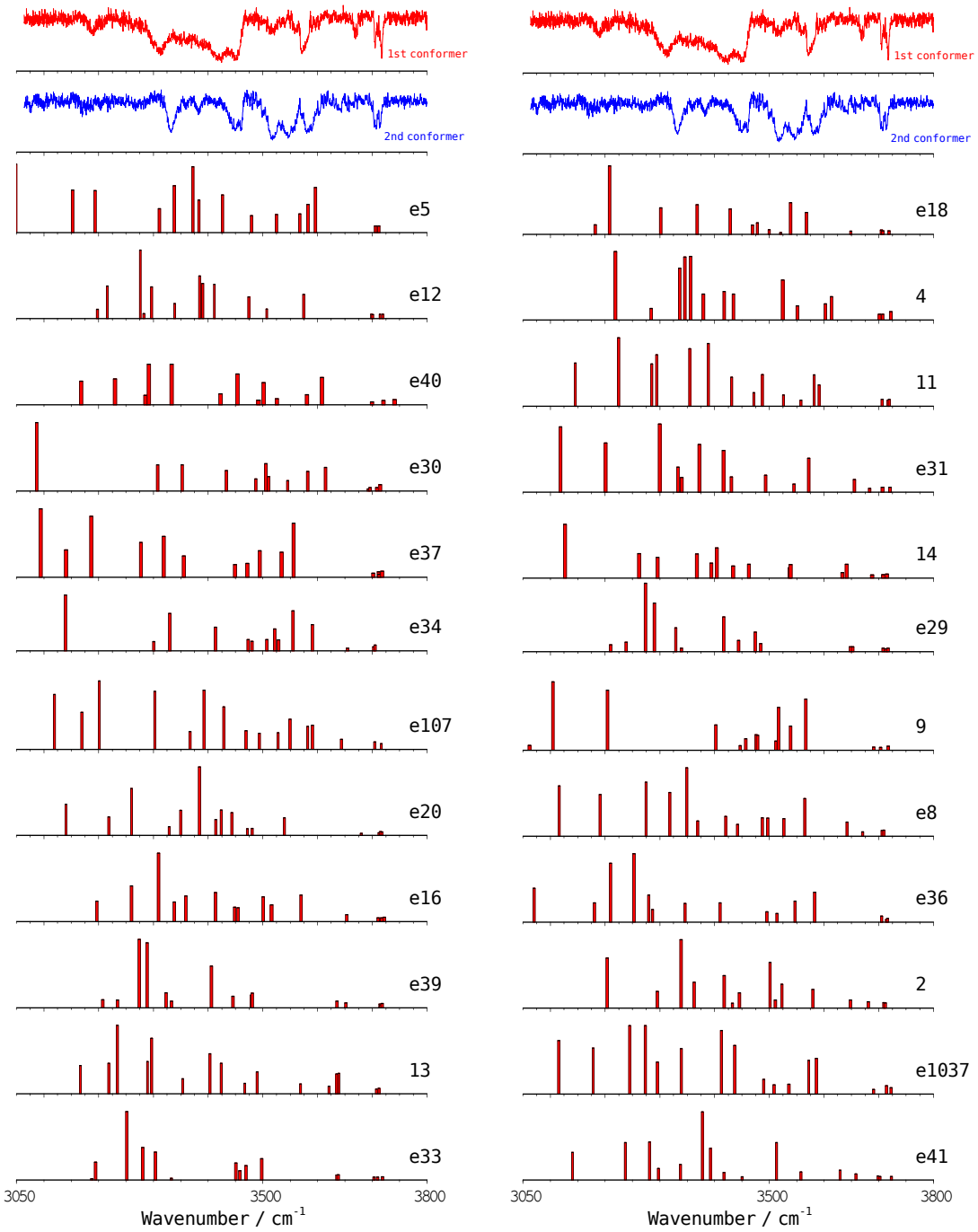

Figure 7.34b. *Experimental IDIRS for propofol$_2$·W$_7$ (upper traces) together with the predicted frequencies for each calculated structure. A correction factor of 0.955 was employed.*

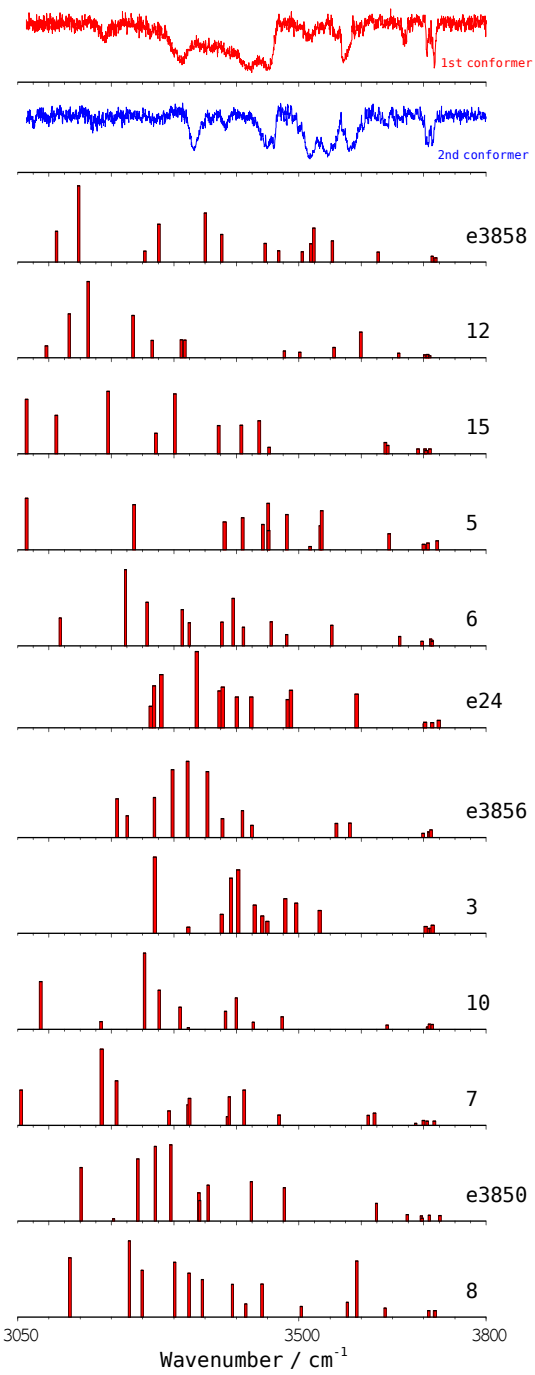

Figure 7.34c. *Experimental IDIRS for propofol$_2$·W$_7$ (upper traces) together with the predicted frequencies for each calculated structure. A correction factor of 0.955 was employed.*

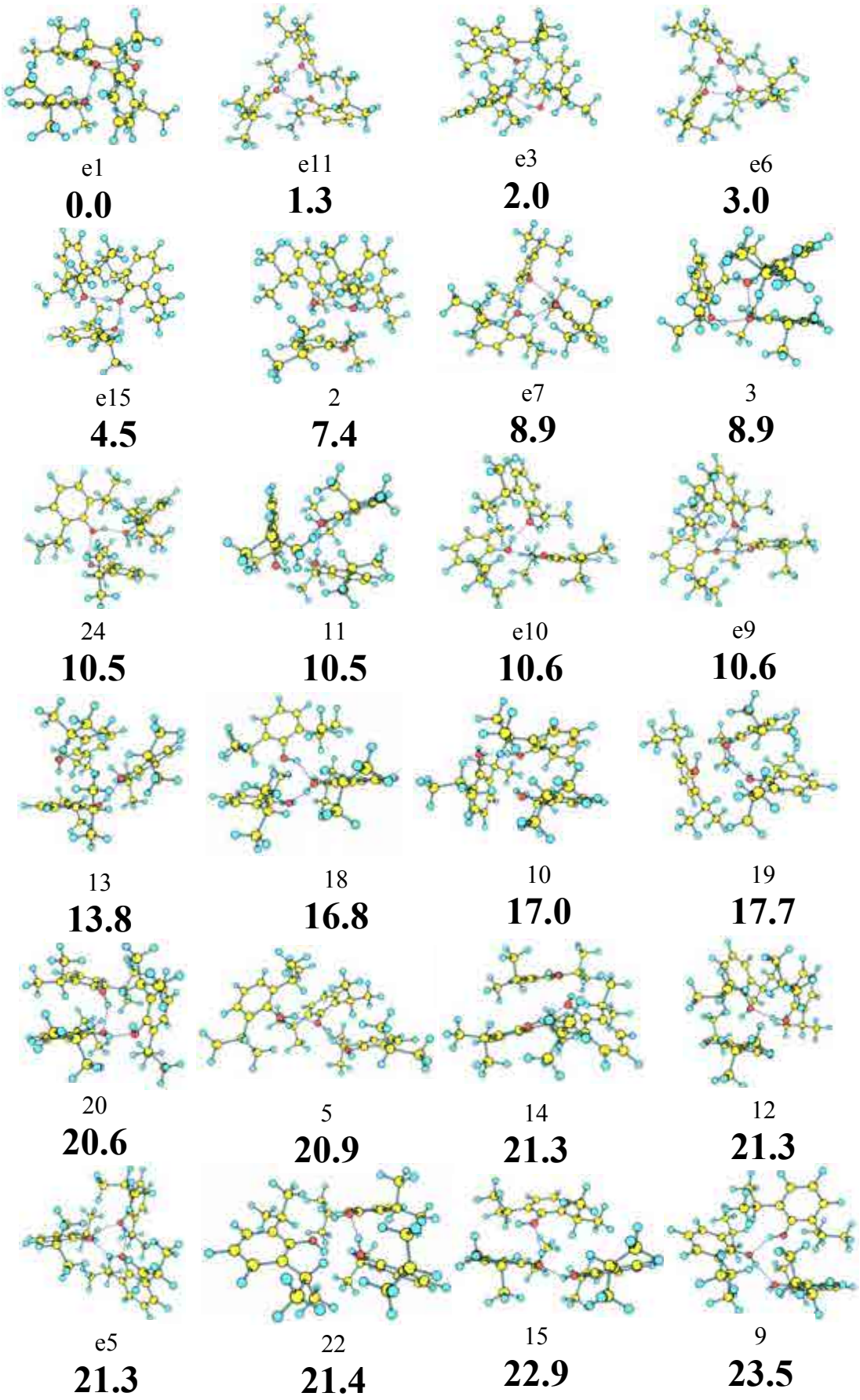

Figure 7.35a. *Propofol$_3$ calculated structures at M06-2x/6-31+G(d).*

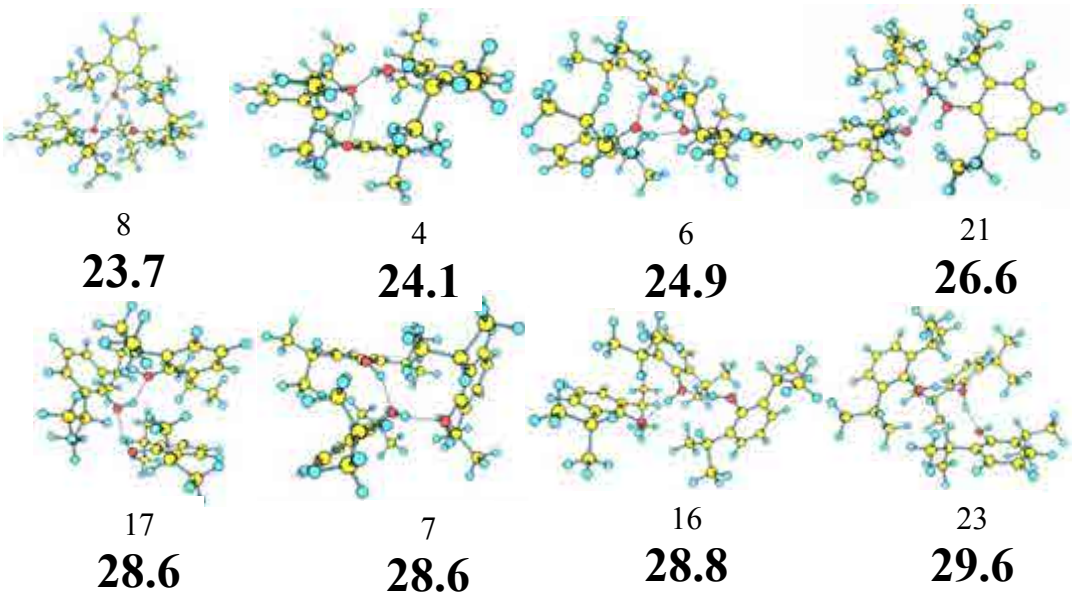

Figure 7.35b. *Propofol$_3$ calculated structures at M06-2x/6-31+G(d).*

Table 7.18. *Propofol$_3$ structures with their relative energies and binding energies calculated at M06-2x/6-31+G(d).*

Structure	*ΔE (kJ/mol)*	*ΔE_{ZPE} (kJ/mol)*	*D_0 (kJ/mol)*	*BSSE (kJ/mol)*
e1	0.00	0.00	-101.63	19.47
e11	-5.29	1.29	-102.03	17.79
e3	-1.29	2.04	-101.20	18.27
e6	-3.96	2.95	-104.08	17.78
e15	4.06	4.53	-102.91	17.37
2	2.45	7.41	-96.32	17.38
e7	2.30	8.89	-101.50	17.73
3	5.68	8.92	-95.13	17.46
24	10.27	10.46	-96.92	17.02
11	6.23	10.54	-97.18	17.10
e10	6.88	10.60	-96.75	17.06
e9	6.88	10.61	-96.73	17.06
13	12.89	13.81	-91.51	15.78
18	13.93	16.80	-87.35	16.96
10	11.97	17.00	-86.62	17.89
19	15.35	17.73	-87.34	16.03
20	19.28	20.64	-83.90	16.97
5	17.79	20.94	-84.04	15.30
14	15.87	21.27	-83.52	16.31
12	21.37	21.29	-83.53	15.48
e5	20.97	21.30	-94.09	16.02
22	16.74	21.40	-87.00	15.59
15	20.96	22.90	-82.07	16.13
9	17.46	23.46	-82.18	15.46
8	19.70	23.66	-89.19	15.26
4	22.20	24.08	-81.54	15.89
6	21.27	24.87	-80.83	15.01
21	23.52	26.61	-83.52	16.36
17	26.71	28.58	-76.70	15.83
7	25.45	28.61	-75.66	16.02
16	27.68	28.82	-76.09	15.79
23	26.05	29.64	-76.532	14.93

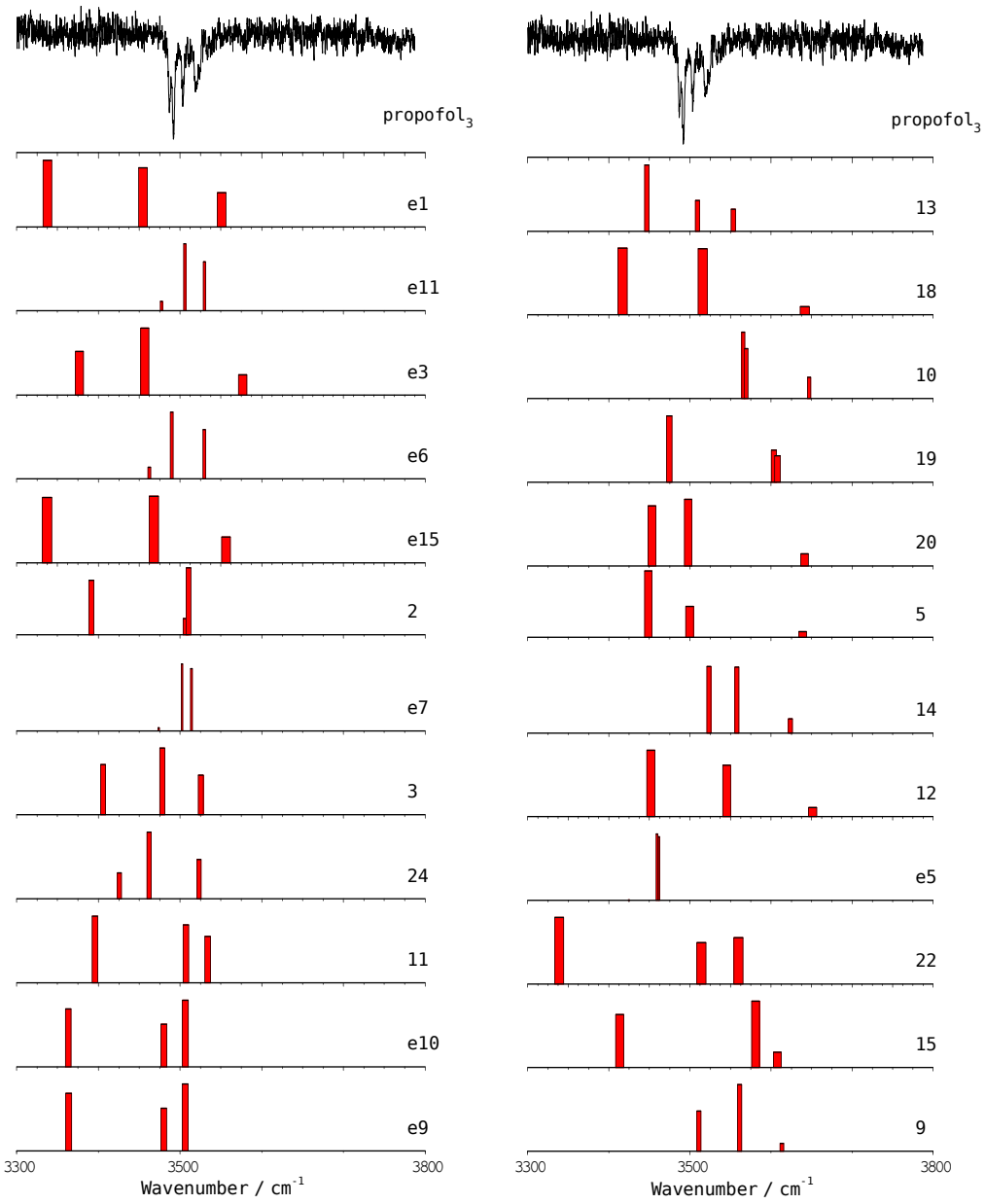

Figure 7.36a. *Experimental IDIRS for propofol$_3$ (upper trace) together with the predicted frequencies for each calculated structure. A correction factor of 0.953 was employed.*

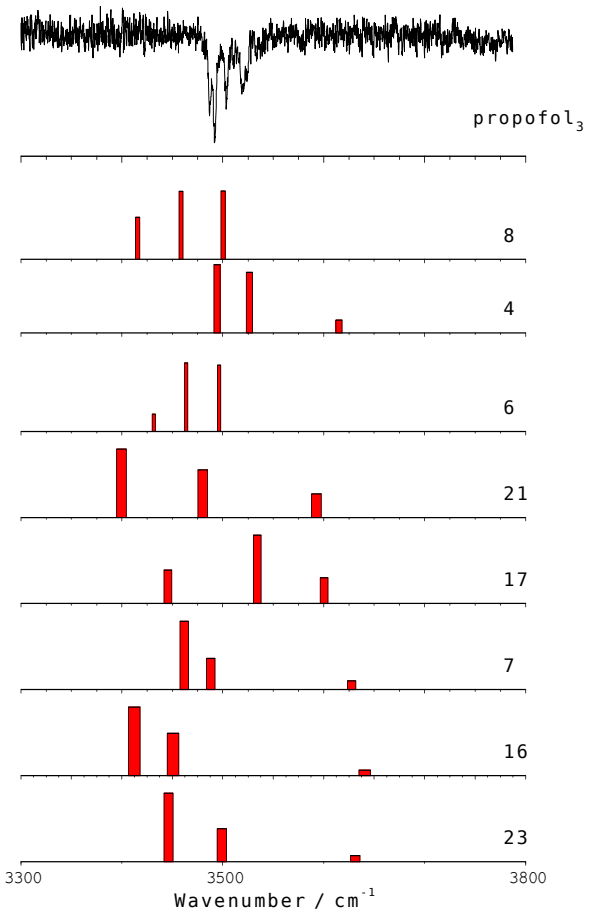

Figure 7.36b. *Experimental IDIRS for propofol$_3$ (upper trace) together with the predicted frequencies for each calculated structure. A correction factor of 0.953 was employed.*

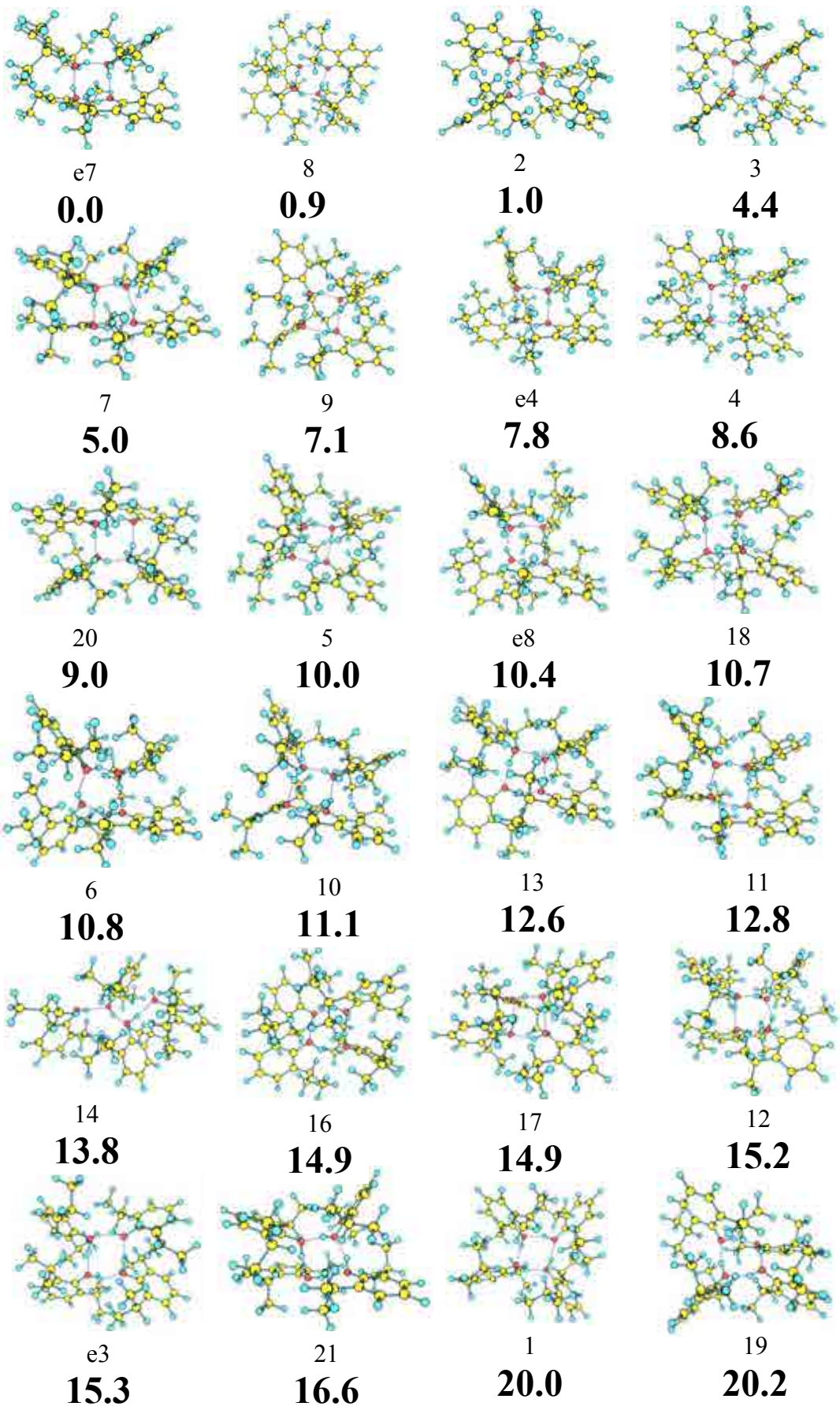

Figure 7.37. *Propofol$_4$ calculated structures at M06-2x/6-31+G(d).*

Table 7.19. *Propofol$_4$ structures with their relative energies and binding energies calculated at M06-2x/6-31+G(d).*

Structure	*ΔE (kJ/mol)*	*ΔE_{ZPE} (kJ/mol)*	*D_0 (kJ/mol)*	*BSSE (kJ/mol)*
e7	0	0	-159.5	30.79
8	3.85	0.90	-160.15	29.64
2	0.11	1.04	-158.60	31.05
3	4.03	4.45	-154.56	31.68
7	6.13	4.96	-155.68	30.46
9	8.57	7.12	-154.01	29.15
e4	10.77	7.81	-152.22	29.84
4	9.14	8.62	-154.99	30.78
20	8.48	9.00	-154.91	30.07
5	9.84	9.99	-150.34	29.95
e8	12.48	10.39	-150.36	29.53
18	10.05	10.67	-152.07	31.65
6	9.65	10.80	-153.26	30.34
10	10.54	11.10	-149.90	29.28
13	12.08	12.61	-148.46	29.21
11	12.37	12.83	-151.02	30.55
14	15.02	13.80	-149.70	27.19
16	16.14	14.94	-148.23	30.82
17	16.14	14.94	-148.24	30.81
12	12.85	15.25	-146.38	29.47
e3	14.85	15.35	-150.56	28.09
21	14.87	16.59	-149.73	30.15
1	23.43	19.97	-140.01	29.90
19	18.50	20.25	-140.73	29.71

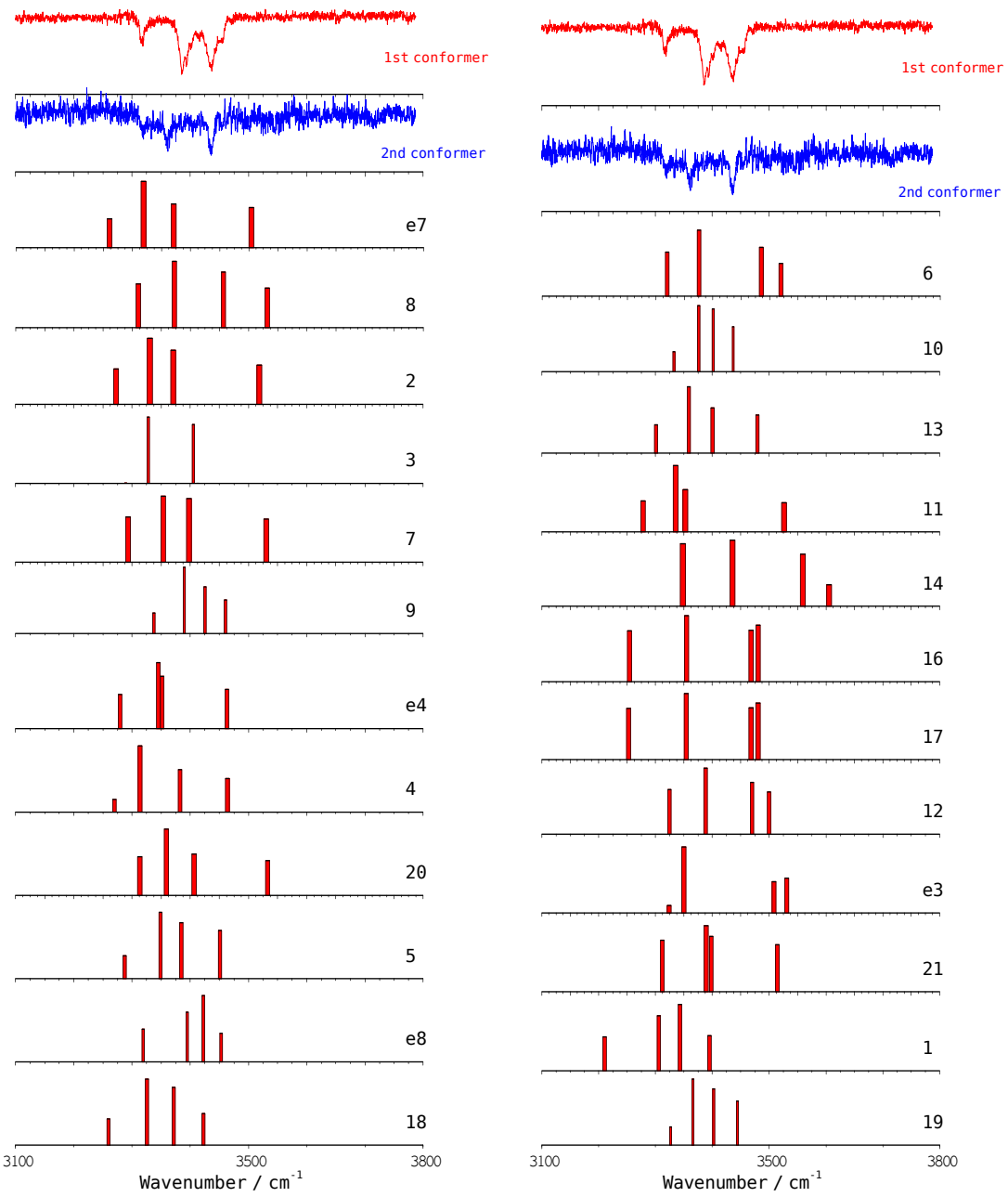

Figure 7.38. *Experimental IDIRS for propofol$_4$ (upper traces) together with the predicted frequencies for each calculated structure. A correction factor of 0.965 was employed.*

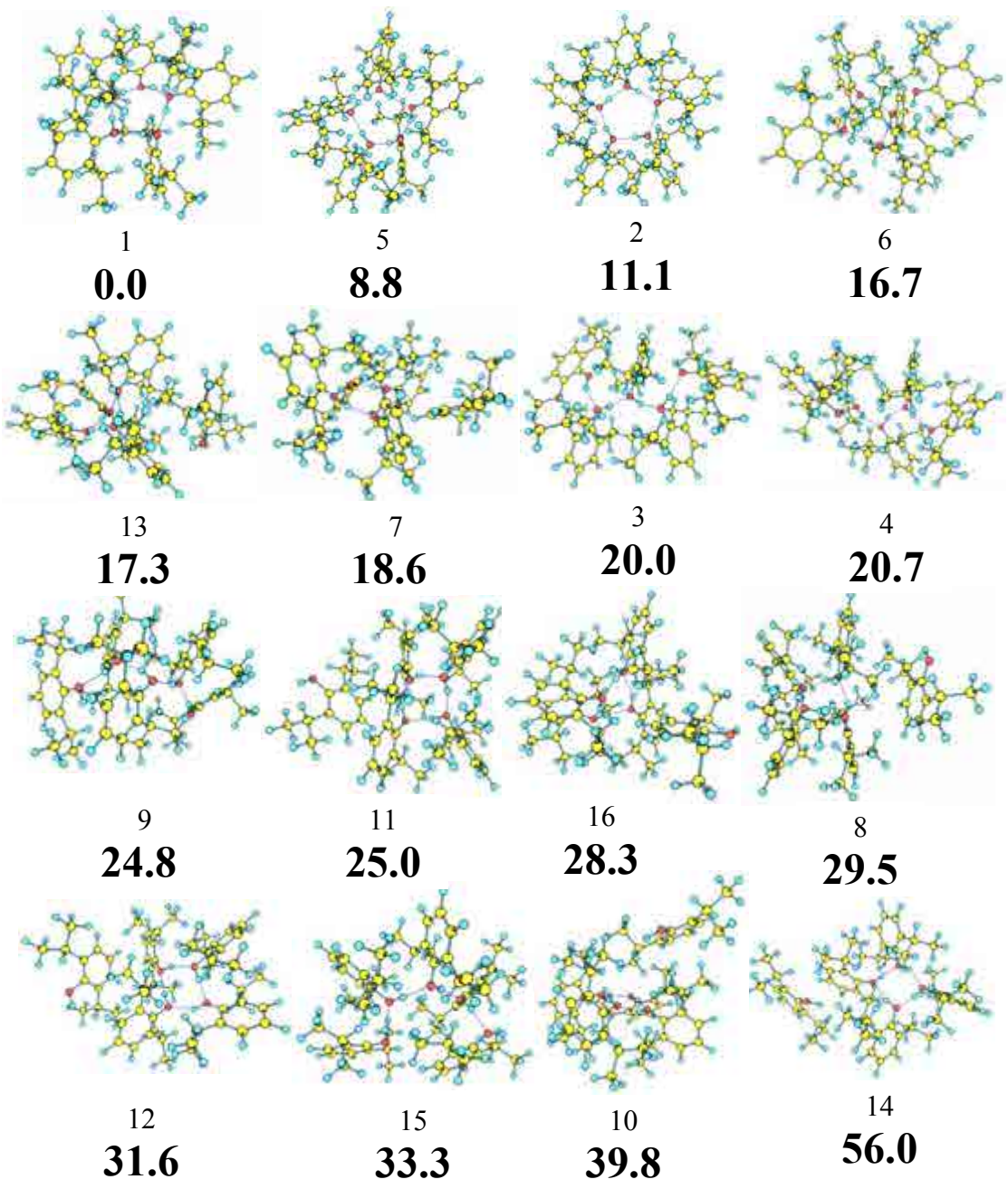

Figure 7.39. *Propofol$_5$ calculated structures at M06-2x/6-31+G(d).*

Table 7.20. *Propofol$_5$ structures with their relative energies and binding energies calculated at M06-2x/6-31+G(d).*

Structure	*ΔE (kJ/mol)*	*ΔE_{ZPE} (kJ/mol)*	*D_0 (kJ/mol)*	*BSSE (kJ/mol)*
1	0	0	-218.34	42.22
5	7.52	8.82	-210.73	40.61
2	15.58	11.11	-208.55	40.10
6	11.42	16.74	-199.73	43.27
13	17.75	17.26	-204.37	38.53
7	23.26	18.55	-204.75	37.26
3	21.22	20.00	-201.64	38.92
4	25.06	20.74	-202.63	37.19
9	28.35	24.77	-202.34	37.16
11	26.80	25.01	-195.79	38.54
16	26.52	28.25	-192.63	39.27
8	28.76	29.51	-191.68	38.96
12	33.37	31.61	-191.87	37.07
15	33.15	33.28	-188.99	37.88
10	41.69	39.85	-184.17	36.55
14	61.63	56.03	-174.52	35.38

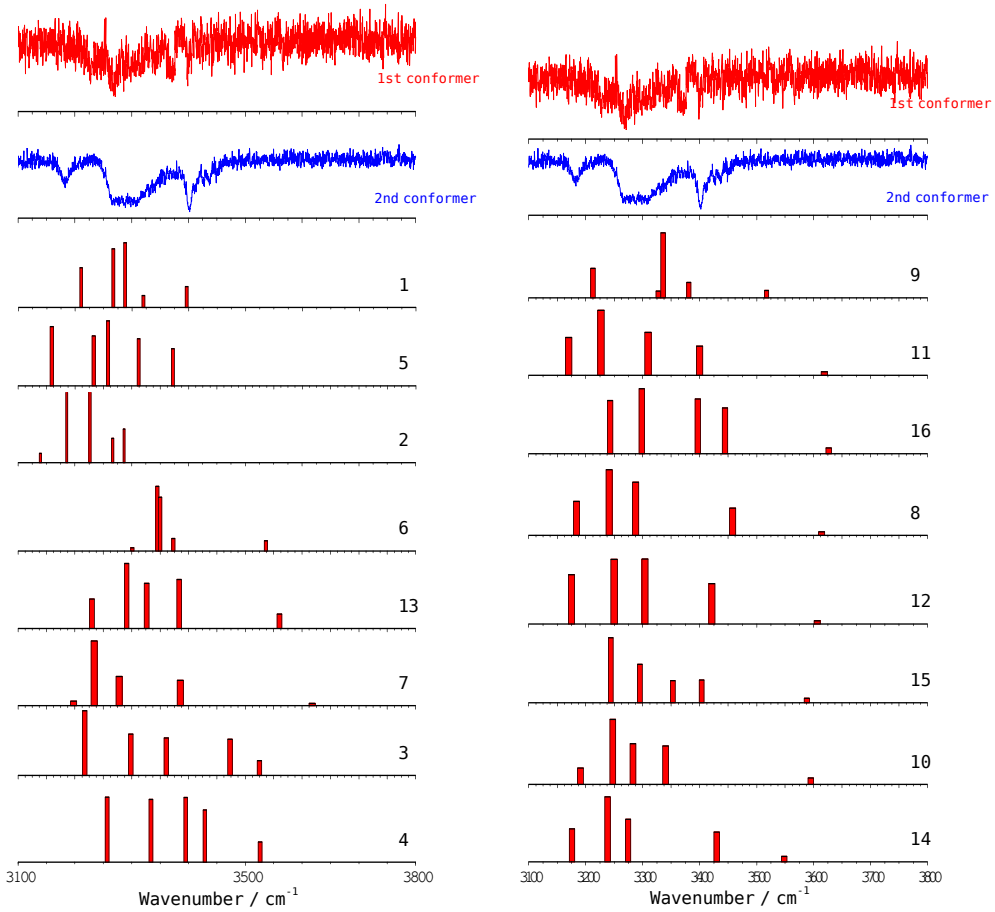

Figure 7.40. *Experimental IDIRS for propofol$_5$ (upper traces) together with the predicted frequencies for each calculated structure. A correction factor of 0.942 was employed.*

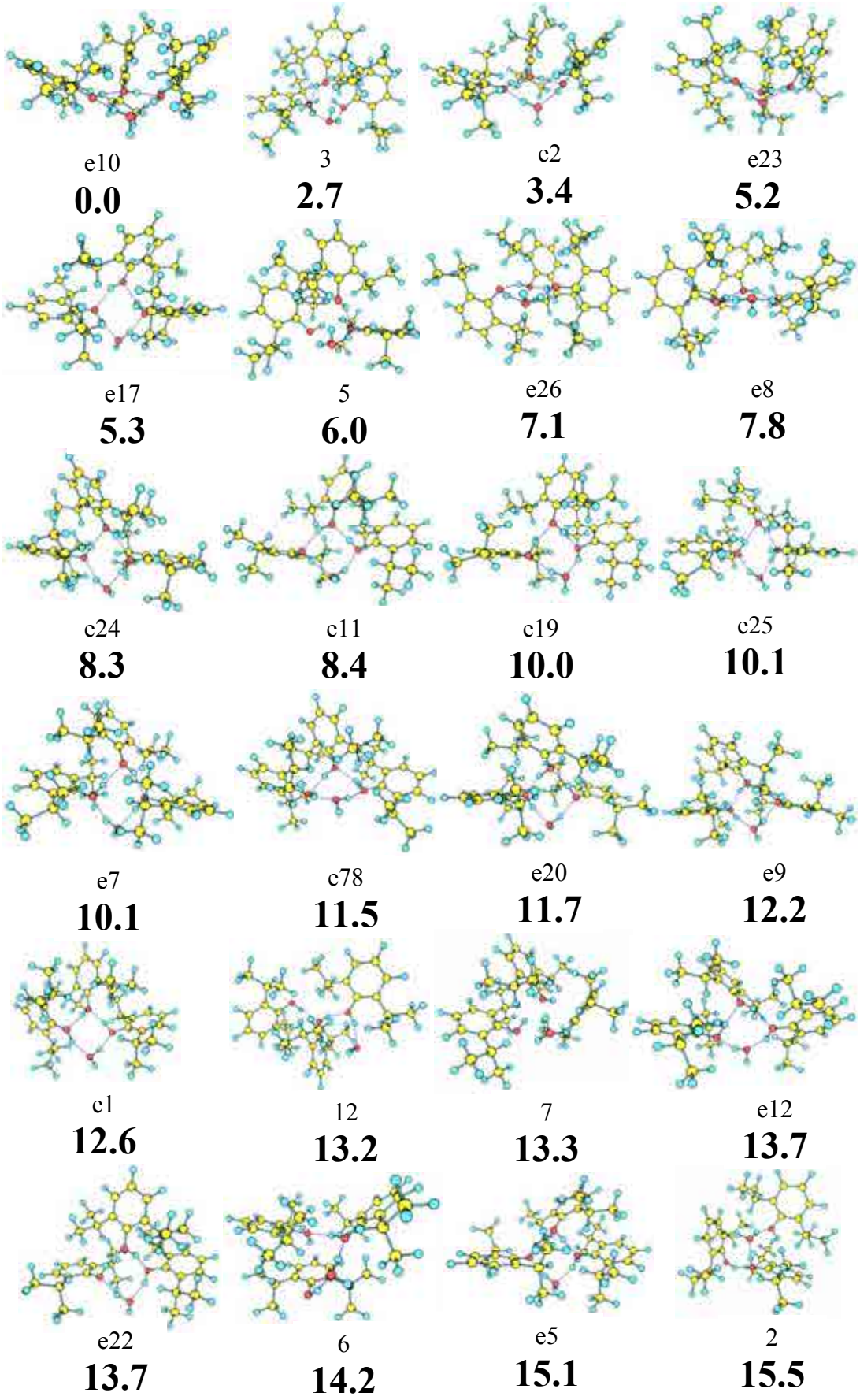

Figure 7.41a. *Propofol$_3$·W$_1$ calculated structures at M06-2x/6-31+G(d).*

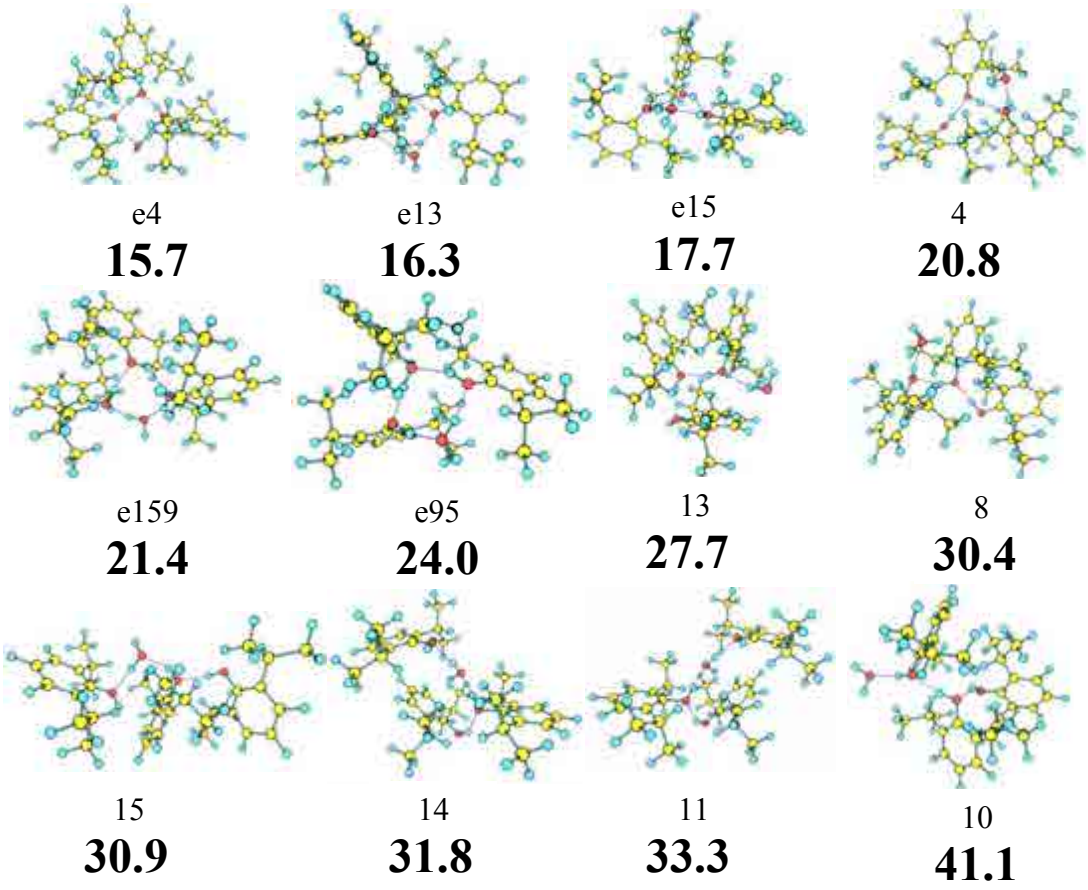

Figure 7.41b. *Propofol$_3$·W$_1$ calculated structures at M06-2x/6-31+G(d).*

Table 7.21. *Propofol$_3$·W$_1$ structures with their relative energies and binding energies calculated at M06-2x/6-31+G(d).*

Structure	*ΔE (kJ/mol)*	*ΔE_{ZPE} (kJ/mol)*	*D_0 (kJ/mol)*	*BSSE (kJ/mol)*
e10	0.00	0.00	-141.41	28.34
3	-0.39	2.74	-139.02	28.00
e2	5.05	3.44	-139.16	27.15
e23	4.68	5.16	-135.87	29.13
e17	4.89	5.30	-136.45	28.81
5	3.40	5.97	-136.07	27.71
e26	5.23	7.08	-133.10	29.57
e8	7.17	7.80	-137.16	28.10
e24	9.34	8.29	-136.56	28.61
e11	8.90	8.38	-133.85	28.34
e19	10.86	9.97	-131.58	28.61
e25	10.74	10.09	-131.17	28.49
e7	11.53	10.14	-131.70	27.91
e78	10.04	11.46	-134.29	27.31
e20	10.80	11.70	-134.02	27.74
e9	10.13	12.17	-130.59	27.40
e1	12.92	12.63	-128.90	28.22
12	13.29	13.16	-130.02	26.57
7	14.63	13.33	-129.97	26.46
e12	14.97	13.66	-132.73	27.08
e22	15.30	13.67	-130.06	26.43
6	14.16	14.15	-128.90	26.69
e5	16.01	15.13	-126.20	28.43
2	17.45	15.50	-125.80	28.45
e4	16.75	15.67	-125.80	27.88
e13	16.00	16.35	-128.32	28.39
e15	19.80	17.67	-128.48	26.91
4	22.41	20.81	-122.72	26.64
e159	20.57	21.36	-131.53	26.75
e95	22.62	23.98	-124.42	28.36
13	28.68	27.67	-114.01	28.49
8	33.57	30.44	-112.29	26.61
15	31.95	30.92	-114.59	24.65
14	33.06	31.77	-111.67	26.32
11	34.50	33.34	-110.57	25.85
10	44.07	41.05	-103.98	24.31

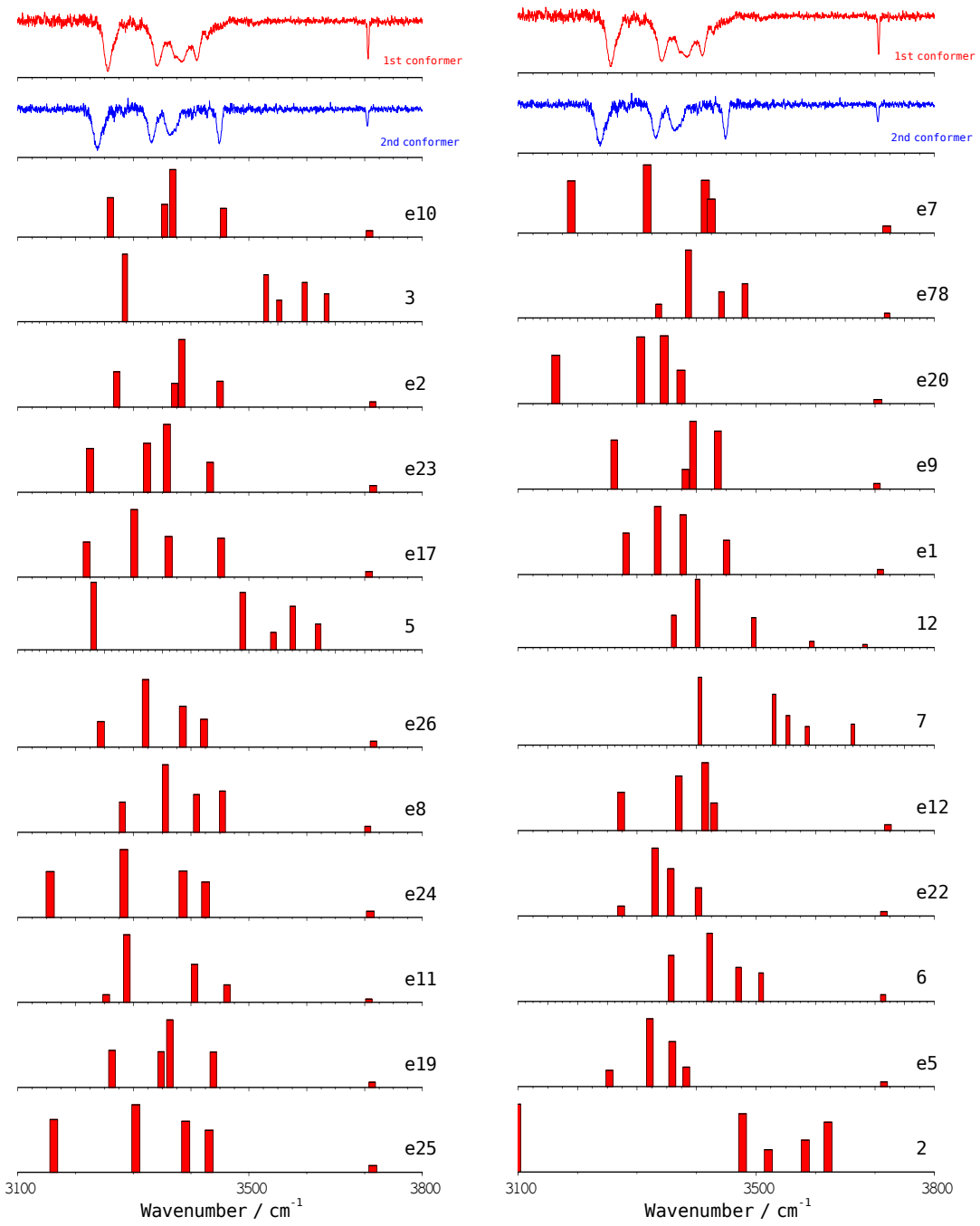

Figure 7.42a. *Experimental IDIRS for propofol$_3$·W$_1$ (upper traces) together with the predicted frequencies for each calculated structure. A correction factor of 0.958 was employed.*

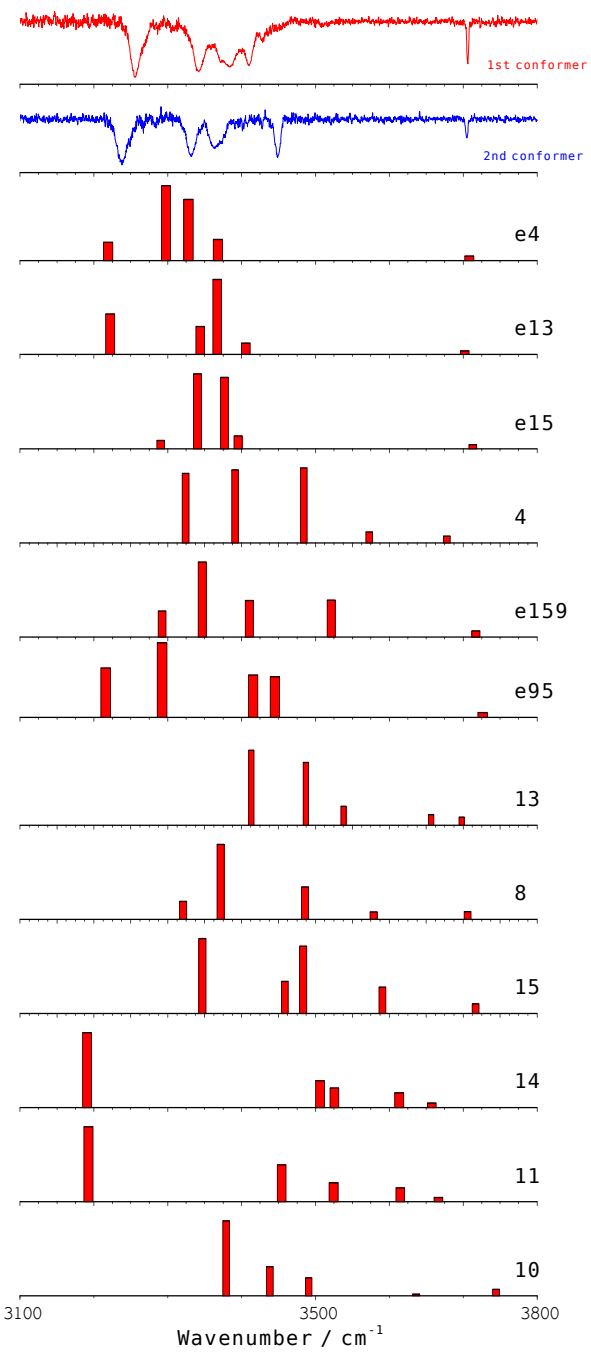

Figure 7.42b. *Experimental IDIRS for propofol$_3$·W$_1$ (upper traces) together with the predicted frequencies for each calculated structure. A correction factor of 0.958 was employed.*

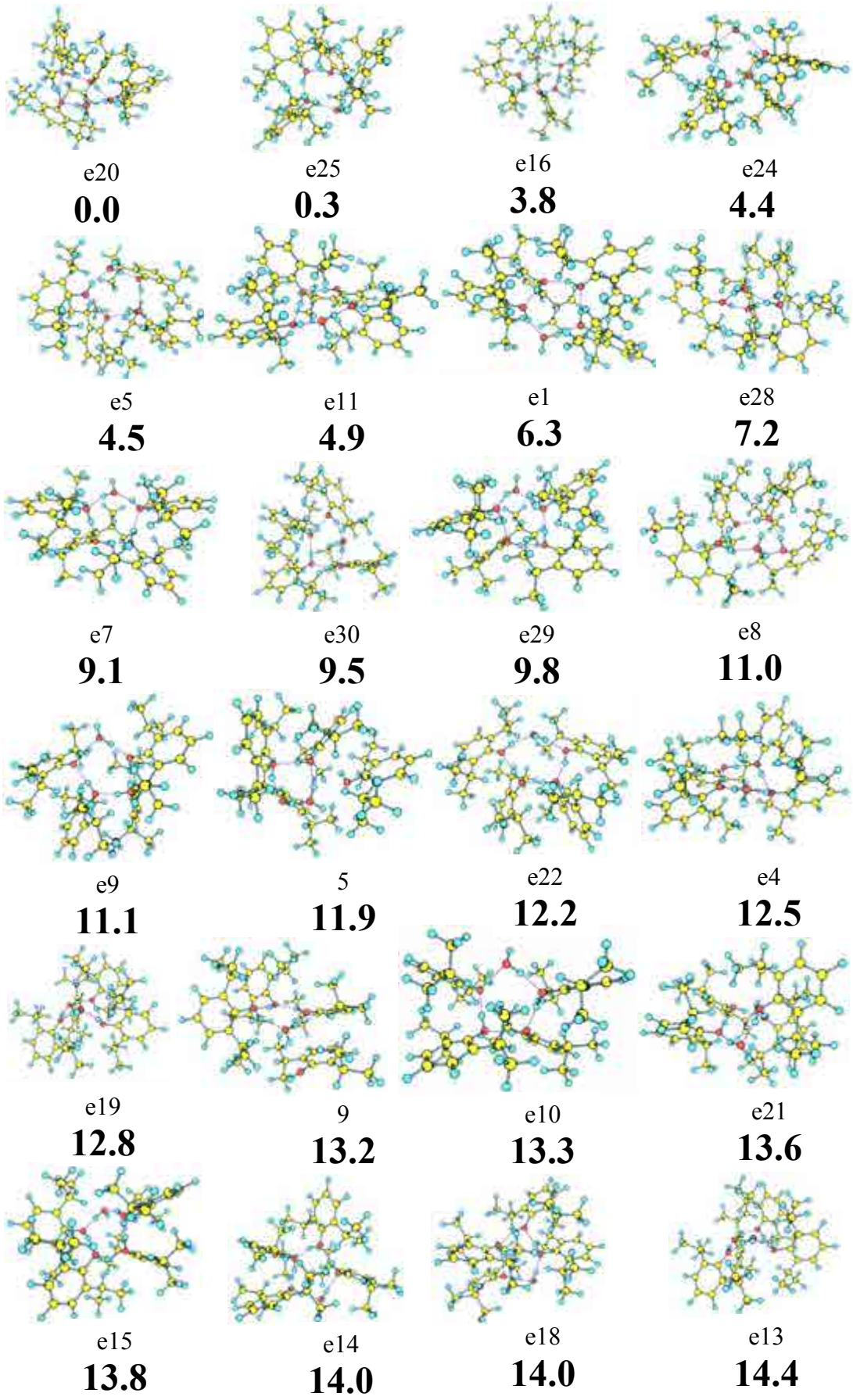

Figure 7.43a. *Propofol$_4$·W$_1$ calculated structures at M06-2x/6-31+G(d).*

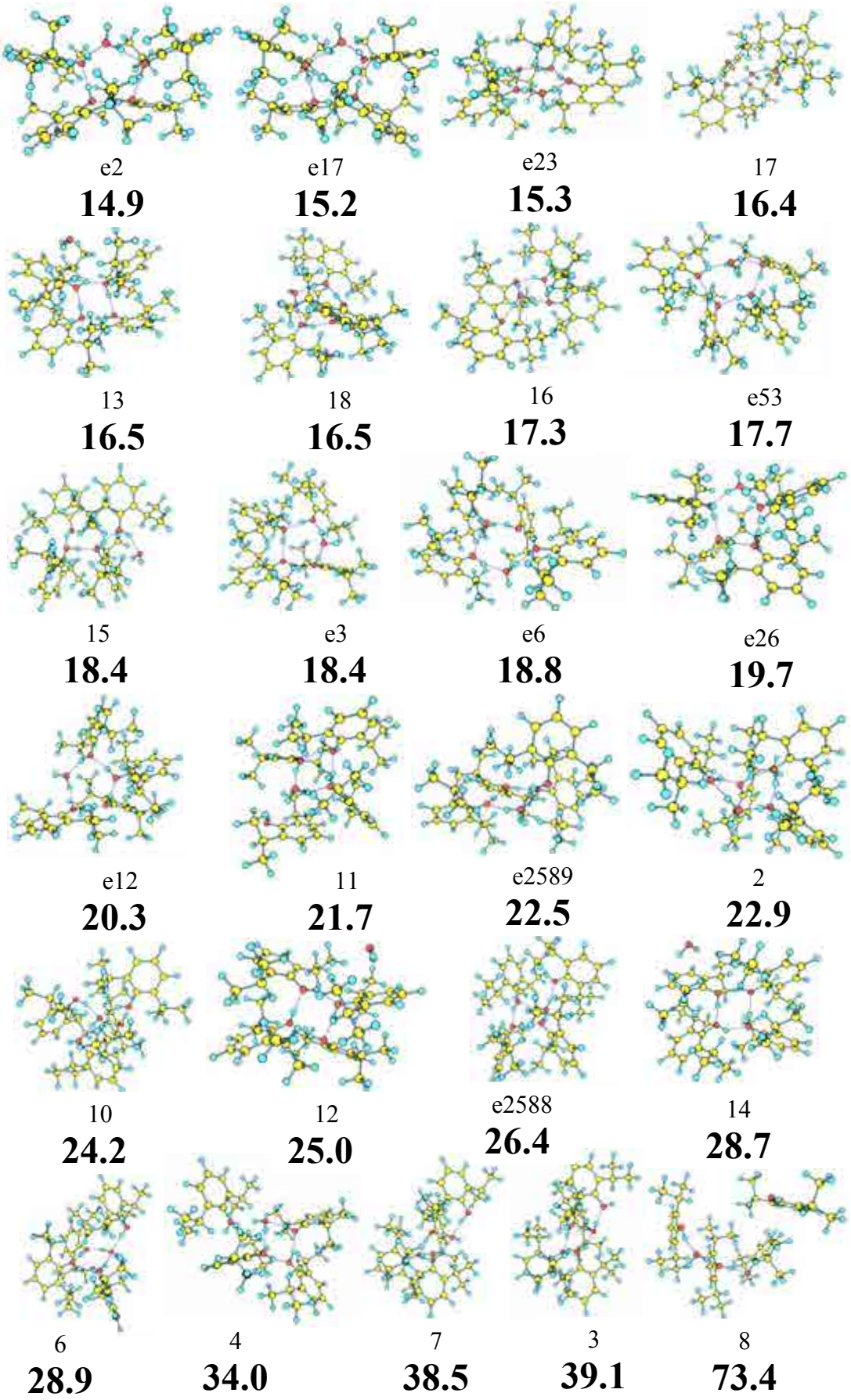

Figure 7.43b. *Propofol$_4$·W$_1$ calculated structures at M06-2x/6-31+G(d).*

Table 7.22. *Propofol$_4$·W$_1$ structures with their relative energies and binding energies calculated at M06-2x/6-31+G(d).*

Structure	*ΔE (kJ/mol)*	*ΔE_{ZPE} (kJ/mol)*	*D_0 (kJ/mol)*	*BSSE (kJ/mol)*
e20	0.00	0.00	-196.07	41.47
e25	1.66	0.35	-196.86	39.92
e16	3.19	3.81	-193.35	39.56
e24	4.77	4.40	-191.70	41.04
e5	6.72	4.51	-193.58	38.63
e11	5.75	4.87	-191.61	41.06
e1	11.23	6.35	-191.45	39.74
e28	8.40	7.21	-188.23	41.68
e7	11.98	9.06	-188.38	40.52
e30	12.74	9.53	-187.57	40.44
e29	11.18	9.83	-187.22	40.08
e8	10.67	10.97	-184.96	40.39
e9	14.37	11.09	-186.10	39.54
5	13.36	11.93	-184.97	40.23
e22	14.60	12.24	-190.16	38.03
e4	13.04	12.47	-187.67	40.30
e19	11.95	12.80	-183.34	40.19
9	16.44	13.17	-186.24	37.73
e10	15.86	13.31	-185.05	38.77
e21	14.01	13.59	-185.91	41.33
e15	16.46	13.78	-182.75	41.01
e14	18.16	14.05	-181.73	40.95
e18	16.08	14.06	-181.49	41.58
e13	14.15	14.39	-182.73	39.61
e2	16.08	14.94	-187.23	39.08
e17	17.64	15.16	-189.29	39.69
e23	17.03	15.33	-182.96	38.84
17	15.01	16.37	-184.30	36.46
13	22.43	16.48	-180.10	40.55
18	17.48	16.54	-180.55	39.64
16	17.75	17.31	-178.62	40.80
e53	19.91	17.68	-184.58	38.17
15	17.93	18.36	-179.36	39.42
e3	19.09	18.39	-179.79	39.36
e6	21.38	18.75	-180.81	37.17
e26	21.17	19.67	-182.28	38.89
e12	21.86	20.34	-178.12	39.08
11	25.19	21.66	-177.17	37.90
e2589	24.53	22.54	-185.12	36.48
2	25.13	22.93	-178.48	39.02
10	25.49	24.20	-179.13	37.11
12	30.58	24.98	-172.71	39.45
e2588	24.81	26.37	-181.64	38.61
14	35.58	28.68	-173.94	38.22
6	29.40	28.93	-171.16	37.04
4	34.47	33.98	-171.01	35.45
7	40.83	38.50	-161.14	37.49
3	39.87	39.08	-159.30	38.35
8	77.41	73.43	-134.99	29.12

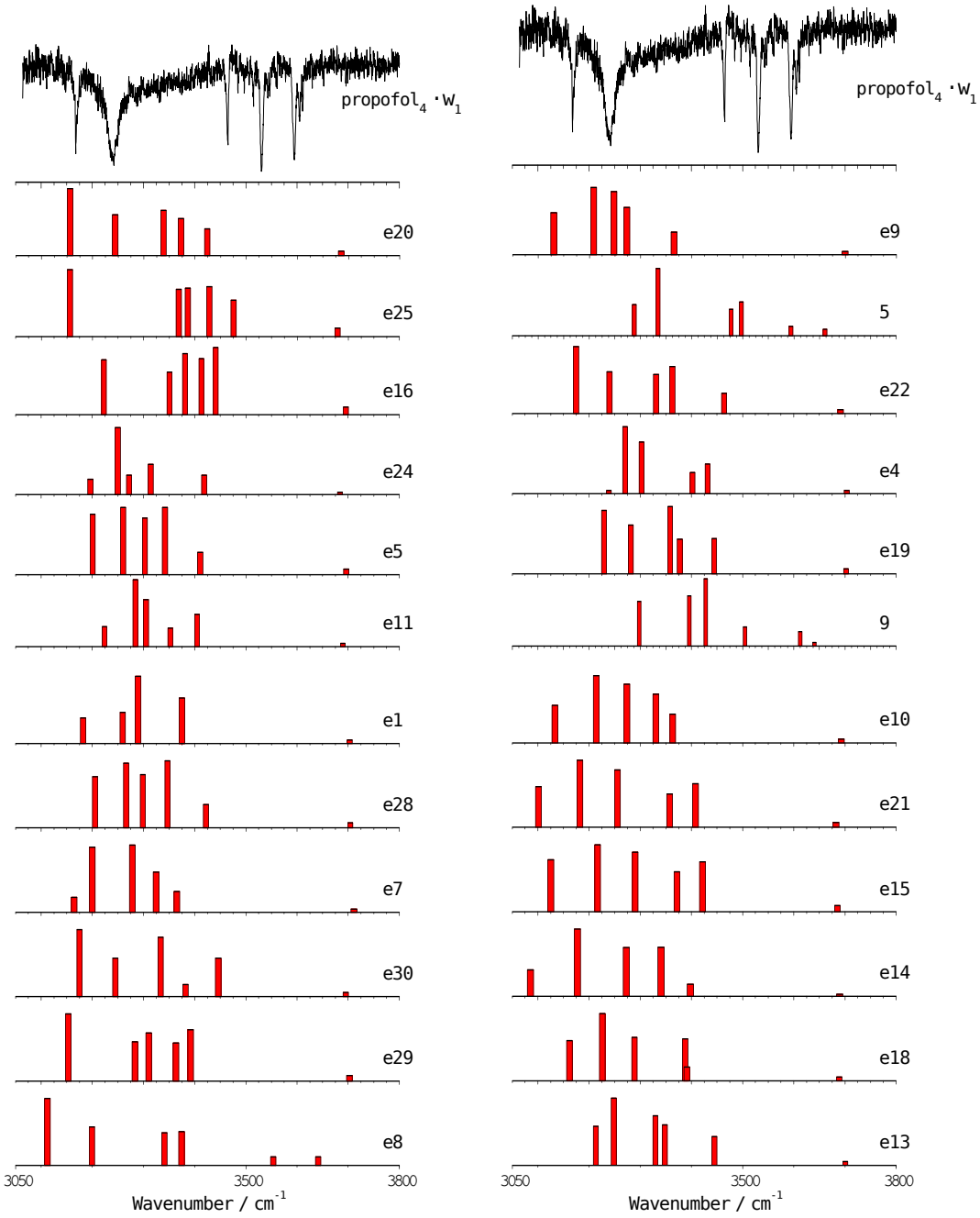

Figure 7.44a. *Experimental IDIRS for propofol$_4$·W$_1$ (upper trace) together with the predicted frequencies for each calculated structure. A correction factor of 0.955 was employed.*

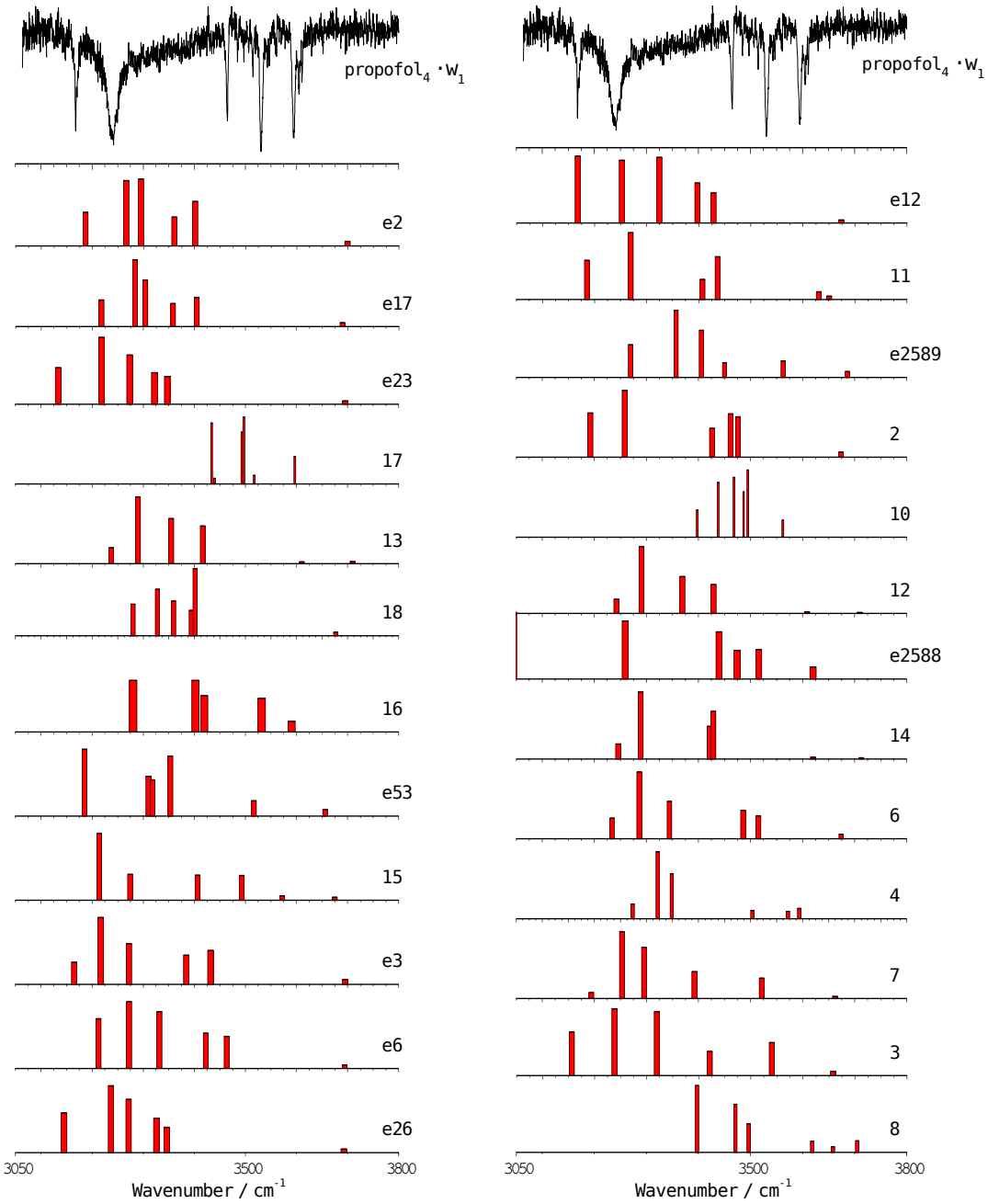

Figure 7.44b. *Experimental IDIRS for propofol$_4$·W$_1$ (upper trace) together with the predicted frequencies for each calculated structure. A correction factor of 0.955 was employed.*

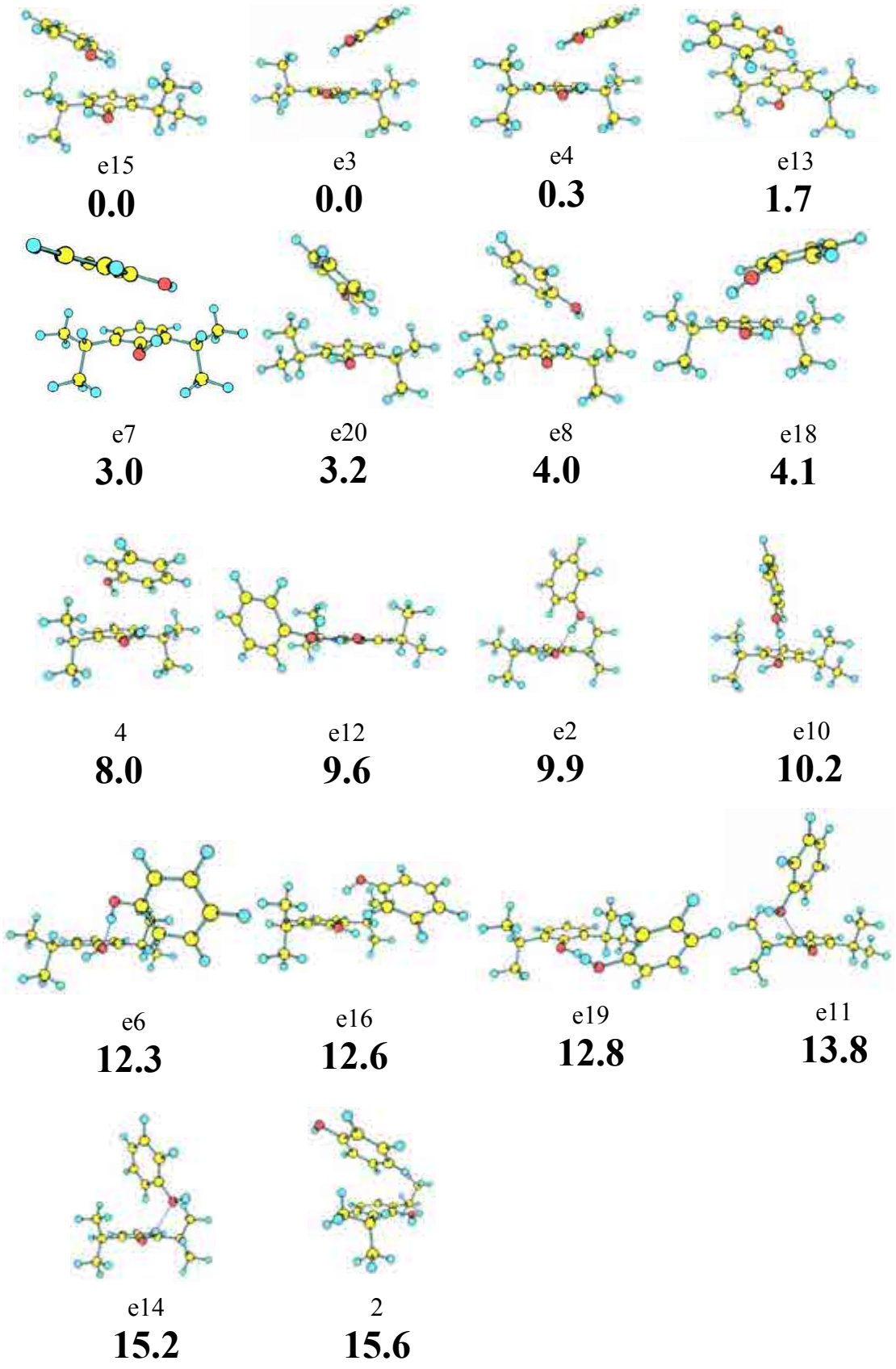

Figure 7.45. *Propofol·phenol calculated structures at M06-2x/6-31+G(d).*

Table 7.23. *Propofol·phenol structures with their relative energies and binding energies calculated at M06-2x/6-31+G(d).*

Structure	*ΔE (kJ/mol)*	*ΔE_{ZPE} (kJ/mol)*	*D_0 (kJ/mol)*	*BSSE (kJ/mol)*
e15	0.00	0.00	-35.21	6.28
e3	0.80	0.01	-34.90	6.59
e4	0.34	0.27	-38.60	6.33
e13	2.67	1.69	-33.94	6.28
e7	2.70	3.01	-31.93	6.97
e20	4.38	3.17	-32.28	6.04
e8	5.54	3.95	-30.47	7.08
e18	4.19	4.12	-31.57	6.22
4	9.34	8.00	-30.93	6.28
e12	8.64	9.56	-27.23	5.11
e2	8.82	9.94	-24.07	7.49
e10	9.92	10.18	-30.12	7.38
e6	12.11	12.30	-22.77	6.43
e16	11.84	12.64	-26.24	6.33
e19	11.50	12.75	-27.37	5.08
e11	14.20	13.81	-21.33	6.36
e14	16.44	15.22	-23.58	6.41
2	17.02	15.65	-22.22	3.63

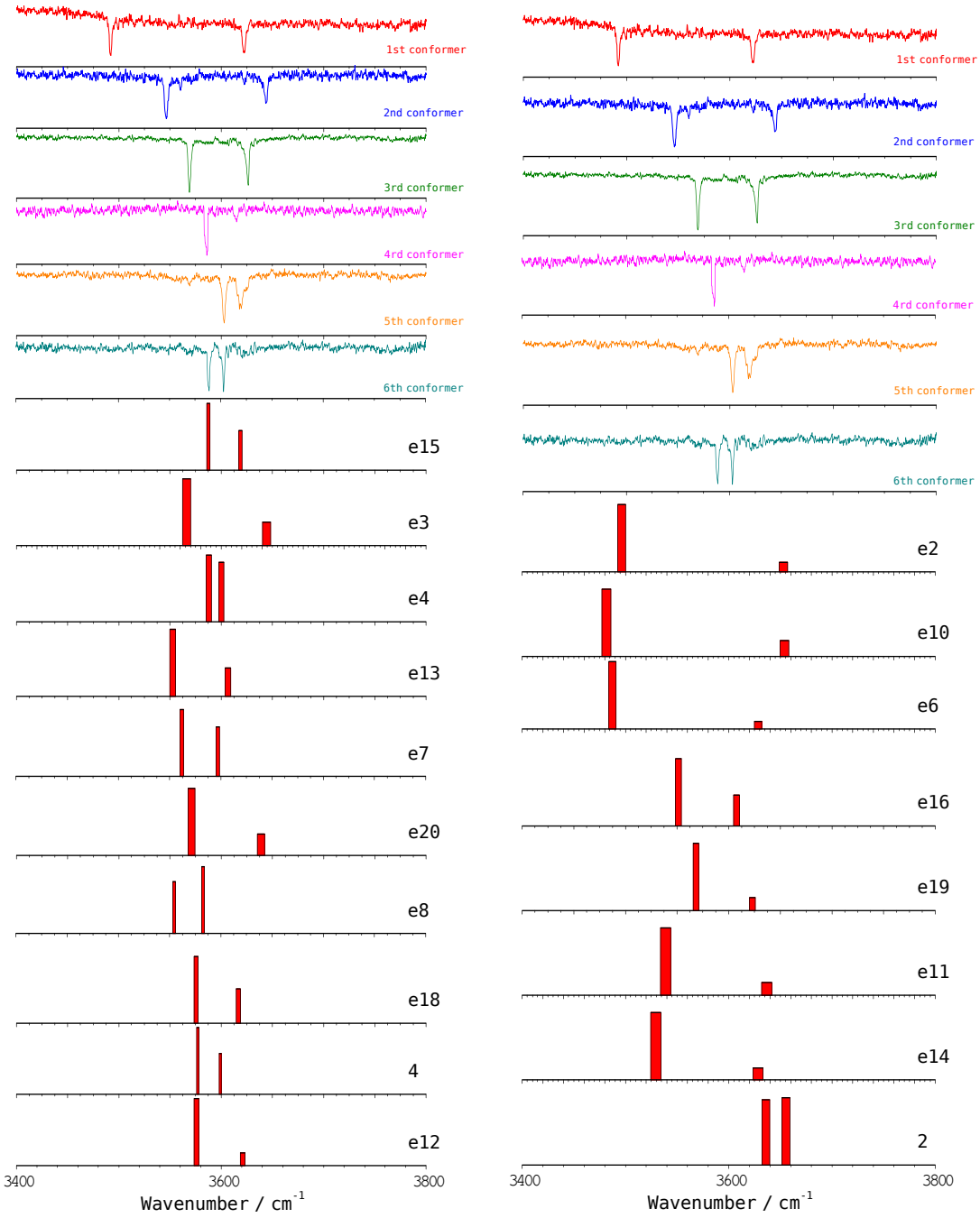

Figure 7.46. *Experimental IDIRS for propofol·phenol (upper traces) together with the predicted frequencies for each calculated structure. A correction factor of 0.952 was employed.*

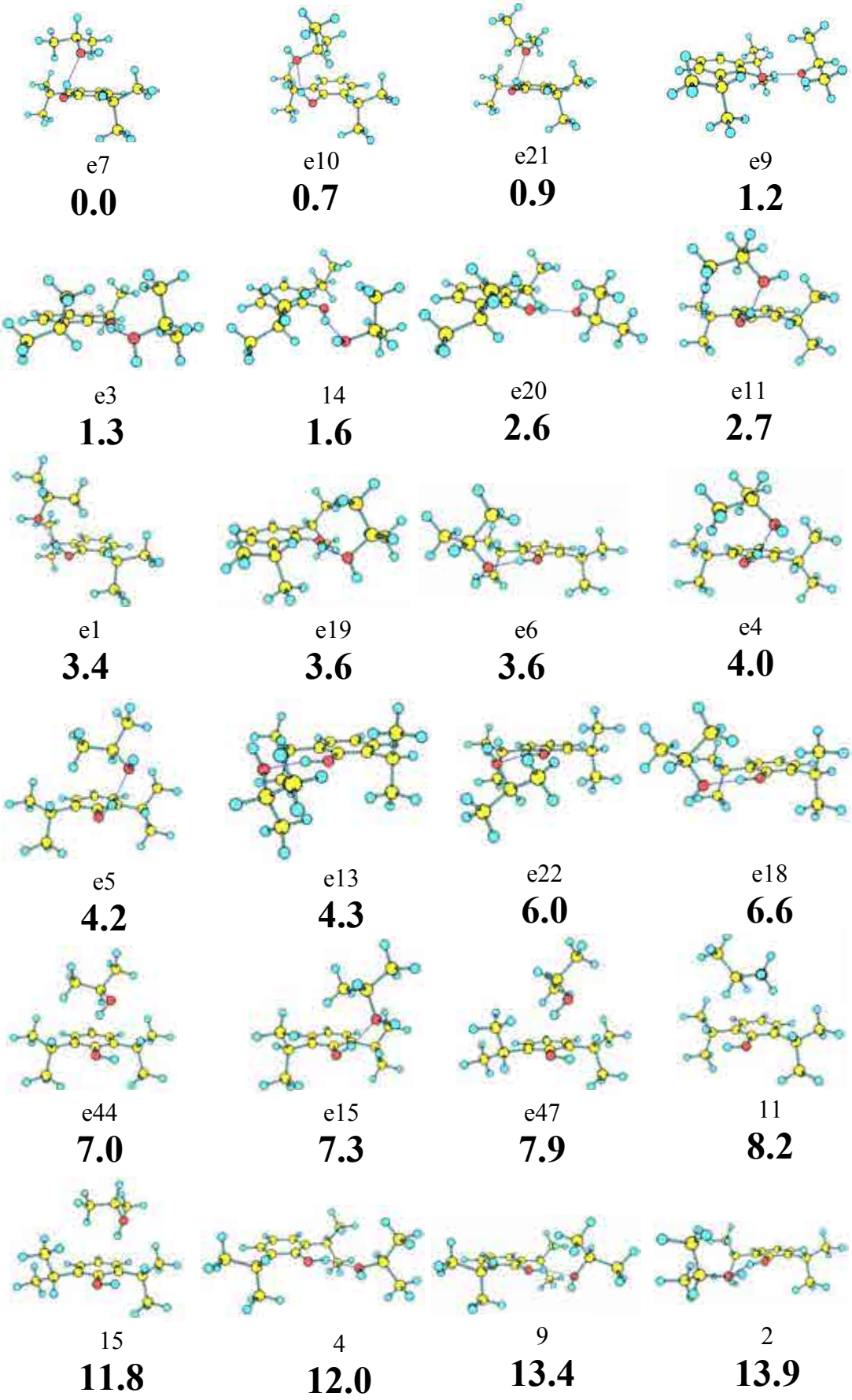

Figure 7.47a. *Propofol·isopropanol calculated structures at M06-2x/6-31+G(d).*

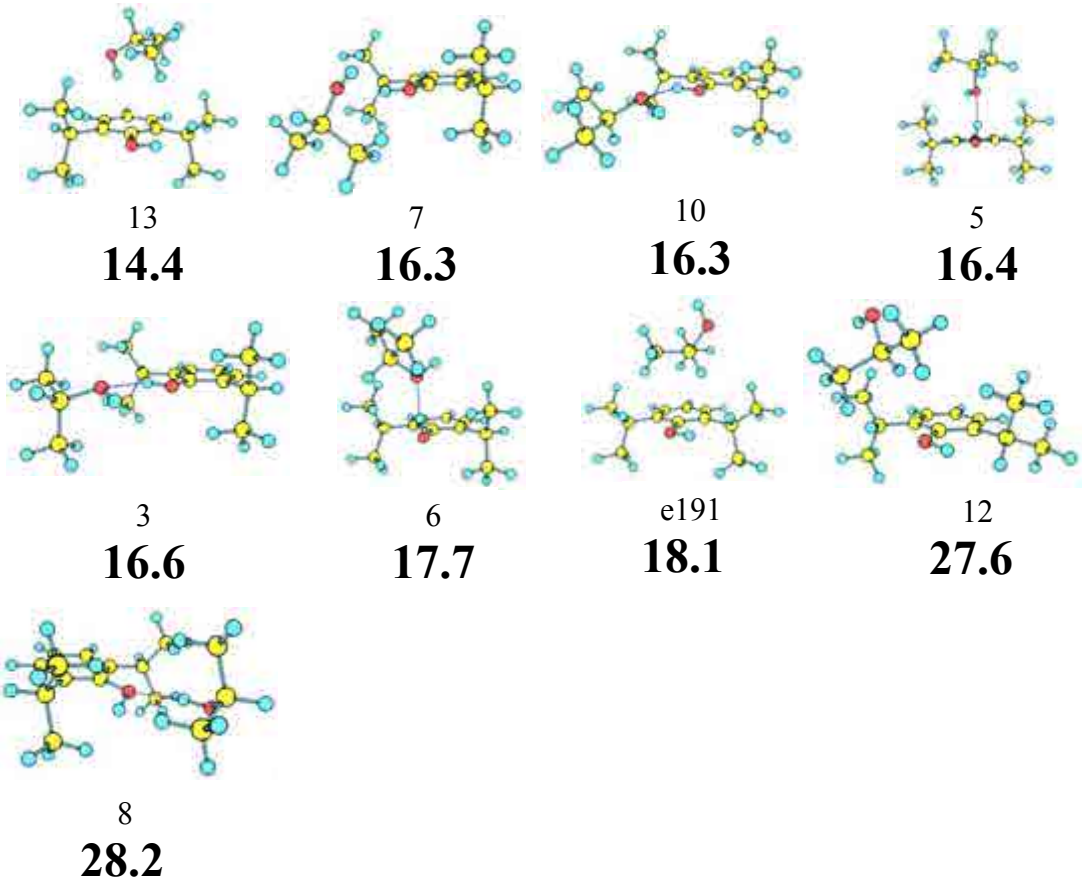

Figure 7.47b. *Propofol·isopropanol calculated structures at M06-2x/6-31+G(d).*

Table 7.24. *Propofol·isopropanol structures with their relative energies and binding energies calculated at M06-2x/6-31+G(d).*

Structure	*ΔE (kJ/mol)*	*ΔE_{ZPE} (kJ/mol)*	*D_0 (kJ/mol)*	*BSSE (kJ/mol)*
e7	0.00	0.00	-33.65	5.49
e10	0.35	0.65	-34.05	5.12
e21	0.74	0.91	-33.48	5.43
e9	-0.71	1.22	-33.12	4.80
e3	-0.84	1.31	-32.83	4.99
14	-1.45	1.62	-32.61	4.91
e20	0.75	2.56	-32.60	4.67
e11	1.47	2.70	-30.40	5.63
e1	3.96	3.37	-30.29	5.07
e19	1.02	3.64	-33.92	4.88
e6	2.81	3.64	-30.89	4.61
e4	2.64	4.03	-29.28	5.42
e5	1.18	4.17	-29.70	5.95
e13	1.44	4.29	-33.26	4.88
e22	3.57	6.00	-32.47	4.65
e18	5.69	6.64	-31.38	4.42
e44	6.94	7.02	-27.09	5.02
e15	6.73	7.28	-30.09	5.07
e47	6.55	7.90	-26.07	4.77
11	9.00	8.21	-26.21	4.71
15	11.46	11.78	-23.17	4.46
4	11.31	12.00	-29.53	4.07
9	13.45	13.35	-28.22	4.03
2	12.08	13.93	-27.72	3.27
13	15.45	14.41	-27.04	4.15
7	17.64	16.30	-27.50	3.68
10	16.09	16.34	-27.81	3.33
5	16.95	16.41	-26.28	4.79
3	15.59	16.61	-27.61	3.26
6	20.36	17.70	-25.71	4.75
e191	18.61	18.07	-18.82	2.93
12	27.46	27.56	-8.52	2.65
8	28.44	28.21	-15.81	4.14

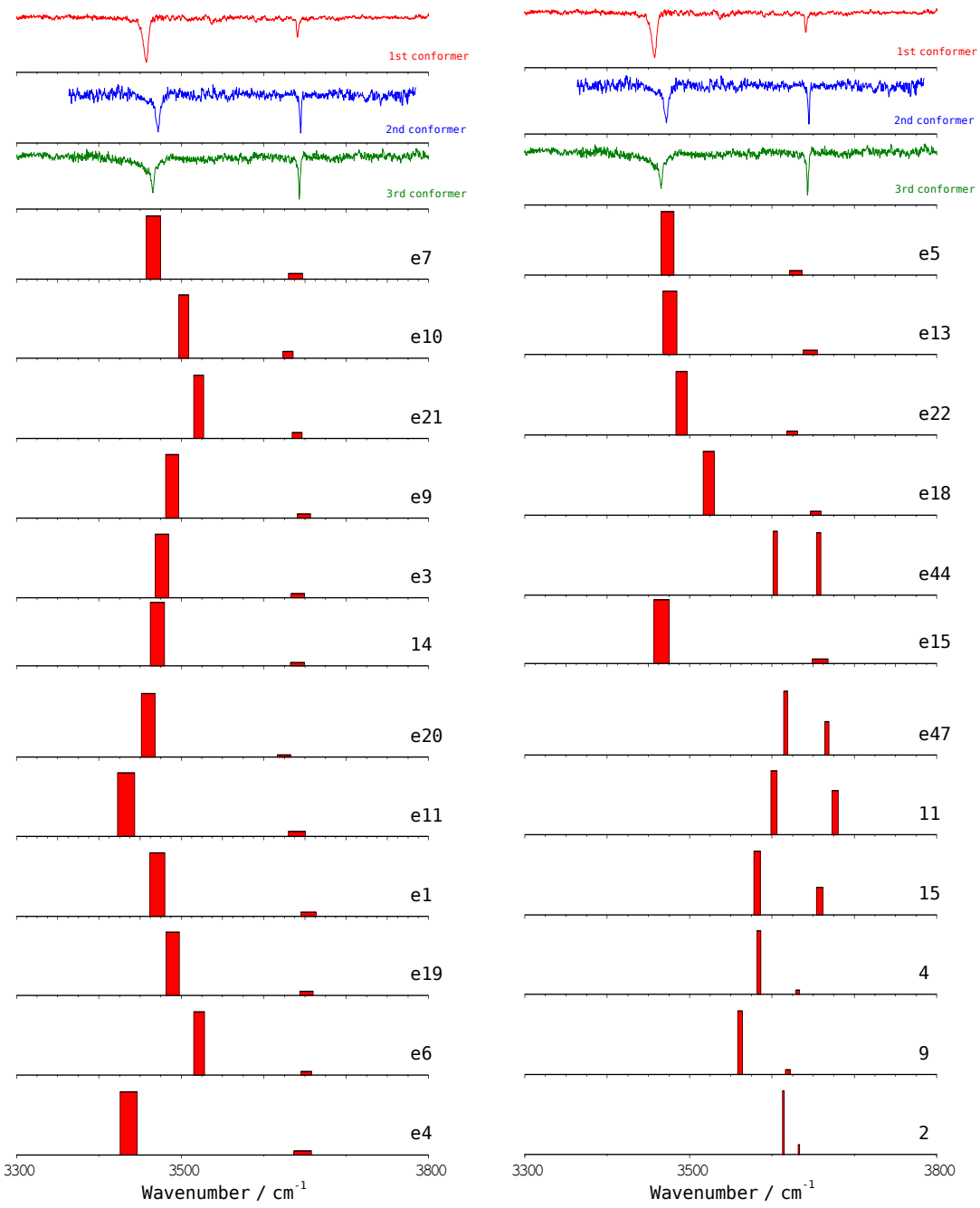

Figure 7.48a. *Experimental IDIRS for propofol·isopropanol (upper traces) together with the predicted frequencies for each calculated structure. A correction factor of 0.956 was employed.*

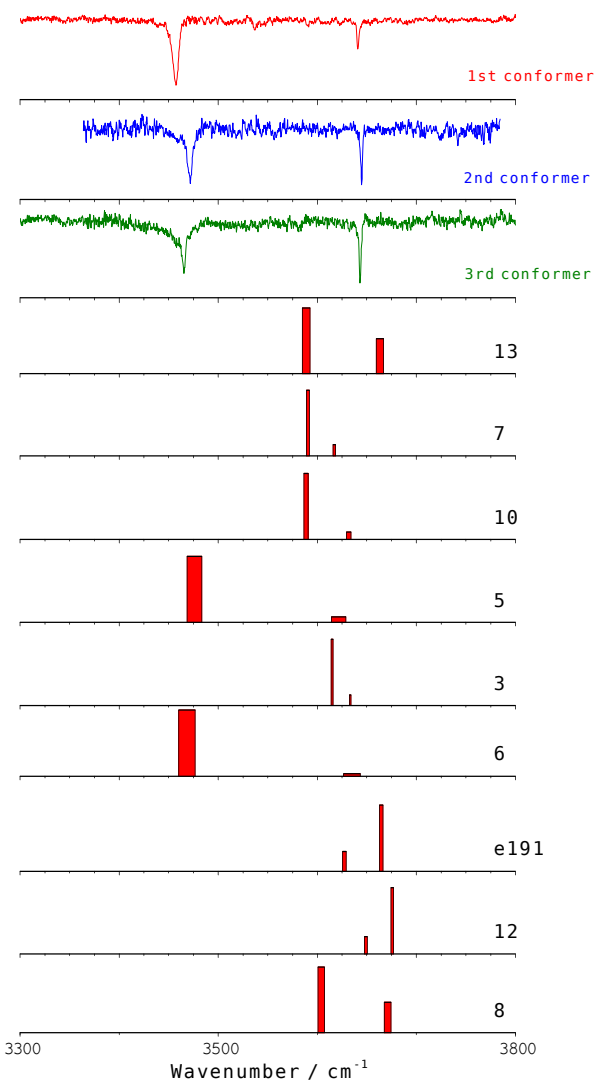

Figure 7.48b. *Experimental IDIRS for propofol·isopropanol (upper traces) together with the predicted frequencies for each calculated structure. A correction factor of 0.956 was employed.*

7.2 – Lifetimes

During this work, the lifetimes of all the propofol clusters were determined as explained in Section 3.1.2.9. The blue dots in the graphics represent the experimental data, while the dotted red line is the best fit. The lifetime in ns is indicated in an insert for each species.

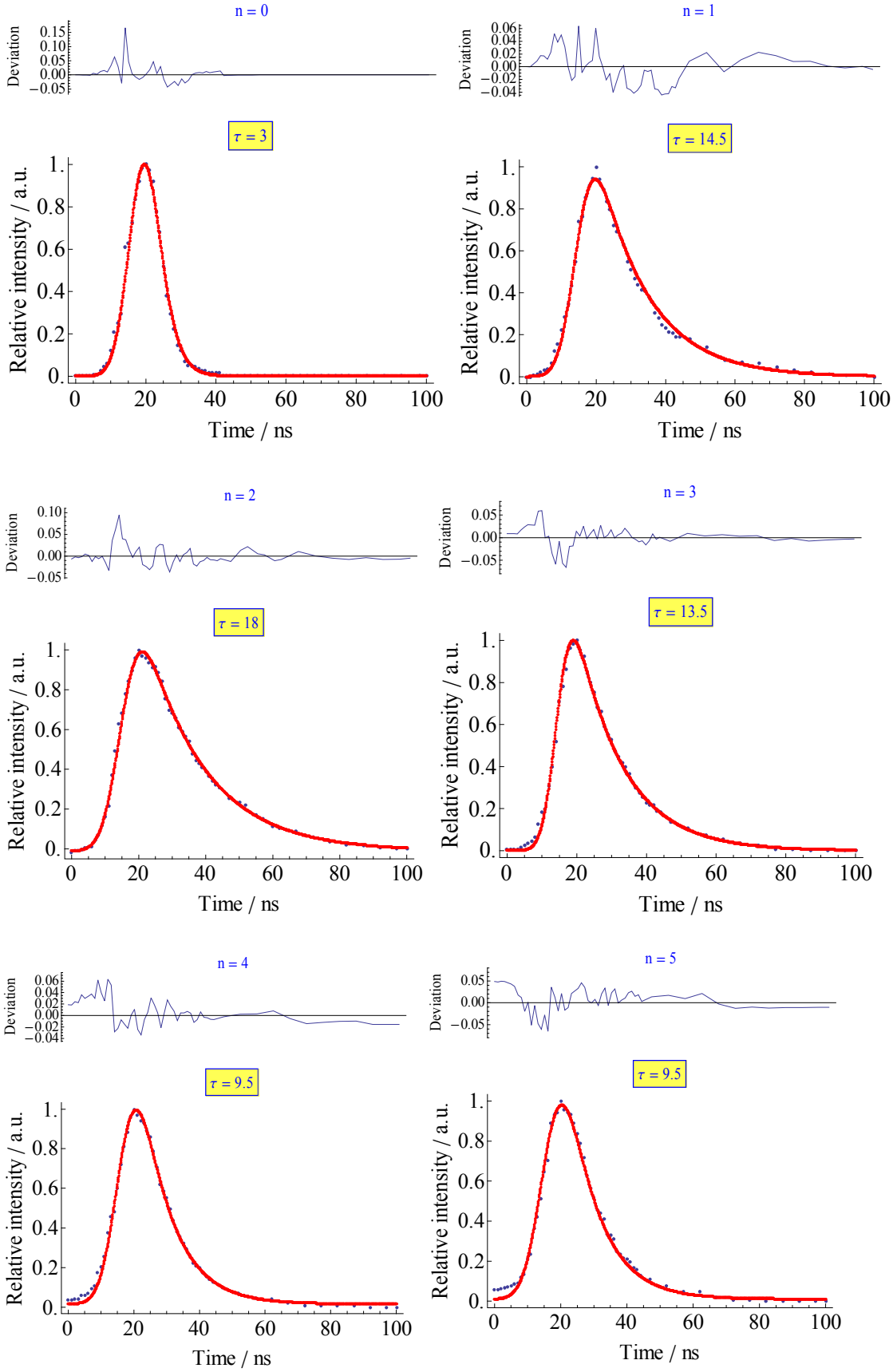

Figure 7.49. *Propofol·W_n, n=0-5, S_1 decays. The lifetime increases from the bare molecule to the propofol·W_{1-3} species and decreases again after introduction of the fourth water molecule. From this point, remains constant with the number of water molecules.*

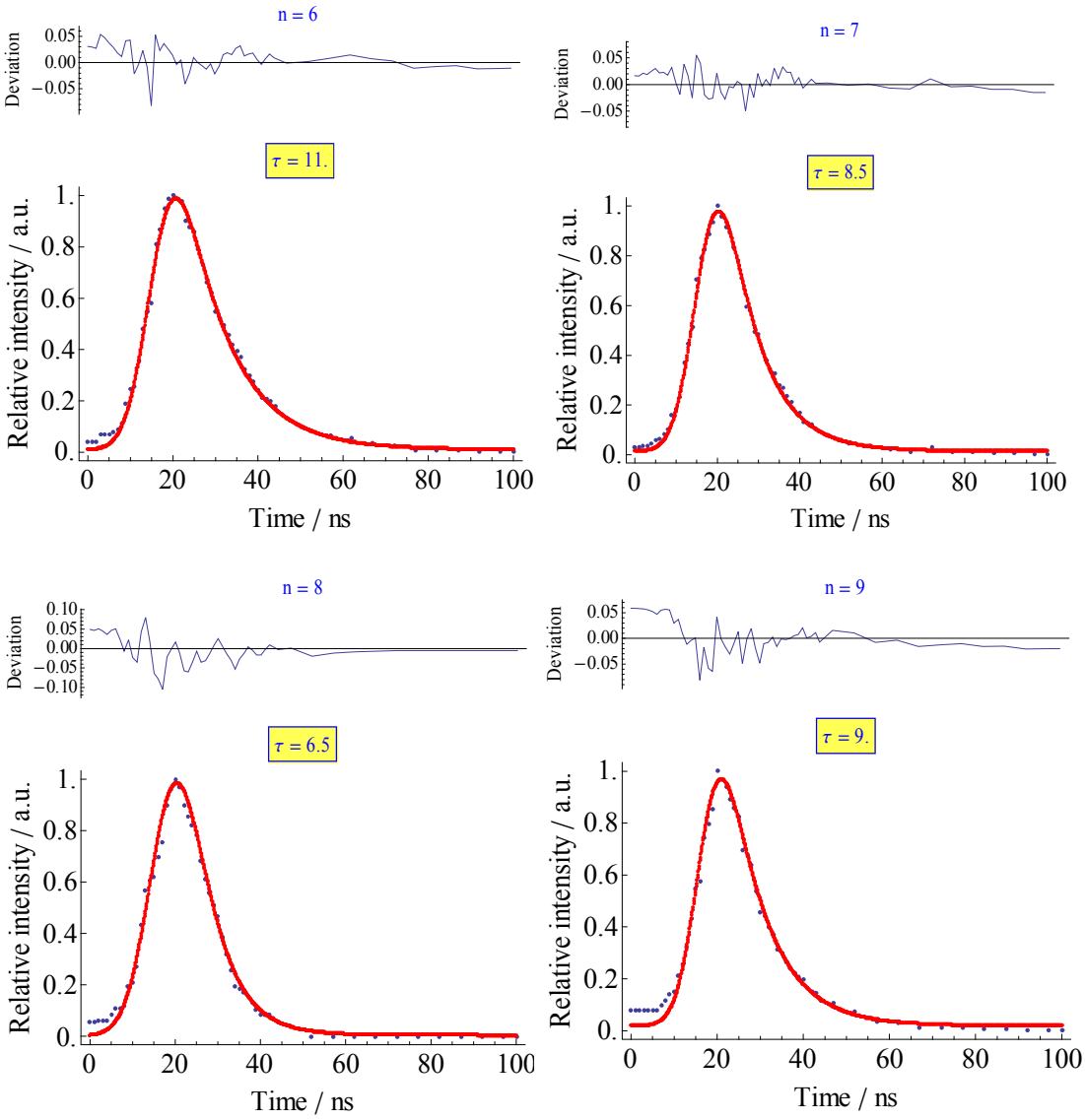

Figure 7.50. *Propofol·W_n, n=6-9, S_1 decays.*

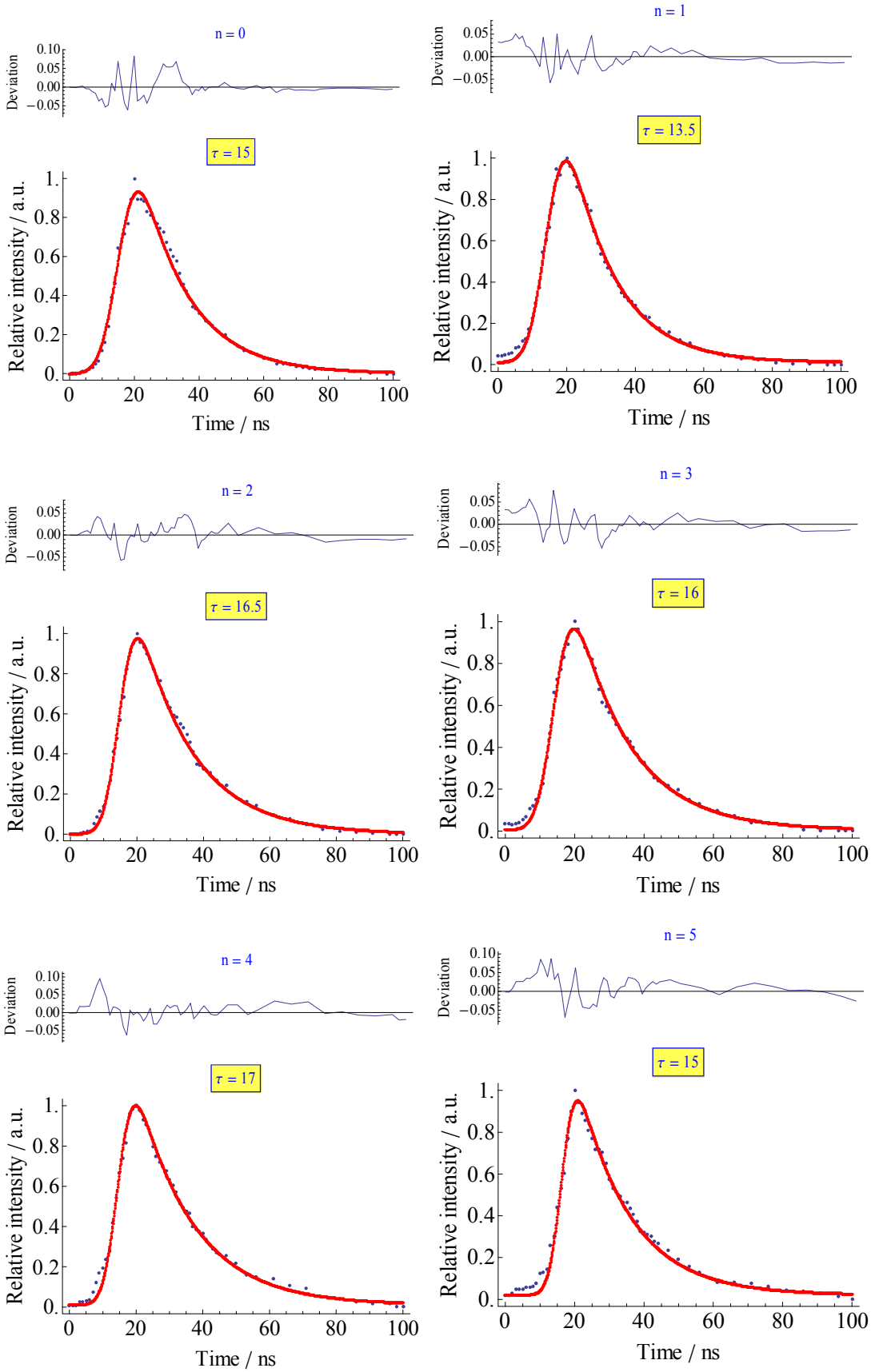

Figure 7.51. *Propofol$_2$·W$_n$, n=0-5, S$_1$ decays. All species present similar lifetimes around 15 ns.*

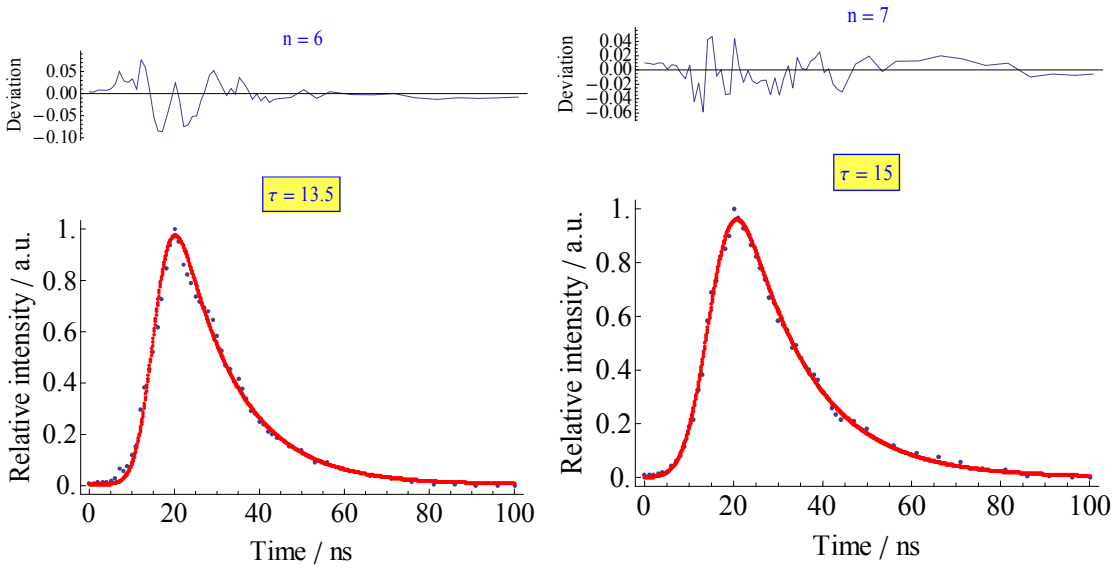

Figure 7.52. *Propofol$_2$·W$_n$, n=6-7, S$_1$ decays. All species present similar lifetimes around 15 ns.*

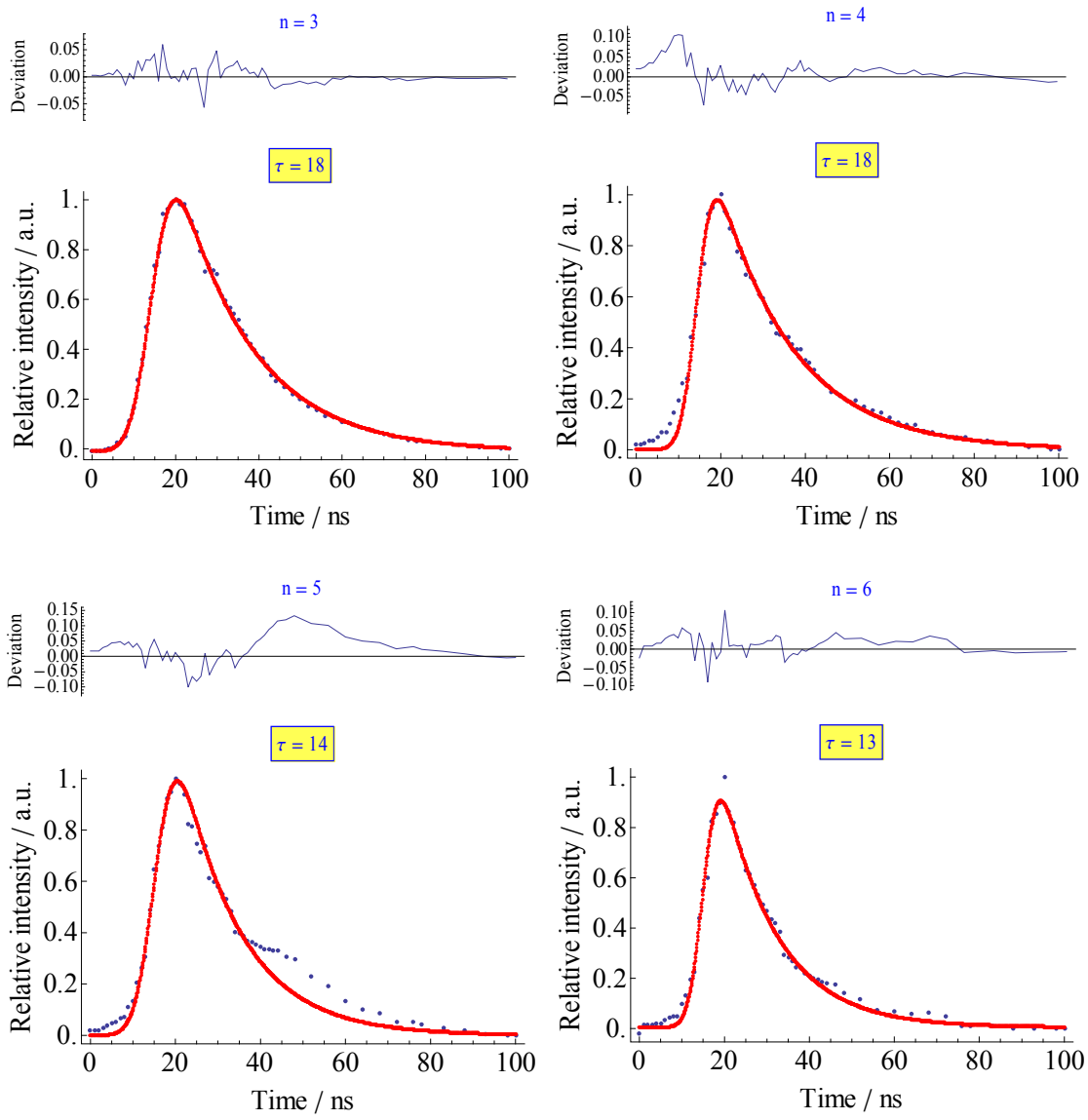

Figure 7.53. *Propofol$_n$, n=3-6, S_1 decays. The lifetime of propofol$_3$ and propofol$_4$ is c.a. 18 ns. For propofol$_5$ and propofol$_6$ the experimental results cannot be fitted to a single-exponential, probably due to intersystem crossing with a triplet state.*

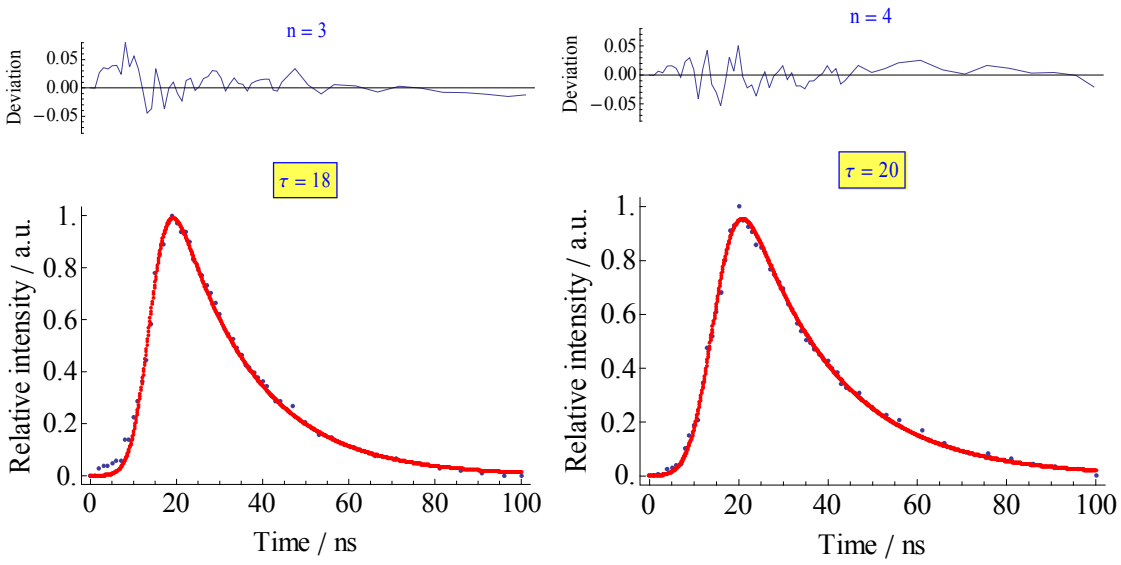

Figure 7.54. *Propofol$_n$·W$_1$ n=3-4, S$_1$ decays. The lifetime is c.a. 18 ns for both species.*

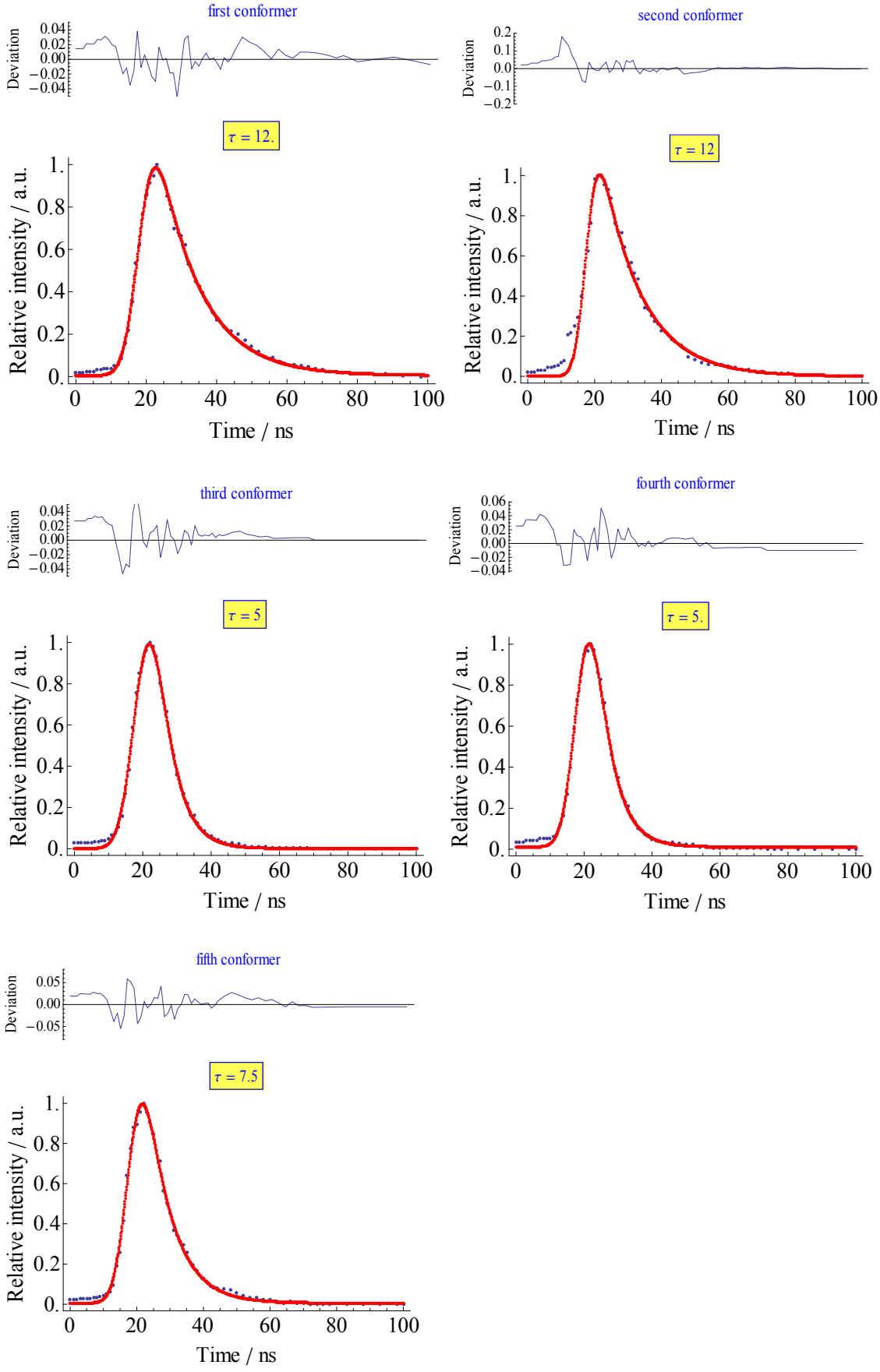

Figure 7.55. *Propofol·phenol S_1 decays. Note that the lifetime is c.a. 12 ns for the first and second conformers.*

7.3 – Calculations

During this work, a large number of calculations were carried out on systems of different size, with up to 186 atoms, and using mainly MP2 and M06-2x with several Pople's basis sets. We present here a compilation of the CPU times required on some of the calculations, as it may serve as a guide in future works. Table 7.30 shows the average time in days, employed to complete 60 optimization cycles (not steps) for each of the structures using 4 processors. It is well known that parallelization of HF and DFT methods is noticeably better than MP2. During this work we reached to the same conclusion: using more than 4 processors when running a MP2 calculation does not speed the calculations, as the time needed for an *opt+freq* calculation with 8 processors is almost the same as using 4 processors. On the other hand, when M06-2x, as well as other DFT methods are used, calculation time decreases almost linearly with the number of processors: for example, a calculation on propofol$_2$·W$_5$ (77 atoms) that takes 3 days and 6 hours with 4 processors takes half that time when using 8 processors (1 day and 15 hours), and less than 20 hours with 16 processors. Thus, the values presented here are obtained in 4-processor calculations, in order to compare with those obtained with MP2.

Finally, the calculations for large systems fail due to the CPHF step convergence problems, and it is necessary to tighten the integrals accuracy, using the "Int=Acc2E=11" option. According to our experience, such option is not required for systems like propofol$_2$·W$_7$ or smaller, while propofol$_3$ or larger systems required such option. This means that, somewhere between 81 and 93 atoms introducing the "Int=Acc2E=11" option is necessary. On the other hand, calculation times may be affected by the integral accuracy increasing the computational cost, although we did not make a systematic evaluation of in which factor.

Table 7.25. *CPU time (in days) employed for 60 optimization cycles using 4 processors for several propofol clusters, using three different Popel basis sets and two different theory levels.*

Molecule	M06-2x / 6-31+G(d)			M06-2x / 6-311++G(d,p)			MP2 / 6-311++G(d,p)		
	Opt	Freq	Total	Opt	Freq	Total	Opt	Freq	Total
Propofol	0.17	0.03	0.20	0.42	0.13	0.54	1.71	1.29	3.00
Propofol·W_1	0.17	0.04	0.21	0.46	0.13	0.58	3.25	2.00	5.25
Propofol·W_2	0.17	0.04	0.21	0.58	0.17	0.75	4.17	2.83	7.00
Propofol·W_3	0.25	0.08	0.33	0.79	0.29	1.08			
Propofol·W_4	0.25	0.08	0.33	0.96	0.33	1.29			
Propofol·W_5	0.33	0.08	0.42	1.08	0.42	1.50			
Propofol·W_6	0.38	0.13	0.50	1.17	0.54	1.71			
Propofol·W_7	0.46	0.17	0.63	1.67	0.75	2.42			
Propofol·W_8	0.46	0.21	0.67	1.79	1.08	2.88			
Propofol·W_9	0.54	0.29	0.83	1.83	1.25	3.08			
$Propofol_2$	1.29	0.71	2.00	5.00	4.25	9.25			
$Propofol_2$·W_1	1.5	0.75	2.25						
$Propofol_2$·W_2	1.54	0.83	2.38						
$Propofol_2$·W_3	1.67	1.13	2.79						
$Propofol_2$·W_4	1.96	1.42	3.38						
$Propofol_2$·W_5	2.13	1.54	3.67						
$Propofol_2$·W_6	2.21	1.75	3.96						
$Propofol_2$·W_7	2.46	1.96	4.42						
$Propofol_3$	5.71	3.50	9.21						
$Propofol_3$·W_1	5.92	3.67	9.59						
$Propofol_4$	11.00	10.33	21.33						
$Propofol_4$·W_1	11.13	11.38	22.51						
$Propofol_5$	24.00	27.00	51.00						
$Propofol_6$	42.00	66.00	108.00						

Figure 7.102 shows a plot of the computational cost of each calculation, against the number of processors. Although only a few clusters where studied with MP2, it is important to note that there is a substantial increment on the amount of time with the addition of a single water molecule, while for M06-2x the increment is hardly noticeable. Furthermore, propofol·W_2 MP2 calculation takes approximately the same time than a $propofol_2$ M06-2X calculation, using the same basis set. MP2 is a widely used level of theory and in this work we demonstrate that M06-2x reproduces reasonably well the experimental results at a reduced computational cost. This observation highlights the importance of finding theories which lead to good results without a high computational cost.

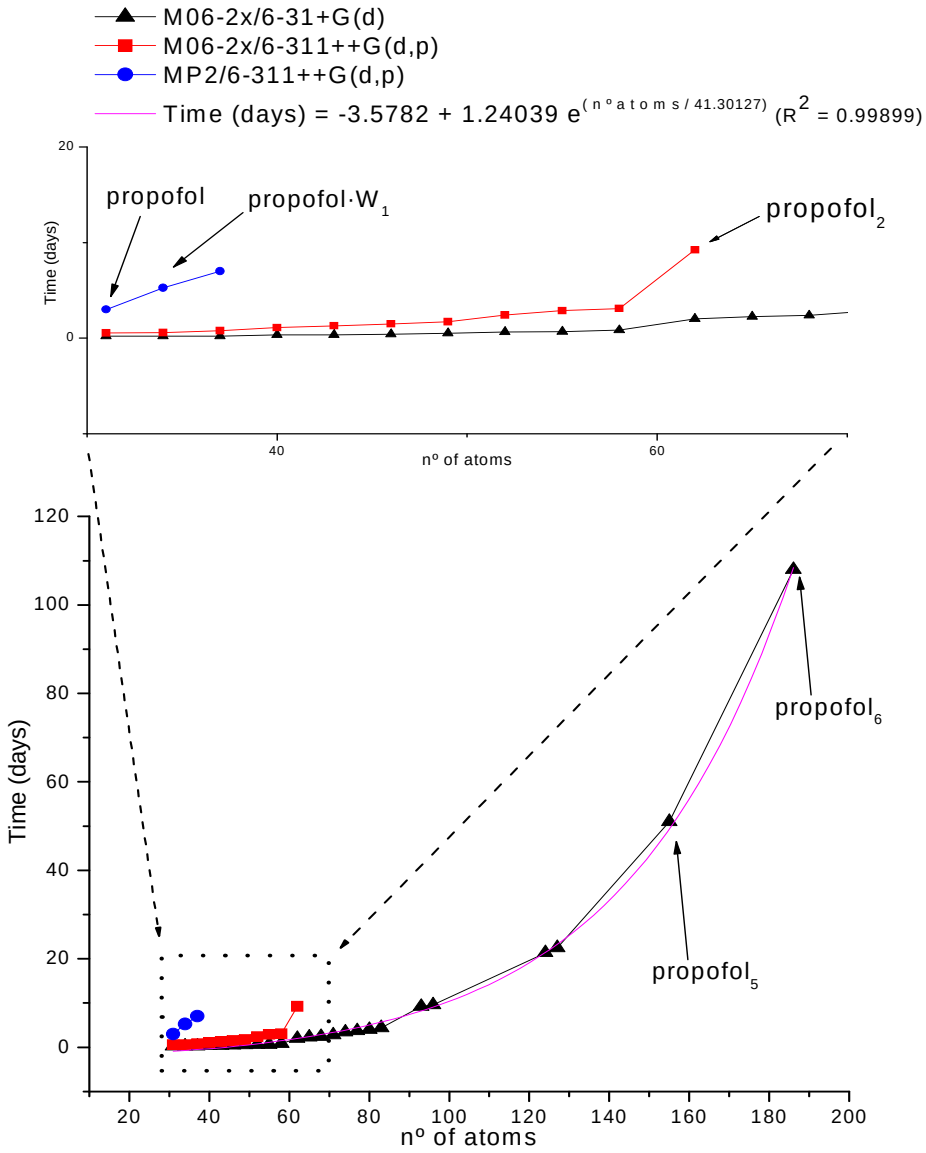

Figure 7.56. *Averaged time needed for an opt+freq calculation using different theories and basis sets, as a function of the number of atoms in the system. The exponential fit gives an estimation of the time needed for big systems (> 60 atoms).*

When M06-2x is employed, an important difference is observed with the basis set used. Calculation of propofol$_2$ is three times more expensive than propofol·W$_9$ if 6-311++G(d,p) is used, while it only doubles if 6-31+G(d) is chosen.

Finally, Figure 7.103 shows a plot of the averaged time needed for 60 optimization cycles (squares), frequency calculation (circles) and the addition of both calculations (triangles), against the number of atoms. The plot clearly indicates that optimization consumes most of the calculation time for systems smaller than propofol$_4$. For larger systems, the frequency calculation is more expensive, although the data in Figure 7.103 do not take into account the increase in the number of cycles required to reach optimization with the size of the system.

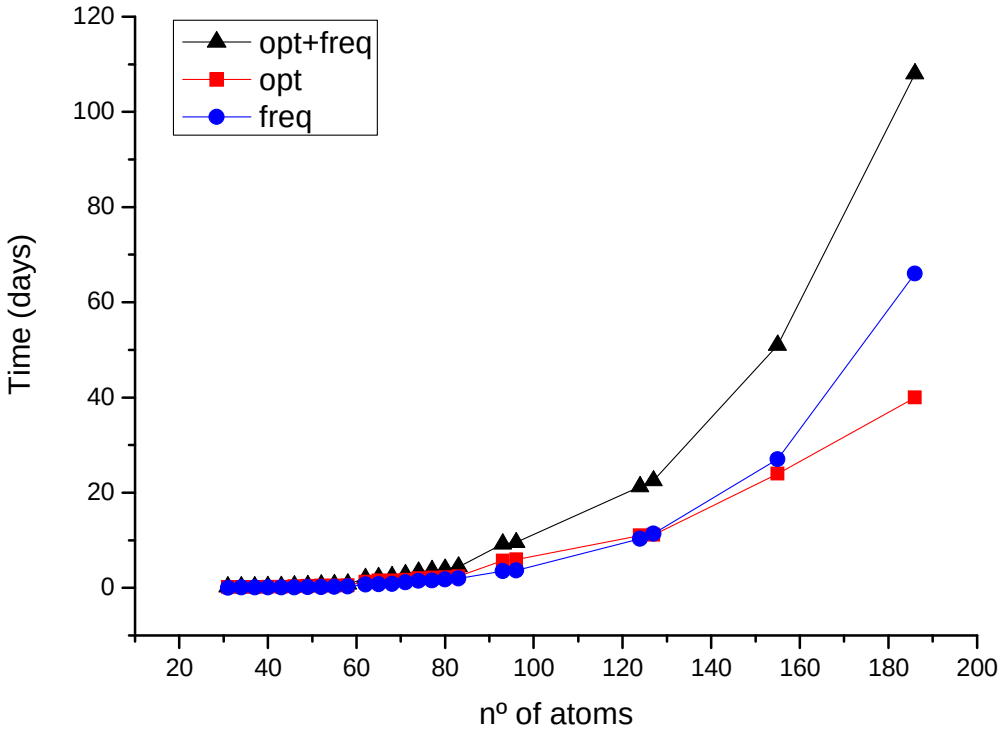

Figure 7.57. *Plot of the CPU-time for 60 optimization cycles and a frequency calculation against the number of atoms in the system, at M06-2x/6-31+G(d) level.*

It is also worthy to note that we have used up to 96 processors for propofol$_6$ calculations thanks to the computational resources and laser facilities from the SGI/IZO-SGIker and I2basque.

7.4 – Additional material

In this section a very short study on propofol·benzocaine and propofol$_2$·benzocaine is shown.

Although there is no biological motivation behind the study, its spectroscopy represents an interesting problem from the physico-chemical point of view, and an experimental challenge due to the variety of solvation points of benzocaine, propofol's isopropyl groups which impose some restrictions when trying to establish a hydrogen bond and the large size of the system.

Thus, this section shows some preliminary results of the spectroscopic exploration of propofol·benzocaine and propofol$_2$·benzocaine.

7.4.1 – Propofol·benzocaine

Figure 7.58 shows some of the calculated structures for this cluster. The most stable structures are those where both molecules are stabilized by dispersive forces and where propofol's OH moiety interacts with the benzocaine's C=O group (structures *e11, e183, e9*). When propofol acts as a proton-donor to the NH_2 group of benzocaine, the relative energy increases in nearly 5 kJ/mol (structure *e118*) because the isopropyl groups prevent propofol-OH···NH_2 reaching the optimal position that maximizes the hydrogen bond. The interaction with benzocaine's oxygen atom (structure *240*) is slightly more favorable. On the other hand, when propofol acts as a proton acceptor from the NH_2 group, the stability decreases in at least to 14 kJ/mol (structure *e185*). Finally, when only dispersive forces are present the structures are at least 25 kJ/mol (structure *3*) less stable that the global minimum.

Figure 7.59 shows a comparison of the *2c-REMPI* spectra of propofol·benzocaine and propofol$_2$·benzocaine. As can be seen, the spectrum of propofol·benzocaine shows only a few well resolved peaks starting at c.a. 34002 cm^{-1}. The increase in the background in the red-most part of the spectrum is surely due to fragmentation from propofol$_2$·benzocaine, whose *2c-REMPI* spectrum does not show any resolved transition.

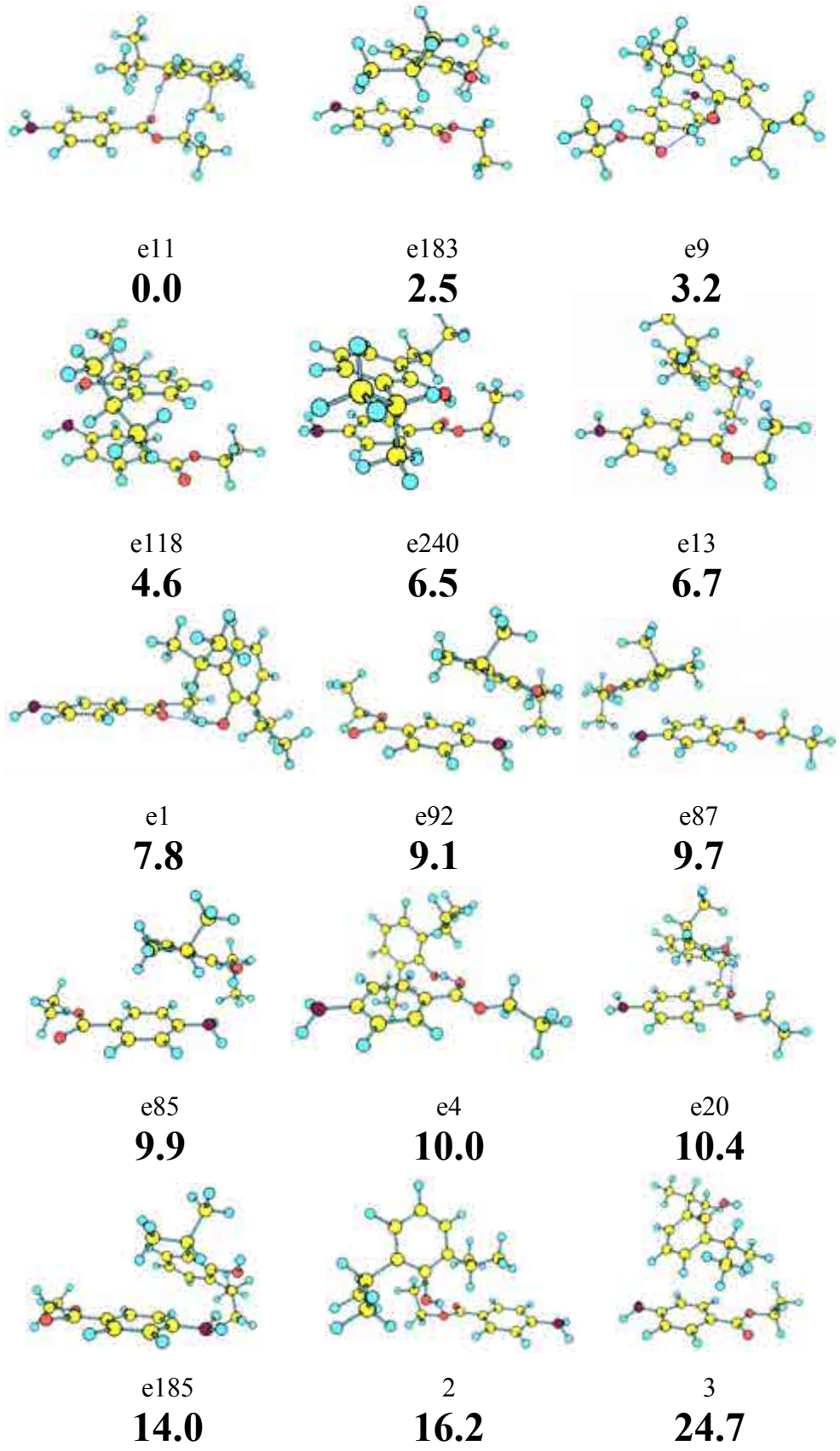

Figure 7.58. *Propofol·benzocaine calculated structures at M06-2x/6-31+G(d) level, with their ZPE-corrected relative energies in bold, in kJ/mol.*

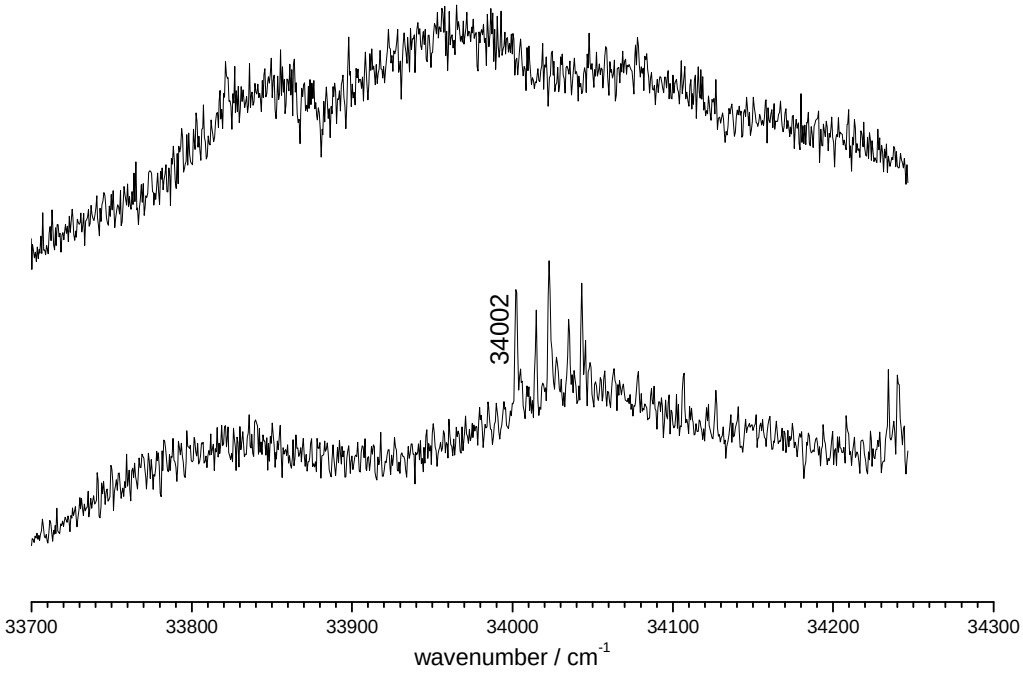

Figure 7.59. *2-color REMPI of propofol·benzocaine (lower trace) and propofol$_2$·benzocaine (upper trace), in the 33700-34300 cm^{-1} region, recorded setting the probe laser at 27972 cm^{-1}.*

Due to the poor S/N and to the weak intensity of the transitions, we were not able to record a *hole burning* experiment, but instead, an IDIR experiment probing each of the transitions was done, obtaining the same IR spectrum in all the cases (figure 7.60), indicating that, very likely, a single conformer is present. The IR spectrum shows three peaks: two of them due to the NH stretching modes and the third one due to propofol molecule's OH stretching.

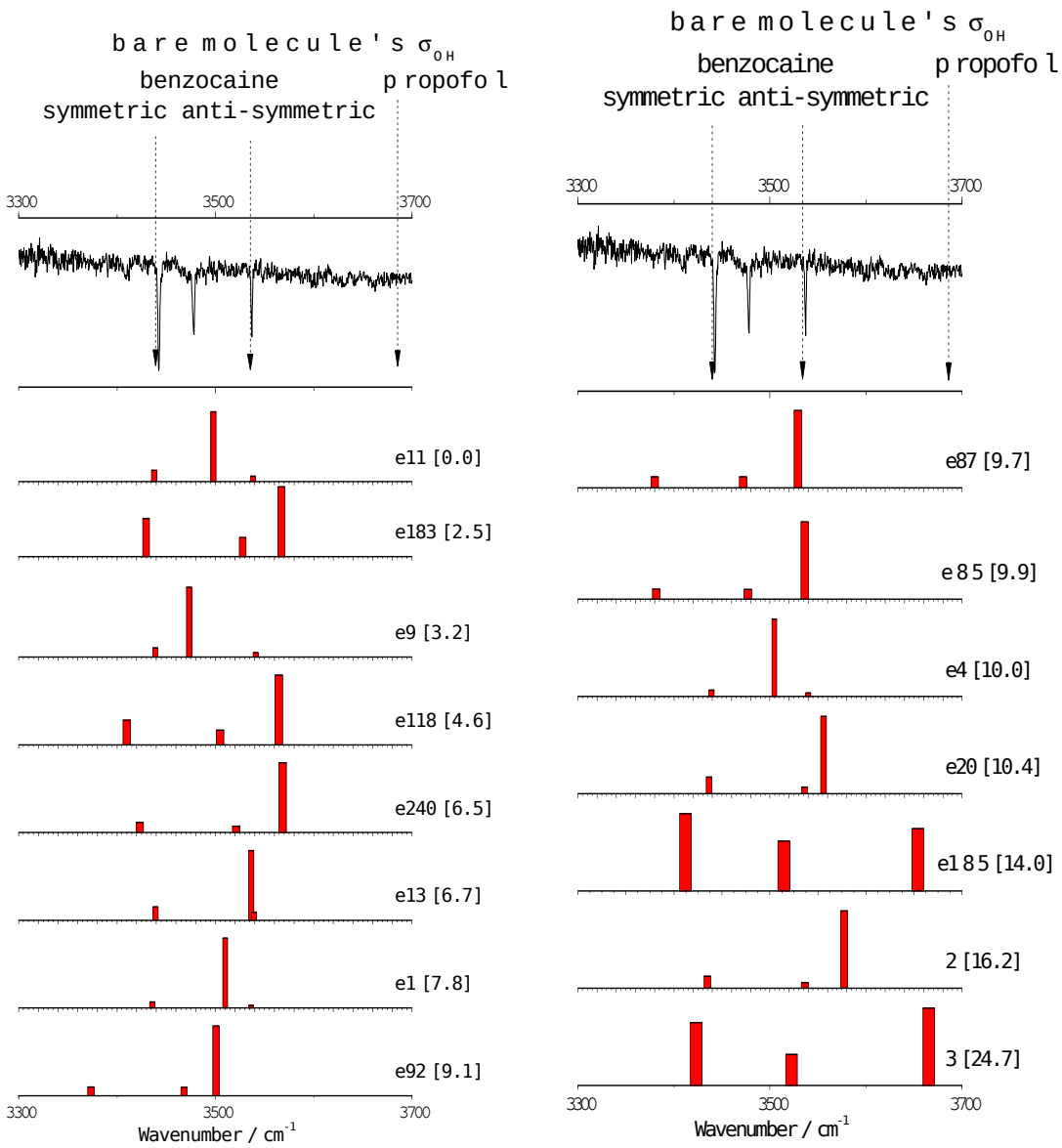

Figure 7.60. *Experimental IDIRS for propofol·benzocaine (upper trace) and the calculated frequencies for each of the calculated structures. The numbers in brackets are the relative energies of the calculated conformers, in kJ/mol. A correction factor of 0.955 was applied.*

Assignment

The three bands in the IDIR spectrum are located at 3443, 3478 and 3537 cm^{-1}. For the propofol bare molecule, the OH stretching appears at 3685 cm^{-1} while for the benzocaine bare molecule the symmetric OH stretching at c.a. 3435 cm^{-1} and the anti-symmetric OH stretching at c.a. 3535 cm^{-1}, when the same correction factor is applied. Such values perfectly match those for the predicted IR spectrum of structure *3*, where the stabilization is only by dispersive forces and thus no hydrogen bond is taking place.

The assignment is quite straightforward, as the only predicted IR spectra that reproduce the experimental results are those where the two NH moieties are free and propofol is hydrogen bonded to the C=O group. Such interaction causes a red shift in the OH stretching mode. Structures *e11 and e9* can reproduce the experimental results and are those where the **propofol molecules is hydrogen bonded to the C=O group**. Figure 7.61 shows the most stable structure for this kind of interaction. These results remark the importance of dispersive forces, as already stated for the propofol dimer.

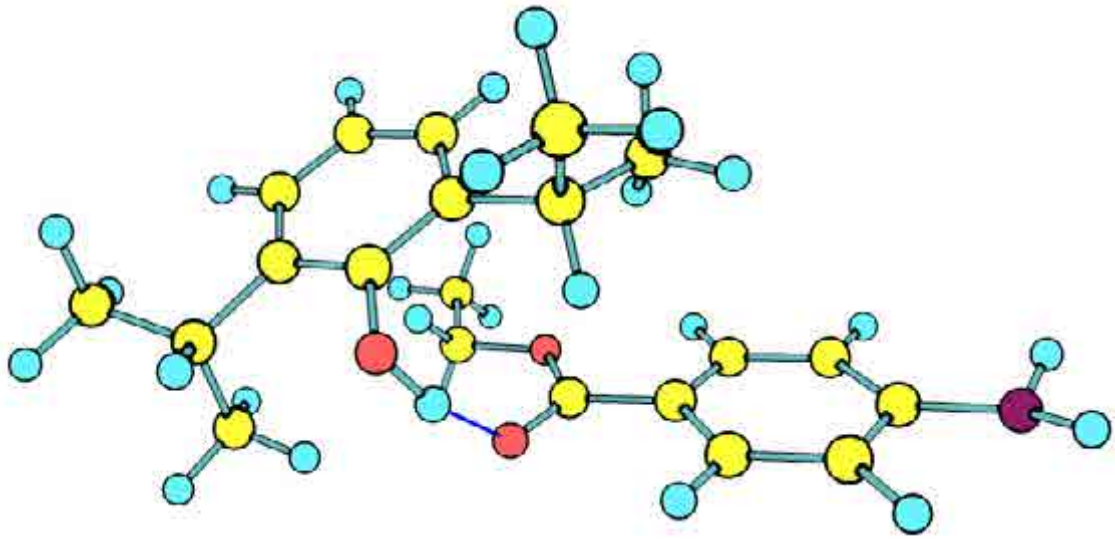

Figure 7.61. *Structure e11 is the most stable one that can reproduce the experimental results. Note the O-H···O=C interaction*

.

7.3.2 – Propofol$_2$·benzocaine

Figure 7.62 shows some of the calculated structures for this cluster. Different interaction-based structures were found, and as can be seen, all of them are stabilized by dispersive forces between the isopropyl groups and the aromatic rings. Apart from this stabilization, the most stable structures are those where one of the propofol molecules acts as a proton donor to the other propofol, while the latter hydrogen bonds to the C=O group (structures *e5, e13, e1*). Instead, if propofol interacts with benzocaine's NH_2 group, the relative energy increases in nearly 5 kJ/mol (structure *e1603*) as encountered for propofol·benzocaine cluster. Other structures where the propofol molecules do not hydrogen bond, and instead, one of the propofol interacts with the NH and the other one to the C=O (structures *e1606, 3*) are found at higher relative energies, up to 20 kJ/mol.

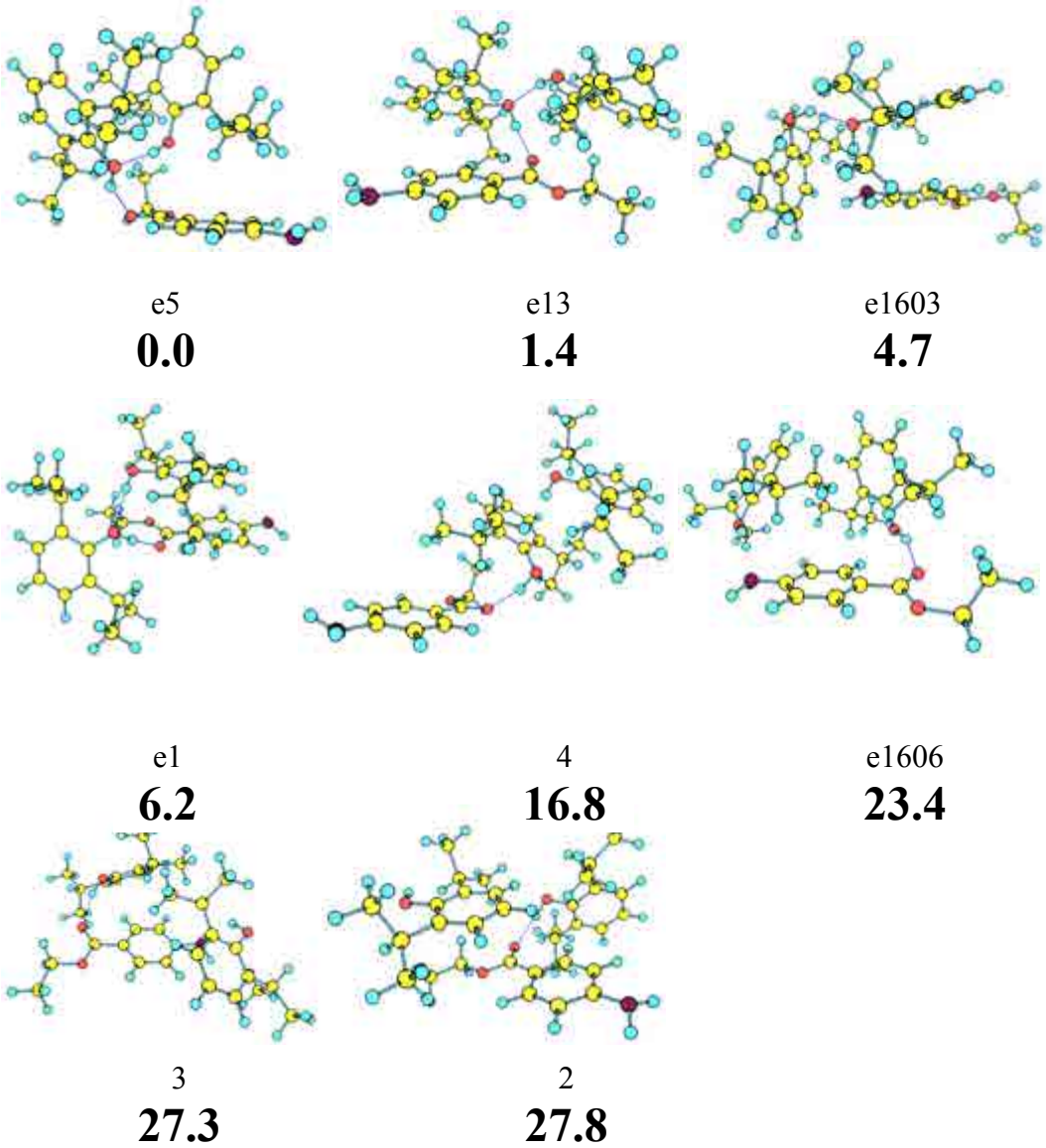

Figure 7.62. *Propofol$_2$·benzocaine calculated structures at M06-2x/6-31+G(d) level, with their ZPE-corrected relative energies in bold, in kJ/mol.*

As previously stated, figure 7.63 shows a non resolved spectrum for propofol$_2$·benzocaine cluster. Nevertheless, we managed to obtain an IDIR spectrum by probing at different wavelength within the broad absorption. As happens with propofol·benzocaine, a single IR spectrum was obtained. An intense peak at c.a. 3560 cm^{-1} is clearly seen and another intense and broad band in the 3380-3420 cm^{-1} region which probably involves more than one OH stretching vibration is also found.

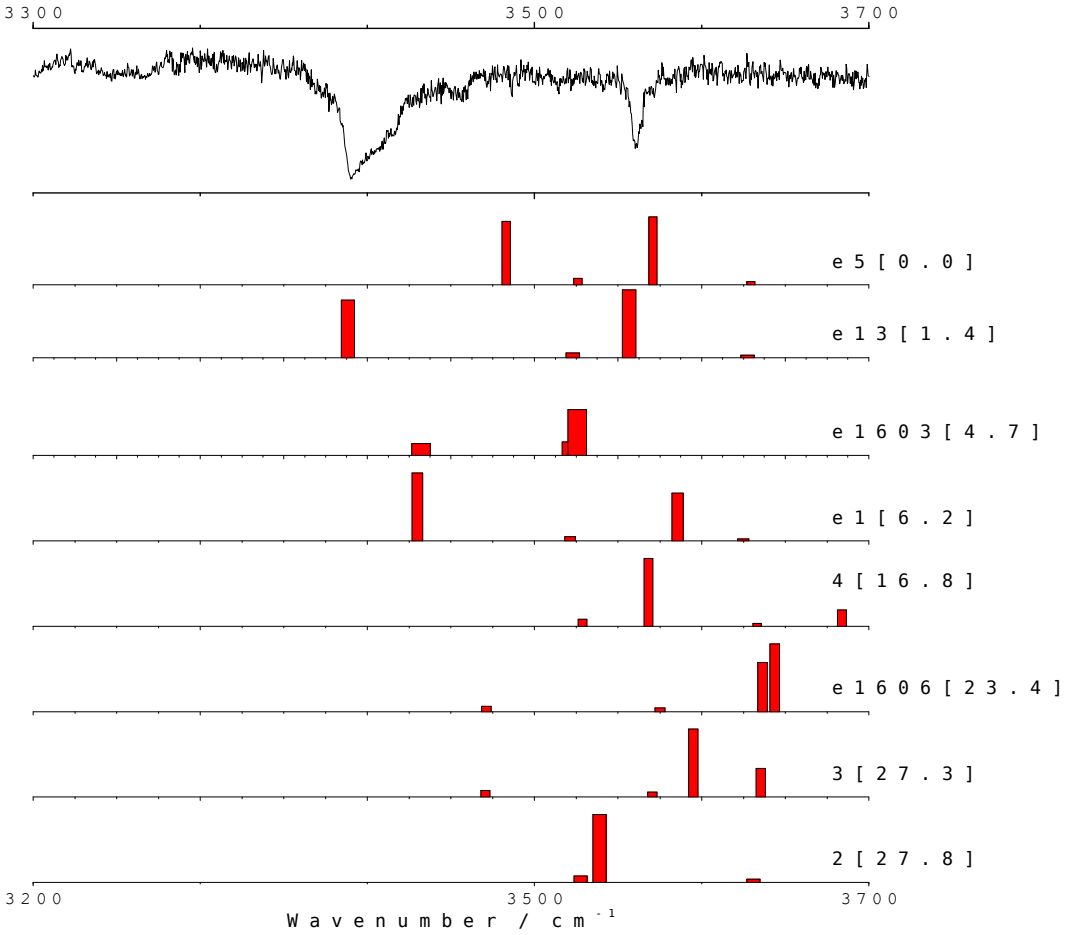

Figure 7.63. *Experimental IDIRS for propofol$_2$·benzocaine (up) and the calculated frequencies for each of the calculated structures. The numbers in brackets are the relative energies of the calculated conformers, in kJ/mol. A correction factor of 0.98 was applied.*

Assignment

Only structures *e13* and *e1* present calculated spectra that reproduce the experimental one. This indicates that the experimental conformer is that where one of the propofol molecules acts as an acid, hydrogen bonded to the other one, while the latter hydrogen bonds to the C=O group. The molecules experiment a great stabilization due to dispersive forces, as their aromatic rings and isopropyl groups are interacting. Figure 7.64 shows structure *e13*, one of the most stable structures for this kind of interaction. It is remarkable how other similar structures based on the same type of interaction, as structure *e5*, where the only difference is that the propofol molecule which is hydrogen bonded to the carboxyl group, is not placed in an optimal position and thus, the hydrogen bond is far away from an ideal one, do not correctly reproduce the experimental results. It is important to note that the relative position of the molecules is determined by the dispersive forces, remarking once again the importance of such interactions, which play the main role in their stacking.

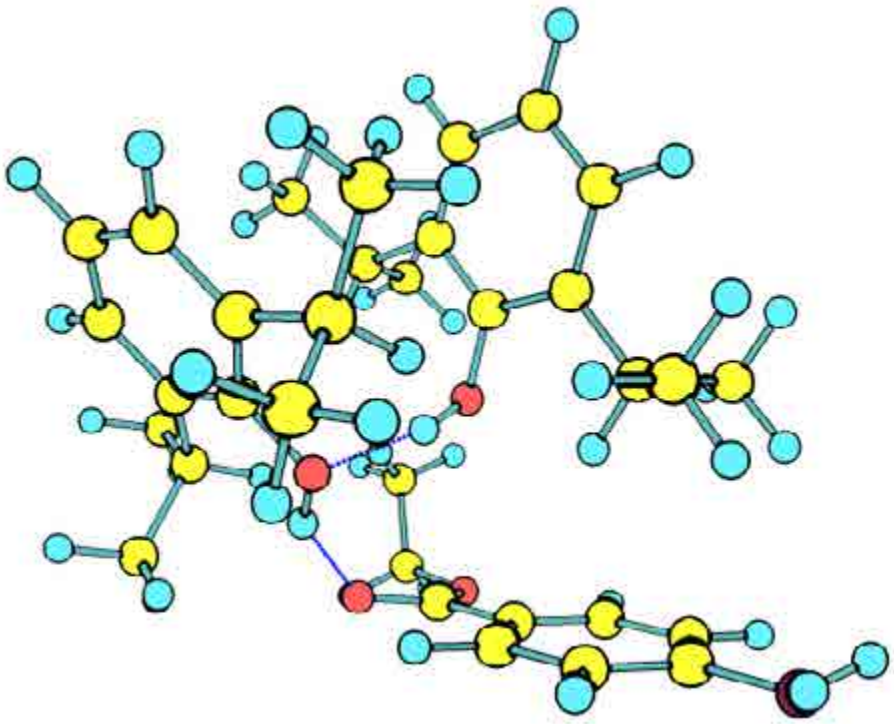

Figure 7.64. *Structure e13 is one of the most stable structures representing the interaction type present for our detected experimental conformer.*

Acknowledgments

I would like to thank Prof. Fernando Castaño for accepting me in his group and specially Dr. José Andrés Fernández for giving me the opportunity of growing up as a scientist thanks to his wise advises and for his help and patience, which I have found to be infinite, to finish this thesis writing. Also, thanks for letting me play basketball in the team ☺

I express my gratitude to Drs. Emilio Cocinero and Judith Milán for their help and for introducing me in the world of theoretical calculations.

One special thank to the Drs. Asier Longarte (a big scientist) and Edurne Aguado for all their support in the lab, dedication and patience.

I also would like to thank the Drs. Maria Nieves Sánchez, Francisco Basterretxea, Roberto Matínez and Alberto Lesarri for the invaluable help.

Another great thanks for my lab-coworkers: Álvaro, Borja, Carola, David, Eduardo, Egoitz, Estela, Esti, Imanol, Jon, Lorena, Patricia, Raúl, Rober, Silvia, Sonia, Veloso, Virginia, who bear with me along this time and who let me have a really good time!!!

I cannot forget Dr. Anouk Risk, Sanders Jaeqx and everyone at FELIX for their amazing work and all the good time.

A special thanks to all of my friends who keep supporting me ☺

And last, but never least, I am indescribably grateful to my family for their love and support.

I also would like to thank the GV for a pre-doctoral research fellowship.

Computational resources and laser facilities from the SGI/IZO-SGIker and I2basque were used for this work.